FOOD PROTEIN-BASED COLLOIDS: STRUCTURE, DIGESTION, AND NUTRIENTS DELIVERY

EDITED BY: Yuan Li, Weilin Liu, Pete Wilde and Jianhua Liu
PUBLISHED IN: Frontiers in Nutrition

frontiers Research Topics

ISSN 1664-8714
ISBN 978-2-88976-785-4
DOI 10.3389/978-2-88976-785-4

About Frontiers

Frontiers is more than just an open-access publisher of scholarly articles: it is a pioneering approach to the world of academia, radically improving the way scholarly research is managed. The grand vision of Frontiers is a world where all people have an equal opportunity to seek, share and generate knowledge. Frontiers provides immediate and permanent online open access to all its publications, but this alone is not enough to realize our grand goals.

Frontiers Journal Series

The Frontiers Journal Series is a multi-tier and interdisciplinary set of open-access, online journals, promising a paradigm shift from the current review, selection and dissemination processes in academic publishing. All Frontiers journals are driven by researchers for researchers; therefore, they constitute a service to the scholarly community. At the same time, the Frontiers Journal Series operates on a revolutionary invention, the tiered publishing system, initially addressing specific communities of scholars, and gradually climbing up to broader public understanding, thus serving the interests of the lay society, too.

Dedication to Quality

Each Frontiers article is a landmark of the highest quality, thanks to genuinely collaborative interactions between authors and review editors, who include some of the world's best academicians. Research must be certified by peers before entering a stream of knowledge that may eventually reach the public - and shape society; therefore, Frontiers only applies the most rigorous and unbiased reviews.
Frontiers revolutionizes research publishing by freely delivering the most outstanding research, evaluated with no bias from both the academic and social point of view. By applying the most advanced information technologies, Frontiers is catapulting scholarly publishing into a new generation.

What are Frontiers Research Topics?

Frontiers Research Topics are very popular trademarks of the Frontiers Journals Series: they are collections of at least ten articles, all centered on a particular subject. With their unique mix of varied contributions from Original Research to Review Articles, Frontiers Research Topics unify the most influential researchers, the latest key findings and historical advances in a hot research area! Find out more on how to host your own Frontiers Research Topic or contribute to one as an author by contacting the Frontiers Editorial Office: frontiersin.org/about/contact

FOOD PROTEIN-BASED COLLOIDS: STRUCTURE, DIGESTION, AND NUTRIENTS DELIVERY

Topic Editors:
Yuan Li, China Agricultural University, China
Weilin Liu, Zhejiang Gongshang University, China
Pete Wilde, Quadram Institute, United Kingdom
Jianhua Liu, Zhejiang University of Technology, China

Citation: Li, Y., Liu, W., Wilde, P., Liu, J., eds. (2022). Food Protein-Based Colloids: Structure, Digestion, and Nutrients Delivery. Lausanne: Frontiers Media SA. doi: 10.3389/978-2-88976-785-4

Table of Contents

frontiers | Frontiers in Nutrition

TYPE Editorial
PUBLISHED 18 July 2022
DOI 10.3389/fnut.2022.982366

OPEN ACCESS

EDITED AND REVIEWED BY
Ken Ng,
The University of Melbourne, Australia

*CORRESPONDENCE
Pete Wilde
peter.wilde@quadram.ac.uk
Jianhua Liu
jhliu@zjut.edu.cn

SPECIALTY SECTION
This article was submitted to Food Chemistry, a section of the journal Frontiers in Nutrition

RECEIVED 30 June 2022
ACCEPTED 04 July 2022
PUBLISHED 18 July 2022

CITATION
Li Y, Liu W, Wilde P and Liu J (2022) Editorial: Food Protein-Based Colloids: Structure, Digestion, and Nutrients Delivery. *Front. Nutr.* 9:982366. doi: 10.3389/fnut.2022.982366

Editorial: Food Protein-Based Colloids: Structure, Digestion, and Nutrients Delivery

Yuan Li[1], Weilin Liu[2], Pete Wilde[2,3]* and Jianhua Liu[4]*

[1]Key Laboratory of Precision Nutrition and Food Quality, Key Laboratory of Functional Dairy, College of Food Science and Nutritional Engineering, China Agricultural University, Beijing, China, [2]School of Food Science and Biotechnology, Zhejiang Gongshang University, Hangzhou, China, [3]Quadram Institute Bioscience, Norwich Research Park, Norwich, United Kingdom, [4]College of Food Science and Technology, Zhejiang University of Technology, Hangzhou, China

KEYWORDS

protein-based colloids, emulsion, gel, digestion, structure

Editorial on the Research Topic
Food Protein-Based Colloids: Structure, Digestion, and Nutrients Delivery

Introduction

There has been much interest over the years in protein-based colloidal systems and utilizing the functionality of protein in food systems has been a target for many researchers and there is a huge literature on their gelling, thickening, emulsifying, and foaming properties. Proteins are seen as a natural alternative to synthetic emulsifiers and stabilizers, which are generally perceived to be artificial and associated with unhealthy ultra-processed foods. Therefore, this earlier research on protein functionality is now being exploited to formulate protein-based colloidal structures with functionalities capable of delivering health benefits. The papers in this special issue reflect very well the current and emerging trends in protein-colloid research in the food and nutrition space.

Protein-based particles

Powder and particulate technology have been used to develop powdered or granulated systems with a low water content, and hence long shelf life and low transport costs, but could be reconstituted easily at point of use. By creating the right structure with the right properties, such colloidal particles can be loaded with bioactive compounds to improve storage stability and functionality. Zhang et al. showed that they could create particles using the maize protein zein complexed with gum Arabic. The particle stability was improved by adding tannic acid to enhance the intermolecular interactions. Similarly, Chen et al. complexed zein with glycosylated lactoferrin to form nanoparticles that could encapsulate the flavone 7,8-dihydroxyflavone (7,8-DHF), which had good stability, high encapsulation efficiency and *in vitro* bioaccessibility of the DHF.

Simple emulsion systems

Proteins can stabilize emulsions, but they are not always as effective as small molecule emulsifiers, but they can add other functionalities to an emulsion. The first example is from Cai et al. where they tried to enhance the functionality of thymol, a natural antibiotic by encapsulating it with lauric acid in a caseinate stabilized emulsion. The caseinate emulsions are highly stable, but readily digestible, making the thymol available to control bacterial growth. Wang Q. et al. found that certain ratios of whey protein and caseinate could stabilize the emulsion against calcium induced aggregation and also improve oxidative stability, potentially offering a solution to improve the nutritional and functional properties of infant formulae.

Pickering emulsions

Pickering emulsions are stabilized by particles which are held at the interface by surface interactions between the three phases (oil, water, and particle). Their application in food systems has been limited, and the most effective Pickering particles are synthetic and not suitable for human consumption. More recent work has focussed on the use of food grade particles, such as protein aggregates to form food-suitable Pickering emulsions. Ren et al. utilized insoluble protein nano-particles from tea residues as natural, sustainable emulsifiers. The emulsions showed tuneable rheological properties as a function of ionic strength. The high stability of Pickering emulsions is further demonstrated by Shen et al. who combined bacterial nano-cellulose and soy protein to create strong, stable particles through anti-solvent precipitation. These particles offered excellent emulsion stability, and improved the bioavailability of curcumin. A similar approach was used by Kiat Wong et al. who also used cellulose and soy protein to form Pickering emulsions which were incorporated into gel beads as a targeted delivery device to control release of the encapsulated bioactive compound. Finally, Wang J. et al. used whey protein aggregates to stabilize emulsions containing the long chain fatty acid DHA. This approach again improved the oxidative stability and delivery of the DHA.

Emulsion gels

Emulsion gels are an interesting composite system as their rheological and functional properties depend on both the emulsion and the gel matrix as well as the interactions between the phases. These areas have been reviewed by Abdullah et al. showing how research on the gel-matrix interactions is being applied to functionalities such as fat replacement, controlled release and probiotic delivery, demonstrating the versatility of these structures to provide multiple functionalities in food products. This was demonstrated by Su et al. who found that high pressure processing could influence interactions between the emulsion and gel phases, altering not only the gel properties but also the delivery of encapsulated curcumin. Similarly, as discussed earlier, the incorporation of Pickering emulsions into gel beads could also be used to control release of bioactives (Kiat Wong et al.).

Emulsifier replacement

There is a drive toward replacing artificial emulsifiers with more natural alternatives. Protein-particles can create very stable Pickering emulsions, but tend to have large droplet size, which is not always desirable in food systems. To address this, the surface activity and structure of the protein molecule itself needs to be altered. Li et al. have reviewed a specific approach of utilizing protein-polyphenol complexes to alter the secondary structure, hydrophobicity and flexibility of the protein. This can significantly improve the emulsifying properties of the protein, leading to finer, more stable emulsions, acting as possible replacements of artificial emulsifiers, whilst also adding further functionalities such as improved oxidative stability and delivery of bioactive compounds.

Plant based systems

Finally, another global food challenge is the move away from animal protein toward plant-based systems. Most plant proteins have poor solubility and require extensive processing to improve functionality. Some of the papers already described are addressing this challenge, to improve the functional properties of plant proteins. All these papers are effectively utilizing the poor solubility of plant proteins, to form particles to either act as functional carriers themselves (Zhang et al.) or to stabilize Pickering emulsions with plant protein-based particles (Kiat Wong et al.; Ren et al.; Shen et al.).

Summary

The utilization of protein-based colloidal systems has been based on many years of fundamental research into the molecular, colloidal, structural, and functional properties of these systems. This research is currently being applied to develop intelligently designed structures with enhanced functionalities, particularly the oxidative stability and bioavailability of beneficial bioactive compounds whilst also addressing the demand for more natural and sustainable food ingredients.

Author contributions

YL, WL, and JL: writing—review and editing. PW: writing—original draft. All authors contributed to the article and approved the submitted version.

Funding

PW gratefully acknowledges the support of the Biotechnology and Biological Sciences Research Council (BBSRC) through the BBSRC Institute Strategic Programme Food Innovation and Health BB/R012512/1.

Conflict of interest

The authors declare that the research was conducted in the absence of any commercial or financial relationships that could be construed as a potential conflict of interest.

Publisher's note

frontiers in Nutrition

ORIGINAL RESEARCH
published: 07 September 2021
doi: 10.3389/fnut.2021.734620

Fabrication of Bacterial Cellulose Nanofibers/Soy Protein Isolate Colloidal Particles for the Stabilization of High Internal Phase Pickering Emulsions by Anti-solvent Precipitation and Their Application in the Delivery of Curcumin

Rui Shen[1], *Dehui Lin*[1]*, *Zhe Liu*[1], *Honglei Zhai*[2] *and Xingbin Yang*[1]

[1] *Shaanxi Engineering Laboratory for Food Green Processing and Safety Control, Shaanxi Key Laboratory for Hazard Factors Assessment in Processing and Storage of Agricultural Products, College of Food Engineering and Nutritional Science, Shaanxi Normal University, Xi'an, China,* [2] *Department of Pediatrics, Children's Nutrition Research Center, Baylor College of Medicine, Houston, TX, United States*

OPEN ACCESS

Edited by:
Jianhua Liu,
Zhejiang University of Technology, China

Reviewed by:
Wei Liu,
Nanchang University, China
Fuguo Liu,
Northwest A and F University, China

***Correspondence:**
Dehui Lin
lindehui504@snnu.edu.cn

Specialty section:
This article was submitted to Food Chemistry, a section of the journal Frontiers in Nutrition

Received: *01 July 2021*
Accepted: *12 August 2021*
Published: *07 September 2021*

Citation:
Shen R, Lin D, Liu Z, Zhai H and Yang X (2021) Fabrication of Bacterial Cellulose Nanofibers/Soy Protein Isolate Colloidal Particles for the Stabilization of High Internal Phase Pickering Emulsions by Anti-solvent Precipitation and Their Application in the Delivery of Curcumin. Front. Nutr. 8:734620. doi: 10.3389/fnut.2021.734620

In this study, the anti-solvent precipitation and a simple complex method were applied for the preparation of bacterial cellulose nanofiber/soy protein isolate (BCNs/SPI) colloidal particles. Fourier transform IR (FT-IR) showed that hydrogen bonds generated in BCNs/SPI colloidal particles *via* the anti-solvent precipitation were stronger than those generated in BCNs/SPI colloidal particles self-assembled by a simple complex method. Meanwhile, the crystallinity, thermal stability, and contact angle of BCNs/SPI colloidal particles *via* the anti-solvent precipitation show an improvement in comparison with those of BCNs/SPI colloidal particles *via* a simple complex method. BCNs/SPI colloidal particles *via* the anti-solvent precipitation showed enhanced gel viscoelasticity, which was confirmed by dynamic oscillatory measurements. Furthermore, high internal phase Pickering emulsions (HIPEs) were additionally stable due to their stabilization by BCNs/SPI colloidal particles *via* the anti-solvent precipitation. Since then, HIPEs stabilized by BCNs/SPI colloidal particles *via* the anti-solvent precipitation were used for the delivery of curcumin. The curcumin-loaded HIPEs showed a good encapsulation efficiency and high 2,2-diphenyl-1-picrylhydrazyl (DPPH) removal efficiency. Additionally, the bioaccessibility of curcumin was significantly increased to 30.54% after the encapsulation using the prepared HIPEs. Therefore, it can be concluded that the anti-solvent precipitation is an effective way to assemble the polysaccharide/protein complex particles for the stabilization of HIPEs, and the prepared stable HIPEs showed a potential application in the delivery of curcumin.

Keywords: BCNs/SPI colloidal particles, anti-solvent precipitation, high internal phase pickering emulsions, antioxidation, delivery of curcumin

INTRODUCTION

Emulsion is a dispersed heterogeneous system composed of two or more completely or partially immiscible liquids, which has been widely used in foods, pharmaceuticals, cosmetics, and other fields (1). Recently, high internal phase emulsions (HIPEs) belonging to the class of concentrated emulsions with more than 74% (v/v) of the internal phase have aroused much interest in the food industry because HIPEs offer a promising approach for converting liquid oil into solid. However, the stability of HIPEs is a critical challenge due to the usual occurrence of phase transitions and an increase in the volume of the internal fraction to a threshold. Traditional HIPEs are usually stabilized by the high dosages (10–50%) of surfactants or small-molecule emulsifiers, which were considered as a metastable system with thermodynamic instability (2, 3). Therefore, Pickering emulsions stabilized by solid particles have attracted great attention because of their outstanding stability, resulting from the irreversible adsorption of particles at an oil–water interface (4, 5). At present, inorganic particles, including silicon dioxide, titanium dioxide, and clay, are widely used as stabilizers for HIPEs due to their efficient emulsifying capacity (6, 7). However, the application of inorganic particles in the food industry is limited due to their toxicity risks (8). Therefore, it is necessary to explore food-grade stabilizers for HIPEs (9).

Recently, various food materials (such as proteins, polysaccharides, and lipids) have been widely used for the development of food-grade particles for Pickering emulsion (10–12). However, it has been demonstrated that the solid particles from proteins or polysaccharides alone display poor emulsification properties as these are used for the stabilization of HIPEs. Thus, chemical modifications are usually used to improve the emulsifying capacity of polysaccharide or protein particles while the chemical modification is unable to adapt to the development of the green food processing industry (13, 14). It has been reported that the complex particles of protein and polysaccharides by the self-assembly can stabilize the HIPE effectively. However, the self-assembly methods would largely affect the properties of complex particles because different self-assembly methods lead to different intermolecular interactions between the complex particles (e.g., the electrostatic interactions, hydrogen bonds, van der Waals' force, and steric hindrance) (15). Thus, it is necessary to investigate the effects of self-assembly methods on the properties of the complex particles.

In this work, bacterial cellulose nanofiber/soy protein isolate (BCNs/SPI) colloidal particles were prepared by using the anti-solvent precipitation and a simple complex method. Then, in this study, the properties of BCNs/SPI colloidal particles, including microstructure, thermostability, contact angle, and rheological behavior, were compared. Meanwhile, BCNs/SPI colloidal particles were used for the stabilization of the HIPEs, and their stability was studied. Afterward, the super stable HIPEs were used for the delivery of curcumin. The present study has investigated the delivery properties, including the antioxidant activity of curcumin, bioaccessibility of curcumin during *in vitro* digestion, and release of free fatty acids (FFAs).

MATERIALS AND METHODS

Materials

Bacterial cellulose (BC) producing strain *Komagataeibacter hansenii* CGMCC 3917 was donated by the Fermentation Technology Innovation Laboratory of Northwest A & F University (Yanglin, Shaanxi, China). SPI (purity 95%), curcumin, and bile extract were purchased from Yuanye Bio-Technology Co., Ltd. (Shanghai, China). Sunflower seed oil was purchased from the local supermarket (Xi'an, China). Porcine mucin, porcine pepsin (≥300 U/mg), and porcine pancreatin (4,000 U/g) were obtained from Aladdin Bio-Technology Co., Ltd. (Shanghai, China), and other chemicals were of analytical grade.

Sodium Dodecyl Sulfate-Polyacrylamide Gel Electrophoresis Measurements

Sodium dodecyl sulfate-polyacrylamide gel electrophoresis (SDS-PAGE) measurements were measured according to the method reported in a previous literature study (16). About 5.0% polyacrylamide stacking gels and 15.0% polyacrylamide running gels were prepared by using a gel kit. Then, the gels were stained with Coomassie Brilliant Blue. Next, the stained gels were faded by using destaining solution (glacial acetic acid: methyl alcohol: water = 10: 45: 45 v: v: v). Finally, the gel imager (Bio-Rad, Hercules, CA, USA) was used for performing scanning and analysis.

The protein composition of SPI was analyzed by using SDS-PAGE and mainly consists of 7S and 11S globulin (**Supplementary Figure 1**). Three electrophoretic bands were separated clearly as shown corresponding to the molecular weights of 72, 68, and 52 kDa, which were observed as the α', α, and β subunits of 7S globulin. Electrophoretic bands corresponding to the molecular weights of 35 and 20 kDa represent the acidic and basic peptides of 11S globulin, respectively.

The Preparation of BCNs

Bacterial cellulose was produced according to the method in our previous study (17). Briefly, *K. hansenii* CGMCC 3917 was cultured at an aerobic environment (30°C) in a fermentation medium (pH 5.0) containing glucose 2% (w/v), yeast extract 0.5% (w/v), K_2HPO_4 0.1% (w/v), $MgSO_4$ 1.5% (w/v), and ethanol 2% (v/v). Cellulose membranes were harvested after the 14-day static cultivation. Then, the membranes were rinsed under running water overnight, followed by the treatment with 0.1 M NaOH solution at 80°C for 2 h. After that, the membranes were washed several times with deionized water until it was natural. Next, BC was hydrolyzed with 2.5 M HCl solution at 70°C for 1 h under magnetic stirring conditions (200 rpm). Afterward, the suspension was washed with deionized water and centrifuged at 10,000 *g* until the pH was neutral. Finally, BCNs suspension was obtained and stored in a fridge at 4°C for a successive study.

Preparation of BCNs/SPI Complex Particles

Bacterial cellulose nanofiber/SPI complex particles were prepared by using the anti-solvent precipitation and a simple complex

method. For the anti-solvent precipitation, SPI stock solution (1.25%, w/v) was obtained by dissolving an SPI powder in ethanol solution (70%, v/v) through stirring at room temperature (25°C). BCNs suspension with the concentration of 0.1% (w/v) was prepared by dissolving BCNs in deionized water. Then, SPI solution and BCNs solution were mixed in the ratio of 1:2.5 (v: v). Next, BCNs/SPI mixtures were prepared in the ratio of 1:5 (w/w) and sheared at 8,000 rpm for 4 min using a high-speed homogenizer (S10, SCIENTZ, Zhejiang, China). Finally, ethanol and excess water were removed by rotary evaporation and centrifugation, and BCNs/SPI colloidal particles with a concentration of 2% were obtained and marked as A-BCNs/SPI. For a simple complex method, SPI stock solution (1.25%, w/v) was obtained by dissolving a powder in deionized water through stirring at room temperature (25°C). BCNs suspension was prepared by dissolving these in the deionized water. Then, BCNs/SPI mixtures were prepared in the ratio of 1:5 (w/w) and sheared at 8,000 rpm for 4 min using a high-speed homogenizer (S10, SCIENTZ, Zhejiang, China). Finally, excess water was removed by centrifugation (4,000 rpm, 10 min), and BCNs/SPI colloidal particles with a concentration of 2% were obtained and marked as S-BCNs/SPI.

Preparation of HIPEs

A-bacterial cellulose nanofiber/soy protein isolate colloidal particles and S-BCNs/SPI colloidal particles were used as a stabilizer to prepare HIPEs, which were marked as A-HIPEs and S-HIPEs, respectively. Oil in water (O/W) HIPEs were prepared with the oil fraction of 75% by one-step homogenization. Briefly, the continuous phase (BCNs/SPI complex particle solution 2%) and dispersed phase sunflower seed oil were homogenized at 25,000 rpm for 3 min using a high-speed homogenizer (S10, SCIENTZ, Zhejiang, China).

The Loading of Curcumin

In this study, three types of systems were used for the loading of curcumin. Type I: curcumin was added into the oil with a concentration of 0.5 mg/ml (w/v), then the curcumin-loaded oil was obtained and marked as cur-oil. Type II: the HIPEs (oil fraction, 75%) stabilized by BCNs/SPI colloidal particles *via* the anti-solvent precipitation were used for the loading of curcumin. Briefly, the continuous phase (A-BCNs/SPI colloidal particle solution, 2%) and dispersed phase (curcumin-loaded oil) were homogenized at 25,000 rpm for 3 min, then the curcumin-loaded HIPEs were obtained and marked as cur-HIPEs. Type III: emulsions (oil fraction, 50%) stabilized by a surfactant (Tween 80 solution, 2%) were used for the loading of curcumin and set as a control group (18). Briefly, the continuous phase (Tween 80 solution, 2%) and dispersed phase (curcumin-loaded oil) were homogenized at 25,000 rpm for 3 min, then the curcumin-loaded emulsion stabilized by Tween 80 was obtained and marked as cur-TEs.

Zeta-Potential Measurements

The particle charge [zeta- (ζ-) potential] of colloidal particles and HIPEs was performed using the nano-zeta potential analyzer (Malvern Instruments Ltd., Malvern, UK). Briefly, the samples were diluted to 0.01% (v/v), and 0.5 ml of diluted dispersion was injected into a measurement cell for measurement. AI and RI of samples were set as 0.010 and 1.590. Each experiment was measured three times.

Particle Size

The particle size and polydispersity index of BCNs, SPI, and BCNs/SPI colloidal particles were measured by using a laser particle analyzer (Brookhaven, NY, USA). The samples were diluted 50-fold before the measurement. And each experiment was measured three times.

Microstructures

The microstructure of BCNs/SPI complex particles was characterized using scanning electron microscopy (S-3400N, HITACHI, Tokyo, Japan) The freeze-dried samples were coated with gold by an E-1045 sputter coater (HITACHI, Tokyo, Japan). The images were collected with 10,000× and 1,000× magnification at an accelerating voltage of 10.0 kV (19).

The microstructures of HIPEs were observed using the Axio Imager Upright Microscope (ZEISS, Oberkochen, Germany). A drop of HIPE was put on the glass microscope slide, then the prepared samples were observed under the microscope (20).

FT-IR Spectroscopy

The FTIR spectra of BCNs/SPI complex particles were recorded using a FT-IR spectrometer (BRUKER, Vertex70, Karlsruhe Germany) at 4,000–400 cm^{-1} with a resolution of 4 cm^{-1} (21).

X-Ray Diffraction

X-ray diffraction (XRD) patterns were recorded using an x-ray diffractometer (Rigaku, Smart Lab, Tokyo, Japan) at 40 kV and 45 mA. The samples were scanned from 5 to 50° with a step of 0.02° 2θ intervals (4).

Thermostability Analysis

The thermostability analysis of colloidal particles was characterized using the thermogravimetric analysis (TGA) and differential scanning calorimetry (DSC). Thermogravimetry (TG) was performed with 5 mg of nanoparticles under nitrogen atmosphere (N_2 flow was 20 ml/min) using a Thermoanalyzer System (Q1000DSC + L NCS + FACS Q600SDT, TA Instrument, New Castle, DE, USA) according to the previous method. The samples were heated from 20 to 800°C for 10°C/min, and the derivative thermogravimetry (DTG) was obtained by using the derivation for the TGA curve (22).

Differential scanning calorimetry (Flash DSC1, Schwerzenbach, Switzerland) was carried out for thermal analysis. About 3 mg of freeze-dried samples were placed in an aluminum pan and measured at the rate of 10°C/min over the range of 20–250°C (23).

Fluorescence Spectroscopy

The fluorescence intensity of samples was determined by using the previously reported method, with some modifications (24). A fluorescence spectrophotometer (F-7000, HITACHI, Tokyo, Japan) was used, the concentration of colloidal particle dispersions was fixed to 2 mg/ml. The emission spectra were

recorded between 290 and 450 nm. The scanning parameters were set as follows: the excitation wavelength of 280 nm, the scanning speed of 100 nm/min, and the slit width of 10 nm for excitation and emission. All data were the average of three runs.

Contact Angle

An optical contact angle measuring device (OCA20, Dataphiscis Instruments GmbH, Filderstadt, Germany) was used for the evaluation of the hydrophilic/hydrophobic characteristics of BCNs, SPI, and BCNs/SPI colloidal particles. In brief, the samples were spread on the tablets and dried at 37°C. Then the dried samples were placed in the equipment platform, 2 μl ultrapure water (pH 7.5) was successively deposited on the surface using a high-precision syringe. The water drop image was recorded *via* a high-speed video camera for a second. After that, the droplet profile data was fitted to the LaPlace–Young equation, and the contact angle was calculated according to the pervious description (25).

Rheological Properties

Dynamic rheometer (ZX7M-AR1000, TA Instruments, New Castle, DE, USA) was used for the measurement of the rheological properties of BCNs/SPI colloidal particles and HIPEs (10). The linear viscoelastic domain of particles was determined *via* an oscillatory stress sweep at a fixed frequency (1 Hz) before carrying out the oscillatory measurements. Then, a storage modulus (G') and loss modulus (G'') were measured from 0.1 to 1,000 Pa at a frequency of 1 Hz. A steady shear flow model was used for the measurement of the viscosity of particles. The viscosity (η) was recorded from 0.1 to 100 s^{-1} at 25°C under the condition of linear mode. For a thixotropic property analysis, the initial shear rate was set at 0.1 s^{-1} for 300 s. Then, the shear rate was increased to 10 s^{-1} for 300 s. Finally, the shear rate was recovered to 0.1 s^{-1} for 300 s, and the viscosity (η) was recorded.

Stability of HIPEs

Long-term storage was performed for testing the stability of HIPEs. Briefly, HIPEs were sealed in a serum bottle for 1 month at room temperature. The visual appearance and droplet size distribution of HIPEs were monitored for 1 month. The particle size and size distribution of HIPEs were determined using a laser particle size analyzer (LS13320, Beckman, Indianapolis, IN, USA). HIPEs were sufficiently diluted by deionized water to avoid multiple scattering. The refractive indexes of oil droplets and water (dispersants) were 1.46 and 1.33, respectively (26).

Retention Rate of Curcumin

The retention rate of curcumin in HIPEs stabilized by A-BCNs/SPI colloidal particles was measured under accelerated oxidation (27). About 1 g of samples were dissolved in 4 ml chloroform and then centrifuged at 3,000 rpm for 10 min, the absorbance of supernatant was read at 419 nm. The curcumin concentration of samples was calculated by the calibration curve of curcumin standards. The retention rate after emulsion formation and retention rate under accelerated oxidation were calculated by Equations (1) and (2), respectively:

$$\text{Retention rate after emulsion formation (\%)} = \frac{c_1}{c_2} \times 100\% \quad (1)$$

$$\text{Retention rate under accelerated oxidation (\%)} = \frac{c_3}{c_1} \times 100\% \quad (2)$$

where c_1 represents the initial concentrations of curcumin encapsulated in HIPEs, c_2 represents the initial concentrations of curcumin loaded in oil, and c_3 represent the concentrations of curcumin loaded in samples under accelerated oxidation.

DPPH Removal Efficiency

About 1 g of samples were mixed with 4 ml ethanol and centrifuged at 3,000 g for 15 min. Then, 1 ml of supernatant was mixed with 3 ml of DPPH solution (1 mM). The mixture was incubated for 30 min in a dark environment. Then, the absorbance was measured with a spectrophotometer (UV-3000, Insmark, Shanghai, China) at 517 nm (28). DPPH removal efficiency was calculated with the following equation.

$$\text{DPPH removal efficiency (\%)} = (1 - \frac{A - A_1}{A_0}) \times 100\% \quad (3)$$

where A represents adsorption after incubation, A_0 represents the adsorption of the initial DPPH solution, and A_1 represents the adsorption of the mix solution.

Lipid Oxidation

The contents of primary lipid oxidation products [lipid hydroperoxide (LH)] and secondary lipid oxidation products [malondialdehyde (MDA)] in oil, cur-oil, HIPEs, and cur-HIPEs were determined under accelerated oxidation (60°C, 10 days) according to the method in a previous study (29).

In vitro Digestion Model

A gastrointestinal tract model was utilized to evaluate the potential gastrointestinal fate of curcumin in a HIPE system (30). The samples were preheated at 37°C and contain the same level of oil.

For the mouth stage, 20 ml of HIPEs was mixed with 20 ml of mucin solution, which was prepared by using PBS with the mucin concentration of 0.03 g/ml. Then, the pH of the whole system was adjusted to 6.8 and incubated in a table concentrator (37°C, 100 rpm) for 10 min.

For the stomach stage, 15 ml of the sample collected from the mouth stage was mixed with 15 ml of simulated gastric fluids (SGFs, 3.2 mg/ml pepsin, 2 mg/ml NaCl), and the pH was adjusted to 2.0. Next, the mixture was incubated in a table concentrator (37°C, 100 rpm) for 120 min.

For the intestine stage, 1.5 ml of simulated intestine fluids (SIFs, 10 mm $CaCl_2$ and 150 mm NaCl) and 3.5 ml of bile salt (20 mg/ml) were added into 30 ml samples from the stomach stage for adjusting the pH to 7.0 using 0.1 M NaOH. Then, 2.5 ml of mixed solutions containing 2.4 mg/ml pancreatin and 3.6 mg/ml lipase were added to the system. Finally, the mixture was

incubated in a water bath with magnetic stirrers (37°C, 100 rpm) for 120 min.

The Release of FFAs

The degree of lipolysis was measured by the release of FFAs (31). During the intestinal digestion, NaOH was added into the whole system to neutralize the FFAs. The consumption of NaOH was recorded for every 10 min. The fraction of FFA release was calculated by Equation 4.

$$\text{FFA}\ (\%) = \frac{V_{\text{NaOH}} \times m_{\text{NaOH}} \times M_{\text{lipid}}}{2 \times W_{\text{lipid}}} \times 100\% \quad (4)$$

where V_{NaOH} is the volume of the NaOH for the neutralization of the FFAs, m_{NaOH} is the concentration of NaOH solutions (0.1 M), M_{lipid} is the average molecular mass of oil, and W_{lipid} is the total content of oil during the intestinal digestion.

Bioaccessibility of Curcumin

After intestinal digestion, the samples were collected for the determination of the bioaccessibility of curcumin. The samples were centrifuged at 10,000 *g* for 30 min. Then, the clear micelle phase and raw digesta, which dissolved curcumin, were measured by using HPLC (32). The curcumin concentration of samples was calculated by the calibration curve of curcumin standards. The bioaccessibility of curcumin was calculated by Equation 5.

$$\textit{Bioaccessbility}\ (\%) = \frac{C_{micelle}}{C_{digest}} \times 100\% \quad (5)$$

where c_{micelle} is the concentration of curcumin in micelle and c_{digest} is the concentration of curcumin in the whole digest.

Statistical Analysis

Analysis of variance (ANOVA) of the data was performed by using the SPSS 22 (SPSS Inc., Chicago, IL, USA), and the data were expressed as mean values ± SD with a CI of 95%. All data were plotted using the Origin 2019 software (Origin Lab Inc., Northampton, MA, USA).

RESULTS AND DISCUSSION

Zeta-Potential and Particle Size Distributions

In this study, the particle size distribution and ζ-potential of BCNs, SPI, and BCNs/SPI colloidal particles were analyzed. As described in **Table 1**, the average size of BCNs/SPI colloidal particles with these two self-assembly methods displayed a significant difference ($p < 0.05$), where the average size of S-BCNs/SPI colloidal particles (1,495.41 ± 248.01 nm) was significantly larger than that of A-BCNs/SPI colloidal particles (1,059.53 ± 104.77 nm). In addition, the polydispersity indexes of complex colloidal particles *via* the anti-solvent precipitation and a simple complex method were 0.27 ± 0.03 and 0.24 ± 0.02, respectively, which were lower than that of BCNs (0.37 ± 0.03) and SPI (0.33 ± 0.02). This result suggests that colloidal particles showed a better distribution in comparison with the single BCNs and SPI. The ζ-potential of SPI and BCNs was −33.07 ± 3.97 and −15.61 ± 0.65 mV, respectively (**Table 1**). For complex particles, the ζ-potential of A-BCNs/SPI (−35.97 ± 1.54 mV) was significantly higher than that of S-BCNs/SPI colloidal particles (−14.80 ± 1.06 mV), suggesting that the repulsive forces between the particles self-assembled by the anti-solvent method were intensively larger than those between BCNs/SPI particles self-assembled by a simple complex method. Thus, particles with weaker repulsive forces were easy aggregated, thus leading to the larger particle sizes as described earlier. Additionally, the ζ-potential of BCNs/SPI self-assembled by the anti-solvent method was higher than that of both BCNs and SPI, indicating that surface patch binding would participate in the formation of BCNs/SPI colloidal particles (33).

TABLE 1 | Average size, polydispersity index (PDI), and zeta- (ζ-) potential of bacterial cellulose nanofibers (BCNs), soy protein isolate (SPI), and BCNs/SPI colloidal particles with different self-assembly mechanisms.

Types	BCNs	SPI	A-BCNs/SPI	S-BCNs/SPI
Average size (nm)	366.71 ± 45.2^{d}	947.24 ± 157.42^{c}	1059.53 ± 104.77^{b}	1495.41 ± 248.01^{a}
PDI	0.37 ± 0.03^{a}	0.33 ± 0.02^{a}	0.27 ± 0.03^{b}	0.24 ± 0.02^{b}
Zeta potential (mV)	−15.61 ± 0.65^{b}	−33.07 ± 3.97^{a}	−35.97 ± 1.54^{a}	−14.80 ± 1.06^{b}

Data are presented as means ± SD with three replications. Different letters (a and b) show a significant difference in the same row.
^{c,d}This indicated a significant difference between the groups.

Microstructure of BCNs, SPI, and BCNs/SPI Colloidal Particles

The morphologies of BCNs, SPI, and BCNs/SPI colloidal particles with different self-assembly methods were observed by using the SEM. As displayed in **Figure 1A**, BCNs revealed an irregularly interconnected 3D network, which was in agreement with our results in a previous study (23). The structure of SPI showed a lamellar structure with smooth surfaces as a result of the sample treatment in SEM analysis (**Figure 1B**). The structure of BCNs/SPI colloidal particles with different self-assembly methods displayed a cross-linked structure with long fibers and an SPI matrix. The structure of BCNs/SPI colloidal particles self-assembled by a simple complex method showed a smooth agglomerate with a less fiber structure (**Figure 1D**). This phenomenon suggested that BCNs were covered by SPI and there were less structural rearrangements. However, BCNs/SPI colloidal particles self-assembled by the anti-solvent precipitation displayed a rough surface, where a large number of fibers passed through and were distributed in an SPI matrix (**Figure 1C**).

Fourier Transform-IR Spectroscopy

In this study, to investigate the changes in the chemical structure of colloidal particles with different self-assembly methods, FT-IR analysis was performed. As shown in **Figure 2A**, in the spectrum of BCNs, a wide band in the range of 3,600–3,000 cm^{-1} belonged to O-H stretching of hydroxyl groups of BCNs, which was in accordance with the reported result (34). The characteristic

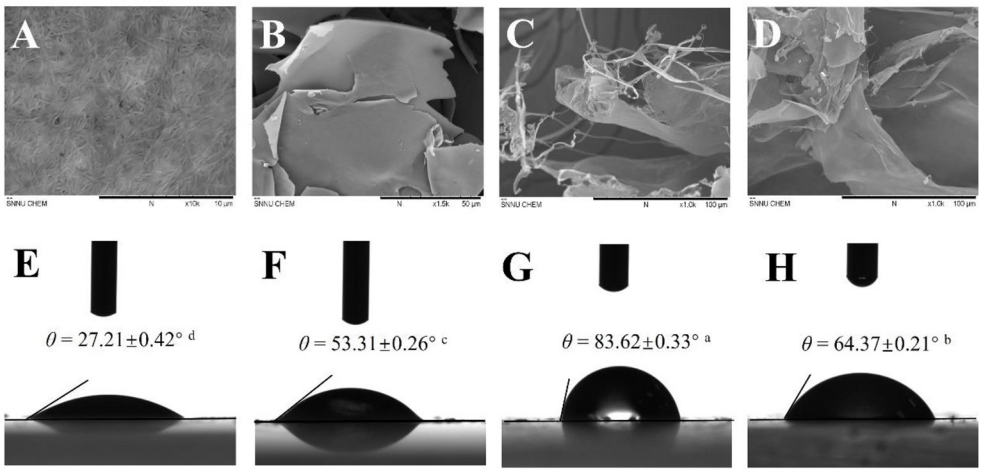

FIGURE 1 | Scanning electron microscopy (SEM) images of bacterial cellulose nanofibers (BCNs) (**A**, at 10.0 K magnification), soy protein isolate (SPI) (**B**, at 1.5 K magnification), A-BCNs/SPI colloidal particles (**C**, at 1.0 K magnification), and S-BCNs/SPI colloidal particles (**D**, at 1.0 K magnification). Water contact angle values of BCNs **(E)**, SPI **(F)**, A-BCNs/SPI colloidal particles **(G)**, and S-BCNs/SPI colloidal particles **(H)**.

peaks at around 2,908 and 1,428 cm^{-1} were associated with the dissymmetric stretching vibration and unsymmetric distortion vibration of methylene (-CH2-). In the spectrum of SPI, the characteristic peak of O-H stretching vibrations exhibited at 3,274 cm^{-1}, and obvious absorption peaks at 1,554 and 1,643 cm^{-1} were assigned to the N-H bending vibration (amide II) and C-O stretching vibration (amide I), respectively (35). The absorption peaks of N-H bending vibration (amide II) and C-O stretching vibration (amide I) in BCNs/SPI colloidal particles self-assembled by the anti-solvent precipitation were observed at 1,523 and 1,615 cm^{-1}, respectively while the corresponding peaks shifted to higher wavenumbers of 1,542 and 1,620 cm^{-1} in BCNs/SPI colloidal particles with a simple complex method, respectively. This result indicated that hydrogen bonds are generated in BCNs/SPI colloidal particles, which is in agreement with the results reported in the literature (36). In addition, the shift distance of A-BCNs/SPI colloidal particles was larger than that of S-BCNs/SPI colloidal particles, indicating that the strengthening of hydrogen bonds generated in BCNs/SPI colloidal particles self-assembled by the anti-solvent method seemed to be stronger than those generated in BCNs/SPI colloidal particles self-assembled by a simple complex method.

X-Ray Diffraction

The crystal properties of BCNs, SPI, and BCNs/SPI colloidal particles were investigated *via* an XRD analysis. As displayed in **Figure 2B**, there were no peaks in the pure SPI, suggesting that amorphous humps were presented in pure SPI, which were in accordance with the reported result (37). There were three characteristic peaks appearing at $2\theta = 14.22$, 16.81, and 22.52° in the XRD profile of BCNs, suggesting that BCNs possess a typical cellulose I structure with a high crystal structure, which was in agreement with our previous result (38). The crystallinity of BCNs/SPI colloidal particles obtained *via* different methods shows a decreased value in comparison with that of BCNs, which was probably due to the interactions between BCNs and SPI (23). Furthermore, the crystallinity of A-BCNs/SPI colloidal particles was higher than that of S-BCNs/SPI colloidal particles, which was likely because the rough surface of fiber structures was largely covered by the SPI in the particles self-assembled by a simple complex method, confirmed by the SEM results as described earlier.

Thermostability

The TGA and DTG curves of BCNs, SPI, and BCNs/SPI colloidal particles were shown in **Figure 2C**. The weight loss stages at relatively low temperatures were associated with the volatilization of the physical and chemical bound water or other volatiles and the dehydration in all samples, and the weight loss was about 1%, which was in agreement with the result reported in the literature (39). With an increase in temperature, the thermograph showed different degradation behaviors between BCNs and BCNs/SPI colloidal particles, where the main degradation of BCNs started at 200°C while the main degradation of BCNs/SPI colloidal particles started at around 150°C, which was attributed to the thermal denaturation of soybean protein components including β-conglycinin and glycinin fractions. Additionally, the main degradation temperature of BCNs/SPI colloidal particles *via* the anti-solvent precipitation was relatively higher than that of BCNs/SPI colloidal particles *via* a simple complex method. Based on the DTG analysis, the main degradation temperature of SPI was 325°C, which was in coincidence with the result reported in the literature (40). The peaks at 360 and 370°C were presented in the curves of BCNs/SPI colloidal particles self-assembled by a simple complex method and the anti-solvent precipitation, respectively. The main degradation temperature of BCNs/SPI colloidal particles *via* different methods increased in comparison with that of SPI, indicating that the thermostability of colloidal particles was improved by BCNs. The present result showed that the temperature of the maximum weight reduction of A-BCNs/SPI colloidal particles was markedly higher

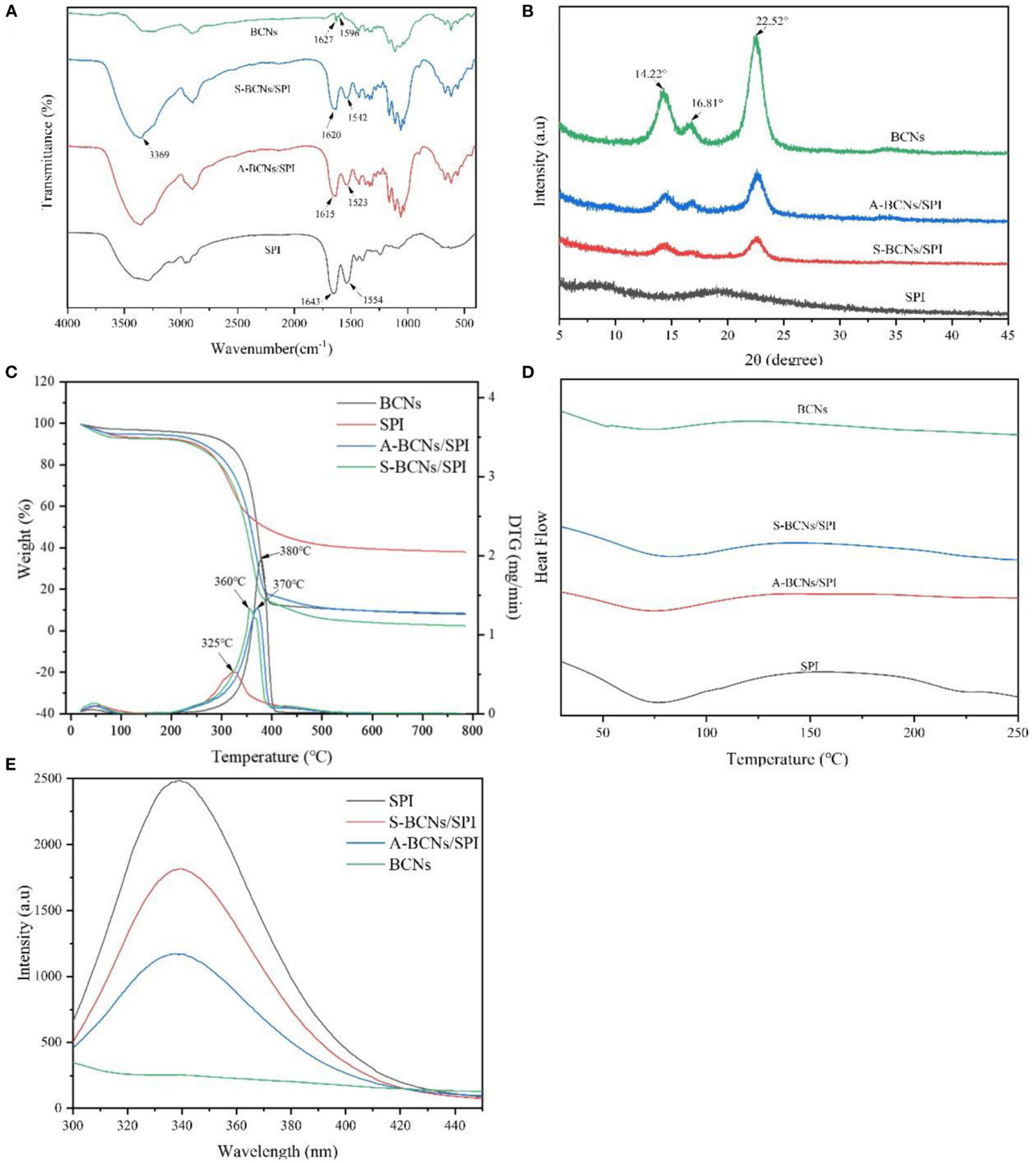

FIGURE 2 | Fourier transform IR (FT-IR) **(A)**, x-ray diffraction (XRD) **(B)**, thermogravimetric analysis (TGA) **(C)**, differential scanning calorimetry (DSC) **(D)**, and fluorescence spectrums **(E)** of SPI, BCNs, and BCNs/SPI colloidal particles prepared by using different self-assembly methods.

than that of S-BCNs/SPI colloidal particles, suggesting that A-BCNs/SPI colloidal particles possessed higher thermal stability in comparison with S-BCNs/SPI colloidal particles. This result was mainly caused by the higher crystallinity of A-BCNs/SPI colloidal particles in comparison with that of S-BCNs/SPI, which was confirmed by the XRD results as described earlier.

The differential scanning calorimetry curve was displayed in **Figure 2D**. Two endothermic peaks at 63.26 and 134.28°C in

BCNs were attributed to the degradation of crystalline water molecules and the degradation of polymers, respectively. A clear endothermic peak at 50–125°C was presented in SPI and complex colloidal particles, which was mainly attributed to β-conglycinin (7S) and glycinin (11S) in SPI (41). This result indicated that the physical interaction between BCNs and SPI was generated during a self-assembly process other than a chemical interaction, which was confirmed by the FT-IR results as described earlier. In addition, with an increase in temperature, a melting peak at 230°C in the DSC curve was observed in SPI and disappeared in the curve of BCNs/SPI colloidal particles, indicating that BCNs improved the thermostability of SPI, which was in consistent with the TGA profile as described earlier.

Contact Angle

The interfacial wettability of colloidal particles is an important property for evaluating the emulsifying capacity of colloidal particles as Pickering stabilizers (42). Contact angle measurement is a direct method for the characterization of the partial wettability of a solid particle. As shown in **Figure 1**, the contact angle values of BCNs and SPI were 27.21° ± 0.42° and 53.31° ± 0.26°, suggesting strong hydrophilicity as a result of the hydroxyl groups of BCNs and SPI, which is in agreement with the FT-IR results as described earlier. Moreover, the contact angle values of colloidal particles were higher than those of both BCNs and SPI. This result was probably due to the hidden and closed surface hydrophobicity groups of SPI getting exposed during the self-assembly process as a result of the presence of hydrogen bonds between the hydroxyl groups of BCNs and carbonyl groups of SPI (43). It has been demonstrated that θ value is much closer to 90°, the wettability of particles facilitates more effective adsorption and accumulation at the droplet surface, which is more suitable for the preparation of stable Pickering emulsion (1). The contact angle of A-BCNs/SPI colloidal particles (83.62° ± 0.33°) was higher than that of S-BCNs/SPI colloidal particles (64.37° ± 0.20°), suggesting that A-BCNs/SPI colloidal particles displayed a better amphiphilic property as a result of their contact angle values closer to 90°. Thus, the emulsifying capacity of A-BCNs/SPI colloidal particles was higher than that of S-BCNs/SPI colloidal particles.

Fluorescence Property

In the present study, the conformational changes of proteins were determined using fluorescence spectroscopy. As shown in **Figure 2E**, the fluorescence intensity of BCNs was much lower than that of SPI, which was likely due to the non-protein structure of BCNs. SPI presented a typical fluorescence emission peak at 340 nm, which was in agreement with a previous study (44). The wavelength of maximum emission did not show a distinct shift in both two types of colloid particles while the fluorescence intensity of colloid particles obviously ($p < 0.05$) decreased as a result of the presence of BCNs, which was in agreement with the reported result that the protein conformation was altered as a result of the interaction with other biopolymers (45). Moreover, the intensity of A-BCNs/SPI colloidal particles was significantly lower than that of S-BCNs/SPI colloidal particles, indicating that the effect of the anti-solvent precipitation on the protein conformation was more dramatically in comparison with that of a simple complex method.

Rheological Properties of BCNs/SPI Colloidal Particles

In this study, the rheological behavior of BCNs/SPI colloidal particles *via* different methods was investigated. As shown in **Figure 3A**, colloidal particles exhibit a storage modulus (G'), which is higher than a loss modulus (G''), indicating that all particles possessed gel-like behaviors of elastic solids, which was in agreement with the reported result (46). The G' of BCNs/SPI colloidal particles self-assembled by the anti-solvent precipitation was higher than that of the colloidal particles self-assembled by a simple complex method at the linear viscoelastic interval, suggesting that the colloidal particles self-assembled by the anti-solvent precipitation had stronger gel viscoelasticity. With an increase in stress, an obvious intersection (yield point) appeared, which indicated the changes of gel viscoelasticity, showing the conversion from gel-like behaviors to sol-like behaviors (47). The corresponding crossover point increased from 106 Pa for S-BCNs/SPI colloidal particles to 958 Pa for A-BCNs/SPI colloidal particles. These results suggested that the texture of colloidal particles using the anti-solvent precipitation was stronger than that of colloidal particles self-assembled using a simple complex method.

Figure 3B describes the dynamical viscosity (η) of colloidal particles as a function of shear rate (dr/dt) at 25°C. It was observed that the apparent viscosity of all colloidal particles displayed a constant decrease with an increase of shear rate at a relatively lower shear rate (0–50 s^{-1}), showing a shear-thinning behavior, suggesting that BCNs/SPI colloidal particles belonged to the category of Newtonian fluid at a relatively lower shear rate (48). However, the apparent viscosity of all colloidal particles displayed stable and unchangeable values at a higher shear rate (60–100 s^{-1}), in accordance with the Non-Newton fluidity. In addition, the viscosity of S-BCNs/SPI colloidal particles was lower than that of A-BCNs/SPI colloidal particles, indicating that BCNs/SPI colloidal particles self-assembled by the anti-solvent precipitation showed stronger gel strength, in agreement with the results of the stress sweep curve as described earlier.

The structural recovery properties of both two types of colloidal particles were shown in **Figure 3C**. The viscosity of A-BCNs/SPI colloidal particles was significantly higher than that of S-BCNs/SPI colloidal particles at all time intervals, which was in agreement with the dynamic viscosity as described earlier. The structural recovery degree was evaluated using the value of maximum viscosity at a third interval divided by the end viscosity of the first interval. The structural recovery degree of A-BCNs/SPI colloidal particles and S-BCNs/SPI colloidal particles was 98.47 and 30.69%, respectively. According to a previous study, the recovery percentage larger than 70% was regarded as a better thixotropic recovery (49). Thus, the result indicated that the structural recovery property of A-BCNs/SPI colloidal particles was better than that of S-BCNs/SPI colloidal particles, which was mainly due to a stronger gel structure demonstrated in the stress sweep as described earlier.

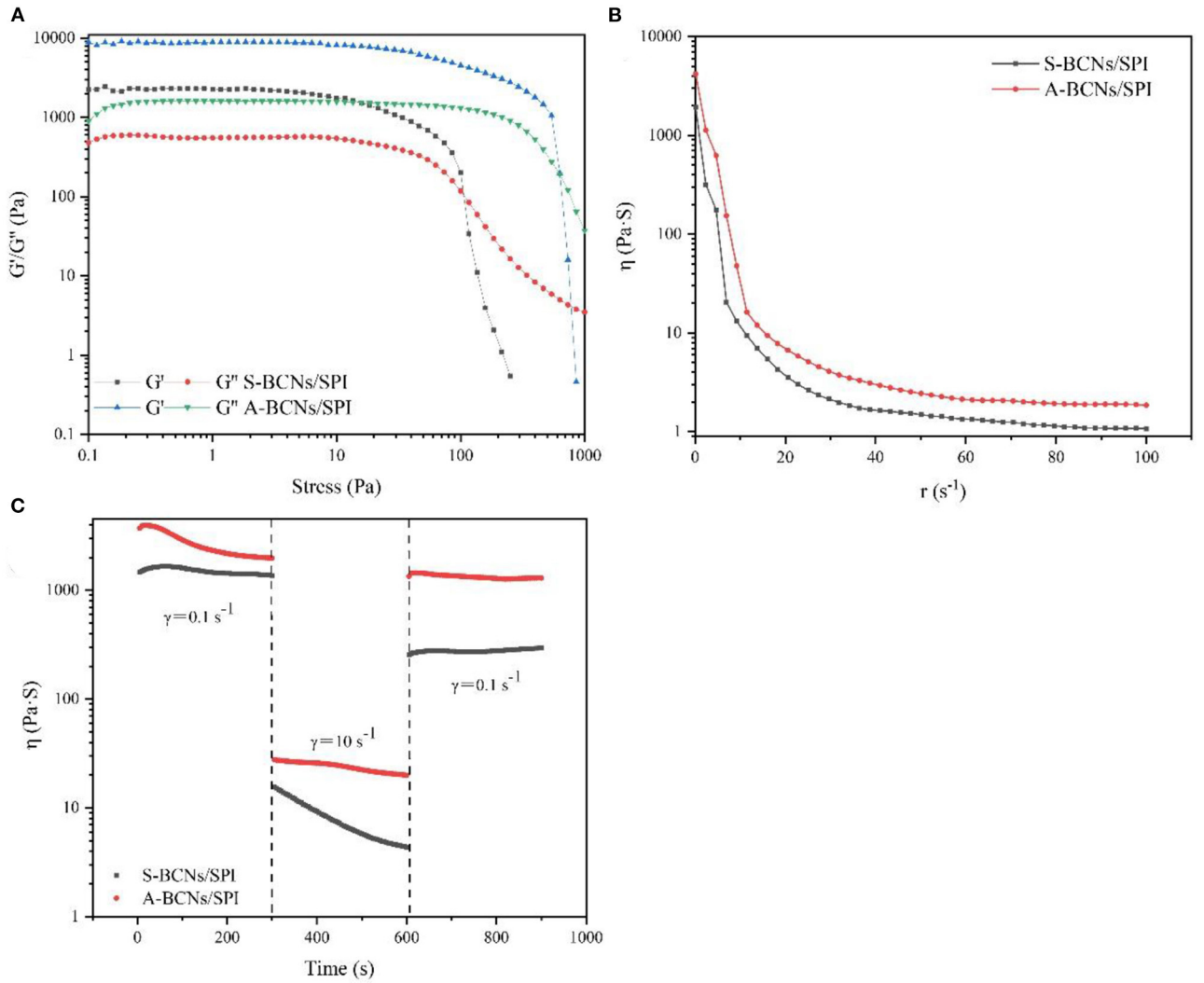

FIGURE 3 | Stress sweeps **(A)**, apparent viscosity **(B)**, and thixotropic recovery **(C)** for BCNs/SPI colloidal particles prepared by using different self-assembly methods.

To better understand the underlying mechanism of BCNs/SPI colloidal particles with different self-assembly methods, we proposed a schematic illustration to explain the formation route of BCNs/SPI colloidal particles with different self-assembly methods (**Supplementary Figure 2**).

Properties of HIPEs Stabilized by the Prepared Two Types of Colloidal Particles

In the present work, the properties of HIPEs stabilized by the prepared BCNs/SPI colloidal particles with different self-assembly methods were investigated. The microstructures of HIPEs stabilized by different types of BCNs/SPI colloidal particles were observed by using an optical microscope. As shown in **Figure 4**, the droplets were interconnected and closely arranged. This is basically consistent with the fact that a gel-like network for HIPEs would be formed (50). It was obvious that HIPEs stabilized by A-BCNs/SPI colloidal particles presented a small and uniform spherical droplet, whereas HIPEs stabilized by S-BCNs/SPI colloidal particles presented uneven spheres. This result was mainly due to a stronger steric force and the surface activity of the A-BCNs/SPI colloidal particles.

The droplet size distribution of these two types of HIPEs was shown in **Figure 4C**, it was observed that both two types of HIPEs showed a single peak, whereas the average sizes of these two types of HIPEs displayed a significant difference, where the average size of HIPEs stabilized by A-BCNs/SPI colloidal particles ($40.54 \pm 2.66\,\mu m$) was lower than that of HIPEs stabilized by S-BCNs/SPI colloidal particles ($73.96 \pm 8.43\,\mu m$). Furthermore, the droplet distribution and average size of HIPEs stabilized by A-BCNs/SPI colloidal particles displayed no significant change after 1 month of storage at room temperature, suggesting that HIPEs stabilized by A-BCNs/SPI colloidal particles were very stable. However, there were dramatic changes in the droplet distribution and average

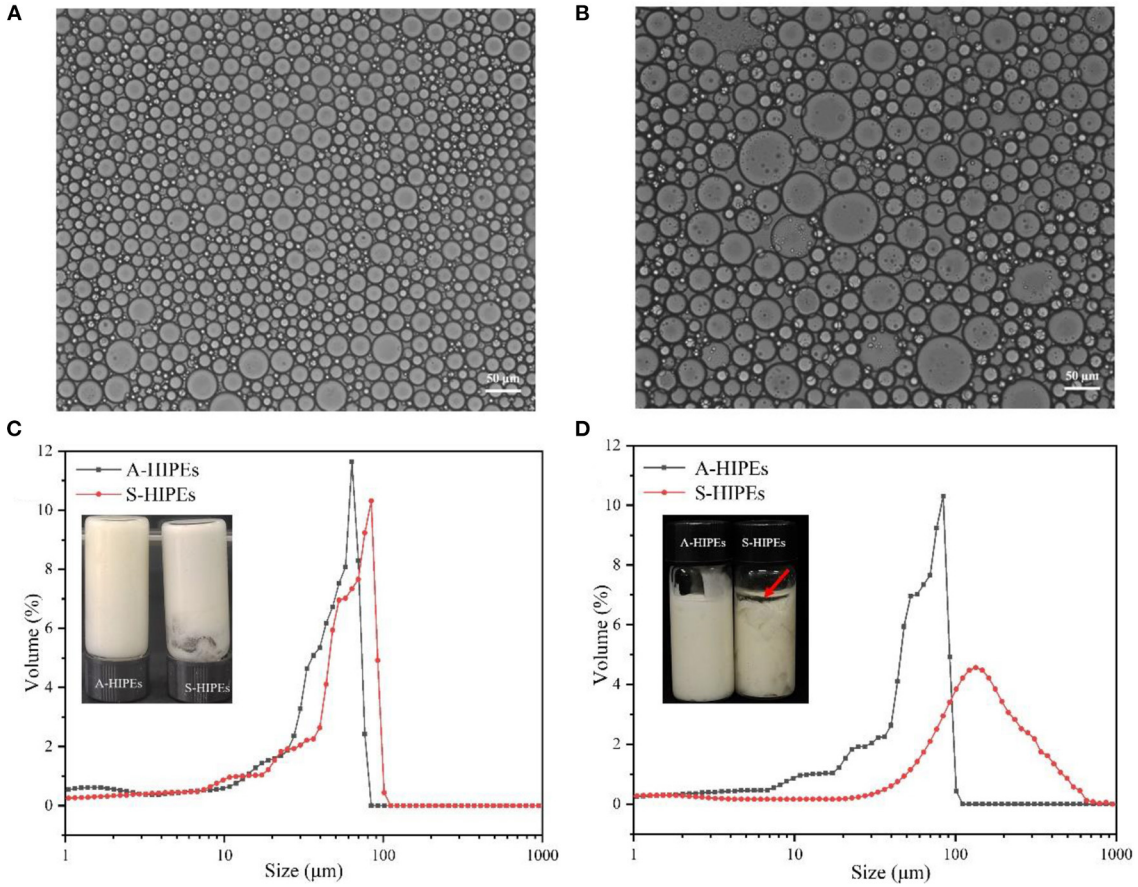

FIGURE 4 | Optical micrographs of A-HIPEs **(A)** and S-HIPEs **(B)**. The bar lengths of optical micrographs represented 50 μm. The appearance and size distribution of the HIPEs stabilized by BCNs/SPI colloidal particles using different self-assembly methods (**C**: new preparation; **D**: 1 month later).

size for HIPEs stabilized by S-BCNs/SPI colloidal particles, where the average size of HIPEs stabilized by S-BCNs/SPI colloidal particles significantly increased after 1 month of storage. Moreover, HIPEs stabilized by S-BCNs/SPI colloidal particles seemed to show an oil layer on the top of HIPEs, denoted by a red arrow (**Figure 4D**). This result suggested that HIPEs stabilized by A-BCNs/SPI colloidal particles were more stable in comparison with those stabilized by S-BCNs/SPI colloidal particles.

The ζ- potential of HIPEs was shown in **Table 2**. Both these types of HIPEs seemed to possess a negative charge, which was mainly due to the colloidal particles with a negative charge in an oil–water interface. The ζ-potential of HIPEs stabilized by A-BCNs/SPI colloidal particles and S-BCNs/SPI colloidal particles were -35.97 ± 1.54 and -24.30 ± 3.84 mV, respectively. It has been reported that the absolute value of ζ-potential >30 can confer stability in which the emulsion system will resist aggregation (51). In this regard, HIPEs stabilized by A-BCNs/SPI colloidal particles showed better stability than those stabilized by S-BCNs/SPI colloidal particles, which were consistent with the results of the droplet distribution and long-term storage test as described earlier.

TABLE 2 | Average size and ζ-potential of A-HIPEs and S-HIPEs.

Types	S-HIPEs	A-HIPEs
Average size (μm)	73.96 ± 8.43^{a}	40.54 ± 2.66^{b}
Zeta potential (mV)	-24.30 ± 3.84^{b}	-35.97 ± 1.54^{a}

Data are presented as means ± SD with three replications. Different letters (a and b) show a significant difference in the same row.

To better understand the internal structures and physicochemical properties of these emulsions, in the present study, the rheological properties of HIPEs stabilized by BCNs/SPI colloidal particles with different self-assembling methods were investigated. **Figure 5** showed the storage modulus (G'), loss modulus (G''), viscosity, and structural recovery properties of HIPEs stabilized by different types of colloidal particles. HIPEs stabilized by different types of colloidal particles showed a storage modulus (G'), which was higher than a loss modulus (G'') in a linear viscoelastic domain while a crossover point at 75.65 Pa was observed in the curve of HIPEs stabilized by S-BCNs/SPI colloidal particles, indicating a weaker structure formed by the S-BCNs/SPI colloidal particles at an interface

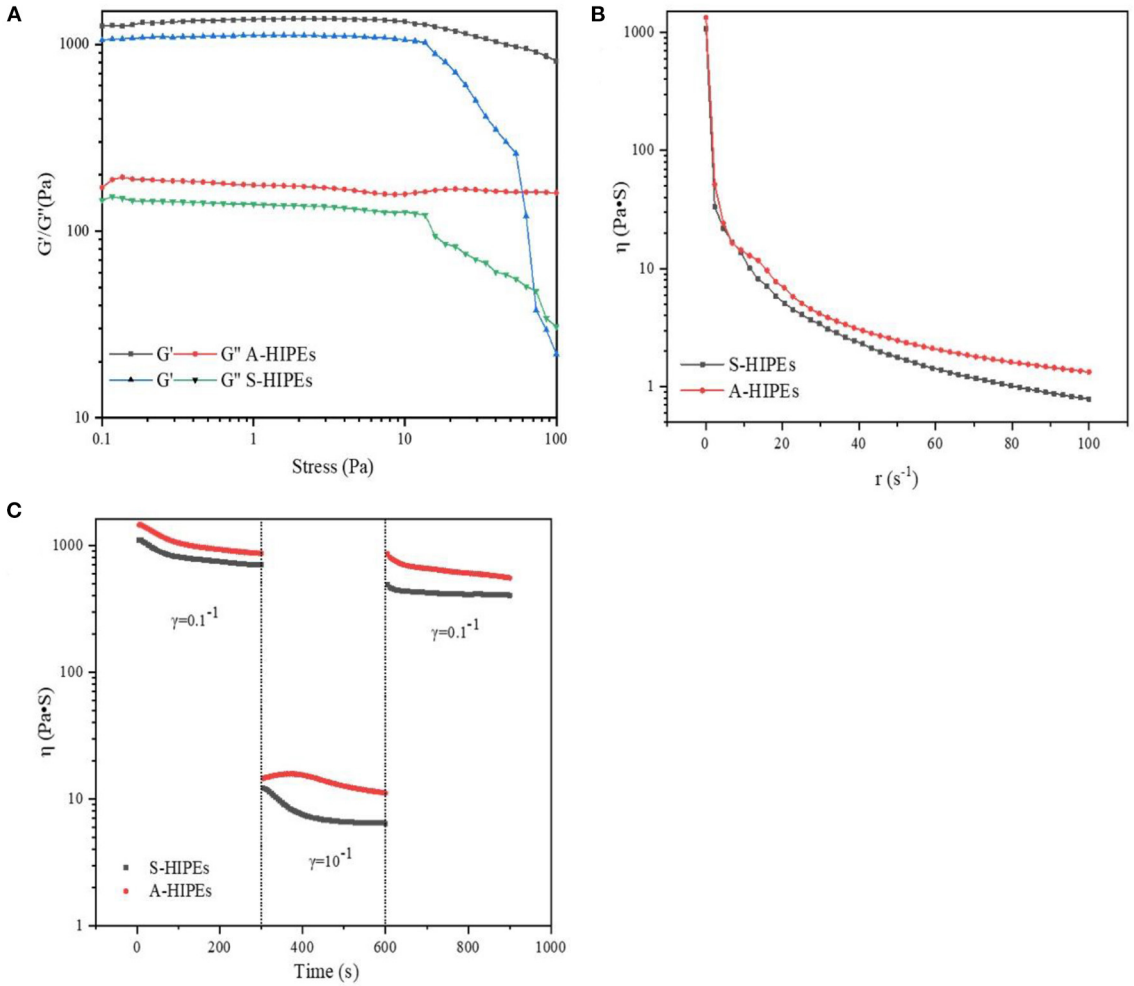

FIGURE 5 | Stress sweeps **(A)**, apparent viscosity **(B)**, and thixotropic recovery **(C)** for HIPEs stabilized by BCNs/SPI colloidal particles with different self-assembly methods.

(5). The stress sweep of HIPEs demonstrated that HIPEs stabilized by A-BCNs/SPI colloidal particles presented better gel viscoelasticity in comparison with the HIPEs stabilized by S-BCNs/SPI colloidal particles. This result was mainly due to an efficient rearrangement of A-BCNs/SPI colloidal particles at an interface into a more ordered network (52). The viscosity test showed that two types of HIPEs presented a characteristic of shear thinning, which was probably due to the squeezing between droplets, leading to a sharp shrink of the continuous phase, in agreement with the result in previous research (1). Additionally, HIPEs stabilized by A-BCNs/SPI colloidal particles displayed a higher viscoelasticity than those stabilized by S-BCNs/SPI colloidal particles, suggesting that the structural recovery degree of HIPEs stabilized by A-BCNs/SPI colloidal particles (99.86%) was significantly higher than that of HIPEs stabilized by S-BCNs/SPI colloidal particles (78.51%). This result was mainly due to improved gel viscoelasticity of HIPEs stabilized by A-BCNs/SPI confirmed by the stress sweep and viscosity test as described earlier.

Loading Properties of Curcumin in Different Systems

In this study, three types of systems (Type I: curcumin was loaded with only bulk oil; Type II: curcumin was loaded with HIPEs stabilized by BCNs/SPI colloidal particles *via* the anti-solvent precipitation; and Type III: curcumin was loaded with emulsions stabilized by Tween-80 solution) were used for the loading of curcumin, and the properties of curcumin-loaded systems were investigated. The encapsulated efficiency and retention rate of curcumin in the three systems were evaluated and compared. As shown in **Figure 6A**, the retention rate of curcumin after the emulsion formation in Type II and Type III systems was 94.18 ± 2.97 and 80.25 ± 2.04%, respectively. After a 10-day storage, the retention rate of curcumin in Type II system showed the highest (69.51 ± 2.14%), followed by that in Type III system (42.22 ± 2.04%), whereas the retention rate of curcumin in Type I system was the lowest (27.90 ± 7.57%). These results suggested that HIPEs stabilized by BCNs/SPI colloidal particles *via* the anti-solvent precipitation displayed better protection for

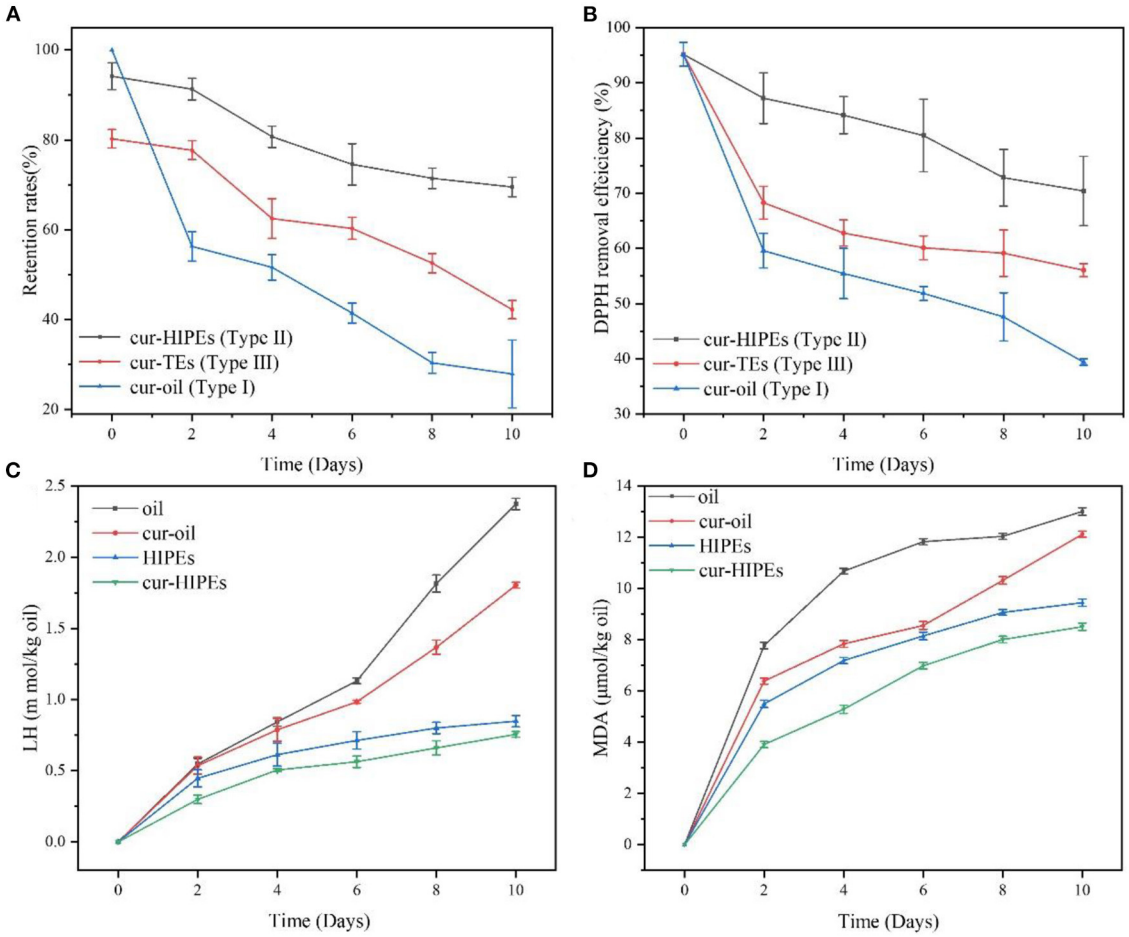

FIGURE 6 | Evolution of lipid hydroperoxides (LHs) **(A)**, malondialdehyde (MDA) **(B)** retention rate **(C)**, and 1,1-diphenyl-2-picrylhydrazyl (DPPH) removal efficiency **(D)** under accelerated storages at 60°C for 10 days.

curcumin in comparison with the emulsion stabilized by Tween-80 and bulk oil.

DPPH removal efficiency was evaluated under accelerated oxidation. As shown in **Figure 6B**, the initial DPPH removal efficiency of all samples was very similar. However, after 10 days of storage, the DPPH removal efficiency of curcumin in Type I system decreased to 39.39 ± 0.58% from 95.15 ± 2.17%. The DPPH removal efficiency of curcumin in Type II system was the highest (70.40 ± 6.28%), followed by that in Type III system (56.15 ± 1.19%), which indicated that the antioxidant ability of curcumin was obviously improved using the system of HIPEs stabilized by BCNs/SPI colloidal particles *via* the anti-solvent precipitation.

Lipid Oxidation

To better understand the change in the antioxidant ability of curcumin-loaded HIPEs stabilized by BCNs/SPI colloidal particles *via* the anti-solvent precipitation under accelerated oxidation, the contents of lipid oxidation markers (LH and MDA) in the samples were detected. As shown in **Figure 6**, LH and MDA contents of bulk oil and cur-oil were significantly increased after the storage for 10 days at 60°C. It was obvious that the antioxidant effects of HIPEs systems were significantly better than those of a bulk oil system, which was mainly attributed to the formation of a solid physical barrier at an oil/water interface because of the irreversible adsorption of BCNs/SPI colloidal particles *via* the anti-solvent precipitation (52). Furthermore, the barriers would protect the oil from oxygen, thus improving the antioxidant effect of the HIPE system. LH and MDA contents of curcumin-loaded oil and curcumin-loaded HIPEs were obviously lower than the bulk oil and HIPEs during the storage, respectively, suggesting that the curcumin decreased the lipid oxidation rate in agreement with the previous result as reported in the literature (5).

Digest Properties of Curcumin in Different Systems

In the present work, three types of systems (Type I: curcumin was loaded with only bulk oil; Type II: curcumin was loaded with HIPEs stabilized by BCNs/SPI colloidal particles *via* the

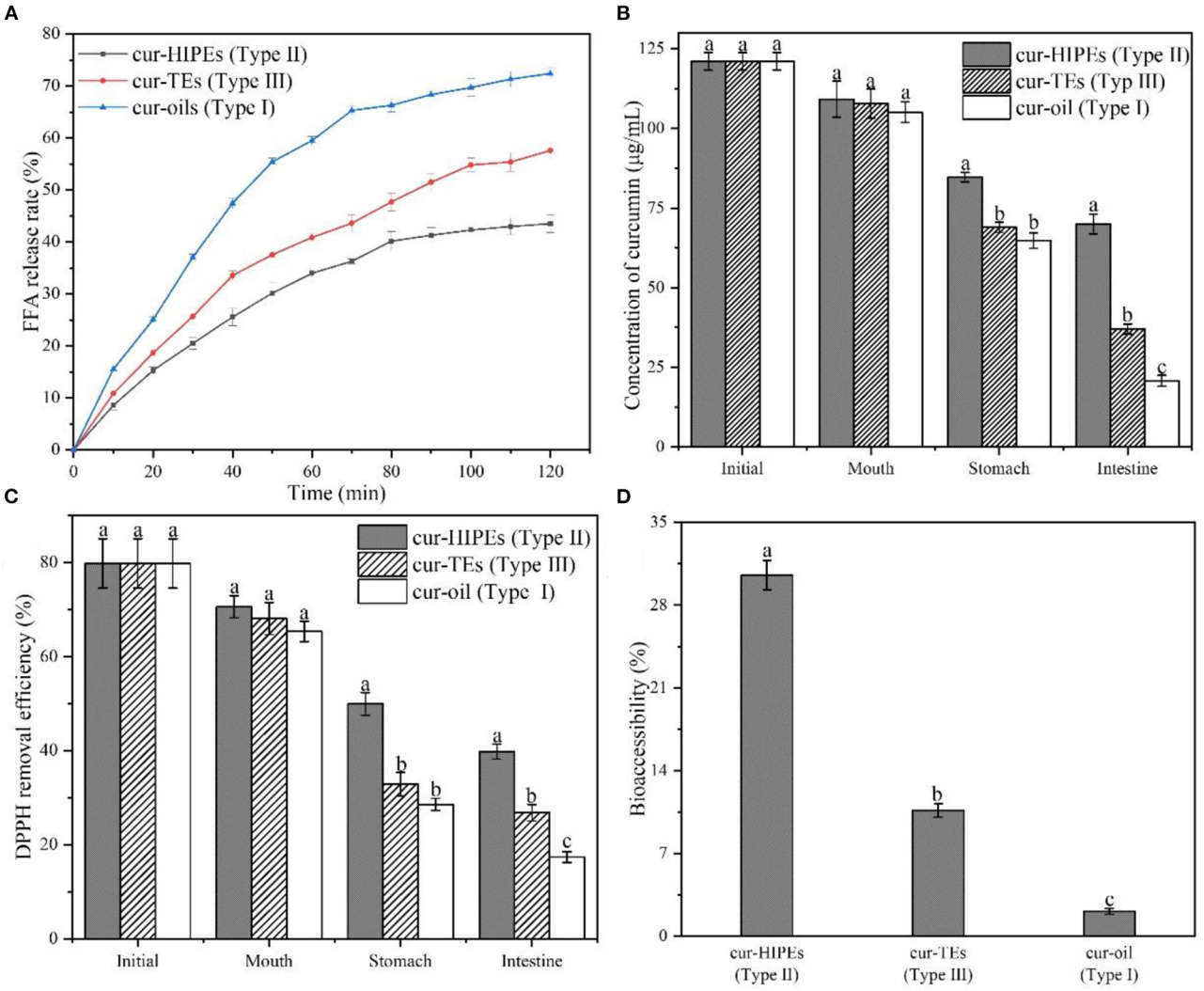

FIGURE 7 | FFA release rate **(A)**, concentration of curcumin **(B)**, 1,1-diphenyl-2-picrylhydrazyl (DPPH) removal efficiency **(C)**, and bioaccessibility of curcumin **(D)** during *in vitro* digestion.

anti-solvent precipitation; and Type III: curcumin was loaded with emulsions stabilized by Tween-80 solution) were used for the delivery of curcumin, and the *in vitro* digestion properties of curcumin-loaded systems were investigated. **Figure 7A** shows the FFA release profiles of curcumin in the three types of systems. For all systems, an increase in the FFA release rate was observed during the simulated gastric digestion, which was due to the conversion of triglyceride into FFAs and glycerides by the absorption of lipase on the surface of an oil droplet in agreement with the previous research (31). Type I system showed the highest FFA release rate (72.40 ± 1.05%) while the FFA release rate of Type II system was the lowest (43.52 ± 1.71%), followed by that of Type III system being 57.58 ± 1.49%. This phenomenon was mainly attributed to the formation of a solid physical barrier in the HIPE system formed by BCNs/SPI colloidal particles because it has been demonstrated that the solid physical barriers were hardly disrupted by surface active bile salts and lipase due to their irreversible adsorption at an oil/water interface (53). In contrast, the adsorption of Tween-80 at an oil/water interface was unstable, and the structure of the emulsion was destroyed during gastric digestion. In contrast, the adsorption of Tween-80 at an oil/water interface was unstable, thus the structure of emulsion was easily disrupted during *in vitro* digestion.

The concentrations of curcumin in different systems during *in vitro* digestion were determined by using HPLC. As shown in **Figure 7B**, the initial curcumin concentration of all systems was similar (121.06 ± 2.71 μg/ml). After *in vitro* digestion, the concentration of curcumin in Type II system was the highest with a value of 69.95 ± 3.14 μg/ml whereas the concentration of curcumin in Type I and Type III systems was 20.73 ± 1.71 and 37.01 ± 1.58 μg/ml, respectively. Thus, after digestion, the retention rate of curcumin in Type II system was the

highest (57.78%) while that of curcumin in Type I and Type III systems was 17.12% and 30.57%, respectively. This result indicated that the HIPEs potentially protect the curcumin from getting destroyed from the simulated digestion fluids during *in vitro* digestion. To investigate the change in the antioxidant ability of curcumin during *in vitro* digestion, DPPH removal efficiency was evaluated. As shown in **Figure 7C**, the DPPH removal efficiency of all systems was 79.81% ± 5.25%. After *in vitro* digestion, the DPPH removal efficiency of curcumin in Type I system was decreased to 17.40% ± 1.15%, whereas the DPPH removal efficiencies of curcumin in Type II and Type III systems were 39.81% ± 1.58% and 26.86% ± 1.75%, respectively. This result suggested that the structure of HIPEs increased the DPPH removal efficiencies of curcumin during *in vitro* digestion, in agreement with the change in curcumin concentration during *in vitro* digestion as shown in **Figure 7C**.

The bioaccessibility of curcumin in different systems during *in vitro* digestion was shown in **Figure 7D**, the bioaccessibility of curcumin in Type I, Type II, and Type III systems was 2.10% ± 0.25, 30.54% ± 1.25, and 10.65% ± 0.56%, respectively. The bioaccessibility of curcumin in Type II system was higher than that of curcumin in Type I and Type III systems. This result was probably obtained by HIPEs having the ability to improve the solubility of curcumin in micelle after *in vitro* digestion. In the HIPE system, the undigested BCNs/SPI colloidal particles may improve the solubility of curcumin in mix micelle (54). In contrast, the solubility of curcumin in mix micelle from Type I and Type III systems was relatively lower, thus leading to the reduced bioaccessibility for curcumin.

CONCLUSION

In this study, BCNs/SPI colloidal particles were prepared by using the anti-solvent precipitation and a simple complex method. The ζ-potential of colloidal particles indicated that the surface patch binding gets induced during the self-assembly of BCNs and SPI. FT-IR analysis showed that BCNs/SPI colloidal particles were assembled by using the anti-solvent precipitation and a simple complex method through hydrogen bonds. Moreover, the intensity of hydrogen bonds generated in BCNs/SPI colloidal particles self-assembled by the anti-solvent precipitation was stronger than those particles self-assembled by a simple complex method. Meanwhile, the droplet size, crystallinity, thermal stability, and contact angle values of composite colloidal particles self-assembled by the anti-solvent precipitation were better than the colloidal particles self-assembled by a simple complex method. Dynamic oscillatory measurements of colloidal particles indicated that the colloidal particles self-assembled by the anti-solvent precipitation have enhanced gel viscoelasticity. The microstructures and long-term stabilization test displayed that HIPEs stabilized by A-BCNs/SPI particles were more stable as compared to those stabilized by S-BCNs/SPI particles. Curcumin-loaded HIPEs stabilized by BCNs/SPI colloidal particles showed better loading effects and antioxidant ability as compared to the oil system and emulsion system stabilized by Tween-80 under accelerated oxidation. Moreover, the bioaccessibility of curcumin in the HIPE system during *in vitro* digestion was higher as compared to that of curcumin in the emulsion system stabilized by Tween-80. Therefore, it can be concluded that the anti-solvent precipitation is an effective way to assemble the polysaccharide/protein particles that are used as high internal phase Pickering stabilizers, and HIPEs stabilized by A-BCNs/SPI showed a potential for the delivery of curcumin.

DATA AVAILABILITY STATEMENT

The original contributions presented in the study are included in the article/**Supplementary Material**, further inquiries can be directed to the corresponding author/s.

AUTHOR CONTRIBUTIONS

RS and DL conceived and designed the experiments. RS and ZL performed the experiments. XY and HZ contributed helpful discussion during the experiment. RS and DL analyzed the data and wrote the manuscript. DL, HZ, and XY reviewed and revised the manuscript. All authors contributed to the article and approved the submitted version.

FUNDING

This study was supported by the National Natural Science Foundation, China (Grant No. C31701662); the Shaanxi Province Agricultural Science and Technology Innovation and Key Project (2021NY-175); the Key Projects of Central Universities, China (Grant No. GK201902012); and the Supporting Program for Youth Talent, China (20190206).

SUPPLEMENTARY MATERIAL

The Supplementary Material for this article can be found online at: https://www.frontiersin.org/articles/10.3389/fnut.2021.734620/full#supplementary-material

REFERENCES

1. Feng X, Dai H, Ma L, Yu Y, Tang M, Li Y, et al. Food-grade gelatin nanoparticles: preparation, characterization, and preliminary application for stabilizing pickering emulsions. *Foods.* (2019) 8:479–92. doi: 10.3390/foods8100479
2. Dickinson E. Colloids in food: ingredients, structure, and stability. *Ann Rev Food Sci Technol.* (2015) 6:211–33. doi: 10.1146/annurev-food-022814-015651
3. Muschiolik G, Dickinson E. Double emulsions relevant to food systems: preparation, stability, and applications. *Comprehens Rev Food Sci Food Saf.* (2017) 16:532–55. doi: 10.1111/1541-4337.12261
4. Chen Q-H, Zheng J, Xu Y-T, Yin S-W, Liu F, Tang C-H. Surface modification improves fabrication of pickering high internal phase emulsions stabilized by cellulose nanocrystals. *Food Hydrocolloids.* (2018) 75:125–30. doi: 10.1016/j.foodhyd.2017.09.005

5. Zeng T, Wu Z-L, Zhu J-Y, Yin S-W, Tang C-H, Wu L-Y, et al. Development of antioxidant pickering high internal phase emulsions (HIPEs) stabilized by protein/polysaccharide hybrid particles as potential alternative for PHOs. *Food Chem.* (2017) 231:122–30. doi: 10.1016/j.foodchem.2017.03.116
6. Liu L, Pu X, Tao H, Chen K, Guo W, Luo D, et al. Pickering emulsion stabilized by organoclay and intermediately hydrophobic nanosilica for high-temperature conditions. *Colloids Surf Physicochem Eng Aspects.* (2021) 610:125694. doi: 10.1016/j.colsurfa.2020.125694
7. Wang F, Yin Y, Chen B, Cuan S, Wang Z, Wang A, et al. Pickering medium internal phase emulsions based on natural clay particles: route to a macroporous adsorbent. *J Mol Liquids.* (2021) 322:114995. doi: 10.1016/j.molliq.2020.114995
8. Wan Z-L, Guo J, Yang X-Q. Plant protein-based delivery systems for bioactive ingredients in foods. *Food Funct.* (2015) 6:2876–89. doi: 10.1039/C5FO00050E
9. Mwangi WW, Lim HP, Low LE, Tey BT, Chan ES. Food-grade pickering emulsions for encapsulation and delivery of bioactives. *Trends Food Sci Technol.* (2020) 100:320–32. doi: 10.1016/j.tifs.2020.04.020
10. Zhou F-Z, Yan L, Yin S-W, Tang C-H, Yang X-Q. Development of pickering emulsions stabilized by Gliadin/Proanthocyanidins Hybrid Particles (GPHPs) and the fate of lipid oxidation and digestion. *J Agric Food Chem.* (2018) 66:1461–71. doi: 10.1021/acs.jafc.7b05261
11. Ruan Q, Guo J, Wan Z, Ren J, Yang X. pH switchable pickering emulsion based on soy peptides functionalized calcium phosphate particles. *Food Hydrocolloids.* (2017) 70:219–28. doi: 10.1016/j.foodhyd.2017.03.023
12. Chen X, Chen Y, Huang Y, Zou L, Liu C, McClements DJ, et al. Hybrid bionanoparticle-stabilized pickering emulsions for quercetin delivery: effect of interfacial composition on release, lipolysis, and bioaccessibility. *Acs Appl Nano Mater.* (2019) 2:6462–72. doi: 10.1021/acsanm.9b01413
13. Tavernier I, Wijaya W, Van der Meeren P, Dewettinck K, Patel AR. Food-grade particles for emulsion stabilization. *Trends Food Sci Technol.* (2016) 50:159–74. doi: 10.1016/j.tifs.2016.01.023
14. von Staszewski M, Pizones Ruiz-Henestrosa VM, Pilosof AMR. Green tea polyphenols-beta-lactoglobulin nanocomplexes: interfacial behavior, emulsification and oxidation stability of fish oil. *Food Hydrocolloids.* (2014) 35:505–11. doi: 10.1016/j.foodhyd.2013.07.008
15. Hu Y-Q, Yin S-W, Zhu J-H, Qi J-R, Guo J, Wu L-Y, et al. Fabrication and characterization of novel pickering emulsions and Pickering high internal emulsions stabilized by gliadin colloidal particles. *Food Hydrocolloids.* (2016) 61:300–10. doi: 10.1016/j.foodhyd.2016.05.028
16. Zhou Y, Teng F, Tian T, Sami R, Wu CL, Zhu Y, et al. The impact of soy protein isolate-dextran conjugation on capsicum oleoresin (*Capsicum annuum* L.) nanoemulsions. *Food Hydrocolloids.* (2020) 108:105818. doi: 10.1016/j.foodhyd.2020.105818
17. Zhai X, Lin D, Zhao Y, Yang X. Bacterial cellulose relieves diphenoxylate-induced constipation in rats. *J Agric Food Chem.* (2018) 66:4106–17. doi: 10.1021/acs.jafc.8b00385
18. Ngwabebhoh FA, Erdagi SI, Yildiz U. Pickering emulsions stabilized nanocellulosic-based nanoparticles for coumarin and curcumin nanoencapsulations: *in vitro* release, anticancer and antimicrobial activities. *Carbohydrate Polymers.* (2018) 201:317–28. doi: 10.1016/j.carbpol.2018.08.079
19. Liu Z, Shen R, Yang X, Lin D. Characterization of a novel konjac glucomannan film incorporated with Pickering emulsions: effect of the emulsion particle sizes. *Int J Biol Macromol.* (2021) 179:377–87. doi: 10.1016/j.ijbiomac.2021.02.188
20. Wang L-J, Yin S-W, Wu L-Y, Qi J-R, Guo J, Yang X-Q. Fabrication and characterization of Pickering emulsions and oil gels stabilized by highly charged zein/chitosan complex particles (ZCCPs). *Food Chem.* (2016) 213:462–9. doi: 10.1016/j.foodchem.2016.06.119
21. Hussain Z, Sajjad W, Khan T, Wahid F. Production of bacterial cellulose from industrial wastes: a review. *Cellulose.* (2019) 26:2895–911. doi: 10.1007/s10570-019-02307-1
22. Gu W, Liu X, Li F, Shi SQ, Xia C, Zhou W, et al. Tough, strong, and biodegradable composite film with excellent UV barrier performance comprising soy protein isolate, hyperbranched polyester, and cardanol derivative. *Green Chem.* (2019) 21:3651–65. doi: 10.1039/C9GC01081E
23. Liu Z, Lin D, Shen R, Yang X. Bacterial cellulose nanofibers improved the emulsifying capacity of soy protein isolate as a stabilizer for pickering high internal-phase emulsions. *Food Hydrocolloids.* (2021) 112:106279. doi: 10.1016/j.foodhyd.2020.106279
24. Song J, Sun C, Zhang J, Xiong Z, Fang Y. Fabrication, characterization, and formation mechanism of Zein- Gum Arabic nanocomposites in aqueous ethanol solution with a high ethanol content. *J Agric Food Chem.* (2020) 68:13138–45. doi: 10.1021/acs.jafc.9b08179
25. Chen X, McClements DJ, Wang J, Zou LQ, Deng SM, Liu W, et al. Coencapsulation of (-)-epigallocatechin-3-gallate and quercetin in particle-stabilized W/O/W emulsion gels: controlled release and bioaccessibility. *J Agric Food Chem.* (2018) 66:3691–9. doi: 10.1021/acs.jafc.7b05161
26. Wang L-J, Hu Y-Q, Yin S-W, Yang X-Q, Lai F-R, Wang S-Q. Fabrication and characterization of antioxidant pickering emulsions stabilized by Zein/Chitosan Complex Particles (ZCPs). *J Agric Food Chem.* (2015) 63:2514–24. doi: 10.1021/jf505227a
27. Pan Y, Li X-M, Meng R, Zhang B. Exploration of the stabilization mechanism and curcumin bioaccessibility of emulsions stabilized by whey protein hydrolysates after succinylation and glycation in different orders. *J Agric Food Chem.* (2019) 68:623–32. doi: 10.1021/acs.jafc.9b07350
28. Wang X, Huang H, Chu X, Han Y, Li M, Li G, et al. Encapsulation and binding properties of curcumin in zein particles stabilized by Tween 20. *Colloids Surf Physicochem Eng Aspects.* (2019) 577:274–80. doi: 10.1016/j.colsurfa.2019.05.094
29. Zhou FZ, Zeng T, Yin SW, Tang CH, Yuan DB, Yang XQ. Development of antioxidant gliadin particle stabilized Pickering high internal phase emulsions (HIPEs) as oral delivery systems and the *in vitro* digestion fate. *Food Funct.* (2018) 9:959–70. doi: 10.1039/C7FO01400G
30. Pan Y, Li X-M, Meng R, Zhang B. Exploration of the stabilization mechanism and curcumin bioaccessibility of emulsions stabilized by whey protein hydrolysates after succinylation and glycation in different orders. *J Agric Food Chem.* (2020) 68:623–32. doi: 10.1021/acs.jafc.9b07350
31. Winuprasith T, Khomein P, Mitbumrung W, Suphantharika M, Nitithamyong A, McClements DJ. Encapsulation of vitamin D-3 in pickering emulsions stabilized by nanofibrillated mangosteen cellulose: impact on *in vitro* digestion and bioaccessibility. *Food Hydrocolloids.* (2018) 83:153–64. doi: 10.1016/j.foodhyd.2018.04.047
32. Huang X-N, Zhou F-Z, Yang T, Yin S-W, Tang C-H, Yang X-Q. Fabrication and characterization of Pickering High Internal Phase Emulsions (HIPEs) stabilized by chitosan-caseinophosphopeptides nanocomplexes as oral delivery vehicles. *Food Hydrocolloids.* (2019) 93:34–45. doi: 10.1016/j.foodhyd.2019.02.005
33. Xiong W, Li J, Li B, Wang L. Physicochemical properties and interfacial dilatational rheological behavior at air-water interface of high intensity ultrasound modified ovalbumin: effect of ionic strength. *Food Hydrocolloids.* (2019) 97:105210. doi: 10.1016/j.foodhyd.2019.105210
34. Yan H, Chen X, Song H, Li J, Feng Y, Sh Z, et al. Synthesis of bacterial cellulose and bacterial cellulose nanocrystals for their applications in the stabilization of olive oil pickering emulsion. *Food Hydrocolloids.* (2017) 72:127–35. doi: 10.1016/j.foodhyd.2017.05.044
35. Lv P, Wang D, Chen Y, Zhu S, Zhang J, Mao L, et al. Pickering emulsion gels stabilized by novel complex particles of high-pressure-induced WPI gel and chitosan: fabrication, characterization and encapsulation. *Food Hydrocolloids.* (2020) 108:105992. doi: 10.1016/j.foodhyd.2020.105992
36. Chen H, Zhao R, Hu J, Wei Z, McClements DJ, Liu S, et al. One-Step dynamic imine chemistry for preparation of chitosan-stabilized emulsions using a natural aldehyde: acid trigger mechanism and regulation and gastric delivery. *J Agric Food Chem.* (2020) 68:5412–25. doi: 10.1021/acs.jafc.9b08301
37. Teng Z, Luo Y, Wang Q. Nanoparticles synthesized from soy protein: preparation, characterization, and application for nutraceutical encapsulation. *J Agric Food Chem.* (2012) 60:2712–20. doi: 10.1021/jf205238x
38. Zhai X, Lin D, Li W, Yang X. Improved characterization of nanofibers from bacterial cellulose and its potential application in fresh-cut apples. *Int J Biol Macromol.* (2020) 149:178–86. doi: 10.1016/j.ijbiomac.2020.01.230
39. Martelli-Tosi M, Masson MM, Silva NC, Esposto BS, Barros TT, Assis OBG, et al. Soybean straw nanocellulose produced by enzymatic or acid treatment as a reinforcing filler in soy protein isolate films. *Carbohydrate Polymers.* (2018) 198:61–8. doi: 10.1016/j.carbpol.2018.06.053
40. Sadare OO, Daramola MO, Afolabi AS. Synthesis and performance evaluation of nanocomposite soy protein isolate/carbon nanotube

(SPI/CNTs) adhesive for wood applications. *Int J Adhesion Adhesives.* (2020) 100:102605. doi: 10.1016/j.ijadhadh.2020.102605
41. Guo Y, Zhang X, Hao W, Xie Y, Chen L, Li Z, et al. Nano-bacterial cellulose/soy protein isolate complex gel as fat substitutes in ice cream model. *Carbohydrate Polymers.* (2018) 198:620–630. doi: 10.1016/j.carbpol.2018.06.078
42. de Folter JWJ, van Ruijven MWM, Velikov KP. Oil-in-water Pickering emulsions stabilized by colloidal particles from the water-insoluble protein zein. *Soft Matt.* (2012) 8:6807–15. doi: 10.1039/c2sm07417f
43. Wagner JR, Sorgentini DA, Anon MC. Relation between solubility and surface hydrophobicity as an indicator of modifications during preparation processes of commercial and laboratory-prepared soy protein isolates. *J Agric Food Chem.* (2000) 48:3159–65. doi: 10.1021/jf990823b
44. Zheng L, Wang Z, Kong Y, Ma Z, Wu C, Regenstein JM, et al. Different commercial soy protein isolates and the characteristics of Chiba tofu. *Food Hydrocolloids.* (2021) 110:106115. doi: 10.1016/j.foodhyd.2020.106115
45. Zhang A, Cui Q, Yu Z, Wang X, Zhao X-H. Effects of transglutaminase glycosylated soy protein isolate on its structure and interfacial properties. *J Sci Food Agric.* (2021) 101:5097–105. doi: 10.1002/jsfa.11155
46. Zou Y, Yan X, Scholten E. Rheological behavior of emulsion gels stabilized by zein/tannic acid complex particles. *Food Hydrocolloids.* (2018) 77:363–371. doi: 10.1016/j.foodhyd.2017.10.013
47. Shi L, Tian H, Wang Y, Hao G, Chen J, Weng W. Effect of pH on properties of golden pompano skin collagen-based fibril gels by self-assembly *in vitro*. *J Sci Food Agric.* (2020) 100:4801–7. doi: 10.1002/jsfa.10539
48. Liu X, Liu Y-Y, Guo J, Yin S-W, Yang X-Q. Microfluidization initiated cross-linking of gliadin particles for structured algal oil emulsions. *Food Hydrocolloids.* (2017) 73:153–61. doi: 10.1016/j.foodhyd.2017.07.001
49. Liu X, Guo J, Wan Z-L, Liu Y-Y, Ruan Q-J, Yang X-Q. Wheat gluten-stabilized high internal phase emulsions as mayonnaise replacers. *Food Hydrocolloids.* (2018) 77:168–75. doi: 10.1016/j.foodhyd.2017.09.032
50. Yang T, Li X-T, Tang C-H. Novel edible pickering high-internal-phase-emulsion gels efficiently stabilized by unique polysaccharide-protein hybrid nanoparticles from Okara. *Food Hydrocolloids.* (2020) 98:105285. doi: 10.1016/j.foodhyd.2019.105285
51. Zhu X-F, Zheng J, Liu F, Qiu C-Y, Lin W-F, Tang C-H. The influence of ionic strength on the characteristics of heat-induced soy protein aggregate nanoparticles and the freeze-thaw stability of the resultant Pickering emulsions. *Food Funct.* (2017) 8:2974–81. doi: 10.1039/C7FO00616K
52. Zhou F-Z, Huang X-N, Wu Z-l, Yin S-W, Zhu J-H, Tang C-H, et al. Fabrication of zein/pectin hybrid particle-stabilized pickering high internal phase emulsions with robust and ordered interface architecture. *J Agric Food Chem.* (2018) 66:11113–23. doi: 10.1021/acs.jafc.8b03714
53. Hur SJ, Decker EA, McClements DJ. Influence of initial emulsifier type on microstructural changes occurring in emulsified lipids during *in vitro* digestion. *Food Chem.* (2009) 114:253–62. doi: 10.1016/j.foodchem.2008.09.069
54. Qian C, Decker EA, Xiao H, McClements DJ. Nanoemulsion delivery systems: influence of carrier oil on beta-carotene bioaccessibility. *Food Chem.* (2012) 135:1440–7. doi: 10.1016/j.foodchem.2012.06.047

Conflict of Interest: The authors declare that the research was conducted in the absence of any commercial or financial relationships that could be construed as a potential conflict of interest.

Publisher's Note: All claims expressed in this article are solely those of the authors and do not necessarily represent those of their affiliated organizations, or those of the publisher, the editors and the reviewers. Any product that may be evaluated in this article, or claim that may be made by its manufacturer, is not guaranteed or endorsed by the publisher.

frontiers in Nutrition

ORIGINAL RESEARCH
published: 04 October 2021
doi: 10.3389/fnut.2021.752207

In vitro Digestion and Swelling Kinetics of Thymoquinone-Loaded Pickering Emulsions Incorporated in Alginate-Chitosan Hydrogel Beads

See Kiat Wong[1], Dora Lawrencia[1], Janarthanan Supramaniam[1], Bey Hing Goh[2,3], Sivakumar Manickam[4], Tin Wui Wong[5], Cheng Heng Pang[6,7,8] and Siah Ying Tang[1,9,10]**

[1] Chemical Engineering Discipline, School of Engineering, Monash University Malaysia, Subang Jaya, Malaysia, [2] Biofunctional Molecule Exploratory Research Group, School of Pharmacy, Monash University Malaysia, Subang Jaya, Malaysia, [3] College of Pharmaceutical Sciences, Zhejiang University, Hangzhou, China, [4] Petroleum and Chemical Engineering, Faculty of Engineering, Universiti Teknologi Brunei, Bandar Seri Begawan, Brunei, [5] Non-Destructive Biomedical and Pharmaceutical Research Centre, Smart Manufacturing Research Institute, Universiti Teknologi MARA, Puncak Alam, Malaysia, [6] Department of Chemical and Environmental Engineering, The University of Nottingham Ningbo China, Ningbo, China, [7] New Materials Institute, The University of Nottingham Ningbo China, Ningbo, China, [8] Municipal Key Laboratory of Clean Energy Conversion Technologies, The University of Nottingham Ningbo China, Ningbo, China, [9] Advanced Engineering Platform, School of Engineering, Monash University Malaysia, Subang Jaya, Malaysia, [10] Tropical Medicine and Biology Platform, School of Science, Monash University Malaysia, Subang Jaya, Malaysia

OPEN ACCESS

Edited by:
Jianhua Liu,
Zhejiang University of Technology, China

Reviewed by:
Weilin Liu,
Zhejiang Gongshang University, China
Yifeng Sheng,
The Chinese University of Hong Kong, Shenzhen, China

***Correspondence:**
Cheng Heng Pang
chengheng.pang@nottingham.edu.cn
Siah Ying Tang
patrick.tang@monash.edu

Specialty section:
This article was submitted to Food Chemistry, a section of the journal Frontiers in Nutrition

Received: *02 August 2021*
Accepted: *10 September 2021*
Published: *04 October 2021*

Citation:
Wong SK, Lawrencia D, Supramaniam J, Goh BH, Manickam S, Wong TW, Pang CH and Tang SY (2021) In vitro Digestion and Swelling Kinetics of Thymoquinone-Loaded Pickering Emulsions Incorporated in Alginate-Chitosan Hydrogel Beads. Front. Nutr. 8:752207. doi: 10.3389/fnut.2021.752207

The present work aimed to investigate the swelling behavior, *in vitro* digestion, and release of a hydrophobic bioactive compound, thymoquinone (TQ), loaded in Pickering emulsion incorporated in alginate-chitosan hydrogel beads using a simulated gastrointestinal model. In this study, oil-in-water Pickering emulsions of uniform micron droplet sizes were formulated using 20% red palm olein and 0.5% (w/v) cellulose nanocrystals-soy protein isolate (CNC/SPI) complex followed by encapsulation within beads. FT-IR was used to characterize the bonding between the alginate, chitosan, and Pickering emulsion. 2% (w/v) alginate-1% (w/v) chitosan hydrogel beads were found to be spherical with higher stability against structural deformation. The alginate-chitosan beads displayed excellent stability in simulated gastric fluid (SGF) with a low water uptake of ∼19%. The hydrogel beads demonstrated a high swelling degree (85%) with a superior water uptake capacity of ∼593% during intestinal digestion in simulated intestinal fluid (SIF). After exposure to SIF, the microstructure transformation was observed, causing erosion and degradation of alginate/chitosan wall materials. The release profile of TQ up to 83% was achieved in intestinal digestion, and the release behavior was dominated by diffusion via the bead swelling process. These results provided useful insight into the design of food-grade colloidal delivery systems using protein-polysaccharide complex-stabilized Pickering emulsions incorporated in alginate-chitosan hydrogel beads.

Keywords: alginate, chitosan, hydrogel beads, Pickering emulsion, *in vitro* digestion

INTRODUCTION

Thymoquinone (TQ), a major essential oil component of *Nigella sativa* seeds, has attracted significant attention in recent years to be used as an alternative to chemical drugs. TQ has been known to possess therapeutic benefits such as anti-oxidant, anti-inflammatory, and anti-cancer with minimal adverse effects and no severe toxicity (1, 2). Furthermore, several studies showed that TQ could induce apoptosis in human colorectal cancer cells by abrogate the stress response pathway sensor CHEK1 (3) and inhibit the proliferation of human colon cancer cells by increasing the phosphorylation states of the mitogen-activated protein kinases (4, 5). These findings suggest that TQ could be a critical component in formulating nutraceutical food products for colon cancer prevention. However, the application of TQ in food systems has been limited because of its high hydrophobicity due to the low dissolution profile when delivered orally. Hence, it exhibits low bioavailability at the target-diseased site (6). In addition, researchers found that TQ also suffers from chemical decomposition and enzymatic degradation in the gastrointestinal tract, which further limits the oral administration of TQ (7). These limitations could be effectively overcome by physically entrapping TQ in delivery colloid carrier systems to enhance its bioavailability and therapeutic ability.

Natural resources such as protein, lipid and polysaccharides have been used as environmentally sustainable biomaterials for the active coating of the bioactive agent (8). One of the prominent carriers for encapsulation, the alginate hydrogel beads, have been investigated extensively over the last decade because of their unique properties such as good aqueous solubility, biocompatibility, biodegradability, and non-toxicity. These characteristics make them helpful in encapsulating food ingredients, drugs, or natural extracts in the food industry and drug delivery system (9–12). The system can encapsulate small and large molecules at high efficiencies (13). It can readily form a three-dimensional gel-like structure, known as the egg-box model, when crosslinking with divalent cations such as Ca^{2+} (14). However, mainly hydrophilic molecules are selected as encapsulants resulting from many free hydroxyl and carboxyl groups along the alginate backbone (15). To encapsulate hydrophobic molecules, chemical modification is required by introducing hydrophobic groups such as lipid into the hydrogel beads matrix.

Emulsions are a mixture of two or more immiscible liquids, often stabilized with surfactants or surface-active particles. They have been widely used in food products due to their excellent stability and high nutritional value (16, 17). Due to the lipophilic property of TQ, an oil-in-water (O/W) emulsion is a perfect carrier system for the encapsulation of TQ. In particular, Pickering emulsions (PE) are emulsions stabilized with solid particles in place of surfactants. PE has shown numerous advantages of robust stabilization against coalescence with enhanced phase separation due to a dense layer of solid particles adsorbed irreversibly around the emulsion droplets (18). Liu and Tang confirmed that soy protein nanoparticles (0.5–6.0%, w/w) could formulate Pickering emulsions with properties tailored by changing the concentration and emulsification process (19). Yi et al. found that the combined use of soy protein isolate (20 mg/mL) and gallic acid (0.5–1.5 mg/mL) as the Pickering stabilizers contributed to great stability, excellent anti-oxidant, and antimicrobial abilities (20). Most recently, Wong et al. demonstrated the preparation of highly stable yet uniform red palm olein-in-water Pickering emulsions using cellulose nanocrystals-soy protein isolate (1.0%:1.0%, w/w) nanoconjugates as the food-based stabilizer (21).

However, protein particles-stabilized PE is often susceptible to changes in pH, especially during gastric digestion. Hence, by dissolving TQ in the oil phase of PE, followed by encapsulating the TQ-loaded PE within the alginate hydrogel matrix, bioactive compounds can be protected from the harsh external environment by improving the bioavailability of orally administered hydrophobic molecules (22, 23). Several studies have demonstrated the application of hydrogel in the immobilization of Pickering emulsion. For instance, Xiao et al. fabricated curcumin-loaded Pickering emulsion alginate hydrogel with improved processing stability and controlled digestion profile (24). In addition, Yan et al. reported the encapsulation of alfacalcidol in alginate beads using Pickering emulsion as a template, and the composite beads exhibited sustained release performance (11). In another study, Lim et al. successfully prepared chitosan-stabilized Pickering emulsions with immobilization efficiency exceeding 99% using calcium-alginate hydrogel (25).

To improve the stability and rigidity of alginate hydrogel beads, chitosan, a deacetylated product of chitin, which is the second most abundant polysaccharide after cellulose, can be employed as a supporting polymer. Chitosan has excellent biocompatibility, biodegradability, and mucoadhesive properties, and it is the only polysaccharide exhibiting cationic character, making it a suitable material in the food and nutraceutical industry (26, 27). When used together in forming hydrogel beads, the cationic amine group ($-NH_3^+$) of chitosan could bind to the carboxylate group ($-COO^-$) of alginate, forming crosslinked alginate-chitosan complexes, providing an enhanced protective coating for the encapsulated moieties (28, 29). It is also reported that the stability of the protein-based delivery system could be benefited from the chitosan coating, where proteins hydrolysis can be decreased during gastrointestinal digestion (30).

To date, the encapsulation of Pickering emulsions in alginate-chitosan beads with a hydrophobic bioactive component is rarely reported, especially when using a polysaccharide-protein complex as the Pickering emulsifier. This study combined the highly efficient encapsulating performance of alginate-chitosan (Alg-Chi) hydrogel beads with cellulose nanocrystals-soy protein isolate (CNC/SPI)-stabilized Pickering emulsion to develop a new delivery formulation for the loading of the hydrophobic bioactive model, TQ. The CNC/SPI-stabilized Pickering emulsion (TPE) was prepared by ultrasonication using a probe based on a previous study (21) and an ionic gelation

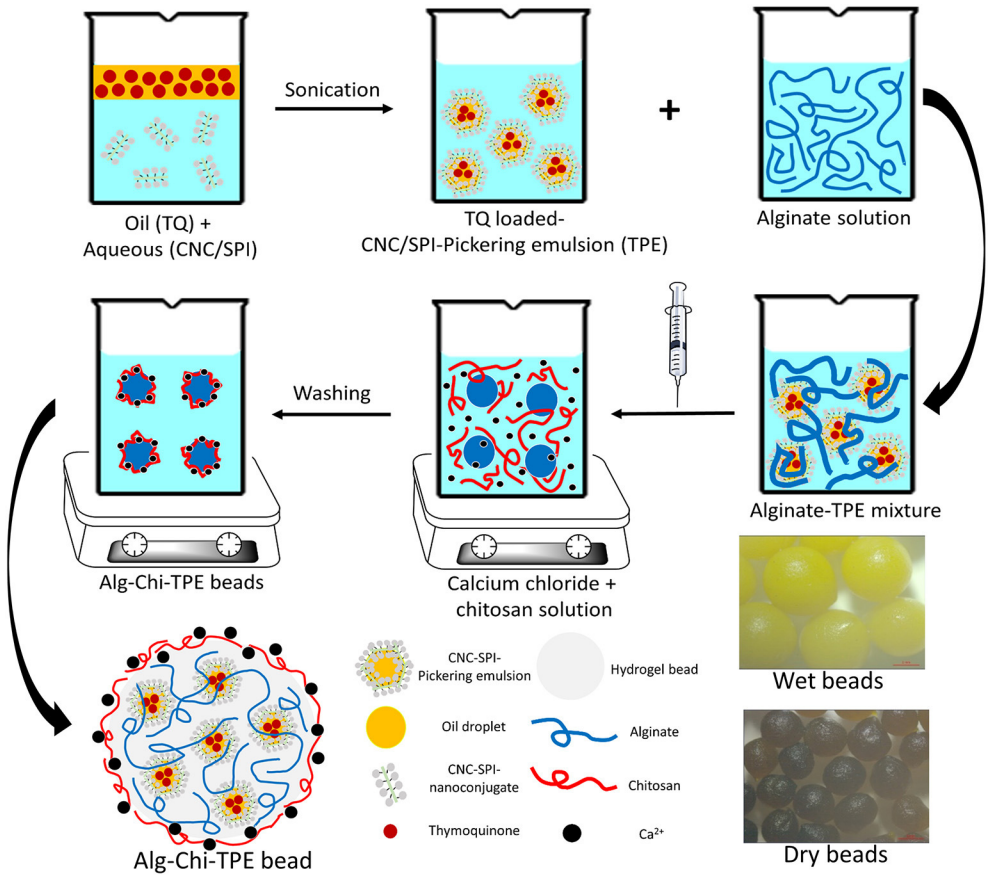

FIGURE 1 | The schematic illustration of the preparation of thymoquinone loaded alginate-chitosan beads by immobilized CNC/SPI-stabilized Pickering emulsion.

method to fabricate Alg-Chi-TPE hydrogel beads, as shown in **Figure 1**. The morphology, encapsulation efficiency, *in vitro* digestion and release performance of Alg-Chi-TPE hydrogel beads were investigated. The findings of the current work could contribute to the practical applications of polysaccharide-protein-based Pickering emulsions in nutraceutical and functional food products.

MATERIALS AND METHODS

Materials

Cellulose nanocrystals (CNC) (freeze-dried) were procured from the University of Maine, United States. Soy protein isolate (SPI) was provided by Shandong Wonderful Industrial Group Co., Ltd. (Shandong, China). Sodium alginate, calcium chloride and low molecular weight chitosan (50–190 kDa) were purchased from Sigma Chemicals Co. (St. Louis, MO, USA). Red palm superolein (275 ppm β-carotene, melting point 19°C) was acquired from Sime Darby Jomalina Sdn. Bhd., Malaysia. Ultrapure water (18.2 MΩ cm^{-1}) was obtained from the Milli-Q® Plus apparatus (Millipore, Billerica, USA) and was used in all the experiments. All other chemicals and reagents used were of analytical grade.

Preparation of Thymoquinone-Loaded Oil-in-Water (O/W) Pickering Emulsion (TPE)

CNC/SPI complex was used as the solid stabilizer in forming O/W Pickering emulsion with red palm olein (deep orange color) as the oil phase and deionized water as the continuous aqueous phase. Thymoquinone (TQ) was firstly dissolved in the oil phase with magnetic stirring at 500 rpm at room temperature for 1 h. Next, emulsions with a fixed oil content were prepared by mixing 20% (v/v) palm olein with aqueous suspensions of 0.5% (w/v) CNC/SPI complex at pH 7, adjusted by 1 M HCl and 1 M NaOH. Subsequently, the mixture was emulsified for 5 min using the ultrasonic horn at 60 W, and the emulsion was stored in glass vials for further usage. The measured average droplet size of formulated TPE was found to be ~23.5 ± 2.2 μm with a zeta potential of 34.3 ± 1.4 mV (21). Pickering emulsions without TQ was prepared similarly as control.

Preparation of Alginate-Chitosan (Alg-Chi) Beads Immobilized TPE

According to a previously described method (31), alginate-chitosan beads immobilized Pickering emulsions (Alg-Chi-TPE) were produced using the ionic gelation method with

modification. Firstly, sodium alginate was dissolved in ultrapure water to give sodium alginate solutions of different concentrations (1%, 2%, 3%, 4% w/v). These sodium alginate solutions were degassed for 30 min to discharge air bubbles before being utilized. Next, freshly prepared Pickering emulsions were added in alginate solutions at a 1:1 (v/v) ratio and mixed homogeneously under magnetic stirring for 10 min to produce Pickering emulsion-alginate solutions with final alginate concentrations (0.5%, 1%, 1.5%, 2% w/v). Then, Pickering emulsion-alginate solution was added dropwise into a mixed solution of 2% (w/v) calcium chloride solution in ultrapure water and 1% (w/v) chitosan solution in 1% (v/v) acetic acid solution under gentle stirring through a 21-gauge needle syringe. The formed beads were hardened in the mixed solution for 30 min before collection and washed with ultrapure water. The mixed and washing solutions were kept to measure the encapsulation efficiency of thymoquinone in the Pickering emulsion-filled alginate-chitosan beads.

Characterization of Alginate-Chitosan (Alg-Chi) Beads Immobilized TPE

Shape and Size of Hydrogel Beads

The shape and average size of freshly formed Alg-Chi-TPE hydrogel beads and dried Alg-Chi-TPE hydrogel beads were investigated using a Stemi microscope (Stemi2000, Zeiss, Germany). The size of the beads was measured using the ZEN2012 Blue software and was averaged based on eight replicates. The shrinking ratio of freshly prepared and dried alginate-chitosan beads was calculated using the following Equation (1).

$$Shrinking\ ratio\ (\%) = \frac{S_f - S_d}{S_f} x\ 100\% \quad (1)$$

Where S_f is the average size of freshly prepared beads and S_d is the average size of dried beads.

FT-IR Spectroscopy

Alg-Chi-TPE hydrogel beads were crushed using mortar and pestle before analysis. The FTIR spectra over the wavelength range of 400–4,000 cm^{-1} were recorded using the attenuated total reflectance Fourier transform infrared (ATR-FT-IR) spectrometer (Nicolet iS10, Thermo Fisher Scientific, USA).

Measurement of Encapsulation Efficiency (EE)

According to the previously described method for O/W emulsions (32), the encapsulation efficiency was analyzed by centrifugation with modification. In brief, 1 mL of O/W emulsion was added dropwise into a mixture of isopropanol and hexane (1:1 v/v, 10 mL) and subjected to vortex for 20 s to break the emulsion. Then, the mixture was centrifuged at 4,500 rpm for 10 min. The amount of thymoquinone in the supernatant was measured at the wavelength of 290 nm by a UV-Vis spectrophotometer (Genesys 10s UV, Thermo Fisher Scientific, USA). O/W emulsion without thymoquinone was prepared similarly and used as a blank. The encapsulation efficiency of thymoquinone in O/W emulsions (EE_e) was calculated based on a standard calibrated curve of thymoquinone based on the following Equation (2).

$$EE_e\ (\%) = \left(\frac{Amount\ of\ thymoquinone\ in\ the\ supernatant}{Amount\ of\ total\ thymoquinone}\right) \times 100\% \quad (2)$$

According to the previously described method for O/W emulsion-filled alginate-chitosan (Alg-Chi-TPE) hydrogel beads, the encapsulation efficiency was calculated by measuring the leakage during the crosslinking process (30). After the hardening process of beads, the absorbance of the mixed solution ($CaCl_2$ and chitosan) and the washing solution was measured at the wavelength of 290 nm by a UV-Vis spectrophotometer (Genesys 10s UV, Thermo Fisher Scientific, USA). The encapsulation efficiency of thymoquinone in Alg-Chi-TPE hydrogel beads (EE_b) was calculated using the following Equation (3).

$$EE_b\ (\%) = \left(1 - \frac{Amount\ of\ thymoquinone\ in\ the\ mixed\ solution}{Amount\ of\ total\ thymoquinone}\right) \times 100\% \quad (3)$$

In vitro Digestion

Simulated digestion of Alg-Chi-TPE hydrogel beads in gastric and intestinal phases was performed according to a previously described method (32) with modification. Simulated gastric fluid (SGF) and simulated intestinal fluid (SIF) were prepared as described below. SGF was prepared by dissolving 2 g of NaCl, 3.2 g of pepsin and 7 ml of 12 M HCl in 1 L of ultrapure water. SIF was prepared by adding pancreatic lipase (4 mg/mL), bile salt (4.3 mg/mL), and 0.6 mM $CaCl_2$ in phosphate buffer solution (pH 7.5). The mixture was stirred until homogenized for 1 h before use. Pepsin is responsible for breaking down protein during gastric digestion, while pancreatic lipase is important in the dietary triacylglycerol breakdown during intestinal digestion.

Water Uptake Study

The water uptake of the Alg-Chi-TPE hydrogel beads was performed in two different digestive media: SGF and SIF. Accurately weighed beads were immersed in 20 mL of respective medium in a sealed conical flask and placed in an incubator shaker (100 rpm) at 37°C. The beads were separated from the medium at specific time intervals, wiped gently with filter paper and weighed. The weight change of the beads to time was determined using the following Equation (4).

$$Water\ uptake\ (\%) = \frac{W_s - W_i}{W_i}\ x\ 100\% \quad (4)$$

Where W_s is the weight of the beads in swollen state and W_i is the initial weight of the untreated beads.

Swelling and Erosion Study

The swelling and erosion of the Alg-Chi-TPE hydrogel beads were performed in two different digestive media: SGF and SIF. Beads were immersed in 20 mL of respective medium in a sealed

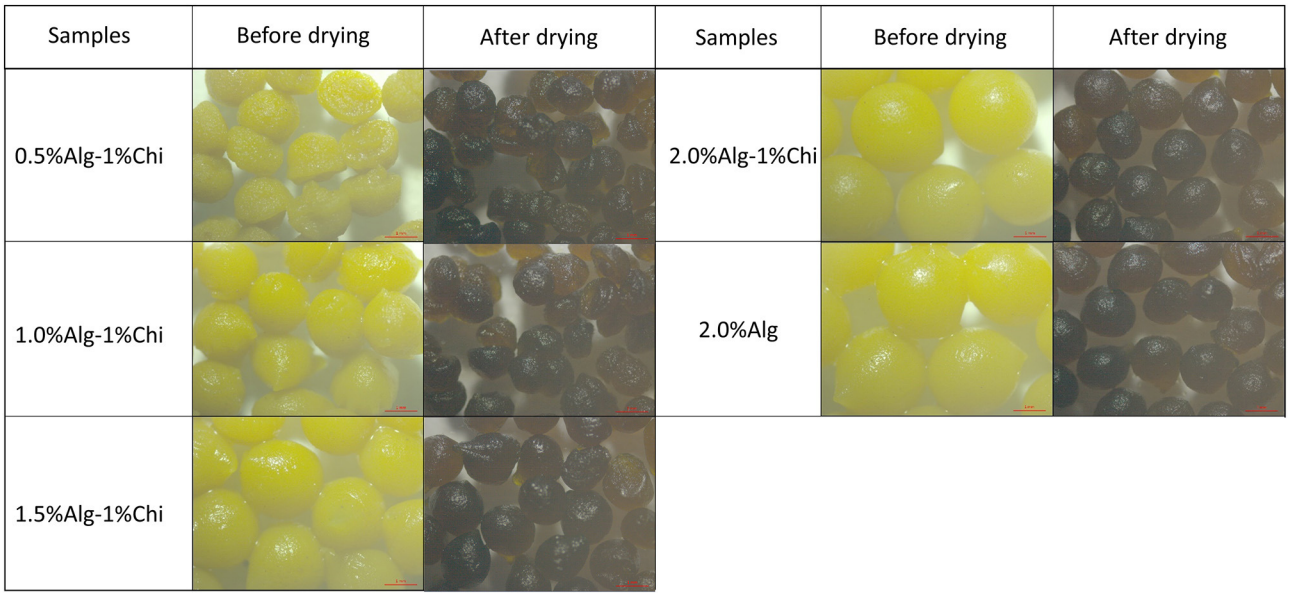

FIGURE 2 | Digital images of wet and dry alginate-chitosan hydrogel beads immobilized Pickering emulsion obtained with different alginate concentrations.

conical flask and placed in an incubator shaker (100 rpm) at 37°C. The beads were removed from the medium at specific time intervals, wiped gently with filter paper, and the diameter was measured. The swelling degree and erosion degree of the beads to time were determined using the following Equations (5) and (6), respectively.

$$Swelling\ (\%) = \frac{D_s - D_i}{D_i}\ x\ 100\% \quad (5)$$

$$Erosion\ \ (\%) = \frac{W_i - W_e}{W_i}\ x\ 100\% \quad (6)$$

Where D_s is the diameter of the beads in the swollen state, D_i is the initial diameter of the untreated beads, W_e is the weight of the dried beads in the swollen state, and W_i is the initial weight of the untreated beads.

Microstructures of Beads After Digestion

The microstructures of Alg-Chi-TPE hydrogel beads after gastric digestion and intestinal digestion were observed through a variable pressure scanning electron microscope (VP-SEM, Hitachi s3400N-II, Japan) and an upright fluorescent microscope (Nikon Eclipse 90i, Nikon Instrument Inc., USA). For VP-SEM preparation, the samples were air-dried, sputter-coated with gold under a vacuum before analysis. The samples were observed at an accelerating voltage of 10 kV. For the fluorescent microscope, the lipid phase of the emulsions was stained with Nile red (0.01% w/v) during the preparation process. A bead was placed on a microscopic slide and gently covered with a coverslip. The edge of beads was observed.

Release Study of Thymoquinone During Digestion

The release of thymoquinone (TQ) from Alg-Chi-TPE hydrogel beads in gastric digestion and intestinal digestion were evaluated according to the method described in section Measurement of Encapsulation Efficiency (EE). In brief, the hydrogel beads were immersed in 20 mL of respective medium in a sealed conical flask and placed in an incubator shaker (100 rpm) at 37°C. The hydrogel beads were treated with SGF for 120 min followed by SIF for another 240 min. Then, at specific time intervals, 2 mL of the medium was withdrawn from the conical flask and topped up with the fresh medium. The release profiles of TQ were fitted to the Peppas model by the following Equation (7) (33).

$$\frac{Mt}{Mi} = kt^n \quad (7)$$

Where Mt/Mi is the cumulative release ratio at time t, k is the kinetic constant, and n is the diffusional exponent.

RESULTS AND DISCUSSION

Fabrication and Characterization of Alginate-Chitosan Beads Immobilized Thymoquinone-Loaded Pickering Emulsion

Thymoquinone (TQ) was first dissolved in the red palm olein phase before the emulsification process. Next, the cellulose nanocrystals-soy protein isolate (CNC/SPI) complex was used as the Pickering stabilizer and dispersed in the aqueous phase. The alginate-chitosan (Alg-Chi) hydrogel beads were then prepared by external gelation method through dripping a mixture of TQ-loaded CNC/SPI-stabilized Pickering emulsion (TPE) with different alginate concentrations into a pre-mixed

TABLE 1 | The mean sizes and the shrinking ratio of Alg-Chi hydrogel beads were determined by ZEN2012 Blue software.

	Wet (mm)	Dry (mm)	Shrinking ratio (%)
0.5% Alg-1.0% Chi	1.598 ± 0.106^{a}	1.138 ± 0.077^{a}	28.65 ± 0.10
1.0% Alg-1.0% Chi	1.987 ± 0.118^{b}	1.383 ± 0.052^{b}	31.84 ± 1.47
1.5% Alg-1.0% Chi	2.339 ± 0.155^{c}	1.554 ± 0.068^{c}	34.96 ± 1.39
2% Alg-1.0% Chi	2.699 ± 0.097^{d}	$1.613 \pm 0.061^{c,d}$	40.13 ± 0.11
2% Alg	$2.651 \pm 0.102^{d,e}$	$1.583 \pm 0.044^{c,d,e}$	40.94 ± 0.63

Values expressed as the mean ± standard deviation. Different letters in the same column indicate significant differences ($p < 0.05$).

$CaCl_2$/chitosan solution (**Figure 1**). The digital images of the wet and dry Alg-Chi-TPE hydrogel beads are shown in **Figure 2**. Both wet and dry beads exhibited uniformly spherical shapes when 2% (w/v) alginate was used. However, when lower alginate concentrations were used, the shape of the beads was deformed, resulting in rough and collapsed surface morphology. This deformation is inevitable when water was evaporated from the wet hydrogel beads during the drying process, causing volume shrinkage of hydrogel beads (34).

Table 1 summarizes the percentage of weight change after the drying process. It could be observed that 2% (w/v) alginate beads exhibit the highest difference in shrinking ratio compared to the rest due to the higher concentration available to form larger wet beads with more water content. Generally, increasing the alginate ratio in beads formulation causes the beads' amplification and weight change. However, hydrogel beads obtained with 2.0% (w/v) alginate concentration displayed the least structural deformation after the drying process and demonstrated better stability than the other hydrogel beads. It is worth noting that the colors of the beads became darker when the beads shrink, which could be due to the increase in the concentration of immobilized TPE within the beads after the water has evaporated.

FTIR spectra of thymoquinone-loaded Pickering emulsion (TPE), Alg, Alg-TPE, Chi, and Alg-Chi-TPE hydrogel beads are shown in **Figure 3A**. The typical bands for the fatty acid hydrocarbon chains of palm olein in TPE could be observed at 2,921, 2,852, and 1,743 cm^{-1} for the asymmetric and symmetric stretching vibrations of C-H (-CH2) and carbonyl group (C=O) from ester (35). The FTIR spectrum of Alg-Chi-TPE beads revealed similar profiles as the TPE with the additional strong peaks at 1,592 and 1,416 cm^{-1}, attributed to the asymmetric and symmetric stretching vibrations of the -CO bond in the carboxylate ($-COO^{-}$) group of alginate (36). The shift observed from 1,603 to 1,592 cm^{-1} and 1,427 to 1,416 cm^{-1} in the spectra could be due to ion-induced alginate gelation by Ca^{2+} and cationic chitosan. The similarities of the palm olein bands revealed no interaction between the Pickering emulsion and wall materials, indicating that the Pickering emulsion is physically entrapped within the Alg-Chi beads system. Chitosan spectrum shows characteristic bands at 1,651 and 1,583 cm^{-1} due to the C=O vibration of the acetylated units ($-CONH_2$ groups) (37). The C=O vibration in the Alg-Chi-TPE spectrum shifted to a lower wavelength (1,651 to 1,592 cm^{-1}), denoting the electrostatic interaction of chitosan with alginate in the hydrogel beads. On the other hand, the FTIR spectra (**Figure 3B**) of Alg-Chi-TPE hydrogel beads with different Alg concentrations displayed similar profiles suggesting that Alg concentration does not affect the physicochemical interactions between the immobilized TPE and the wall materials.

According to Equation (2), the encapsulation efficiency (EE_e) of thymoquinone (TQ) in the freshly prepared Pickering emulsion system was determined to be >99%. This is reasonable since TQ first fully dissolves in the oil phase before turning into an O/W emulsion. Alternatively, based on the hydrogel shells formed by external gelation that immobilized the O/W emulsion loaded with TQ, the TQ's encapsulation efficiency (EE_b) according to Equation (3) of the Alg-Chi-TPE beads was determined to be 89.18 ± 3.63%, revealing an excellent loading efficiency using hydrogel beads. A decrease in the encapsulation efficiency could be due to the release of TQ during the ionic gelation and the hardening process.

Effects of Digestion on Alginate-Chitosan Beads Immobilized Thymoquinone-Loaded Pickering Emulsions

Figure 4 illustrates the water uptake of Alg-Chi-TPE hydrogel beads with different Alg concentrations in simulated gastric fluid (SGF) and simulated intestinal fluid (SIF). All hydrogel beads exhibited a weight increase of ∼15% after 30 min of gastric digestion. The increase in weight can be justified where the void regions within the hydrogel beads get filled up by water due to osmotic pressure asserting on the hydrogel beads. The water uptake ratio of all the beads continued to rise to a maximum of 23% for beads formed with 2.0% (w/v) Alg. The water uptake is minimal at the low pH of gastric fluid because alginate precipitates to form alginic molecules in the form of aggregates linked by hydrogen bonding leading to higher stability (38). When the hydrogel beads were introduced to the gastric digestive fluid, denser alginate structures were believed to be due to the weakened electrostatic repulsion among the alginate molecules. The pH of the SGF was maintained at pH 1.5, and the pK_a of alginate was at about 3.5, causing the alginate to reduce its negative charges (39).

The water uptake of beads was accelerated during intestinal digestion, which is ideal for digesting oils. Hydrogel beads obtained with 0.5% and 1.0% (w/v) alginate were disintegrated and deformed, where the weight measurement of the swollen beads could not proceed (**Figure 4B**). Generally, the water uptake ability of all beads during intestinal digestion improved with

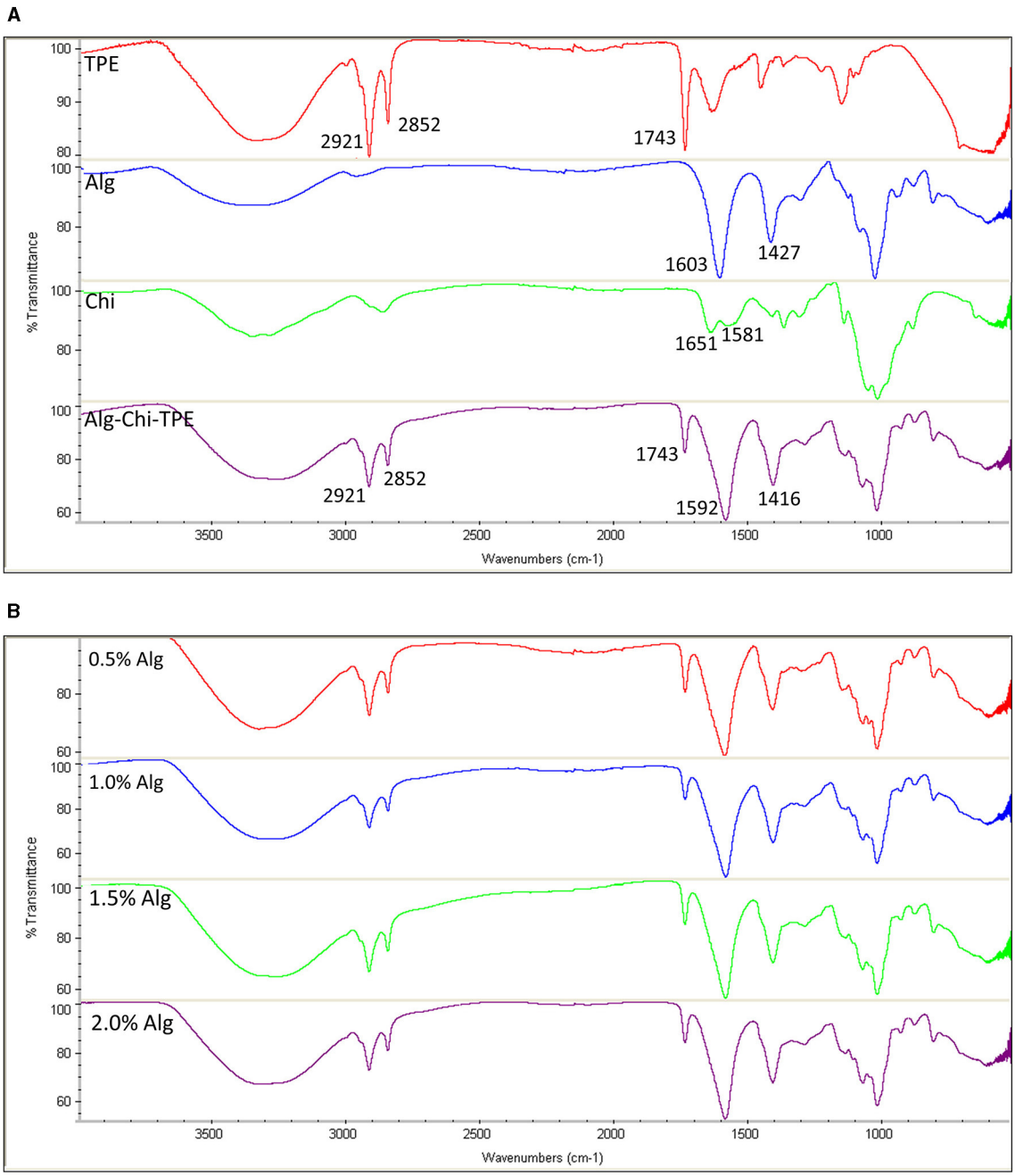

FIGURE 3 | FTIR spectra of **(A)** TPE, Alg, Chi, and Alg-Chi-TPE beads **(B)** different alginate concentrations (0.5–2.0% w/v).

increasing alginate concentration. The water uptake ratios of 2.0% (w/v) alginate and 2.0% (w/v) alginate-chitosan beads were significantly different at 120 min ($P < 0.05$) and continued to achieve 643 and 593%, respectively at 240 min, demonstrating substantial intestinal digestion of hydrogel beads in SIF. The destabilization of the alginate polymer network at intestinal pH is due to the ion exchange between Na^+ ions in the intestinal digestion fluid and Ca^{2+} ions in the hydrogel beads (40). The calcium ions dissociate and form calcium phosphate salts which no longer crosslink with the alginate matrix, leading to the structural degradation of the hydrogel matrix. On the other hand, the ionization of alginate at intestinal pH produces electrostatic repulsion forces between alginate chains, increasing weight gain (32).

Table 2 shows the swelling and erosion degrees of Alg-TPE and Alg-Chi-TPE hydrogel beads after 120 min of gastric

digestion and up to 240 min of intestinal digestion. The swelling degree measures the diameter of the swollen beads after treatment. The swelling degree for both hydrogel beads reduced after 120 min of gastric digestion, demonstrating the shrinking of beads. The shrinking occurs due to the dissociation of Ca^{2+} ions at low pH, the COO^- groups become protonated, resulting in the formation of hydrogen bonds within the alginate chains (41). In contrast, the swelling degree increased tremendously

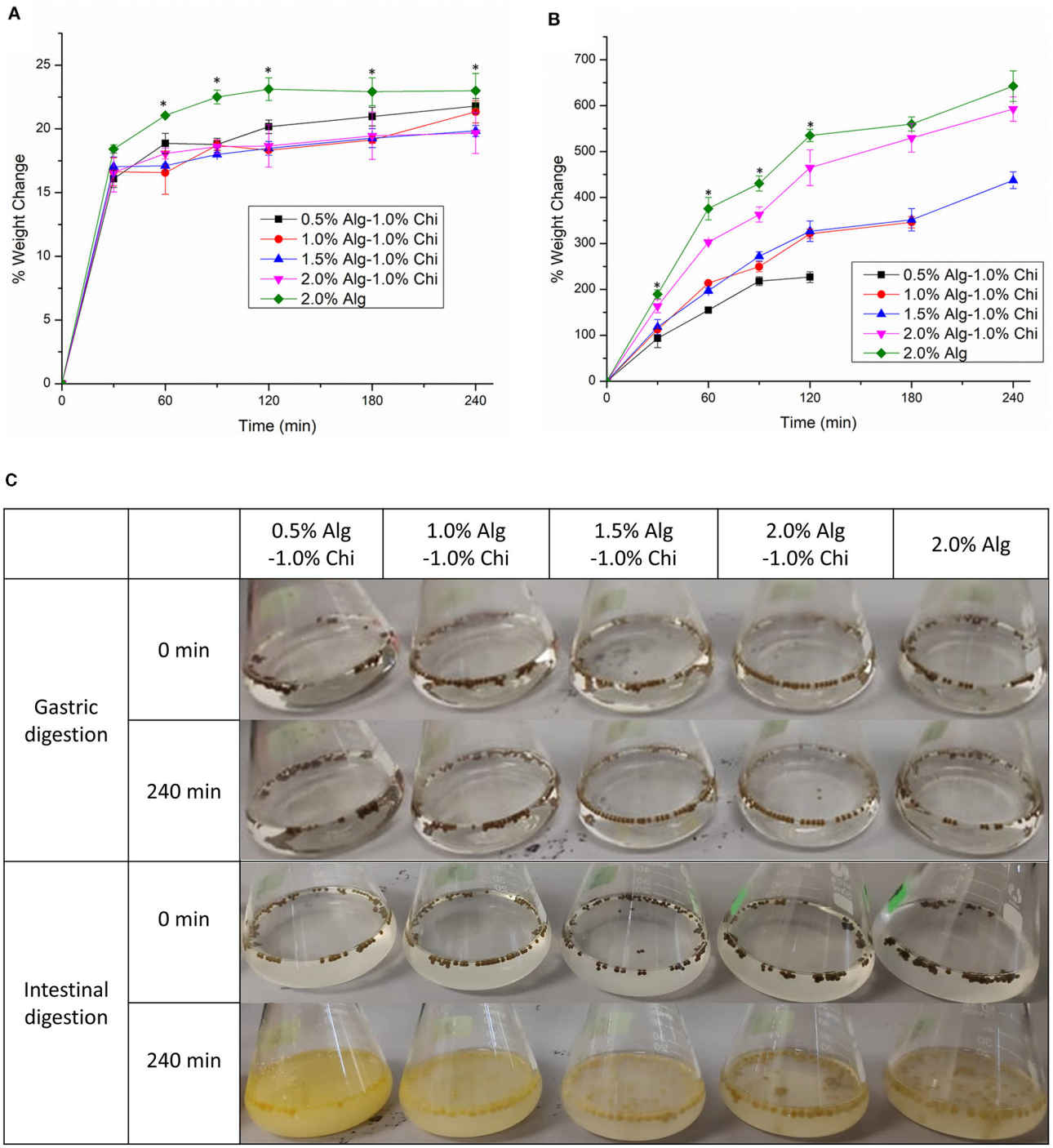

FIGURE 4 | The water uptake of alginate-chitosan hydrogel beads immobilized Pickering emulsion obtained with different alginate concentrations during **(A)** gastric digestion **(B)** intestinal digestion. **(C)** The visual appearance of beads before and after gastric and intestinal digestion. Error bars represent the standard deviation of three replicates. *Marks significant differences ($p < 0.05$). A comparison was made between 2.0% Alg and 2.0–1.0% Chi.

TABLE 2 | The swelling and erosion degrees of alginate hydrogel beads and alginate-chitosan hydrogel beads during gastric digestion and intestinal digestion.

	2.0% Alg		2.0% Alg-1.0% Chi	
Time (min)	**Swelling (%)**	**Erosion (%)**	**Swelling (%)**	**Erosion (%)**
SGF-120	-3.38 ± 3.76^{a}	8.24 ± 0.48^{c}	-9.12 ± 3.32^{b}	6.56 ± 0.84^{d}
SIF-30	27.51 ± 4.92^{a}	4.49 ± 0.45^{c}	18.64 ± 4.03^{b}	3.83 ± 1.04^{d}
SIF-60	56.27 ± 6.74^{a}	6.23 ± 0.61^{c}	48.55 ± 5.29^{a}	4.66 ± 0.56^{d}
SIF-120	75.06 ± 7.92^{a}	7.81 ± 0.23^{c}	54.75 ± 5.47^{b}	5.76 ± 0.79^{d}
SIF-180	90.13 ± 7.02^{a}	12.18 ± 0.90^{c}	68.72 ± 6.82^{b}	7.66 ± 0.85^{d}
SIF-240	100.23 ± 8.83^{a}	15.13 ± 0.77^{c}	85.22 ± 6.01^{b}	13.83 ± 1.01^{c}

Values expressed as the mean ± standard deviation. Different letters in the same row indicate significant differences ($p < 0.05$). A comparison was made between 2.0% Alg and 2.0–1.0% Chi. SGF—gastric digestion, and SIF—intestinal digestion.

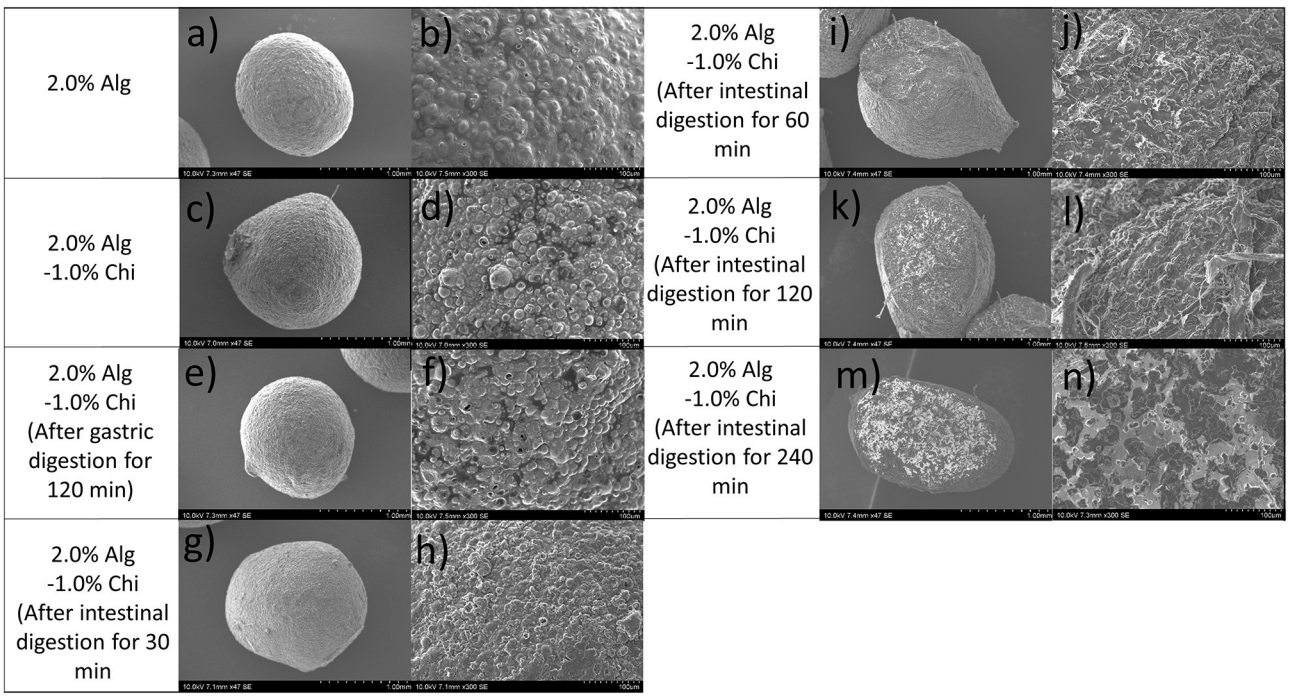

FIGURE 5 | SEM images of **(a,b)** 2.0% Alg hydrogel beads, **(c,d)** 2.0% Alg-1.0% Chi hydrogel beads, **(e,f)** 2.0% Alg- 1.0% Chi hydrogel beads after 120 min gastric digestion, **(g–n)** 2.0%- 1.0% Chi hydrogel beads after 30-240 min intestinal digestion at ×47 magnification (left) and ×300 magnification (right).

to around 100 and 85% after 240 min of intestinal digestion for Alg-TPE and Alg-Chi-TPE hydrogel beads, respectively. This observation is in line with other studies where alginate-based hydrogel beads shrunk during gastric digestion and swell during intestinal digestion, possibly due to the changes in electrostatic forces of the wall matrix at different pH (31, 40). It is worth noting that the hydrogel beads with chitosan illustrated a lower swelling degree than the hydrogel beads without chitosan. The addition of chitosan onto alginate leads to the formation of a more entangled system developed by the blending of both polymers forming polyelectrolyte complexes between the amino groups of chitosan and carboxylate groups of alginate (31). These factors improved the stability of Alg-Chi-TPE hydrogel beads and exhibited increased resistance to osmotic pressure.

On the other hand, the erosion degree measures the weight loss of the dried hydrogel beads after treatment. From **Table 2**, the erosion degrees for both Alg-TPE and Alg-Chi-TPE hydrogel beads after gastric digestion were 8.24 and 6.56%, respectively ($P < 0.05$). A significant reduction in the weight of hydrogel beads can be related to the syneresis effect in an acidic environment where shrinkage is favored (42). Nevertheless, the erosion degree of the hydrogel beads in an alkaline environment begins to rise with time, with the maximum erosion degree of 13.83% at 240 min for hydrogel beads coated with chitosan and 15.13% for hydrogel beads without chitosan. The erosion degree for hydrogel beads coated with chitosan was lower than hydrogel beads without chitosan, demonstrating enhanced stability of the hydrogel beads when chitosan was introduced. As the treatment continues, the degradation, and dissolution of the bead matrix

were enhanced over time. As a result, the final weight of the dried and treated hydrogel beads became lower, displaying time-dependent erosion properties.

The hydrogel beads prepared by 2.0% alginate were used to study the effects of digestion on the microstructures and bioactive release profile based on the swelling performance reported above. Scanning electron micrographs of dry alginate hydrogel (Alg-TPE) beads, chitosan-coated alginate (Alg-Chi-TPE) beads and Alg-Chi-TPE beads after specific digestion in SGF or SIF are illustrated in **Figure 5**. The Alg-TPE and Alg-Chi-TPE hydrogel beads exhibited spherical shape after air drying, and a detailed examination of the surface structure revealed a rough and folded appearance. There was not much difference between alginate and alginate-chitosan beads in terms of surface structure. However, a closer observation on SEM images with higher magnification (x300) illustrated the presence of more rough surfaces with irregular dents on the crosslinked alginate-chitosan hydrogel beads (**Figures 5b,d**). This could be attributed to the effect of chitosan polymer coating onto the surface of the alginate matrix, creating patchy-like textures associated with a shielding effect by the insoluble chitosan layer. The results can be correlated to the lower swelling profile of chitosan-coated alginate beads than the uncoated beads [swelling degree of 85 vs. 100% at 2.0% (w/v) alginate concentration].

As shown in **Figures 5d,f**, there is no significant variation in the microstructure of beads after gastric digestion with similar roughness and compact surfaces. This observation agrees with the swelling behaviors of hydrogel beads, where alginate displayed excellent stability in a medium of low pH. The stability of the alginate-chitosan beads or capsules depends strongly on the differences in their assembly (43) and the amount of chitosan bound to the capsules (44). The present study employed a one-step preparative procedure by dropping the emulsion-alginate mixture into a chitosan solution containing calcium chloride. Hydrogel bead formation was achieved by the ionic gelation effect, and chitosan formed the outer layer of the beads. An earlier

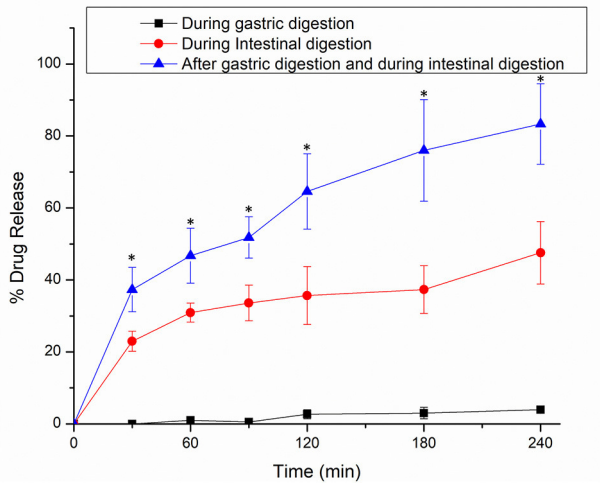

FIGURE 7 | *In vitro* release profiles of thymoquinone from alginate-chitosan hydrogel beads immobilized Pickering emulsion in SGF, SIF, and 2 h in SGF followed by SIF. Error bars represent the standard deviation of three replicates. *Marks significant differences ($p < 0.05$). A comparison was made between 2 h in SGF followed by SIF and SGF/SIF.

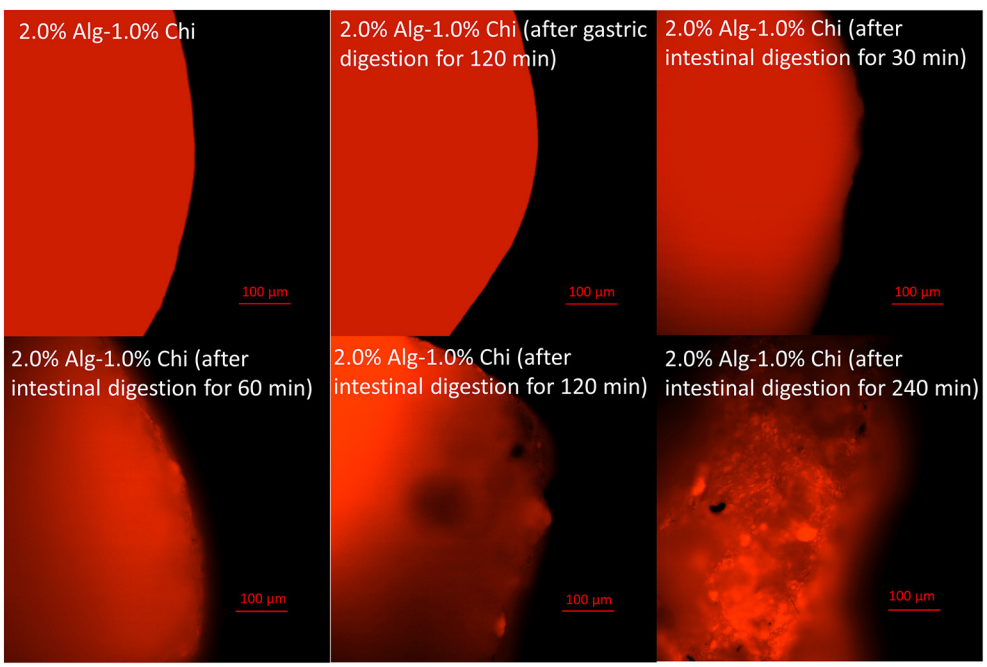

FIGURE 6 | Fluorescent images of alginate-chitosan hydrogel beads immobilized Pickering emulsion surface after gastric and intestinal digestion (scale bar, 100 µm).

TABLE 3 | Diffusional exponent (*n*), correlation coefficient (R^2), and the transport mechanism of thymoquinone release profile.

	n	R^2	Transport mechanism
During gastric digestion	1.147	0.947	Case-II transport
During intestinal digestion	0.311	0.991	Fickian diffusion
After gastric digestion and during intestinal digestion	0.298	0.999	Fickian diffusion

study reported that the chitosan molecules could diffuse into the alginate matrix, creating a 3D hydrogel network interconnected by alginate molecules, chitosan polymer bridges, and cationic calcium ions (45). The SEM micrographs revealed minimal changes in the surface morphology of alginate-chitosan beads upon 120 min exposure to SGF. A similar observation was also made in a previous work conducted by Li et al. (46). In addition, Chew et al. concluded that the chitosan-alginate coacervated beads appear to resist in an acidic medium where the structure remains intact because of the ionic bonds of calcium-alginate-chitosan complexation through electrostatic interactions (47).

The micrographs of Alg-Chi-TPE hydrogel beads at a different time point of intestinal digestion are illustrated in **Figures 5g–n**. After 30 min of intestinal digestion, the microstructure of hydrogel beads displayed a smoother surface, indicating the degradation of the hydrogel bead wall materials (**Figures 5g,h**). The compact structure gradually transforms into a heterogeneous structure with disorderly folded and significant dents when the intestinal digestion time increased to 120 min. The change in the microstructures of hydrogel beads could be due to the swelling process, which coincides with the erosion and dissolution of swollen beads (32). A slight deformation on the morphology of hydrogel beads (spherical to oval) after 60 min of intestinal digestion (**Figures 5i,j**) could be related to the swelling process and erosion of beads where the degradation of chitosan-coated alginate matrix as the wall materials of the beads has begun. At 240 min of intestinal digestion, micrographs of hydrogel beads (**Figures 5m,n**) with severe cleavages and uneven surfaces could be observed in the later stage. As shown in **Figure 6**, the fluorescent micrographs showed a similar microstructure of beads after gastric digestion without any substantial difference. However, the micrographs of beads displayed significant changes at different time points of intestinal digestion. The original compact surface has gradually transformed into a loose structure, indicating the loss of lipid phase from the beads. These results suggest that the digestion could start from the surface toward the center of the beads (48), causing the release of immobilized Pickering emulsion within the beads into the external medium.

Release of Thymoquinone From Alginate-Chitosan Beads Immobilized Thymoquinone-Loaded Pickering Emulsion

The release of encapsulated thymoquinone (TQ) from the hydrogel beads was achieved during gastrointestinal digestion. The TQ release profiles from Alg-Chi-TPE hydrogel beads in three different digestion systems [SGF, SIF, and SIF after pre-soaked in SGF for 2 h (SGF/SIF)] are presented in **Figure 7**. The release curves in SIF and SGF/SIF media showed a burst release in the initial stage (0–30 min) and then a slow release in the following stage (30–240 min). In the first 30 min, hydrogel beads in SGF/SIF medium demonstrated a faster release of TQ than in the SIF medium (37 vs. 23%, $P < 0.05$), while TQ releases in the SGF medium is undetected. Only about 4% of TQ was detected after the end of gastric digestion (240 min). The total TQ release in SIF medium and SGF/SIF medium was 48 and 83%, respectively ($P < 0.05$), showing the extensive release of TQ when the hydrogel beads were pre-soaked in the SGF medium before introducing to the SIF medium. The introduction of intestinal fluid at an alkaline pH and the extensive water uptake properties of the hydrogel beads could account for the initial rapid release (11). In addition, the presence of lipase in SIF could initiate the lipolysis process, breaking down lipid droplets into triacylglycerol molecules, mixed micelles, non-digested fat droplets, or smaller fractions of free fatty acids (49, 50), thus releasing TQ in short-chain fatty acids that could be absorbed in the small intestine.

By comparing the TQ release in the SIF medium alone and SGF/SIF medium, it can be denoted that two possible mechanisms regulate the bioactive release out of the hydrogel beads: the swelling process and the diffusion process (31). When the hydrogel beads were soaked in the SGF medium, a syneresis process occurs, resulting in the shrinking of beads. These shrunk beads with lesser volume were later transferred into the SIF medium to initiate intestinal digestion. Following the changes in different pH, the external gelation network structure of hydrogel beads was affected, producing more enormous pores/cleavages, accelerating the swelling process. Then, the encapsulated TQ can be released by diffusion process through the increasingly large openings. During the later stage (60–240 min), the rate of swelling of the beads decreased, and the diffusion process determines the amount of bioactive release.

The results were analyzed using the Peppas model to distinguish the release mechanisms of TQ from the alginate beads. For hydrogel beads, the diffusional exponent (n) specifies the mechanism of release. The calculation of the n value was measured up to the initial 60% release of the bioactive. If the values of n are equal or <0.43, the release is associated with Fickian diffusion. If n values are within 0.43 to 0.85, the release is indicated with Fickian diffusion and Case-II transport (caused by the swelling process). If the values of n are more than 0.85, the release is solely contributed by Case-II transport (32, 51). The results shown in **Table 3** indicate that the TQ release from Alg-Chi-TPE hydrogel beads in gastric digestion is associated with Case-II transport since the n value is more significant than 0.85. Thus, the swelling of hydrogel beads only controlled the bioactive release in the gastric stage. In contrast, the n values for TQ release

in intestinal digestion, with and without gastric treatment, were lesser than 0.43, indicating that the Fickian diffusion governs the release. The n values in both cases are relatively similar, suggesting that the diffusion of bioactive molecules mainly dominates the release mechanism out of the beads as the digestive medium hydrates the beads.

CONCLUSION

This work demonstrates *in vitro* digestion and hydrophobic thymoquinone (TQ) release from alginate-chitosan hydrogel beads immobilized Pickering emulsion (Alg-Chi-TPE). 2.0% (w/v) alginate hydrogel beads with spherical shape demonstrated the highest stability against structural deformation during the drying process. The presence of chitosan in beads formation improved the wall materials properties, providing a lower swelling degree and a rougher microstructure. Alg-Chi-TPE hydrogel beads demonstrated good stability during gastric digestion, and the release of encapsulated TQ was observed during intestinal digestion. Up to 83% of total TQ was released from the hydrogel beads after 2 h gastric digestion followed by 4 h treatment in the simulated intestinal fluid. The bioactive release mechanisms were incorporated with the Peppas model, which exhibited a Case-II transport caused by the swelling process during gastric digestion and Fickian diffusion during intestinal digestion. This study contributes to a better understanding of the swelling and digestion behaviors of alginate-chitosan hydrogel beads immobilized with food-grade Pickering emulsions to release a hydrophobic bioactive compound. This provides valuable information about its potential application in developing the colloids-based nutraceutical delivery system.

DATA AVAILABILITY STATEMENT

The original contributions presented in the study are included in the article/supplementary material, further inquiries can be directed to the corresponding author/s.

AUTHOR CONTRIBUTIONS

SKW: conceptualization, methodology, investigation, data curation, formal analysis, and original draft writing. DL and JS: writing-review and editing. CHP and SYT: funding acquisition and validation. BHG, SM, TWW, and CHP: resources and review. SYT: supervision and project administration. All authors contributed to the article and approved the submitted version.

FUNDING

The authors gratefully express gratitude to all parties which have contributed toward the success of this project, both financially and technically, especially the S&T Innovation 2025 Major Special Programme (Grant No. 2018B10022) and the Ningbo Natural Science Foundation Programme (Grant No. 2018A610069) funded by the Ningbo Science and Technology Bureau, China, as well as the UNNC FoSE Faculty Inspiration Grant, China. The Zhejiang Provincial Department of Science and Technology is also acknowledged for this research under its Provincial Key Laboratory Programme (2020E10018). This project was supported by the Tropical Medicine and Biology Platform, School of Science and Advanced Engineering Platform, School of Engineering, Monash University Malaysia.

REFERENCES

1. Darakhshan S, Pour AB, Colagar AH, Sisakhtnezhad S. Thymoquinone and its therapeutic potentials. *Pharmacol. Res.* (2015) 95:138–58. doi: 10.1016/j.phrs.2015.03.011
2. El-Far AH, Al Jaouni SK, Li W, Mousa SA. Protective roles of thymoquinone nanoformulations: potential nanonutraceuticals in human diseases. *Nutrients.* (2018) 10:1369. doi: 10.3390/nu10101369
3. Gali-Muhtasib H, Kuester D, Mawrin C, Bajbouj K, Diestel A, Ocker M, et al. Thymoquinone triggers inactivation of the stress response pathway sensor CHEK1 and contributes to apoptosis in colorectal cancer cells. *Cancer Res.* (2008) 68:5609–18. doi: 10.1158/0008-5472.CAN-08-0884
4. Jrah-Harzallah H, Ben-Hadj-Khalifa S, Almawi WY, Maaloul A, Houas A, Mahjoub T. Effect of thymoquinone on 1, 2-dimethyl-hydrazine-induced oxidative stress during initiation and promotion of colon carcinogenesis. *Eur J. Cancer.* (2013) 49:1127–35. doi: 10.1016/j.ejca.2012.10.007
5. El-Najjar N, Chatila M, Moukadem H, Vuorela H, Ocker M, Gandesiri M, et al. Reactive oxygen species mediate thymoquinone-induced apoptosis and activate ERK and JNK signaling. *Apoptosis.* (2010) 15:183–95. doi: 10.1007/s10495-009-0421-z
6. Negi P, Rathore C, Sharma G, Singh B, Katare OP. Thymoquinone a potential therapeutic molecule from the plant *Nigella sativa*: role of colloidal carriers in its effective delivery. *Recent Pat Drug Deliv Formul.* (2018) 12:3–22. doi: 10.2174/1872211311666171129121128
7. Schneider-Stock R, Fakhoury IH, Zaki AM, El-Baba CO, Gali-Muhtasib HU. Thymoquinone: fifty years of success in the battle against cancer models. *Drug Discov Today.* (2014) 19:18–30. doi: 10.1016/j.drudis.2013.08.021
8. Liu W, Mei J, Xie J. Shelf-life extension of refrigerated turbot (*Scophthalmus maximus*) by using weakly acidic electrolyzed water and active coatings containing daphnetin emulsions. *Front. Nutr.* (2021) 8:418. doi: 10.3389/fnut.2021.696212
9. Li Q, Liu CG, Huang ZH, Xue FF. Preparation characterization of nanoparticles based on hydrophobic alginate derivative as carriers for sustained release of vitamin D3. *J Agric Food Chem.* (2011) 59:1962–7. doi: 10.1021/jf1020347
10. Yan H, Chen X, Li J, Feng Y, Shi Z, Wang X, et al. Synthesis of alginate derivative via the Ugi reaction and its characterization. *Carbohydr Polym.* (2016) 136:757–63. doi: 10.1016/j.carbpol.2015.09.104
11. Yan H, Chen X, Feng M, Shi Z, Zhang W, Wang Y, et al. Entrapment of bacterial cellulose nanocrystals stabilized Pickering emulsions droplets in alginate beads for hydrophobic drug delivery. *Colloids Surf B.* (2019) 177:112–20. doi: 10.1016/j.colsurfb.2019.01.057
12. Kim S, Jeong C, Cho S, Kim SB. Effects of thermal treatment on the physical properties of edible calcium alginate gel beads: response surface methodological approach. *Foods.* (2019) 8:578. doi: 10.3390/foods8110578
13. Jeong C, Kim S, Lee C, Cho S, Kim SB. Changes in the physical properties of calcium alginate gel beads under a wide range of gelation temperature conditions. *Foods.* (2020) 9:180. doi: 10.3390/foods9020180

14. Chan ES. Preparation of Ca-alginate beads containing high oil content: influence of process variables on encapsulation efficiency and bead properties. *Carbohydr Polym.* (2011) 84:1267–75. doi: 10.1016/j.carbpol.2011.01.015
15. Yang JS, Xie YJ, He W. Research progress on chemical modification of alginate: a review. *Carbohydr Polym.* (2011) 84:33–39. doi: 10.1016/j.carbpol.2010.11.048
16. Wu Y, Li Y, Wang R, Zhao Y, Liu H, Wang JJ. Characterization of a novel food grade emulsion stabilized by the by-product proteins extracted from the head of giant freshwater prawn (*Macrobrachium rosenbergii*). *Front Nutr*. (2021) 8:359. doi: 10.3389/fnut.2021.676500
17. Low LE, Wong SK, Tang SY, Chew CL, De Silva HA, Lee JMV, et al. Production of highly uniform Pickering emulsions by novel high-intensity ultrasonic tubular reactor (HUTR). *Ultrason Sonochem*. (2019) 54:121–8. doi: 10.1016/j.ultsonch.2019.02.008
18. Low LE, Siva SP, Ho YK, Chan ES, Tey BT. Recent advances of characterization techniques for the formation, physical properties and stability of Pickering emulsion. *Adv Colloid Inter Sci.* (2020) 277:102117. doi: 10.1016/j.cis.2020.102117
19. Liu F, Tang CH. Soy protein nanoparticle aggregates as Pickering stabilizers for oil-in-water emulsions. *J Agric Food Chem.* (2013) 61:8888–98. doi: 10.1021/jf401859y
20. Yi F, Wu K, Yu G, Su C. Preparation of Pickering emulsion based on soy protein isolate-gallic acid with outstanding antioxidation and antimicrobial. *Colloids Surf B Biointerfaces.* (2021) 206:111954. doi: 10.1016/j.colsurfb.2021.111954
21. Wong SK, Supramaniam J, Wong TW, Soottitantawat A, Ruktanonchai UR, Tey BT, et al. Synthesis of bio-inspired cellulose nanocrystals-soy protein isolate nanoconjugate for stabilization of oil-in-water Pickering emulsions. *Carbohydr Res.* (2021) 504:108336. doi: 10.1016/j.carres.2021.108336
22. Elmowafy M, Samy A, Raslan MA, Salama A, Said RA, Abdelaziz AE, et al. Enhancement of bioavailability and pharmacodynamic effects of thymoquinone via nanostructured lipid carrier (NLC) formulation. *AAPS Pharmscitech*. (2016) 17:663–72. doi: 10.1208/s12249-015-0391-0
23. Lei L, Zhang Y, He L, Wu S, Li B, Li Y. Fabrication of nanoemulsion-filled alginate hydrogel to control the digestion behavior of hydrophobic nobiletin. *LWT*. (2017) 82:260–7. doi: 10.1016/j.lwt.2017.04.051
24. Xiao J, Shi C, Li Y, Pan Y, Huang Q. Pickering emulsions immobilized within hydrogel matrix with enhanced resistance against harsh processing conditions and sequential digestion. *Food Hydrocoll.* (2017) 62:35–42. doi: 10.1016/j.foodhyd.2016.07.025
25. Lim HP, Ho KW, Singh CKS, Ooi CW, Tey BT, Chan ES. Pickering emulsion hydrogel as a promising food delivery system: synergistic effects of chitosan Pickering emulsifier and alginate matrix on hydrogel stability and emulsion delivery. *Food Hydrocoll.* (2020) 103:105659. doi: 10.1016/j.foodhyd.2020.105659
26. Tampucci S, Castagna A, Monti D, Manera C, Saccomanni G, Chetoni P, et al. Tyrosol-enriched tomatoes by diffusion across the fruit peel from a chitosan coating: a proposal of functional food. *Foods.* (2021) 10:335. doi: 10.3390/foods10020335
27. Wang Y, Chen H, Wang J, Xing L. Preparation of active corn peptides from zein through double enzymes immobilized with calcium alginate–chitosan beads. *Process Biochem.* (2014) 49:1682–90. doi: 10.1016/j.procbio.2014.07.002
28. Baysal K, Aroguz AZ, Adiguzel Z, Baysal BM. Chitosan/alginate crosslinked hydrogels: preparation, characterization application for cell growth purposes. *Int J Biol Macromol.* (2013) 59:342–8. doi: 10.1016/j.ijbiomac.2013.04.073
29. Tan PY, Tan TB, Chang HW, Tey BT, Chan ES, Lai OM, et al. Effects of storage and yogurt matrix on the stability of tocotrienols encapsulated in chitosan-alginate microcapsules. *Food Chem.* (2018) 241:79–85. doi: 10.1016/j.foodchem.2017.08.075
30. Bourbon AI, Pinheiro AC, Cerqueira MA, Vicente AA. Influence of chitosan coating on protein-based nanohydrogels properties and *in vitro* gastric digestibility. *Food Hydrocoll.* (2016) 60:109–18. doi: 10.1016/j.foodhyd.2016.03.002
31. Pasparakis G, Bouropoulos N. Swelling studies *in vitro* release of verapamil from calcium alginate calcium alginate–chitosan beads. *Int J Pharm.* (2006) 323:34–42. doi: 10.1016/j.ijpharm.2006.05.054
32. Sun R, Xia Q. *In vitro* digestion behavior of (W1/O/W2) double emulsions incorporated in alginate hydrogel beads: microstructure, lipolysis, and release. *Food Hydrocoll*. (2020) 107:105950. doi: 10.1016/j.foodhyd.2020.105950
33. Lao LL, Peppas NA, Boey FYC, Venkatraman SS. Modeling of drug release from bulk-degrading polymers. *Int J Pharm*. (2011) 418:28–41. doi: 10.1016/j.ijpharm.2010.12.020
34. Jeddi MK, Mahkam M. Magnetic nano carboxymethyl cellulose-alginate/chitosan hydrogel beads as biodegradable devices for controlled drug delivery. *Int J Biol Macromol.* (2019) 135:829–38. doi: 10.1016/j.ijbiomac.2019.05.210
35. Rohman A, Riyanto S, Sasi AM, Yusof FM. The use of FTIR spectroscopy in combination with chemometrics for the authentication of red fruit (Pandanus conoideus Lam) oil from sunflower and palm oils. *Food Biosci*. (2014) 7:64–70. doi: 10.1016/j.fbio.2014.05.007
36. Voo WP, Lee BB, Idris A, Islam A, Tey BT, Chan ES. Production of ultra-high concentration calcium alginate beads with prolonged dissolution profile. *RSC Adv*. (2015) 5:36687–95. doi: 10.1039/C5RA03862F
37. Vasile FE, Romero AM, Judis MA, Mazzobre MF. *Prosopis alba* exudate gum as excipient for improving fish oil stability in alginate–chitosan beads. *Food Chem.* (2016) 190:1093–101. doi: 10.1016/j.foodchem.2015.06.071
38. Ching SH, Bansal N, Bhandari B. Alginate gel particles–a review of production techniques and physical properties. *Crit Rev Dood Sci Nutri.* (2017) 57:1133–52. doi: 10.1080/10408398.2014.965773
39. Li Y, Hu M, Du Y, Xiao H, McClements DJ. Control of lipase digestibility of emulsified lipids by encapsulation within calcium alginate beads. *Food Hydrocoll.* (2011) 25:122–30. doi: 10.1016/j.foodhyd.2010.06.003
40. Lin D, Kelly AL, Maidannyk V, Miao S. Effect of structuring emulsion gels by whey or soy protein isolate on the structure, mechanical properties, and *in-vitro* digestion of alginate-based emulsion gel beads. *Food Hydrocoll.* (2021) 110:106165. doi: 10.1016/j.foodhyd.2020.106165
41. Rayment P, Wright P, Hoad C, Ciampi E, Haydock D, Gowland P, et al. Investigation of alginate beads for gastro-intestinal functionality, part 1: *in vitro* characterisation. *Food Hydrocoll.* (2009) 23:816–22. doi: 10.1016/j.foodhyd.2008.04.011
42. Ramdhan T, Ching SH, Prakash S, Bhandari B. Time dependent gelling properties of cuboid alginate gels made by external gelation method: effects of alginate-$CaCl_2$ solution ratios pH. *Food Hydrocoll*. (2019) 90:232–40. doi: 10.1016/j.foodhyd.2018.12.022
43. Li Y, McClements DJ. Controlling lipid digestion by encapsulation of protein-stabilized lipid droplets within alginate–chitosan complex coacervates. *Food Hydrocoll.* (2011) 25:1025–33. doi: 10.1016/j.foodhyd.2010.09.024
44. Gåserød O, Sannes A, Skjåk-Bræk G. Microcapsules of alginate–chitosan. II. A study of capsule stability and permeability. *Biomaterials.* (1999) 20:773–83. doi: 10.1016/S0142-9612(98)00230-0
45. Gåserød O, Smidsrød O, Skjåk-Bræk G. Microcapsules of alginate-chitosan–I: a quantitative study of the interaction between alginate and chitosan. *Biomaterials.* (1998) 19:1815–25. doi: 10.1016/S0142-9612(98)00073-8
46. Li XY, Jin LJ, McAllister TA, Stanford K, Xu JY, Lu YN, et al. Chitosan–alginate microcapsules for oral delivery of egg yolk immunoglobulin (IgY). *J Agric Food Chem.* (2007) 55:2911–7. doi: 10.1021/jf062900q
47. Chew SC, Tan CP, Long K, Nyam KL. *In-vitro* evaluation of kenaf seed oil in chitosan coated-high methoxyl pectin-alginate microcapsules. *Ind Crops Prod.* (2015) 76:230–6. doi: 10.1016/j.indcrop.2015.06.055
48. van Leusden P, den Hartog G, Bast A, Postema M, van der Linden E, Sagis LM. Lipase diffusion in oil-filled, alginate micro-and macrobeads. *Food Hydrocoll.* (2018) 85:242–7. doi: 10.1016/j.foodhyd.2018.07.028
49. Li Y, McClements DJ. New mathematical model for interpreting pH-stat digestion profiles: impact of lipid droplet characteristics on *in vitro* digestibility. *J Agric Food Chem.* (2010) 58:8085–92. doi: 10.1021/jf101325m
50. Nik AM, Wright AJ, Corredig M. Micellization of beta-carotene from soy-protein stabilized oil-in-water emulsions under *in vitro* conditions of lipolysis. *J Am Oil Chem Soc.* (2011) 88:1397–407. doi: 10.1007/s11746-011-1806-z
51. Ritger PL, Peppas NA. A simple equation for description of solute release II. Fickian and anomalous release from swellable devices.

J Control Release. (1987) 5:37–42. doi: 10.1016/0168-3659(87)90035-6

Conflict of Interest: The authors declare that the research was conducted in the absence of any commercial or financial relationships that could be construed as a potential conflict of interest.

Publisher's Note: All claims expressed in this article are solely those of the authors and do not necessarily represent those of their affiliated organizations, or those of the publisher, the editors and the reviewers. Any product that may be evaluated in this article, or claim that may be made by its manufacturer, is not guaranteed or endorsed by the publisher.

frontiers in Nutrition

REVIEW
published: 02 November 2021
doi: 10.3389/fnut.2021.765589

Recent Progress on Protein-Polyphenol Complexes: Effect on Stability and Nutrients Delivery of Oil-in-Water Emulsion System

Minghui Li[1], *Christos Ritzoulis*[2,3], *Qiwei Du*[1], *Yefeng Liu*[4], *Yuting Ding*[1], *Weilin Liu*[3]* *and Jianhua Liu*[1]*

[1] College of Food Science and Technology, Zhejiang University of Technology, Hangzhou, China, [2] Department of Food Science and Technology, International Hellenic University, Thermi, Greece, [3] School of Food Science and Biotechnology, Zhejiang Gongshang University, Hangzhou, China, [4] Hangzhou Huadong Medicine Group Pharmaceutical Research Institute Co. Ltd., Hangzhou, China

OPEN ACCESS

Edited by:
Miguel Angel Prieto Lage, University of Vigo, Spain

Reviewed by:
Javier E. Alvarez, University of Vigo, Spain
Franklin Chamorro, University of Vigo, Spain
Marta Barral Martínez, University of Vigo, Spain

***Correspondence:**
Jianhua Liu
jhliu@zjut.edu.cn
Weilin Liu
lwl512@zjgsu.edu.cn

Specialty section:
This article was submitted to Food Chemistry, a section of the journal Frontiers in Nutrition

Received: 27 August 2021
Accepted: 28 September 2021
Published: 02 November 2021

Citation:
Li M, Ritzoulis C, Du Q, Liu Y, Ding Y, Liu W and Liu J (2021) Recent Progress on Protein-Polyphenol Complexes: Effect on Stability and Nutrients Delivery of Oil-in-Water Emulsion System. Front. Nutr. 8:765589. doi: 10.3389/fnut.2021.765589

Oil-in-water emulsions are widely encountered in the food and health product industries. However, the unsaturated fatty acids in emulsions are easily affected by light, oxygen, and heat, which leads to oxidation, bringing forward difficulties in controlling emulsion quality during transportation, storage, and retail. Proteins are commonly used as emulsifiers that can enhance the shelf, thermal and oxidation stability of emulsions. Polyphenols are commonly found in plants and members of the family have been reported to possess antioxidant, anticancer, and antimicrobial activities. Numerous studies have shown that binding of polyphenols to proteins can change the structure and function of the latter. In this paper, the formation of protein–polyphenol complexes (PPCs) is reviewed in relation to the latters' use as emulsifiers, using the (covalent or non-covalent) interactions between the two as a starting point. In addition, the effects polyphenol binding on the structure and function of proteins are discussed. The effects of proteins from different sources interacting with polyphenols on the emulsification, antioxidation, nutrient delivery and digestibility of oil-in-water emulsion are also summarized. In conclusion, the interaction between proteins and polyphenols in emulsions is complicated and still understudied, thereby requiring further investigation. The present review results in a critical appraisal of the relevant state-of-the-art with a focus on complexes' application potential in the food industry, including digestion and bioavailability studies.

Keywords: protein, polyphenol, interaction, oil-in-water emulsion, antioxidant, stability, nutrient delivery, ligand

INTRODUCTION

Oil-in-water emulsions are widely used in the food industry and often play specific functions such as flavor carriers or as functional substances. Functional oils in oil-in-water emulsions (fish oil, algal oil, etc.) are rich in polyunsaturated fatty acids such as eicosapentaenoic acid (EPA) and docosahexaenoic acid (DHA), which are beneficial for the health of elderly and young children. These oils have health functions such as lowering cholesterol and promoting brain

development. However, oil-in-water emulsion systems are generally unstable, as they are prone to oxidation, stratification, breakage and other phenomena in the process of storage, transportation and processing, making the emulsions' quality decline. The instability of unsaturated oils in oil-in-water emulsion systems is mainly caused by oxidation, and the oxidation itself is mainly due to three processes: autoxidation, photosensitive oxidation and enzymatic oxidation; of these the autoxidized chain reaction is the most significant (1). Free radicals are mainly responsible for the oil automatic oxidation. Free radicals are mainly derived from normal metabolic processes in cells and generated by the reaction between metal ions (cobalt, copper, iron, etc.) and oil during the processing (2). The outer layer of the free radical electron shell has an unpaired electron, which has a strong affinity to free electrons, so it can play the role of a strong oxidant. The chain reaction of free radicals causes the auto-oxidation of oils and fats. When the oil in the emulsion is autoxidized, the stability of the emulsion decreases and the flavor deteriorates, resulting in stratifying and other phenomena (3). Therefore, it is necessary to improve the oxidative stability of oil-in-waters emulsion in the application process of food industry.

Efficient emulsifiers can form a layer on the oil-water interface of droplets and protect again coalescence, hence increase the storage stability of the emulsion. Proteins are often used as emulsifiers to improve emulsion stability. Some milk protein-derived proteins, such as whey proteins, can form interfacial layers able to offer protection against not only coalescence, but also to inhibit the oxidation of oil-in-water emulsions during storage and transportation (4).

Some milk proteins have strong antioxidant ability. In oil-in-water emulsions, the antioxidant capacity of interfacial emulsifiers could have a conspicuous influence on the rate of lipid oxidation by affecting the reactivity and location of the pro-oxidative transition metals, lipid hydroperoxide and free radicals (5, 6). For example, caseins have been shown to have significant antioxidant properties in oil-in-water emulsions, and the antioxidant activity of casein has mainly been attributed to its ability to bind pro-oxidants (7).

Polyphenols have antibacterial, anti-cancer, cardiovascular disease-preventive, anti-oxidative, and other health-related and functional properties (8). However, phenolic compounds are apt to oxidize to quinones under oxygen, ozone, or polyphenol oxidase (9). Therefore, polyphenols have strong antioxidant properties but poor emulsifying ability. The interaction between polyphenols and proteins improves protein antioxidant activity and also broadens the application of polyphenols. A previous research reported that, compared to egg white protein, egg white protein (EWP)-epigallocatechin gallate (EGCG) complexes could significantly improve the emulsifying properties and the stability of emulsions (10). Proteins, interacting covalently and/or non-covalently with polyphenols, could change the structure and function of the former, which affects their role as emulsifiers in oil-in-water emulsions. Milk proteins α-casein (α-CS) and β-CS interactions with tea polyphenols were analyzed by spectral analysis (identifying substances and determining their chemical composition and relative content) and docking experiments (studying the interaction between molecules). It was found that the interactions change the secondary structure of proteins and improve their antioxidant activity, which is consistent with the previous cases (11).

The present paper reviews the formation of complexes between proteins and polyphenols through covalent and non-covalent interactions. Both these modes of action induce PPCs (protein-polyphenol complexes) to have good interfacial properties on the surface of the emulsion. For example, PPCs can form a thick film on the surface of the oil droplets, which can prevent the oxidation of the oil droplet and improve the stability of the emulsion. Therefore, they can be used as emulsifying agents that enhance the oxidation stability, emulsification stability and thermal stability of oil-in-water emulsions. Moreover, after PPCs are formed, the particle size and electric potential are reduced, making it potentially easier to attach to the surface of oil droplets and be used to resist enzymes in the stomach environment, and then allow them to slowly release in the intestines. Of course, their relevant effectiveness in the presence of bile salts remains to be examined. In addition, the emulsions can be used to carry bioactive substances in oil, so the oil droplets loaded with PPCs will also be more conducive to the transportation and release of active substances.

To sum up, understanding the interactions between protein and polyphenol offers the potential to substantially improve the mode of utilization of proteins in the food industry, and their applications in stabilizing oil-in-water emulsions can open new possibilities in functional food design. PPCs also have a great significance in improving the storage stability of the oil-in-water emulsions, and their application in the food industry.

Abbreviations: ABTS, 2,2'-azino-bis (3-ethylbenzothiazoline-6-sulfonic acid); ACN, Anthocyanin; $LO^{\cdot}$, Alkoxyl; β-LG, β-lactoglobulin; BSA, Bovine serum albumin; C, (+)-catechin; CA, Catechin acid; CD, Circular dichroism; CI, Creaming index; CS, Casein; CT, Catechin; DHA, Docosahexaenoic acid; DPPH, 1,1-diphenyl-2-picrylhydrazyl; DSC, Differential scanning calorimetry; EAI, Emulsifying activity index; EGC, (-)-epigallocatechin; EGCG, (-)-epigallocatechin gallate; EPA, Eicosapentaenoic acid; ESI, Emulsion stability index; FPP, Flaxseed polyphenols; FPI, Flaxseed protein isolate; FRAP, Ferric reducing activity power; GA, Gallic acid; GSP, Gliadin-grape seed proanthocyanidins; GTNP, Gliadin and TA nanoparticles; HIPE, High internal phase emulsion; LF, Lactoferrin; LOOH, Lipid hydroperoxide; MALDI–TOF–MS, Matrix-assisted laser desorption/ionization time-of-flight mass spectrometry; O/W, Oil-in-water; ORAC, Oxygen radical absorbance capacity; OVA, Ovalbumin; $LOO^{\cdot\cdot}$, Peroxyl; PPCs, Protein–polyphenol complexes; RBP, Rice bran protein; SDS–PAGE, Sodium dodecyl sulfate-polyacrylamide gel electrophoresis; SP, Soybean protein; SPI, Soy protein isolate; TA, Tannin acid; TBARS, Thiobarbituric acid reactive substance; Td, Decomposition temperature.

PROTEIN–POLYPHENOL COMPLEXES (PPCs)

Formation Mechanisms of Protein–Polyphenol Complexes

The interactions between protein and polyphenol can be divided into reversible interactions and irreversible interactions. Reversible interactions are carried out by non-covalent bonds such as hydrogen bonds, hydrophobic bonds and van der Waals forces, while irreversible interactions are generally the

ones where proteins and polyphenols combine into complexes by covalent bonding, thus affecting the respective structural properties of proteins and polyphenols (12). Among the two kinds of interactions, the non-covalent interactions are the most abundant in nature. Interactions involving non-covalent bonds are susceptible to environmental factors, such as changes in temperature and pH, which will affect the binding of protein and polyphenols.

Covalent Interactions

The covalent interactions between proteins and polyphenols are usually through C–N or C–S linkage (**Figure 1**). Under alkaline conditions, polyphenols form the corresponding quinones in the presence of enzymes and oxygen (13). In the process of forming PPCs, the polyphenols' enzymatic oxidation intermediate products, such as half quinone radicals of nucleophilic residues, interact with amino acids (e.g., methionine, lysine) on the protein side chain. Finally, protein and polyphenol form covalent bonds (14). If polyphenols are partially oxidized and then combined with proteins, they may also form complexes with proteins, at times improving the latter's emulsification and antioxidant properties (15). For example, oxidized tannin (TA) and catechin acid (CA) can covalently combine with porcine plasma proteolytic products as to form complexes under alkaline conditions, improving the emulsifying and antioxidant properties of polypeptides (9).

Proteins are reported to bind to polyphenols by enzymatic and non-enzymatic methods (3, 15). Non-enzymatic methods mainly involve free radical grafting, hydrogen peroxide and ascorbic acid as redox systems. The free radical grafting process

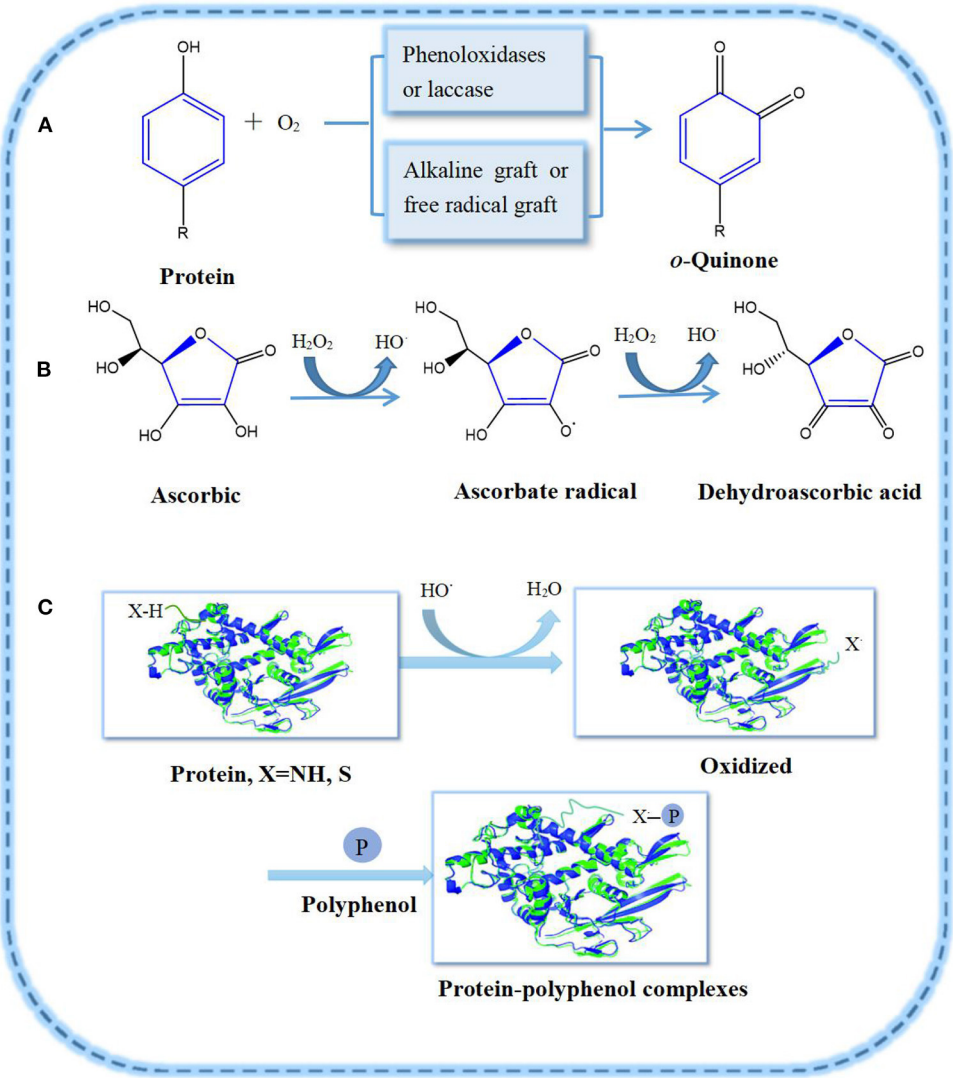

FIGURE 1 | Oxidation of polyphenols and their covalent graft reactions with proteins: **(A)** Polyphenol oxidation pathway; **(B)** Ascorbic acid oxidation system; **(C)** Protein-polyphenol radical grafting reaction.

involves proteins binding to polyphenols and is considered as a better method to produce high active PPCs, as it can improve the antioxidant activity of proteins more efficiently than the alkaline method (3). Feng et al. (16) grafted ovalbumin (OVA) with catechins such as (+)-catechin (C), (-)-epigallocatechin (EGC) and (-)-epigallocatechin gallate (EGCG) as to form covalent complexes. The binding of OVA to polyphenols was confirmed by sodium dodecyl sulfate-polyacrylamide gel electrophoresis (SDS–PAGE) and matrix-assisted laser desorption/ionization time-of-flight mass spectrometry (MALDI–TOF–MS). Covalent interaction of gelatin-gallic acid/catechin (gelatin–GA/CT), β-lactoglobulin–catechin (β-LG–CT), α-lactalbumin–CT, and lactoferrin–chlorogenic acid/epigallocatechin gallate/gallic acid (LF–CA/EGCG/GA) were successfully prepared *via* this method, and the effect of polyphenol modification on the structural and functional properties of these proteins have been estimated (17–19).

Non-covalent Interactions

The non-covalent interactions (**Figure 2**) between protein and polyphenols mainly occur via hydrogen bonds, hydrophobic interactions and electrostatic interactions (20). Hydrogen bonding and hydrophobic interactions are the main forces involved in the non-covalent synthesis of complexes between proteins and polyphenols (20, 21).

Hydrogen Bonds

The polyphenols can be used as hydrogen donors to form a hydrogen bond with the C = O group of the protein (22). When interacting with proteins, as long as hydrogen bonds are formed through carbon-oxygen double bonds, interaction forces between proteins and polyphenols are exerted, resulting in bonding. Besides, hydrogen bonds also form via the interactions between the OH groups of polyphenols and oxygen or nitrogen, especially the hydroxyl (–OH) and amino ($–NH_2$) groups of proteins (23).

It has been shown that casein residues (Phe23, Phe24, Phe28, Phe32, and Val31) can interact with catechins via hydrogen bonds (24). In addition, the main mode of interaction between plant proteins such as pea protein and grape seed pro-anthocyanidins is hydrogen bonding, and the interaction between pea protein and pro-anthocyanidins can make emulsion more stable (25), which also extends the application field of non-covalent interactions between protein and polyphenols in emulsion systems.

Hydrophobic Interactions

Surface hydrophobicity (H_0) is an important parameter affecting the surface-related functions of proteins (26). The hydrophobic interaction between proteins and polyphenols is one of the main forces involved in the formation of PPCs, hence plays an important role in the formation of non-covalent protein–polyphenol complexes. Several researchers, such as Yuksel et al. (27), Hasni et al. (11), and Staszawski et al. (28), reported that the interaction between proteins and polyphenols is mainly accomplished through hydrophobic forces. They also reported that cytochrome adsorbed on a gel column containing

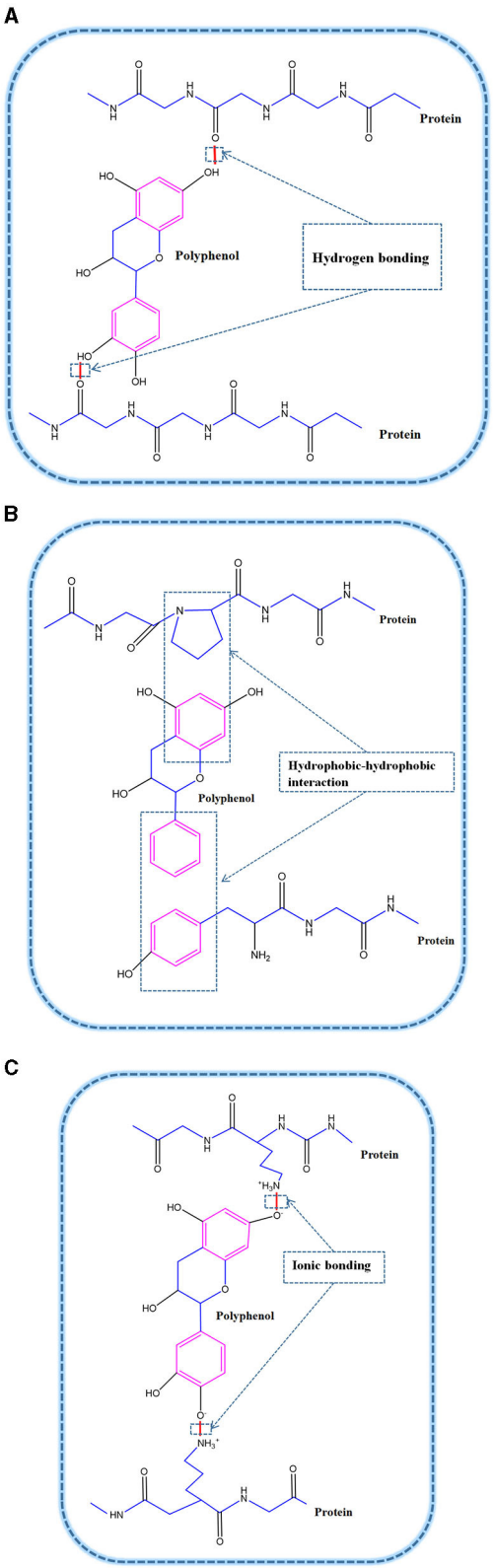

FIGURE 2 | Non-covalent interactions between proteins and polyphenols: **(A)** Hydrogen bonding; **(B)** Hydrophobic-hydrophobic interaction; **(C)** Ionic bonding.

immobilized polyphenols could be eluted by anion and non-anion eluents, thus proving that hydrophobic interaction between proteins and tannin acid (TA) may be influenced by surfactants.

In addition, studies have shown that some hydrophobic amino acids, such as leucine and glycine, can interact with the non-polar aromatic rings of polyphenols, highlighting the nature of the main PPCs hydrophobic interactions (12, 29). Through docking studies, Kanakis et al. (29) found that tea polyphenols had a weak binding hydrophobic interaction with β-lactoglobulin (LG) in emulsions. In addition, they discovered that the hydrophobic interaction of polyphenols with β-LG altered the secondary structure of the protein (29), making it more stable, a property beneficial to the stability of relevant PPCs-stabilized emulsions. Therefore, hydrophobic interactions between proteins and polyphenols can change the structure and interfacial environment of proteins.

Ionic Binding Forces

Amino acids are the structural units of proteins, which possess different electrically charged, uncharged polar, and hydrophobic side chains. The charges side chains may interact with polyphenols via ionic binding interactions (30). The ionic bond and force interaction between proteins and polyphenols are mostly due to the attractions between the positively-charged amino acids, such as lysine, and the negative-hydroxyl groups of polyphenols. For example, Han et al. (30) reported that lysine, having a higher positive charge than hemoglobin or immune protein, demonstrated stronger ionic interactions with catechin (CT). Therefore, the degree of ionic interaction between proteins with different side chain groups and polyphenols is different, which will further influence the functional differences of protein-polyphenols complexes. Of course, as the charges of proteins and (conditionally) of PPCs are strongly dependent on pH, these interactions are pH-specific.

EFFECTS OF PROTEIN–POLYPHENOLS INTERACTION ON THE PROTEIN STRUCTURE AND ITS FUNCTIONAL PROPERTIES

Changes in Protein Structural Properties

When proteins interact with polyphenols to form PPCs, the secondary, tertiary and quaternary structures of proteins can be affected. The polyphenols can change the secondary conformation of proteins mainly by the conversion between α-helical, β-sheet, β-turn, and random coil (11). Ge et al. (31) used circular dichroism (CD) to analyze the secondary structure of soybean soluble protein bound with tea polyphenols. They found that tea polyphenols increased the content of α-helix and the loose structure of random coils disappeared, which contributed to a stabler conformation of the protein (31). Liu et al. (32) analyzed and determined the structure of lactoferrin (LF) after coupling with polyphenols and measuring by CD. Moreover, they also found that the wavelength band of far-UV caused by conjugation and the negative peak-to-peak position related to α-helix increased. The complexes of LF and CA or EGCG caused a small change in the band intensity from 210 to 230 nm. It can be concluded that the conjugation of LF with polyphenols gave rise to an increased fraction in α-helix with a parallelly-decreasing fraction in the random coil structure, indicating restructure behavior effect on LF. Nevertheless, it was reported that the interaction of CA with bovine serum albumin (BSA) would cause a decreased fraction of α-helix together with increased portions of other structures, which might be influenced by the differences in the physicochemical characteristics between LF and BSA, as well as by the methods used to prepare these conjugates (13).

Information can be obtained about the conformational and/or dynamic changes of proteins during their interaction with phenolics by fluorescence spectroscopy analysis. The structures of LF–EGCG, LF–CA, and LF–GA complexes were measured by fluorescence spectrophotometer, and it can be concluded that the conjugation phenomenon of LF-polyphenol complexes may change the tertiary structure of LF (32). Usually, the maximum emission wavelength of LF is 342 nm, while the measured maximum emission wavelength of LF–EGCG, LF–CA, and LF–GA are 351, 345, and 344 nm, respectively (32). The fluorescence intensity of the interaction between LF and polyphenols decreased significantly, and the maximum emission wavelength showed a red shift caused by the transfer of tryptophan residues to a more hydrophilic environment. It could be deduced that the interaction between LF and polyphenols induced conformational changes that might lead to the unfolding and denaturation of LF. It should be stressed that the derivatization of polyphenols will also affect the protein. Klaus et al. (33) showed that the binding of derivatization chlorogenic acid (CA) to β-LG affected the protein amino acid composition in experiment involving rats; while high derivatization level could affect the nutritional quality of β-LG. It might be the concentration of the reactants that causes the structural change. An explanation for this is that the interaction between protein and polyphenols is affected by the type of protein, or by differences between *in vitro* and *in vivo* experiments (33). Therefore, the effect of polyphenols on proteins is different on a case-by-case basis: Some proteins are not affected by the interaction with polyphenols, while they are influenced by external factors like the concentration of the reaction solution.

Changes in Protein Functional Properties

Protein–polyphenol complexes not only affect the structure of proteins but also change their functional properties. For example, the interactions between proteins and polyphenols can improve their emulsification properties and oxidation resistance capacity.

The interactions between proteins and polyphenols can significantly increase the stability of protein-based colloid systems and protein-stabilized emulsions (34). Liu et al. (35) showed that the average diameter and polydispersity index of the droplets coated with LF–polyphenol complexes were less than those coated with LF alone. According to this report, the emulsifying properties of LF have been greatly improved after being covalently modified by EGCG. Staszewski et al. (6, 28)

also showed that the stability of oil-in-water emulsion emulsified by sunflower protein–CA complexes was higher than that of plain sunflower protein. These might be because the combination of polyphenols with LF increases its surface hydrophobicity and enhances its surface activity, and/or leads to the formation of a thicker interfacial layer. Other research also showed that the improvement of emulsification performance might be due to the increase of protein flexibility, solubility, and surface hydrophobicity, thus improving the ability of protein adsorption on oil-water surfaces (36).

Whey protein is one of the main proteins of milk, has good emulsifying properties and is widely used in the food processing industry (37). Whey protein can stabilize emulsions on its own, while studies have shown that it has a strong non-covalent affinity to tannic acid (TA), leading to complexes that will not only affect the secondary structure of the protein, but will also reduce the stability of emulsions (38). However, other studies have shown that the covalent and non-covalent interactions between TA and other proteins, such as gliadin, can improve the emulsification ability of the protein (39), thus enhancing the stability of the emulsion produced with the relevant PPCs. These are cases where the non-covalent interactions between protein and polyphenol are not good for the stability of oil-in-water emulsions, while covalent binding between protein and polyphenol is beneficial to the stability of emulsions, and has a profound influence on the latter's during storage. Of course, such examples relate to very few proteins and should not be generalized. It should be noted that phenolic acids and flavonoids reacting with soy protein may destroy amino acids (Lys, tryptophan) and amino acid residues (cysteine residues) in protein molecules, thus affecting the availability of the protein's amino acids (13).

Antioxidant activity is one of the most important properties of protein–polyphenol complexes. The following studies concluded that protein–polyphenol complexes exhibited stronger antioxidant activity than the unmodified proteins. Sun et al. (40) showed that the antioxidant capacity of EWP was significantly improved when coupled with catechin (CT) and CA. Studies have shown that under the same protein concentration, the DPPH free radical scavenging capabilities of EWP-CT and EWP-CA are 38.0 and 67.7%, respectively, which were 2.5- and 4.5 fold than that of unmodified EWP (40). As reported earlier, Staszewski et al. (6) also concluded that the combination of tea polyphenols with β-LG could improve the oxidation stability of oil-in-water emulsions, while the complexes had stronger antioxidant activities than the pure β-LG. This can be attributed to the fact that the compound-stabilized emulsion had lower concentrations of hydroperoxide, which can account for its better stability (6). You et al. (41) also found that 2,2'-azino-bis (3-ethylbenzothiazoline-6-sulfonic acid) (ABTS) radical scavenging activity, ferric reducing activity power (FRAP), and oxygen radical absorbance capacity (ORAC) of ovotransferrin–CT complexes were increased by 4–5 times as compared to those of native ovotransferrin (14). In addition, Feng et al. (16) revealed that complexes of ovalbumin (OVA) with EGCG, EGC, or CT synthesized by free-radical grafting showed stronger ORAC, 1,1-diphenyl-2-picrylhydrazyl (DPPH) and ABTS radical scavenging activities than OVA alone. Gu et al. (42) measured the antioxidant activities of EWP, of the mixture of EWP and CT, and of the EWP–CT complexes by reference to the previous ABTS free radical scavenging ability experiment, and the results showed that the antioxidant activity of EWP–CT complexes were much higher than those of pure EWP. Moreover, the complexes of EWP and tea polyphenols could enhance the antioxidant activity of EWP (43). In this work, the DPPH radical scavenging activity of EWP was significantly improved ($P < 0.05$) after covalent conjugating with TP alkaline/free radical methods (44). In addition, the thiobarbituric acid reactive substance (TBARS) of FPI and FPI–FPP were measured in the design of the antioxidant performance test of PPCs, and the results of 15 days-old specimens showed that the TBARS of the FPI–FPP complexes were significantly lower than that of FPI (34). Furthermore, the antioxidant capacities of PPCs were improved because of the introduction of hydroxyl groups from polyphenols into proteins (23, 41, 43). Therefore, protein–polyphenol complexes can be used to enhance antioxidant properties with an aim to improve the oxidative stability of several lipid-based foods.

Many foods need heat treatment such as sterilization, pasteurization, and cooking in the process of manufacture or use, so it is useful to detect the effect of heating on the stability of emulsions (35). The addition of polyphenols affects the thermal stability of the protein. For example, after free radical grafting of LF with EGCG, CA, and GA, respectively, the melting temperature of LF increased from 5 to 15.2°C (32). The melting temperature of milk protein also increased with the addition of EGCG, which improved the stability of the produced emulsion (45). They also verified that covalent complexes had better thermal stabilities than non-covalent complexes, as shown by the thermal decomposition temperature (T_d). This suggested that covalently modified milk proteins needed less energy to unfold, because they are more stable. This might be due to the spatial expansion of milk protein in the chemically modified part of EGCG. In addition, studies showed that the stability of emulsion stabilized with LF was low when compared to that of LF–CA complex emulsions (35). This might be due to the spatial expansion of LF above the thermal denaturation temperature, resulting in a strong hydrophobic force between lipid droplets. As a result, the droplets flocculated/coalesced. However, the emulsion coated with LF–CA was highly stable to high temperature processing. Differential scanning calorimetry (DSC) measurements of protein thermal behavior showed that the denaturation temperatures of LF–CA complexes were higher than that of natural LF.

The interaction between proteins and certain polyphenols will also affect the functional properties of proteins due to structural differences between the different polyphenols and the relevant interactions. For example, some researchers have reported that egg protein and tea polyphenol complexes can increase the resilience of air/water surfaces and enhance foamability (46). In addition, Li et al. (36) showed that the binding between LF and procyanidins improved the foaming properties of LF, which could be used to improve the quality-related properties of natural functional foods. Other researchers considered tannic acid (TA) and caseinate (CS) complexes, and found that complexes would actually decrease their foamability (47).

TYPES OF PROTEIN–POLYPHENOL COMPLEXES

Animal Proteins and Polyphenols

Animal protein mainly comes from poultry, livestock and fish meat, and from eggs and milk. The dominant proteins are the caseins (extracted from milk), which can be better absorbed and utilized by adults (48). Compared with plant protein, animal protein has more essential amino acids. The interactions between animal proteins (such as the previously-mentioned EWP, CN, OVA and LF) and polyphenols (such as CA, CT, and EGCG) not only enhanced most of the studied functional properties of protein (**Table 1**), but also expanded the application of animal proteins in food and cosmetic industry. For example, EWP has a high surface activity and is often used as a foaming agent in food industry (50). Quan et al. (14) also showed that EWP enhances emulsion stability, and is often used in food as an emulsifier. In addition, Sun et al. (40) found that the covalent complexes between EWP and polyphenols (CT or CA) can significantly improve the antioxidant activity and emulsifying performance of EWP, thus improving the oxidative and coalescence stability of emulsions. Moreover, LF is often used to interact with polyphenols, polysaccharides or other proteins to improve its emulsifying properties. Recent reports suggested that the complexes formed by LF and some reactive small molecules such as polyphenols can improve the emulsion antioxidation properties (51). Furthermore, Liu et al. (32) calculated the emulsifying activity index (EAI) and emulsion stability index (ESI) parameters of the unmodified LF and LF–polyphenol complexes, and the results showed that the ESI of LF–EGCG was improved and the emulsion stability was higher than that of LF (32). In addition, gelatin–anthocyanin complexes can change the functional properties of hydrophilic gelatin proteins and thus improves the stability of emulsions (49).

Plant Proteins and Polyphenols

The use of plant protein to replace animal protein is becoming the trend of more and more food companies (**Table 2**). Because of its good surface activity, pea protein can be used as a natural emulsifier for application in emulsions; however, it was shown to exhibit inferior oxidation inhibition effect compared to other proteins (48). Other studies reported that the interactions between pea protein and proanthocyanidins can improve the antioxidant ability of pea protein, thus improving the stability of oil-in-water emulsions (25). Rice bran protein (RBP), composed of albumin, globulin, gliadin, and glutenin, is a complete protein. However, most of rice bran is still used as animal feed, which is a serious waste of resources. RBP–CT complexes can affect the structural and functional properties of RBP, improve its emulsifying performance, and thus enhance the stability of relevant oil-in-water emulsions (36). The study showed that the addition of CT reduced the incidence of RBP α-helix and β-sheet. The surface hydrophobicity of RBP was enhanced and the interfacial tension between oil and water was decreased. In addition, the emulsion stabilized by RBP–CT had smaller particle size and better emulsifying properties (36).

Microbial Proteins and Polyphenols

Generally, microorganisms can use sugar, volatile fatty acids, and carbon dioxide and nitrogen sources to form amino acids. Under the appropriate energy supply, the amino acids are then converted to microbial proteins (**Table 2**). Microorganisms contain a multitude of enzymes that can break down food, so microbial proteins are often present in the form of enzymes.

TABLE 1 | Typical animal protein-polyphenol complexes.

Complexes	Combining with the way	Characterization methods	Functions	References
EWP/CA/CT	Covalent: free radical graft; alkaline methods	Circular dichroic (CD) spectroscopy; fluorescence analysis	Improving antioxidant activity and emulsifying performance	(40, 44)
LF-EGCG	Covalent: free radical graft	FTIR spectroscopy; DSC measurement; fluorescence spectroscopy	Improving solubility and emulsifying properties	(32)
Gelatin-Anthocyanin	Non-covalent interaction: hydrogen	Circular dichroism (CD); isothermal titration calorimetry (ITC)	Improving antioxidant activity	(49)

TABLE 2 | Typical plant and microbial protein-polyphenol complexes.

Complexes	Combining with the way	Characterization methods	Functions	References
OVA-CT/EGC/EGCG	Covalent: free radical graft	Circular dichroic(CD) spectroscopy; DSC measurement; FTIR spectroscopy	Improving antioxidant activity and interfacial accumulation	(16)
PP-PC	Non-covalent interaction: hydrogen; hydrophobic interactions	Isothermal titration calorimetry analysis; molecular docking	Antioxidants	(25)
RBP-CC	Non-covalent interaction: hydrogen; hydrophobic binding	FTIR spectroscopy	Higher viscosity and viscoelasticity; Increased hydrophobicity	(36)
Lysozyme-Proanthocyanidins	Non-covalent interaction: hydrogen	Gel permeation chromatography	Improve protein foam stability	(21)

Microbial proteins have a high affinity to polyphenols (such as proanthocyanidins) at a suitable pH. Lysozyme is a spherical food protein (52). Prigent et al. (21) showed that the affinity between lysozyme and proanthocyanidins was strong at higher pH, and the stabler form of lysozyme–proanthocyanidins complexes appeared at higher pH (pH 7.5). In addition, microbial proteins can be produced thousands of times more efficiently than in animals or in plants (53), hence the microbial protein–polyphenol materials may have wider development prospects in the food industry.

EFFECT OF PROTEIN–POLYPHENOL COMPLEXES ON STABILITY OF EMULSIONS

Zeta-Potential and Particle Size

The protein adsorbed on the surface of the oil droplets in an oil-in-water emulsion may provide charges on the surface of oil droplets. The ζ-potential is a measure of the surface charge density of a particle, which typically relates to the ζ-potential of the emulsion system onto whose droplets the proteins are adsorbed (54). Li et al. (36) measured the ζ-potential of RBP and RBP–CT complexes and found that it first increased and then decreased with increasing polyphenol concentration. When the polyphenol concentration was 0.15 (%, W/V) and protein concentration was 0.1 (%, W/V), the ζ-potential reached its maximum value. RBP–CT complexes emulsions exhibited significantly higher ($p < 0.05$) absolute ζ-potential, suggesting greater negative charge density at the interface. The increased absolute ζ-potential of emulsions led to a high energy obstacle between emulsion droplets, thereby providing good electrostatic stabilization. The increase in absolute ζ-potential is because catechins let the secondary structure of RBP change, and then protein structure becomes extended, decreasing the exposure of the positively charged groups, hence increasing the apparent negative charge of the protein (36). The pI values of EWP–CT and EWP–CA complexes were mildly lower than those of EWP, suggesting that CT and CA complexes changed the surface charge characteristics of EWP. It can be explained that CT or CA complexes possibly decreased the number of exposed positive groups on the surfaces of the protein, or increased the number of exposed negative groups (40). This is consistent with the findings of Li et al. (36).

The addition of polyphenols can induce protein aggregation and depolymerization, so the particle size of PPCs may change with the addition of polyphenols. Research showed that the average diameter of β-CG–EGCG co-assembled nanoparticles increased in the presence of EGCG. Moreover, scanning electron microscopy confirmed that the particle size gradually increased with the increase of EGCG concentration (55). Staszawski et al. (6) measured the distribution size of β-LG and tea polyphenol particles in emulsions prepared with similar materials. They concluded that β-LG formed nanocomplexes with polyphenols, with β-LG–polyphenols particles being larger than pure β-LG ones. The increase in particle size was attributed to the binding of polyphenols with proteins occurring on the hydrophobic side chain and near-plane side chain, which is mainly due to the aforementioned accumulation of polyphenol rings on the hydrophobic side chain (6). Finally, the complexes of polyphenols with proteins are evenly dispersed an oil-in-water emulsion, and have higher stability.

By measuring the droplet size of PPCs, one may obtain information on the stability of the oil-in-water emulsions containing protein–polyphenol. The particle size may be related to the pH value. Feng et al. (16) studied the particle size of oil droplets of OVA and OVA–polyphenol when the pH were 3.5 and 7. The particle size of OVA-stabilized oil droplets under the two pH values was double than that of oil droplet, which might be due to droplet aggregation and/or coalescence. However, the stable droplet size of OVA–polyphenol complexes were all smaller than that of OVA, and there was little difference between pH 3.5 and 7. This showed that the conjugation of OVA and polyphenol had beneficial stability effects against droplet aggregation and coalescence (16).

Rheology and Gel Texture

Rheological properties are among the most important attributes of food emulsions, and are closely related to their texture, sensory properties, and shelf life (16, 32). The gelling properties of the proteins contribute substantially to the stability of the emulsion rheology. The researchers thought that the improved emulsion stability may be due to the formation of gel-like microstructure, which has been significant in stabilizing emulsions prepared by SPI and whey protein (26, 56). Emulsions stabilized by OVA showed a higher viscosity with a more distinct pseudoplastic behavior as compared with those stabilized by OVA–CT complexes, as evidenced by their higher consistency coefficient (k) but lower rheological index (n). This showed that OVA-coated emulsions were more prone to flocculate, which manifested in their larger particle size (16).

Studies have shown that water or oil crystallization will cause phase separation during freeze-thaw processes, and the increase of emulsion viscosity can prevent this phenomenon (45). Protein gels can also enhance the stability of the emulsion by forming a three-dimensional network structure (14). Many plant polyphenols are able to interact with proteins, thus improve the gelling properties (57). Gels formed by covalent interactions are more rigid and heat stable than those formed by non-covalent interactions. The complexes formed by the binding of β-LG and tea polyphenols significantly enhanced the gelation ability of β-LG, because tea polyphenols enhanced the gelation speed of the protein (28). Tea polyphenols can also increase the whey protein gel hardness or viscosity, depending on the case (58). Yan et al. (59) reported that the conjugate of GA or rutin into gelatin from walleye pollock (*Theragra chalcogramma*) skin at a concentration of 20 mg/g dry gelatin significantly increased gel strength. In addition, the viscous modulus and elastic modulus of gelatin gel were improved by the crosslinking of carboxyl group skeletal and C–N–C group of gelatin molecules with rutin or GA.

Microstructure

Microstructure refers to the structure of substances, organisms, cells under the microscope, and also refers to structures in

the nano scale, the molecular scale, the atomic scale, and even the subatomic scale. Through the electron microscope, it can be found that protein sample which is not conjugated to polyphenols exhibited a morphology characteristic without fibrillar or sheet-like structures (50). For example, soybean protein (SP) has a variety of structures which can interact with tea polyphenols to form complexes, and the microstructure of soybean protein can be observed by scanning electron microscopy (60). This work showed that the study of SP microstructure can be used to study the function of complexes in emulsions. In addition, Cryo-SEM images of soy protein isolate-anthocyanin (SPI–ACN) composite nanoparticles and emulsion showed that the SPI–ACN composite nanoparticles were spherical and had diameters ranging from 200 to 500 nm. In addition, increasing the amount of ACN at low temperatures led to the formation of highly porous structures (61). The researchers suggested that this might be due to the covalent interactions between ACN and SPI, which then untied the protein-peptide chain, then the latter interacting with adjacent droplets, eventually forming emulsions in a bridging flocculation-type induced structure (62). The structure of the bridged emulsion was the typical structure of the protein-stabilized emulsion, which can accelerate the formation of the network structure of the emulsion and thus enhanced the stability of the emulsion. In addition, the emulsion stabilized by SPI–ACN showed that the droplets dispersed were good without obvious coalescence. With the increase of ACN, the particle size of droplets decreased significantly. Moreover, it was observed that SPI–ACN adhered to the surface of emulsion droplets densely.

Furthermore, Gu et al. (3) prepared β-CG–EGCG assembled particles in an ethanol-mediated process and used this assemble complexes to stabilize a high internal phase emulsion (HIPE). Using scanning electron microscopy, they found that the spherical composite nanoparticles gradually increased when the concentration of EGCG–β-CG particles increased. From the optical microscope observation, it could be inferred that most of the droplets in these HIPEs were closely packed, and in many cases, two adjacent droplets shared the same interface layer, again in a bridging flocculation-type of structure. High internal emulsion thus showed a more homogeneous and stable state (3).

Creaming and Flocculation

Food emulsions usually consist of aqueous (continuous) and oil (dispersed) phases (63). The presence of two phases in the emulsion causes flocculation and aggregation of the emulsion during processing, storage and transportation (64). Such temporal instability can be followed by permanent destabilization via coalescence and/or Ostwald ripening. As a result, the emulsions tend to revert to the original two phases state. The protein–polyphenol complexes are added to the emulsion as an emulsifier and adsorbed on the surface of the emulsion droplets to form a dense film. It can reduce the interfacial tension of the protein on the surface of the droplet, which reduces the coalescence rate, as well as reduces the extent of flocculation of the emulsion, thus enhancing its stability. Thus, the emulsion can be prevented from instability caused by such causes as coalescence or Ostwald ripening (15, 63). Therefore, under such interactions, the emulsification of protein and the stability of the emulsion stabilized by protein–polyphenol complexes would be improved (42, 43).

One of the key factors to produce emulsion is the density difference between lipid phase and water phase. The creaming index (CI) is known as a useful indicator in terms of quantifying the extent of separation of lipids from the water phase in an emulsion (65). It is typically a function of the density difference, particle size, continuous phase viscosity and extent of flocculation, among others. Ju et al. (65) proposed that the emulsion formed by SPI–ACN complexes nanoparticles had higher stability at room temperature, which might be due to its low CI value. Therefore, it can be considered that the enhancement of emulsion stability might be attributed to the change of protein microstructure after interacting with polyphenol, which was of significance in stabilizing SPI emulsions or whey protein and chitin emulsions (26, 56). Zhu et al. (39) studied the interaction between gliadin and TA nanoparticles (GTNP) in order to stabilize the emulsion, and measured the relevant CI. The results showed that the CI of majority of the studied emulsions increased significantly within short term and subsequently stabilized. For example, the CI of GTNP complexes appeared to plateau at 10 h, whereas the CI of the other emulsions appeared to plateau within 5 h, which indicated the slowest creaming rate of the GTNP complexes-stabilized emulsions. This is due to the observation that the particle size of gliadin–TA complexes decreased, due to the best emulsification properties of the complexes (39).

According to related studies, β-LG and CT covalent complexes formed by the free radical method can stabilize the oil-in-water emulsion more effectively than β-LG itself (18). Chen et al. (66) showed that the porcine plasma protein-CA complexes could be rapidly adsorbed to the oil surface to form an interfacial film, which indicated an improved emulsifying property of the complexes. The improvement of the emulsifying properties of the protein–polyphenol complexes can also reduce the flocculation and eventual instability of emulsions (14). Therefore, the stability of the emulsions can be conditionally enhanced by the interaction of proteins and polyphenols, thus alleviating the flocculation and coalescence of the produced emulsions.

Antioxidant Ability

Oil-in-water emulsions are easy to be oxidized during storage and processing. This is mainly because the interaction between lipid oxidation products and amino groups on proteins can accelerate protein oxidation (67). Some researchers have reported that transition metals are the main oxidants of oil-in-water emulsions (68). In emulsions, transition metals mainly promote oxidation by decomposing lipid hydroperoxides on the droplet surface into free radicals. Some proteins are good emulsifiers, but they do not often display strong antioxidant capacity. However, after combination with polyphenols, their antioxidant capacity can be greatly enhanced (14, 50).

More and more researchers have been carrying out in-depth studies on the antioxidant properties of protein–polyphenol complexes. The ability of protein–polyphenol complexes to control droplet oxidation have been demonstrated in a number

of works. The concentration of hydrogen peroxide in plain β-LG stabilized fish oil emulsion from 20 to 214meq/kg oil during the 30 days storage process (18). On the other hand, the hydrogen peroxide content of the emulsions formed by β-LG-polyphenol complexes never exceeded 40 meq/kg oil during the 30 days storage process, which suggested that β-LG and polyphenols complexes are highly efficient antioxidants. That was because β-LG and polyphenols complexes formed a surface film on the droplet interface, the adsorbed entities blocking the free radicals before entering the oil droplet surface, thus avoiding oxidation. The interface region formed by the complexes was the contact region between lipid and water, which was also the key region for the development of oxidation (69). PPCs were captured and located at this interface as antioxidants to prevent lipid oxidation.

In addition, continuous phase proteins in oil-in-water emulsion can also inhibit lipid oxidation by scavenging free radicals. Although many amino acids can participate in free radical scavenging, cysteine and tyrosine are reported to be the two most important free radical scavengers. However, proline and cysteine are the main binding sites of protein to polyphenols. Free radicals are another main factor leading to oxidation of droplets of oil-in-water emulsion. Waraho et al. (70) concluded that protein–polyphenol complexes can make an important contribution to free radical scavenging. They showed that OVA–CT complexes can scavenge free radicals and/or inactivate promoters such as transition metals at the lipid–water interface (70), thereby preventing lipid hydroperoxide (LOOH) from decomposing into alkoxyl ($LO^{'}$) and peroxyl ($LOO^{''}$) free radicals. In addition, the activity of these highly active free radicals, which extracted hydrogen from unsaturated fatty acid (LH) to form new free radicals was inhibited (5). In addition, compared with the OVA stabilized fish oil emulsion, the interfacial protein content (F_{ip}) of the OVA–CT complexes-stabilized fish oil emulsion increased significantly, while the continuous phase protein content (F_{cp}) decreased significantly. This might be due to the decrease in the interfacial tension of the protein after the CT grafting reaction, which can be due to the partial negation of the protein hydrophobicity: the covalent interactions involved the non-polar parts of the protein, leading to a stronger binding to the lipid-water interface once adsorbed (45). Therefore, the lipid droplets in the emulsion stabilized by the conjugate could have a denser and defect-free interface film, thus effectively preventing the penetration and diffusion of the oxidation initiators and thus arresting them from reacting with ω-3 polyunsaturated fatty acids.

Thermal Stability and Salt Stability

In some situations, the thermally-induced denaturation of proteins is detrimental to the stability of emulsions (71). After heat treatment, flocculation and coalescence often occur in oil-in-water emulsion droplets which were stabilized by proteins, and thereby affected the function of bioactive substances in the emulsion. Droplet flocculation could be attributed to the unfolding of the globular proteins adsorbed onto the lipid droplet surfaces when heated above their thermal denaturation temperature (72). This will result in increased exposure of surface-active groups (such as hydrophobic and sulfhydryl groups), which will increase the attractive interaction between droplets. The PPCs can effectively protect the emulsions from heat treatment because of the interfacial film formed on the surface of the emulsion droplets. The stability of β-carotene-containing emulsion stabilized by LF and LF–polyphenol complexes was determined at 100°C for 20 min (32). The study showed that the emulsion stabilized by protein showed poor thermal stability, which could be attributed to the unfolding of the LF macromolecules. The thermal denaturation of the adsorbed globular protein led to the increase of the hydrophobicity of the lipid droplet surface, which generated a strong hydrophobic attraction between the lipid droplets. Schmelz et al. (72) showed that LF-coated emulsions formed gels when temperatures exceeded 70°C, which was because the enhancement of hydrophobic attractions induced extensive flocculation of denatured protein-coated droplets. However, the emulsions coated by LF–CA and LF–EGCG complexes were highly stable to heat, and their particle size distribution did not change much with heating. In addition, DSC results showed that protein–polyphenol complexes had higher denaturation temperatures than protein alone. Thus, the emulsion stabilized by protein–polyphenol complexes had better thermal stability. It is worth noting that, precisely because of the higher thermal stability of the covalent complexes, the covalently-modified protein was relatively easy to expand, requiring very little energy toward that aim (45). It also presented a new challenge for the study of thermal stability of modified proteins in emulsions.

Under low salt concentrations, the average particle sizes of the emulsions were relatively small, but under higher salt concentrations, the average particle sizes increase, which is related to the electrostatic shielding effect. That is, when salt is added into the aqueous phase, counterions are gathered around the charged surface groups, and the size and range of electrostatic repulsion between oil droplets are reduced (63). In addition, the effects of EWP, EWP + CT physical mixtures (not essentially interacting) and EWP–CT covalent complexes on emulsion were investigated (as mentioned above). For the emulsion stabilized by EWP alone or EWP+CT mixtures, the average particle size of the emulsion increased significantly when the concentration of NaCl increased from 50 mm to 100 mM, while for the emulsion with stable EWP–CT conjugates, the average particle size of the emulsion increased significantly only when the concentration of NaCl increased from 100 to 200 mM NaCl. These results showed that the emulsions stabilized by EWP–CT complexes had better salt stability than the other two systems, which might be due to the stronger spatial repulsions caused by the presence of polyphenols. Therefore, the oil-in-water emulsions stabilized by EWP–CT had better thermal stability and salt stability.

Digestive Characteristics

Studies of protein–polyphenol compound interactions aim to better analyze and understand phenomena that take place during digestion (43). The oil droplets, coated by protein–polyphenol complexes, enter the gastrointestinal tract, where they are exposed to continuous alterations in shear fields, pH, enzymic, salt and surfactant environments. Digestion simulations have

been extensively used in order to probe such processes (**Figure 4**). These studies aim to comprehend the basis of bioavailability and fat absorption process from emulsions, and to lay a foundation for the research of functional foods (73).

Jiang et al. (62) found that all protein components in casein (CS) or WPI were fragmented into small peptides during a simulated gastrointestinal pepsin–pancreatin digestion. In both CS and WPI samples, the treatment with increasing concentrations of catechin acid (CA) resulted in lighter peptide bands, suggesting improved digestibility. In addition, for all CS samples, only a few small peptides remained present in the electrophoretic graph after 1 h of simulated gastric hydrolysis and almost no peptides were found after subsequent pancreatic hydrolysis. With the increase of CA content, more and more proteins were digested into smaller peptides which were lysed after 1 h of digestion (62). It can be illustrated that the addition of CA promoted digestibility of both WPI and CS. When the emulsion drops were digested in the stomach, the pH value, ionic strength and enzyme activity of the environment of the gastrointestinal would change, and the particle sizes of the emulsions showed an increasing trend in the gastric digestion stage (7). In the stomach stage, due to the relatively low gastric pH value, the absolute value of the ζ-potential of the emulsion decreased, thus reducing the electrostatic repulsion between the lipid droplets, promoting flocculation. Microscopy images showed that the droplets formed by mixtures of LF and LF–EGCG was more physically stable under this environment, and the droplet formed by the covalent complexes was less stable and the droplets were of uniform size distributions. The results showed that the covalent bonds of EGCG and LF could improve the stability of the systems during the digestive process. The absolute value of the ζ-potential of the three emulsions was increased, so the electrostatic repulsion between emulsion droplets also increased. Microscopic image suggested that LF–EGCG covalent complexes can render oil-in-water emulsions more stable during intestinal digestion.

In addition, the extent of emulsion destruction depends on the amount of free fatty acids released during intestinal digestion (65). The amount of free fatty acids released from protein–polyphenol emulsions was generally used to reflect the decomposition of oil-in-water emulsion during digestion. Studies have shown that LF–EGCG covalent complexes can delay the release of fatty acids to some extent when *in vitro* measuring the fat digestibility and digestibility of different samples in small intestine by automatic pH titration (7). In the same way, Zhou et al. (74) also reported that the free fatty acid released from emulsions stabilized by gliadin were restrained when proanthocyanins were added, which is because proanthocyanin also found their way at the interface along the proteins. Moreover, studies showed that the release rate of free fatty acids in fish oil emulsions stabilized by gliadin-grape seed proanthocyanidins (GSP) complexes was lower than that of normal emulsions. It can be concluded that the digestion time of normal emulsion was 20 min, and that of complexes stabilized emulsion was longer, with free fatty acid release rates of 92.5 and 63.3%, respectively (49). The results showed that the digestibility of emulsion stabilized with gliadin–GSP was lower than that of free gliadin.

Nutrient Delivery Capacity

Oil-in-water emulsion delivery systems are potentially competent of delivering functional oils or lipophilic active substances, which can improve their solubilities and bio-availabilities, and availably control release (**Figure 3**) (75). PPCs can be adhered to oil-in-water (O/W) interfaces, supplying emulsions with both protein surface activity and polyphenol antioxidant activity. Recently, protein-polyphenol complexes have shown that they possessed the binding affinity toward both hydrophobic and hydrophilic compounds because of the amphiphilic properties of their protein parts (76). Previous studies have shown that PPCs can be utilized as carriers for liposomes (77), micelles (78), and cyclodextrin/lipid complexes (79). These have been aroused interest in the application of protein–polyphenol complexes-based emulsifiers to create emulsion-based delivery systems for encapsulation of bioactive compounds such as carotenoids, curcumin, and lutein (15). In addition, this emulsion can be used in yogurt, beverage, and iron supplements and other products, and has good prospects for development.

It is well-known that β-carotene has been widely studied in industry and academia because of its unique antioxidant and vitamin A-promoting bioactivity. People have tried to design delivery systems of β-carotene as to improve its dispersion and chemical stability, and finally enhance its functionality (**Figure 4**). At the same time, oil-in-water emulsions have been proved to be effective delivery systems for fat-soluble bioactive components. β-Carotene stabilization was been reported in oil-in-water nano-emulsions by conjugate-based delivery systems such as α-lactalbumin–CT (18), β-LG–CT (19), and LF–CT (32). Gu et al. (42) studied and determined the ability of EWP–CT complexes synthesized by a free radical method to form and stabilize β-carotene emulsion transport systems. The results showed that the particle sizes of β-carotene emulsion stabilized by EWP–CT increased more than those of EWP. It can be assumed that the EWP–CT complexes produced smaller droplets during the homogenization process, mainly because the complexes reduced the interfacial tension of the protein. Such processes are also known to favor droplet re-coalescence and destruction during homogenization (80). Therefore, the fact that the use of EWP–CT complexes led to larger droplets was probably due to other factors. First of all, the adsorption rate of EWP–CT complexes products to the droplet surface during homogenization could be slow because of their high molecular weight or their surface chemistry change, which might lead to more re-coalescence in the homogenizer. Secondly, the properties of the interface layer formed by EWP–CT complexes, such as their thickness, hydrophobicity or charge, might change the aggregation stability of droplets. For example, the formation of complexes might change the colloidal interactions between droplets. The complexes of polyphenols with proteins could also increase the hydrophobic attraction between droplets. On the contrary, the covalent binding of polyphenols with proteins should increase the thickness of the interface coating, thus increasing the spatial repulsion between droplets. The

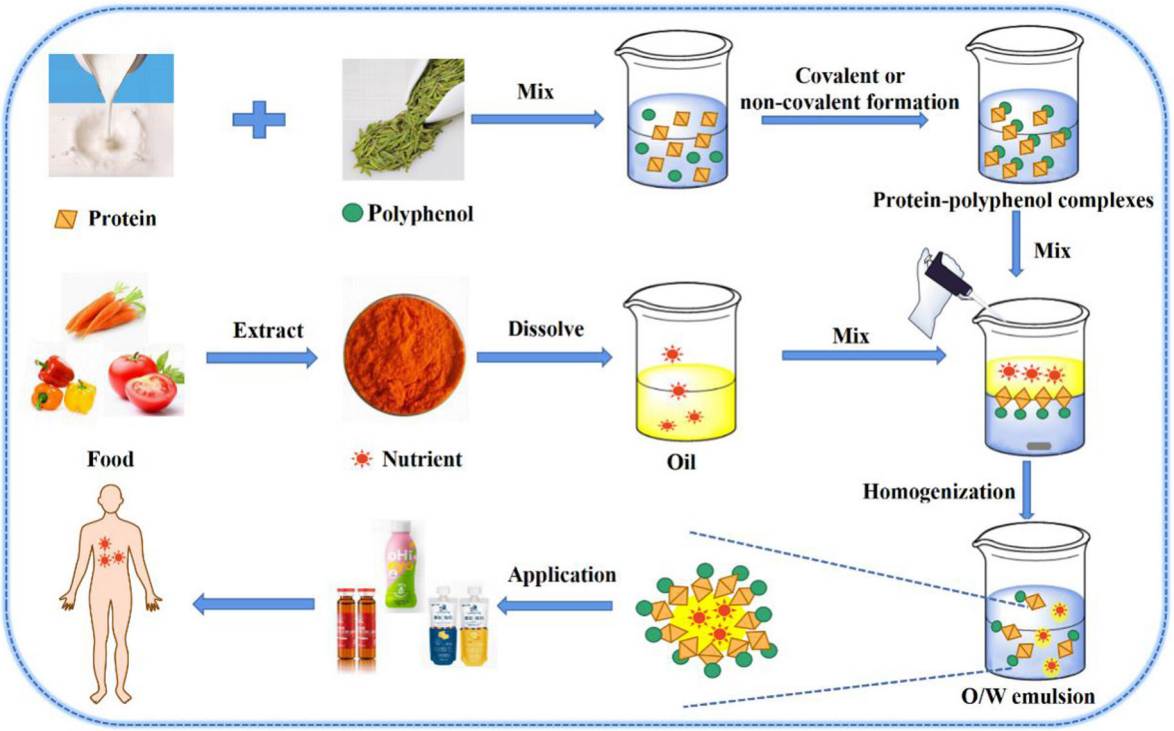

FIGURE 3 | O/W emulsion nutrient delivery system: Protein-polyphenol complexes load nutrients in O/W emulsion.

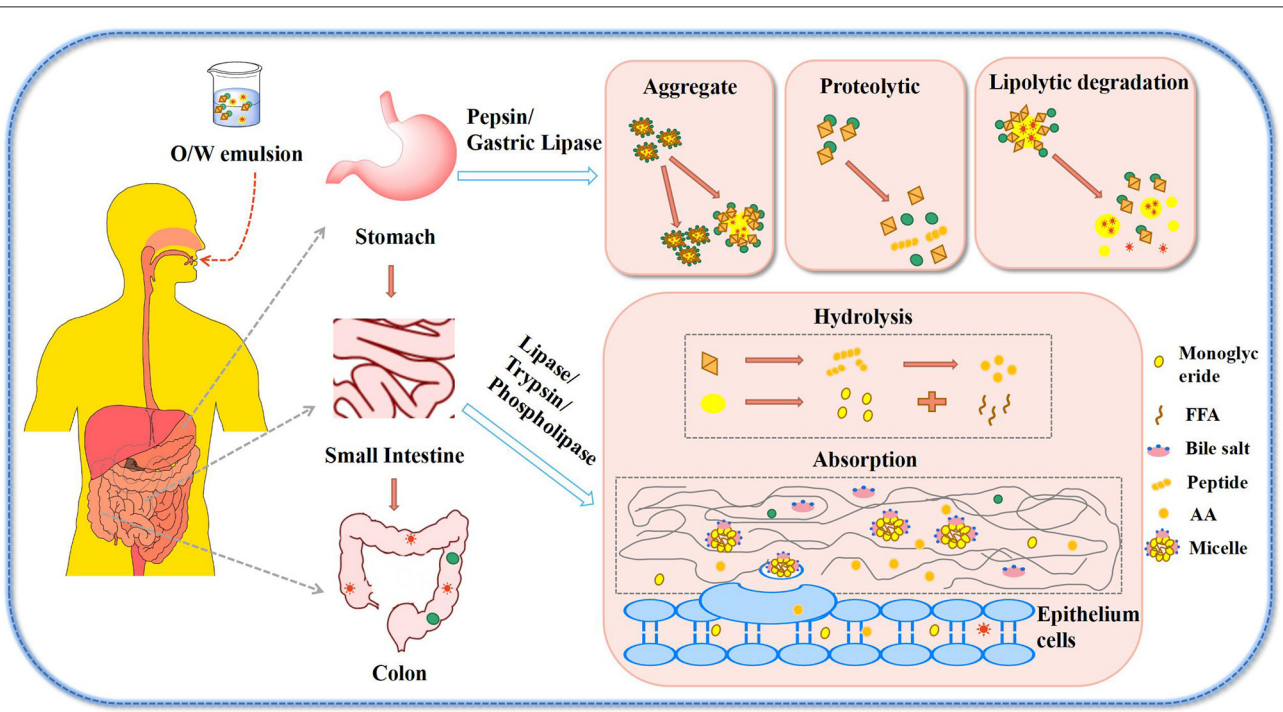

FIGURE 4 | Digestive behavior of protein-polyphenol stabilized O/W emulsion.

differences in particle size and potential of different proteins and polyphenols have been described above. The average particle size and stability of each emulsion was related to the type of protein and polyphenol.

Moreover, Yi et al. (19) also improved the retention of β-carotene in emulsions by free radical methods. The Z-average diameters of β-carotene emulsion coated with α- LA (158.8 nm) and α-LA–CT (162.7 nm) were different. The PDI values of α-LA and α-LA-CT stabilized nano-emulsions were 0.109 and 0.118, respectively. Compared with the α-LA ζ-potential of −57.5 ($P < 0.05$), the ζ-potential of α-LA–CT complexes was as low as −61.9 ($P < 0.05$), which was consistent with the results of Gu et al. (42). This was due to the negative charge of catechins at neutral pH. Because the density of β-carotene-loaded oil droplets was quite different from that of dispersions, the nanoparticles that tended to rise and aggregate on the surface may be excited by gravity, which might be due to the great difference in density between β-carotene-loaded oil droplets and dispersions, so it could be caused by gravity. Nano-emulsions are essentially thermodynamically stable colloidal dispersions. The diameter stability of nano-emulsion is very important for its application in food, because its texture, appearance and taste depend on the stability of structure. In addition, temperature might be an important factor determining the physical stability of β-carotene nano-emulsions (18). It has also been reported that the diameter increment of nanoparticles or emulsions increases with increasing temperature, which was due to the fact that the temperature effect leads to faster movement at higher temperatures, thus increasing gravity flocculation (19, 81).

It was also found that α-LA–CT binding strongly inhibited the degradation of β-carotene in the emulsion at different temperatures. For example, the nano-emulsion prepared with α-LA–CT conjugates had only 4.4% β-carotene degradation in the first 2 days at 50°C, and 71.3% β-carotene degraded after 16 days, while at the end of the measurement (30 days at 50°C), there was still 56.7% β-residual carotene in the sample. α-LA–CT complexes had excellent antioxidant activity, and its mechanism was proposed: The complexes had a good ability to scavenge hydroxyl radicals and protect β-carotene from degradation. Secondly, the natural transition metal (Fe^{3+}) in aqueous phase might be the main factor leading to the oxidation and degradation of β-carotene (81). The protein–polyphenol complexes can be used as powerful metal ion binders and reducers, as shown by the relevant results, which could inhibit Fe^{3+} from its role as an oxidizer, and protect β-carotene from degradation. In short, compared with the nutrient emulsion based on protein, the emulsion loaded with protein-polyphenol complexes had a strong nutrient transport capacity, less loss and strong stability.

CONCLUSIONS

In this paper, the interaction mechanism between protein and polyphenols was reviewed, initially being divided into covalent interaction and non-covalent interactions. Hydrogen bond and hydrophobic interactions are the main driving forces for the formation of such protein-polyphenol complexes (PPCs). The interactions between proteins and polyphenols affect the structural and functional properties of proteins. The PPCs can reduce the number of proteins α-helix and change the interfacial properties of protein. The interface region formed by the PPCs on the surface of oil droplets is essentially the contact region between lipid and water. The change of the interfacial properties of the emulsion affects the emulsification, thermal stability and oxidation resistance of the emulsion, thus affecting the function of the complexes in the emulsion. Studies have shown that when protein and polyphenol are complexed, a layer of film forms on the surface of oil droplets, thus preventing the entry of free radicals and some metal ions, and improving the stability of emulsion oxidation.

Moreover, the size of oil droplets coated with PPCs is small, which suggests prevention of coalescence and flocculation of the oil droplets, thus improving the emulsion stability. In addition, the PPCs could make the particle size of the emulsion smaller, which improves the bioavailability of nutrient. Furthermore, PPCs play an important role in the process of lipid to nutrient delivery. As a broad rule, the lipid delivery capacity of oil-in-water emulsions is enhanced in the presence of PPCs, while the retention rate of nutrients is higher. Through this study, it can be concluded that protein–polyphenol complexes play an important role in improving the stability, digestion characteristics and the ability of nutrient delivery of oil-in-water emulsions. This paper can provide guidelines for enhancing the application potential of PPCs, especially in improving stability and nutrients delivery of oil-in-water emulsion system in the food industry.

AUTHOR CONTRIBUTIONS

ML: conceptualization and writing original draft. CR, JL, QD, and WL: writing—review & editing and supervision. YL and YD: supervision. All authors contributed to the article and approved the submitted version.

FUNDING

This work was financially supported by the National Natural Science Foundation of China (Grant No. 31972104) and National Key R&D Program of China (2019YFD0901603).

REFERENCES

1. Weitz D, Weintraub H, Fisher E, Schwartzbard AZ. Fish oil for the treatment of cardiovascular disease. *Cardiol Rev.* (2010) 18:258–63. doi: 10.1097/CRD.0b013e3181ea0de0
2. Mariutti LR, Bragagnolo N. Influence of salt on lipid oxidation in meat and seafood products: a review. *Food Res Int.* (2017) 94:90–100. doi: 10.1016/j.foodres.2017.02.003
3. Gu L, Peng N, Chang C, McClements DJ, Su Y, Yang Y. Fabrication of surface-active antioxidant food biopolymers: conjugation of

catechin polymers to egg white proteins. *Food Biophys.* (2017) 12:198–210. doi: 10.1007/s11483-017-9476-5
4. Nielsen NS, Horn AF, Jacobsen C. Effect of emulsifier type, pH and iron on oxidative stability of 5% fish oil-in-water emulsions. *Euro J Lipid Sci Technol.* (2013) 115:874–89. doi: 10.1002/ejlt.201200303
5. Chityala PK, Khouryieh H, Williams K, Conte E. Effect of xanthan/enzyme-modified guar gum mixtures on the stability of whey protein isolate stabilized fish oil-in-water emulsions. *Food Chem.* (2016) 212:332–40. doi: 10.1016/j.foodchem.2016.05.187
6. Staszewski MV, Victor MPRH, Pilosof AMR. Green tea polyphenols-b-lactoglobulin nanocomplexes: interfacial behavior, emulsification and oxidation stability of fish oil. *Food Hydrocoll.* (2014) 35:505–11. doi: 10.1016/j.foodhyd.2013.07.008
7. Liu J, Liu W, Salt LJ, Ridout MJ, Ding Y, Wilde PJ. Fish oil emulsions stabilized with caseinate glycated by dextran: physicochemical stability and gastrointestinal fate. *J Agric Food Chem.* (2019) 67:452–62. doi: 10.1021/acs.jafc.8b04190
8. Khan H, Sureda A, Belwal T, Cetinkaya S, Suntar I, Tejada S, et al. Polyphenols in the treatment of autoimmune diseases. *Autoimmun Rev.* (2019) 18:647–57. doi: 10.1016/j.autrev.2019.05.001
9. Chen Y, Jiang S, Chen Q, Liu Q, Kong B. Antioxidant activities and emulsifying properties of porcine plasma protein hydrolysates modified by oxidized tannic acid and oxidized chlorogenic acid. *Proc Biochem.* (2019) 79:105–13. doi: 10.1016/j.procbio.2018.12.026
10. He W, Xu H, Lu Y, Zhang T, Li S, Lin X, et al. Function, digestibility and allergenicity assessment of ovalbumin–EGCG conjugates. *J Funct Foods.* (2019) 61:103490. doi: 10.1016/j.jff.2019.103490
11. Hasni I, Bourassa P, Hamdani S, Samson G, Carpentier R, Tajmir-Riahi HA. Interaction of milk α- and β-caseins with tea polyphenols. *Food Chem.* (2011) 126:630–9. doi: 10.1016/j.foodchem.2010.11.087
12. Ozdal T, Capanoglu E, Altay F. A review on protein-phenolic interactions and associated changes. *Food Res Int.* (2013) 51:954–70. doi: 10.1016/j.foodres.2013.02.009
13. Harshadrai MR, Dörte C, Sascha R, Jürgen K. Interactions of different phenolic acids and flavonoids with soy protein. *Int J Biol Macromol.* (2002) 30:137–50. doi: 10.1016/S0141-8130(02)00016-8
14. Quan TH, Benjakul S, Sae-leaw T, Balange AK, Maqsood S. Protein-polyphenol conjugates: antioxidant property, functionalities and their applications. *Trends Food Sci Technol.* (2019) 91:507–17. doi: 10.1016/j.tifs.2019.07.049
15. Liu F, Ma C, Gao Y, McClements DJ. Food-Grade covalent complexes and their application as nutraceutical delivery systems: a review. *Compr Rev Food Sci Food Saf.* (2017) 16:76–95. doi: 10.1111/1541-4337.12229
16. Feng J, Cai H, Wang H, Li C, Liu S. Improved oxidative stability of fish oil emulsion by grafted ovalbumin-catechin conjugates. *Food Chem.* (2018) 241:60–9. doi: 10.1016/j.foodchem.2017.08.055
17. Umile GS, Francesca L, Francesco P, Giuseppe C, Manueia C, Ortensia LP, et al. Synthesis of antioxidant polymers by grafting of gallic acid and catechin on gelatin. *Biomacromolecules.* (2009) 10:1923–30. doi: 10.1021/bm900325t
18. Yi J, Zhang Y, Liang R, Zhong F, Ma J. Beta-carotene chemical stability in nanoemulsions was improved by stabilized with beta-lactoglobulin-catechin conjugates through free radical method. *J Agric Food Chem.* (2015) 63:297–303. doi: 10.1021/jf5056024
19. Yi J, Fan Y, Zhang Y, Zhao L. Characterization of catechin-alpha-lactalbumin conjugates and the improvement in beta-carotene retention in an oil-in-water nanoemulsion. *Food Chem.* (2016) 205:73–80. doi: 10.1016/j.foodchem.2016.03.005
20. Le Bourvellec C, Renard CM. Interactions between polyphenols and macromolecules: quantification methods and mechanisms. *Crit Rev Food Sci Nutr.* (2012) 52:213–48. doi: 10.1080/10408398.2010.499808
21. Prigent SV, Voragen AG, van Koningsveld GA, Baron A, Renard CM, Gruppen H. Interactions between globular proteins and procyanidins of different degrees of polymerization. *J Dairy Sci.* (2009) 92:5843–53. doi: 10.3168/jds.2009-2261
22. Buitimea-Cantua NE, Gutierrez-Uribe JA, Serna-Saldivar SO. Phenolic-Protein interactions: effects on food properties and health benefits. *J Med Food.* (2018) 21:188–98. doi: 10.1089/jmf.2017.0057
23. Yildirim-Elikoglu S, Erdem YK. Interactions between milk proteins and polyphenols: binding mechanisms, related changes, and the future trends in the dairy industry. *Food Rev Int.* (2017) 34:665–97. doi: 10.1080/87559129.2017.1377225
24. Chanphai P, Tajmir-Riahi HA. Tea polyphenols bind serum albumins: a potential application for polyphenol delivery. *Food Hydrocoll.* (2019) 89:461–7. doi: 10.1016/j.foodhyd.2018.11.008
25. Dai T, Li T, Li R, Zhou H, Liu C, Chen J, et al. Utilization of plant-based protein-polyphenol complexes to form and stabilize emulsions: pea proteins and grape seed proanthocyanidins. *Food Chem.* (2020) 329:127219. doi: 10.1016/j.foodchem.2020.127219
26. Tang CH, Liu F. Cold, gel-like soy protein emulsions by microfluidization: emulsion characteristics, rheological and microstructural properties, gelling mechanism. *Food Hydrocoll.* (2013) 30:61–72. doi: 10.1016/j.foodhyd.2012.05.008
27. Yuksel Z, Avci E, Erdem YK. Characterization of binding interactions between green tea flavanoids and milk proteins. *Food Chem.* (2010) 121:450–6. doi: 10.1016/j.foodchem.2009.12.064
28. Staszewski MV, Jara FL, Ruiz ALTG, Jagus RJ, Carvalho JE, Pilosof AMR. Nanocomplex formation between β-lactoglobulin or caseinomacropeptide and green tea polyphenols: impact on protein gelation and polyphenols antiproliferative activity. *J Funct Foods.* (2012) 4:800–9. doi: 10.1016/j.jff.2012.05.008
29. Kanakis CD, Hasni I, Bourassa P, Tarantilis PA, Polissiou MG, Tajmir-Riahi HA. Milk beta-lactoglobulin complexes with tea polyphenols. *Food Chem.* (2011) 127:1046–55. doi: 10.1016/j.foodchem.2011.01.079
30. Han Y, Lin Z, Zhou J, Yun G, Guo R, Richardson JJ, et al. Polyphenol-Mediated assembly of proteins for engineering functional materials. *Angew Chem Int Ed Engl.* (2020) 59:15618–625. doi: 10.1002/anie.202002089
31. Ge G, Guo W, Zheng J, Zhao M, Sun W. Effect of interaction between tea polyphenols with soymilk protein on inactivation of soybean trypsin inhibitor. *Food Hydrocoll.* (2021) 111:106177. doi: 10.1016/j.foodhyd.2020.106177
32. Liu FG, Sun CX, Yang W. Structural characterization and functional evaluation of lactoferrin-polyphenol conjugates formed by free-radical graft copolymerization. *R Soc Chem.* (2015) 520:15641–51. doi: 10.1039/C4RA10802G
33. Klaus J, Petzke SS, Sascha R, Harshadrai Rawel M, Jürgen K. Chlorogenic acid moderately decreases the quality of whey protein in rats. *J Agric Food Chem.* (2005) 53:3714–20. doi: 10.1021/jf048186z
34. Pham LB, Wang B, Zisu B, Adhikari B. Complexation between flaxseed protein isolate and phenolic compounds: effects on interfacial, emulsifying and antioxidant properties of emulsions. *Food Hydrocoll.* (2019) 94:20–9. doi: 10.1016/j.foodhyd.2019.03.007
35. Liu F, Wang D, Sun C, McClements DJ, Gao Y. Utilization of interfacial engineering to improve physicochemical stability of beta-carotene emulsions: multilayer coatings formed using protein and protein-polyphenol conjugates. *Food Chem.* (2016) 205:129–39. doi: 10.1016/j.foodchem.2016.02.155
36. Li D, Zhao Y, Wang X, Tang H, Wu N, Wu F, et al. Effects of (+)-catechin on a rice bran protein oil-in-water emulsion: Droplet size, zeta-potential, emulsifying properties, rheological behavior. *Food Hydrocoll.* (2020) 98:105306. doi: 10.1016/j.foodhyd.2019.105306
37. Geng F, Wang J, Liu D, Jin Y, Ma M. Identification of N-Glycosites in chicken egg white proteins using an omics strategy. *J Agric Food Chem.* (2017) 65:5357–64. doi: 10.1021/acs.jafc.7b01706
38. Chen Y, Li Z, Yi X, Kuang H, Ding B, Sun W, et al. Influence of carboxymethylcellulose on the interaction between ovalbumin and tannic acid via noncovalent bonds and its effects on emulsifying properties. *Lwt.* (2020) 118:108778. doi: 10.1016/j.lwt.2019.108778
39. Zhu XW, Chen YT, Hu YX, Han Y, Xu JT, Zhao YL, et al. Tuning the molecular interactions between gliadin and tannic acid to prepare Pickering stabilizers with improved emulsifying properties. *Food Hydrocoll.* (2021) 111:106179. doi: 10.1016/j.foodhyd.2020.106179
40. Sun J, Jing H, Mu Y, McClements DJ, Dong S, Xu B. Fabrication of antioxidant emulsifiers from natural ingredients: conjugation of egg white proteins with catechin and chlorogenic acid. *Food Hydrocoll.* (2020) 108:106019. doi: 10.1016/j.foodhyd.2020.106019
41. You J, Luo Y, Wu J. Conjugation of ovotransferrin with catechin shows improved antioxidant activity. *J Agric Food Chem.* (2014) 62:2581–7. doi: 10.1021/jf405635q
42. Gu L, Su Y, Zhang M, Chang C, Li J, McClements DJ, et al. Protection of beta-carotene from chemical degradation in emulsion-based delivery systems using

antioxidant interfacial complexes: catechin-egg white protein conjugates. *Food Res Int.* (2017) 96:84–93. doi: 10.1016/j.foodres.2017.03.015
43. Czubinski J, Dwiecki K. A review of methods used for investigation of protein-phenolic compound interactions. *Int J Food Sci Technol.* (2017) 52:573–85. doi: 10.1111/ijfs.13339
44. Jing H, Sun J, Mu Y, Obadi M, McClements DJ, Xu B. Sonochemical effects on the structure and antioxidant activity of egg white protein-tea polyphenol conjugates. *Food Funct.* (2020) 11:7084–94. doi: 10.1039/D0FO01636E
45. Wei Z, Yang W, Fan R, Yuan F, Gao Y. Evaluation of structural and functional properties of protein–EGCG complexes and their ability of stabilizing a model β-carotene emulsion. *Food Hydrocoll.* (2015) 45:337–50. doi: 10.1016/j.foodhyd.2014.12.008
46. Sui X, Sun H, Qi B, Zhang M, Li Y, Jiang L. Functional and conformational changes to soy proteins accompanying anthocyanins: focus on covalent and non-covalent interactions. *Food Chem.* (2018) 245:871–8. doi: 10.1016/j.foodchem.2017.11.090
47. Zhan F, Li J, Wang Y, Shi M, Li B, Sheng F. Bulk, foam, and interfacial properties of tannic acid/sodium caseinate nanocomplexes. *J Agric Food Chem.* (2018) 66:6832–9. doi: 10.1021/acs.jafc.8b00503
48. Mariotti F. Animal and plant protein sources and cardiometabolic health. *Adv Nutr.* (2019) 10:S351–66. doi: 10.1093/advances/nmy110
49. Su YR, Tsai YC, Hsu CH, Chao AC, Lin CW, Tsai ML, et al. Effect of grape seed proanthocyanidin-gelatin colloidal complexes on stability and *in vitro* digestion of fish oil emulsions. *J Agric Food Chem.* (2015) 63:10200–8. doi: 10.1021/acs.jafc.5b04814
50. Duan X, Li M, Shao J, Chen H, Xu X, Jin Z, et al. Effect of oxidative modification on structural and foaming properties of egg white protein. *Food Hydrocoll.* (2018) 75:223–8. doi: 10.1016/j.foodhyd.2017.08.008
51. Liu F, Zhang S, Li J, McClements DJ, Liu X. Recent development of lactoferrin-based vehicles for the delivery of bioactive compounds: complexes, emulsions, and nanoparticles. *Trends Food Sci Technol.* (2018) 79:67–77. doi: 10.1016/j.tifs.2018.06.013
52. Prigent SVE, Voragen AGJ, Visser AJWG, van Koningsveld GA, Gruppen H. Covalent interactions between proteins and oxidation products of caffeoylquinic acid (chlorogenic acid). *J Sci Food Agric.* (2007) 87:2502–10. doi: 10.1002/jsfa.3011
53. Bajpai P. Nutritional benefits of single-cell proteins. *Springer Briefs Mol Sci.* (2017) 8:59–63. doi: 10.1007/978-981-10-5873-8_8
54. Shanmugam A, Ashokkumar M. Ultrasonic preparation of stable flax seed oil emulsions in dairy systems-Physicochemical characterization. *Food Hydrocoll.* (2014) 39:151–62. doi: 10.1016/j.foodhyd.2014.01.006
55. Peng LP, Tang CH. Outstanding antioxidant pickering high internal phase emulsions by co-assembled polyphenol-soy beta-conglycinin nanoparticles. *Food Res Int.* (2020) 136:109509. doi: 10.1016/j.foodres.2020.109509
56. Liu F, Tang CH. Soy protein nanoparticle aggregates as pickering stabilizers for oil-in-water emulsions. *J Agric Food Chem.* (2013) 61:8888–98. doi: 10.1021/jf401859y
57. Zhang XQ, My DD, Philip C, Adrian S, Greg GQ, Leif L. Chemical cross-linking gelatin with natural phenolic compounds as studied by high-resolution NMR spectroscopy. *Biomacromolecules.* (2010) 11:1125–32. doi: 10.1021/bm1001284
58. Staszewski MV, Jagus RJ, Pilosof AMR. Influence of green tea polyphenols on the colloidal stability and gelation of WPC. *Food Hydrocoll.* (2011) 25:1077–84. doi: 10.1016/j.foodhyd.2010.10.004
59. Yan M, Li B, Zhao X, Yi J. Physicochemical properties of gelatin gels from walleye pollock (*Theragra chalcogramma*) skin cross-linked by gallic acid and rutin. *Food Hydrocoll.* (2011) 25:907–14. doi: 10.1016/j.foodhyd.2010.08.019
60. Chen G, Wang S, Feng B, Jiang B, Miao M. Interaction between soybean protein and tea polyphenols under high pressure. *Food Chem.* (2019) 277:632–8. doi: 10.1016/j.foodchem.2018.11.024
61. Wang R, Liu J, Guo S. Binding of phytate to soybean protein during the heat treatment of soymilk and its effect on protein aggregation. *Food Hydrocoll.* (2018) 84:368–78. doi: 10.1016/j.foodhyd.2018.06.031
62. Jiang L, Liu Y, Li L, Qi B, Ju M, Xu Y, et al. Covalent conjugates of anthocyanins to soy protein: unravelling their structure features and *in vitro* gastrointestinal digestion fate. *Food Res Int.* (2019) 120:603–9. doi: 10.1016/j.foodres.2018.11.011
63. McClements DJ. Emulsion design to improve the delivery of functional lipophilic components. *Annu Rev Food Sci Technol.* (2010) 1:241–69. doi: 10.1146/annurev.food.080708.100722
64. Mao LK, Wang D, Liu FG, Gao YX. Emulsion design for the delivery of β-Carotene in complex food system. *Crit Rev Food Sci Nutr.* (2016) 58:770–84. doi: 10.1080/10408398.2016.1223599
65. Ju M, Zhu G, Huang G, Shen X, Zhang Y, Jiang L, et al. A novel pickering emulsion produced using soy protein-anthocyanin complex nanoparticles. *Food Hydrocoll.* (2020) 99:105329. doi: 10.1016/j.foodhyd.2019.105329
66. Chen Y, Wang C, Liu H, Liu Q, Kong B. Enhanced physical and oxidative stability of porcine plasma protein hydrolysates-based oil-in-water emulsions by adding oxidized chlorogenic acid. *Coll Surf A Physicochem Eng Aspects.* (2018) 558:330–7. doi: 10.1016/j.colsurfa.2018.08.067
67. Estevez M, Kylli P, Puolanne E, Kivikari R, Heinonen M. Fluorescence spectroscopy as a novel approach for the assessment of myofibrillar protein oxidation in oil-in-water emulsions. *Meat Sci.* (2008) 80:1290–6. doi: 10.1016/j.meatsci.2008.06.004
68. Dimakou CP, Kiokias SN, Tsaprouni IV, Oreopoulou V. Effect of processing and storage parameters on the oxidative deterioration of oil-in-water emulsions. *Food Biophys.* (2007) 2:38–45. doi: 10.1007/s11483-007-9027-6
69. Laguerre M, Giraldo LJ, Lecomte J, Figueroa-Espinoza MC, Barea B, Weiss J, et al. Chain length affects antioxidant properties of chlorogenate esters in emulsion: the cutoff theory behind the polar paradox. *J Agric Food Chem.* (2009) 57:11335–42. doi: 10.1021/jf9026266
70. Waraho T, McClements DJ, Decker EA. Mechanisms of lipid oxidation in food dispersions. *Trends Food Sci Technol.* (2011) 22:3–13. doi: 10.1016/j.tifs.2010.11.003
71. Demetriades K, Coupland JN, McClements DJ. Physicochemical properties of whey protein-stabilized emulsions as affected by heating and ionic strength. *J Food Sci.* (1997) 62:462–7. doi: 10.1111/j.1365-2621.1997.tb04407.x
72. Schmelz T, Lesmes U, Weiss J, McClements DJ. Modulation of physicochemical properties of lipid droplets using β-lactoglobulin and/or lactoferrin interfacial coatings. *Food Hydrocoll.* (2011) 25:1181–9. doi: 10.1016/j.foodhyd.2010.11.005
73. Singh H, Ye A, Horne D. Structuring food emulsions in the gastrointestinal tract to modify lipid digestion. *Prog Lipid Res.* (2009) 48:92–100. doi: 10.1016/j.plipres.2008.12.001
74. Zhou FZ, Yan L, Yin SW, Tang CH, Yang XQ. Development of pickering emulsions stabilized by gliadin/proanthocyanidins hybrid particles (GPHPs) and the fate of lipid oxidation and digestion. *J Agric Food Chem.* (2018) 66:1461–71. doi: 10.1021/acs.jafc.7b05261
75. Adjonu R, Doran G, Torley P, Agboola S. Formation of whey protein isolate hydrolysate stabilised nanoemulsion. *Food Hydrocoll.* (2014) 41:169–77. doi: 10.1016/j.foodhyd.2014.04.007
76. Chanphai P, Bourassa P, Kanakis CD, Tarantilis PA, Polissiou MG, Tajmir-Riahi HA. Review on the loading efficacy of dietary tea polyphenols with milk proteins. *Food Hydrocoll.* (2018) 77:322–8. doi: 10.1016/j.foodhyd.2017.10.008
77. Landi-Librandi AP, Chrysostomo TN, Caleiro Seixas Azzolini AE, Marzocchi-Machado CM, de Oliveira CA, Lucisano-Valim YM. Study of quercetin-loaded liposomes as potential drug carriers: *in vitro* evaluation of human complement activation. *J Liposome Res.* (2012) 22:89–99. doi: 10.3109/08982104.2011.615321
78. Liu W, Guo R. Interaction between flavonoid, quercetin and surfactant aggregates with different charges. *J Colloid Interface Sci.* (2006) 302:625–32. doi: 10.1016/j.jcis.2006.06.045
79. Xu XR, Yu HT, Yang Y, Hang L, Yang XW, Ding SH. Quercetin phospholipid complex significantly protects against oxidative injury in ARPE-19 cells associated with activation of Nrf2 pathway. *Eur J Pharmacol.* (2016) 770:1–8. doi: 10.1016/j.ejphar.2015.11.050
80. McClements DJ, Gumus CE. Natural emulsifiers-Biosurfactants, phospholipids, biopolymers, and colloidal particles: molecular and physicochemical basis of functional performance. *Adv Colloid Interface Sci.* (2016) 234:3–26. doi: 10.1016/j.cis.2016.03.002
81. Soukoulis C, Bohn T. A comprehensive overview on the micro- and nano-technological encapsulation advances for enhancing the chemical stability and bioavailability of carotenoids. *Crit Rev Food Sci Nutr.* (2018) 58:1–36. doi: 10.1080/10408398.2014.971353

Conflict of Interest: YL was employed by company Hangzhou Huadong Medicine Group Pharmaceutical Research Institute Co. Ltd.

The remaining authors declare that the research was conducted in the absence of any commercial or financial relationships that could be construed as a potential conflict of interest.

Publisher's Note: All claims expressed in this article are solely those of the authors and do not necessarily represent those of their affiliated organizations, or those of the publisher, the editors and the reviewers. Any product that may be evaluated in this article, or claim that may be made by its manufacturer, is not guaranteed or endorsed by the publisher.

frontiers in Nutrition

ORIGINAL RESEARCH
published: 03 January 2022
doi: 10.3389/fnut.2021.806623

Establishment and Characterization of Stable Zein/Glycosylated Lactoferrin Nanoparticles to Enhance the Storage Stability and *in vitro* Bioaccessibility of 7,8-Dihydroxyflavone

Yufeng Chen[1,2], *Xiaojing Gao*[1], *Shucheng Liu*[2], *Qiuxing Cai*[3], *Lijun Wu*[1], *Yi Sun*[1], *Guobin Xia*[4]* *and Yueqi Wang*[3,5]*

[1] College of Food Science and Technology, Zhejiang University of Technology, Hangzhou, China, [2] Guangdong Provincial Key Laboratory of Aquatic Product Processing and Safety, College of Food Science and Technology, Guangdong Ocean University, Zhanjiang, China, [3] College of Food Engineering, Beibu Gulf University, Qinzhou, China, [4] Department of Pediatrics Section of Neonatology, Texas Children's Hospital, Houston, TX, United States, [5] Key Lab of Aquatic Product Processing, Ministry of Agriculture and Rural Affairs of the People's Republic of China, South China Sea Fisheries Research Institute, Chinese Academy of Fishery Sciences, Guangzhou, China

OPEN ACCESS

Edited by:
Weilin Liu,
Zhejiang Gongshang University, China

Reviewed by:
Qian Li,
Hubei University of Technology, China
Hujun Xie,
Zhejiang Gongshang University, China

***Correspondence:**
Guobin Xia
gxxia@texaschildrens.org
Yueqi Wang
wangyueqi@scsfri.ac.cn

Specialty section:
This article was submitted to Food Chemistry, a section of the journal Frontiers in Nutrition

Received: 01 November 2021
Accepted: 29 November 2021
Published: 03 January 2022

Citation:
Chen Y, Gao X, Liu S, Cai Q, Wu L, Sun Y, Xia G and Wang Y (2022) Establishment and Characterization of Stable Zein/Glycosylated Lactoferrin Nanoparticles to Enhance the Storage Stability and in vitro Bioaccessibility of 7,8-Dihydroxyflavone. Front. Nutr. 8:806623. doi: 10.3389/fnut.2021.806623

In this work, the lactoferrin (LF) was glycosylated by dextran (molecular weight 10, 40, and 70 kDa, LF 10K, LF 40K, and LF 70K) *via* Maillard reaction as a stabilizer to establish zein/glycosylated LF nanoparticles and encapsulate 7,8-dihydroxyflavone (7,8-DHF). Three zein/glycosylated LF nanoparticles (79.27–87.24 nm) with low turbidity (<0.220) and polydispersity index (PDI) (<0.230) were successfully established by hydrophobic interactions and hydrogen bonding. Compared with zein/LF nanoparticles, zein/glycosylated LF nanoparticles further increased stability to ionic strength (0–500 mM NaCl) at low pH conditions. Zein/glycosylated LF nanoparticles had nanoscale spherical shape and glycosylated LF changed surface morphology of zein nanoparticles. Besides, encapsulated 7,8-DHF exhibited an amorphous state inside zein/glycosylated LF nanoparticles. Most importantly, zein/glycosylated LF nanoparticles had good water redispersibility, high encapsulation efficiency (above 98.50%), favorable storage stability, and bioaccessibility for 7,8-DHF, particularly LF 40K. Collectively, the above research provides a theoretical reference for the application of zein-based delivery systems.

Keywords: zein, glycosylated lactoferrin, nanoparticles, bioaccessibility, 7,8-dihydroxyflavone

INTRODUCTION

An infrequent flavone monomeric compound existing in *Godmania aesculifolia* and *Tridax procumbens*, 7,8-dihydroxyflavone (7,8-DHF) (**Supplementary Figure 1**), was authenticated as a high-affinity tropomyosin receptor kinase B (TrkB) agonist (1, 2). It could mimic the physiologic roles of brain-derived neurotrophic factor (BDNF) and its downstream signaling pathway (3). Current literature confirm that 7,8-DHF can relieve a lot of BDNF-relevant human sickness, such

as obesity, Parkinson's disease, Alzheimer's disease, and depression (4–8). However, methylation, sulfation, and glucuronidation of 7,8-DHF in the intestinal tract and liver caused its extremely low oral bioavailability (9). In our previous research, we testified that the permeability coefficient of 7,8-DHF was lower than 3×10^{-6} cm/s, and it had an active efflux mediated by multidrug resistance-related proteins (MRPs, especially MRP 2 outflow) and P-glycoprotein (P-gp) (10). Thus, the low chemical instability, low oral bioavailability, and high intestinal efflux of 7,8-DHF restricted its application as a functional component in the food industry.

Encapsulating 7,8-DHF within well-designed nano-sized carriers might be a promising alternative to overcome the chemical instability and low bioavailability in food industry. In our previous study, decorative liposomes were fabricated to encapsulate 7,8-DHF with improved stability, *in vitro* bioaccessibility, and permeability coefficient across Caco-2 cell monolayers (11). Recently, food-grade protein nanoparticles have been increasingly applied in encapsulating health-promoting naturally occurring flavonoids. For instance, epigallocatechin gallate and curcumin were encapsulated by zein and caseinate (12, 13). Particularly, zein has been the present research hotspot focus on hydrophobic flavonoids delivery by antisolvent precipitation (ASP) (14). Penalva *et al*. has fabricated zein nanoparticles for encapsulating resveratrol to improve its chemical instability and oral bioavailability (19.2-time increase in rats) (15). Besides, astilbin-encapsulated zein nanoparticles improved the absolute bioavailability of astilbin from 0.32 to 4.40% (16).

Nevertheless, when exposed to a certain temperature, ionic strength, and pH range, zein nanoparticles are highly susceptible to aggregation because of the strong hydrophobic attractions between them. To address the abovementioned issues, in our previous study, we used lactoferrin (LF) as a stabilizer to confirm it had good stability in fabricating zein nanoparticles at high salt concentration and wide pH range compared with other proteins. However, at low pH range, salt tolerance of zein/LF complex nanoparticles was poor (17). Thus, in our study, we want to employ the Maillard reaction to form LF-polysaccharides conjugates to overcome the above issues. The Maillard reaction is a non-enzymatic reaction that involves the condensation of the carbonyl group of a reducing carbohydrate with a free amino group of a protein (either an N-terminal amino group or a lysine residue), it is greatly accelerated by heat and alkaline conditions.

Above all, the first objective of our research was to explore the effect of selected glycosylated LF by Maillard reaction on the stability of protein-based zein nanoparticles. Subsequently, the chemical structure and microstructure of zein/glycosylated LF nanoparticles to encapsulate 7,8-DHF were explored by a series of characterization techniques. Moreover, storage stability, *in vitro* digestion, and related bioaccessibility of 7,8-DHF encapsulated nanoparticles were evaluated for potential food and pharmaceutical formulas applications.

MATERIALS AND METHODS

Materials and Chemicals

In this study, 7,8-DHF (≥98%) was bought from TCI Co., Ltd. (Tokyo, Japan). LF (≥98%) was bought from Glycarbo Co., Ltd. (Tokyo, Japan). Pancreatin (4 × USP specification) and zein (≥95%) and was purchased from Sigma-Aldrich (MO, USA). Dextran (10, 40, and 70 kDa) and kaempferol (>98%) and was received from Aladdin Co., Ltd. (Shanghai, China). Pepsin (activity 3,000–3,500 U/mg) and bile salts and were obtained from Sangon Biotech Co., Ltd. (Shanghai, China). Other chemicals and reagents used were of analytical grade.

Lactoferrin-Dextran Conjugates Generation *via* Maillard Reaction

Dextran (1%, w/v, 10, 40, or 70 kDa) and LF (1%, w/v) were all alone solubilized and stirred overnight at 4°C in phosphate-buffered solution (PBS, 0.01 M, pH = 7.4). Subsequently, they were blended at a 1:1 mass ratio for freeze-drying. The lyophilized mixtures proceeded Maillard reaction in a sealed desiccator containing saturated KBr solution (48 h, 60°C, and 79% relative humidity). After conjugation, the LF-dextran conjugates (LF 10K, 40K, and 70K) were lyophilized again and preserved at −20°C before study.

Lactoferrin-Dextran Conjugates Characterization

Sodium Dodecyl Sulfate-Polyacrylamide Gel Electrophoresis

A 5% stacking gel and an 8% acrylamide separating gel were used for sodium dodecyl sulfate-polyacrylamide gel electrophoresis (SDS-PAGE). Furthermore, 5 μl of LF, LF 10K, LF 40K, and LF 70K solutions (according to 2 mg/ml LF) were blended with 20 μl of protein loading buffer and then heated together for 5 min in burning water. Each gel lane was loaded with 10 μl sample and performed at 80–120 mV for electrophoresis. At the end of electrophoresis, each gel was dyed with Coomassi bright blue R-250 solution (0.25%, w/v), and decolorized by decolorizing agent (50% methanol, 40% distilled water, and 10% acetic acid, v/v).

Conjugation Efficiency

To measure the conjugation efficiency of the samples, o-phthaldialdehyde (OPA) method was applied (18). Briefly, 4.0 ml of OPA working solution was blended with 200 μl of LF and three glycosylated LF water solutions (according to 2 mg/ml LF) after 3 min reaction at 37°C for measuring at 340 nm absorbance. The amino content standard curve was established *via* a suitable range concentration of L-leucine (0.25–2.5 mM). The conjugation efficiency was calculated by the following formula:

$$\text{Conjugation efficiency (\%)} = \left(1 - \frac{\text{amine groups after conjugation (mM)}}{\text{amine groups before conjugation (mM)}}\right) \times 100 \quad (1)$$

Browning

The degree of browning caused by the Maillard reaction was assessed using a UV-vis spectrophotometer at 420 nm

absorbance, LF, LF 10K, LF 40K, and LF 70K were dissolved in distilled water (according to 1 mg/ml LF) for measuring.

Zeta Potential

Zeta potential was characterized using a dynamic light scattering (DLS) instrument (Nano-ZS 90 analyzer, UK) at 25°C. LF, LF 10K, LF 40K, and LF 70K were dissolved in deionized water (according to 2 mg/ml LF) for determining by Smoluchowski model.

Circular Dichroism

Secondary structural characters of non-conjugates and conjugates under analysis (according to 0.2 mg/ml LF) were detected using a CD spectrometer (J-1500, JASCO, Tokyo, Japan). The secondary structure scanning region was 190–260 nm with 0.1 cm path length, the scanning speed was 50 nm/min, and bandwidth was 1.0 nm. The data were evaluated by Spectra Manager™ II Software equipped with CD spectrometer.

Fourier-Transform Infrared Spectroscopy

Pre-dried LF, LF 10K, LF 40K, and LF 70K under analysis was produced using adding 99% KBr disc and scanned on a Fourier-transform infrared (FTIR) spectrometer (Avatar 370, Nicolet, Madison, WI, USA). Spectral sweep band was ranged from 4,000 to 500 cm^{-1} at a 4 cm^{-1} resolution. The analytical results were obtained by OMNIC version 8.0 software.

Zein/Glycosylated LF Composite Nanoparticles Preparation

To prepare zein/glycosylated LF composite nanoparticles by ASP method, zein was dissolved in 80% ethanol/water solution to prepare the stock solution (1% zein, w/v). Then, the mother liquor was quickly added into three glycosylated LF aqueous solutions (antisolvent) with a 1:3 volume ratio under continuous stirring at 800 rpm for 30 min, whereafter, ethanol was eliminated by a rotary evaporator at an appropriate temperature. As control samples, zein/LF and zein nanoparticles were prepared based on the above method using LF aqueous solution and deionized water as an antisolvent, respectively. The final concentration of zein, LF, and glycosylated LF in each nanoparticle were all 2.5 mg/ml. Final nanoparticles were reserved at 4°C for subsequent research. Zein/LF nanoparticles were named as Zein/LF, zein/glycosylated LF nanoparticles with different molecular weight dextran were denominated as zein/LF 10K, 40K, and 70K, respectively.

Physical Stability of Zein/Glycosylated LF Composite Nanoparticles

pH Influence

The influence of pH on the stability of each colloidal particle was evaluated within a pH 3–9 range using either 2 M HCl or NaOH.

Ionic Strength Influence

Each zein colloidal particle was blended with NaCl to obtain samples within 0, 25, 50, 100, 200, and 500 mM NaCl concentrations at different pH (pH 3–9) and stored after 24 h for observing.

Temperature Influence

The temperature influence on the stability of each colloidal particle was tested by heating for 60 min at 95°C and then, cooled at 25°C.

Storage Time Influence

Each freshly zein colloidal particle was stored at room temperature for 1 month.

Particle size changes within complex dispersions were recorded using DLS at 25°C. The light intensity at a fixed scattering angle was 90 degrees, and the refractive index of water was set at 1.45.

Encapsulation of 7,8-DHF Into Complex Particles

In the current study, 7,8-DHF encapsulation was conducted in the above methods described in section Zein/Glycosylated LF Composite Nanoparticles Preparation. Zein and 7,8-DHF were dissolved at 10:1 and 5:1 mass ratios in 80% ethanol-water solution, respectively. The mass ratio of LF or glycosylated LF to zein was 1:1 in the final reaction system. 7,8-DHF encapsulation in zein, zein/LF, and zein/glycosylated LF nanoparticles were denoted as DHF-zein, DHF-zein/LF, DHF-zein/LF 10K, DHF-zein/LF 40K, and DHF-zein/LF 70K, respectively. Loaded complex particles were reserved at 4°C, other samples were lyophilized for 48 h to conduct an in-depth study.

Polydispersity Index, Particle Size, Zeta Potential, and Turbidity

Polydispersity index (PDI) and particle size of fresh dispersions were characterized based on section Physical Stability of Zein/Glycosylated LF Composite Nanoparticles. Zeta potential was tested according to section Zeta Potential. The turbidity of complex particles was tested at 600 nm using a UV spectrophotometer at 25°C.

Entrapment Efficiency Determination

The entrapment efficiency (EE) of encapsulated 7,8-DHF was assessed by ultra-performance liquid chromatography (UPLC) based on our previously described method (19, 20) and then calculated depending on the following equation:

$$\text{EE } (\%) = \frac{\text{loaded } 7,8-\text{DHF}}{\text{initial } 7,8-\text{DHF}} \times 100 \quad (2)$$

Transmission Electron Microscopy

The 10-fold diluted freshly loaded colloidal particles were deposited on a copper grid with a 200-mesh formvar-carbon coating. Then, the samples were dried in air and dyed with 2% uranyl acetate. Transmission electron microscopy (TEM) (JEM-1200 EX, Tokyo, Japan) was performed for microscopic observation at 120 kV accelerating voltage.

Field Emission Scanning Electron Microscope

The surface morphology of lyophilized nanoparticles was captured by using a field emission scanning electron microscope

(FE-SEM) (GeminiSEM 300, ZEISS, Germany). Before analysis, a gold layer with 3–6 nm thickness was covered on the sample surfaces. The electron microscope acceleration voltage was 15.0 kV.

Differential Scanning Calorimetry

Thermal behavior of 7,8-DHF, lyophilized glycosylated LF and freeze-dried nanoparticles were studied *via* differential scanning calorimetry (DSC) (Mettler Toledo, Zurich, Switzerland). About 2–8 mg of samples were accurately weighed and hermetically sealed in aluminum pots, an empty crucible under the same condition was used as a reference. Scanning calorimetry was performed at a range of 25–200°C in N_2 atmosphere with a 10°C/min heating rate under 30 ml/min flow.

X-Ray Diffraction

The crystalline characteristic of selected samples was evaluated on an X-ray diffractometer (Bruker D8, Karlsruhe, Germany). This diffractometer tube current and accelerating voltages were 40 mA and 40 kV, respectively. Soller slit and divergence slit were set at 2.5 and 0.5 degrees, respectively, the 2θ angle ranged from 5 to 90 degrees.

Fourier-Transform Infrared

All analyzed colloidal dispersions were proceeded according to the method described in section Fourier-Transform Infrared Spectroscopy.

Storage Stability of 7,8-DHF

Furthermore, 7,8-DHF, DHF-zein, DHF-zein/LF, DHF-zein/LF 10K, DHF-zein/LF 40K, and DHF-zein/LF 70K were conducted at 50°C for 72 h under dark and 25°C for 15 days under light. At an appropriate point-in-time, a certain amount of suspension was acquired for measuring by UPLC. The storage stability equation was figured as follow:

$$\text{Retention rate } (\%) = \frac{\text{retained } 7,8-\text{DHF concentration}}{\text{initial } 7,8-\text{DHF concentration}} \times 100 \quad (3)$$

In vitro Simulated Gastrointestinal Digestion

Based on the study of Yuan *et al. via* some amendments (21), briefly, 10 ml of simulated gastric fluid (SGF, 3.2 mg/ml pepsin and 2 mg/ml NaCl, pH = 2.5) and 10 ml of 7,8-DHF, DHF-zein, DHF-zein/LF, DHF-zein/LF 10K, DHF-zein/LF 40K, and DHF-zein/LF 70K were mingled for incubating in a 37°C water bath shaker for 60 min at 100 rpm. After SGF digestion, 10 ml of above-mentioned simulated gastric digestive fluids were modulated to pH 7.4 *via* 2 M NaOH. Ten milliliter of simulated intestinal fluid (SIF, 5 mg/ml bile salts, 4 mg/ml pancreatin, 6.8 mg/ml K_2HPO_4, and 8.8 mg/ml NaCl, and pH = 7.4) was blended to incubate for 120 min at same temperature and speed. Finally, the final digestive solution was centrifuged by 20,000 × g centrifugal force for 1 h, and the supernatant was collected. The bioaccessibility (%) was calculated based on the following equation:

$$\text{Bioaccessibility } (\%) = \frac{7,8-\text{DHF concentration in the supernatant phases}}{7,8-\text{DHF concentration in the formulation}} \times 100 \quad (4)$$

Besides, the digesta were gathered for acquiring particle size at designed point-in-time (30, 60, 120, and 180 min). And the final digesta were freeze-dried for FE-SEM observation.

Statistical Analysis

Mean ± SD was presented *via* at least three times for all data. One-way ANOVA was utilized to assess the significant difference among groups ($p < 0.05$). Unpaired two-tailed Student's *t*-test ($^{***}p < 0.001$, $^{**}p < 0.01$, and $^{*}p < 0.05$), was applied to analyze the significant differences between two groups. Data analysis was carried out by using the GraphPad Prism 8.0 (GraphPad Sofware, San Diego, CA, USA) and Origin 2021 (Origin Lab Co., Northampton, MA, USA).

RESULTS AND DISCUSSION

Preparation and Characterization of Glycosylated LF *via* Maillard Reaction

As seen in **Figure 1A**, the molecular weight of LF and glycosylated was tested through SDS-PAGE. The major molecular weight band in native LF was at about 80 kDa (lane 0), which was in agreement with the previous literature (22). Compared with LF, after glycosylation with dextran, the bands of three LF-dextran conjugates at 80 kDa were reduced and the color became weaker, while the bands at the high molecular weight (between 85 and 270 kDa) became darker and stronger, resulting in high mobility in molecular weight. It indicated that LF and dextran generated high molecular weight glycosylated proteins (Lane 1–3) through the Maillard reaction. At the same time, it was found that the intensity and color of the bands in the high molecular weight region of LF 10K and 40K were stronger and darker than that of LF 70K, indicating that with the increase of molecular weight and the decreasing number of reductive carbonyl terminal inside dextran led to the weakening of Maillard reaction, and short polysaccharide chains were easier to conjugate to LF protein than long polysaccharide chains.

This result was confirmed by OPA results. The Maillard reaction occurs when the free amino group of the protein is covalently linked to the carbonyl group of the reducing sugar to form a Schiff base (23). As seen from **Figure 1B**, the grafting efficiency of LF with 10, 40, and 70 kDa dextran was about 24.96, 16.54, and 11.39%, respectively. The data certified that the molecular weight of dextran influenced the conjugation efficiency of LF. A similar result has been reported in the covalent binding of ovalbumin and dextran (18). The color depth of Maillard reaction products can intuitively reflect the degree of Maillard reaction, and the absorbance value at 420 nm is used as an indicator of the number of Browning products (24). As seen in **Figure 1B**, the absorbance

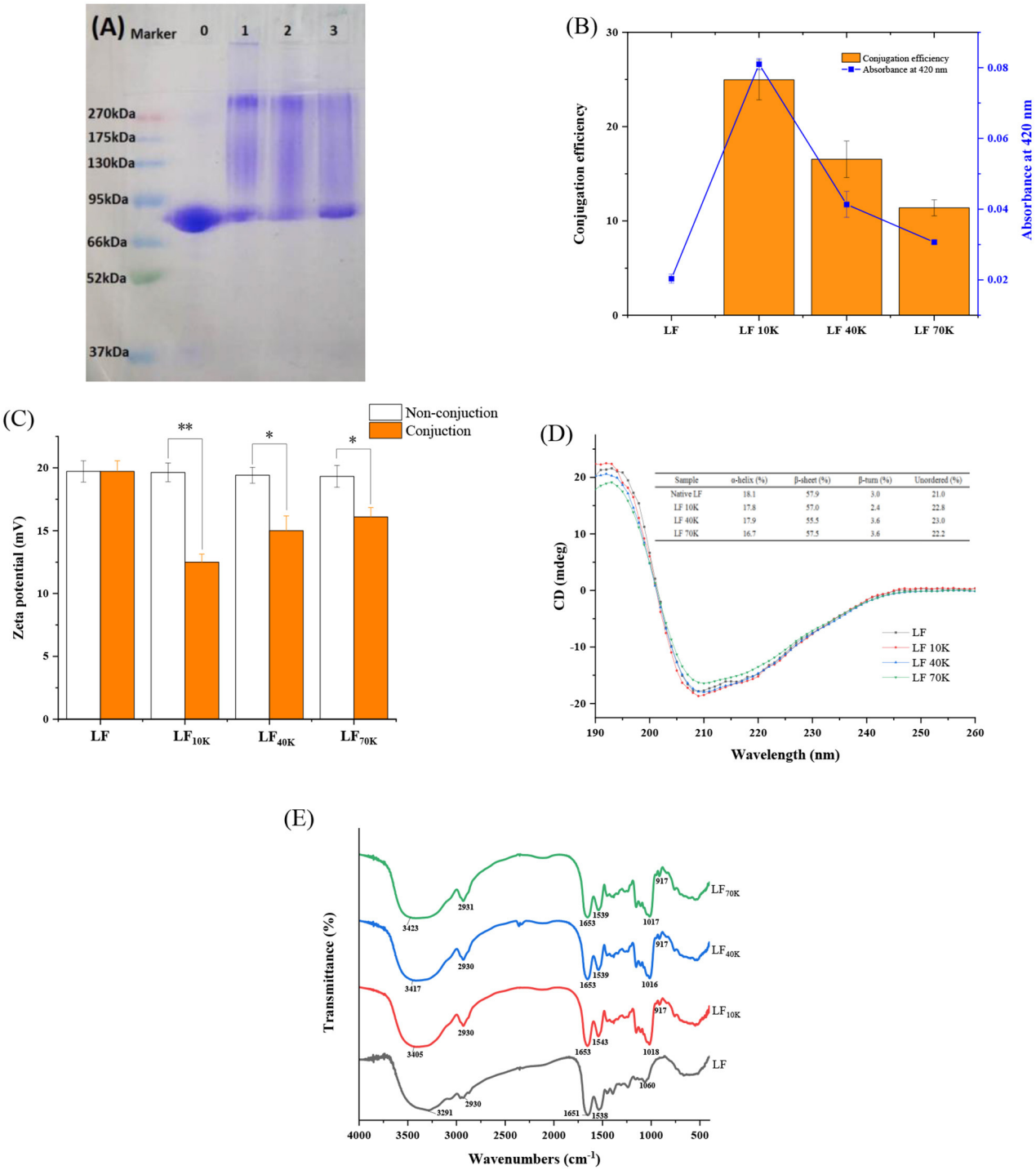

FIGURE 1 | Characterization of glycosylated lactoferrin (LF) *via* Maillard reaction. sodium dodecyl sulfate-polyacrylamide gel electrophoresis (SDS-PAGE) profiles, lane 0, LF; lane 1, LF 10K; lane 2, LF 40K; lane 3, LF 70K **(A)**. Conjugation efficiency and browning **(B)**. Zeta potential, non-conjunction means the mix of LF and dextran with 10, 40, or 70 kDa **(C)**. Circular dichroism (CD) spectra **(D)**. Fourier-transform infrared (FTIR) spectra **(E)**.

at 420 nm of the glycosylated substances of LF to dextran with 10, 40, and 70 kDa was about 0.081, 0.041, and 0.030, respectively. Furthermore, zeta potential of glycosylated LF was significantly less than that of non-conjugated LF mixes and LF ($p < 0.05$) (**Figure 1C**), which was due to the positive -NH_2 group in LF participating in the formation of Schiff base,

resulting in the decrease of amount of positively charged -NH_2 groups.

Circular dichroism spectroscopy can reflect the influence of glycosylation on the secondary structure change of LF. As observed from **Figure 1D**, CD scanning in the far-ultraviolet region of LF showed the negative band at 208 and 215 nm, and a maximum band at 190–195 nm, which was a typical α-helix and β-sheet structure for LF (25, 26). The inserts about secondary structure composition in **Figure 1D** showed that the α-helix and β-sheet of LF decreased (fall off 1.1–7.7% and 0.7–4.1% corresponding to α-helix and β-sheet, respectively), while the unordered structure increased after glycosylation (went up 5.4–8.7%), indicating that glycosylated secondary structure of LF was changed by Maillard reaction to some extent (**Figure 1E**). In FTIR spectroscopy, 3,300–3,600 cm^{-1} absorption peak was signified to the N-H stretching coupled with hydrogen bonding (27). The spectra of LF exhibited 3,291 cm^{-1} absorption peak, which was identical with the result of anterior research (28). As compared with LF, glycosylated LF had a significant blue-shift, and the absorption peak of LF 10K, 40K, and 70K were increased by 114, 126, and 132 cm^{-1}, respectively, which implied -NH_2 groups of LF took part in glycosylation reaction. Moreover, the major peak at 950–1,150 cm^{-1} reflected O-H deforming vibration and C-O stretching (29). We found that the absorption peak of the native LF at 1,060 cm^{-1} occurred at 42, 44, and 43 cm^{-1} redshifts corresponding to LF 10K, 40K, and 70K, respectively. As we know, dextran was rich in O-H and C-O bonds, thus illustrating reduced carbonyl group of dextran was involved in the LF Maillard reaction. In addition, after the Maillard reaction, C=O (amide I band, characteristic peak of LF was at 1,652 and 1,651 cm^{-1}) and C–N stretching vibration (amide II band, characteristic peak of LF was at 1,538 and 1,538 cm^{-1}) have been changed (30). Above all, the secondary and chemical structure of LF protein changes has been changed after glycosylation reaction.

Physical-Chemical Stability Study on Zein/Glycosylated LF Nanoparticles

According to our previous research about Zein/LF (17), in our research, the selected mass ratio of glycosylated LF to zein was 1:1, and the ASP method was used to construct zein/glycosylated LF nanoparticles for the study of physicochemical stability. Zein nanoparticles and zein/LF were used as the control.

pH Influence

As observed from **Figure 2A**, our previous study has proved that bare zein nanoparticles occurred severe aggregation at pH 5.0–7.0 accompanied by a large rise in particle size. Besides, the addition of LF greatly prevented zein nanoparticles from aggregation at pH 5.0–7.0 due to that LF provided strong electrostatic repulsion and steric exclusion (17). In addition, glycosylated LF adding exhibited the same stabilizing effect compared with native LF at a pH range of 3–9, no matter what zein/LF 10K, 40K, and 70K. This might be ascribed to the shielding effect of particle surface charge by protein-carbohydrate layer. The same result was found in caseinate-carbohydrate conjugates coating zein nanoparticles (31). Above all, glycosylated LF acted as protein emulsifiers, exhibited the same advantages for zein nanoparticle stabilization at pH 3–9 compared with LF.

Ionic Strengths Influence at Different pH Condition

Colloidal systems will undergo different ionic environments in the commercial food products and human digestive tract. Thus, ionic strengths stability testing is necessary to evaluate the functionality of colloidal particles (**Figures 2B–E**) (32). Previously, it has been proved that zein unitary system is highly sensitive to ionic strength, even at a low level of salt. Although the zein/LF binary system with the addition of LF has been improved, it was still highly sensitive to the ionic strength to produce aggregation at low pH (3–5) (17). However, under the presence of LF 10K, 40K, and 70K, the particle size of zein/glycosylated LF nanoparticles maintained stable at a broad pH range of 3–9 when adding 0–500 mM NaCl, particularly zein/LF 40K and 70K. The mean particle size of zein/LF 40K and zein/LF 70K was below 250 and 200 nm, respectively, at a pH range of 3–9 when adding 0–500 mM NaCl, zein/LF 70K showed the best stabilization effect. These results showed that with the increase of the molecular weight of dextran, its chain length increased correspondingly, resulting in a greater steric hindrance, which prevented the agglomeration effect of nanoparticles. At the same time, the interface layer formed by glycosylated LF coating particle surface played a role in shielding the external charge. It is demonstrated that zein/glycosylated LF nanoparticles as nutritional ingredients will remain certainly stable in commercial products, it is also manifested that they as colloidal delivery systems may improve the stability and bioaccessibility of bioactive compounds through the human gastrointestinal tract with relatively high ionic strengths.

Thermal Treatment Influence

Heat treatment was often applied to sterilize and pasteurize food or beverages. As seen in **Figure 2F** and **Supplementary Figure 2** (photograph), after heating at 95°C for 60 min, the average particle size of bare zein nanoparticles was above 400 nm. A previous study has shown that bare zein nanoparticles are highly sensitive to under heating conditions (33). However, under the same heating conditions, the particle size of zein/LF, zein/LF 10K, zein/LF 40K, and zein/LF 70K had no significant change, indicating the presence of native or glycosylated LF improved thermal stability of zein nanoparticles.

Long-Term Storage Influence

In daily commodity circulation, it is critical to evaluate the long-term stability of colloidal particles in room temperature circumstances. As seen from **Figure 2G**, individual zein nanoparticles displayed highly instability accompanied by aggregation range from pH 3.0 to 9.0 after 1-month storage. However, whatever the presence of native or glycosylated LF, the composite nanoparticles were stable to prevent aggregation for 30 days storage, demonstrating glycosylated LF coating exhibited same effect at increasing the long-term storage stability for zein nanoparticles compared with native LF.

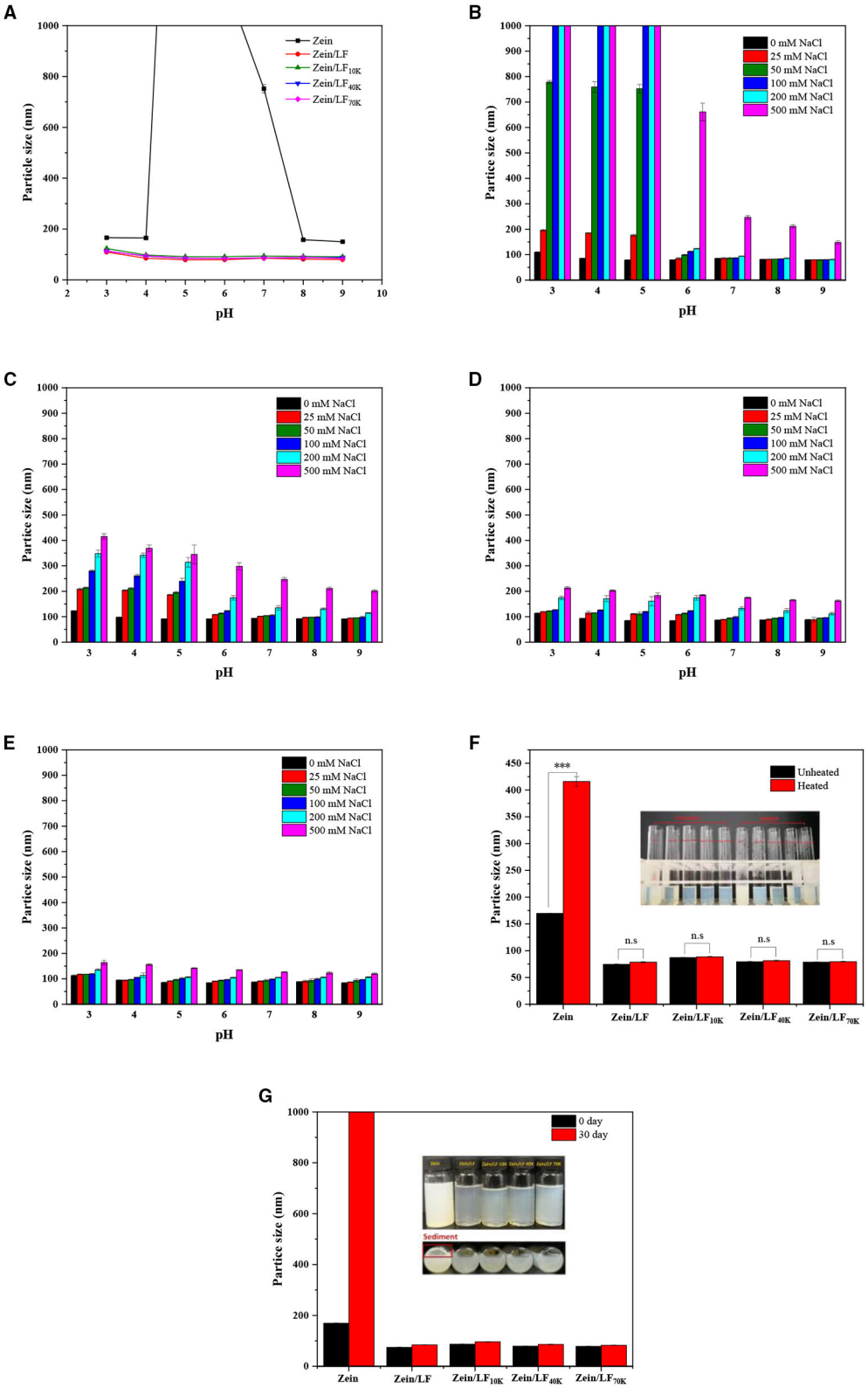

FIGURE 2 | Particle size of colloidal particles at pH 3-9 condition **(A)**. Particle size of colloidal particles under 0-500 mM NaCl concentrations at pH 3-9 condition, zein/LF **(B)**, zein/LF 10K **(C)**, zein/LF 40K **(D)**, zein/LF 70K **(E)**. Particle size of colloidal particles under thermal treatments **(F)**. Particle size of colloidal particles in 1-month storage at 25°C **(G)**.

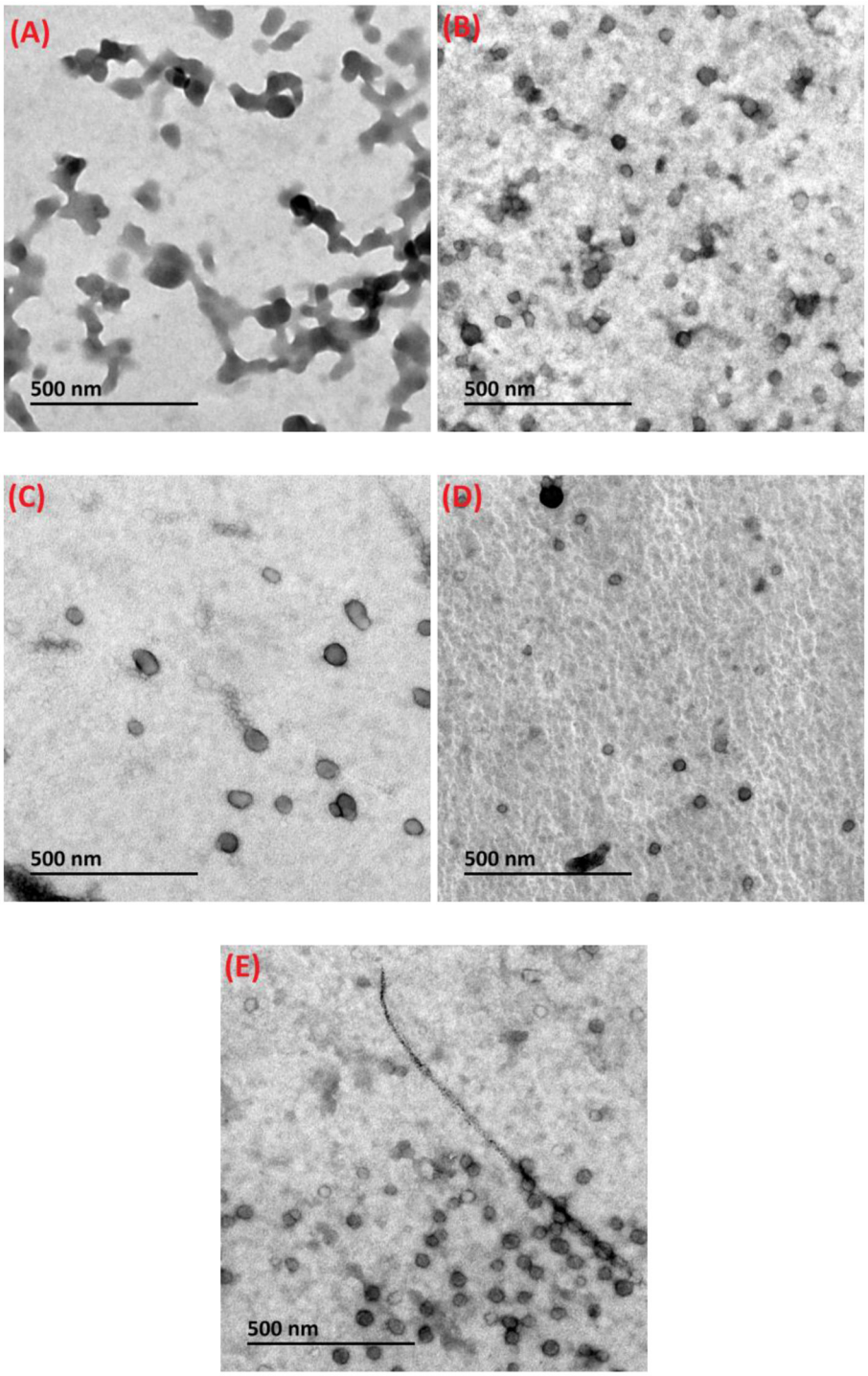

FIGURE 3 | Transmission electron microscopy (TEM) images of dihydroxyflavone (DHF)-zein **(A)**, DHF-zein/LF **(B)**, DHF-zein/LF 10K **(C)**, DHF-zein/LF 40K **(D)**, and DHF-zein/LF 70K **(E)**. Pictures were taken at ×50,000 magnifications.

Encapsulation of 7,8-DHF

The influence of *via* glycosylated LF with different molecular weight (LF 10K, 40K, and 70K) and 7,8-DHF concentration on EE, PDI, particle size, zeta potential, and turbidity within different delivery systems are summarized in **Table 1**. Without 7,8-DHF, zeta potential of bare zein particles was 4.66 mv, the increase of positive charge occurred when supplementation with glycosylated LF, displaying 21.63–23.45 mv zeta potential, which

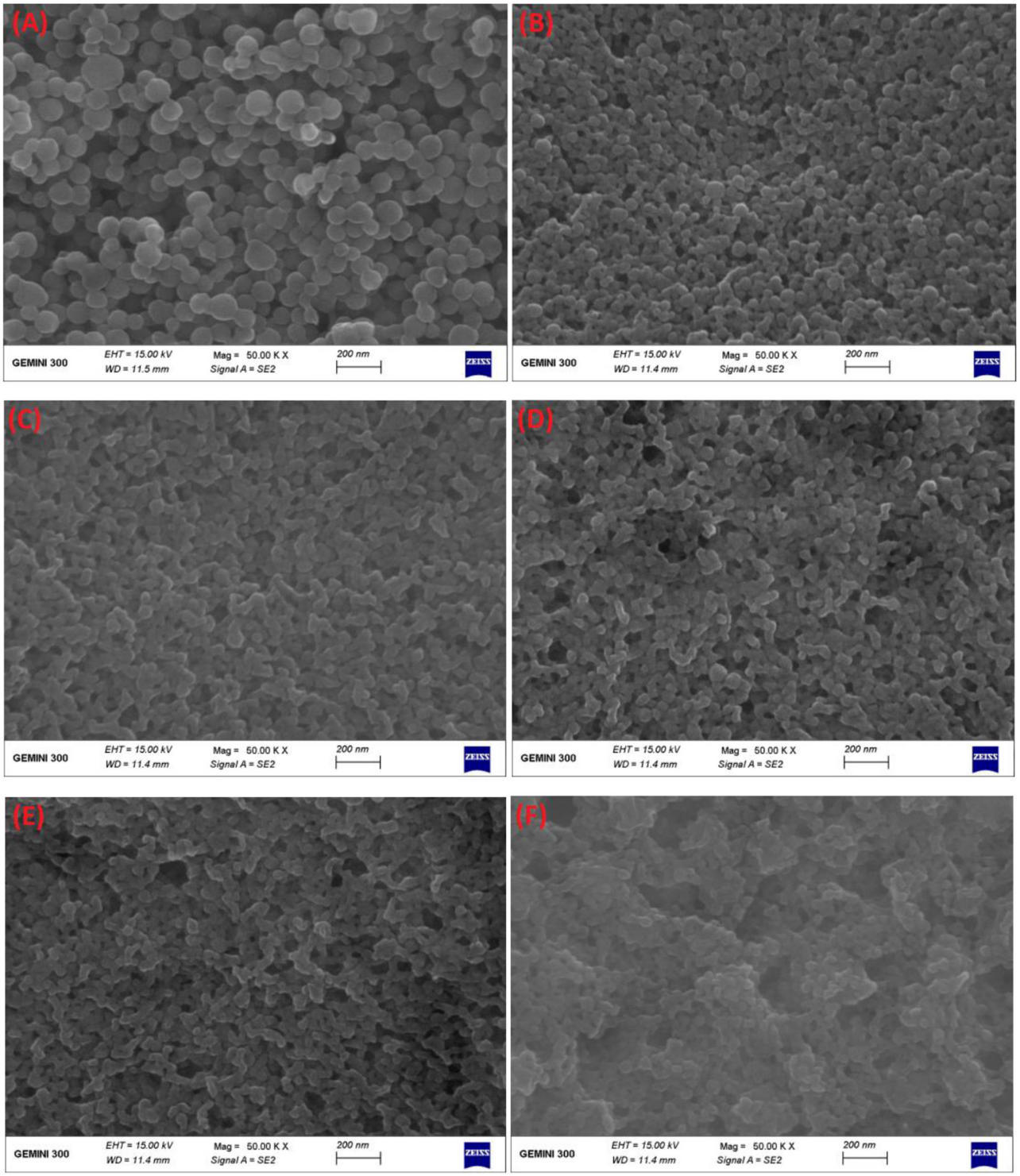

FIGURE 4 | Field emission scanning electron microscope (FE-SEM) images of bare zein nanoparticles **(A)**, DHF-zein **(B)**, DHF-zein/LF **(C)**, DHF-zein/LF 10K **(D)**, DHF-zein/LF 40K **(E)**, and DHF-zein/LF 70K **(F)**. Pictures were taken at ×50,000 magnifications.

was due to amino acid residue ($-NH^{3+}$) in LF 10K, 40K, and 70K. But zeta potential values of zein/glycosylated LF nanoparticles were all lower than that of zein/LF, furtherly clarifying that amino acid residue in LF participated in the Maillard reaction. Homogeneous colloid systems (79.27–87.24 nm) came true by reducing the surface hydrophobicity of the zein protein

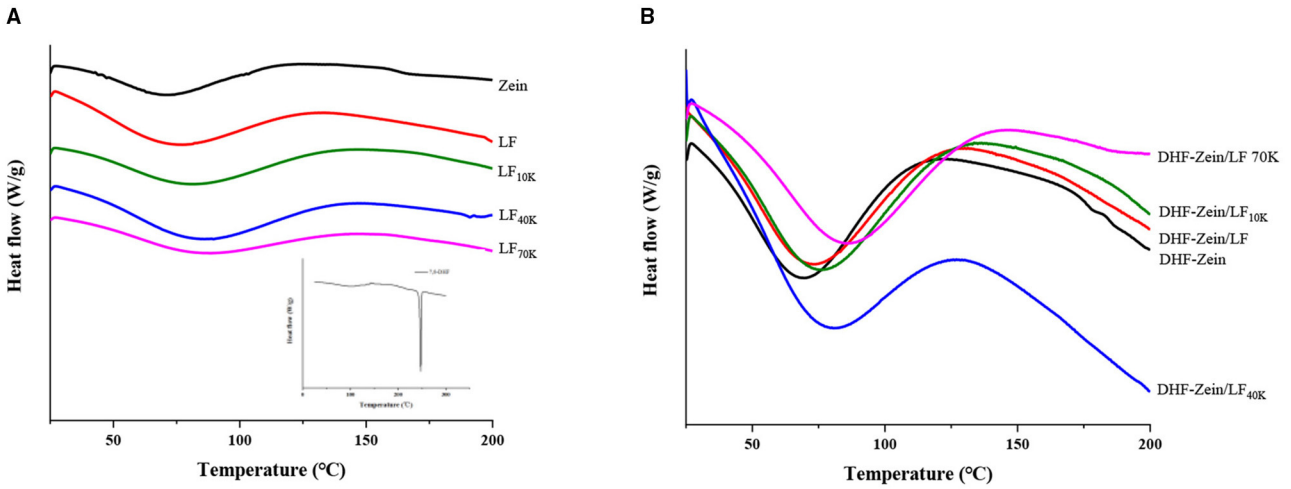

FIGURE 5 | Differential scanning calorimetry (DSC) analysis of samples, such as individual zein, LF, glycosylated LF, and 7,8-DHF **(A)**, DHF-zein, DHF-zein/LF, DHF-zein/LF 10K, DHF-zein/LF 40K, and DHF-zein/LF 70K **(B)**.

when adding LF 10K, 40K, and 70K in contrast to bare zein nanoparticle (169.56 nm). In addition, compared with zein/LF, the particle size of zein/LF 10K, 40K, and 70K was larger, which was due to long polysaccharide chains conjugated to the surface of LF protein. In addition, turbidity and PDI showed a similar trend to particle size The decrease manifested that there is more glycosylated LF coating on the surface of zein nanoparticles, which inhibits their micro-aggregation. At the 7,8-DHF to zein mass ratio was 1:5, EE of zein, zein/LF, zein/LF 10K, zein/LF 40K, and zein/LF 70K was 37.27, 66.10, 72.41, 84.75, and 83.61%, respectively. Above outcomes manifested that the addition of LF glycosylation further increased EE of 7,8-DHF ($p < 0.05$), particularly LF 40K and 70K. An identical result was discovered at the mass ratio of 7,8-DHF to zein 1:10 (the EE of DHF-zein/LF 10K, 40K, and 70K were all above 98%). In general, as 7,8-DHF was embedded, it could disturb mutual effect among hydrophobic groups of zein, leading to the stability of zein particles, with the accompanying decline in particle size (116.9–119.7 nm). However, the particle size of DHF-Zein/LF 10K, 40K, and 70K slightly increased compared with unloaded nanoparticles but were all below 100 nm, displaying a small nanoscale size. In addition, 7,8-DHF encapsulation led to the increase of PDI and turbidity of nanoparticles, a homologous tendency was reported by Sun et al. (34). After the lyophilized DHF-zein/LF 10K, 40K, and 70K were redissolved in the distilled water, the redispersibility was good, the redissolved nanoparticles still maintained a good EE (above 93.43%), zeta potential (above 18.43 mV), particle size (below 108.2 nm), PDI (below 0.281), and turbidity (below 0.267) value, which was owed to that hydrophilic glycosylated LF adsorbing adequately on the surface of the zein resulted in a decrease in the surface hydrophobicity. Collectively, zein/glycosylated LF nanoparticles were a high-quality colloidal delivery for 7,8-DHF, particularly zein/LF 40K and 70K.

Micromorphology

The microstructural features of loaded composite nanoparticles were analyzed *via* TEM. As observed from **Figure 3A**, the diameter of DHF-zein was above 100 nm, which was consistent with the DLS conclusions. In addition, DHF-zein was interconnected, which may be due to the hydrophobic interaction among zein particles after they were diluted 10 times, resulting in aggregation. However, after the addition of glycosylated LF, DHF-zein/LF 10K, 40K, and 70K showed a spherical shape in the range of 70–100 nm (**Figures 3B–E**) and were homogeneously dispersed, indicating that the adsorption of glycosylated LF could increase the electrostatic repulsion and spatial repulsion effect. Thus, the aggregation of DHF-zein could be prevented. In addition, the average particle size of DHF-zein/glycosylated LF was relatively larger than that of DHF-zein/LF, especially DHF-zein/LF 10K.

Furthermore, FE-SEM was applied to observe the differences in surface microscopic morphology of each composite nanoparticle (**Figure 4**). As seen from **Figure 4A**, zein nanoparticles and DHF-zein were typically of spherical shapes with uniform in size (35), but the surface morphology of DHF-zein emerged slightly rough, it was consistent with a preceding study about curcumin (36). However, after adding glycosylated LF, DHF-zein/LF 10K, 40K, and 70K were significantly changed with irregular and rough surfaces in comparison to zein nanoparticles and DHF-zein (**Figures 4D–F**). This appearance was probably due to our hypothesis that glycosylated LF was adsorbed on the surface of DHF-zein by some non-covalent forces. This result was consistent with that of native LF adsorbed on the surface of DHF-zein (**Figure 4C**). In addition, compared with bare zein nanoparticles, the average particle size of the binary system was decreased after encapsulating, which was consistent with the results measured by DLS.

TABLE 1 | Entrapment efficiency (EE), zeta potential, particle size, polydispersity index (PDI), and turbidity of 7,8-dihydroxyflavone (7,8-DHF) in different colloidal systems.

(Zein or LF): 7,8-DHF (w/w)	Colloidal systems	EE (%)	Zeta potential (mV)	Particle size (nm)	PDI	Turbidity
Without 7,8-DHF	Zein	–	4.66 ± 0.13^{a}	169.6 ± 0.54^{a}	0.262 ± 0.005^{bc}	1.465 ± 0.05^{a}
	Zein/LF	–	26.93 ± 0.33^{c}	74.6 ± 0.65^{c}	0.199 ± 0.008^{b}	0.140 ± 0.03^{c}
	Zein/LF 10K	–	21.63 ± 0.46^{c}	87.24 ± 0.16^{c}	0.227 ± 0.014^{a}	0.219 ± 0.06^{c}
	Zein/LF 40K	–	23.45 ± 0.32^{c}	79.27 ± 0.96^{c}	0.213 ± 0.010^{b}	0.134 ± 0.03^{c}
	Zein/LF 70K	–	23.17 ± 0.12^{c}	78.67 ± 0.51^{c}	0.205 ± 0.004^{b}	0.125 ± 0.07^{c}
5:1	Zein	37.27 ± 1.36^{d}	10.23 ± 0.13^{b}	119.7 ± 5.69^{b}	0.361 ± 0.010^{d}	0.451 ± 0.07^{b}
	Zein/LF	66.10 ± 2.63^{c}	24.14 ± 0.36^{c}	84.3 ± 1.21^{c}	0.384 ± 0.021^{d}	0.206 ± 0.04^{c}
	Zein/LF 10K	72.41 ± 2.12^{c}	18.74 ± 0.16^{c}	98.1 ± 1.41^{c}	0.371 ± 0.014^{c}	0.287 ± 0.06^{c}
	Zein/LF 40K	84.75 ± 3.52^{b}	20.41 ± 0.26^{c}	88.41 ± 2.01^{c}	0.363 ± 0.024^{d}	0.174 ± 0.02^{c}
	Zein/LF 70K	83.61 ± 2.88^{b}	20.31 ± 0.31^{c}	87.98 ± 2.16^{c}	0.357 ± 0.030^{d}	0.168 ± 0.03^{c}
10:1	Zein	46.38 ± 2.46^{d}	11.24 ± 0.14^{b}	116.9 ± 1.76^{b}	0.291 ± 0.020^{c}	0.401 ± 0.08^{b}
	Zein/LF	98.31 ± 4.12^{a}	25.41 ± 0.43^{c}	82.3 ± 1.01^{c}	0.321 ± 0.014^{d}	0.145 ± 0.05^{c}
	Zein/LF 10K	98.66 ± 3.54^{a}	19.74 ± 0.23^{c}	95.6 ± 1.41^{c}	0.345 ± 0.037^{bc}	0.230 ± 0.09^{c}
	Zein/LF 40K	99.41 ± 4.14^{a}	21.45 ± 0.31^{c}	85.79 ± 0.87^{c}	0.334 ± 0.047^{d}	0.138 ± 0.02^{c}
	Zein/LF 70K	99.21 ± 4.14^{a}	21.31 ± 0.51^{c}	85.64 ± 1.26^{c}	0.330 ± 0.034^{d}	0.127 ± 0.06^{c}
10:1	Redissolved Zein/LF	92.66 ± 3.54^{a}	24.31 ± 0.32^{c}	103.6 ± 1.41^{c}	0.265 ± 0.037^{bc}	0.165 ± 0.05^{c}
	Redissolved Zein/LF 10K	93.43 ± 2.56^{a}	18.43 ± 0.41^{c}	108.2 ± 1.43^{c}	0.273 ± 0.024^{bc}	0.267 ± 0.04^{c}
	Redissolved Zein/LF 40K	94.21 ± 3.21^{a}	21.01 ± 0.24^{c}	105.3 ± 1.75^{c}	0.281 ± 0.021^{bc}	0.154 ± 0.03^{c}
	Redissolved Zein/LF 70K	94.25 ± 4.35^{a}	21.13 ± 0.32^{c}	105.7 ± 1.24^{c}	0.278 ± 0.042^{bc}	0.152 ± 0.03^{c}

Values are the means ± SD (n = 3). Different letters in the same column indicate significant differences ($p < 0.05$) based on one-way ANOVA followed by Tukey's honest significant difference post-hoc tests.

Differential Scanning Calorimetry

As a thermal and crystallographic analysis technique, DSC was used to understand the thermal behavior associated with phase transformation of biomaterials *via* thermodynamic characterization (37). As shown in **Figure 5A**, for the pure 7,8-DHF, the embedded thermograms showed a narrow and sharp peak at 246.24°C, which might be attributed to the melting of 7,8-DHF crystals (38). Besides, compared with other flavonoids, such as curcumin (39), the endothermic peak of 7,8-DHF was higher. The DSC curve of zein exhibited broad endothermic peaks at around 71.12°C, this result was less than the reports of Dai et al. (40), which showed that endothermic peaks of zein were at around 81.16°C. Furthermore, the characteristic endothermal peak of LF, LF 10K, LF 40K, and LF 70K was at around 75.41, 80.56, 86.22, and 88.12°C, respectively, confirming that glycosylation reactions jointed with polysaccharides improved the thermostability of LF. After Maillard reaction, its affinity with bound water became strong (41), and the polysaccharide chain was longer, the binding water ability was stronger. After 7,8-DHF encapsulation, no distinctive endothermic peaks of 7,8-DHF in DHF-zein, DHF-zein/LF, DHF-zein/LF 10K, DHF-zein/LF 40K, and DHF-zein/LF 70K were discovered, which suggested that 7,8-DHF changed from the crystalline state to the amorphous state. Some similar observations have been reported about curcumin (42) and β-carotene (43). Besides, the endothermic peak of DHF-zein was decreased from 71.12 to 68.57°C compared with bare zein nanoparticles (**Figure 5B**), the decrease in melting temperatures might be attributed to intermolecular interactions between 7,8-DHF and zein. In addition, Wei et al. reported the existence of resveratrol declined the thermal stability of zein nanoparticles (44). Most intriguingly, after adding native LF and glycosylated LF, the endothermic peak of DHF-zein/LF, DHF-zein/LF 10K, DHF-zein/LF 40K, and DHF-zein/LF 70K was shifted to 72.61, 75.74, 80.89, and 85.60°C (**Figure 5B**), indicating that they improved the thermal stability of DHF-Zein nanoparticles, particularly LF 70K.

X-Ray Diffraction

X-ray diffraction ranging from 5 to 90 degrees at 2θ values was applied to examine the physical state of 7,8-DHF in different nanoparticles. As known in **Figure 6**, 7,8-DHF was extremely crystalline with multiple sharp diffraction peaks at the 5–40 degrees range. In contrast, when the diffraction angles of zein and LF in the 2θ range were 9.3 and 19.6 degrees and 9.7 and 18.6 degrees, respectively, two flat humps without sharp diffraction maximum have appeared in the XRD spectrum, besides, LF 10K, 40K, and 70K had similar peak pattern to native LF, indicating that glycosylated LF were all in an amorphous form (40). However, no distinctly characteristic diffraction maximum for 7,8-DHF was found in zein/glycosylated LF composite nanoparticles. Such behavior indicated 7,8-DHF was completely loaded into zein/LF 10K, 40K, 70K, and existing in an amorphous state. This discovery confirmed the results based on DSC analysis. Furthermore, similar outcomes were discovered by previous studies about coenzyme Q10, curcumin, and resveratrol (45–47). Astonishingly, in contrast to DHF-zein, the diffraction peak of DHF-zein/LF and 70K at 19.6 degrees was remarkably increased and the peaks of DHF-zein/LF 10K and 40K at these diffraction angles almost disappeared. This result can be explained that due to changes in the interactions (hydrophobic effect, hydrogen

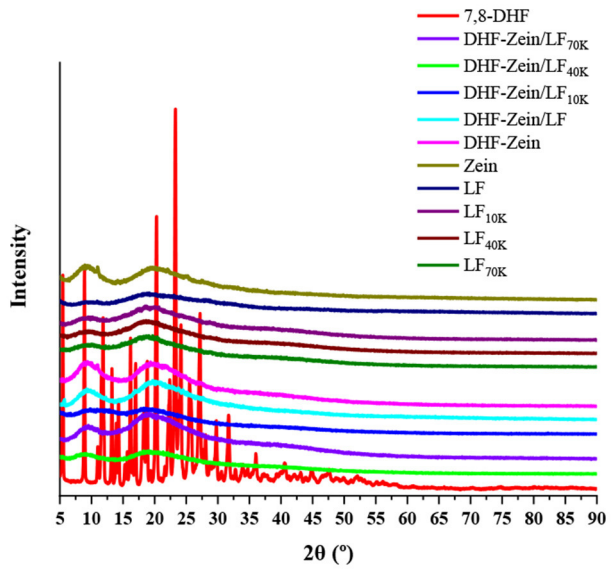

FIGURE 6 | X-ray diffraction (XRD) spectra of free 7,8-DHF, zein, LF, glycosylated LF DHF-zein, DHF-zein/LF, DHF-zein/LF 10K, DHF-zein/LF 40K, and DHF-zein/LF 70K.

bonding, and electrostatic interaction) along with zein, LF and glycosylated LF within the different systems, distinguishable behaviors of in DHF-zein, DHF-zein/LF, DHF-zein/LF 10K, DHF-zein/LF 40K, and DHF-zein/LF 70K were observed (44).

Fourier-Transform Infrared

Fourier-transform infrared is a versatile tool for monitoring changes within the functional groups of biopolymers and evaluating interactive force among components post-particle formation. As shown in **Figure 7**, the O–H group stretching characteristic peak of zein was 3,306 cm^{-1} (**Figure 7A**) (48). When zein was combined with glycosylated LF to form zein/LF 10K, 40K, and 70K, the hydrogen bonds characteristic peaks were transformed from 3,306 to 3,406 cm^{-1} and 3,404 and 3,417 cm^{-1}, respectively, indicating the hydrogen bonds existed in the binding of zein and glycosylated LF. Besides, the forming hydrogen bonds were stronger than that of Zein/LF. In addition, 2,953 cm^{-1} is considered to be the hydrophobic C–H group stretching vibration peak in zein (49). After the formation of zein/LF 10K, 40K, and 70K, their characteristic peaks redshifted from 2,953 to 2,932 cm^{-1} and 2,930 and 2,931 cm^{-1}, indicating that stronger hydrophobic interactions existed in the formation of zein/glycosylated LF nanoparticles compared with Zein/LF. According to Liu et al. report (35), the 1,652 cm^{-1} peak of zein was the C=O stretching (amide I). In addition, 1,538 cm^{-1} peak was primarily associated with the bending of N–H coupled with the stretching of C–N (amide II). With LF 10K, 40K, and 70K incorporation, the amide I and amide II characteristic peaks of zein/glycosylated LF nanoparticles had no change, elucidating that zein/glycosylated LF nanoparticles formation was not involved in electrostatic interaction (46). Additionally, hydrophobic interaction and hydrogen bonds among glycosylated LF and zein were confirmed by the result of DSC about the increasing endothermic peak temperature of nanoparticles.

As shown in **Figure 7A**, the peaks at 3,114, 1,626, 1,575, 1,405, 1,195, and 1,071 cm^{-1} were the typical peaks of 7,8-DHF, which has been confirmed in our foregoing research (11). Expectedly, these characteristic peaks of 7,8-DHF have vanished in DHF-zein, DHF-zein/LF, DHF-zein/LF 10K, DHF-zein/LF 40K, and DHF-zein/LF 70K, indicating that these nanoparticles successfully encapsulated for 7,8-DHF. Moreover, compared with the unloaded nanoparticles, the wavenumbers of the main characteristic peaks of the loaded nanoparticles were all changed, indicating that the presence of 7,8-DHF could also change the non-covalent binding ability of the composite carriers to some extent.

A Graphic Illustration for the Formation and Stability Mechanism of Nanoparticles

Diverse technologies, such as EE, PDI, particle size, zeta potential, turbidity, TEM, FE-SEM, DSC, XRD, and FTIR were applied to make clear formation and stability mechanism of zein/glycosylated LF delivery system (**Figure 8**). After zein was rapidly added into glycosylated LF (mass ratio 1:1), sufficient glycosylated LF acted as a shielding effect (electrostatic repulsion) and steric hindrance stabilizer was coated onto the surface of zein particles to stop their sedimentation, showing a low PDI, turbidity, and size based on DLS and UV. Especially in the high ionic strengths (0–500 mM NaCl) at wide pH 3–9 range condition, glycosylated LF played a stabilizing role *via* above-mentioned shielding effect and steric hindrance. And some internal drives (hydrogen bonding and hydrophobic effect) participated in the formation of zein/glycosylated LF nanoparticles according to FTIR and FE-SEM. Employing EE, XRD, DSC, TEM analysis, 7,8-DHF was successfully encapsulated in zein/glycosylated LF nanoparticles with relatively uniform sphericity, displaying a good entrapment efficiency.

Storage Stability of 7,8-DHF

To prevent food nutraceuticals from degradation by heat or light exposure is challenging but critically necessary during storage. To meet this application end, short and long storage were investigated under varying storage environments for DHF-zein/LF 10K, 40K, and 70K. As exhibited in **Figure 9A**, free 7,8-DHF was mostly degraded at 25°C with light exposure for 15 days post-storage. Encapsulation of the 7,8-DHF in zein nanoparticles strengthened the storage stability (12.35%) of 7,8-DHF. The addition of LF and glycosylated LF further significantly enhanced the stability of encapsulated 7,8-DHF, in particular glycosylated LF, among them, the retention percentage of DHF-Zein/LF 40K was highest (43.21%). As seen from **Figure 9B**, at 50°C under dark circumstances, a similar effect was observed. The active groups of 7,8-DHF were possibly protected within the hydrophobic lumen of zein/glycosylated LF nanoparticles as a mechanism (50), especially DHF-zein/LF 70K (46.33%). The above results were in conformance to preceding studies that introduced curcumin being embedded in zein and quaternized chitosan complexes, along with work showing that quercetagetin

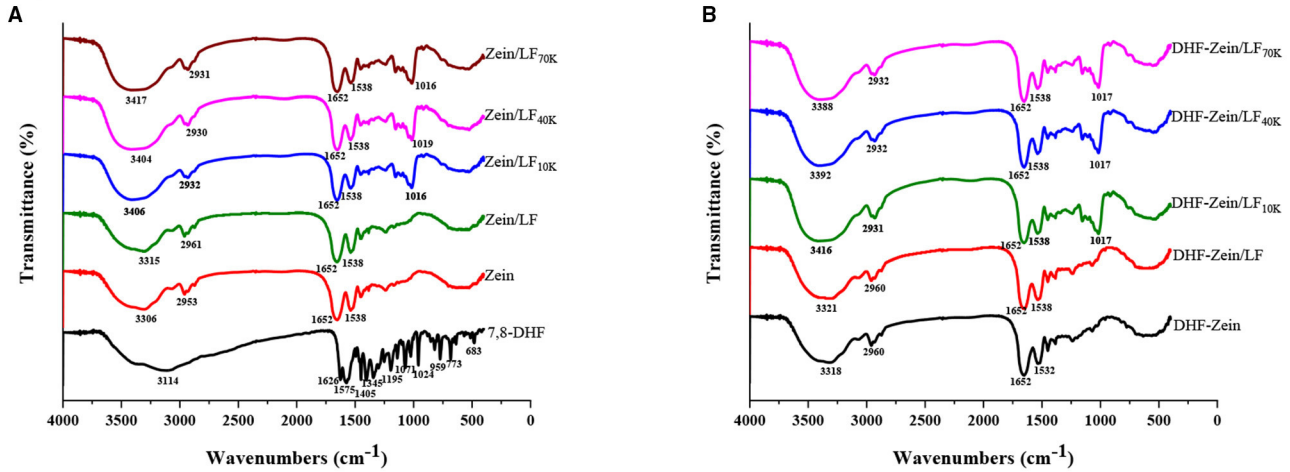

FIGURE 7 | Fourier-transform infrared spectra of free 7,8-DHF, zein, zein/LF, zein/LF 10K, zein/LF 40K, zein/LF 70K **(A)**, DHF-zein, DHF-zein/LF, DHF-zein/LF 10K, DHF-zein/LF 40K, and DHF-zein/LF 70K **(B)**.

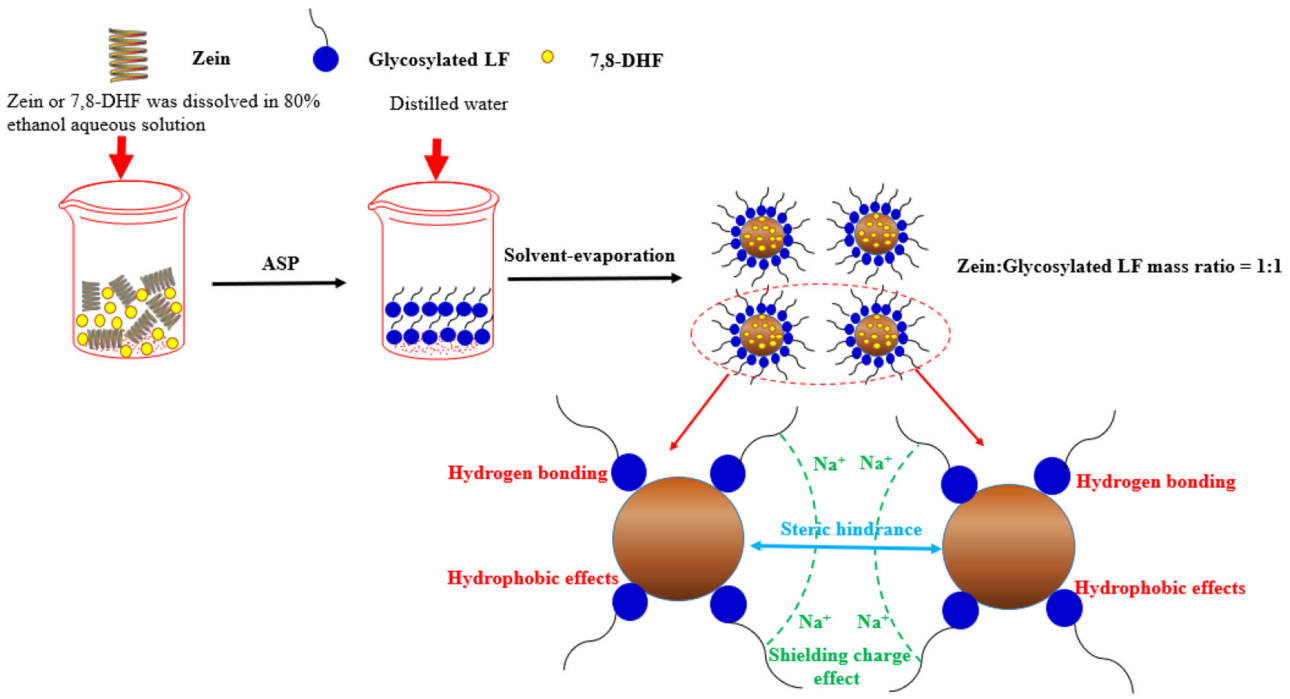

FIGURE 8 | An illustration of the formation and stability mechanism of DHF-zein/glycosylated LF.

was loaded within the zein-hyaluronic acid binary complex. Generally, the smaller the particle, the more susceptible it is to environmental factors, such as oxygen, light, and temperature. Therefore, the higher chemical stability of 7,8-DHF encapsulated in zein/glycosylated LF colloidal systems was probably due to the antioxidant activity of Maillard reaction products, which inhibited the chemical degradation of 7,8-DHF during storage. Above all, the existence of glycosylated LF enhanced the storage stability of 7,8-DHF.

In vitro Simulated Gastrointestinal Digestion

Effective protection of encapsulated nutritional ingredients throughout the gastrointestinal tract (GIT) is critical to assess carrier systems. In this study, an *in vitro* GIT model was applied to explore the digestive fate and bioaccessibility of 7,8-DHF in nanoparticles. Particle size changes for colloidal carriers were monitored at a specific digestion time (30, 60, 120, and 180 min),

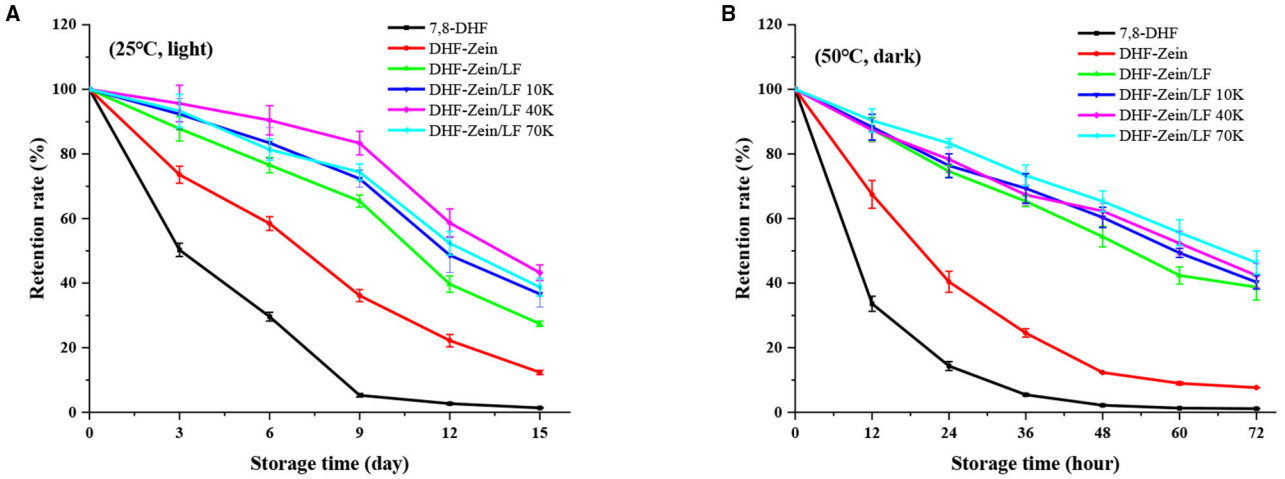

FIGURE 9 | Storage stability of free 7,8-DHF, DHF-zein, DHF-zein/LF, DHF-zein/LF 10K, DHF-zein/LF 40K, and DHF-zein/LF 70K at 25°C under light **(A)** and at 50°C under dark **(B)**.

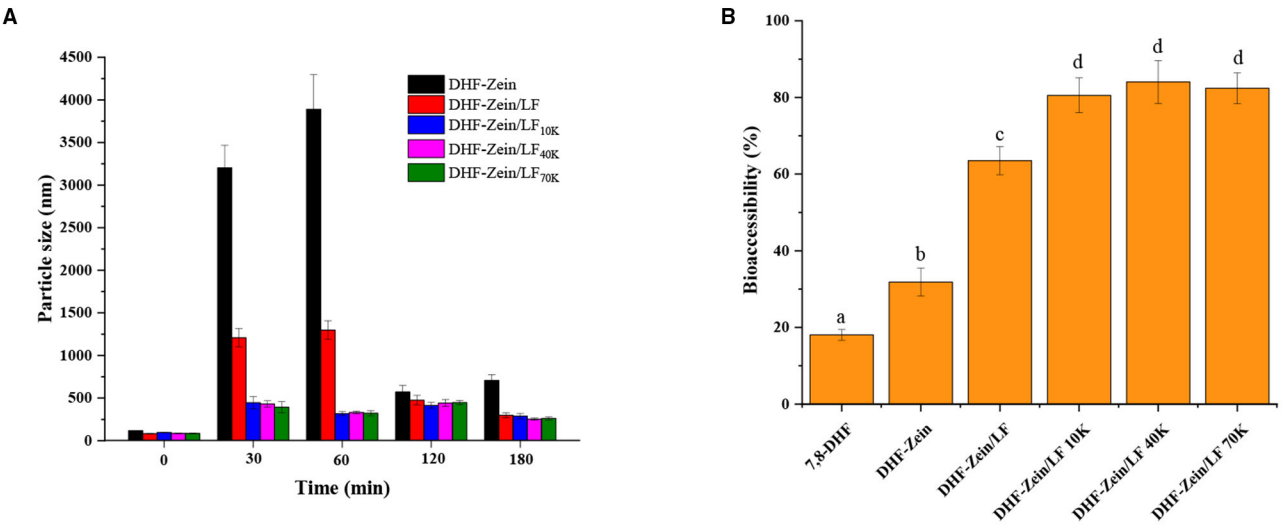

FIGURE 10 | Influence of *in vitro* digestion time on the particle size of DHF-zein, DHF-zein/LF, DHF-zein/LF 10K, DHF-zein/LF 40K, and DHF-zein/LF 70K **(A)**. *In vitro* bioaccessibility **(B)**.

and the results were observed in **Figure 10A**, the mean particle size of DHF-zein was increased markedly after 60 min SGF digestion compared with original particle size ($p < 0.05$). This finding was possibly due to that the nanoparticles were subjected to ionic strength along with low pH and partially digested *via* pepsase. The low pH and ionic strength exposure likely weakened electrostatic repulsion forces among zein nanoparticles. Besides, its particle size reduction in DHF-zein post-SIF-exposure was ascribed to the fact that SIF contained bile salt, a compound with strong emulsifying abilities. Bile salt can combine many biopolymer molecules and contribute to bridging flocculation (48). An identical consequence was observed by Zou et al. report for curcumin loaded in zein nanoparticles (51). Similarly, as depicted in **Figure 10A**, DHF-zein/LF occurred aggregation in the SIF digestion, this result was in accord with that of pH and salt stability, which was due to the attenuated electrostatic repulsion among them. But its particles were smaller than DHF-zein after SIF digestion. Most importantly, under the presence of glycosylated LF, the mean particle size of DHF-zein/LF 10K, 40K, and 70K was mildly increased after SGF digestion, then remained fixedness during SIF digestion compared with DHF-zein and DHF-zein/LF, illustrating that the presence of glycosylated LF improved the intestinal instability of these nanoparticles. This might be due to that the glycosylated LF coating on the nanoparticles provided a greater steric repulsion that conquers attractive force (such as hydrophobic

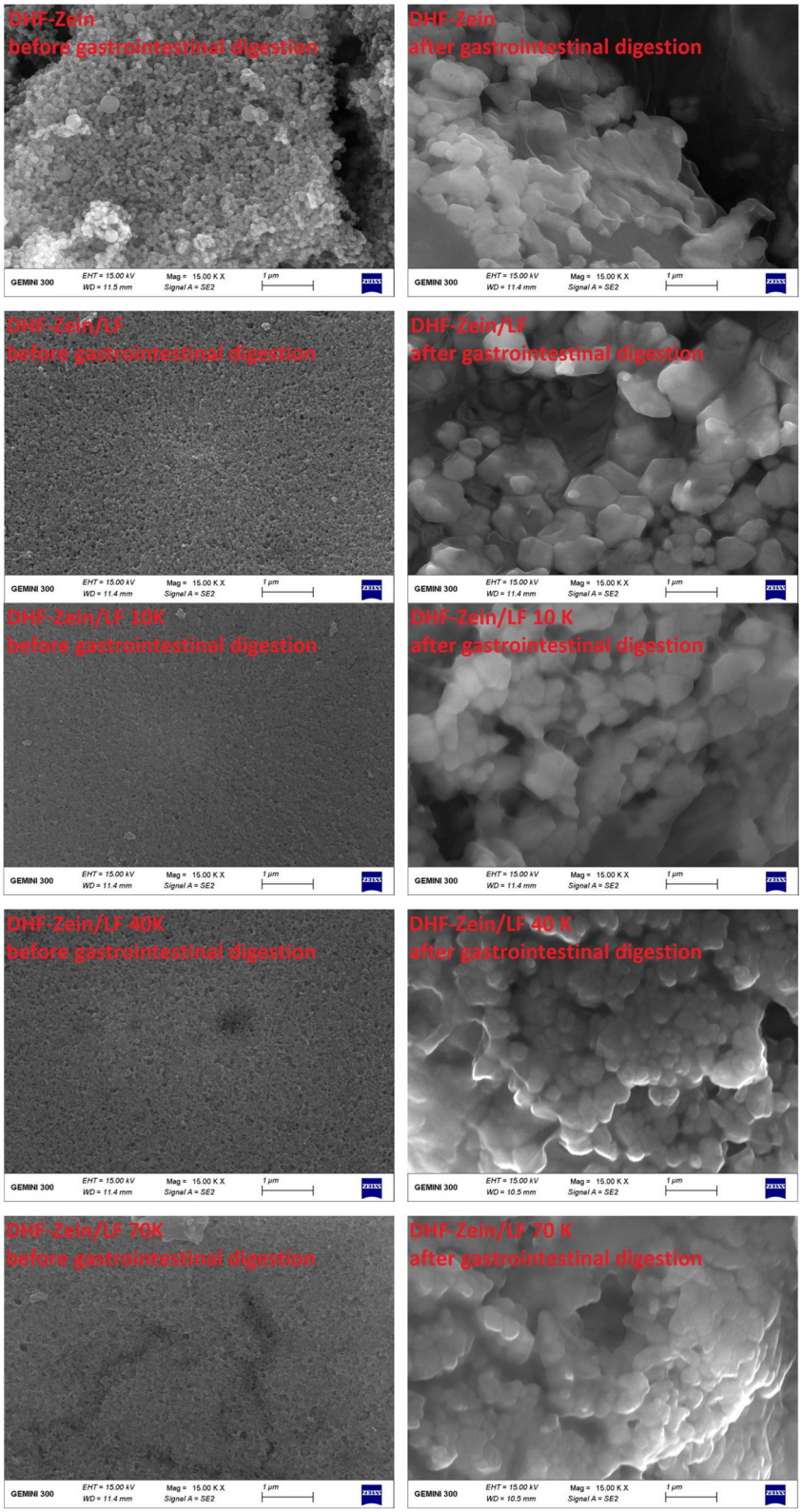

FIGURE 11 | Influence of *in vitro* digestion on the FE-SEM images of DHF-zein, DHF-zein/LF, DHF-zein/LF 10K, DHF-zein/LF 40K, and DHF-zein/LF 70K. Pictures were taken at ×15,000 magnifications.

interactions or Van der Waals), which aroused the interfacial layer surrounding the colloids by shielding effect against the ionic strength and enzyme. **Supplementary Figure 3** was about particle size distribution of each sample in origin, SGF and SIF digestion. In the SGF digestion, DHF-zein and DHF-zein/LF were mainly distributed in the range of 4,000–10,000 nm and 1,000–2,000 nm, respectively, and DHF-zein/glycosylated LF was mainly distributed in the range of 100–1,000 nm. Nevertheless, in the SIF digestion, particle size distribution of each sample tended to accordance, but there was bimodal particle size distribution with DHF-zein and DHF-zein/LF above 5,000 nm.

The FE-SEM microscopic observation furtherly confirmed that subjecting to GIT has a significant effect on the morphology of 7,8-DHF-loaded nano-complexes (**Figure 11**). DHF-zein had a spherical shape in initial conditions, after *in vitro* GIT, no spherical particle and a plate-like structure were found. This finding was unanimous to the conclusions of the anterior study (52). For DHF-zein/LF, after gastrointestinal digestion, their form changed from spherical to rectangular, this was because of a lot of aggregation in SGF digestion. However, it was amusing to notice a notably different morphology for DHF-Zein/glycosylated LF after digestion especially DHF-zein/LF 40K and 70K. They exhibited a relatively spherical morphology just like the cross-linked structure of large nanoparticles. Above all, glycosylated LF could effectively protect 7,8-DHF in delivery systems throughout GIT.

After being exposed to simulated gastrointestinal conditions, the bioaccessibility of 7,8-DHF was assayed after centrifugation and collection of micelle phases. As exhibited in **Figure 10B**, as its crystalline characteristic, the solubility of free 7,8-DHF was relatively low, its bioaccessibility was about 18.06% after digestion. As expected, the bioaccessibility of DHF-zein was raised to 31.85% ($p < 0.05$). In the presence of LF, its bioaccessibility increased to about 63.51%, there was a three-fold increase in comparison with free 7,8-DHF ($p < 0.05$). Most importantly, in the existence of glycosylated LF, the bioaccessibility of DHF-zein/LF 10K, 40K, and 70K all reached above 80%, particularly DHF-zein/LF 40K reached the maximum (84.05%). The higher bioaccessibility of encapsulated 7,8-DHF may be due to the following points. First, the amorphous form of 7,8-DHF is known to have a higher bioaccessibility and solubility than its crystalline form (53). Second, the partial digestion of glycosylated LF may lead to water-soluble peptides generation that can solubilize and bind to 7,8-DHF. Third, the surface of long-chain polysaccharides through steric hindrance and external charge shielding protected particles from ionic strength, enzymolysis, and interattraction. Above all, our results displayed that encapsulating 7,8-DHF in zein/glycosylated LF nanoparticles can promote a considerable increase in its *in vitro* bioaccessibility.

CONCLUSIONS

In the present study, three zein/glycosylated LF composite spherical nanoparticles (78.67–87.24 nm) were successfully fabricated by ASP method with low PDI (<0.230) and turbidity (<0.220) values. Glycosylated LF could result fully stabilize zein nanoparticles against precipitation or aggregation, exhibiting high stability to salt at a wide pH range of 3.0–9.0. Besides, zein/glycosylated LF exhibited good thermostability and long-term storage, particularly zein/LF 40K and 70K. These zein/glycosylated LF nanoparticles were formed by hydrophobic interactions and hydrogen bonding and successfully used to encapsulate hydrophobic 7,8-DHF through DSC, EE, FIRT, and XRD. Furthermore, zein/glycosylated LF nanoparticles had good redispersibility and increase EE of 7,8-DHF, the encapsulation of 7,8-DHF improved its short- or long-term storage stability. Most astonishingly, 7,8-DHF loaded in zein/glycosylated LF nanoparticles promoted its *in vitro* bioaccessibility, particularly DHF-zein/LF 40K. Overall, these results indicate that zein/glycosylated LF nanoparticles are efficient at encapsulating, retaining, and delivering 7,8-DHF and may therefore be utilized in dietary supplements and functional foods.

DATA AVAILABILITY STATEMENT

The original contributions presented in the study are included in the article/**Supplementary Material**, further inquiries can be directed to the corresponding author/s.

AUTHOR CONTRIBUTIONS

YC: conceptualization, methodology, resources, funding acquisition, and writing—original draft preparation. XG: software and formal analysis. LW and YS: investigation and data curation. QC: project administration. SL, YW, and GX: validation, writing—review and editing and supervision. All authors have read and agreed to the published version of the manuscript.

FUNDING

The authors are grateful for the grant provided by the Zhejiang Province Public Welfare Technology Application Research Project—National Cooperation Project (Grant Number LGJ21C20001), the Fund of Key Laboratory of Aquatic Product Processing, Ministry of Agriculture and Rural Affairs, China (Grant Number NYJG202104), the Fund of Guangdong Provincial Key Laboratory of Aquatic Product Processing and Safety (Grant Number GDPKLAPPS2101), the Guangxi Natural Science Foundation Program (grant number 2018GXNSFBA294015), the Zhejiang Province Xinmiao Talents Program (Grant Number 2021R403035), and the National College Students Innovation and Entrepreneurship Training Program (Grant Number 2021052 and 2021011).

SUPPLEMENTARY MATERIAL

The Supplementary Material for this article can be found online at: https://www.frontiersin.org/articles/10.3389/fnut.2021.806623/full#supplementary-material

REFERENCES

1. Andero R, Ressler K-J. Fear extinction and BDNF: translating animal models of PTSD to the clinic. *Genes Brain Behav.* (2012) 11:503–12. doi: 10.1111/j.1601-183X.2012.00801.x
2. Colombo P-S, Flamini G, Christodoulou M-S, Rodondi G, Vitalini S, Passarella D, et al. Farinose alpine Primula species: phytochemical and morphological investigations. *Phytochemistry.* (2014) 98:151–9. doi: 10.1016/j.phytochem.2013.11.018
3. Jang S, Liu X, Yepes M, Shepherd K-R, Miller G-W, Liu Y, et al. A selective TrkB agonist with potent neurotrophic activities by 7,8-dihydroxyflavone. *P Natl Acad Sci USA.* (2010) 107:2687–92. doi: 10.1073/pnas.0913572107
4. Li X-H, Dai C-F, Chen L, Zhou W-T, Han H-L, Dong Z-F. 7,8-dihydroxyflavone ameliorates motor deficits via suppressing α-synuclein expression and oxidative stress in the MPTP-induced mouse model of Parkinson's disease. *Cns Neurosci Ther.* (2016) 22:617–24. doi: 10.1111/cns.12555
5. Aytan N, Choi J, Carreras I, Crabtree L, Nguyen B, Lehar M, et al. Protective effects of 7,8-dihydroxyflavone on neuropathological and neurochemical changes in a mouse model of Alzheimer's disease. *Eur J Pharmacol.* (2018) 828:9–17. doi: 10.1016/j.ejphar.2018.02.045
6. Chan C-B, Tse M-C-L, Liu X, Zhang S, Schmidt R, Otten R, et al. Activation of muscular TrkB by its small molecular agonist 7,8-dihydroxyflavone sex-dependently regulates energy metabolism in diet-induced obese mice. *Chem Biol.* (2015) 22:355–68. doi: 10.1016/j.chembiol.2015.02.003
7. Chen C, Wang Z, Zhang Z, Liu X, Kang SS, Zhang Y, et al. The prodrug of 7,8-dihydroxyflavone development and therapeutic efficacy for treating Alzheimer's disease. *Proc Natl Acad Sci USA.* (2018) 115:578–83. doi: 10.1073/pnas.1718683115
8. Zhang J, Yao W, Dong C, Yang C, Ren Q, Ma M, et al. Comparison of ketamine, 7,8-dihydroxyflavone, and ANA-12 antidepressant effects in the social defeat stress model of depression. *Psychopharmacology.* (2015) 232:4325–35. doi: 10.1007/s00213-015-4062-3
9. Liu C, Chan C-B, Ye K. 7,8-dihydroxyflavone, a small molecular TrkB agonist, is useful for treating various BDNF-implicated human disorders. *Transl Neurodegener.* (2016) 5:1–9. doi: 10.1186/s40035-015-0048-7
10. Chen Y, Xue F, Xia G, Zhao Z, Chen C, Li Y, et al. Transepithelial transport mechanisms of 7,8-dihydroxyflavone, a small molecular TrkB receptor agonist, in human intestinal Caco-2 cells. *Food Funct.* (2019) 10:5215–27. doi: 10.1039/C9FO01007F
11. Chen Y, Xia G, Zhao Z, Xue F, Gu Y, Chen C, et al. 7,8-Dihydroxyflavone nano-liposomes decorated by crosslinked and glycosylated lactoferrin: storage stability, antioxidant activity, in vitro release, gastrointestinal digestion and transport in Caco-2 cell monolayers. *J Funct Foods.* (2020) 65:103742. doi: 10.1016/j.jff.2019.103742
12. Yan X, Zhang X, McClements D-J, Zou L, Liu X, Liu F. Co-encapsulation of epigallocatechin gallate (EGCG) and curcumin by two proteins-based nanoparticles: role of EGCG. *J Agr Food Chem.* (2019) 67:13228–36. doi: 10.1021/acs.jafc.9b04415
13. Ding J, Xu Z, Qi B, Cui S, Wang T, Jiang L, et al. Fabrication and characterization of soybean oil bodies encapsulated in maltodextrin and chitosan-EGCG conjugates: an *in vitro* digestibility study. *Food Hydrocolloid.* (2019) 94:519–27. doi: 10.1016/j.foodhyd.2019.04.001
14. Ma M, Yuan Y, Yang S, Wang Y, Lv Z. Fabrication and characterization of zein/tea saponin composite nanoparticles as delivery vehicles of lutein. *LWT.* (2020) 125:109270. doi: 10.1016/j.lwt.2020.109270
15. Penalva R, Esparza I, Larraneta E, González-Navarro C-J, Gamazo C, Irache J-M. Zein-based nanoparticles improve the oral bioavailability of resveratrol and its anti-inflammatory effects in a mouse model of endotoxic shock. *J Agr Food Chem.* (2015) 63:5603–11. doi: 10.1021/jf505694e
16. Zheng D, Zhang Q. Bioavailability enhancement of astilbin in rat through zein-caseinate nanoparticles. *J Agr Food Chem.* (2019) 67:5746–53. doi: 10.1021/acs.jafc.9b00018
17. Chen Y, Zhao Z, Xia G, Xue F, Chen C, Zhang Y. Fabrication and characterization of zein/lactoferrin composite nanoparticles for encapsulating 7,8-dihydroxyflavone: Enhancement of stability, water solubility and bioaccessibility. *Int J Biol Macromol.* (2020) 146:179–92. doi: 10.1016/j.ijbiomac.2019.12.251
18. Feng J, Wu S, Wang H, Liu S. Improved bioavailability of curcumin in ovalbumin-dextran nanogels prepared by Maillard reaction. *J Funct Foods.* (2016) 27:55–68. doi: 10.1016/j.jff.2016.09.002
19. Chen Y, Xia G, Zhao Z, Xue F, Chen C, Zhang Y. Formation, structural characterization, stability and *in vitro* bioaccessibility of 7,8-dihydroxyflavone loaded zein-/sophorolipid composite nanoparticles: effect of sophorolipid under two blending sequences. *Food Funct.* (2020) 11:1810–25. doi: 10.1039/C9FO02704A
20. Chen Y, Peng J, Wang Y, Wadhawan D, Wu L, Gao X, et al. Development, characterization, stability and bioaccessibility improvement of 7,8-dihydroxyflavone loaded zein/sophorolipid/polysaccharide ternary nanoparticles: comparison of sodium alginate and sodium carboxymethyl cellulose. *Foods.* (2021) 10:2629. doi: 10.3390/foods10112629
21. Yuan Y, Li H, Liu C, Zhang S, Xu Y, Wang D. Fabrication and characterization of lutein-loaded nanoparticles based on zein and sophorolipid: enhancement of water solubility, stability, and bioaccessibility. *J Agr Food Chem.* (2019) 67:11977–85. doi: 10.1021/acs.jafc.9b05175
22. Wang B, Timilsena Y-P, Blanch E, Adhikari B. Lactoferrin: structure, function, denaturation and digestion. *Crit Rev Food Sci.* (2019) 59:580–96. doi: 10.1080/10408398.2017.1381583
23. Hafsa J, Smach M-A, Mrid R-B, Sobeh M, Majdoub H, Yasri A. Functional properties of chitosan derivatives obtained through Maillard reaction: a novel promising food preservative. *Food Chem.* (2021) 349:129072. doi: 10.1016/j.foodchem.2021.129072
24. Tan J, Liu T, Yao Y, Wu N, Du H, Xu M, et al. Changes in physicochemical and antioxidant properties of egg white during the Maillard reaction induced by alkali. *LWT.* (2021) 143:111151. doi: 10.1016/j.lwt.2021.111151
25. Fan F, Liu M, Shi P, Xu S, Lu W, Du M. Effects of thermal treatment on the physicochemical properties and osteogenic activity of lactoferrin. *J Food Process Pres.* (2019) 43:e14068. doi: 10.1111/jfpp.14068
26. Li M, Li X, McClements D-J, Shi M, Shang Q, Liu X, et al. Physicochemical and functional properties of lactoferrin-hyaluronic acid complexes: effect of non-covalent and covalent interactions. *LWT.* (2021) 151:112121. doi: 10.1016/j.lwt.2021.112121
27. Jiang W, Zhou Z, Wang D, Zhou X, Tao R, Yang Y, et al. Transglutaminase catalyzed hydrolyzed wheat gliadin grafted with chitosan oligosaccharide and its characterization. *Carbohyd Polym.* (2016) 153:105–14. doi: 10.1016/j.carbpol.2016.07.097
28. Liu F, Sun C, Yang W, Yuan F, Gao Y. Structural characterization and functional evaluation of lactoferrin-polyphenol conjugates formed by free-radical graft copolymerization. *Rsc Adv.* (2015) 5:15641–51. doi: 10.1039/C4RA10802G
29. Raychaudhuri R, Pandey A, Das S, Nannuri S-H, Joseph A, George S-D, et al. Nanoparticle impregnated self-supporting protein gel for enhanced reduction in oxidative stress: a molecular dynamics insight for lactoferrin-polyphenol interaction. *Int J Biol Macromol.* (2021) 189:100–13. doi: 10.1016/j.ijbiomac.2021.08.089
30. Lancelot E, Fontaine J, Grua-Priol J, Assaf A, Thouand G, Le-Bail A. Study of structural changes of gluten proteins during bread dough mixing by Raman spectroscopy. *Food Chem.* (2021) 358:129916. doi: 10.1016/j.foodchem.2021.129916
31. Davidov-Pardo G, Joye I-J, Espinal-Ruiz M, McClements D-J. Effect of maillard conjugates on the physical stability of zein nanoparticles prepared by liquid antisolvent coprecipitation. *J Agr Food Chem.* (2015) 63:8510–18. doi: 10.1021/acs.jafc.5b02699
32. Li H, Yuan Y, Zhu J, Wang T, Wang D, Xu Y. Zein/soluble soybean polysaccharide composite nanoparticles for encapsulation and oral delivery of lutein. *Food Hydrocolloid.* (2020) 103:105715. doi: 10.1016/j.foodhyd.2020.105715
33. Hu K, McClements D-J. Fabrication of biopolymer nanoparticles by antisolvent precipitation and electrostatic deposition: zein-alginate core/shell nanoparticles. *Food Hydrocolloid.* (2015) 44:101–8. doi: 10.1016/j.foodhyd.2014.09.015
34. Sun C, Dai L, Gao Y. Binary complex based on zein and propylene glycol alginate for delivery of quercetagetin. *Biomacromolecules.* (2016) 17:3973–85. doi: 10.1021/acs.biomac.6b01362
35. Liu F, Ma C, McClements D-J, Gao Y. A comparative study of covalent and non-covalent interactions between zein and

polyphenols in ethanol-water solution. *Food Hydrocolloid.* (2017) 63:625–34. doi: 10.1016/j.foodhyd.2016.09.041
36. Hasankhan S, Tabibiazar M, Hosseini S-M, Ehsani A, Ghorbani M. Fabrication of curcumin-zein-ethyl cellulose composite nanoparticles using antisolvent co-precipitation method. *Int J Biol Macromol.* (2020) 163:1538–45. doi: 10.1016/j.ijbiomac.2020.08.045
37. Yoon H, Seo T, Lim S. Stabilization of aqueous dispersion of CoQ_{10} nanoparticles using maize starches. *Food Hydrocolloid.* (2014) 35:144–9. doi: 10.1016/j.foodhyd.2013.05.008
38. Narwal S, Kumar A, Chaudhary M, Budhwar V. Formulation of eutectic mixture of curcumin with salicylic acid for improving its dissolution profile. *Res J Pharm Technol.* (2021) 14:1875–9. doi: 10.52711/0974-360X.2021.00331
39. Hu K, Huang X, Gao Y, Huang X, Xiao H, McClements D-J. Core-shell biopolymer nanoparticle delivery systems: synthesis and characterization of curcumin fortified zein-pectin nanoparticles. *Food Chem.* (2015) 182:275–81. doi: 10.1016/j.foodchem.2015.03.009
40. Dai L, Sun C, Wei Y, Zhan X, Mao L, Gao Y. Formation and characterization of zein-propylene glycol alginate-surfactant ternary complexes: effect of surfactant type. *Food Chem.* (2018) 258:321–30. doi: 10.1016/j.foodchem.2018.03.077
41. Luo Y, Zhang B, Whent M, Yu L-L, Wang Q. Preparation and characterization of zein/chitosan complex for encapsulation of α-tocopherol, and its *in vitro* controlled release study. *Colloids Surf B Biointerf.* (2011) 85:145–52. doi: 10.1016/j.colsurfb.2011.02.020
42. Jiang F, Yang L, Wang S, Ying X, Ling J, Ouyang X-K. Fabrication and characterization of zein-alginate oligosaccharide complex nanoparticles as delivery vehicles of curcumin. *J Mol Liq.* (2021) 342:116937. doi: 10.1016/j.molliq.2021.116937
43. Wang M, Fu Y, Chen G, Shi Y, Li X, Zhang H, et al. Fabrication and characterization of carboxymethyl chitosan and tea polyphenols coating on zein nanoparticles to encapsulate β-carotene by anti-solvent precipitation method. *Food Hydrocolloid.* (2018) 77:577–87. doi: 10.1016/j.foodhyd.2017.10.036
44. Wei Y, Yu Z, Lin K, Sun C, Dai L, Yang S, et al. Fabrication and characterization of resveratrol loaded zein-propylene glycol alginate-rhamnolipid composite nanoparticles: physicochemical stability, formation mechanism and *in vitro* digestion. *Food Hydrocolloid.* (2019) 95:336–48. doi: 10.1016/j.foodhyd.2019.04.048
45. Dai L, Sun C, Li R, Mao L, Liu F, Gao Y. Structural characterization, formation mechanism and stability of curcumin in zein-lecithin composite nanoparticles fabricated by antisolvent co-precipitation. *Food Chem.* (2017) 237:1163–71. doi: 10.1016/j.foodchem.2017.05.134
46. Wei Y, Zhang L, Yu Z, Lin K, Yang S, Dai L, et al. Enhanced stability, structural characterization and simulated gastrointestinal digestion of coenzyme Q10 loaded ternary nanoparticles. *Food Hydrocolloid.* (2019) 94:333–44. doi: 10.1016/j.foodhyd.2019.03.024
47. Huang X, Dai Y, Cai J, Zhong N, Xiao H, McClements D-J, et al. Resveratrol encapsulation in core-shell biopolymer nanoparticles: impact on antioxidant and anticancer activities. *Food Hydrocolloid.* (2017) 64:157–65. doi: 10.1016/j.foodhyd.2016.10.029
48. Dai L, Li R, Wei Y, Sun C, Mao L, Gao Y. Fabrication of zein and rhamnolipid complex nanoparticles to enhance the stability and *in vitro* release of curcumin. *Food Hydrocolloid.* (2018) 77:617–28. doi: 10.1016/j.foodhyd.2017.11.003
49. Khan M-A, Chen L, Liang L. Improvement in storage stability and resveratrol retention by fabrication of hollow zein-chitosan composite particles. *Food Hydrocolloid.* (2021) 113:106477. doi: 10.1016/j.foodhyd.2020.106477
50. Wang W, Liu F, Gao Y. Quercetagetin loaded in soy protein isolate–κ-carrageenan complex: fabrication mechanism and protective effect. *Food Res Int.* (2016) 83:31–40. doi: 10.1016/j.foodres.2016.02.012
51. Zou L, Zheng B, Zhang R, Zhang Z, Liu W, Liu C, et al. Enhancing the bioaccessibility of hydrophobic bioactive agents using mixed colloidal dispersions: curcumin-loaded zein nanoparticles plus digestible lipid nanoparticles. *Food Res Int.* (2016) 81:74–82. doi: 10.1016/j.foodres.2015.12.035
52. Parris N, Cooke P-H, Hicks K-B. Encapsulation of essential oils in zein nanospherical particles. *J Agr Food Chem.* (2005) 53:4788–92. doi: 10.1021/jf040492p
53. Muhoza B, Zhang Y, Xia S, Cai J, Zhang X, Su J. Improved stability and controlled release of lutein-loaded micelles based on glycosylated casein via Maillard reaction. *J Funct Foods.* (2018) 45:1–9. doi: 10.1016/j.jff.2018.03.035

Conflict of Interest: The authors declare that the research was conducted in the absence of any commercial or financial relationships that could be construed as a potential conflict of interest.

Publisher's Note: All claims expressed in this article are solely those of the authors and do not necessarily represent those of their affiliated organizations, or those of the publisher, the editors and the reviewers. Any product that may be evaluated in this article, or claim that may be made by its manufacturer, is not guaranteed or endorsed by the publisher.

frontiers in Nutrition

ORIGINAL RESEARCH
published: 13 January 2022
doi: 10.3389/fnut.2021.812119

Encapsulation of Docosahexaenoic Acid Oil Substantially Improves the Oxylipin Profile of Rat Tissues

Jun Wang[1,2], *Jordane Ossemond*[1,2], *Yann Le Gouar*[1,2], *Françoise Boissel*[1,2], *Didier Dupont*[1,2] *and Frédérique Pédrono*[1,2]*

[1] French National Research Institute for Agriculture, Food and Environment (INRAE), Mixed Research Units of Science and Technology of Milk and Eggs (STLO), Rennes, France, [2] Institut Agro, Agrocampus Ouest, Rennes, France

Docosahexaenoic acid (DHA) is a major n-3 polyunsaturated fatty acid (PUFA) particularly involved in cognitive and cardiovascular functions. Due to the high unsaturation index, its dietary intake form has been considered to improve oxidation status and to favor bioaccessibility and bioavailability as well. This study aimed at investigating the effect of DHA encapsulated with natural whey protein. DHA was dietary provided as triacylglycerols to achieve 2.3% over total fatty acids. It was daily supplied to weanling rats for four weeks in omelet as food matrix, consecutively to a 6-hour fasting. First, when DHA oil was encapsulated, consumption of chow diet was enhanced leading to promote animal growth. Second, the brain exhibited a high accretion of 22.8% DHA, which was not improved by dietary supplementation of DHA. Encapsulation of DHA oil did not greatly affect the fatty acid proportions in tissues, but remarkably modified the profile of oxidized metabolites of fatty acids in plasma, heart, and even brain. Specific oxylipins derived from DHA were upgraded, such as Protectin Dx in heart and 14-HDoHE in brain, whereas those generated from n-6 PUFAs were mainly mitigated. This effect did not result from oxylipins measured in DHA oil since DHA and EPA derivatives were undetected after food processing. Collectively, these data suggested that dietary encapsulation of DHA oil triggered a more efficient absorption of DHA, the metabolism of which was enhanced more than its own accretion in our experimental conditions. Incorporating DHA oil in functional food may finally improve the global health status by generating precursors of protectins and maresins.

Keywords: DHA, encapsulation, oxylipin, brain, heart, rat

OPEN ACCESS

Edited by:
Weilin Liu,
Zhejiang Gongshang University, China

Reviewed by:
Belur Lokesh,
Central Food Technological Research Institute (CSIR), India
Dr.Sugasini Dhavamani,
University of Illinois at Urbana-Champaign, United States
Yufeng Chen,
Zhejiang University of Technology, China

***Correspondence:**
Frédérique Pédrono
frederique.pedrono@agrocampus-ouest.fr

Specialty section:
This article was submitted to Food Chemistry, a section of the journal Frontiers in Nutrition

Received: *09 November 2021*
Accepted: *15 December 2021*
Published: *13 January 2022*

Citation:
Wang J, Ossemond J, Le Gouar Y, Boissel F, Dupont D and Pédrono F (2022) Encapsulation of Docosahexaenoic Acid Oil Substantially Improves the Oxylipin Profile of Rat Tissues. Front. Nutr. 8:812119. doi: 10.3389/fnut.2021.812119

INTRODUCTION

Docosahexaenoic acid (DHA, 22:6n-3) is an essential n-3 polyunsaturated fatty acid (PUFA), mainly known for its health benefits on brain and heart. This bioactive compound presents a large range of beneficial outcomes inherent to the modulation of both membrane structure and cell functions. Therefore, DHA improves neurological activities by enhancing neurogenesis and synaptic plasticity, or by reducing neuroinflammation (1). Its high body level is related to the lower risk of developing cardiovascular disease (2, 3) and myocardial infarction as well (4). The functionality of DHA is likely to be mostly implemented through the synthesis of derivatives such as oxidized metabolites of FA (oxylipins) or endocannabinoid-like mediators. These derivatives may be generated either from DHA itself or from other FA, such as arachidonic acid (ARA, 20:4n-6),

dihomo-α-linolenic acid (DGLA, 20:3n-6), linoleic acid (LA, 18:2n-6), and eicosapentaenoic acid (EPA, 20:5n-3). DHA accumulates, indeed, in cell membranes concomitantly with the reduction of n-6 FA, principally ARA, or is retroconverted into EPA. Therefore, the effect of DHA may be attributed both to the rise of its own derivatives and the decline of derivatives synthesized from other FA. Many studies have reviewed the importance of the dietary supply of DHA as a strategy to increase tissue DHA concentrations (5–7). Although modulating the FA content in brain still represents a challenge comparatively to other tissues, dietary interventions may be effective in targeting serum lipid pools important for brain DHA uptake (8). Thereby, several works have shown a higher (9–11) or equal (12–14) bioavailability of DHA esterified to phospholipids (PL) in comparison to DHA esterified to triacylglycerols (TAG). Other works are more controversial (15, 16), insomuch as a higher concentration of circulating DHA would not predict brain accretion of DHA (17–19). Furthermore, dietary supplementation of DHA was shown to generate higher levels of its oxygenated derivatives as oxylipins (20, 21). These lipid mediators are synthesized from PUFA by cyclooxygenase, lipoxygenase, or cytochrome P450 ω-hydroxylase or epoxygenase enzymes, or by non-enzymatic autoxidation (22). The oxylipin pattern depends both on the dietary intake of n-6 or n-3 PUFA, and on the endogenous synthesis of long-chain PUFA considering enzyme competition between n-6 and n-3 families in tissues. The structural diversity of oxylipins is notably high for most of the PUFA and foreshadows a diversity of biological functions as well. Hence, these essential signaling messengers are usually involved in physiological responses to maintain homeostasis, contain infection or restrain inflammation process by acting through specific membrane receptors (23, 24). More particularly, oxygenation of DHA forms docosanoids, including specialized pro-resolving mediators (SPM) such as maresins, D-resolvins, and protectins (25). The literature reports their bioactive implying on pathophysiological process as they improve immune response, resolution of neuro-inflammation, or other metabolic disorders including diabetes, atherosclerosis, non-alcoholic fatty liver disease, or hepatic steatosis (26–30). These pleiotropic properties justify the interest for DHA, and its food intake other than based on PL or TAG esterification has to be considered as well.

An alternative approach to optimize dietary DHA intake is the use of functional food based on encapsulation. The food-grade delivery system was originally developed to protect bioactive ingredients notably from degradation such as oxidation. Many techniques using different encapsulant materials were processed in diverse food matrices for this purpose (31). Nevertheless, controlling the colloidal state of lipophilic molecules underlies the control of composition, size, and surface characteristics of particles, to ensure the required bioavailability. Pickering emulsification of food oil has recently received substantial interest as it relies more specifically on adsorption of bioparticles rather than synthetic surfactants to the oil-water interface, which confers resistance to droplet coalescence and improves the stability of emulsion (32–34). In this study, Pickering emulsion was prepared with natural whey protein to encapsulate DHA enriched-TAG, as previously described (35). Although fermented milk products are widely used as a vector of encapsulated nutrients, our previous study showed that eggs present an interesting bioavailability of DHA according to the recipe (omelet, hard-boiled egg, or mousse) (36). In the present study, DHA was therefore encapsulated in heat-denatured whey proteins. Whey protein isolate is commonly used in food industry due to a variety of functionalities such as emulsification or gelation properties. The heat-denatured form was favored in this study considering the cooking process that needed to be applied during the food manufacture. For this reason, whey protein-based microcapsules of DHA oil were incorporated into eggs and baked thereafter as omelets. Then, the rats were daily fed with DHA enriched-omelet for four weeks. The effect of encapsulation was finally assessed on DHA accretion, specifically in brain and heart, and subsequently on FA derivative formation such as oxylipins.

Abbreviations: ALA, α-Linolenic acid (18:3n-3); ARA, Arachidonic acid (20:4n-6); Control, omelet without DHA supplementation; DGLA, Dihomo-α-linolenic acid (20:3n-6); DHA, Docosahexaenoic acid (22:6n-3); DHEA, Docosahexaenoyl ethanolamide; DMA, Dimethylacetal; DPA, Docosapentaenoic acid (22:5n-3); 5,6-EET, (±)5(6)-Epoxy-8Z,11Z,14Z-eicosatrienoic acid; 8,9-EET, (±)8(9)-Epoxy-5Z,11Z,14Z-eicosatrienoic acid; 11,12-EET, (±)11(12)-Epoxy-5Z,8Z,14Z-eicosatrienoic acid; 14,15-EET, (±)14(15)-Epoxy-5Z,8Z,11Z-eicosatrienoic acid; EN-DHA-O, Encapsulated DHA oil in omelet; EPA, Eicosapentaenoic acid (20:5n-3); FA, Fatty acid; FAME, Fatty acid methyl ester; H-diet, Habituation diet; 14-HDoHE, (±)14-Hydroxy-4Z,7Z,10Z,12E,16Z,19Z-docosahexaenoic acid; 17-HDoHE, (±)17-Hydroxy-4Z,7Z,10Z,13Z,15E,19Z-docosahexaenoic acid; 18-HEPE, (±)18-Hydroxy-5Z,8Z,11Z,14Z,16E-eicosapentaenoic acid; 5-HETE, 5(S)-Hydroxy-5Z,8Z,11Z,13E-eicosatetraenoic acid; 8-HETE, (±)8-Hydroxy-5Z,9E,11Z,14Z-eicosatetraenoic acid; 12-HETE, 12(S)-Hydroxy-5Z,8Z,10E,14Z-eicosatetraenoic acid; 15-HETE, 15(S)-Hydroxy-5Z,8Z,11Z,13E-eicosatetraenoic acid; 9-HODE, 9-Hydroxy-10E,12Z-octadecadienoic acid; 13-HODE, 13-Hydroxy-9Z,11E-octadecadienoic acid; LA, Linoleic acid (18:2n-6); 5-oxo-ETE, 5-oxo-6E,8Z,11Z,14Z-eicosatetraenoic acid; PGD_2, Prostaglandin D_2; PDx, Protectin Dx; PGE_2, Prostaglandin E_2; $6kPGF_1\alpha$, 6-keto prostaglandin $F_1\alpha$; $PGF_2\alpha$, Prostaglandin $F_2\alpha$; 15d-PGJ_2, 15-deoxy-delta-12,14-prostaglandin J_2; PL, Phospholipid; PUFA, Polyunsaturated fatty acids; RBC, Red blood cells; TAG, Triacylglycerol; T-diet, Treatment diet; TXB_2, Thromboxane B_2; UN-DHA-O, Unencapsulated DHA oil in omelet.

MATERIALS AND METHODS

Animal Experiment

All handling protocols performed complied with the European Union Guideline for animal care and use (2010/63/CEE; decree 2013-118). The present project was authorized by the French Ministry of Higher Education and Research under the number 27678-2020100615388160 v3. Male Wistar rats (3 weeks-old) were supplied by the Janvier Labs Breeding Center (Le Genest-Saint-Isle, France). The animal experiment was performed at ARCHE Biosit (University of Rennes I, Campus of Villejean, Rennes, France). They were randomly divided into 3 groups of 8 animals and housed in pairs. They were acclimated for one week with the habituation diet (H-diet) and were then fed with the treatment diet (T-diet) for four weeks (**Figure 1**). During this period, the rats were daily fasted from 9 a.m. to 3 p.m. Each group then received 3g per rat of omelet containing no DHA, DHA oil, or encapsulated-DHA oil. Thereby, the rats

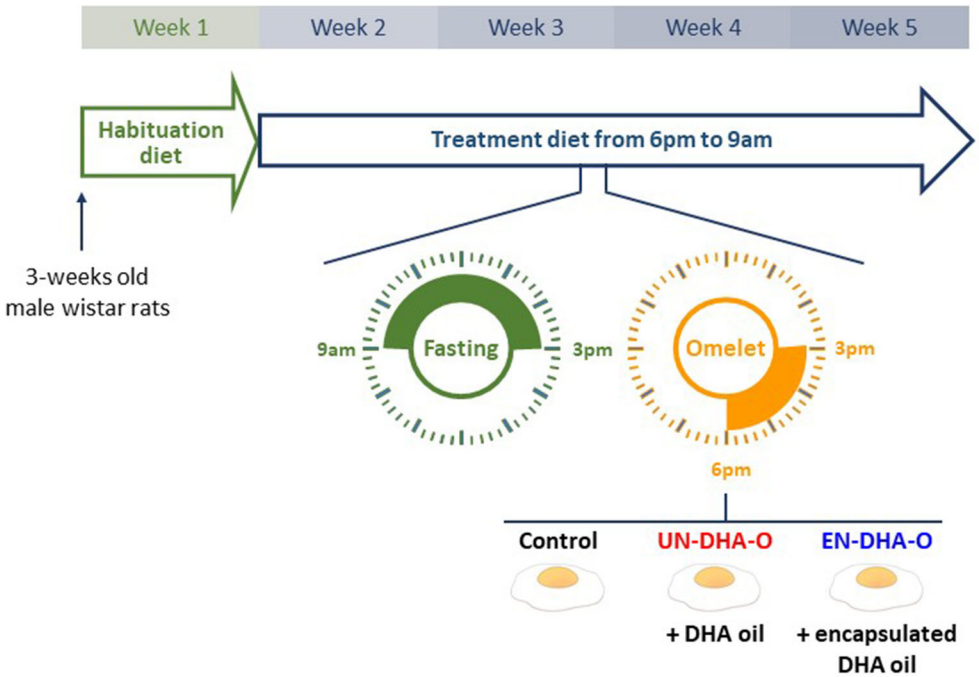

FIGURE 1 | The experimental design. Rats were acclimated with the habituation diet for one week. They were then fed with the treatment diet (T-diet) for four weeks. During this period, the rats were daily fasted for 6 hours before receiving 3g of omelet containing DHA as oil (UN-DHA-O) or as encapsulated oil (EN-DHA-O).

were separated for three hours by a plexiglass plate positioned in the middle of the cage, allowing individual consumption of omelet serving while guaranteeing eye and smell contact between congeners. At 6 p.m., the T-diet was restored until the next morning. The animals had access to water *ad libitum*. Rodent chows (H-diet and T-diet) were distributed *ad libitum* as well at the indicated time slots. After four weeks of experiment, the fasted rats were anesthetized with intraperitoneal injections of ketamine (100 mg/kg, Imalgene®1000, Mérial, Lyon, France) and xylazine (10mg/kg, Rompun® 2%, Bayer Animal Health, Puteaux, France). Blood was collected in heparin tubes by cardiac puncture. Plasma was separated from red blood cells (RBC) by centrifugation (2000 rpm, 15 min, 15 °C). Eyes were sampled in phosphate buffer saline whereas liver, heart, and brain (frontal cortex was studied here) were snap-frozen and stored at −80 °C until analysis.

Diet

Diets were rodent chows prepared according to the AIN-93-G formulation and made at the Unité de Préparation des Aliments Expérimentaux of INRAE (Jouy en Josas, France) (37). The H-diet was composed of 20.6% proteins, 64.8% carbohydrates, and 5% lipids. The T-diet was composed of 20.8% proteins, 65.1% carbohydrates, and 4.5% lipids. Both diets contained 5.1% fibers and 4.5% mineral and vitamin mix (**Table 1**) (38). Pellets were formulated by adding a mixture of vegetable oils specific for each diet (**Table 1**), considering the consumption of eggs during the 4-week period of treatment.

TABLE 1 | The composition of diets **(A)** and oil mix **(B)**.

%	H-diet	T-diet
A		
Starch	54.6	54.9
Sucrose	10.2	10.2
Cellulose	5.1	5.1
Casein	20.6	20.8
Oil mix	5.0	4.5
Mineral mix	3.5	3.5
Vitamin mix	1.0	1.0
B		
Linseed	1.4	2.9
Sunflower	8.6	8.8
Olive	13.5	12.6
Rapeseed	25.0	25.2
Palm	51.5	50.5

The composition of dry diets based on the AIN-93-G is presented for the habituation and the treatment diets. Both diets contained a mixture of vegetable oils formulated according to the daily consumption of eggs.

The T-diet was designed similarly to the H-diet to achieve the same final FA profile per day. Food consumption was previously estimated at 20 g per day of rodent chow combined with 3 g omelet serving over this growth period. In that condition, egg was supposed to contribute to the height of 0.5% lipids and T-diet of 4.5% lipids. The mixture of vegetable oils was adjusted in

T-diet as a consequence in considering the FA profile of egg. The portion of linseed was thus increased between H-diet and T-diet to compensate the low level of 18:3n-3 (α-linolenic acid, ALA) in omelet, in order to maintain the ratio n-6/n-3 to 5 with 3.4% of 18:3n-3 in average.

DHA Encapsulation and Omelets

DHA oil was prepared enzymatically from fish oil and was composed of DHA-enriched TAG containing 615 μg/mg DHA, 31 μg/mg docosapentaenoic acid n-3 (DPAn-3, 22:5n-3), and 36 μg/mg EPA, accounting for 76.5, 3.9, and 4.5% of total FA, respectively (Polaris, Quimper, France). DHA oil was daily encapsulated with heat-denatured whey protein isolate as described previously (35). The supplementation of proteins was therefore 300 μg per day, corresponding to less than 0.1% of proteins from eggs.

The omelet was daily prepared with a whole egg (Moisan aviculture, Plestan, France) homogenized by ultraturrax (10 000 rpm, 30 sec). Then, encapsulated-DHA oil (EN-DHA-O), heat-denatured whey protein isolate dispersion alone (Control) or completed with the DHA oil (UN-DHA-O) were added and mixed by stirring (500 rpm, 5 min). The eggs were finally molded and cooked in a water bath (80°C, 10 min).

Fatty Acid and Dimethylacetal Analysis

The lipids from omelets and tissues were extracted according to the Folch's method (39). DHA oil, vegetable oils, and lipids from omelets and tissues were saponified with 0.5 mol/L NaOH in methanol at 70°C for 20 min and methylated with BF_3 (14 % in methanol) at 70°C for 15 min (**Supplementary Figure 1**). Fatty acid methyl esters (FAMEs) and dimethylacetals (DMAs) were extracted with pentane and then separated by a QP 2010-SE gas chromatograph coupled to a mass spectrometer (Shimadzu, Marne-La-Vallée, France) equipped with a BPX70 capillary column (120 m, 0.25 mm i.d., 0.25 μm film, SGE Trajan, Chromoptic, Paris). Helium was used as carrier gas at a constant velocity of 27,5 cm/sec. The temperature of injector was adjusted to 250°C. The column temperature ramped from 50 to 175°C at 20 °C/min and then from 175 to 240°C at 2 °C/min. The mass spectrometer was operated under electron ionization at 0.2 keV and 200 °C source temperature. Analyses were performed in scan mode over the m/z range of 30–450 amu. Components were identified by using the National Institute of Standards and Technology (NIST) mass spectral library (version 2.01) in addition to commercial standards. Concentrations were determined by using 17:0 as the internal standard and were calculated by standard curves of either FAME or DMA. Results were expressed as a mass percentage of the total FA or total DMA, and as concentrations for total FA and total DMA as well.

Oxylipin Analysis

Oxidized metabolites of PUFA were quantified in DHA oil, omelets as well as plasma, heart, and brain by liquid chromatography combined with tandem mass (LC-QQQ) by the MetaToul lipidomic core facility (Justine Bertrand-Michel and Pauline Le Faouder, I2MC, Inserm 1048, MetaboHUB-ANR-11-INBS-0010 Toulouse, France). Briefly, frozen tissues (250 mg) were crushed with a FastPrep ®-24 Instrument (MP Biomedical, Illkirch-Graffenstaden, France) in 500 μL of Hank's balanced salt solution (Thermo Fisher Scientific, Illkirch-Graffenstaden, France). After 2 crush cycles (6.5 m/sec, 30 sec), cold methanol (300μL) and internal standard (5 μL of LXA4-d5, LTB4-d4 and 5HETE-d8) were added to homogenates. After centrifugation (15 min at 2000 g at 4°C), supernatants were diluted in 2 mL H_2O and then submitted to solid phase extraction using OASIS HLB 96-well plate (30 mg/well, Waters, Saint-Quentin-en-Yvelines, France) pretreated with methanol (1 mL), equilibrated with 10% methanol (1 mL), and washed after sample application with 10% methanol (1 mL). Lipid mediators were finally eluted with 1 mL of methanol and reconstituted in 10 μL methanol prior to LC-QQQ analysis (40). They were separated on a ZorBAX SB-C18 column (50 mm, 2.1 mm i.d., 1.8 μm film) using Agilent 1,290 Infinity HPLC system coupled to an ESI-triple quadruple G6460 mass spectrometer (Agilent Technologies, Les Ulis, France). Data were acquired in multiple reactions monitoring mode with optimized conditions (ion optics and collision energy). Peak detection, integration, and quantitative analysis were done using Mass Hunter Quantitative analysis software (Agilent Technologies) based on calibration lines built with eicosanoid standards (Interchim, Montluçon, France).

Statistics

The results are expressed as the mean ± SEM of 8 animal samples per group. Data analysis was performed using R software. Correlations were evaluated by Pearson correlation coefficients and the analysis of variance was done by ANOVA followed by a *post hoc* test depending on the normality of the data distribution. The significance of the effect observed with the DHA oil or the encapsulated-DHA oil was marked by an asterisk or different letters when $p < 0.05$.

RESULTS

Diet Characteristics

The animals were accommodated with the H-diet for one week. This rodent chow was composed of monoenes (18:1n-9) and saturates (16:0 and 18:0) as major FA, and contained 17.0% LA (18:2n-6) and 3.4% ALA corresponding to a ratio of 5 (**Table 2**). This composition contrasts with the breeding rodent chow, which classically contains 50% LA and 9% ALA. The composition of the T-diet was close to the H-diet but was reduced in lipid content considering the daily supply of eggs. Specifically, ALA was increased (4.3% of the total FA) to achieve a n-6/n-3 ratio of 4 in the T-diet since the supply of omelet reduces the n-3 FA content (only 0.4–0.5% of 18:3n-3). Overall, the FA profile of omelets was closed to the FA profile of rodent chow. LA and ALA were however lower in omelets as compared to the H-diet and T-diet, balanced by a greater proportion of 18:0. The T-diet was designed according to the FA profile of omelets, considering the expected daily consumption of both omelet and rodent chow. After one week of acclimation with H-diet, the T-diet was distributed during the 4-week treatment with eggs. Each group of animals received 3g omelet per day, the supplementation of which differed according

TABLE 2 | The fatty acid composition of the diets and the omelets.

%	Diets		Omelets		
	H-diet	T-diet	Control	UN-DHA-O	EN-DHA-O
12:0	0.1	0.1	0.0	0.0	0.0
14:0	0.6	0.6	0.3	0.3	0.3
16:0	26.2	25.7	25.3	22.5	22.1
18:0	3.4	3.4	8.0	7.1	7.2
20:0	0.4	0.4	0.0	0.0	0.0
22:0	0.2	0.2	0.0	0.0	0.0
24:0	0.1	0.1	0.0	0.0	0.0
Saturates	**31.0**	**30.5**	**33.6**	**29.9**	**29.6**
14:1n-5	0.0	0.0	0.1	0.0	0.1
n-5	**0.0**	**0.0**	**0.1**	**0.0**	**0.1**
16:1n-7	0.2	0.2	2.9	2.6	2.6
18:1n-7	1.4	1.4	2.0	1.8	1.8
n-7	**1.6**	**1.6**	**4.9**	**4.4**	**4.4**
16:1n-9	0.0	0.0	0.7	0.6	0.6
18:1n-9	46.2	45.7	42.2	37.9	37.2
20:1n-9	0.5	0.4	0.1	0.2	0.3
22:1n-9	0.3	0.3	0.0	0.0	0.0
24:1n-9	0.0	0.0	0.0	0.2	0.2
n-9	**47.0**	**46.4**	**43.0**	**38.9**	**38.3**
18:2n-6	17.0	17.2	14.8	13.0	12.9
20:4n-6	0.0	0.0	2.0	1.9	1.9
22:4n-6	0.0	0.0	0.0	0.1	0.1
22:5n-6	0.0	0.0	0.3	0.6	0.6
n-6	**17.0**	**17.2**	**17.1**	**15.6**	**15.5**
18:3n-3	3.4	4.3	0.5	0.4	0.5
20:5n-3	0.0	0.0	0.0	0.5	0.5
22:5n-3	0.0	0.0	0.0	0.5	0.5
22:6n-3	0.0	0.0	0.8	9.8	10.6
n-3	**3.4**	**4.3**	**1.3**	**11.2**	**12.1**

Lipids from croquettes and omelets were extracted according to the Folch's method. The fatty acid profile performed by GC-MS was determined for the habituation and the treatment diets, and the different omelets prepared with unencapsulated-DHA oil or encapsulated-DHA oil.

Bold values correspond to the sum of fatty acids per family.

Colored values correspond to the type of omelets: black for control, red for UN-DHA-O and blue for EN-DHA-O.

to the input form of DHA oil. DHA was integrated to the recipe to reach 10% of the total FA of omelet, while only 0.8% of endogenous DHA was measured from control eggs (**Table 2**).

Food Intake and Animal Growth

The animals were fasted for 6 h before receiving individually the portion of omelets, the consumption of which was complete for each group of rats during the entire experiment. The T-diet intake was followed as well and a significant increase in the food consumption was observed from the first week with EN-DHA-O (**Figure 2A**). More precisely, the cumulative intake of the T-diet over the 4-week experiment was increased by 6% with UN-DHA-O and by 20% with EN-DHA-O compared with the control. This behavior was coupled with the animal growth since the final weight of rats fed EN-DHA-O was significantly higher by 15% than the control group (**Figure 2B**). Food efficiency ratio, calculated by the ratio between body weight gain and food intake (T-diet and omelet), was not different between groups and averaged 38.4, 37.9, and 39.3% for Control, UN-DHA-O, and EN-DHA-O respectively, over the four-week experiment (**Figure 2C**). Likewise, the weights of organs were also significantly augmented in the EN-DHA-O group by 24% for liver, by 19% for heart, and by 6% for brain as compared with the control group (**Figure 2D**). Nevertheless, when the organ weights were normalized with body weights of animals, no significant differences were obtained between groups, which subtends that the raise in organ weights resulted from rat growth. The weight gain of animals resulted presumably from an increased energy intake, since the FA proportion was similar between groups. The FA profile was indeed estimated in the view of the measured consumption of the T-diet per group on the one hand, and the complementary omelet on the other (**Table 3**). The FA profile combining T-diet and omelet was similar to the FA profile of the H-diet and no major difference in FA proportions or n-6/n-3 ratio was observed between groups. In addition, both diets enriched in DHA oil accounted for a supplementation of TAG-DHA of 2.3%, since the FA was supplied equivalently between the groups through the distribution of 3g omelet per day.

The first ascertainment showed an effect of the EN-DHA-O diet on food intake and rat growth, so we further investigated the effect of encapsulation of DHA on lipid metabolism.

Effect of Diets on the Metabolism of FA

The FA metabolism and particularly the accretion of DHA in tissues were then explored to assess the importance of encapsulation of the DHA oil in the diet. The analysis focused on blood, liver, heart, brain, and eyes. First, the diet supplementation of DHA induced a significant increase in DHA in tissues, except for the brain and the eyes (**Figure 3**). Encapsulation of the DHA oil globally tends to increase the DHA accretion in blood and heart (**Supplementary Tables 1–3**). In liver, a decrease in the DHA proportion was observed with EN-DHA-O, but coupled with a slight increase in the FA content, the DHA concentration was not changed. The impact of the diets was also estimated on precursors of DHA, minorly present in the DHA oil. Thus, EPA was significantly increased by the DHA supplementation in plasma, RBC, and liver without any significant effect of the encapsulation of the DHA oil. The same result was observed with DPA n-3 only in plasma (**Figure 3**). Second, the proportion of n-6 FA was significantly decreased with the DHA-enriched diets in all tissues, depending on the considered FA. The main effect was obtained in heart on the entire n-6 family (**Supplementary Table 2**) and in eyes especially on ARA (**Supplementary Table 3**). Only the eyes exhibited a significant effect of the encapsulation of the DHA oil by slightly reducing ARA from 11.8% in UN-DHA-O to 10.9% in EN-DHA-O. Otherwise, no major effect of the DHA supplementation was observed on the FA profiles. Analyses were further performed on particular lipids or derivatives.

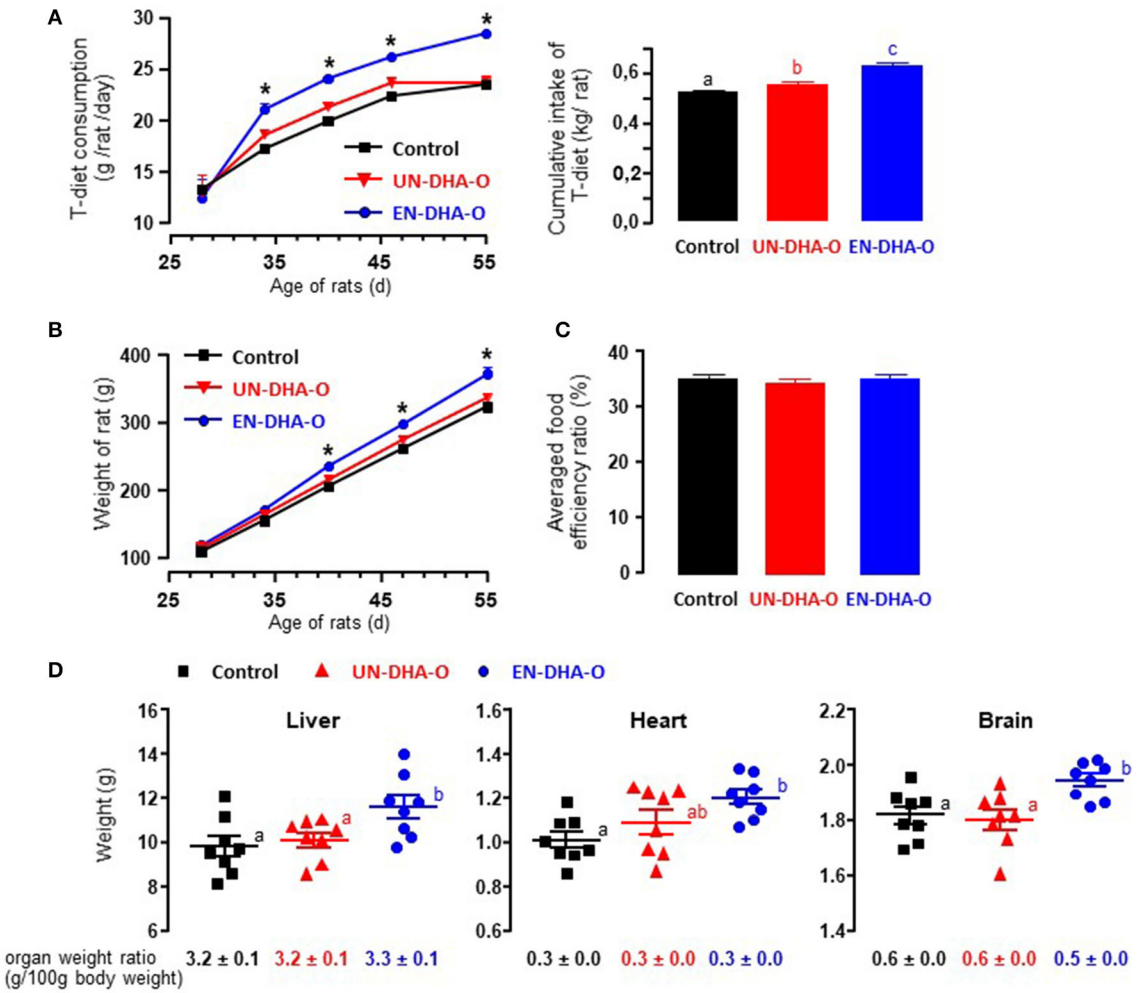

FIGURE 2 | The food intake **(A),** the growth **(B)**, the food efficiency ratio **(C)**, and the tissue weights **(D)** of rats. Food consumption of T-diet and animal growth were followed during the four-week experiment. Food efficiency ratio averaged over the four-week experiment was calculated with the daily consumption of T-diet and omelets over the weight gain of growing animals. The effect of diets was determined as well on the tissue weight prior to lipid analysis. a, b, c and ab indicate significant differences between the three groups when $p < 0.05$; ab means no difference with a and no difference with b. * indicates significant differences between EN-DHA-O and both Control and UN-DHA-O when $p < 0.05$.

Effect of Diets on the DMA Profile

The brain and heart are particularly rich in plasmalogens, which are specific etherlipids known as reservoirs of polyunsaturated FA. DMA compounds are derived from the aldehyde chain of plasmalogens present at the *sn*-1 position of the glycerol and were synthesized through the lipid saponification and methylation steps. They co-eluted with FAME. The DMA profile was thus analyzed to quantify plasmalogens (**Table 4**). Therefore, the DMAs were only measured in brain, heart, RBC, and eyes. The brain contained an average of 2 μg of DMA per mg of tissues, against 0.4μg/mg in heart and 0.1μg/mg in RBC and eyes. Moreover, the alkenyl chain was discriminant between tissues. For instance, in brain, the major DMA was composed of 18:0 (53% in all groups), then 16:0 (22%), 18:1n-9 (15%), and 18:1n-7 (10%). The profile of DMA was completely different in heart with 63% of 16:0, then 18:1n-9 (23%) and 18:0 (13%). Nonetheless, no effect of the diet was measured on the DMA profile. Surprisingly in eyes, the DMA content was reduced by half with the DHA supplementation passing from 0.12μg/mg to 0.06μg/mg and 0.07μg/mg with the UN-DHA-O and EN-DHA-O diets, respectively. Moreover, a switch in the DMA profile was observed in favoring 16:0-DMA (+13.9% with UN-DHA-O and +8.3% EN-DHA-O) to the detriment of 18:1-DMA, but without impacting the 18:0-DMA. No change of the DMA profile was, however, observed by encapsulation of the DHA oil.

Effect of Diets on Oxidized Metabolites of PUFA

Considering the slight effect of diets on the FA profiles in tissues, we further investigated the oxidized metabolites. First of all, oxylipins were quantified in DHA oil and food matrices

TABLE 3 | The fatty acid composition of the daily intake of T-diet and omelets.

%	T-diet with different omelets		
	Control	**UN-DHA-O**	**EN-DHA-O**
12:0	0.1	0.1	0.1
14:0	0.5	0.5	0.5
16:0	25.6	25.4	25.4
18:0	4.5	4.4	4.4
20:0	0.3	0.3	0.3
22:0	0.1	0.1	0.1
24:0	0.1	0.1	0.1
Saturates	**31.2**	**30.9**	**30.9**
16:1n-7	0.8	0.8	0.8
18:1n-7	1.6	1.5	1.5
n-7	**2.4**	**2.3**	**2.3**
16:1n-9	0.2	0.2	0.2
18:1n-9	44.8	44.8	44.8
20:1n-9	0.4	0.4	0.4
22:1n-9	0.2	0.2	0.2
24:1n-9	0.0	0.1	0.1
n-9	**45.6**	**45.7**	**45.7**
18:2n-6	16.6	16.6	16.6
20:4n-6	0.5	0.5	0.4
22:5n-6	0.1	0.2	0.2
n-6	**17.2**	**17.3**	**17.2**
18:3n-3	3.4	3.4	3.5
20:5n-3	0.0	0.1	0.1
22:5n-3	0.0	0.1	0.1
22:6n-3	0.2	2.5	2.5
n-3	**3.6**	**6.1**	**6.2**
n-6/n-3	4.9	4.9	4.8
Total	**100.0**	**102.3**	**102.3**
		TAG-DHA + 2.3%	

The fatty acid profile was calculated per group of omelets on the base of the treatment diet consumption, and was averaged per day on the four-week experimental period. This profile corresponds to the combination between FA consumed from the T-diet and FA supplied by the 3g omelet.

Bold values correspond to the sum of fatty acids per family.

Colored values correspond to the type of omelets: black for control, red for UN-DHA-O and blue for EN-DHA-O.

as well (**Table 5**). Eight oxidized metabolites from n-6 and n-3 PUFA were measured, mainly from LA and DHA. Hence, DHA oil contained a majority of 13-HODE and 9-HODE derived from LA, followed by 17-HDoHE and 14-HDoHE derived from DHA. Much less present, few oxylipins of ARA and 18-HEPE from EPA were detected as well. When oxylipins were then measured in omelets, 13-HODE, 9-HODE, and 5-HETE were the only oxidized metabolites quantified in all groups, even in DHA-enriched omelets, where the DHA oil was added. No oxylipins from DHA and EPA were detected in UN-DHA-O and EN-DHA-O, whereas a small amount of these compounds was expected considering the supplementation with the DHA oil.

We further analyzed the oxylipin pattern of animal tissues after the 4-week experiment. First, in plasma, three oxylipins were measured and derived from DHA but also from ARA and LA (**Table 6**). Overall, the supplementation of DHA strongly modulated the concentrations of oxylipins, and the encapsulation of the DHA oil greatly emphasized this effect. More specifically, 14-HDoHE derived from DHA was reduced by half with UN-DHA-O and by 6 with EN-DHA-O, as 14-HDoHE was negatively correlated with the DHA proportions in plasma (**Supplementary Figure 2**). In parallel, 17-HDoHE was not affected by the diet, as well as with 9-HODE from LA, whereas 13-HODE was reduced by the DHA supplementation without any influence of its encapsulation. Last, the greatest effect was the decrease in ARA derivatives by 76% with UN-DHA-O and by 93% with EN-DHA-O as compared with the control. Some of the oxylipins even became undetectable with the DHA encapsulation such as PGE_2 or 8-HETE.

The analyses were then completed by oxidized metabolites from heart (**Table 7**). Oxylipins were altogether more numerous but quantitatively less important than in plasma. No significant effect of the diets was observed this time on 14- and 17-HDoHE derived from DHA, but another derivative named PDx was remarkably increased with the DHA encapsulation. Absent in the control, PDx reached 2.1 pg/mg with UN-DHA-O and was multiplied by 8 with EN-DHA-O. The same applied to 18-HEPE derived from EPA, since it was absent in the control and the UN-DHA-O groups but reached 20.7 pg/mg with EN-DHA-O. In contrast, the cardiac concentrations of eicosanoids derived from ARA were globally decreased with the DHA supplementation, and particularly with the DHA encapsulation for $PGF_{2\alpha}$ and PGE_2. Finally, the most remarkable effect was achieved by an eicosanoid from DGLA termed 6keto-$PGF_{1\alpha}$, which was reduced by half with UN-DHA-O and by five with EN-DHA-O.

At last, in brain, no effect of the DHA oil supplementation was observed on measured oxidized metabolites (**Table 8**). But more interestingly, three oxylipins were significantly increased when the DHA oil was encapsulated. Therefore, 14-HDoHE derived from DHA was almost doubled with EN-DHA-O as compared with the control and the UN-DHA-O groups, while 8-HETE and 5,6-EET, positively correlated in brain ($R^2 = 0.5845$, $p < 0.001$, not shown), were more reasonably raised with EN-DHA-O. To conclude, the DHA supplementation globally modulated the oxylipin pattern of tissues, but the modulation was particularly prominent when the DHA oil was encapsulated.

DISCUSSION

In this study, DHA esterified to TAG was encapsulated with natural whey proteins in producing Pickering emulsion. Egg was chosen as a food matrix to favor the bioavailability of DHA (36), but we used cooked egg as omelet to determine the tissue accretion of encapsulated DHA in using rats as experimental model. Overall, the DHA supplementation increased the DHA

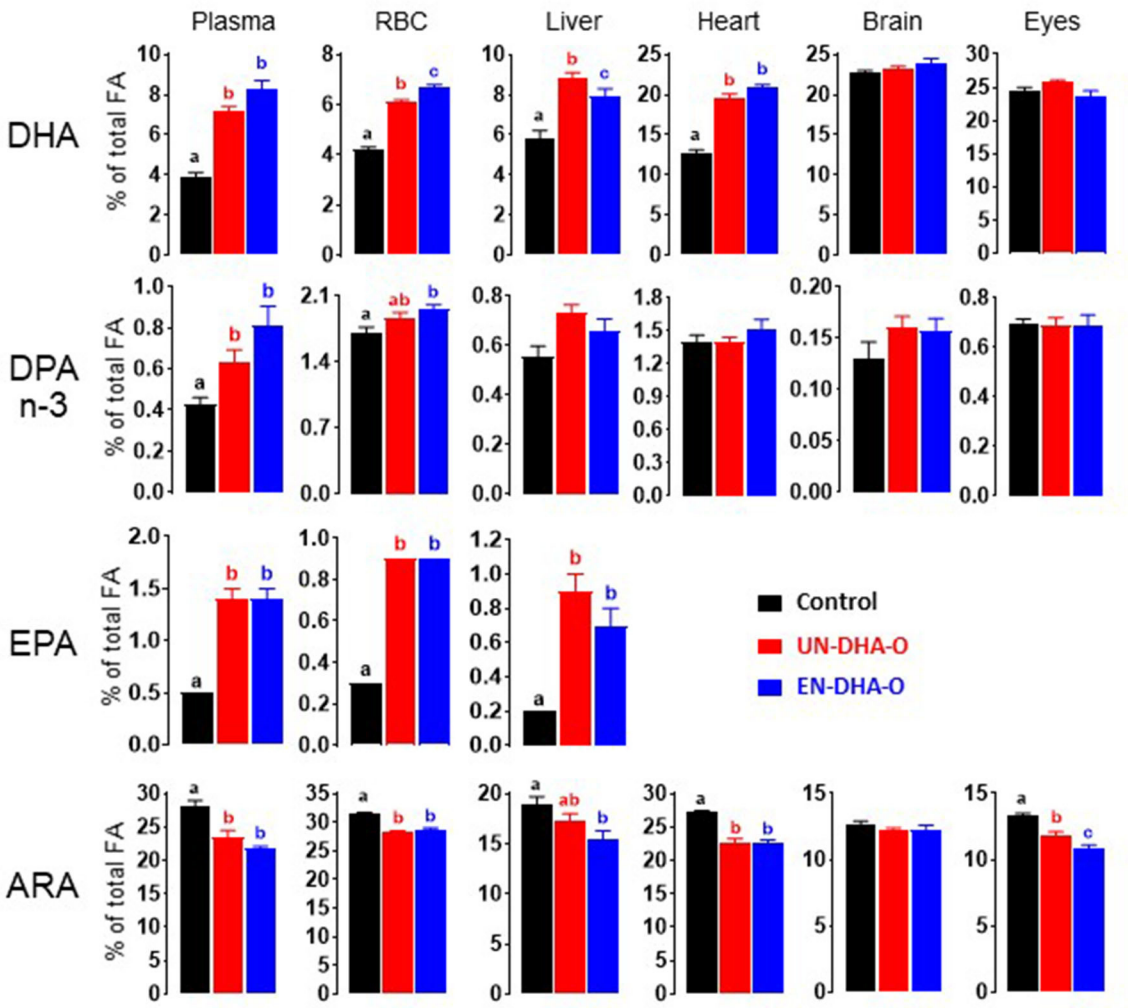

FIGURE 3 | The effect of form of the DHA intake on the FA profile of rat tissues after 4 weeks of treatment. Lipids from rat tissues were extracted according to the Folch's method and the fatty acid profile was then determined by gas chromatography-mass spectrometry (GC-MS). The main results on n-3 PUFA and arachidonic acid are presented. a, b, c and ab indicate significant differences between the three groups when $p < 0.05$; ab means no difference with a and no difference with b.

concentration in tissues except brain and eyes. EPA was increased as well in plasma, RBC, and liver. This FA was possibly synthesized from n-3 precursors such as ALA present in T-diet. Nevertheless, this raise was inherent to the DHA supplementation in omelets, considering that EPA was minorly present in DHA oil and was potentially generated by retro-conversion of DHA or of DPA n-3. DPA n-3 was also minorly present in DHA oil, to the same extent than EPA. However, its metabolism differed since DPA n-3 was weakly accumulated in tissues. As EPA was directly provided by egg food and easily synthesized from ALA, retro-conversion may not be favored in our conditions of work, although the importance of retro-conversion to produce EPA is still under discussion (41–43). Now, considering more specifically DHA, accretion was measured whereas rats were fed from weaning during 4 weeks of growth with an optimized diet. In these conditions, the DHA supplementation did not improve significantly DHA accretion in brain, as the DHA concentration was already high in the tissue, reaching more than 20% of total FA regardless of the diet. Our result contrasts with other studies where DHA proportion in brain was significantly increased by around 20% when rats fed a DHA enriched-diet as compared with the control (19, 44–46). First, it has to be mentioned that important differences between studies were also highlighted by other authors concerning mouse models, where comparisons were difficult considering strains, brain regions, ages, and diet conditions (47). Then, it must be noted that this effect was observed in the literature while the DHA proportion in brain was usually close to 10–15% of the total FA, which greatly differs from our DHA proportion reaching 22.8% in the control group. Additionally, many of the studies on DHA were designed with a low n-3 PUFA diet, favoring DHA half-life in brain and synthesis rate from the liver. In our study, the experimental design favored a higher concentration of DHA in frontal cortex, which was not significantly improved by the dietary DHA supplementation. This effect may result from ALA supplied from the T-diet in complement to the low

TABLE 4 | The dimethylacetal profile of RBC, heart, brain, and eyes.

	%	16:0-DMA	18:0-DMA	18:1n-9-DMA	18:1n-7-DMA	μg/mg
RBC	**Control**	29.2 ± 0.3	33.2 ± 0.3	31.6 ± 0.3	6.0 ± 0.1	0.12 ± 0.00
	UN-DHA-O	30.3 ± 0.3	32.6 ± 0.4	31.8 ± 0.5	5.3 ± 0.2	0.12 ± 0.00
	EN-DHA-O	30.0 ± 0.5	33.0 ± 0.4	31.6 ± 0.7	5.4 ± 0.3	0.13 ± 0.00
Heart	**Control**	63.2 ± 1.0	13.4 ± 1.0	23.4 ± 1.2	0.0 ± 0.0	0.38 ± 0.01
	UN-DHA-O	64.2 ± 1.8	13.6 ± 1.5	22.2 ± 1.4	0.0 ± 0.0	0.36 ± 0.02
	EN-DHA-O	62.2 ± 1.3	15.1 ± 0.7	22.7 ± 1.5	0.0 ± 0.0	0.42 ± 0.02
Brain	**Control**	22.2 ± 0.9	52.6 ± 0.7	14.9 ± 0.4	10.3 ± 0.3	2.17 ± 0.07
	UN-DHA-O	21.5 ± 0.7	51.7 ± 0.6	16.3 ± 0.7	10.5 ± 0.4	2.49 ± 0.13
	EN-DHA-O	21.6 ± 0.5	52.7 ± 0.6	15.4 ± 0.6	10.3 ± 0.4	2.30 ± 0.11
Eyes	**Control**	26.8 ± 0.3^{a}	34.3 ± 0.4	20.0 ± 0.4^{a}	18.9 ± 0.2^{a}	0.12 ± 0.00^{a}
	UN-DHA-O	40.7 ± 2.1^{b}	34.8 ± 3.0	11.1 ± 2.4^{b}	13.4 ± 2.2^{b}	0.06 ± 0.00^{b}
	EN-DHA-O	35.1 ± 1.3^{b}	34.8 ± 0.6	15.9 ± 0.8^{ab}	14.2 ± 1.0^{ab}	0.07 ± 0.01^{b}

Lipids of tissues were extracted by the Folch's method and the dimethylacetal profile was determined by GC-MS.
a, b, c and ab indicate significant differences between the three groups when $p < 0.05$; ab means no difference with a and no difference with b.
Colored values correspond to the type of omelets: black for control, red for UN-DHA-O and blue for EN-DHA-O.

TABLE 5 | The oxidized derivatives of fatty acids from DHA oil and omelets.

			Omelets (ng/3 g omelet)			
FA		**DHA oil (ng/mL)**	**Control**	**UN-DHA-O**	**EN-DHA-O**	**Expected***
LA	13-HODE	36.61	6.61	4.03	6.15	1.81
	9-HODE	31.27	6.20	2.92	4.78	1.55
ARA	15-dPGJ$_2$	0.52	0.00	0.00	0.00	0.03
	15-HETE	Trace	Trace	Trace	Trace	Trace
	5-HETE	0.94	2.16	1.19	1.53	0.05
EPA	18-HEPE	2.21	0.00	0.00	0.00	0.1
DHA	17-HDoHE	17.57	0.00	0.00	0.00	0.87
	14-HDoHE	13.07	0.00	0.00	0.00	0.65

*The oxidized metabolites of fatty acids were quantified by LC-QQQ as mentioned in methods on DHA oil used to prepare omelets. * A column named "expected" results from calculations on oxylipin concentrations expected after supplementation of egg with DHA oil, considering the oxylipin pattern from DHA oil.*
Colored values correspond to the type of omelets: black for control, red for UN-DHA-O and blue for EN-DHA-O.

level of PL-DHA from eggs. It was indeed shown that DHA synthesis from ALA may be sufficient to maintain brain DHA concentrations in the absence of dietary DHA consumption (48). Here, a high level of DHA in brain was possibly conditioned by an important *de novo* synthesis from dietary ALA and favored by the daily fasting as well. Short-term fasting was shown to enhance DHA concentrations in serum without dietary supplementation with DHA (49). The authors suggested that an increase in the expression of FA transporters specific for DHA likely mediated an enrichment of PUFA in hepatic TAG. This enrichment may foster secretion of DHA from the liver as 2-DHA-lysoPL for recirculation, subsequently promoting brain DHA accretion. Hepatic lipase was actually shown to play a major role in generating 1-lyso-2-DHA-*sn*-glycerophosphocholine, one of the main forms of DHA transported through the blood brain barrier for brain DHA enrichment (50). However, in our study, encapsulation of dietary DHA was shown to significantly improve neither bioavailability nor brain accretion of DHA. This result contrasts with other works based on whey protein or lipid emulsions. When rats were treated by gavage with encapsulated linseed oil, DHA was enhanced in cardiac sarcoplasmic reticulum by 28 and 94% with protein and phospholipid-based emulsions, respectively (51). When DHA was supplied as fish oil, the DHA was more accumulated in tissues with encapsulated oil than with native oil (52). Nevertheless, the effect was high with lipid emulsion and much less important with whey protein emulsion. More specifically in brain, the DHA accretion was upgraded from 11.4% with native fish oil to 12.6% with whey protein encapsulation. If the nature of encapsulation plays a major role in the tissue delivery of DHA, methods of administration may impact the bioavailability of DHA as well. In many studies, animals were fed encapsulated oil by gavage. In this study, we

TABLE 6 | The oxidized derivatives of fatty acids from plasma.

ng/mL of plasma		Control	UN-DHA-O	EN-DHA-O
LA	13-HODE	13.47 ± 1.90[a]	8.04 ± 1.01[b]	7.29 ± 1.21[b]
	9-HODE	2.56 ± 0.30	1.71 ± 0.13	1.72 ± 0.25
ARA	$PGF_{2\alpha}$	0.39 ± 0.09[a]	0.00 ± 0.00[b]	0.00 ± 0.00[b]
	PGE_2	0.78 ± 0.16[a]	0.19 ± 0.02[b]	0.00 ± 0.00[c]
	PGD_2	0.59 ± 0.21[a]	0.00 ± 0.00[b]	0.00 ± 0.00[b]
	TXB_2	7.88 ± 2.76[a]	1.59 ± 0.41[b]	0.77 ± 0.08[c]
	15-HETE	2.98 ± 0.51[a]	1.15 ± 0.12[b]	0.64 ± 0.08[c]
	8-HETE	2.03 ± 0.33[a]	0.54 ± 0.13[b]	0.00 ± 0.00[c]
	12-HETE	384.28 ± 76.32[a]	90.73 ± 22.97[b]	25.05 ± 3.25[c]
	5-HETE	4.48 ± 0.28[a]	2.30 ± 0.14[b]	1.53 ± 0.13[c]
DHA	14-HDoHE	42.30 ± 7.53[a]	20.41 ± 4.20[b]	6.82 ± 0.87[c]
	17-HDoHE	3.70 ± 0.73	2.91 ± 0.36	2.06 ± 0.26

The oxidized metabolites of fatty acids were quantified in plasma by LC-QQQ as mentioned in methods.
a, b and c indicate significant differences between the three groups when $p < 0.05$.
Colored values correspond to the type of omelets: black for control, red for UN-DHA-O and blue for EN-DHA-O.

TABLE 7 | The oxidized derivatives of fatty acids from heart.

pg/mg protein		Control	UN-DHA-O	EN-DHA-O
LA	13-HODE	772.1 ± 93.6	709.4 ± 64.9	765.3 ± 58.5
	9-HODE	220.4 ± 28.9	223.6 ± 17.7	248.3 ± 20.0
DGLA	$6kPGF_{1\alpha}$	437.7 ± 96.6[a]	194.6 ± 28.1[b]	88.1 ± 6.7[c]
ARA	$PGF_{2\alpha}$	118.1 ± 20.8[a]	51.8 ± 8.8[b]	23.6 ± 3.9[c]
	PGE_2	82.2 ± 11.6[a]	39.1 ± 7.2[b]	24.0 ± 2.3[c]
	PGD_2	42.8 ± 6.4[a]	20.0 ± 3.1[b]	22.5 ± 3.4[b]
	TXB_2	94.8 ± 18.5	55.3 ± 7.4	44.5 ± 6.1
	15-HETE	494.2 ± 50.6[a]	270.8 ± 22.0[b]	313.6 ± 30.9[b]
	8-HETE	109.4 ± 14.8	88.6 ± 7.9	95.9 ± 10.7
	12-HETE	3,562.0 ± 441.1	3,213.5 ± 926.4	4,335.8 ± 536.1
	5-HETE	532.0 ± 66.0[a]	325.7 ± 19.1[b]	274.6 ± 18.2[b]
	14,15-EET	55.6 ± 11.4[a]	0.0 ± 0.0[b]	0.0 ± 0.0[b]
	5-oxo-ETE	514.4 ± 60.7[a]	306.5 ± 18.9[b]	222.5 ± 14.8[b]
	11,12-EET	102.2 ± 14.8[a]	68.9 ± 5.2[ab]	48.0 ± 6.3[b]
	8,9-EET	179.3 ± 37.2	110.9 ± 10.9	78.0 ± 9.4
	5,6-EET	248.3 ± 59.7[a]	121.1 ± 18.4[ab]	70.9 ± 16.6[b]
EPA	18-HEPE	0.0 ± 0.0[a]	0.0 ± 0.0[a]	20.7 ± 3.6[b]
DHA	PDx	0.0 ± 0.0[a]	2.1 ± 2.1[a]	17.4 ± 3.1[b]
	14-HDoHE	1,754.9 ± 383.6	1,743.4 ± 323.6	2,961.9 ± 354.3
	17-HDoHE	2486.1 ± 646.4	2178.8 ± 429.8	3218.1 ± 395.3

The oxidized metabolites of fatty acids were quantified in heart by LC-QQQ as mentioned in methods.
a, b, c and ab indicate significant differences between the three groups when $p < 0.05$; ab means no difference with a and no difference with b.
Colored values correspond to the type of omelets: black for control, red for UN-DHA-O and blue for EN-DHA-O.

integrated functional food with a cook processing. The daily preparation was constraining but, in that way, omelets were baked with natural compounds and no additives.

In view of the results on FA profiles, we further analyzed DMA derived from plasmalogens. These etherlipids, and more precisely those derived from phosphatidylethanolamine, are known as carriers of long-chain PUFA in brain. Zhao et al. showed in mouse cortex that plasmenylethanolamine was composed of 30% DHA, 25% DPAn-3, and 10% EPA (53). In brain, we found the major alkenyl chains described in plasmalogen species, as the authors highlighted that plasmenylethanolamine mainly contained 18:0 and 16:0 at the *sn*-1 position when DHA was

TABLE 8 | The oxidized derivatives of fatty acids from brain.

pg/mg protein		Control	UN-DHA-O	EN-DHA-O
LA	13-HODE	103.2 ± 14.2	108.6 ± 12.0	154.0 ± 19.6
DGLA	6kPGF$_{1\alpha}$	272.3 ± 39.7	324.4 ± 57.6	428.7 ± 64.2
ARA	PGF$_{2\alpha}$	3,641.1 ± 367.7	4,062.1 ± 266.9	4,184.5 ± 187.4
	PGE$_2$	401.0 ± 39.8	499.0 ± 40.3	540.3 ± 71.4
	PGD$_2$	3,040.4 ± 249.4	3,679.7 ± 307.1	3,644.2 ± 254.5
	TXB$_2$	577.0 ± 53.4	637.4 ± 53.3	715.8 ± 109.6
	15-HETE	716.0 ± 69.6	782.2 ± 65.2	861.5 ± 52.1
	8-HETE	147.3 ± 15.0^{a}	151.8 ± 8.3^{a}	218.9 ± 25.5^{b}
	12-HETE	3557.6 ± 438.4	4908.4 ± 679.7	5055.1 ± 472.0
	5-HETE	840.3 ± 85.9	834.8 ± 72.2	1046.5 ± 206.8
	14,15-EET	223.4 ± 20.5	217.3 ± 22.3	272.9 ± 37.8
	5-oxo-ETE	588.5 ± 75.7	569.6 ± 66.6	705.5 ± 55.3
	11,12-EET	279.2 ± 36.6	267.3 ± 26.1	297.5 ± 47.1
	8,9-EET	380.9 ± 44.4	370.4 ± 33.9	554.7 ± 95.2
	5,6-EET	566.1 ± 90.9^{ab}	446.0 ± 54.2^{b}	730.1 ± 73.0^{a}
DHA	14-HDoHE	382.6 ± 47.1^{a}	385.5 ± 63.2^{a}	597.1 ± 61.1^{b}
	17-HDoHE	375.8 ± 49.1	581.6 ± 113.7	645.8 ± 55.4

The oxidized metabolites of fatty acids were quantified in brain by LC-QQQ as mentioned in methods.
a, b, c and ab indicate significant differences between the three groups when $p < 0.05$; ab means no difference with a and no difference with b.
Colored values correspond to the type of omelets: black for control, red for UN-DHA-O and blue for EN-DHA-O.

esterified at the *sn*-2 position. But overall, our diets did not change the DMA profile in brain, heart, or RBC, although the DHA proportion was increased in heart and RBC with the DHA supplementation. A previous work showed that the plasmalogen content in brain may be increased by dietary DHA through a potent stimulation of dihydroxyacetone phosphate acyl transferase activity (54). This effect was however presumed as relevant at the beginning of the life but not during aging. In our study, DHA supplementation consistently affected the DMA structures and concentrations in eyes, but surprisingly in reducing the DMA content. We also found equivalent proportions between saturated DMA (around 35% for both 16:0-DMA and 18:0-DMA) and between monounsaturated DMA (around 15% for both 18:1n-9-DMA and 18:1n-7-DMA), on the contrary to other studies performed on mice (55), where the diet enriched in fat modulated as well the DMA profile. DHA supplementation may shift the balance between plasmalogens, since few phospholipid species coexist in retina and other structures in eyes (56). Some authors showed in mouse cerebral cortex that DHA-enriched diet reduced the n-6 PUFA content in plasmenylethanolamine, the concentration of which tended to decrease in the tissue, whereas a substantial raise in peroxidation products was observed as well (57). Considering all the data, high concentrations of DHA in eye may explain a lower content of plasmalogens, which are considered as scavenger agents to protect against oxidation (58). Nevertheless, the discrepancy between control and DHA-enriched diets remains difficult to explain. The regulation of dietary FA on enzymes involved in plasmalogen metabolism has to be further investigated.

Finally, many studies showed that DHA enriched-diets modulate the production of mediators derived from FA such as oxylipins. Oxidized metabolites are miscellaneous and mainly generated by cyclooxygenase, lipoxygenase, and cytochrome P450 (23). In this study, we first determined the oxylipin pattern of DHA oil. We found eight compounds primarily derived from LA with 13- and 9-HODE, and from DHA with 17- and 14-HDoHE. When quantification was performed on omelets, half of the oxylipins were lost. Only 13-HODE, 9-HODE, and 5-HETE were still quantified. DHA supplementation was not discriminant as the oxylipin profile was similar between the three omelets. However, in DHA-enriched omelets, all oxylipins were expected in spite of the small amount of DHA oil added in egg preparation. Thus, this result suggests that food processing destroyed most of the oxidized derivatives of PUFA supplied by DHA oil in DHA-enriched omelets, while promoting non-enzymatic oxidation by generating specific hydroxylated FA such as HODE and HETE from egg FA. In such conditions, all groups of animals fed a similar amount of oxylipins derived from omelets. Quantification of oxylipins was performed on one set of food, but we may consider a consumption of 8 to 15 ng oxylipins per day per rat. On this basis, we further evaluated the impact of DHA encapsulation. Our data showed that DHA supplementation modified the oxylipin patterns in plasma and heart, and to a lesser extent in brain. The dietary effect on n-6 metabolites dominated over the effect on docosanoids generated from DHA. But most importantly, we demonstrated a very high influence of DHA oil encapsulation on the oxylipin concentrations in tissues, even in brain. Precisely, 14-HDoHE was drastically reduced in plasma and raised in brain with DHA encapsulation. 14-HDoHE is subsequently generated by 12-lipoxygenase and glutathione peroxidase (59). Other studies showed an increase in 14-HDoHE consecutive to a n-3 enriched-diet in brain (20, 60) or in plasma

(61, 62). Blood concentration was enhanced in pathological conditions such as morbid obesity (63) or metabolic syndrome (61), whereas the local level of 14-HDoHE was usually reduced in inflammatory conditions such as in arthritis (64), periodontitis (65), or pulmonary inflammation (66). 14-HDoHE was shown to be involved in the resolution of inflammation, to participate in the immune response or the platelet activation in reducing thrombus formation (67, 68). If the mechanism of action of 14-HDoHE still remains unclear, a cerebral increase in 14-HDoHE may be a good marker to prevent potent neuroinflammation. In heart, the level of 14-HDoHE tended to increase but more importantly, the accumulation of PDx was favored with DHA oil encapsulation. This poxytrin is generated by the action of 15-lipoxygenase on DHA and displays a pleiotropic function in inhibiting inflammation, cyclooxygenases 1 and 2, production of reactive oxygen species, and RNA virus replication (69). PDx also improved the liver steatosis status (70) and lowered hepatic gluconeogenesis in an obese mouse model (71), making it a potential therapeutic agent for lipid-induced and obesity-linked insulin resistance and type 2 diabetes (72). More specifically, PDx may be a resolution mediator of kidney fibrosis and cardiac failure (73). Only healthy functions have been attributed to PDx, which makes the DHA supplementation a valuable approach to improve health tissue before potential injury. DHA oil used in our study was prepared enzymatically by esterification of glycerol with enriched DHA oil extracted from fish. The DHA content was high but other PUFA such as EPA was lowly detected. Although minorly present, EPA from the DHA-enriched diets displayed a remarkable impact on cardiac tissues as we found 18-HEPE with DHA supplementation but only when DHA oil was encapsulated. 18-HEPE is generated from EPA through catalysis of COX-2/aspirin or cytochrome P450 as a precursor of resolvin E1. It accumulated as well in brain (60) or plasma (61, 62) after a diet enriched in n-3 PUFA. Its blood concentration decreased with the obesity-linked inflammation status (61, 63), whereas it raised in inflammatory arthritis (64). 18-HEPE was also particularly concentrated in plasma of fat-1 mice compared with wild-type mice, and it was shown to protect against pulmonary metastasis of melanoma (74). More specifically, 18-HEPE was highly correlated with the coronary plaque regression on patients with coronary artery disease supplemented with high dose of n-3 PUFA for 30 months (75). Collectively in heart, the increase in PDx and 18-HEPE, together with the reduction of n-6 eicosanoids triggered by both DHA supply and oil encapsulation, emphasized the upgraded status on cardiac tissues on a short-term supplementation. Encapsulation of DHA oil with whey protein as Pickering emulsion showed in our study that the delivery system was efficient to modulate derivatives of PUFA in tissues, as compared to non-encapsulated DHA oil. This effect was presumed to be mediated by a different rate of absorption of DHA oil. Indeed, when the same omelets were digested by using an *in vitro* model of static digestion for adults, lipolysis of DHA-TAG was enhanced when DHA oil was encapsulated (unpublished result). Emulsions presenting the lowest droplet size prior to digestion exhibit a better rate of lipolysis compared to coarser emulsion (76). The same observation was assigned to nanoemulsion as compared with microemulsion where the release of oil took place either by interfacial transfer or degradation of the vehicle driving the lipids out (77). The breakdown of encapsulated oil depends as well on differences in emulsion structure and surface area available for catalytic activity. Many encapsulant materials are available (78) but the best delivery system of marine oil has to be developed and experienced. The subsequent lipolysis rate and thus absorption into the intestine greatly influenced the bioavailability of DHA as demonstrated with volunteers submitted to fish oil supplementation (79, 80).

Reducing lipid droplet size affects satiety as well by increasing FA sensing in small intestine or by enhancing peptide secretion like cholecystokinin or peptide YY during digestion (81). In our work, encapsulation of DHA oil heightened the growth of animals coupled with a change in eating behavior. We observed that the rats were particularly enthusiastic to eat DHA-enriched omelets and especially in the EN-DHA-O group. Yet, a study on volunteers showed that palatability was negatively impacted by the highest concentrations of DHA when fish oil was added to ground beef. Moreover, panelists were distinctly sensitive depending on the FA as EPA had a greater impact on off-flavor perception than DHA (82). Nonetheless, contrary to the fishy flavors triggered by bulk fish oil, more sophisticated preparation of oil such as encapsulation may improve palatability of food. Encapsulating DHA oil possibly mitigated the unpleasant taste leading to a better acceptance of DHA-enriched omelet. Now, the origin of oil may influence food intake as well. In considering a longer-term supplementation, the eating behavior was shown to be influenced by the effect of DHA on the reward system regulating appetite (83). Chalon et al. demonstrated that the mesolimbic dopaminergic pathway was overactivated in rats deficient in n-3 PUFA (84). Lacking n-3 PUFA increased reward sensitivity as well in patients with intrauterine growth restriction. This pathology affects brain responses to palatable food creating an impulsive eating behavior, reversible with n-3 PUFA supplementation (85). The alimentary impact was partly explained by the leptin pathway involved in the anorexigenic system. Indeed, DHA-TAG enhanced leptin secretion in obese mice, consequently reducing hyperphagia in regulating appetite (86). Conversely, one study counteracted this data on patients with haemodialysis suffering from anorexia (87). Implying of DHA was suggested to be attributed to its derivatives such as the endocannabinoid docosahexaenoyl ethanolamide (DHEA). Positively correlated to appetite, DHEA was suspected to act as an activator of the orexigenic pathway, possibly by antagonizing the putative anorectic effects of linoleoyl ethanolamide. If data are controversial in presenting DHA or derivatives either as an enhancer or as an inhibitor of appetite, other effects on food reward circuit are still poorly described. Aside from the neuronal implication, DHEA was otherwise shown to improve glucose intake of myoblasts *in vitro* through the activation of the endocannabinoid system (88). A similar result was observed on sows-fed DHA-enriched fish oil during gestation.

Intestinal glucose uptake was therefore increased in offspring, in association with the n-3 PUFA enrichment of jejunum tissues (89). This effect was partly mediated by the raise in brush border membrane glucose transporters. Transposed to our work, the effect of DHA encapsulation on animal growth was possibly facilitated by the modulation of intestinal transport functions as well. All together, these data suggest that encapsulation of DHA oil may upgrade the food palatability of omelets, improve appetite for the T-diet, and favor growth in promoting energy metabolism. For as much, it remains difficult to interpret the effect of encapsulation observed on derivatives of PUFA, more than on PUFAs themselves. The molecular mechanism requires further research for understanding.

To conclude, we used a rat model to assess the efficacy of a food-graded delivery system by encapsulating DHA oil into whey protein. In our experimental conditions, the brain displayed a great proportion of 22.8% DHA, which was not enhanced by dietary supplementation of DHA oil, as compared to other tissues. Overall, the encapsulation of DHA oil did not modulate the FA profile as compared to the literature, but remarkably modified the oxylipin pattern in plasma, heart, and even brain. Specific oxidized metabolites derived from DHA were upgraded while those from n-6 PUFA were essentially mitigated. This effect was independent of oxylipins present in DHA oil as food processing induced the loss of the specific oxidized metabolites from DHA and EPA. Finally, this work showed that encapsulation of DHA oil remains a key factor for DHA metabolism in generating precursors of protectins and maresins, thus improving the global health status.

DATA AVAILABILITY STATEMENT

The original contributions presented in the study are included in the article/**Supplementary Material**, further inquiries can be directed to the corresponding author/s.

ETHICS STATEMENT

The animal study was reviewed and approved by French Ministry of Higher Education and Research.

AUTHOR CONTRIBUTIONS

DD and FP conceived the study. FP designed the experimental work. JW performed the experiments with the help of JO, YL, and FB. JW and FP analyzed the data and wrote the manuscript. DD reviewed the manuscript. All authors contributed to the article and approved the submitted version.

ACKNOWLEDGMENTS

This research was financially supported by the National Research Institute for Agriculture, Food and Environment (INRAE).

SUPPLEMENTARY MATERIAL

The Supplementary Material for this article can be found online at: https://www.frontiersin.org/articles/10.3389/fnut.2021.812119/full#supplementary-material

REFERENCES

1. Weiser MJ, Butt CM, Mohajeri MH. Docosahexaenoic Acid and Cognition throughout the Lifespan. *Nutrients.* (2016) 8:99. doi: 10.3390/nu8020099
2. Holub BJ. Docosahexaenoic acid (DHA) and cardiovascular disease risk factors. *Prostaglandins Leukot Essent Fat Acids.* (2009) 81:199–204. doi: 10.1016/j.plefa.2009.05.016
3. Ajith TA, Jayakumar TG. Omega-3 fatty acids in coronary heart disease: Recent updates and future perspectives. *Clin Exp Pharmacol Physiol.* (2019) 46:11–8. doi: 10.1111/1440-1681.13034
4. Richard D, Oszust F, Guillaume C, Millart H, Laurent-Maquin D, Brou C, et al. Infusion of docosahexaenoic acid protects against myocardial infarction. *Prostaglandins Leukot Essent Fat Acids.* (2014) 90:139–43. doi: 10.1016/j.plefa.2014.01.001
5. Gerbi A, Bernard M, Gleize B, Coste TC, Maixent JM, Lan C, et al. Dose dependent accretion of docosahexaenoic acid (DHA) in cardiac membranes of rats fed egg yolk powder enriched in DHA. *Cell Mol Biol.* (2004) 50:855–60. doi: 10.1170/T579
6. Aghaei N, Safamehr A, Mehmannavaz Y, Chekaniazar S. Blood and tissue fatty acid compositions, lipoprotein levels, performance and meat flavor of broilers fed fish oil: changes in the pre- and post-withdrawal design. *Animal.* (2012) 6:2031–40. doi: 10.1017/S1751731112000924
7. Hajjaji N, Schubnel V, Bougnoux P. Determinants of DHA incorporation into tumor tissue during dietary DHA supplementation. *Lipids.* (2011) 46:1063–9. doi: 10.1007/s11745-011-3573-x
8. Lacombe RJS, Chouinard-Watkins R, Bazinet RP. Brain docosahexaenoic acid uptake and metabolism. *Mol Asp Med.* (2018) 64:109–34. doi: 10.1016/j.mam.2017.12.004
9. Maki KC, Reeves MS, Farmer M, Griinari M, Berge K, Vik H, et al. Krill oil supplementation increases plasma concentrations of eicosapentaenoic and docosahexaenoic acids in overweight and obese men and women. *Nutr Res.* (2009) 29:609–15. doi: 10.1016/j.nutres.2009.09.004
10. Ulven SM, Kirkhus B, Lamglait A, Basu S, Elind E, Haider T, et al. Metabolic effects of krill oil are essentially similar to those of fish oil but at lower dose of EPA and DHA, in healthy volunteers. *Lipids.* (2011) 46:37–46. doi: 10.1007/s11745-010-3490-4
11. Ramprasath VR, Eyal I, Zchut S, Jones PJ. Enhanced increase of omega-3 index in healthy individuals with response to 4-week n-3 fatty acid supplementation from krill oil versus fish oil. *Lipids Health Dis.* (2013) 12:178. doi: 10.1186/1476-511X-12-178
12. Carnielli VP, Verlato G, Pederzini F, Luijendijk I, Boerlage A, Pedrotti D, et al. Intestinal absorption of long-chain polyunsaturated fatty acids in preterm infants fed breast milk or formula. *Am J Clin Nutr.* (1998) 67:97–103. doi: 10.1093/ajcn/67.1.97
13. Schuchardt J, Schneider I, Meyer H, Neubronner J, von Schacky C, Hahn A. Incorporation of EPA and DHA into plasma phospholipids in response to different omega-3 fatty acid formulations - a comparative bioavailability study of fish oil vs. krill oil. *Lipids Health Dis.* (2011) 10:145. doi: 10.1186/1476-511X-10-145
14. Yurko-Mauro K, Kralovec J, Bailey-Hall E, Smeberg V, Stark JG, Salem N. Similar eicosapentaenoic acid and docosahexaenoic acid plasma levels achieved with fish oil or krill oil in a randomized double-blind four-week bioavailability study. *Lipids Health Dis.* (2015) 14:99. doi: 10.1186/s12944-015-0109-z
15. Ghasemifard S, Turchini GM, Sinclair AJ. Omega-3 long chain fatty acid "bioavailability": A review of evidence and methodological considerations. *Prog Lipid Res.* (2014) 56:92–108. doi: 10.1016/j.plipres.2014.09.001

16. Gázquez A, Larqué E. Towards an optimized fetal DHA accretion: differences on maternal DHA supplementation using phospholipids vs. triglycerides during pregnancy in different models. *Nutrients.* (2021) 13:511. doi: 10.3390/nu13020511
17. Gázquez A, Ruíz-Palacios M, Larqué E, DHA. supplementation during pregnancy as phospholipids or TAG produces different placental uptake but similar fetal brain accretion in neonatal piglets. *Br J Nutr.* (2017) 118:981–8. doi: 10.1017/S0007114517002951
18. Adkins Y, Laugero KD, Mackey B, Kelley DS. Accretion of dietary docosahexaenoic acid in mouse tissues did not differ between its purified phospholipid and triacylglycerol forms. *Lipids.* (2019) 54:25–37. doi: 10.1002/lipd.12115
19. Destaillats F, Oliveira M, Bastic Schmid V, Masserey-Elmelegy I, Giuffrida F, Thakkar S, et al. Comparison of the incorporation of DHA in circulatory and neural tissue when provided as triacylglycerol (TAG), monoacylglycerol (MAG) or Phospholipids (PL) provides new insight into fatty acid bioavailability. *Nutrients.* (2018) 10:620. doi: 10.3390/nu10050620
20. Ostermann AI, Schebb NH. Effects of omega-3 fatty acid supplementation on the pattern of oxylipins: a short review about the modulation of hydroxy-, dihydroxy-, and epoxy-fatty acids. *Food Funct.* (2017) 8:2355–67. doi: 10.1039/C7FO00403F
21. Gabbs M, Zahradka P, Taylor CG, Aukema HM. Time course and sex effects of α-linolenic acid-rich and DHA-rich supplements on human plasma oxylipins: a randomized double-blind crossover trial. *J Nutr.* (2021) 151:513–22. doi: 10.1093/jn/nxaa294
22. Gabbs M, Leng S, Devassy JG, Monirujjaman M, Aukema HM. Advances in our understanding of oxylipins derived from dietary PUFAs. *Adv Nutr.* (2015) 6:513–40. doi: 10.3945/an.114.007732
23. An J-U, Kim S-E, Oh D-K. Molecular insights into lipoxygenases for biocatalytic synthesis of diverse lipid mediators. *Prog Lipid Res.* (2021) 83:101110. doi: 10.1016/j.plipres.2021.101110
24. Chiang N, Serhan CN. Specialized pro-resolving mediator network: an update on production and actions. *Essays Bioch.* (2020) 64:443–62. doi: 10.1042/EBC20200018
25. Hajeyah AA, Griffiths WJ, Wang Y, Finch AJ, O'Donnell VB. The biosynthesis of enzymatically oxidized lipids. *Front Endocrinol.* (2020) 11:591819. doi: 10.3389/fendo.2020.591819
26. Zaloga GP. Narrative review of n-3 polyunsaturated fatty acid supplementation upon immune functions, resolution molecules and lipid peroxidation. *Nutrients.* (2021) 13:662. doi: 10.3390/nu13020662
27. Devassy JG, Leng S, Gabbs M, Monirujjaman M, Aukema HM. Omega-3 polyunsaturated fatty acids and oxylipins in neuroinflammation and management of Alzheimer disease. *Adv Nutr.* (2016) 7:905–16. doi: 10.3945/an.116.012187
28. Li C, Wu X, Liu S, Shen D, Zhu J, Liu K. Role of resolvins in the inflammatory resolution of neurological diseases. *Front Pharmacol.* (2020) 11:612. doi: 10.3389/fphar.2020.00612
29. Duan J, Song Y, Zhang X, Wang C. Effect of ω-3 polyunsaturated fatty acids-derived bioactive lipids on metabolic disorders. *Front Physiol.* (2021) 12:646491. doi: 10.3389/fphys.2021.646491
30. Maciejewska-Markiewicz D, Stachowska E, Hawryłkowicz V, Stachowska L, Prowans P. The role of resolvins, protectins and marensins in non-alcoholic fatty liver disease (NAFLD). *Biomolecules.* (2021) 11:937. doi: 10.3390/biom11070937
31. Gruskiene R, Bockuviene A, Sereikaite J. Microencapsulation of bioactive ingredients for their delivery into fermented milk products: a review. *Molecules.* (2021) 26:4601. doi: 10.3390/molecules26154601
32. Chevalier Y, Bolzinger M-A. Emulsions stabilized with solid nanoparticles: Pickering emulsions. *Colloids Surfaces A Physicochem Eng Aspects.* (2013) 439:23–34. doi: 10.1016/j.colsurfa.2013.02.054
33. Low LE, Siva SP, Ho YK, Chan ES, Tey BT. Recent advances of characterization techniques for the formation, physical properties and stability of Pickering emulsion. *Adv Colloid Interface Sci.* (2020) 277:102117. doi: 10.1016/j.cis.2020.102117
34. Wu J, Ma G-H. Recent Studies of Pickering Emulsions: Particles Make the Difference. *Small.* (2016) 12:4633–48. doi: 10.1002/smll.201600877
35. Wang J, de Figueiredo Furtado G, Monthean N, Dupont D, Pédrono F, Madadlou A. CaCl2 supplementation of hydrophobised whey proteins: assessment of protein particles and consequent emulsions. *Int Dairy J.* (2020) 110:104815. doi: 10.1016/j.idairyj.2020.104815
36. Pineda-Vadillo C, Nau F, Guérin-Dubiard C, Bourlieu C, Capozzi F, Bordoni A, et al. *In Vivo* digestion of egg products enriched with dha: effect of the food matrix on DHA bioavailability. *Foods.* (2020) 10:6. doi: 10.3390/foods10010006
37. Reeves PG, Nielsen FH, Fahey GC. AIN-93 purified diets for laboratory rodents: final report of the american institute of nutrition ad hoc writing committee on the reformulation of the AIN-76A rodent diet. *J Nutr.* (1993) 123:1939–51. doi: 10.1093/jn/123.11.1939
38. Potier de. Courcy G, Durand G, Abraham J, Gueguen L. Recommandations sur les conditions d'alimentation des animaux de laboratoire (rats et souris). *Sci Aliments.* (1989) 9:209–17.
39. Folch J, Lees M, Stanley GHS, A. simple method for the isolation and purification of total lipids from animal tissues. *J Biol Chem.* (1957) 226:497–509. doi: 10.1016/S0021-9258(18)64849-5
40. Le Faouder P, Baillif V, Spreadbury I, Motta J-P, Rousset P, Chêne G, et al. LC–MS/MS method for rapid and concomitant quantification of pro-inflammatory and pro-resolving polyunsaturated fatty acid metabolites. *J Chromatogr B.* (2013) 932:123–33. doi: 10.1016/j.jchromb.2013.06.014
41. Metherel AH, Bazinet RP. Updates to the n-3 polyunsaturated fatty acid biosynthesis pathway: DHA synthesis rates, tetracosahexaenoic acid and (minimal) retroconversion. *Prog Lipid Res.* (2019) 76:101008. doi: 10.1016/j.plipres.2019.101008
42. Metherel AH, Irfan M, Klingel SL, Mutch DM, Bazinet RP. Compound-specific isotope analysis reveals no retroconversion of DHA to EPA but substantial conversion of EPA to DHA following supplementation: a randomized control trial. *Am J Clin Nutr.* (2019) 110:823–31. doi: 10.1093/ajcn/nqz097
43. Brenna JT, DHA. retroconversion revisited: dietary DHA spares endogenous EPA. *Am J Clin Nutr.* (2019) 110:789–90. doi: 10.1093/ajcn/nqz125
44. Lindquist DM, Asch RH, Schurdak JD, McNamara RK. Effects of dietary-induced alterations in rat brain docosahexaenoic acid accrual on phospholipid metabolism and mitochondrial bioenergetics: An in vivo 31 P MRS study. *J Psychiatr Res.* (2017) 95:143–6. doi: 10.1016/j.jpsychires.2017.08.014
45. Ross BM, Malik I, Babay S. Dietary omega-3 polyunsaturated fatty acid supplementation in an animal model of anxiety. *Prostaglandins Leukot Essent Fat Acids.* (2016) 114:17–20. doi: 10.1016/j.plefa.2016.09.004
46. Lin YH, Shah S, Salem N. Altered essential fatty acid metabolism and composition in rat liver, plasma, heart and brain after microalgal DHA addition to the diet. *J Nutr Biochem.* (2011) 22:758–65. doi: 10.1016/j.jnutbio.2010.06.008
47. Joffre C, Grégoire S, De Smedt V, Acar N, Bretillon L, Nadjar A, et al. Modulation of brain PUFA content in different experimental models of mice. *Prostaglandins Leukot Essent Fat Acids.* (2016) 114:1–10. doi: 10.1016/j.plefa.2016.09.003
48. Domenichiello AF, Chen CT, Trepanier M-O, Stavro PM, Bazinet RP. Whole body synthesis rates of DHA from α-linolenic acid are greater than brain DHA accretion and uptake rates in adult rats. *J Lipid Res.* (2014) 55:62–74. doi: 10.1194/jlr.M042275
49. Marks KA, Marvyn PM, Aristizabal Henao JJ, Bradley RM, Stark KD, Duncan RE. Fasting enriches liver triacylglycerol with n-3 polyunsaturated fatty acids: implications for understanding the adipose–liver axis in serum docosahexaenoic acid regulation. *Genes Nutr.* (2015) 10:39. doi: 10.1007/s12263-015-0490-2
50. Sugasini D, Yang P, Ng D, Khetarpal S A, Vitali C, Rader D J, et al. Potential role of hepatic lipase in the accretion of docosahexaenoic acid (DHA) by the brain. *Biochimica et Biophysica Acta (BBA) - Mol Cell Biol Lipids.* (2021) 1866:159002. doi: 10.1016/j.bbalip.2021.159002
51. Sugasini D. Rats fed linseed oil in microemulsion forms enriches the cardiac sarcoplasmic reticulum lipids with docosahexaenoic acid and lower calcium transport. *J Funct Foods.* (2013) 5:1863–72. doi: 10.1016/j.jff.2013.09.007
52. Sugasini D, Lokesh BR. Enhanced incorporation of docosahexaenoic acid in serum, heart, and brain of rats given microemulsions of fish oil. *Mol Cell Biochem.* (2013) 382:203–16. doi: 10.1007/s11010-013-1736-1

53. Zhao Y-C, Zhou M-M, Zhang L-Y, Cong P-X, Xu J, Xue C-H, et al. Recovery of brain DHA-containing phosphatidylserine and ethanolamine plasmalogen after dietary DHA-enriched phosphatidylcholine and phosphatidylserine in SAMP8 mice fed with high-fat diet. *Lipids Health Dis.* (2020) 19:104. doi: 10.1186/s12944-020-01253-3
54. André A, Juanéda P, Sébédio JL, Chardigny JM. Plasmalogen metabolism-related enzymes in rat brain during aging: influence of n-3 fatty acid intake. *Biochimie.* (2006) 88:103–11. doi: 10.1016/j.biochi.2005.06.010
55. Albouery M, Buteau B, Grégoire S, Martine L, Gambert S, Bron AM, et al. Impact of a high-fat diet on the fatty acid composition of the retina. *Exp Eye Res.* (2020) 196:108059. doi: 10.1016/j.exer.2020.108059
56. Acar N, Gregoire S, Andre A, Juaneda P, Joffre C, Bron AM, et al. Plasmalogens in the retina: In situ hybridization of dihydroxyacetone phosphate acyltransferase (DHAP-AT) – the first enzyme involved in their biosynthesis – and comparative study of retinal and retinal pigment epithelial lipid composition. *Exp Eye Res.* (2007) 84:143–51. doi: 10.1016/j.exer.2006.09.009
57. Sun GY, Appenteng MK Li R, Woo T, Yang B, Qin C, Pan M, et al. Docosahexaenoic acid (DHA) supplementation alters phospholipid species and lipid peroxidation products in adult mouse brain, heart, and plasma. *Neuromol Med.* (2021) 23:118–29. doi: 10.1007/s12017-020-08616-0
58. Almsherqi ZA. Potential role of plasmalogens in the modulation of biomembrane morphology. *Front Cell Dev Biol.* (2021) 9:673917. doi: 10.3389/fcell.2021.673917
59. Guichardant M, Calzada C, Bernoud-Hubac N, Lagarde M, Véricel E. Omega-3 polyunsaturated fatty acids and oxygenated metabolism in atherothrombosis. *Biochimica et Biophysica Acta (BBA) - Mol Cell Biol Lipids.* (2015) 1851:485–95. doi: 10.1016/j.bbalip.2014.09.013
60. Rey C, Delpech JC, Madore C, Nadjar A, Greenhalgh AD, Amadieu C, et al. Dietary n-3 long chain PUFA supplementation promotes a pro-resolving oxylipin profile in the brain. *Brain Behav Immun.* (2019) 76:17–27. doi: 10.1016/j.bbi.2018.07.025
61. Barden AE, Mas E, Croft KD, Phillips M, Mori TA. Specialized proresolving lipid mediators in humans with the metabolic syndrome after n−3 fatty acids and aspirin. *Am J Clin Nutr.* (2015) 102:1357–64. doi: 10.3945/ajcn.115.116384
62. Schuchardt JP, Ostermann AI, Stork L, Fritzsch S, Kohrs H, Greupner T, et al. Effect of DHA supplementation on oxylipin levels in plasma and immune cell stimulated blood. *Prostaglandins Leukot Essent Fat Acids.* (2017) 121:76–87. doi: 10.1016/j.plefa.2017.06.007
63. Schulte F, Asbeutah AA, Benotti PN, Wood GC, Still C, Bistrian BR, et al. The relationship between specialized pro-resolving lipid mediators, morbid obesity and weight loss after bariatric surgery. *Sci Rep.* (2020) 10:20128. doi: 10.1038/s41598-020-75353-6
64. Barden AE, Moghaddami M, Mas E, Phillips M, Cleland LG, Mori TA. Specialised pro-resolving mediators of inflammation in inflammatory arthritis. *Prostaglandins Leukot Essent Fat Acids.* (2016) 107:24–9. doi: 10.1016/j.plefa.2016.03.004
65. Wang C-W, Colas RA, Dalli J, Arnardottir HH, Nguyen D, Hasturk H, et al. Maresin 1 Biosynthesis and proresolving anti-infective functions with human-localized aggressive periodontitis leukocytes. *Infect Immun.* (2016) 84:658–65. doi: 10.1128/IAI.01131-15
66. Kilburg-Basnyat B, Reece SW, Crouch MJ, Luo B, Boone AD, Yaeger M, et al. Specialized pro-resolving lipid mediators regulate ozone-induced pulmonary and systemic inflammation. *Toxicol Sci.* (2018) 163:466–77. doi: 10.1093/toxsci/kfy040
67. Crouch MJ, Kosaraju R, Guesdon W, Armstrong M, Reisdorph N, Jain R, et al. Frontline Science: A reduction in DHA-derived mediators in male obesity contributes toward defects in select B cell subsets and circulating antibody. *J Leukoc Biol.* (2019) 106:241–57. doi: 10.1002/JLB.3HI1017-405RR
68. Yamaguchi A, Stanger L, Freedman CJ, Standley M, Hoang T, Adili R, et al. 12-LOX-derived oxylipins regulate platelet activation and thrombus formation through a PKA-dependent signaling pathway. *J Thromb Haemost.* (2021) 19:839–51. doi: 10.1111/jth.15184
69. Lagarde M, Guichardant M, Bernoud-Hubac N. Anti-inflammatory and anti-virus potential of poxytrins, especially protectin DX. *Biochimie.* (2020) 179:281–4. doi: 10.1016/j.biochi.2020.09.008
70. Jung TW, Kyung EJ, Kim H-C, Shin YK, Lee SH, Park ES, et al. Protectin DX Ameliorates hepatic steatosis by suppression of endoplasmic reticulum stress via AMPK-induced ORP150 expression. *J Pharmacol Exp Ther.* (2018) 365:485–93. doi: 10.1124/jpet.117.246686
71. Jung TW, Kim H-C, Abd El-Aty AM, Jeong JH. Protectin DX suppresses hepatic gluconeogenesis through AMPK-HO-1-mediated inhibition of ER stress. *Cell Signal.* (2017) 34:133–40. doi: 10.1016/j.cellsig.2017.03.013
72. White PJ, St-Pierre P, Charbonneau A, Mitchell PL, St-Amand E, Marcotte B, et al. Protectin DX alleviates insulin resistance by activating a myokine-liver glucoregulatory axis. *Nat Med.* (2014) 20:664–9. doi: 10.1038/nm.3549
73. Perazza LR, Mitchell PL, Lizotte F, Jensen BAH, St-Pierre P, Trottier J, et al. Fish oil replacement prevents, while docosahexaenoic acid-derived protectin DX mitigates end-stage-renal-disease in atherosclerotic diabetic mice. *FASEB J.* (2021) 35:e21559. doi: 10.1096/fj.202100073R
74. Li J, Chen C-Y, Arita M, Kim K, Li X, Zhang H, et al. An omega-3 polyunsaturated fatty acid derivative, 18-HEPE, protects against CXCR4-associated melanoma metastasis. *Carcinogenesis.* (2018) 39:1380–8. doi: 10.1093/carcin/bgy117
75. Welty FK, Schulte F, Alfaddagh A, Elajami TK, Bistrian BR, Hardt M. Regression of human coronary artery plaque is associated with a high ratio of (18-hydroxy-eicosapentaenoic acid + resolvin E1) to leukotriene B^4. *FASEB J.* (2021) 35:e21448. doi: 10.1096/fj.202002471R
76. Armand M, Pasquier B, André M, Borel P, Senft M, Peyrot J, et al. Digestion and absorption of 2 fat emulsions with different droplet sizes in the human digestive tract. *Am J Clin Nutr.* (1999) 70:1096–106. doi: 10.1093/ajcn/70.6.1096
77. Dey T. kumar, Ghosh S, Ghosh M, Koley H, Dhar P. Comparative study of gastrointestinal absorption of EPA & DHA rich fish oil from nano and conventional emulsion formulation in rats. *Food Res Int.* (2012) 49:72–9. doi: 10.1016/j.foodres.2012.07.056
78. Venugopalan VK, Gopakumar LR, Kumaran AK, Chatterjee NS, Soman V, Peeralil S, et al. Encapsulation and protection of omega-3-rich fish oils using food-grade delivery systems. *Foods.* (2021) 10:1566. doi: 10.3390/foods10071566
79. Haug IJ, Sagmo LB, Zeiss D, Olsen IC, Draget KI, Seternes T. Bioavailability of EPA and DHA delivered by gelled emulsions and soft gel capsules. *Eur J Lipid Sci Technol.* (2011) 113:137–45. doi: 10.1002/ejlt.201000450
80. Raatz SK, Redmon JB, Wimmergren N, Donadio JV, Bibus DM. Enhanced absorption of n-3 fatty acids from emulsified compared with encapsulated fish oil. *J Am Diet Assoc.* (2009) 109:1076–81. doi: 10.1016/j.jada.2009.03.006
81. Maljaars PWJ, van der Wal RJP, Wiersma T, Peters HPF, Haddeman E, Masclee AAM. The effect of lipid droplet size on satiety and peptide secretion is intestinal site-specific. *Clin Nutr.* (2012) 31:535–42. doi: 10.1016/j.clnu.2011.12.003
82. Jiang T, Busboom JR, Nelson ML, Mengarelli R. Omega-3 fatty acids affected human perception of ground beef negatively. *Meat Sci.* (2011) 89:390–9. doi: 10.1016/j.meatsci.2011.04.026
83. Maher T, Clegg ME. Dietary lipids with potential to affect satiety: Mechanisms and evidence. *Crit Rev Food Sci Nutr.* (2019) 59:1619–44. doi: 10.1080/10408398.2017.1423277
84. Chalon S. Omega-3 fatty acids and monoamine neurotransmission. *Prostaglandins Leukot Essent Fat Acids.* (2006) 75:259–69. doi: 10.1016/j.plefa.2006.07.005
85. Reis RS, Dalle Molle R, Machado TD, Mucellini AB, Rodrigues DM, Bortoluzzi A, et al. Impulsivity-based thrifty eating phenotype and the protective role of n-3 PUFAs intake in adolescents. *Transl Psychiatry.* (2016) 6:e755–e755. doi: 10.1038/tp.2016.16
86. Cao W, Liu F, Li RW, Yang R, Wang Y, Xue C, et al. Triacylglycerol rich in docosahexaenoic acid regulated appetite via the mediation of leptin and intestinal epithelial functions in high-fat, high-sugar diet-fed mice. *J Nutr Biochem.* (2021) 99:108856. doi: 10.1016/j.jnutbio.2021.108856
87. Friedman AN, Kim J, Kaiser S, Pedersen TL, Newman JW, Watkins BA. Association between plasma endocannabinoids and appetite in hemodialysis patients: a pilot study. *Nutr Res.* (2016) 36:658–62. doi: 10.1016/j.nutres.2016.03.009

88. Kim J, Carlson ME, Watkins BA. Docosahexaenoyl ethanolamide improves glucose uptake and alters endocannabinoid system gene expression in proliferating and differentiating C2C12 myoblasts. *Front Physiol.* (2014) 5:100. doi: 10.3389/fphys.2014.00100
89. Gabler NK, Radcliffe JS, Spencer JD, Webel DM, Spurlock ME. Feeding long-chain n-3 polyunsaturated fatty acids during gestation increases intestinal glucose absorption potentially via the acute activation of AMPK. *J Nutr Biochem.* (2009) 20:17–25. doi: 10.1016/j.jnutbio.2007.11.009

Conflict of Interest: The authors declare that the research was conducted in the absence of any commercial or financial relationships that could be construed as a potential conflict of interest.

Publisher's Note: All claims expressed in this article are solely those of the authors and do not necessarily represent those of their affiliated organizations, or those of the publisher, the editors and the reviewers. Any product that may be evaluated in this article, or claim that may be made by its manufacturer, is not guaranteed or endorsed by the publisher.

frontiers in Nutrition

ORIGINAL RESEARCH
published: 25 February 2022
doi: 10.3389/fnut.2022.839761

Fabrication and Characterization of Ultra-High-Pressure (UHP)-Induced Whey Protein Isolate/κ-Carrageenan Composite Emulsion Gels for the Delivery of Curcumin

Jiaqi Su[1†], Linlin Wang[1†], Wenxia Dong[1], Jiao Wei[1], Xi Liu[1], Jinxin Yan[2], Fazheng Ren[1], Fang Yuan[1] and Pengjie Wang[3*]*

[1] Beijing Higher Institution Engineering Research Center of Animal Product, Key Laboratory of Precision Nutrition and Food Quality, Key Laboratory of Functional Dairy, Ministry of Education, College of Food Science and Nutritional Engineering, China Agricultural University, Beijing, China, [2] College of Biological & Environmental Sciences, Zhejiang Wanli University, Ningbo, China, [3] Department of Nutrition and Health, China Agricultural University, Beijing, China

OPEN ACCESS

Edited by:
Jianhua Liu,
Zhejiang University of Technology, China

Reviewed by:
Zihao Wei,
Ocean University of China, China
Bao Zhang,
Hefei University of Technology, China

***Correspondence:**
Fang Yuan
yuanfang0220@cau.edu.cn
Pengjie Wang
wpj1019@cau.edu.cn

[†]These authors have contributed equally to this work

Specialty section:
This article was submitted to Food Chemistry, a section of the journal Frontiers in Nutrition

Received: 20 December 2021
Accepted: 19 January 2022
Published: 25 February 2022

Citation:
Su J, Wang L, Dong W, Wei J, Liu X, Yan J, Ren F, Yuan F and Wang P (2022) Fabrication and Characterization of Ultra-High-Pressure (UHP)-Induced Whey Protein Isolate/κ-Carrageenan Composite Emulsion Gels for the Delivery of Curcumin. Front. Nutr. 9:839761. doi: 10.3389/fnut.2022.839761

The emulsion gels have attracted extensive interests due to their unique physical characters, remarkable stability, and control release properties of flavor and functional components compared to emulsions in liquid. In the current work, whey protein isolate (WPI)/κ-carrageenan (κ-CG) composite emulsion gels were fabricated based on the ultra-high-pressure (UHP) technology, in replacement of the traditional thermal, acid, or enzyme processing. Uniform composite emulsion gels could be fabricated by UHP above 400 MPa with minimum WPI and κ-CG concentrations of 8.0 and 1.0 wt%, respectively. The formation of UHP-induced emulsion gels is mostly attributed to the hydrophobic interaction and hydrogen bonding. The emulsion gels with different textures, rheology properties, and microstructures could be fabricated through adjusting the formulations (WPI concentration, κ-CG concentration, and oil phase fraction) as well as processing under different conditions (pressure and time). Afterward, curcumin-loaded emulsion gels were fabricated and subjected to an *in vitro* simulated gastrointestinal digestion in order to investigate the gastrointestinal fate of curcumin. *In vitro* simulated digestion results demonstrated that the UHP treatment significantly retarded the release of curcumin but had little impact on the bioaccessibility of curcumin. The results in this work provide useful information for the construction of emulsion gels through a non-thermal process, which showed great potential for the delivery of heat-sensitive bioactive components.

Keywords: emulsion gel, ultra-high-pressure, whey protein isolate, κ-carrageenan, *in vitro* digestion, curcumin

INTRODUCTION

Generally, emulsions with a relatively low oil volume fraction are expected to exhibit liquid-like flow behavior. However, when a viscoelastic biopolymer solution or gel functions as a continuous phase, or an emulsion behaves as a viscoelastic material due to the structuring induced by inter-droplet attractions between the droplets or crowded arrangement of droplets, a complex colloidal material may therefore formed as both an emulsion and a gel. Such kind of soft-solid colloid

material with a three-dimensional network structure is referred to as "emulsion gel" (1). As a typical semisolid system, the emulsion gels are able to exhibit the mechanical properties of both liquid and solid, as well as higher physical and oxidative stability compared with traditional emulsions. Moreover, the gel-like structure also enables the emulsions with better controlled properties, making them the ideal carriers for the encapsulation of hydrophobic bioactives.

The protein is one of the commonly used materials to construct food-grade emulsion gels. Protein-based emulsion gels can be classified into two types: (1) Emulsion-filled protein gel: Protein in the aqueous phase forms a polymer network in which oil droplets are uniformly dispersed, and the gel properties mainly depend on the nature of the protein matrix and (2) Protein-stabilized emulsion gel: Protein in the aqueous phase does not form a network structure but promotes the aggregation of droplets, while the gel properties mainly depend on the physical properties of the filled oil droplets. Actually, these two extreme structures typically coexist in a protein-based emulsion gel. That is, both the cross-linked protein molecules and the partially aggregated droplets are responsible for the formation of gel structures in these emulsion gels. To date, a variety of proteins were used to prepare emulsion gels, including whey protein (2), sodium caseinate (3), soy protein isolate (4), porcine serum protein (5), and so on.

As reported by abundant research studies, the protein-based emulsions can be converted into emulsion gels through several treatments (4–7), among which thermal treatment is the most commonly used one. However, the high temperatures (commonly higher than 65°C) would promote the degradation of thermally sensitive ingredients and result in the Maillard reaction within food if reducing sugar is involved, which have adverse effects on the quality, appearance, and flavor of food. Unlike heat-induced emulsion gels, cold-induced emulsion gels induced by acid or salt can be fabricated under mild conditions, and the process is more controllable, but the introduction of hydrogen and salt ions would also affect the microstructure and texture of gels, and further lead to the bad sensory characteristics of final food products, which limit the application of these gels in actual food systems.

Ultra-high-pressure (UHP) is a novel food processing technology that employs a pressure-transfer medium (such as water) to denature biological macromolecules and kill microbes under an extremely high pressure (100∼1,000 MPa) (8). As a non-thermal processing technology, the UHP has been widely used in food processing and food sterilization due to its several advantages such as high efficiency, low consumption, safe operation, less pollution, and maximum retention of flavor substances in food (9). The UHP treatment under relatively low pressure can facilitate the unfolding of proteins, and the bridge flocculation would occur between the protein-coated oil droplets *via* non-covalent bonds. However, by further increasing the pressure, the unfolded monomers dissociated from the partial dimer would polymerize into more stable aggregates, the free sulfhydryl groups on the surface of oil droplets are liable to form disulfide bonds, thereby stabilizing the emulsions. In this case, a three-dimensional network structure can be constructed through non-covalent interactions between adjacent molecules, for instance, hydrogen bonding, disulfide bonding, Van der Waals force, and hydrophobic interaction force (10), enabling the encapsulation of water or other components. Besides, the formation of gel-network structure also contributes to improve the texture property, nutritional value, and functionality of food.

Due to its rich functional properties, such as emulsifying and gelling property, whey protein isolate (WPI) has been widely used in food industries. The WPI solution is liable to convert into gels, whose properties are dominated by multiple causal factors, e.g., protein composition, temperature, pH, ionic strength, etc. (11). Unfortunately, the gels fabricated from individual WPI exhibit low resistance against extreme environmental conditions, leading to a poor stability during storage as well as low bioavailability of encapsulated bioactive compounds. One of the promising methods to solve this problem is to incorporate polysaccharide within WPI gels, which is supposed to enhance the gel strength. Moreover, the complexation of protein and polysaccharide is beneficial to enhance of their functional properties, endowing them with improved interfacial properties and better protective effects on encapsulated sensitive compounds against processing and storage conditions. It is also capable of delivering bioactive compounds to specific gastrointestinal targets with optimal kinetics under mild conditions, achieving controlled release by chewing, pH changes, and enzymatic action. The previous research has confirmed that β-lactoglobulin and β-lactoglobulin-κ-carrageenan (CG) complexes can be induced into semisolid soft gels using UHP under a certain pressure treatment of 400 MPa (12). Chen et al. (13) have also reported that the UHP induction significantly improved the water holding capacity and increased the gel strength of chicken breast myosin/κ-CG composite emulsion gels with high pressure processing under 200 MPa.

To date, numerous studies have shown that complexation can occur between the amino groups on WPI and anionic polysaccharides by ion exchange (14–16). κ-CG is a polymeric hydrophilic anionic polysaccharide extracted from the cell wall of marine red algae, consisting of a repeating unit composed of the disaccharide, β-(1-3)-d-galactose-4-sulfate, and α-(1-4)-3,6-anhydro-d-galactose (17). The high sulfate content (around 15∼40%) and an average relative molecular mass higher than 100 kDa endow κ-CG with a great potential in gelation (18). The previous research have reported that a cohesive κ-CG network can be fabricated in the presence of salt ions and cations such as K^+, $Ca2^+$, and NH^{4+}, and the resulting spiral gels exert good controlled release properties of functional components. Verbeken et al. (19) believe that κ-CG is present in the composite gel in a manner that exists in the interstitial space of the protein network. The UHP can change the molecular structure and spatial conformation of polysaccharides, thereby affecting their physicochemical properties and forming gels (20–22). Therefore, it is theoretically feasible to construct WPI-κ-CG composite gels through UHP treatment.

Curcumin is a natural polyphenolic compound existed in the rhizome of the perennial herb curcuma longa (23). The health benefits of curcumin can be attributed to its various biological activities such as anti-inflammatory, anti-oxidant, anti-bacterial,

anti-tumor activities, and so on (24). The potential health benefits of curcumin have generated a great interest in incorporating it into food, health-care products, and drugs. However, curcumin is extremely susceptible to oxidative deterioration due to the existence of hydroxy groups. Moreover, curcumin has also been shown to have poor solubility in aqueous phase, leading to a low compatibility to food matrix and reduced bioavailability (25). One of the effective methods to solve these problems is to encapsulate curcumin within delivery systems (26).

To date, the fabrication of emulsion gel is mostly limited to the induction by heat, enzyme, acid, and ion, and the research on the UHP-induced gel materials based on biological macromolecules concentrates mainly on the hydrogel, which partly stimulate the current work. The aims of this study were to prepare WPI and WPI/κ-CG emulsion gels by UHP induction and to find the effects of pressure, WPI, and κ-CG concentration. The mechanism of gel formation was also explored. The effects of UHP treatment conditions and gel composition on the *in vitro* digestive release rate of curcumin embedded in emulsion gels were studied for the first time, which provided evidence for the application of UHP-induced emulsion gels in the embedding and sustained release of functional ingredients.

MATERIALS AND METHODS

Materials

The whey protein isolate was obtained from Davisco International, Inc, containing more than 95% protein. The κ-CG was acquired from CPKelco, Inc. Medium-chain fatty acid triglyceride (MCT) was purchased from Musim Mastika Oils and Fats. Curcumin (Cur, 98%) was purchased from the China National Medicine Group (Shanghai, China). Fluorescent dyes (Nile Red and Nile blue) were obtained from Sigma-Aldrich. All other chemicals used were of analytical grade.

Preparation of Emulsion Gels

For WPI emulsion gels, a WPI solution (20 wt%) was prepared by dispersing 3.2 g WPI powder in 16 mL deionized water and stirring overnight to achieve complete dissolution. The WPI solution was then adjusted to pH 7.0 with 0.1M NaOH prior to mixing with 4 mL MCT oil under the shearing with an Ultra-Turrax (IKA, Germany) at a high speed of 10,000 r/min for 5 min. The resulting coarse emulsion was further homogenized three times using a Niro-Soavi Panda two-stage valve homogenizer (Parma, Italy) at 50 MPa. Afterward, a centrifuge tube containing 50 mL emulsion sample was placed in a nylon bag for vacuum sealing. The sample was immersed in the pressure-transfer medium water contained in the sample chamber of the UHP equipment. The boost rate and depressurization rate was set as 6.5 MPa/s and 20 MPa/s, respectively. The whole process took about 20 s $\sim$ 2 min.

For WPI/κ-CG composite emulsion gels, an equal volume of WPI solution and κ-CG solution were mixed and stirred to swell overnight, then the mixed solution was treated on the basis of the method described above.

The WPI, κ-CG, and MCT concentrations, as well as the processing conditions (pressure and time) were summarized in **Table 1**.

Rheology Analysis

The rheological properties of the samples were measured using a DHR-2 rheometer (TA Instruments, UK) at 25°C with a steel parallel plate coded as PP-40 (40 mm diameter, gap 1 mm). The emulsion gel samples were subjected to a dynamic frequency sweep test with the frequency oscillation varied from 0.1 to 100 rad/s at a 1% strain. All the dynamic tests were performed within the linear viscoelastic region. The elastic modulus (G') and loss modulus (G'') were recorded.

Texture Profile Analysis

The textures of samples were determined using a texture analyzer (TMS-Pro, FTC, America) operated under texture profile analysis (TPA) mode. The emulsion gel samples were taken out from centrifuge tubes and cut into cylinders (diameter 1.8 cm, height 2.0 cm) prior to placing in petri dishes. The samples were compressed to a distance of 1.0 cm with a P/6 probe at a speed of 100 mm·min^{-1}. The interval between two consecutive compression cycles was 10 s. The hardness, springiness, chewiness, gumminess, and cohesiveness were calculated to characterize the textural properties of the samples. The TPA measurements were carried out for 5 independent replicates at 25°C.

Fluorescence Spectroscopy

The Fluorimetric experiment was performed using an F-7000 fluorescence spectrophotometer (F-7000, Hitachi, Japan). The emulsion samples were diluted to 0.2 mg/mL (calculated on the basis of WPI) prior to placing in a quartz cell. The excitation wavelength was set as 290 nm, and the emission spectra were collected between 300 and 450 nm with a scanning speed of 100 nm·min^{-1}. Both excitation and the emission slit widths were set at 5 nm. Each individual emission spectrum was the average of three runs.

Circular Dichroism Spectroscopy

The Far-UV circular dichroism (CD) spectra of emulsion samples were recorded using a CD spectropolarimeter (Pistar π-180, Applied Photophysics Ltd. UK) in the far UV region ranged from 190 to 260 nm. The samples were diluted to 0.2 mg/mL (calculated on the basis of WPI) prior to placing in a quartz cell with a 1.0 mm optical path length. A constant nitrogen flush was applied during data acquisition. The secondary structure contents of the samples were estimated using Dichroweb: theonline Circular Dichroism Website http://dichroweb.cryst.bbk.ac.uk (27).

Fourier Transform Infrared Spectroscopy

The Fourier transform infrared spectroscopy (FTIR) was employed to evaluate the vibration of functional groups of emulsion gel samples. Briefly, 2.0 mg lyophilized sample was mixed with 198 mg pure potassium bromide (KBr) powder. The mixture was grounded into fine powder and pressed into a

TABLE 1 | Composition and treatment of WPI/κ-CG composite emulsion gels.

Sample ID	Composition			Treatment	
	WPI concentration (wt%)	κ-CG (wt%)	MCT fraction (v/v)	Processing pressure (MPa)	Pressure processing time (min)
1	8	1	20	600	30
2	10				
3	12				
4	14				
5	16				
6	12	0.75			
7		0.6			
8		0.5			
9		0.4			
10				200	
11				400	
12	12	1		600	
13				600	20
14					10

transparent thin slice. Afterward, the samples were subjected to FTIR analysis using a Spectrum 100 Fourier transform infrared spectrometer (PerkinElmer, UK). All the samples were scanned from 400 to 4,000 cm^{-1}, and scanning was performed 16 times with a resolution of 4 cm^{-1}. Pure KBr slice was measured as a baseline.

Microstructure Observation

The microstructure of emulsion gel samples was observed using a field emission scanning electron microscope (SEM, SU8010, Hitachi) and a confocal laser scanning microscopy (CLSM) (Leica TCS SP5, Leica MicrosystemsInc., Heidelberg, Germany).

For SEM observation, the lyophilized samples were adhered onto a specimen and sputter-coated with a gold layer to avoid charging under the electron beam. The samples were examined at an acceleration voltage of 3.0 kV using a JSM-6701F instrument.

For CLSM observation, the two dyes, Nile Blue (0.2 wt%) and Nile Red (0.2 wt%), were dissolved in absolute ethanol and sonicated for 5 min to ensure the complete dissolution, applying as dyes of WPI and MCT, respectively. A mixed staining solution prepared by mixing an equal volume of Nile Blue and Nile Red dye solution was used to dye the emulsion samples. The dyed samples were subsequently placed in the groove of concave microscope slides and gently covered with a cover slip prior to observe with a 100-fold oil mirror. A Helium–Neon (He–Ne) laser excitation source was excited at 633 nm for the Nile blue, whereas an argon laser excitation source was excited at 488 for the Nile red. The combined pictures originated from two channels were acquired through ZEN Imaging Software.

Determination of Molecular Force

A WPI solution (20 wt%) and a κ-CG solution (2 wt%) were prepared with NaCl, urea, and propylene glycol solutions at concentrations of 0.4, 0.8, 1.2, 1.6, and 2.0 mol/L, respectively. Afterward, the above-mentioned solutions were employed to prepare emulsion samples with the method described in section Preparation of Emulsion Gels before subjecting to a UHP-treatment at 600 MPa for 30 min to form emulsion gels. The molecular structure of emulsion gel samples was determined by measuring the texture properties of each sample with a TPA analysis as described in section Texture Profile Analysis (TPA).

Preparation of Curcumin-Loaded Emulsion Gels

An oil phase was formed by dissolving 1.0 g curcumin powder in 200 mL of MCT oil prior to ultrasonic-treating for 20 min with a JY32-11N Ultrasonic homogenizer (Ningbo Scientz Biotechnology Co. Ltd, China) to achieve complete dissolution. The curcumin-loaded emulsion gels were fabricated with the same method described in section Preparation of Emulsion Gels.

In vitro Digestion Behavior

Simulation Gastrointestinal Digestion

A simulated gastrointestinal tract (GIT) model was used to determine the potential gastrointestinal fate of emulsion gels. The results of our preexperiments have shown that the simulated mouth digestion had almost no effect on the digestion of emulsion gels; the simulated mouth digestion phase was not involved in the following experiments. However, the emulsion gels were broken into small fragments using a MJ-BL25B2 blender before the experiment to better simulate the initial state of samples in stomach.

Gastric phase: 1.0 g of broken emulsion gel samples were mixed with 10 ml of simulated gastric fluid (SGF), which contained NaCl (2 mg/mL), HCl (4 mL/L), and pepsin (3.2 mg/mL). Then, the pH of the mixtures was adjusted to pH 1.5 and stirred at 37°C for 60 min at 100 rpm.

Small intestine phase: 20 mL of gastric digestion juice were adjusted to pH 7.0 prior to mixing with an equal volume of simulated intestinal fluid (SIF) containing K_2HPO_4 (6.8 mg/ml), NaCl (8.775 mg/ml), bile salts (10 mg/ml), and pancreatin (3.2 mg/ml). Then, the pH of the mixture was adjusted to pH 7.0 and continuously shook (100 rpm) at 37°C for 120 min.

Droplet Size Determination

To explore the changes in the droplet size and size distribution of emulsion gels after SGF and SIF digestion, the SGF and SIF digestion juices were measured using a Zetasizer Nano-ZS90 (Malvern Instruments, Worcestershire, UK) based on the principle of dynamic light scattering (DLS).

Release of Curcumin

The release of curcumin was characterized after SIF digestion according to the method described in a previous work. An aliquot of SIF digestion juice was subjected to centrifugation with a CL10 centrifuge (Thermo Scientific, Pittsburgh, PA, USA) at 16,000 rpm for 30 min at 4°C. The supernatant containing solubilized curcumin was collected, on behalf of the "micelle" fraction. The micelle solution was then mixed with an equal volume of ethanol, vortexed, and centrifuged at 4,000 rpm for 10 min at 25°C. The top layer was then collected, whereas the bottom layer was subjected to the above-mentioned process again to ensure the complete extraction of curcumin. The digestive fluid was regularly sampled with an interval of 30 min. The concentration of curcumin extracted from the initial emulsion and micelle fraction was measured using a UV–visible spectrophotometer (Shimadzu, Model UV 1800; Japan) at 446 nm. The release rate (%) was calculated with the following formula:

$$Release\ rate\ (\%) = \frac{C_1}{C_0} \times 100$$

Where C_1 and C_0 were the content of curcumin in the micelle fraction and initial emulsion gel samples, respectively.

TABLE 2 | The physical state of WPI/κ-CG composite emulsion gels with different formulations.

WPI concentration (wt%)	κ-CG concentration (wt%)	Mass ratios between WPI and κ-CG	Texture and shape
8	1	8:1	Soft, sticky, collapse after placement, water seepage
10	1	10:1	Soft, sticky, poor elasticity, lightly seepage after placement
12	1	12:1	Soft, poor elasticity, brittle
14	1	14:1	Relatively hard, deform after extrusion, rough surface, fragile
16	1	16:1	Hard, deform after extrusion, rough surface, fragile
12	0.75	16:1	Soft and sticky, poor elasticity, water seepage after placement
12	0.6	20:1	Very soft and sticky, poorly collapsed after placement, more water seepage
12	0.5	24:1	Very soft and sticky, poor elasticity, obvious collapse after placement, more water seepage
12	0.4	30:1	Very soft and sticky, collapses immediately after placement, obvious fluidity

Statistical Analysis

The samples were prepared in duplicate, and the measurements were performed in triplicate. The data were analyzed using the software package statistical product and service solutions (SPSS) 18.0 (SPSSInc., Chicago, USA). The results were reported as the mean value and SD of two separate injections. The statistical differences were determined by one-way ANOVA with Duncan procedure, and the differences of main effects were identified to be significant with $p < 0.05$.

RESULTS AND DISCUSSIONS

Apparent Characteristics of Emulsion Gels With Different Processing Conditions

The WPI/κ-CG composite emulsion gels with a WPI concentration lower than 12% were found with water leakage phenomenon, as shown in **Table 2**. It could be concluded that 12% was the minimum concentration for the formation of homogenized emulsion gels, and therefore was chosen to fabricate emulsion gels with different WPI/κ-CG ratios. The appearance photographs of WPI and WPI/κ-CG composite emulsion gel samples with different processing conditions were shown in **Figure 1**. Unlike a WPI emulsion, the WPI/κ-CG composite emulsions could be constructed into emulsion gels with an extremely low WPI level under UHP treatment. However, the WPI/κ-CG composite emulsion gel formed by a critical WPI concentration (12%) processed at 600 MPa for 30 min was more soft and viscous compared with the emulsion gels formed by WPI emulsions with an equal WPI concentration. Besides, the WPI/κ-CG composite gels with relatively low concentration of WPI and κ-CG were moister, accompanied by the occurrence of a water leakage phenomenon.

Overall, the WPI/κ-CG composite emulsion gels were more brittle with a higher mobility, and easily destroyed (different degrees of collapses occurred after standing for 10 min). However, the introduction of κ-CG contributed to increase the hardness and decrease the mobility of the WPI emulsion gels, as well as mitigate the water leakage phenomenon. For example, the emulsion gels formed with 10% (w/v) WPI and 1% (w/v)

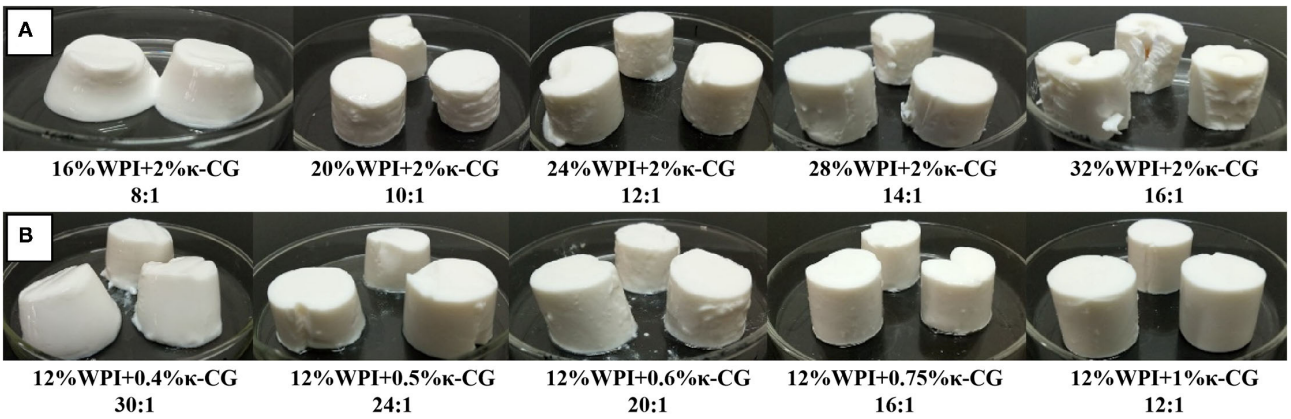

FIGURE 1 | Visual appearance of WPI emulsion gels **(A)** and WPI/κ-CG composite emulsion gels **(B)** composed of different components.

κ-CG were deformed after extrusion when the oil fraction was 30% (w/w), but were cracked or even broken when the oil fraction exceeded 40% (w/w). The high brittleness of WPI/κ-CG composite gels indicated that κ-CG can promote the formation of a fine strand network, which endowed the gel with a decreased stress and an increased fracture strain (20). In summary, the addition of κ-CG could have a positive impact on the formation of gel structure in WPI emulsions.

Rheological Properties of Emulsion Gels

In this experiment, the storage modulus G' (elastic modulus) and the loss modulus G" (viscous modulus) were determined to characterize the rheological properties of the WPI and WPI/κ-CG emulsion gels. G' is a measure of the energy stored and subsequently released in each deformation cycle, which is on behalf of the elastic properties of the samples, and G" is a measure of the amount of heat dissipation, representing the viscous properties of the samples. As shown in **Figure 2**, the dynamic strain sweep tests were conducted on the emulsion gel samples. Considering the fact that all the samples were determined with a linear viscoelastic region between 1 and 10% strain, 1% strain was selected as a fixed strain value in the frequency sweep tests. The critical strain value (γ_c) was decreased as the treatment pressure and time increased, as well as the WPI and κ-CG concentration. At the same time, the strain-amplitude dependence type of emulsion gels changed from a strain thinning type (G' and G" decreasing) to a weak strain overshoot type (G' decreasing, G" increasing followed by decreasing), indicating that the structure in emulsion gels was changed and the stress that the gel structure can withstand was reduced (28).

The dynamic frequency sweep test was conducted to evaluate the frequency dependence of the G' and G' of emulsion gel samples with different compositions and processing conditions. As shown in **Figure 2**, the moduli were found to be in a frequency-dependent manner. It could be also observed that G' was higher than G" in all the emulsion gel samples, revealing that these samples behaved between true gels and weak gels (29, 30). Besides, the G' was highly closed to G' for samples with relatively low WPI and κ-CG concentrations. However, the difference between G' and G" was increased as the increasing WPI and κ-CG concentration as well as treatment pressure, which indicated that the emulsion samples further converted into true gels (31).

Table 3 shows the fitting result of the storage modulus and power-law model to describe the angular frequency (ω) dependence on the modulus. The G' *versus* ω of the samples fitted well to the power law model after the UHP treatment, with a pressure higher than 400 MPa. As the treatment pressure and time were increased, the K' and K'/n' was increased, suggesting that the UHP treatment promoted the formation of non-covalent bonds and enhanced the gel strength of the samples (32, 33). When the WPI concentration was 12% (w/v), the modulus of the samples showed a better imitative effect with a κ-CG concentration higher than 0.5% (w/v). For the samples with better gel properties, the fitting parameter n' for power law model was decreased as the WPI and κ-CG concentration increase, accompanied by a significantly increased K' value. This was consistent with the report of Elsevier (34), who had proposed that the rheological behavior of emulsions can be regulated by the protein/polysaccharide ratio, and a higher protein/polysaccharide ratio is beneficial for the interactions between protein molecules.

Texture Analysis of Emulsion Gels

The texture properties of emulsion gel samples were determined and the results are shown in **Figure 3**. Obviously, the hardness, elasticity, chewiness, and adhesiveness of composite emulsion gels were increased with the increase of treatment pressure and time. The elasticity reflects the structural damage extent of the samples after initial compression. A relatively low elasticity indicates a serious damage occurred in emulsion gels during compression. The cohesiveness was used to characterize the difficulty to destroy the gel structure of samples. The more compact the gel structure is, the higher the cohesion (35, 36). Compared with other samples, the emulsion gels under the treatment of 400 MPa had a lower elasticity but

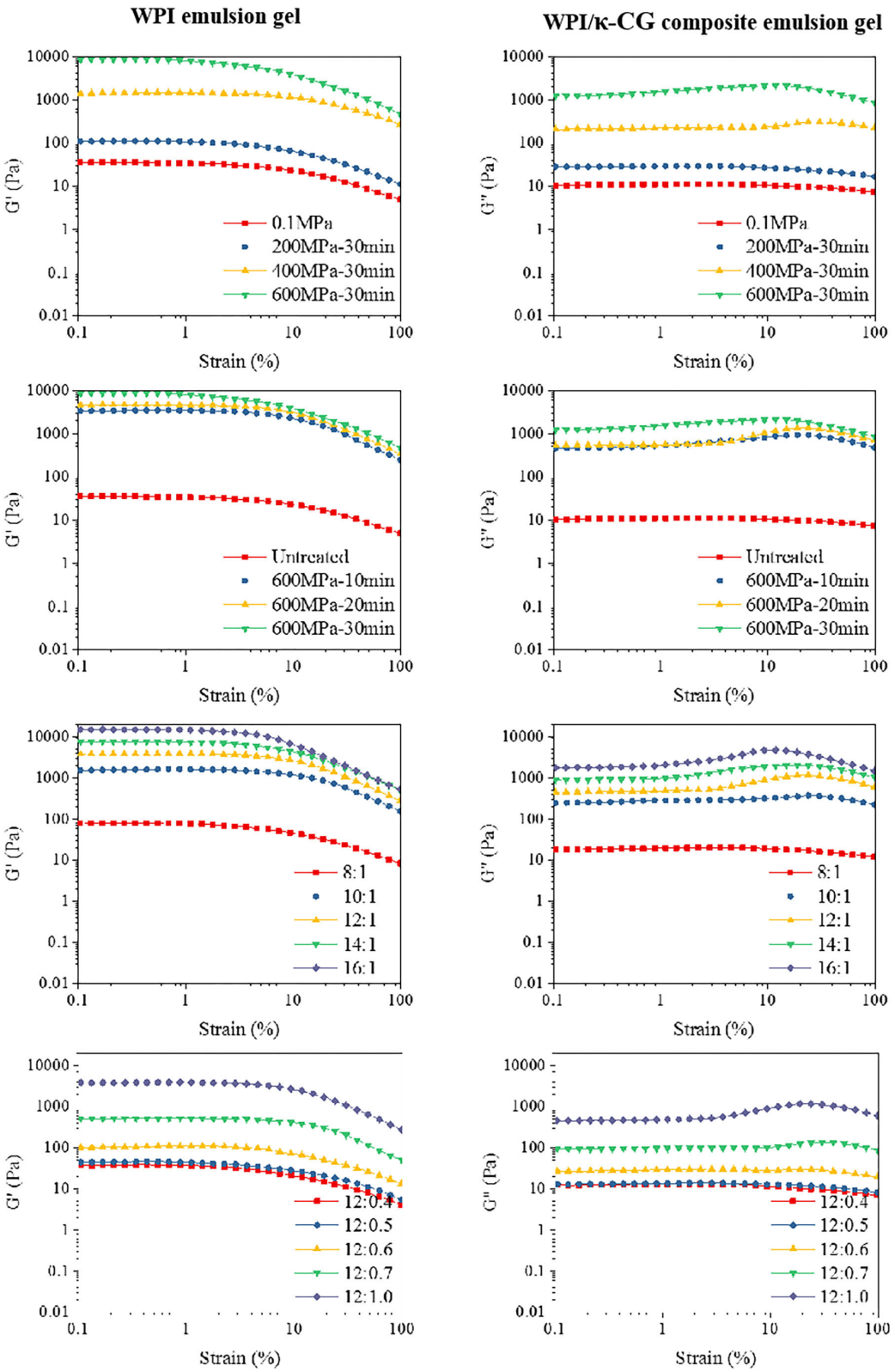

FIGURE 2 | Strain scan curves of WPI and WPI/κ-CG composite emulsion gels [The concentration ratio number "a:b" in the figure represents "WPI%(w/v):κ-CG%(w/v)" in aqueous phase.].

TABLE 3 | Power Law parameters for WPI/κ-CG composite emulsion gel of different processing conditions and composition ratios.

Processing conditions	WPI concentrations (wt%)	κ-CG concentrations (wt%)	$G' = K' \bullet \omega^{n'}$			
			K'	n'	R^2	K'/n'
—	12	1	17.95288 ± 1.60542	0.32318 ± 0.02539	0.87605	55.55071
200 MPa−30 min			59.67279 ± 2.26976	0.11821 ± 0.01331	0.75812	504.8032
400 MPa−30 min			993.69014 ± 12.08667	0.11641 ± 0.00427	0.96466	8536.124
600 MPa−10 min			2109.82495 ± 19.75605	0.11257 ± 0.0033	0.97716	18742.34
600 MPa−20 min			3710.52839 ± 30.47441	0.08493 ± 0.00302	0.96614	43689.25
600 MPa−30 min			5364.19299 ± 65.84353	0.10253 ± 0.00439	0.95248	52318.28
	8		42.16605 ± 2.42844	0.25085 ± 0.01731	0.89503	168.0927
	10		834.01794 ± 8.61492	0.13879 ± 0.00351	0.98347	6009.208
	14		5795.58181 ± 109.61936	0.08898 ± 0.00691	0.85814	65133.53
	16		11001.57157 ± 63.66716	0.0879 ± 0.00212	0.98427	125160.1
	12	0.4	18.81607 ± 1.27015	0.12802 ± 0.0233	0.56204	146.9776
		0.5	4.9251 ± 1.55024	0.81397 ± 0.0759	0.88812	6.050714
		0.6	47.86639 ± 3.908	0.31371 ± 0.02334	0.88784	152.5817
		0.7	337.98244 ± 7.21355	0.15368 ± 0.00712	0.94709	2199.261

an extremely higher cohesiveness, which might be explained by the fact that 400 MPa is close to the critical pressure of gel formation. Although the sample treated under 400 MPa also exhibited a gel-like property, the regularity of the gel network and the strength of interaction between the networks were very weak, thereby decreasing the gel strength of the sample.

As the WPI concentration was increased, the gel properties of the samples were enhanced. Especially, the growth in cohesiveness was slowed down, accompanied by a reduced elasticity as well as the occurrence of broken phenomenon during the secondary chewiness. On the other hand, the increase in the κ-CG concentration also led to the increase in gel strength. As reported by Schmitt and Turgeon (37), highly negative-charged polysaccharide can increase the hardness of a gel, but also making them more brittle and difficult to recover after shearing. However, the recovery ability of a gel is dominated by the interaction strength between protein and polysaccharide. The emulsion gel samples containing 10% (w/v) WPI and 1% (w/v) κ-CG have the same WPI/κ-CG ratio with samples containing 12% (w/v) WPI and 1.2% (w/v) κ-CG; however, only the latter one showed a decreased gel strength. This phenomenon suggested that although WPI and κ-CG had a synergistic effect on the formation of composite emulsion gels, an excessively high WPI/κ-CG concentration would lead to the formation of an excessively compact gel structure, decreasing their protective effects against external force.

Fluorescence Spectral Analysis

The emulsions with a WPI and κ-CG concentration of 20 wt% (w/w) and 2 wt% (w/w) were prepared with the same method described above prior to treating with different pressure and time. The samples were in a liquid state since the concentration of WPI and κ-CG were not high enough to form a gel structure. The samples were performed a fluorescence spectral analysis in order to evaluate the structure change of WPI in emulsions during UHP treatment.

It is well-known that the endogenous fluorescence of protein is mainly ascribed to the tryptophan (Trp), tyrosine (Tyr), and phenylalanine (Phe) in protein, with a fluorescence intensity ratio of 100:9:0.5. This signifies that the fluorescent character of protein containing Trp mainly depends on the existence of Trp. β-lactoglobulin, the main component of WPI, is able to fluoresce under excitation mostly due to the hidden Trp19, rather than Trp61 at the surface, while the fluorescence of α-lactalbumin derives from its four Trp residues. The maximum emission wavelength (λ_{max}) of the emulsion samples was about 328 nm, which is between 320 and 350 nm, the maximum emission range of Trp.

The high-pressure treatment will denature the protein molecules, and the microenvironment of fluorescent amino acid groups can be transferred from the polar hydrophilic surface to the hydrophobic interior, thereby increasing the fluorescence intensity of WPI and WPI/κ-CG in emulsions. As shown in **Figure 4**, the fluorescence intensity was increased with the increasing processing pressures (0.1∼600 MPa) and time (0∼40 min). The fluorescence intensity was obviously increased when the pressure was higher than 200 MPa, which indicated that the WPI was denatured at this moment. Either WPI emulsions or WPI/κ-CG composite emulsions, the fluorescence intensity curve of the sample treated at 600 MPa for 20 and 30 min was nearly coincident. Presumably, the WPI molecules had cross-linked with each other and formed a relatively stable intermolecular structure under this condition, while the molecular structure of WPI was further destroyed by UHP

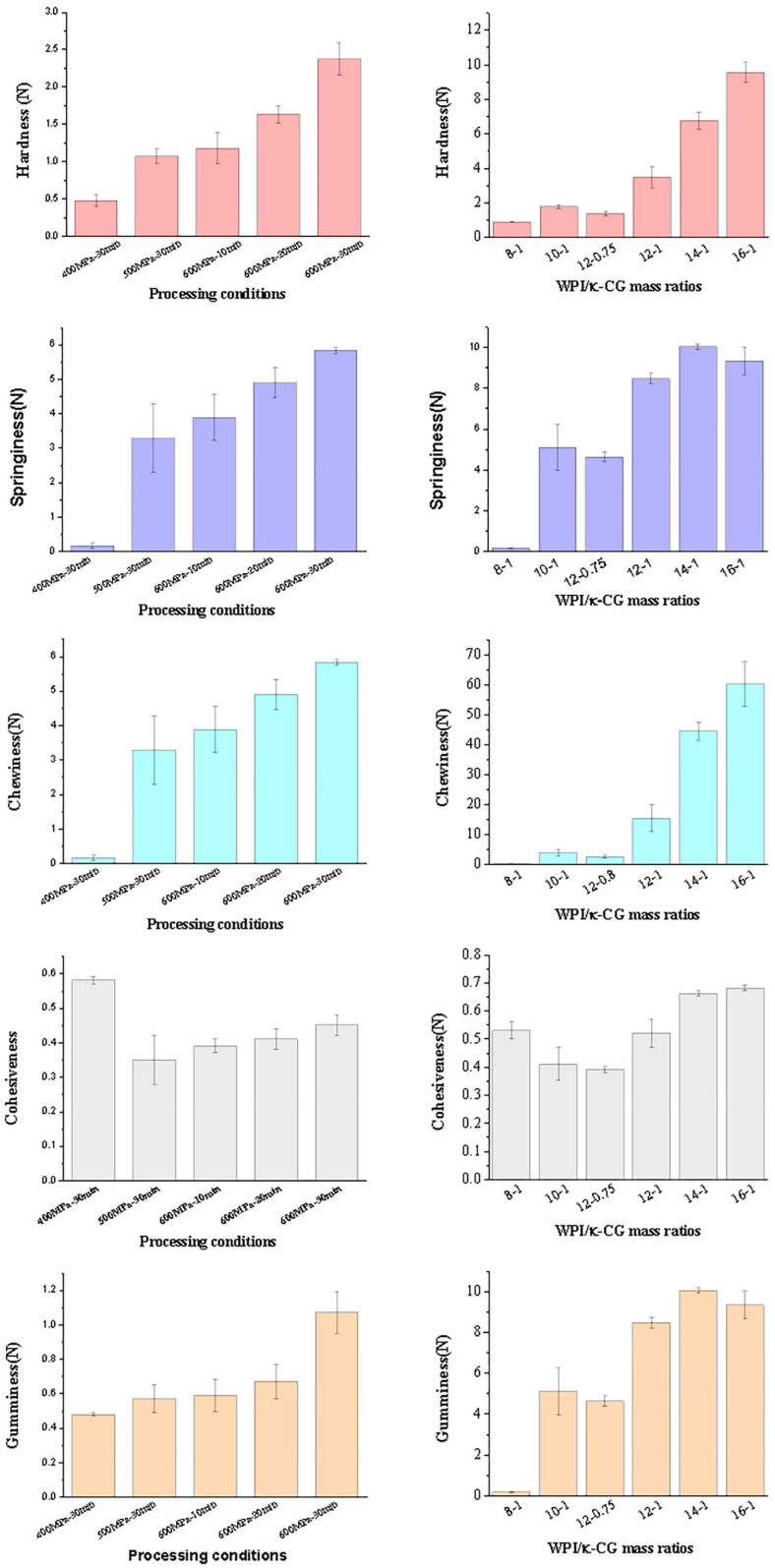

FIGURE 3 | Texture of emulsion gels of different processing conditions and composition ratios [The concentration ratio number "a:b" in the figure represents "WPI%(w/v):κ-CG%(w/v)" in aqueous phase.].

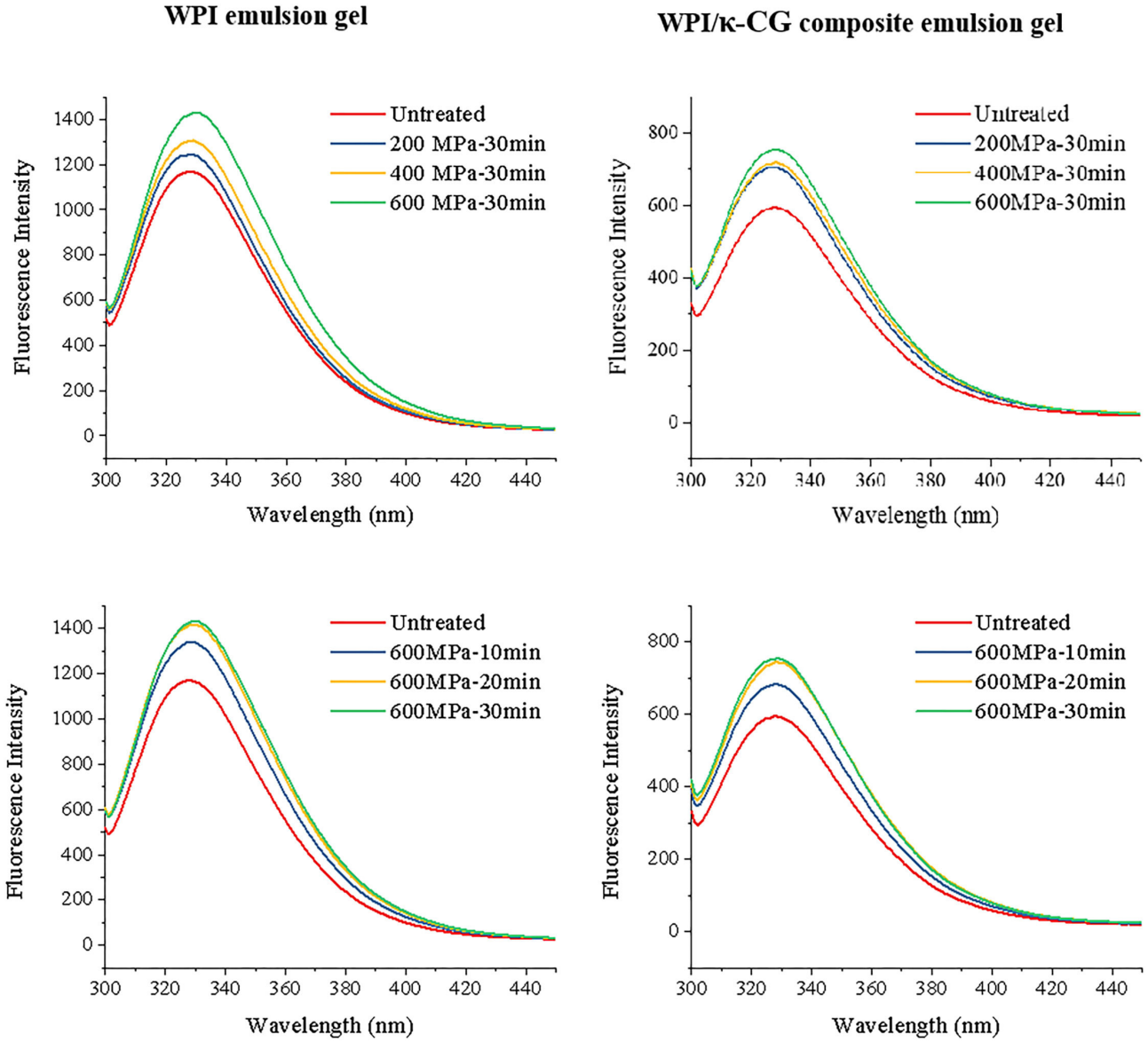

FIGURE 4 | Fluorescence spectra of WPI and WPI/κ-CG composite emulsions with different processing conditions.

treatment, thereby leading to an enhancement in fluorescence. The fluorescence intensity (I_f) of the untreated WPI/κ-CG emulsion was about 594.98, which was much lower than that of the WPI emulsion (1168.38), corresponding to a λ_{max} value of 328 nm. The phenomenon is so-called quenching of protein. The quenching would be ascribed to the Trp, Tyr, or Phe in protein, which were covered up during the binding process of nonfluorescent molecular κ-CG with WPI, preventing the exposure of these chromophore. Similar phenomenon was also reported in a previous research (38), where κ-CG could modify the tertiary structure of peanut protein, as well as adsorb onto the surface of peanut protein, which prevents the exposure of Trp to the aqueous phase.

Effect of UHP on Secondary Structure of Protein

Table 4 shows the secondary structure of WPI in WPI and WPI/κ-CG solution with or without UHP treatment, calculated by DICHROWEB. The results indicated that the α-coil content was significant decreased, while the β-sheet, β-turn, and random-coil contents were increased (among them, the content of β-sheet increased most significantly) when WPI and κ-CG were combined under atmospheric pressure. Considering the fact that κ-CG is not able to induce the damage in the secondary structure of WPI molecules under normal pressure, it can be deduced that the interaction between κ-CG and WPI promoted the production of intermolecular β-sheets between WPI molecules.

TABLE 4 | Changes in secondary structure of WPI and WPI/κ-CG complexes.

Sample	Pressure (MPa)	Time (min)	α-coil (%)	β-sheet (%)	β-turn (%)	Random-coil (%)
WPI	0.1	0	19.1	29.6	21.1	30.3
	200	30	18.5	29.0	21.6	30.9
	400	30	19.6	27.3	21.8	31.4
	600	10	18.0	28.1	22.1	31.9
		20	17.8	27.9	22.2	32.1
		30	17.1	28.1	22.2	32.2
WPI/κ-CG	0.1	0	11.6	34.7	21.9	31.8
	200	30	11.7	34.6	21.9	31.9
	400	30	10.7	34.7	22.3	32.4
	600	10	11.5	34.3	22.1	32.1
		20	10.3	34.9	22.3	32.6
		30	10.7	34.7	22.3	32.4

The intramolecular and intermolecular hydrogen bonds are responsible for the α-helix and β-sheet of protein, respectively, which are strongly influenced by hydrophobic and electrostatic interactions (39–41). Li et al. (42) have proposed that the higher electrostatic repulsion between protein molecules may be the reason for the decrease of random coil content and the increase of α-helix content in secondary structure. Therefore, the change of secondary structure content in this experiment was mostly due to the fact that the electrostatic interaction between WPI and κ-CG reduced the electrostatic repulsion between WPI molecules. Examples of polysaccharides affecting the secondary structures of proteins are abundant and the effect of polysaccharides on the secondary structure of proteins was verified to be related to the types of proteins and polysaccharides. For example, the acacia gum was found to be able to cause about 70% loss of α-helix in β-lactoglobulin (43), and pectin was also found to change the α-helix content of β-lactoglobulin (44).

The α-helix and β-sheet content of WPI in WPI emulsion was decreased at a relatively low pressure of 200 MPa but increased at 400 MPa. This was mostly due to the fact that the secondary structure of WPI was unfolded at a low pressure, while the increased pressure facilitated the refolding of protein molecules and the intermolecular interactions between protein molecules, which jointly contributed to the formation of the gel network. This phenomenon was consistent with a previous report by Acero-Lopez et al. (45) who have reported that the treatment at 200 MPa converted the secondary structure of ovotransferrin from α-helix, β-sheet, β-turn, and aggregate chains into intermolecular β-sheet or aggregated strands, leading to the rearrangement of ovotransferrin under high-pressure conditions. With the UHP treatment under 600 MPa, the content of α-helix and β-sheet was decreased, which could be explained by the fact that the high pressure damaged the gel network in emulsions. Moreover, the β-turn and random coil were increased with the increase of the processing pressure and time, which was agreed with a previous research of Maria et al. (46).

Compared with WPI emulsions, the WPI/κ-CG composite emulsions showed a relatively small change, and the change tended to occur under relatively high pressure. For example, the decrease of α-helix and β-sheet was found until the pressure was increased to 400 MPa. Besides, under the treatment of 600 MPa, the α-helix and β-sheet contents showed a trend of decrease-increase and decrease-increase-decrease, respectively, with the increase of treatment time. This phenomenon could be ascribed to the fact that the intermolecular interactions existed in the WPI/κ-CG composite emulsions are not liable to be destroyed by the UHP treatment since the κ-CG molecules were beneficial to protect the secondary structure of WPI.

Fourier Transform Infrared Spectroscopy

The FTIR spectroscopy is often used to analyze the composition of functional groups and the conformational changes in biomacromolecules. The conformation and flexibility of biomacromolecules, such as proteins and polysaccharides, are responsible for their intermolecular interactions, chemical properties, and functional properties (47). **Figure 5** depicts the FTIR spectra of WPI and WPI/κ-CG composite emulsions with or without the UHP treatment under different processing pressure and time. For both WPI and WPI/κ-CG composite emulsion gel samples, as the treatment pressure or time increases, a red shift could be seen in the broad absorption peaks in 3,200∼3,500 cm^{-1} region (amide A band), which is the characteristic for the intermolecular vibration of hydrogen bond O-H stretching. Taking WPI emulsion gels as an example, the absorption peak of the sample without high-pressure treatment was at the wave number of 3293.02 cm^{-1}, which was shifted to a higher wave numbers at 3304.35 cm^{-1}, 3394.43 cm^{-1}, and 3397.17 cm^{-1} after UHP treatment under 400 MPa for 30 min, 600 MPa for 10 min, and 600 MPa for 30 min, respectively. Therefore, it could be inferred that the UHP treatment could impact the hydrogen bonding of WPI molecules, weakening their affinity to water molecules, as well as enhancing the interactions between WPI molecules. Compared with WPI emulsion gels, a red shift in the corresponding absorption peak of WPI/κ-CG composite gels could be also observed, which was mostly due to the hydroxyl vibration of κ-CG (44). Moreover, the sharper absorption peak characterizing N-H stretching vibration gradually occurred in the spectra

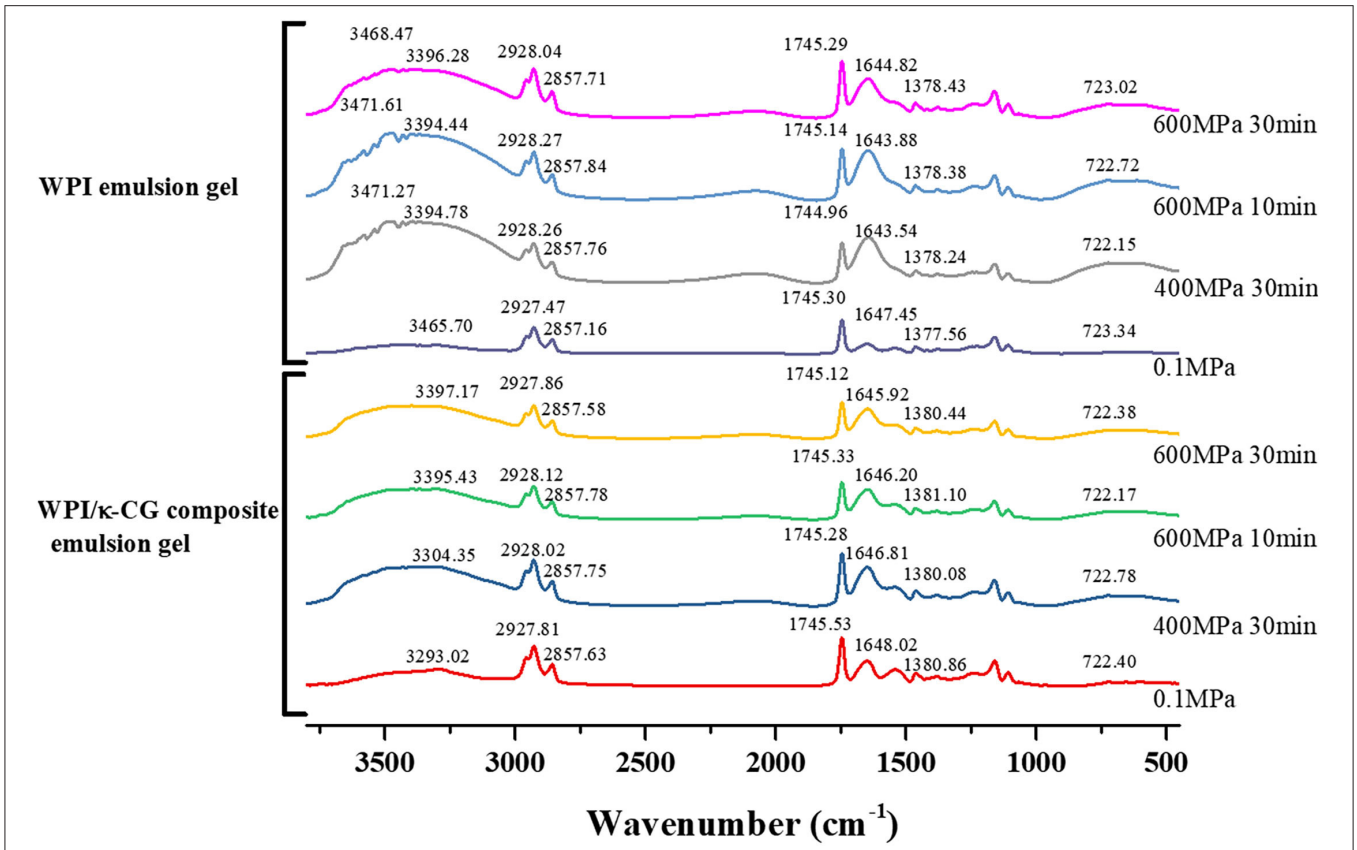

FIGURE 5 | Fourier transform infrared spectroscopy (FTIR) spectra of samples treated with different pressure and time.

of WPI/κ-CG composite gels near the wave number of 3,470 cm^{-1}, which would be blue shifted when the N-H group of the WPI participated in the formation of hydrogen bond in an α chain.

It could be observed that the untreated emulsion sample had a peak at the wavenumber of 1542.27 cm^{-1}, which was associated with the stretching vibration of C–N group and bending vibration of N–H group (amide II). After treated by UHP, a decrease in the intensity of the absorption peak for amide II occurred. At the same time, the peak at 1648.02 cm^{-1}, which was the characteristic peak of amide I (C=O stretching vibration and C-N bending vibration), was red shifted with a significantly increased intensity. These phenomena suggested that an increase in the coiled structure of emulsion gel samples, in other words, a decrease in the ordered structure, due to the formation of WPI/κ-CG complex (48, 49). According to the report of Timilsena et al. (50) negatively charged sulfate groups in κ-CG were able to combine with the positively charged amide groups in polypeptide chains to form polyelectrolyte complexes, leading to higher amplitudes in amide I. Therefore, it could be deduced that the κ-CG and WPI molecules in composite emulsions were combined with each other, exerting a synergistic effect on the formation of the gel structure. As the processing pressure and time increases, the absorption peak near 1542.27 cm^{-1} in the amide II region was red shifted, which might be due to the fact that the hydrophilic groups containing in κ-CG molecules could affect the intermolecular hydrogen bond between WPI molecules.

Microstructure of Emulsion Gels

The SEM images of emulsion gels were captured using SEM to characterize their microstructure. As depicted in **Figure 6**, for samples without UHP treatment, nanosized particles were suspended and aggregated in emulsions, forming large particle aggregations. However, after UHP treatment, clear filament-like cross-linked structure or spherical aggregate with large cavity was formed as the processing pressure and time increase. It could be also observed that the greater the intermolecular bond and the larger the reactivity of protein side chains, the more regular the connection of the WPI molecules, in agreement with several previous reports (51, 52). Previous experiments have confirmed that the emulsion gel formed under 400 MPa was softer, moister, and more liquid-like than the emulsion gel formed under 600 MPa, which could be also explained by the microstructure of these emulsion gels. The regular three-dimensional gel network could provide a good support for the gel structures in emulsions, endowing them with an enhanced hardness and elastic properties. A large amount of moisture was

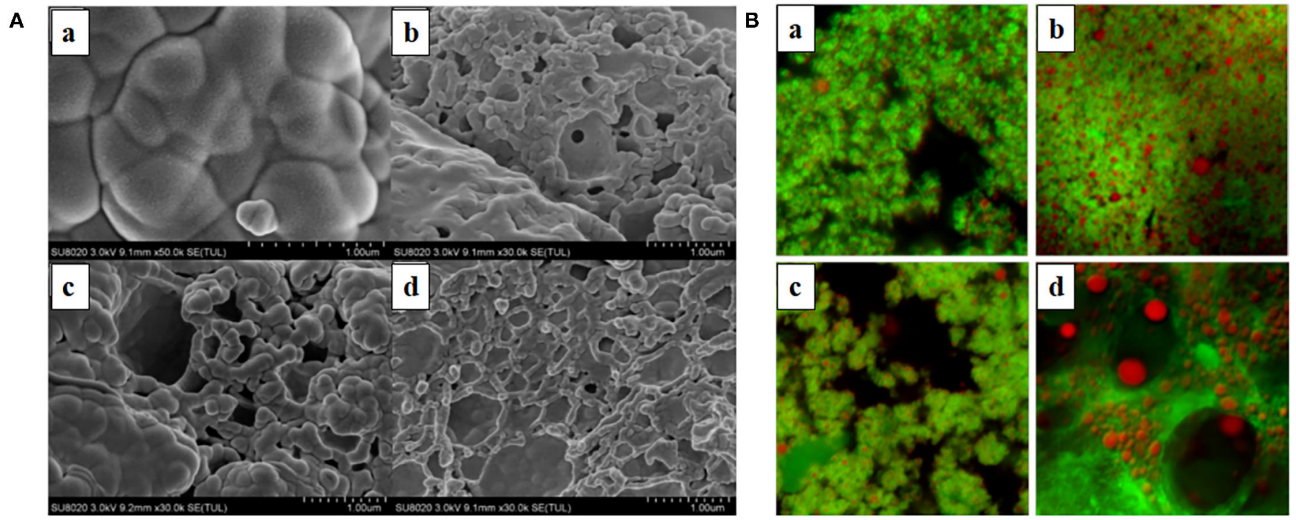

FIGURE 6 | Emission scanning electron microscope (SEM) **(A)** and confocal laser scanning microscopy (CLSM) **(B)** images of emulsion gels treated with different pressure and time. The MCT concentration was 20% (w/w), and the aqueous phase contained 10% (w/v) WPI and 1% (w/v) κ-CG. a–d were the images of untreated and UHP-treated emulsion gel samples under 400 MPa for 30 min, 600 MPa for 10 min, and 600 MPa for 30 min, respectively.

blocked within the pore formed by WPI, hindering the freely flow of water molecules.

For composite gels containing κ-CG, only a low concentration of WPI was required to form an emulsion gel with relatively high hardness with the UHP treatment under 600 MPa for 30 min, suggesting that the electrostatic interaction between κ-CG and WPI was beneficial to the formation of gel structure in emulsions. It could be also found that the gel network of WPI/κ-CG composite emulsion was loose and disordered with large and uneven cavities. This might be due to the fact that the gel structure in emulsion gels induced by UHP treatment depended on the protein unfolding and aggregation rate. The introduction of κ-CG molecules enhanced the viscosity of emulsions, hindering the movement of protein molecules and the aggregation of WPI molecules (53). Another possible explanation might be that the WPI concentration employed in the composite emulsion gel was not sufficient to form a dense network structure.

Figure 6B shows the CLSM image of samples with a magnification of 100x. The MCT was stained with Nile Red (presenting in blue), whereas the WPI was stained by Nile Blue (presenting in red). The size of oil droplets was increased as the processing pressure increases, which indicated that the UHP treatment contributed to the aggregation and coalescence of oil droplets. When the processing pressure was higher than 400 MPa, the oil droplets were embedded within a regular network composed of WPI molecules. Moreover, unlike the emulsion gel treated under 400 MPa for 30 min, whose gel network was indistinct, the emulsion gel treated under 600 MPa for 30 min exhibited a clear structure with obvious boundary. However, the droplet size was not uniform and large cavities could be seen, further confirming the results obtained by SEM observation.

Intermolecular Force of Emulsion Gels Induced by UHP

In this experiment, three kinds of bond cleavage agents, NaCl, urea, and propylene glycol were used to destroy the main non-covalent bonds in emulsion gels. These bond cleavage agents are able to cause the irreversible molecular rearrangement of WPI, which was manifested as the texture changes in emulsion gel samples. The addition of NaCl into emulsion gels introduced a large amount of Na^+, which could adsorb onto the surface of protein molecules and lead to an electrical shielding effect, thereby reducing the electrostatic interactions between protein molecules. Urea was primarily used to destroy the hydrogen bonds in emulsion gel samples, replacing protein-protein and protein-water interactions through forming more stable protein-urea hydrogen bonds; in this case, more hydrophobic residues were exposed, preventing the formation of gel networks (54). The propylene glycol was used to inhibit the hydrophobic interaction in emulsion gels. Since the materials utilized in the current work (WPI and κ-CG) were biological macromolecules, the Van der Waals force could be ignored (too weak). Although the SD of the data in this section was relatively large due to the inevitable systematic errors (e.g., slight thickness difference or sample tilting when the gel was too soft), significant changes could be found in the texture of emulsion gels, as shown in **Figure 7**.

The existence of a low level of ion can effectively weak the intermolecular repulsion through combining with amino acids and water molecules. As the NaCl level increases, the strength of emulsion gels was remarkably increased. However, an extremely high NaCl level led to the reduction in the attractive forces as well as the increase in the repulsion or dissociation between protein molecules, thereby weakening the cross-linking between protein chains (55). As shown in **Figure 7**, NaCl with a concentration of 0.4 mol/L contributed to increase the hardness of emulsion

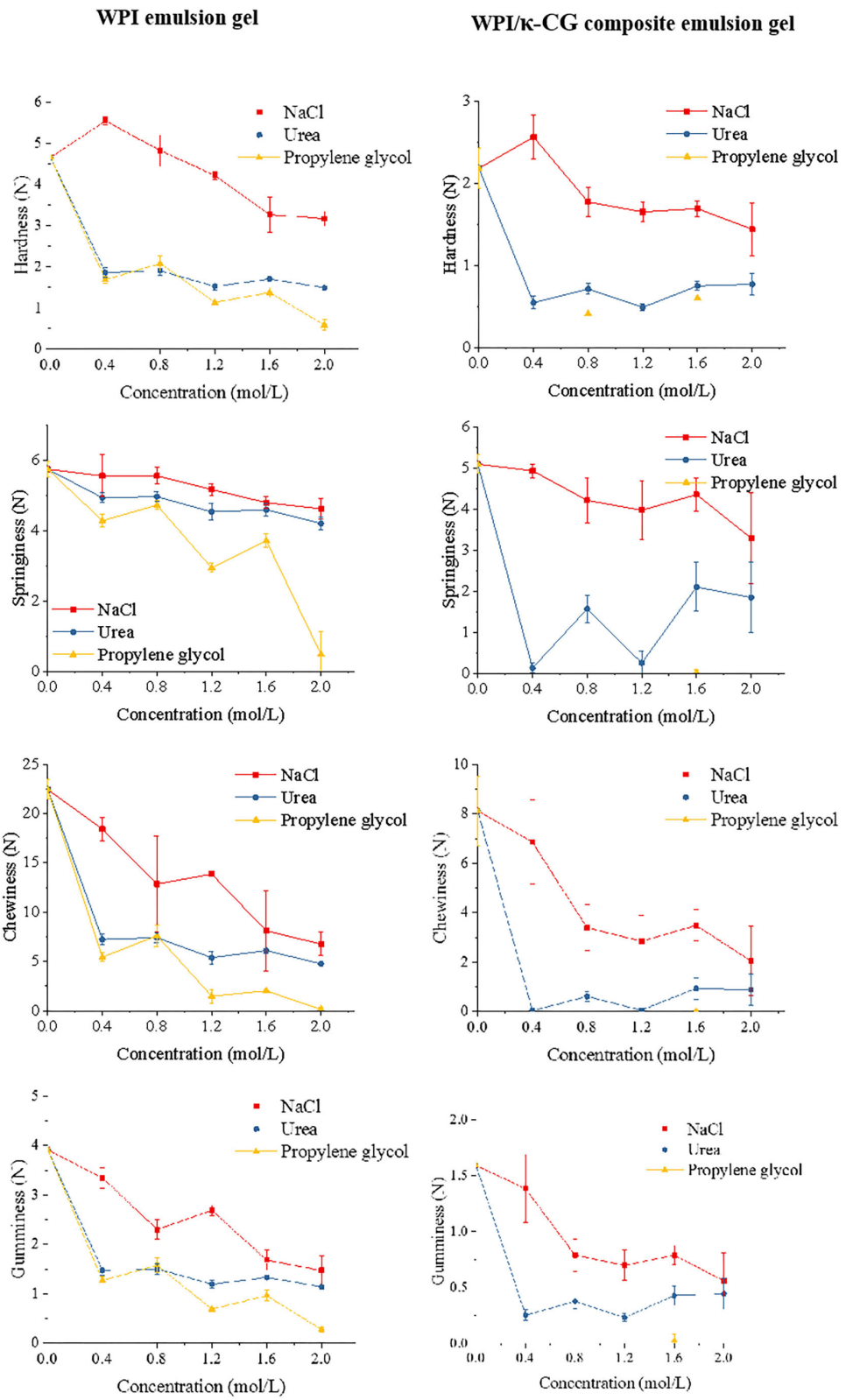

FIGURE 7 | Effect of different concentrations of NaCl, urea, and propylene glycol on the texture properties of emulsion gels.

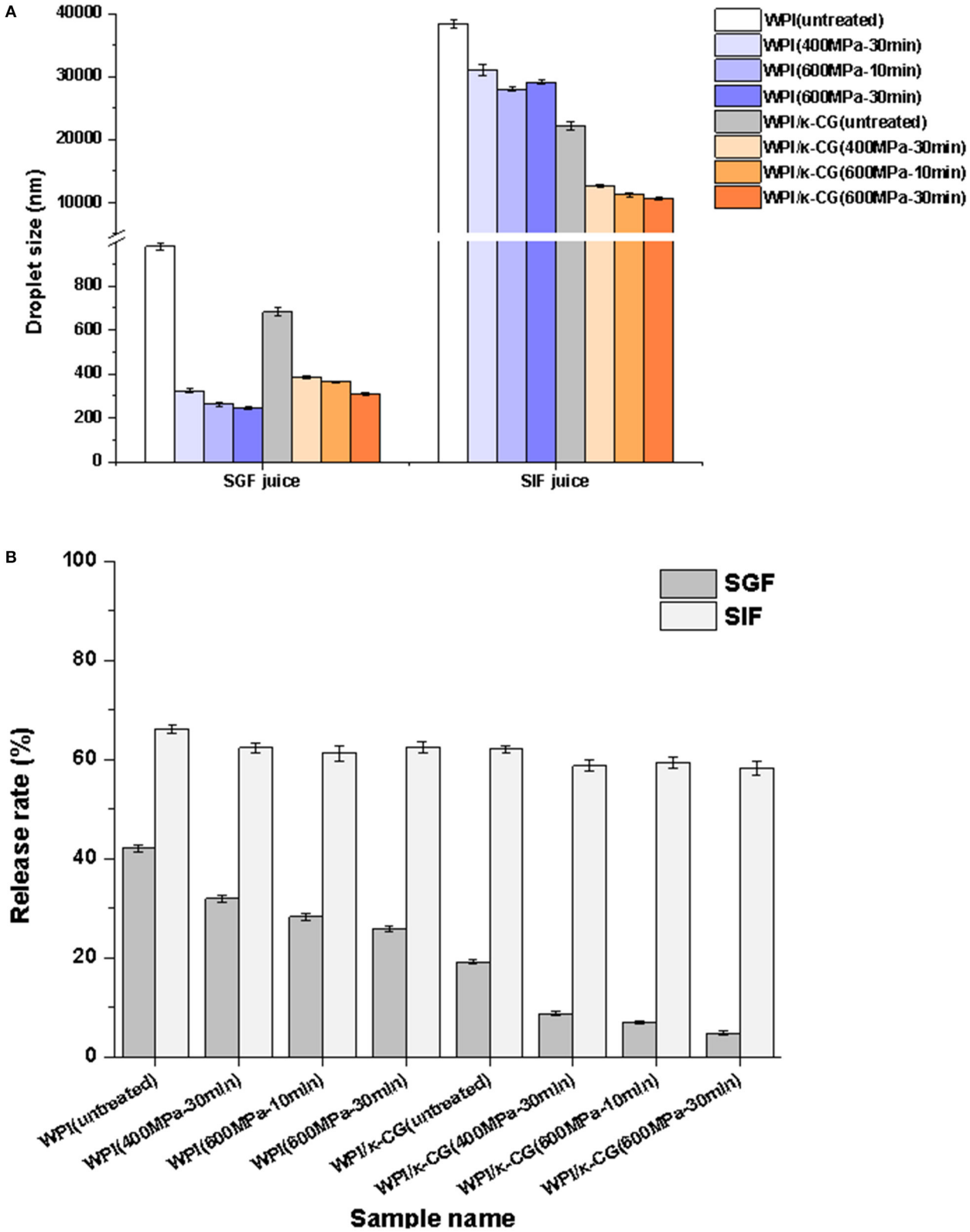

FIGURE 8 | (A,B) Droplet size after simulated gastric fluid (SGF) and simulated intestinal fluid (SIF) digestion and bioacessibility of curcumin of WPI and WPI/κ-CG composite emulsion gels with different treatments.

gels, whereas the hardness was significantly decreased as the NaCl concentration was further increased. With the addition of urea, the WPI emulsion gel could remain in its texture. It could be also observed that the elastic was nearly unchanged in WPI emulsion gel, but changed obviously in WPI/κ-CG composite emulsion gel. This phenomenon indicated that κ-CG promoted the formation of intermolecular hydrogen bonds, which led to the destruction of gel structure during the initial compression process in the TPA measurement mode. Noteworthily, the effect of propylene glycol on the texture of emulsion gel was most obvious, indicating that the hydrophobic interaction is the critical factor that affected the formation of these emulsion gels. Moreover, the WPI/κ-CG composite gel treated with propylene glycol was excessively soft, even not achieving the requirement for a TPA measurement, indicating that the hydrophobic interaction is the most important factor that affects the formation of the gel structure in composite gels.

In vitro Gastrointestinal Digestion

Figure 8A presents the changes in the droplet size of WPI and WPI/κ-CG emulsion gels after SGF and SIF digestion. Apparently, whether for WPI or WPI/κ-CG emulsion gels, the UHP treatment samples exhibited a significant decrease in the droplet size compared to that of untreated samples after SGF and SIF digestion. It could be also observed that there was also a significant difference in the particle size of emulsion gels with different processing conditions. For the same sample, the increase in both treatment time and pressure led to a decrease in the droplet size of SGF and SIF digestion juice. One of possible explanations might be that the UHP treatment led to a more compact structure in these emulsion gels, which would further inhibit the digestion. Moreover, the droplet size of WPI emulsion gels was significantly smaller than that of WPI-κ-CG composite emulsion gels after SGF digestion. On the contrary, the WPI emulsion gels were determined with larger droplet size compared with that of WPI-κ-CG composite emulsion gels after SIF digestion. This result might be attributed to the difference in the droplet size of the untreated WPI emulsion and WPI-κ-CG composite emulsion.

The lipid would be hydrolyzed into diacylglycerols and monoglycerols during digestion, leading to the release of free fatty acid (FFA). The released FFA at the oil/water interface is liable to combine with bile salts and phospholipids to form micelles. The curcumin in micelles is considered to be solubilized and bioaccessible. As presented in **Figure 8B**, the cumulative release of curcumin in UHP-treated emulsion gels was slightly decreased compared to that of untreated emulsions. Moreover, the treatment pressure and time had nearly no effect on the cumulative release of curcumin in emulsion gels during *in vitro* simulated digestion. Interesting enough, the incorporation of κ-CG was confirmed to contribute to the controlled release of curcumin. Most of the curcumin encapsulated within WPI/κ-CG composite emulsion gels was released in SIF stage, whereas the majority of curcumin was released during SGF stage in WPI emulsion gels.

CONCLUSIONS

In this work, the WPI/κ-CG composite emulsion gels were successfully prepared through UHP treatment. The structure of the emulsion gels was mainly maintained by hydrophobic interaction and hydrogen bonding. The UHP treatment can lead to the denaturation of WPI in the emulsion gels. As the pressure increases, the secondary structure of WPI undergoes a process of destruction-forming, and the UHP treatment under a longer time can cause a secondary destruction. Moreover, κ-CG was able to combine with WPI through electrostatic interaction, protecting the WPI molecules against denaturation to a certain extent. The results also confirmed that the UHP treatment significantly retarded the release of curcumin but was beneficial to the controlled release of curcumin. These findings not only developed a non-thermal process to fabricate emulsion gels, but also provided useful information for the development of protein/polysaccharide composite emulsion gels as effective delivery systems for the encapsulation of thermal sensitive functional components.

DATA AVAILABILITY STATEMENT

The original contributions presented in the study are included in the article/supplementary material, further inquiries can be directed to the corresponding author/s.

AUTHOR CONTRIBUTIONS

JS: conceptualization, methodology, and writing-original draft preparation. LW and XL: visualization and investigation. WD: data curation. JW: software. JY: visualization. FR: supervision. FY and PW: writing-reviewing and editing. All authors contributed to the article and approved the submitted version.

FUNDING

This research was funded by the National Natural Science Foundation of China (No. 31901625) and the National Natural Science Foundation of China (No. 31371836).

REFERENCES

1. Dickinson E. Emulsion gels: the structuring of soft solids with protein-stabilized oil droplets. *Food Hydrocoll.* (2012) 28:224–41. doi: 10.1016/j.foodhyd.2011.12.017
2. Mantovani RA, Cavallieri ALF, Cunha RL. Gelation of oil-in-water emulsions stabilized by whey protein. *J Food Eng.* (2016) 175:108–16. doi: 10.1016/j.jfoodeng.2015.12.011
3. de Oca-Ávalos JM, Huck-Iriart C, Candal RJ, Herrera ML. Sodium caseinate/sunflower oil emulsion-based gels for structuring food. *Food Bioprocess Technol.* (2016) 9:981–92. doi: 10.1007/s11947-016-1687-0
4. Wang X, He Z, Zeng M, Qin F, Adhikari B, Chen J. Effects of the size and content of protein aggregates on the rheological and structural properties

of soy protein isolate emulsion gels induced by CaSO4. *Food Chem.* (2017) 221:130–8. doi: 10.1016/j.foodchem.2016.10.019
5. Li W, Huang M, Wang P, Xu X. Rheological and nuclear magnetic resonance characterization of porcine plasma protein-stabilized gel-like emulsion affected by pH and heating. *LWT Food Sci Technol.* (2017) 75:460–5. doi: 10.1016/j.lwt.2016.09.025
6. Wang P, Cui N, Luo J, Zhang H, Guo H, Wen P, et al. Short communication: stable water-in-oil emulsions formulated with polyglycerol polyricinoleate and glucono-δ-lactone-induced casein gels. *Food Hydrocoll.* (2016) 57:217–20. doi: 10.1016/j.foodhyd.2016.01.013
7. Lim SH, Kim HR, Choi SJ, Moon TW. Lipid oxidation of sodium caseinate-stabilized emulsion-gels prepared using microbial transglutaminase. *Food Sci Biotechnol.* (2015) 24:2023–6. doi: 10.1007/s10068-015-0267-9
8. Trujillo AJ, Capellas M, Buffa M, Royo C, Gervilla R, Felipe X, et al. Application of high pressure treatment for cheese production. *Food Res Int.* (2000) 33:311–6. doi: 10.1016/S0963-9969(00)00042-9
9. Daryaei H, Balasubramaniam VM. Microbial decontamination of food by high pressure processing. In: *Demirci A, Ngadi MO, editors. Microbial Decontamination in the Food Industry*. Cambridge: Wood Publishing Limited (2012). p. 370–406. doi: 10.1533/9780857095756.2.370
10. He XH, Liu HZ, Liu L, Zhao GL, Wang Q, Chen QL. Effects of high pressure on the physicochemical and functional properties of peanut protein isolates. *Food Hydrocoll.* (2014) 36:123–9. doi: 10.1016/j.foodhyd.2013.08.031
11. Smulders PEA. *Formation and Stability of Emulsions Made with Proteins and Peptides: Industrial Proteins*, Vol. 5. Wageningen: ProQuest Dissertations Publishing (2000). p. 13–15.
12. Li XY, Mao LK, He XY, Yuan F. Characterization of β-lactoglobulin gels induced by high pressure processing. *Innovat Food Sci Emerg Technol.* (2018) 47:335–45. doi: 10.1016/j.ifset.2018.03.022
13. Chen X, Chen C G, Zhou Y Z, Li P J, Ma F, Nishiumi T, et al. Effects of high pressure processing on the thermal gelling properties of chicken breast myosin containing κ-CG. *Food Hydrocoll.* (2014) 40:262–72. doi: 10.1016/j.foodhyd.2014.03.018
14. Tang CH, Chen L, Foegeding EA. Mechanical and water-holding properties and microstructures of soy protein isolate emulsion gels induced by CaCl2, glucono-δ-lactone (GDL), and transglutaminase: influence of thermal treatments before and/or after emulsification. *J Agric Food Chem.* (2011) 59:4071–7. doi: 10.1021/jf104834m
15. Wagoner TB, Foegeding EA. Whey protein–pectin soluble complexes for beverage applications. *Food Hydrocoll.* (2017) 63:130–8. doi: 10.1016/j.foodhyd.2016.08.027
16. Liu K, Li Q M, Pan L H, Qian X P, Zhang H L, Zha X Q, et al. The effects of lotus root amylopectin on the formation of whey protein isolate gels. *Carbohydrate Polymers.* (2017) 175:721–7. doi: 10.1016/j.carbpol.2017.08.041
17. Necas J, Bartosikova L. κ-CG: a review. *Veterinarni Medicina*. (2013) 58:187–205. doi: 10.17221/6758-VETMED
18. Velde FV, Lourenco ND, Pinheiro HM. κ-CG: a food-grade and biocompatible support for immobilization techniques. *Adv Synthesis Catal.* (2010) 344:815–35. doi: 10.1002/1615-4169(200209)344:8<815::AID-ADSC815>3.0.CO;2-H
19. Verbeken D, Neirinck N, Meeren PVD, Dewettinck K. Influence of κ-CG on the thermal gelation of salt-soluble meat proteins. *Meat Sci.* (2005) 70:161–6. doi: 10.1016/j.meatsci.2004.12.007
20. Moreno HM, Herranz B, Borderías JA, Tover CA. Effect of high pressure treatment on the structural, mechanical and rheological properties of glucomannan gels. *Food Hydrocoll.* (2016) 60:437–44. doi: 10.1016/j.foodhyd.2016.04.015
21. Herranz B, Moreno HM, Javier Borderías A, Tovar CA. Structural and rheological properties of weakly deacetylated glucomannan gels after high-pressure treatment. *Int J Food Properties.* (2017) 20:1–9. doi: 10.1080/10942912.2017.1361972
22. Kudla E, Tomasik HP. The modification of starch by high pressure. Part II: compression of starch with additives. *Starch.* (1992) 44:253–9. doi: 10.1002/star.19920440704
23. Heger M, Golen R F V, Broekgaarden M. The molecular basis for the pharmacokinetics and pharmacodynamics of curcumin and its metabolites in relation to cancer. *Pharmacol Rev.* (2014) 66:222–307. doi: 10.1124/pr.110.004044
24. Wilken R, Veena MS, Wang MB, Srivatsan ES. Curcumin: a review of anti-cancer properties and therapeutic activity in head and neck squamous cell carcinoma. *Mol Cancer.* (2011) 10:1–19. doi: 10.1186/1476-4598-10-12
25. Ahmed K, Li Y, McClements DJ, Xiao H. Nanoemulsion- and emulsion-based delivery systems for curcumin: encapsulation and release properties. *Food Chem.* (2012) 132:799–807. doi: 10.1016/j.foodchem.2011.11.039
26. Mcclements DJ. Advances in fabrication of emulsions with enhanced functionality using structural design principles. *Curr Opin Colloid Interface Sci.* (2012) 17:235–45. doi: 10.1016/j.cocis.2012.06.002
27. Lobley A, Whitmore L, Wallace BA. DICHROWEB: an interactive website for the analysis of protein secondary structure from circular dichroism spectra. *Bioinformatics.* (2002) 18:211–2. doi: 10.1093/bioinformatics/18.1.211
28. Hyun K, Nam JG, Wilhellm M. Large amplitude oscillatory shear behavior of PEO-PPO-PEO triblock copolymer solutions. *Rheol Acta.* (2006) 45:239–49. doi: 10.1007/s00397-005-0014-x
29. Lapasin R, Pricl S. Rheology of industrial polysaccharides: theory and applications. *Springer Sci Business Media.* (1995) 276:108. doi: 10.1007/978-1-4615-2185-3
30. Rosalina I, Bhattacharya M. Dynamic rheological measurements and analysis of starch gels. *Carbohydrate Polym.* (2002) 48:191–202. doi: 10.1016/S0144-8617(01)00235-1
31. Morris E R, Nishinari K, Rinaudo M. Gelation of gellan - a review. *Food Hydrocoll.* (2012) 28:373–411. doi: 10.1016/j.foodhyd.2012.01.004
32. Wang Y, Chang Y, Xue Y, Li Z, Wang Y, Xue C. Rheology and microstructure of heat-induced fluid gels from Antarctic krill (Euphausia superba) protein: effect of pH. *Food Hydrocoll.* (2016) 52:510–9. doi: 10.1016/j.foodhyd.2015.07.032
33. Nicole M, Zhang C, Joseph H, Eeric K, Hua Y. Soybean oil volume fraction effects on the rheology characteristics and gelation behavior of Glucono-δ-Lactone and calcium sulfate-induced tofu gels. *J Texture Studss.* (2016) 47:112–30. doi: 10.1111/jtxs.12166
34. Katafis S. *Modern Biopolymer Science: Bridging the Divide Between Fundamental Treatise and Industrial Application*. London: Academic Press (2009).
35. Lau MH, Tang J, Paulson AT. Texture profile and turbidity of gellan/gelatin mixed gels. *Food Res Int.* (2000) 33:665–71. doi: 10.1016/S0963-9969(00)00111-3
36. Zhu JH, Yang XQ, Ahmad I, Li L, Wang XY, Liu C. Rheological properties of κ-CG and soybean glycinin mixed gels. *Food Res Int.* (2008) 41:219–28. doi: 10.1016/j.foodres.2007.11.009
37. Schmitt C, Turgeon SL. Protein/polysaccharide complexes and coacervates in food systems. *Adv Colloid Interface Sci.* (2011) 167:63–70. doi: 10.1016/j.cis.2010.10.001
38. Zhao H, Zhou F, Peng W, Zheng J, Dziugan P, Zhang B. The effects of κ-CG on stability of arachin and the interactions between them. *Food Hydrocoll.* (2015) 43:763–8. doi: 10.1016/j.foodhyd.2014.08.006
39. Zhang Z, Yang Y, Tang X, Chen Y, You Y. Chemical forces study of heat-induced myofibrillar protein gel as affected by partial substitution of NaCl with KCl, MgCl2 and CaCl2. *CyTA J Food.* (2016) 14:239–47. doi: 10.1080/19476337.2015.1091038
40. Gu B, Zhang F, Wang Z, Wang Z, Zhou H. The solvation of NaCl in model water with different hydrogen bond strength. *J Chem Phys.* (2008) 129:1157. doi: 10.1063/1.3002485
41. Levy-Moonshine A, Amir EAD, Keasar C. Enhancement of beta-sheet assembly by cooperative hydrogen bonds potential. *Bioinformatics.* (2009) 25:2639–45. doi: 10.1093/bioinformatics/btp449
42. Li J, Zhang Y, Fan Q, Teng C, Xie W, Shi Y, et al. Combination effects of NaOH and NaCl on the rheology and gel characteristics of hen egg white proteins. *Food Chem.* (2018) 250:1–6. doi: 10.1016/j.foodchem.2018.01.031
43. Gravelle AJ, Marangoni AG, Barbut S. The influence of particle size and protein content in particle-filled myofibrillar protein gels. *Meat Muscle Biol.* (2017) 1:109–21. doi: 10.22175/mmb2016.11.0004
44. Girard M, Turgeon SL, Gauthier SF. Thermodynamic parameters of β-lactoglobulin-pectin complexes assessed by isothermal titration calorimetry. *J Agric Food Chem.* (2003) 51:4450–5. doi: 10.1021/jf0259359

45. Acero-Lopez A, Ullah A, Offengenden M, Jung S, Wu J. Effect of high pressure treatment on ovotransferrin. *Food Chem.* (2012) 135:2245–52. doi: 10.1016/j.foodchem.2012.07.071
46. De Maria S, Ferrari G, Maresca P. Effects of high hydrostatic pressure on the conformational structure and the functional properties of bovine serum albumin. *Innovat Food Sci Emerg Technol.* (2016) 33:67–75. doi: 10.1016/j.ifset.2015.11.025
47. Qazvini N T, Bolisetty S, Adamcik J, Mezzenga R. Self-healing fish gelatin/sodium montmorillonite biohybrid coacervates: structural and rheological characterization. *Biomacromolecules.* (2012) 13:2136–47. doi: 10.1021/bm3005319
48. Yakimets I, Wellner N, Smith AC, Wilson RH, Farhat I, Mitchell J. Mechanical properties with respect to water content of gelatin films in glassy state. *Polymer.* (2005) 46:12577–85. doi: 10.1016/j.polymer.2005.10.090
49. Sinthusamran S, Benjakul S, Swedlund PJ, Swedlund PJ, Hemar Y. Physical and rheological properties of fish gelatin gel as influenced by κ-CG. *Food Biosci.* (2017) 20:88–95. doi: 10.1016/j.fbio.2017.09.001
50. Derkacha SR, Ilyinb SO, Maklakovaa AA, Kulichikhinb VG, Malkinb AY. The rheology of gelatin hydrogels modified by κ-CG. *LWT Food Sci Technol.* (2015) 63:612–9. doi: 10.1016/j.lwt.2015.03.024
51. Cao Y, Xia T, Zhou G, Xu X. The mechanism of high pressure-induced gels of rabbit myosin. *Innovat Food Sci Emerg Technol.* (2012) 16:41–6. doi: 10.1016/j.ifset.2012.04.005
52. Chen HH, Xu SY, Wang Z. Interaction between flaxseed gum and meat protein. *J Food Eng.* (2007) 80:1051–9. doi: 10.1016/j.jfoodeng.2006.08.017
53. Lefevre F, Fauconneau B, Ouali A, Culioli J. Thermal gelation of brown trout myofibrils: effect of muscle type, heating rate and protein concentration. *J Food Sci.* (2008) 63:299–304. doi: 10.1111/j.1365-2621.1998.tb15730.x
54. Das A, Mukhopadhyay C. Atomistic mechanism of protein denaturation by urea. *J Phy Chem B.* (2008) 112:7903–8. doi: 10.1021/jp800370e
55. Ganasen P, Benjakul S. Physical properties and microstructure of pidan yolk as affected by different divalent and monovalent cations. *J Food Biochem.* (2011) 43:77–85. doi: 10.1016/j.lwt.2009.06.007

Conflict of Interest: The authors declare that the research was conducted in the absence of any commercial or financial relationships that could be construed as a potential conflict of interest.

Publisher's Note: All claims expressed in this article are solely those of the authors and do not necessarily represent those of their affiliated organizations, or those of the publisher, the editors and the reviewers. Any product that may be evaluated in this article, or claim that may be made by its manufacturer, is not guaranteed or endorsed by the publisher.

frontiers in Nutrition

ORIGINAL RESEARCH
published: 17 March 2022
doi: 10.3389/fnut.2022.842850

Delivery of Curcumin Using Zein-Gum Arabic-Tannic Acid Composite Particles: Fabrication, Characterization, and *in vitro* Release Properties

Yiquan Zhang[1,2†], *Guiqiao Liu*[1,2†], *Fazheng Ren*[1,2], *Ning Liu*[1,2], *Yi Tong*[3*], *Yi Li*[3], *Anni Liu*[3], *Lida Wu*[3] *and Pengjie Wang*[1,2*]

[1] *Key Laboratory of Precision Nutrition and Food Quality, Key Laboratory of Functional Dairy, Beijing Higher Institution Engineering Research Center of Animal Product, College of Food Science and Nutritional Engineering, China Agricultural University, Beijing, China,* [2] *Department of Nutrition and Health, China Agricultural University, Beijing, China,* [3] *Jilin COFCO Biochemistry Co., Ltd., Changchun, China*

The application of curcumin (Cur) in fat-free food is limited due to its poor water solubility, stability, and bioaccessibility. In this study, zein-gum arabic-tannic acid (zein-GA-TA) composite particles with high physical stability were fabricated to deliver Cur (ZGT-Cur). Their stability and *in vitro* release properties were also evaluated. The results showed that the thermal and photochemical stability of Cur was improved after loading into composite particles. Meanwhile, the retention rate of Cur in ZGT-Cur composite particles was enhanced compared with Z-Cur or ZG-Cur particles. Fourier transform infrared (FTIR) spectroscopy confirmed that the hydrogen bond within the particles was greatly enhanced after the addition of tannic acid (TA). The *in vitro* antioxidant activity of Cur in ZGT-Cur composite particles was higher in terms of 2,2'-azino-bis (ABTS) (93.64%) and 1,1-diphenyl-2-picrylhydrazyl (DPPH) (50.41%) compared with Z-Cur or ZG-Cur particles. The bioaccessibility of Cur in ZGT-Cur composite particles was 8.97 times higher than that of free Cur. Therefore, the particles designed in this study will broaden the application of Cur in the food industry by improving its stability and bioaccessibility.

Keywords: tannic acid, composite particles, stability, curcumin, bioaccessibility

OPEN ACCESS

Edited by:
Weilin Liu,
Zhejiang Gongshang University, China

Reviewed by:
Zhili Wan,
South China University of Technology, China
Yufeng Chen,
Zhejiang University of Technology, China
Shima Saffarionpour,
University of Toronto, Canada

***Correspondence:**
Yi Tong
tongyi@cofco.com
Pengjie Wang
wpj1019@cau.edu.cn

†These authors have contributed equally to this work

Specialty section:
This article was submitted to Food Chemistry, a section of the journal Frontiers in Nutrition

Received: *24 December 2021*
Accepted: *21 January 2022*
Published: *17 March 2022*

Citation:
Zhang Y, Liu G, Ren F, Liu N, Tong Y, Li Y, Liu A, Wu L and Wang P (2022) Delivery of Curcumin Using Zein-Gum Arabic-Tannic Acid Composite Particles: Fabrication, Characterization, and in vitro Release Properties. Front. Nutr. 9:842850. doi: 10.3389/fnut.2022.842850

INTRODUCTION

Curcumin (Cur) is a yellow phenolic pigment extracted from the rhizome of turmeric (*Curcuma longa* L.) (1). Cur has been utilized as a spice, food colorant, and traditional herbal medicine in the form of turmeric, and it has been reported that Cur has significant antioxidant, anti-inflammatory, and anti-aging effects (2). However, poor water-solubility and low bioaccessibility limit its applications (3). Nanoparticles are effective carriers to improve the water solubility, stability, and bioaccessibility of Cur (4). Zein is a water-insoluble plant protein with good alcohol solubility and biocompatibility (5). Zein particles are widely used as carriers of fat-soluble nutrients.

However, zein contains a large number of hydrophobic amino acids, which promote aggregation through surface hydrophobicity. This may lead to the precipitation

of zein particles and greatly limits its applications (6). To overcome this limitation, a combination of zein with a hydrophilic polysaccharide may represent a valid strategy. These hydrophilic polysaccharides include gum arabic (GA) (7), pectin (8), hyaluronic acid, (9), and carrageenan (10). It has been shown that zein-GA composite nanoparticles had higher stability over a wide pH range (7). Nevertheless, zein-GA composite particles were found to be very sensitive to a micro-environment containing salt ions, and therefore they easily aggregate and precipitate (11, 12). This was because ions will weaken the electrostatic interaction between zein and the GA and lead to the desorption of GA from the zein particles (13). Therefore, inhibiting the desorption of GA from the surface of zein particles is an effective strategy to stabilize the composite particles. As a kind of plant polyphenol, tannic acid (TA) has good water solubility. TA contains a large number of hydroxyl groups that have a strong binding ability with carbonyl groups on proteins (14). In this way, they form relatively stable hydrogen bonds, crosslinking between different protein domains (15). The introduction of hydroxyl groups might stabilize the shell-core structure of composite particles in high ionic strength environments.

In our previous work, we designed zein-gum arabic-TA (zein-GA-TA) composite particles with high physical stability based on the physicochemical properties of TA (16). The introduction of TA could link the protein part of GA crosslinked with the protein on the surface of the zein particles through hydrogen bonding. The designed zein-GA-TA composite particles could be stable to salt ions due to the introduction of TA. This study aimed to evaluate the physicochemical stability and bioaccessibility of Cur after loading into the zein-GA-TA composite particles.

MATERIALS AND METHODS

Materials

Zein, GA, TA, Cur, porcine pepsin (≥400 U/mg), and porcine pancreatin (1,500 U/mg) were purchased from Sigma-Aldrich (St. Louis, MO, USA). Anhydrous ethanol (EtOH) was purchased from Beijing Chemical Plant (Beijing, China). The 2,2'-azino-bis (ABTS) and 1,1-diphenyl-2-picrylhydrazyl (DPPH) free radical scavenging capacity test kits were purchased from Solarbio Technology Co., Ltd. (Beijing, China), other chemicals were of analytical grade.

The Preparation of ZGT-Cur Composite Particles

The composite particles were prepared using the method of Li et al. (7) with slight modifications. Different amount of Cur (zein:Cur = 100:1, 50:1, 20:1, 10:1, 5:1, and 2:1, w/w) were added to the 0.5% zein stock solution and stirred overnight to obtain the mixed solution of Cur and zein. The above mixture was added to 200 ml GA solution (zein:GA = 1:2, w/w). EtOH and excess water were removed by rotary evaporator at 45°C to achieve a final concentration of 0.5%, and then TA (zein:TA = 5:1, w/w) was added to the dispersion of ZG-Cur composite particles to obtain Cur-loaded zein-GA-TA composite particles. The ZGT-Cur composite particles with different mass ratios of zein and Cur are named ZGT-$Cur_{100:1}$, ZGT-$Cur_{50:1}$, ZGT-$Cur_{20:1}$, ZGT-$Cur_{10:1}$, ZGT-$Cur_{5:1}$, and ZGT-$Cur_{2:1}$, respectively.

Particle Size, Polydispersity Index, and ζ-Potential

Particle size, PDI, and ζ-potential were measured by a Nano Zetasizer (Malvern, Instruments, Malvern, UK) (17). The prepared ZGT-Cur composite particle dispersion solution (100 μl) was diluted 200 times to avoid multiple scattering effects. The above indices were determined after the sample was balanced in the instrument for 120 s. All samples were measured at 25°C.

Microstructure

The microstructure of samples was observed by a field emission scanning electron microscope (SEM) (SU8010, Hitachi, Tokyo, Japan). The freeze-dried sample was coated with gold before observation to avoid charging under the electron beam, and then images were collected with a magnification of 100,000× at 10 kV accelerating voltage (18).

Encapsulation Efficiency (EE, %) and Loading Capacity (LC, %) of Cur

The EE and LC of Cur in ZGT-Cur composite particles were measured by spectrophotometry using a spectrophotometer (UV-8000, Shimadzu Japan) (19). ZGT-Cur samples were dissolved in 80% (v/v) aqueous EtOH and extracted by ultrasonic treatment. Then the absorbance of the solution was measured at 425 nm, and the Cur content was calculated according to the Cur absorbance-concentration standard curve. The EE and LC of Cur were calculated by Equations (1) and (2), respectively.

$$\mathrm{EE}\ (\%) = \left(1 - \frac{m_1}{m_{\mathrm{Total}}}\right) \times 100 \quad (1)$$

$$\mathrm{LC}\ (\%) = \frac{m_2}{M} \times 100 \quad (2)$$

where m_1 represents the mass of free Cur, m_{Total} represents the initial total mass of Cur, m_2 represents the mass of Cur in the nanoparticles, and M represents the mass of the sample.

Turbiscan Stability and Storage Time Stability

Turbiscan (Formulaction, L'Union, France) was used to determine and quantify the instability mechanism of composite particle dispersion (20). The samples were measured with an interval of 10 min at 25°C for 24 h.

To evaluate the storage stability of the particles, different concentrations of ZGT-Cur composite particles were stored at 25°C for 30 days, and their particle size, PDI, and ζ-potential were measured.

Thermal Degradation of Cur

The samples (10 ml) were put into a transparent glass bottle, heated in 25, 45, 65, and 85°C water baths for 2 h, respectively, then the above samples were cooled to room temperature (25°C), and the Cur content was calculated according to the standard

curve (21). The retention rate of Cur was calculated according to Equation (3).

$$\text{Retention rate after heating (\%)} = \frac{\text{Residue mass of curcumin}}{\text{Initial mass of curcumin}} \times 100 \quad (3)$$

Photodegradation Kinetics of Cur

The samples (10 ml) were added into a transparent glass bottle and placed in a UV lightbox with a light intensity of 0.35 W/m^2 and a constant temperature of 25°C. The residual amount of Cur in the samples was determined at 0, 30, 60, 90, and 120 min., respectively (21). The degradation kinetic parameters were fitted according to the first-order kinetic Equations (4) and (5) (22).

$$\text{Ln}\,(C/C_0) = -kt \quad (4)$$

$$t_{1/2} = \text{Ln}(2)/k \quad (5)$$

where C represents the Cur concentration at each time point, C_0 represents initial Cur concentration, k represents the Cur degradation rate, and $t_{1/2}$ represents the Cur half-life.

Fourier Transform Infrared (FTIR) Spectroscopy

The FTIR spectra of the samples were determined by an FTIR spectrometer (Nicolet iS5, Thermo Scientific, USA). Lyophilized samples (2 mg) were accurately weighed and mixed with 198 mg potassium bromide (KBr) powder. The mixture was ground into powder with a mortar, and then the powder was pressed into uniform transparent disks with a tablet press. Finally, the samples were measured with a wave-number range of 4,000–500 cm^{-1} and a resolution of 4 cm^{-1} (23).

Fluorescence Spectroscopy

The fluorescence intensity of the samples was measured by fluorescence spectrometry (F-7000, Shimadzu, Japan) (24). The samples were diluted to a concentration of 0.2 mg/ml with deionized water before testing. The excitation wavelength was 280 nm (excitation tryptophan fluorescence), the emission wavelength range was 280–450 nm, the scan speed was 100 nm/min, the excitation and emission slit width was 5 nm, and deionized water was used as the blank.

X-Ray Diffraction

The X-ray diffraction pattern of the samples was recorded by an X-ray diffractometer (D2, AXS, Bruker, Germany). The angle range was 4–50° and the scan rate was 4°/min (25).

In vitro Antioxidant Activity

The samples (0.1 g) were mixed with 4 ml of 80% (v/v) aqueous EtOH, followed by centrifugation at 1,000 rpm for 30 min, and then tested with ABTS and DPPH kits (Solarbio, Beijing, China).

Determination of Cur Bioaccessibility

After 6 h *in vitro* gastrointestinal digestion, the digestive solution was centrifuged at 18,000 rpm for 1 h, the supernatant micelle was taken to determine the content of Cur (26). The bioaccessibility of Cur was determined according to Equation (6).

$$\text{Bioaccessibility (\%)} = \frac{M_{micelle}}{M_{digest}} \times 100 \quad (6)$$

where $M_{micelle}$ is the mass of Cur in the micelle, and M_{digest} is the mass of Cur in the digest.

Statistical Analysis

SPSS statistics 24 software (SPSS Inc., Chicago, IL, USA) was used for one-way ANOVA, and Duncan's test was used to analyze the significance of the difference between multiple groups of samples. The significance level was $p < 0.05$. All experiments were conducted in triplicate, and the results were expressed by mean ± SD.

RESULTS AND DISCUSSION

Particle Size, PDI, and ζ-Potential of ZGT-Cur Composite Particles

The particle size, PDI, and ζ-potential of ZGT-Cur composite particles under different mass ratios of zein and Cur are shown in **Figures 1A,B**. When the ratio of zein:Cur was reduced from 100:1 to 2:1, the size of the ZGT-Cur composite particles was increased from 137.3 ± 2.20 nm to 145.93 ± 6.5 nm, but did not show a significant difference ($p > 0.05$). The molecular weight of Cur was small, and the addition of Cur did not affect the particle size of the composite particles (27). The trend of PDI was similar to that of the particle size, and the dispersions containing Cur were homogeneous colloidal systems. The mass ratio of zein to Cur had no significant effect on the ζ-potential of ZGT-Cur composite particles (**Figure 1B**), which agreed with the results reported by Chen et al. (13). The above results indicated that the ratio of zein to Cur had no impact on the particle properties of ZGT-Cur.

Microstructure of ZGT-Cur Composite Particles

The effects of zein and Cur with different mass ratios on the microstructure of ZGT-Cur are observed by SEM, as shown in **Figure 2**. When the mass ratio of zein to Cur was reduced from 100:1 to 2:1, the particle size and micromorphology of ZGT-Cur composite particles show no statistical difference. However, the dimensions shown in **Figure 2** differ somewhat from those measured using dynamic light scattering (DLS). This phenomenon may be due to the different detection principles of DLS and SEM. DLS provides the hydration diameter of particles in solution, whereas that obtained by SEM shows the images of the dried particles (28). This is consistent with that described in other literature (29). The particles readily aggregated during the drying process. The results of the microstructure also confirmed that the ratio of zein to Cur had no effect on the particle size of ZGT-Cur.

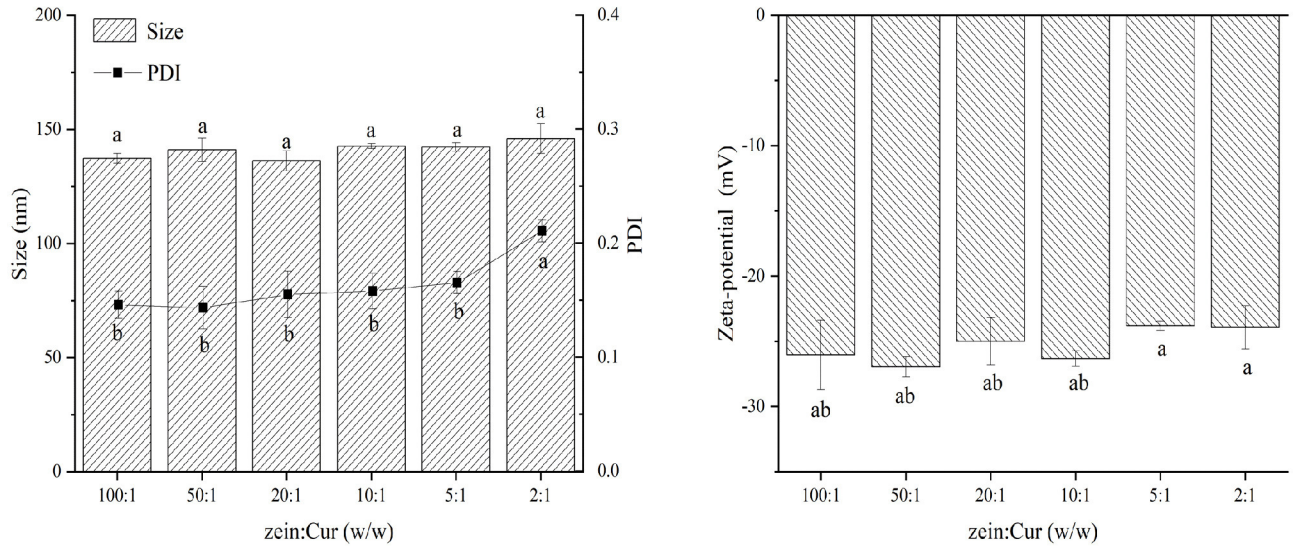

FIGURE 1 | The effect of mass ratio of zein to GA **(A,B)** on the hydration diameter, polydispersity index (PDI), and zeta-potential of ZGT-Cur composite nanoparticles. Different small letters indicate a significant difference ($p < 0.05$), the same below.

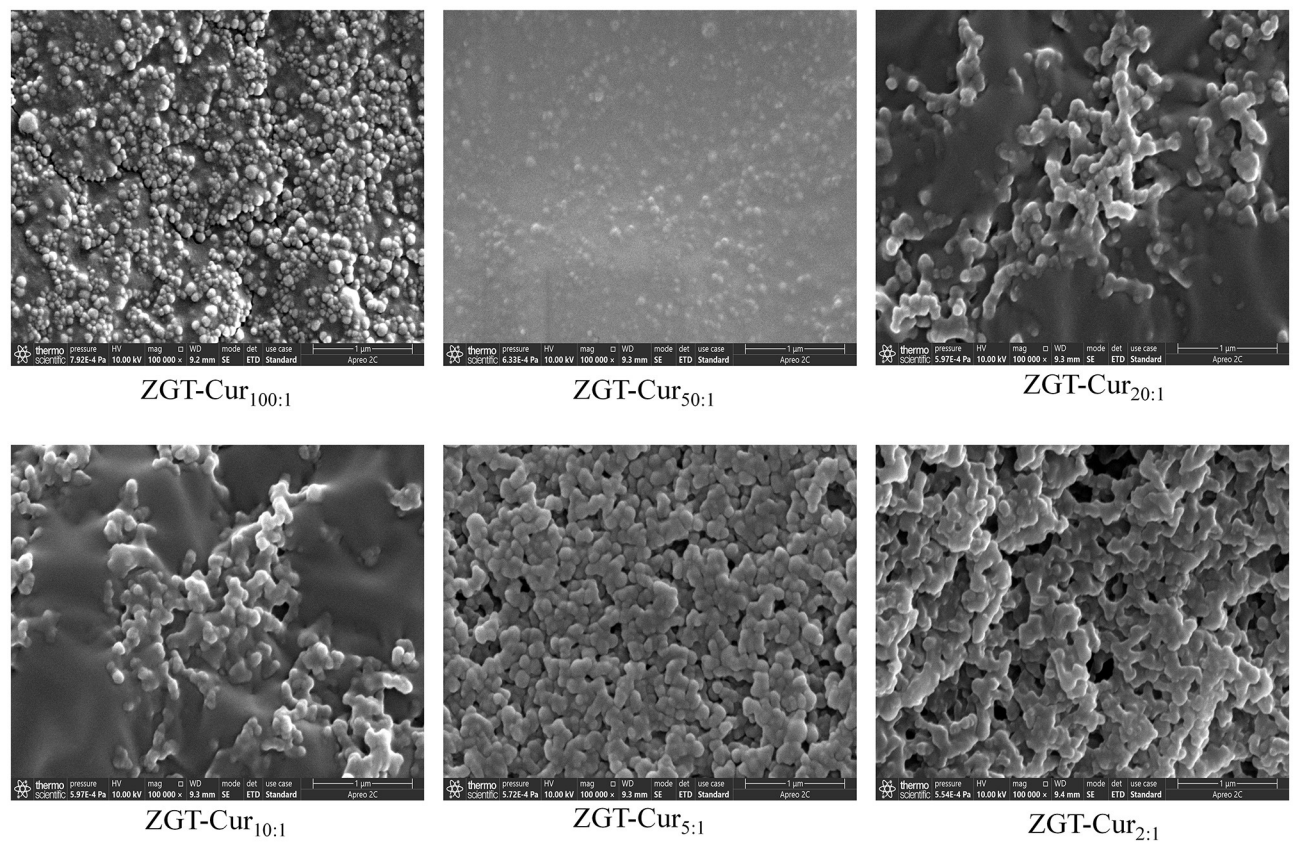

FIGURE 2 | Microstructure of ZGT-curcumin (Cur) composite particles with a different mass of zein to Cur.

EE (%) and LC (%) of Cur

The EE and LC are often used to evaluate the application potential of the carrier delivery system. **Figure 3** shows the EE and LC of Cur in the ZGT-Cur composite particles. The EE of the composite particles showed a decreasing trend as the mass ratio of zein to Cur decreased (**Figure 3**). The excessive addition of Cur exceeded the encapsulation ability of the composite particles, resulting in a decrease in EE (10). When the mass ratio of zein to Cur was 100:1, the EE and LC were 93.32 ± 0.29% and 0.62 ± 0.01%, respectively. However, when the mass ratio of zein to Cur was 2:1, the EE was decreased to 67.63 ± 0.06%, and the LC was increased to 4.38 ± 0.13%. As the addition of Cur was increased, the LC of the composite particles was also increased, which is consistent with the results of Chen et al. (30).

Storage Stability of Composite Particles

Figure 4 shows the backscattered light intensity of ZGT-Cur, Z-Cur, and ZG-Cur. As can be seen from **Figure 4**, the slight increase of backscattered light intensity of Z-Cur and ZG-Cur particles at the bottom and on the top of the bottle indicated that a small number of particles have gathered. The backscattered light intensity of ZGT-Cur composite particles did not change significantly, indicating that the particles did not precipitate or aggregate.

Figure 5 shows the particle size of ZGT-Cur, Z-Cur, and ZG-Cur during storage for 30 days. The particle sizes of ZGT-Cur, Z-Cur, and ZG-Cur composite particles were significantly different ($p < 0.05$; **Figure 5**). The size of Z-Cur particles was increased from 96.94 ± 0.26 nm at 0 day to 1,544.00 ± 228.11 nm at 30 days ($p < 0.05$) and precipitation was observed at the same time. The size of the ZG-Cur particles was increased from 105.13 ± 0.68 nm to 263.10 ± 3.12 nm ($p < 0.05$). The stability of the nanoparticles was destroyed to some extent during storage, and the increase in particle size during storage was due to particle aggregation and expansion (31). However, the size of the ZGT-Cur composite particles did not change significantly during storage, and the particle size of ZGT-Cur was 123.97 ± 1.27 nm at 30 days. The above results showed that the stability of ZGT-Cur was better than Z-Cur and ZG-Cur, and TA had a certain ability to resist aggregation.

Thermal Degradation of Cur

Thermal treatment is an important procedure in food processing. Heat treatment has an important effect on the content of functional components (32). As can be seen from **Figure 6**, the retention rate of Cur in all samples has decreased gradually as the heating temperature is increased. The retention rates of free Cur at 45, 65, and 85°C were 93.1, 89.1, and 73.9%, respectively. When GA was included in the particles, the retention rates of Cur in ZG-Cur were improved from 77.6 to 83.0% at 85°C. It has also been reported that the addition of polysaccharides can improve the retention rate of Cur (21). When TA was added, the retention rates of Cur in ZGT-Cur composite particles

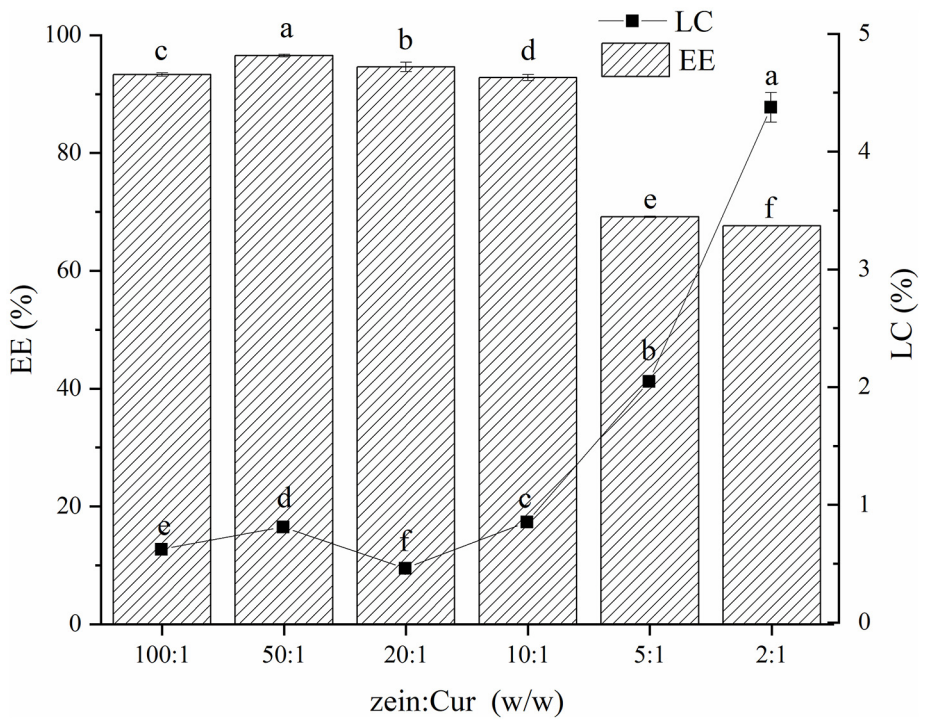

FIGURE 3 | Encapsulation efficiency and loading capacity of curcumin (Cur) in ZGT-Cur composite nanoparticles at different mass ratios of zein to curcumin.

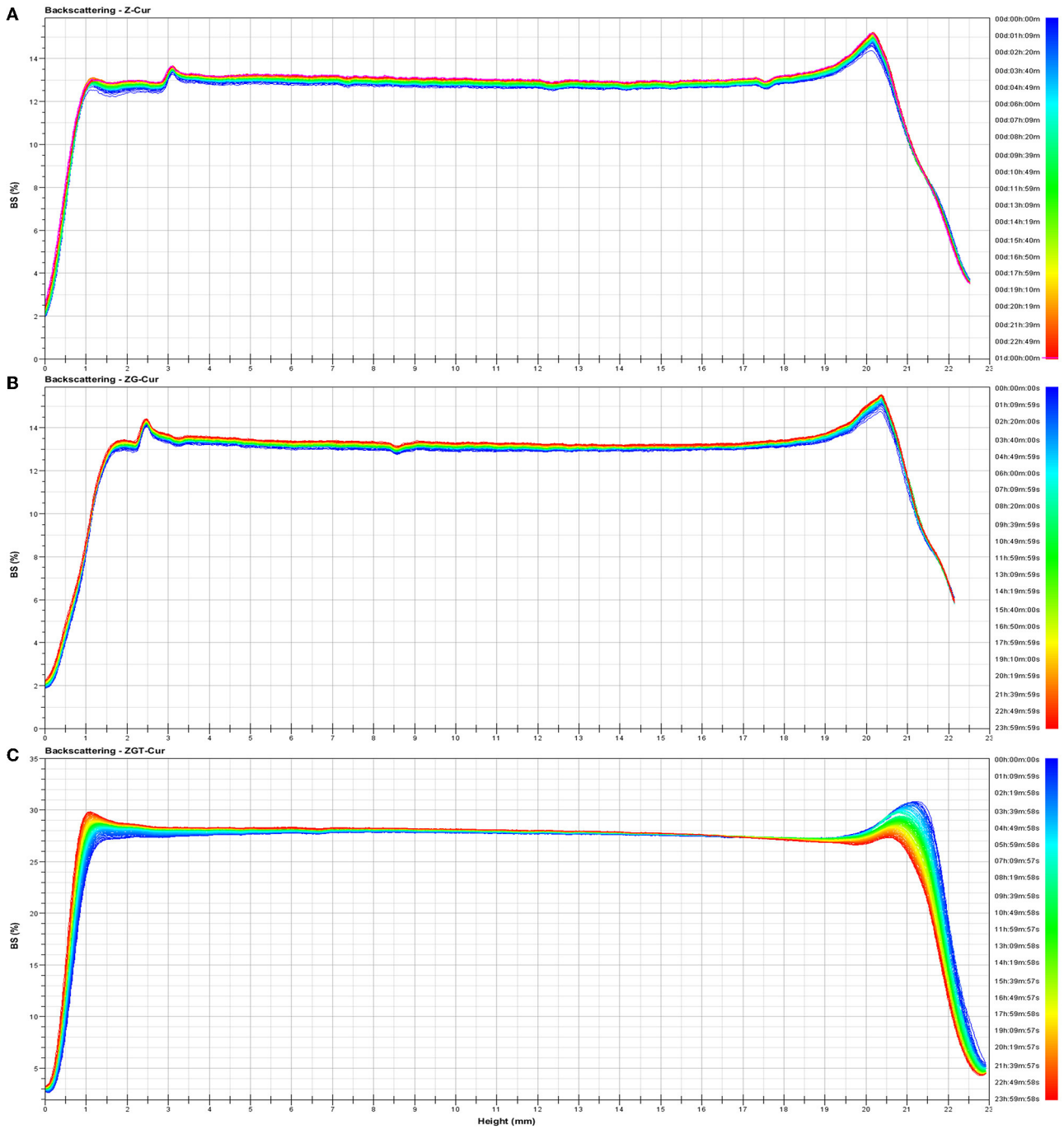

FIGURE 4 | Backscattering changes of Z- curcumin (Cur) **(A)**, ZG-Cur **(B)**, and ZGT-Cur **(C)** composite particle dispersions. Moreover, x-axis means height (mm), y-axis means BS (%).

were further improved to 98.8, 97.67, and 94.3% at 45, 65, and 85°C, respectively. The above results showed that TA could improve the thermal stability of Cur in ZGT-Cur composite particles. Similar results can also be observed in a previous study (33).

Photodegradation

As shown in **Figure 7**, the first-order kinetic curves of each sample are different. The fitted curves of Cur, Z-Cur, and ZG-Cur composite particles had larger slopes, while the fitted curve of ZGT-Cur composite particles had a smaller slope and the

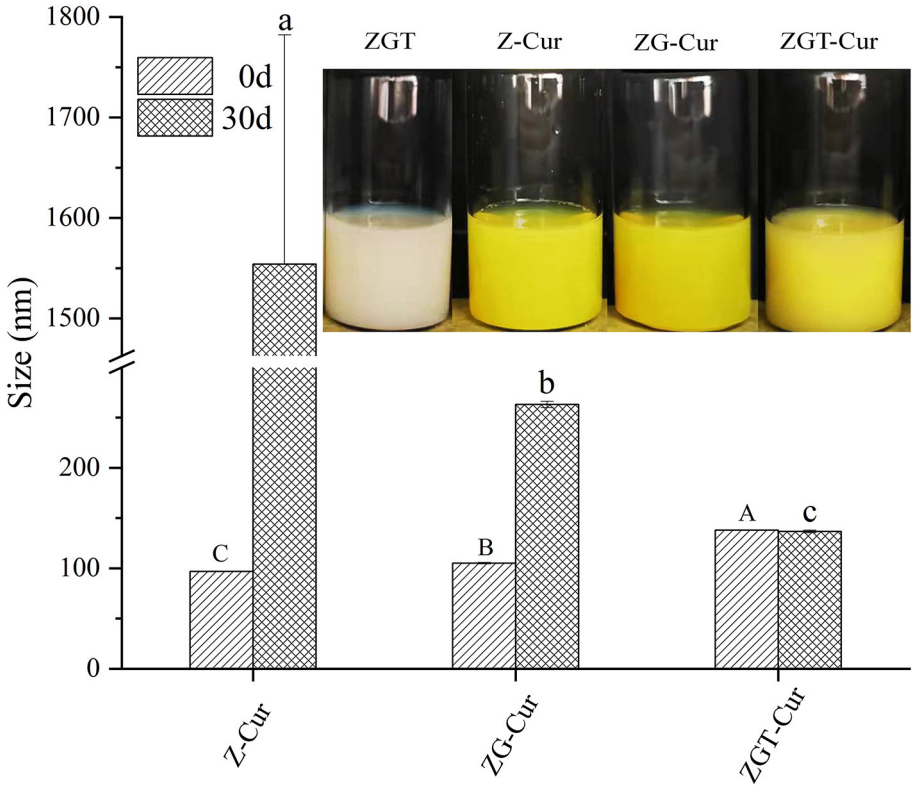

FIGURE 5 | Effect of different storage times (0 and 30 days) on composite particle size.

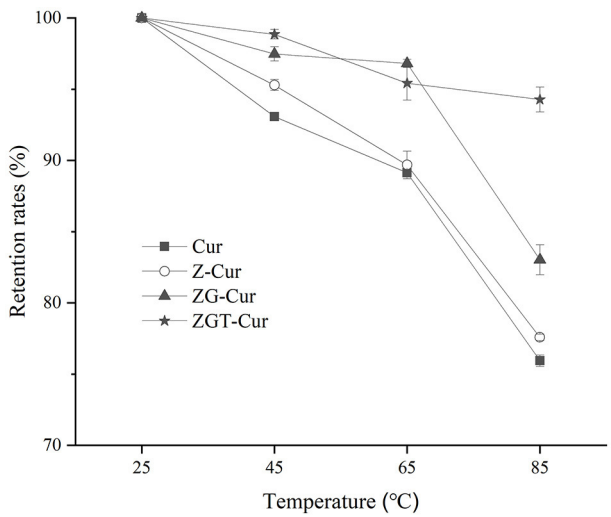

FIGURE 6 | Effect of different temperatures (25, 45, 65, and 85°C) on retention rates of Cur in composite particles.

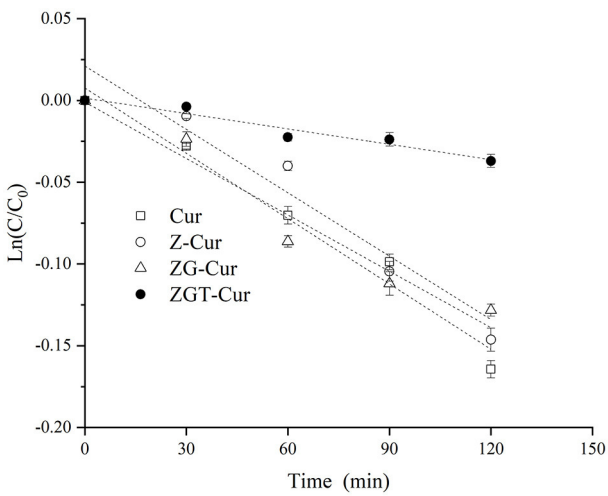

FIGURE 7 | First-order kinetic curve fitting of curcumin degradation during UV irradiation.

curve was less steep. This indicated that the degradation rate of Cur in the ZGT-Cur composite particles containing TA was slower.

The coefficient of determination (R^2) of the fitting curve of each sample was >0.95, and the degradation rate of Cur for each sample was between 0.00030 and 0.00118 min^{-1} (**Table 1**). The degradation rate of free Cur was 0.00118 min^{-1}, and the half-life

was 586 min. When Cur was encapsulated by zein, the half-life of Cur in Z-Cur increased significantly to 621 min ($p < 0.05$). The aromatic groups and disulfide bonds in zein molecules can absorb UV light, thus enhancing the UV-light resistant ability of Cur (34). When zein was further encapsulated with GA, the degradation rate of Cur in ZG-Cur was slowed down and the half-life was increased significantly to 680 min ($p < 0.05$). This was because the addition of GA provided more physical barriers for Cur. Similar findings were also reported by Yu et al. (35) who pointed out that Cur encapsulated in composite particles showed better photostability. The half-life of Cur in ZGT-Cur composite particles was 2,312 min, which was 2.9 times that of ZG-Cur composite particles. These results indicated that the degradation rate and half-life of Cur can be significantly slowed down by encapsulation and the UV stability of Cur can be further improved when TA is included in the composite particles. Similar results were reported for the UV-light resistant ability of Cur, which was also improved after embedding (21).

TABLE 1 | Parameters of the first-order model for curcumin degradation during UV irradiation.

Sample	R^2	Degradation rate (min^{-1})	Half-life period (min)
Cur	0.974	0.00118 ± 0.000015^a	586 ± 8^d
Z-Cur	0.957	0.00112 ± 0.000015^b	621 ± 9^c
ZG-Cur	0.984	0.00102 ± 0.000010^c	680 ± 7^b
ZGT-Cur	0.976	0.00030 ± 0.000010^d	2312 ± 77^a

The different small letters indicate a significant difference ($p < 0.05$).

FTIR Spectroscopy Analysis

The interactions of Cur, zein, GA, and TA in the preparation of ZGT-Cur composite particles can be evaluated by the peak shift and peak intensity of the FTIR spectra. As shown in **Figure 8A**, Cur has characteristic peaks at 3,506, 1,627, 1,428, 1,281, and 1,028 cm^{-1}. This was consistent with the results reported by Feng et al. (23). There were no Cur characteristic peaks in the peak spectra of ZG-Cur and ZGT-Cur composite particles,

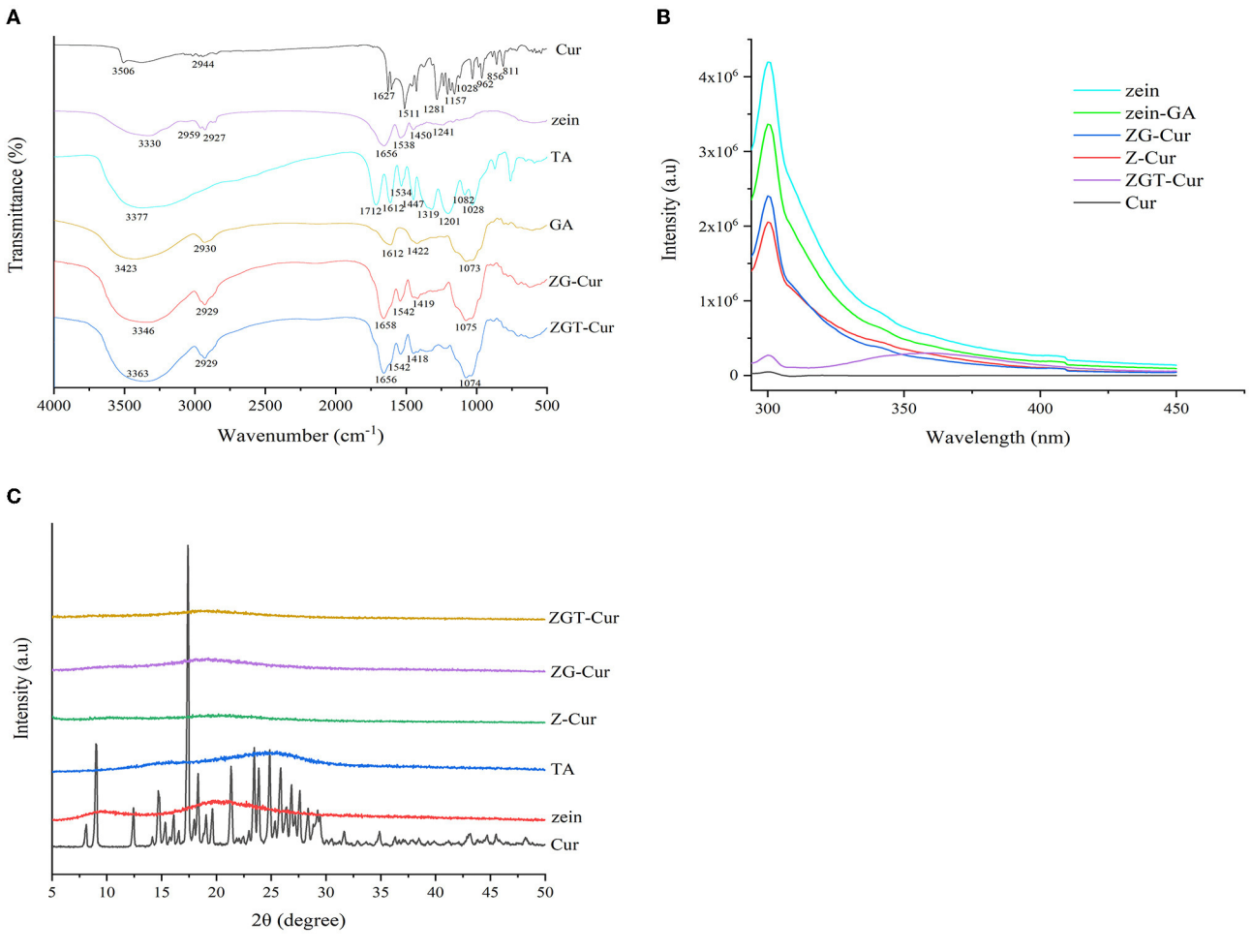

FIGURE 8 | Fourier transform infrared **(A)**, fluorescence spectrums **(B)**, and X-ray diffraction **(C)** spectra of the materials used to prepare the ZGT-curcumin (Cur) particles.

indicating that Cur was encapsulated by the biopolymers. TA had a characteristic peak at 3,377 cm^{-1} and ZG-Cur composite particles had a wide peak at 3,346 cm^{-1}. However, ZGT-Cur composite particles containing TA had an absorption peak at 3,362 cm^{-1}, indicating that TA and ZG-Cur were bound by hydrogen bonding (36). The introduction of TA did not change the N-H and C-N tensile vibration of zein and ZG-Cur secondary amide groups at 1,542 cm^{-1}, indicating that TA did not affect the secondary structure of zein. ZGT-Cur contained the characteristic peak of GA at 1,074 cm^{-1}, but did not contain the characteristic peak of TA at the wavelength of 1,534–1,712 cm^{-1}. Therefore, it was speculated that TA was wrapped inside by GA and interacted with the zein.

Fluorescence Property

As shown in **Figure 8B**, zein has a strong fluorescence intensity at 300 nm. Compared with zein, the fluorescence intensity of zein-GA composite particles was decreased, indicating that the combination of GA to zein was reduced the fluorescence intensity of zein. When loading Cur by zein or zein-GA, a decrease of zein fluorescence intensity was also observed, which also showed that there was a combination of zein, GA, and Cur. The fluorescence quenching of the tyrosine of zein was caused by the specific interaction between the fluorophore and Cur (24). However, compared with the effect of GA on zein fluorescence intensity, Cur had a greater effect on the zein fluorescence intensity. The result indicated that the interaction force between zein and Cur was stronger. After TA was added to ZG-Cur, the fluorescence intensity of ZGT-Cur composite particles was further reduced at 300 nm and a new emission peak was generated at 360 nm, which again showed that TA bound to zein. Hydrogen bonds were formed mainly between the phenolic hydroxyl group of TA and the amide group of the protein (37).

X-Ray Diffraction

The physical state of Cur before and after embedding can be detected by X-ray diffraction. As shown in **Figure 8C**, there are two wide diffraction peaks appearing at $2\theta = 9.5^{\circ}$ and $2\theta = 19.7^{\circ}$ in the XRD profile of zein, and TA had a wide diffraction peak at 25.2° indicating that zein and TA are amorphous structures. However, the characteristic diffraction peaks of Cur did not appear in the X-ray diffraction spectra of ZGT-Cur, ZG-Cur, and Z-Cur composite particles, and the peak intensity produced by the composite particles was very weak. The above results showed that the structure of Cur changed from crystalline to amorphous, indicating that the interaction between Cur and the composite particles had an impact on the crystal form. Similar findings were also found in the study of zein-carrageenan particles embedded with Cur (38).

In vitro Antioxidant Activity

In this study, the free radical scavenging abilities of six different composite particles were evaluated. The DPPH radical scavenging rates of Z-Cur and ZG-Cur were 4.26 and 3.29%, respectively (**Figure 9**). The DPPH free radical scavenging rate of ZGT-Cur composite particles was hugely raised to 50.41% ($p < 0.05$). The trend of the ABTS radical scavenging ability of the composite particles was similar to that of the DPPH radical scavenging ability. It had been shown that encapsulation of Cur with nanoparticles was an effective way to improve its antioxidant capacity, because the composite particles promoted the structure of Cur conjugated diene and provided protons for free radicals (39). The content of Cur within the composite particles was similar, therefore, the addition of TA can improve the antioxidant capacity of Cur-loaded composite particles. Meanwhile, TA and Cur might have an antioxidant synergistic effect. As previously reported, TA-crosslinked nanoparticles enhanced the antioxidant capacity of eugenol (33).

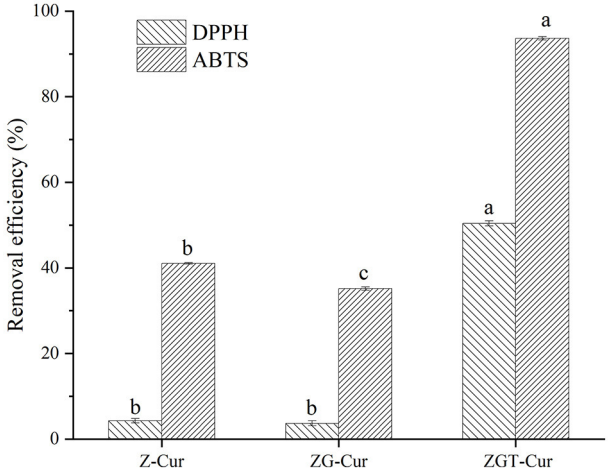

FIGURE 9 | 1,1-diphenyl-2-picrylhydrazyl (DPPH) and 2,2'-azino-bis (ABTS) removal efficiency of composite particles.

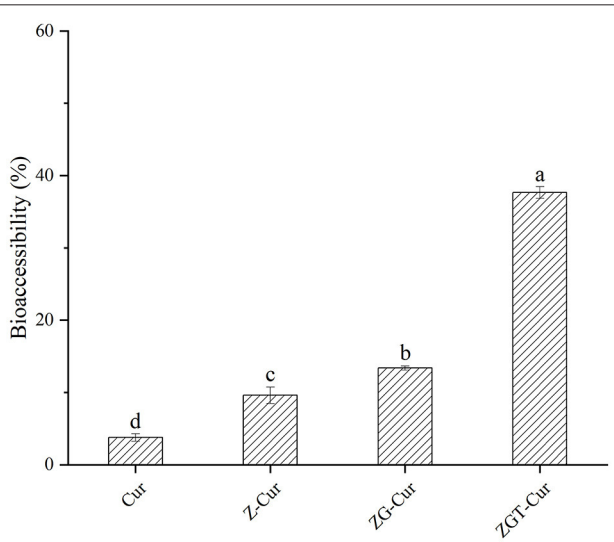

FIGURE 10 | Bioaccessibility of curcumin (Cur) in composite particles.

In vitro Bioaccessibility

Cur is highly hydrophobic so that it can only be absorbed after dissolution in gastrointestinal fluid. The gastroenteric fluid

contains surfactants, bile salts, and enzymes that together form mixed micelles during the dissolution of Cur (40). As can be seen from **Figure 10**, after 6 h of simulated *in vitro* digestion, the bioaccessibility of free Cur is 3.78%. When Cur was embedded with zein, the bioaccessibility of Cur was increased to 9.62%. After embedding Cur with zein-GA composite particles, the bioaccessibility of Cur was further improved to 13.38%, which was 2.54 times higher than that of free Cur. When TA was added, the bioaccessibility of Cur in ZGT-Cur composite particles was increased to 37.67%. It could be that the hydrogen bond interaction between TA, zein, GA, and Cur can make more Cur exist in ZGT-Cur composite particles, and the stable carrier structure can play a key role in controlled release. It was found that the combination of TA and pectin may enhance the absorption of Cur by inhibiting the function of osmotic glycoprotein (41).

CONCLUSION

In this article, Cur-loaded zein-GA-TA composite particles were prepared, and the particle characteristics, bioaccessibility, and antioxidant properties of ZGT-Cur composite particles were studied. As expected, the ZGT-Cur composite particles significantly improved the physical stability, antioxidant activity, thermal, and photochemical stability of Cur, compared to Cur-loaded in zein or zein-GA particles. Overall, ZGT-Cur composite particles delivery systems provide insight into improving the bioaccessibility of Cur, which is worthy of further exploration.

DATA AVAILABILITY STATEMENT

The original contributions presented in the study are included in the article/supplementary material, further inquiries can be directed to the corresponding authors.

AUTHOR CONTRIBUTIONS

YZ and GL conceptualized the manuscript. FR contributed to methodology. NL contributed to investigation. PW contributed to data curation and project administration. YT contributed to formal analysis. YZ wrote the original draft. YL wrote the review and edited the manuscript. AL contributed to resources and reviewed. LW supervised the work. All authors contributed to the article and approved the submitted version.

FUNDING

This research was funded by the National Natural Science Foundation of China (no. 3190625).

REFERENCES

1. Tsuda T. Curcumin: an effective or deceptive dietary factor? challenges for functional food scientists. *J Agr Food Chem.* (2018) 66:1059–60. doi: 10.1021/acs.jafc.7b05878
2. Mahmood K, Zia KM, Zuber M, Salman M, Anjum MN. Recent developments in curcumin and curcumin based polymeric materials for biomedical applications: a review. *Int J Biol Macromol.* (2015) 81:877–90. doi: 10.1016/j.ijbiomac.2015.09.026
3. Stanić Z. Curcumin, a compound from natural sources, a true scientific challenge–a review. *Plant Food Hum Nutr.* (2017) 72:1–12. doi: 10.1007/s11130-016-0590-1
4. Davidov-Pardo G, Joye IJ, McClements DJ. Nanotechnology for increased micronutrient bioavailability. *Trends Food Sci Technol.* (2014) 40:168–82. doi: 10.1016/j.tifs.2014.08.006
5. Liu Z, Cao X, Ren S, Wang J, Zhang H. Physicochemical characterization of a zein prepared using a novel aqueous extraction technology and tensile properties of the zein film. *Ind Crop Prod.* (2019) 130:57–62. doi: 10.1016/j.indcrop.2018.12.071
6. Chen X, Fu S, Hou J, Guo J, Wang J, Yang X. Zein based oil-in-glycerol emulgels enriched with β-carotene as margarine alternatives. *Food Chem.* (2016) 211:836–44. doi: 10.1016/j.foodchem.2016.05.133
7. Li J, Xu X, Chen Z, Wang T, Wang L, Zhong Q. Biological macromolecule delivery system fabricated using zein and gum arabic to control the release rate of encapsulated tocopherol during in vitro digestion. *Food Res Int.* (2018) 114:251–7. doi: 10.1016/j.foodres.2018.08.073
8. Jiang Y, Zhang C, Yuan J, Wu Y, Li F, Li D, et al. Effects of pectin polydispersity on zein/pectin composite nanoparticles (ZAPs) as high internal-phase Pickering emulsion stabilizers. *Carbohyd Polym.* (2019) 219:77–86. doi: 10.1016/j.carbpol.2019.05.025
9. Chen S, Han Y, Wang Y, Yang X, Sun C, Mao L, et al. Zein-hyaluronic acid binary complex as a delivery vehicle of quercetagetin: fabrication, structural characterization, physicochemical stability and *in vitro* release property. *Food Chem.* (2019) 276:322–32. doi: 10.1016/j.foodchem.2018.10.034
10. Sun X, Pan C, Ying Z, Yu D, Duan X, Huang F, et al. Stabilization of zein nanoparticles with k-carrageenan and tween 80 for encapsulation of curcumin. *Int J Biol Macromol.* (2020) 146:549–59. doi: 10.1016/j.ijbiomac.2020.01.053
11. Wang L, Zhang Y. Heat-induced self-assembly of zein nanoparticles: fabrication, stabilization and potential application as oral drug delivery. *Food Hydrocolloids.* (2019) 90:403–12. doi: 10.1016/j.foodhyd.2018.12.040
12. Chen H, Zhong Q. A novel method of preparing stable zein nanoparticle dispersions for encapsulation of peppermint oil. *Food Hydrocolloids.* (2015) 43:593–602. doi: 10.1016/J.Foodhyd.2014.07.018
13. Chen G, Fu Y, Niu F, Zhang H, Li X, Li X. Evaluation of the colloidal/chemical performance of core-shell nanoparticle formed by Zein and gum Arabic. *Colloids Surfaces A*. (2018) 560:130–5. doi: 10.1016/j.colsurfa.2018.10.006
14. Hasni I, Bourassa P, Hamdani S, Samson G, Carpentier R, Tajmir-Riahi H. Interaction of milk α- and β-caseins with tea polyphenols. *Food Chem*. (2011) 126:630–9. doi: 10.1016/j.foodchem.2010.11.087
15. Siebert KJ, Troukhanova NV, Lynn PY. Nature of polyphenol–protein interactions. *J Agr Food Chem.* (1996) 1:80–5. doi: 10.1021/jf9502459
16. Zhang Y, Huang J, Ren F, Li Y, Tong Y, Wen P, et al. A novel method for stabilizing Zein Gel particles to salt ion-induced aggregation. *Molecules.* (2021) 26:1458. doi: 10.3390/molecules26051458
17. Zou L, Zhang Z, Zhang R, Liu W, Liu C, Xiao H, et al. Encapsulation of protein nanoparticles within alginate microparticles: impact of pH and ionic strength on functional performance. *J Food Eng.* (2016) 178:81–9. doi: 10.1016/j.jfoodeng.2016.01.010
18. Hasankhan S, Tabibiazar M, Hosseini SM, Ehsani A, Ghorbani M. Fabrication of curcumin-zein-ethyl cellulose composite nanoparticles using antisolvent co-precipitation method. *Int J Biol Macromol.* (2020) 163:1538–45. doi: 10.1016/j.ijbiomac.2020.08.045
19. Wei Y, Sun C, Dai L, Mao L, Yuan F, Gao Y. Novel Bilayer Emulsions Costabilized by Zein Colloidal Particles and Propylene Glycol Alginate. 2.

Influence of Environmental Stresses on Stability and Rheological Properties. *J Agr Food Chem.* (2019) 67:1209–21. doi: 10.1021/acs.jafc.8b04994
20. Santos J, Alcaide-González MA, Trujillo-Cayado LA, Carrillo F, Alfaro-Rodríguez MC. Development of food-grade Pickering emulsions stabilized by a biological macromolecule (xanthan gum) and zein. *Int J Biol Macromol.* (2020) 153:747–54. doi: 10.1016/j.ijbiomac.2020.03.078
21. Dai L, Li R, Wei Y, Sun C, Mao L, Gao Y. Fabrication of zein and rhamnolipid complex nanoparticles to enhance the stability and *in vitro* release of curcumin. *Food Hydrocolloid.* (2018) 77:617–28. doi: 10.1016/j.foodhyd.2017.11.003
22. Mercali GD, Gurak PD, Schmitz F, Marczak LDF. Evaluation of non-thermal effects of electricity on anthocyanin degradation during ohmic heating of jaboticaba (Myrciaria cauliflora) juice. *Food Chem.* (2015) 171:200–5. doi: 10.1016/j.foodchem.2014.09.006
23. Feng S, Sun Y, Wang D, Sun P, Shao P. Effect of adjusting pH and chondroitin sulfate on the formation of curcumin-zein nanoparticles: synthesis, characterization and morphology. *Carbohyd Polym.* (2020) 250:116970. doi: 10.1016/j.carbpol.2020.116970
24. Li L, Yao P. High dispersity, stability and bioaccessibility of curcumin by assembling with deamidated zein peptide. *Food Chem.* (2020) 319:126577. doi: 10.1016/j.foodchem.2020.126577
25. Khan MA, Yue C, Fang Z, Hu S, Cheng H, Bakry AM, et al. Alginate/chitosan-coated zein nanoparticles for the delivery of resveratrol. *J Food Eng.* (2019) 258:45–53. doi: 10.1016/j.jfoodeng.2019.04.010
26. Zou L, Zheng B, Zhang R, Zhang Z, Liu W, Liu C, et al. Enhancing the bioaccessibility of hydrophobic bioactive agents using mixed colloidal dispersions: curcumin-loaded zein nanoparticles plus digestible lipid nanoparticles. *Food Res Int.* (2016) 81:74–82. doi: 10.1016/j.foodres.2015.12.035
27. Zhang D, Jiang F, Ling J, Ouyang X, Yang G. Delivery of curcumin using a zein-xanthan gum nanocomplex: fabrication, characterization, and *in vitro* release properties. *Colloids Surfaces B.* (2021) 204:111827. doi: 10.1016/j.colsurfb.2021.111827
28. Liang H, Zhou B, He L, An Y, Lin L, Li Y, et al. Fabrication of zein/quaternized chitosan nanoparticles for the encapsulation and protection of curcumin. *RSC Adv.* (2015) 5:13891–900. doi: 10.1039/c4ra14270e
29. Wang G, Yu B, Wu Y, Huang B, Yuan Y, Liu C. Controlled preparation and antitumor efficacy of vitamin E TPGS-functionalized PLGA nanoparticles for delivery of paclitaxel. *Int J Pharmaceut.* (2013) 446:24–33. doi: 10.1016/j.ijpharm.2013.02.004
30. Chen H, Xu B, Zhou C, Yagoub AEA, Cai Z, Yu X. Multi-frequency ultrasound-assisted dialysis modulates the self-assembly of alcohol-free zein-sodium caseinate to encapsulate curcumin and fabricate composite nanoparticles. *Food Hydrocolloid.* (2022) 122:107110. doi: 10.1016/j.foodhyd.2021.107110
31. Jiang F, Yang L, Wang S, Ying X, Ling J, Ouyang XK. Fabrication and characterization of zein-alginate oligosaccharide complex nanoparticles as delivery vehicles of curcumin. *J Mol Liq.* (2021) 335:116937. doi: 10.1016/j.molliq.2021.116937
32. Chen S, Han Y, Jian L, Liao W, Zhang Y, Gao Y. Fabrication, characterization, physicochemical stability of zein-chitosan nanocomplex for co-encapsulating curcumin and resveratrol. *Carbohyd Polym.* (2020) 236:116090. doi: 10.1016/j.carbpol.2020.116090
33. Jia C, Cao D, Ji S, Zhang X, Muhoza B. Tannic acid-assisted cross-linked nanoparticles as a delivery system of eugenol: the characterization, thermal degradation and antioxidant properties. *Food Hydrocolloid.* (2020) 104:105717. doi: 10.1016/j.foodhyd.2020.105717
34. Luo Y, Wang T, Teng Z, Chen P, Sun J, Wang Q. Encapsulation of indole-3-carbinol and 3,3′-diindolylmethane in zein/carboxymethyl chitosan nanoparticles with controlled release property and improved stability. *Food Chem.* (2013) 139:224–30. doi: 10.1016/j.foodchem.2013.01.113
35. Yu Y, Wu M, Wang C, Wang Z, Chen T, Yan J. Constructing biocompatible carboxylic curdlan-coated zein nanoparticles for curcumin encapsulation. *Food Hydrocolloids.* (2020) 108:106028. doi: 10.1016/j.foodhyd.2020.106028
36. Deng Z, Wang S, Pei Y, Zhou B, Li J, Hou X, et al. Tuning of molecular Interactions between zein and tannic acid to modify sunflower sporopollenin exine capsules: enhanced stability and targeted delivery of bioactive macromolecules. *Acs Applied Bio Materials.* (2021) 4:2686–95. doi: 10.1021/acsabm.0c01623
37. Ali SS, Zia MK, Siddiqui T, Khan FH. Binding interaction of sheep alpha-2-macroglobulin and tannic acid: a spectroscopic and thermodynamic study. *Spectrochim Acta A.* (2018) 204:748–53. doi: 10.1016/j.saa.2018.06.024
38. Chen S, Li QK, McClements DJ, Han YH, Dai L, Mao L, et al. Co-delivery of curcumin and piperine in zein-carrageenan core-shell nanoparticles: formation, structure, stability and *in vitro* gastrointestinal digestion. *Food Hydrocolloid.* (2020) 99:105334. doi: 10.1016/j.foodhyd.2019.105334
39. Meng R, Wu Z, Xie Q, Cheng J, Zhang B. Preparation and characterization of zein/carboxymethyl dextrin nanoparticles to encapsulate curcumin: physicochemical stability, antioxidant activity and controlled release properties. *Food Chem.* (2021) 340:127893. doi: 10.1016/j.foodchem.2020.127893
40. Yu HL, Huang QR. Improving the oral bioavailability of curcumin using novel organogel-based nanoemulsions. *J Agr Food Chem.* (2012) 60:5373–9. doi: 10.1021/jf300609p
41. Zhang Q, Wang H, Feng Z, Lu Z, Su C, Zhao Y, et al. Preparation of pectin-tannic acid coated core-shell nanoparticle for enhanced bioavailability and antihyperlipidemic activity of curcumin. *Food Hydrocolloid.* (2021) 119:106858. doi: 10.1016/j.foodhyd.2021.106858

Conflict of Interest: YT, YL, AL, and LW are employed by Jilin COFCO Biochemistry Co., Ltd.

The remaining authors declare that the research was conducted in the absence of any commercial or financial relationships that could be construed as a potential conflict of interest.

Publisher's Note: All claims expressed in this article are solely those of the authors and do not necessarily represent those of their affiliated organizations, or those of the publisher, the editors and the reviewers. Any product that may be evaluated in this article, or claim that may be made by its manufacturer, is not guaranteed or endorsed by the publisher.

frontiers | Frontiers in Nutrition

ORIGINAL RESEARCH
published: 08 April 2022
doi: 10.3389/fnut.2022.859293

Improving Anti-listeria Activity of Thymol Emulsions by Adding Lauric Acid

Qizhen Cai[1], Yun Zhang[1], Xiaofeng Fang[1], Suyun Lin[2], Zhirong He[3], Shengfeng Peng[1] and Wei Liu[1,4]**

[1] State Key Laboratory of Food Science and Technology, Nanchang University, Nanchang, China, [2] Jiangxi Key Laboratory of Natural Products and Functional Food, College of Food Science and Engineering, Jiangxi Agricultural University, Nanchang, China, [3] Jiangxi Danxia Biol Technol Co., Ltd., Yingtan, China, [4] National R&D Center for Freshwater Fish Processing, Jiangxi Normal University, Nanchang, China

In this study, a novel emulsion, thymol (Thy) and lauric acid (LA) emulsion (Thy/LA-Emulsion) was prepared by homogenizing eutectic solvent (Thy/LA mixture) and caseinate solution. The effects of different thymol and lauric acid mass ratio on the formation, stability, and antibacterial activity of emulsions were studied. Compared with thymol alone, adding lauric acid (25, 50, and 75%) could enhance the antibacterial efficacy of the emulsions. Among them, Thy/$LA_{25\%}$-Emulsion could be stored at room temperature for a month without the increase of particle size, indicating that the addition of LA had not impacted the stability of emulsions. Meanwhile, Thy/$LA_{25\%}$-Emulsion exhibited a greater inhibition zone (3.06 ± 0.12 cm) and required a lower concentration (0.125 mg/mL) to completely inhibit the growth of *Listeria monocytogenes*. Consequently, Thy/$LA_{25\%}$-Emulsion demonstrated the best antibacterial activity and physicochemical stability due to its long-term storage stability. Our results suggest that Thy/$LA_{25\%}$-Emulsion may become a more functional natural antibacterial agent with greater commercial potential owing to its cheaper raw materials, simpler production processes, and better antibacterial effect in the food industry.

Keywords: Thymol, lauric acid, emulsion, *Listeria monocytogenes*, antibacterial

OPEN ACCESS

Edited by:
Jianhua Liu,
Zhejiang University of Technology, China

Reviewed by:
Oana Lelia Pop,
University of Agricultural Sciences and Veterinary Medicine of Cluj-Napoca, Romania
Dehui Lin,
Shaanxi Normal University, China

***Correspondence:**
Suyun Lin
ncusklinsuyun@163.com
Wei Liu
liuwei@ncu.edu.cn

Specialty section:
This article was submitted to Food Chemistry, a section of the journal Frontiers in Nutrition

Received: *21 January 2022*
Accepted: *07 March 2022*
Published: *08 April 2022*

Citation:
Cai Q, Zhang Y, Fang X, Lin S, He Z, Peng S and Liu W (2022) Improving Anti-listeria Activity of Thymol Emulsions by Adding Lauric Acid. Front. Nutr. 9:859293. doi: 10.3389/fnut.2022.859293

INTRODUCTION

Approximately 600 million consumers get sick from the food contaminated by foodborne pathogens alone according to recognized outbreaks every year (1). Among the common foodborne pathogen infections, *Listeria monocytogenes* in bacteria has the highest fatality rate, which is up to 20–30% (2, 3). Consequently, it is essential to adopt effective measures to prevent foodborne illnesses caused by pathogens. Antibacterial agents with broad-spectrum and high-efficiency bactericidal effects are one of the hotspots of current research studies. However, the most commonly used kind of antibacterial agents, synthetic ones, still face a wide range of disadvantages, such as toxic residues, environmental pollution caused by their slow biodegradation, the high cost–benefit ratio, and the risk of microbial resistance (4, 5). Nowadays, consumers prefer natural antibacterial agents as substitutes for chemical preservatives to inhibit bacteria and the studies on developing natural antibacterial agents are still in great demand.

Essential oils (EOs), volatile odoriferous oils, one of the alternatives to chemical preservatives, are aromatic oily liquids originated from a variety of plants, which possess diverse properties, including antibacterial, antifungal, antiviral, anti-inflammatory, antioxidant, and insecticidal activity (6–10). Earlier, EOs were acquainted with potential natural antimicrobial agents and were recommended as "natural food additives" in food preservation. Nowadays, EOs are used as preservatives in the food industry to extend the shelf life of food (11). Thymol (2-isopropyl-5-methylphenol), a natural essential oil and phenolic compound, is a component derived from some medicinal plants, such as *Thymus*, *Origanum*, and *Coridithymus* (12). Thymol (Thy) has been proved to display considerable antibacterial activity against various bacteria and yeasts by disrupting bacterial membrane, leading to bacterial lysis and leakage of components inside microbial cells, resulting in cell death (13). Therefore, Thy was selected to develop an antibacterial agent in this study. Nevertheless, the utilization of Eos, especially Thy, in the food industry is partially limited owing to their poor solubility (14, 15) and instability (16) when exposed to light, oxygen, high temperature, and moisture, which might contribute to the degradation of EOs during the processing, transportation, storage, and consumption, or even a risk of forming toxic derivatives (17). Another reason that hinders the extensive utilization of EOs is that the antibacterial effect of a single kind of EOs is usually limited, and when sufficient amounts are added to exert potent antibacterial effects, they can affect food quality and lead to negative sensory effects (18).

To reduce the concentration of EOs without compromising their antibacterial ability, several synergies of diverse antibacterial compounds with EOs has been widely discussed, such as the synergistic effects of various EOs (19, 20), EOs and antibiotics (12, 21, 22), EOs and other antimicrobial agents [drugs (23), medium-chain fatty acids (MCFs) (24), polyphenols (25), etc.]. Among them, the MCFs are saturated fatty acids with 6–12 carbon atoms, including octanoic acid, capric acid, and lauric acid, which exist in nature in the form of medium-chain triglycerides, mainly in breast milk, milk and its products, coconut oil and palm oil, and little in other natural foods (26). Accompanied with antibacterial ability, MCFs have been demonstrated to restrain diverse foodborne pathogens, including *Escherichia coli*, *Salmonella*, and *Staphylococcus aureus* (27–29). According to a previous study (24), the synergistic activity of MCFs and EOs can not only enhance their antibacterial effect, but also lessen its unique odor and irritation by replacing a portion of EOs, and meanwhile minimize the loss of nutrients and quality of food by decreasing the number of antibacterial agents. Moreover, it is more in line with the prevailing market in terms of economic benefits because of the relatively lower price of MCFs. Nevertheless, the problems of poor solubility and instability of EOs remain unsolved by synergy with MCFs.

Several encapsulation systems (30, 31) have been developed to conquer the problem, such as liposomes, polymer particles, solid lipid nanoparticles, cyclodextrin, emulsions, and nanofibers. Using emulsions to encapsulate EOs is one of the feasible ways to widen their application, where the emulsions are claimed to be able to control release, target transport, and improve the solubility and stability of EOs (32, 33). In addition, emulsions can offer high drug-loading efficacy, which fits well with the prevailing market demand as the number of active substances in the antibacterial delivery system should be maximized. To the best of our knowledge, there are no previous reports concerning the influence of lauric acid (LA) on the formation, stability, and antibacterial activity of Thymol-based emulsions.

In this study, we attempted to resolve this dilemma by developing a novel emulsion, that is, by homogenizing the Thymol/Lauric acid (Thy/LA) solutions with caseinate solutions. And the optimal ratio of Thy/LA and their optimal proportion in the oil phase were selected. Finally, the impact of different mass Thy/LA ratios on emulsion stability and antibacterial effect was evaluated.

MATERIALS AND METHODS

Materials

Thymol (98%) and lauric acid (98%) were purchased from Aladdin Biochemical Technology Co., Ltd (Shanghai, China). Sodium caseinate (NaCS) was provided by Sigma Chemical Company (St. Louis, MO, United States). Yeast extract and tryptone were donated by Oxoid (Beijing, China). Agar powder was obtained from Solar Science and Technology Company (Beijing, China). All other reagents used were of analytical grade.

Preparation of Thy/LA-Emulsion

Briefly, 2 wt% NaCS solution was obtained by adding NaCS powder into phosphate-buffered solution (5 mM, pH 6.5) and then kept stirring for 4 h at room temperature. Thy and LA were mixed at different mass ratios (The ratios of LA are 0, 25, 50, 75, and 100 wt%.). Afterward, the mixtures were obtained by stirring at 65°C until a homogeneous liquid was formed. The final oil phases were prepared by mixing Thy/LA solutions and corn oil in various ratios (The ratios of corn oil are 0, 10, 20, 40, and 60 wt%.). The Thy/LA crude emulsions (Φ = 10%) were fabricated by stirring at 12,000 rpm for 3 min with a high shear dispersive machine (ULTRA TURRAX T18 Digital, IKA, Staufen, Germany). The final emulsion was obtained after passing through a microfluidizer (M-110EH30, Microfluidic Corp., Newton, MA, United States) at 70 MPa two times. In addition, the oil phase of the control group was prepared by mixing Thy and corn oil at corresponding mass ratios.

Determination of Characterization of Thy/LA-Emulsion

The mean particle diameters ($d_{3,2}$) and particle size distribution of the emulsions were measured by a laser diffraction instrument (Mastersizer 3000, Malvern Instruments Ltd., Worcestershire, United Kingdom) according to our previous method (34). The operating parameters used were as follows: lights obscuration was from 8 to 13%; the stirring speed was set as 3,500 rpm/s. Phosphate-buffered solution (5 mM, pH 6.5) was used throughout the test.

The ζ-potential of the emulsions was measured by using dynamic light scattering and electrophoresis (Nano ZS, Malvern

Instruments, Worcestershire, United Kingdom) at 25°C. The emulsions were diluted 10-fold by using phosphate-buffered solution (5 mM, pH 6.5) to obtain an appropriate light intensity for reliable measurements.

Determination of Thermal Property of Thy/LA-Emulsion

According to a previous method (35), differential scanning calorimetry (DSC X7000, Hitachi, Japan) was used to characterize the phase transitions during the melting process of Thy/LA mixed solution. By freeze-drying Thy/LA mixed solution, the powder was collected as the sample. The powder (1.8 mg) was weighed into an aluminum sample pan. The aluminum sample pan was heated from −10°C to 80°C at 10°C/min.

Cryo-Scanning Electron Microscope

According to a previous method (36), the effect of LA addition on microstructure of Thy/LA-Emulsion was determined using cryo-scanning electron microscope (cryo-SEM) (HATACHI SU8010). The emulsions with conductive carbon glue were placed on a table, coated, frozen in liquid nitrogen slush, and then sublimated and gold-plated by using the cryogenic preparation and transmission system. The operating conditions of SEM were as follows: temperature, −140°C; accelerating voltage, 5 kV.

Determination of *in vitro* Antibacterial Activity

Microorganisms

Two kinds of typical foodborne gram-negative bacteria [Escherichia *coli,* (10003, *E. coli)* and *Salmonella enterica* subsp. *enterica serovar Typhimurium* (22956, *S. Typhimurium*)] and two kinds of typical foodborne gram-positive bacteria [*Staphylococcus aureus* (21600, *S. aureus*) and *Listeria monocytogenes* (21635, *L. monocytogenes*)] were used to evaluate the antibacterial activity of the emulsions. The stock cultures were transferred 50 μl into 5 ml sterile Luria–Bertani broth (LB), which were revived at 37°C for 24 h to 10^{-9} cfu/ml. The cultures were diluted to 10^{-4} to 10^{-6} cfu/ml before use.

Determination of Minimum Inhibitory Concentrations and Minimum Bactericidal Concentrations

The minimum inhibitory concentrations (MICs) and minimum bactericidal concentrations (MBCs) of all Emulsions and Thy/LA mixed solution were determined by 96-well plate microdilution method based on a previous method (37). The different proportions of emulsion were diluted to 0.016–2 mg/ml in sterile LB, and Thy/LA mixed solutions were diluted to 0.0078–1 mg/ml in sterile LB quickly after heating, which were all prepared in a 96-well plate by an identical twofold serial dilution. Then 100 μl bacterial inoculum was added to each well, and the 96-well plates were incubated at 37°C for 24 h. The MIC was defined as the lowest concentration of an emulsion that inhibits the visible growth of bacteria. To determine MBC, 100 μl of culture broth with invisible growth was taken from each well and transferred to Luria–Bertani agar plate, and then incubated at 37°C for 48 h. The MBC was defined as the lowest concentration that bacteria did not grow at all on the agar surface.

Determination of the Zone of Inhibition

The zones of inhibition of all emulsions were measured by the Oxford cup method (38). Initially, 20 ml Luria–Bertani agar was poured into a 90-mm sterile Petri dish. After solidification, the diluted test strains (1 ml) were transferred into the agar surface and distributed evenly over the agar surface by a sterile bent glass rod. Then, 100 μl emulsion was taken and transferred into the sterilized Oxford cup (6 mm) that was located in the center of the dish. After standing for 5 min, the dish was incubated at 37°C for 48 h. The zone of inhibition (mm) was measured by a Vernier micrometer.

Determination of Growth Curve

To study the growth curves of all emulsions, the aerobic plate count was employed (39). Overnight test strains were diluted and transferred into sterile LB in sterile centrifuge tubes. Afterward, the emulsion was added to the tube at concentrations of 0, 2 MBC, MBC, 1/2 MBC, and 1/4 MBC. After incubating at 37°C, the mixtures were taken and transferred into the agar surface at 0, 4, 8, 12, and 24 h, respectively. After incubating at 37°C for 24 h, the colony number was calculated to draw the growth curve of Thy/LA-Emulsion.

Statistical Analysis

All experiments were repeated at least three times. The mean and standard deviation were analyzed by statistical analysis software (SSPS, version 17.0). Statistical differences between experiments were detected by the least significant difference test ($p < 0.05$).

RESULTS AND DISCUSSION

The Characterization and Antibacterial Activity of Thymol/Lauric Acid Mixture

Initially, the effect of Thy/LA mass ratio (The ratios of LA are 0, 25, 50, 75, and 100%.) on appearance, thermal properties by using differential scanning calorimetry (DSC) and antibacterial activity of Thy/LA was evaluated. The appearance of Thy/LA at different mass ratios is displayed in **Figure 1**. The state of mixtures depended on different mass Thy/LA ratios at room temperature, where Thy/$LA_{25\%}$ was a clear and transparent liquid and Thy/$LA_{50\%}$ and Thy/$LA_{75\%}$ were solid-like. These results are consistent with DSC thermograms exhibited in **Figure 1**. All mixtures displayed a single endothermic melting peak, and their melting point decreased as the content of LA decreased, which was lower than LA alone or Thy alone. This suggests that Thy and LA mutually inhibit crystallization, thus reducing the melting point of the mixed system, indicating that they have formed an eutectic solution rather than a simple eutectic mixture (40).

The antibacterial effects of Thy and LA with different proportions are illustrated in **Table 1**. At a concentration of less than 1 mg/ml, LA using alone did not show any antibacterial effect on four bacteria, while Thy exhibited a strong antibacterial effect on them, indicating that Thy had a

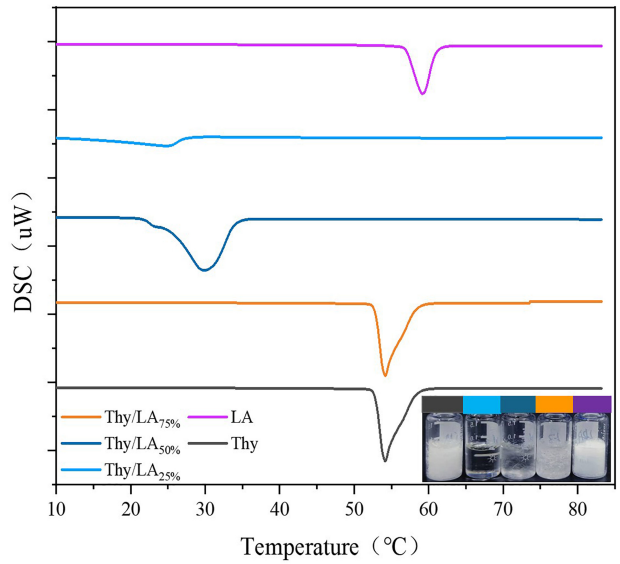

FIGURE 1 | Differential scanning calorimetry (DSC) thermograms of thymol/lauric mixture (Thy/LA) with different mass ratios and the appearance of thymol/lauric acid mixture with different mass ratios at room temperature. All line colors correspond to the samples. *n* = 3.

TABLE 1 | The minimum inhibitory concentration (MIC) and minimum bactericidal concentration (MBC) of different mass thymol/lauric acid ratios against four foodborne pathogens *n* = 3.

Bacteria		Thy	Thy/$LA_{25\%}$	Thy/$LA_{50\%}$	Thy/$LA_{75\%}$	LA
Listeria monocytogenes	MIC(mg/mL)	0.25	0.0625	0.0625	0.25	–
	MBC(mg/mL)	0.5	0.125	0.125	0.5	–
Escherichia coli	MIC(mg/mL)	1	1	1	–	–
	MBC(mg/mL)	1	1	1	–	–
Staphylococcus aureus	MIC(mg/mL)	0.5	0.25	0.5	0.5	1
	MBC(mg/mL)	1	0.5	0.5	1	–
Salmonella	MIC(mg/mL)	1	0.5	0.5	1	–
	MBC(mg/mL)	1	1	0.5	–	–

"–" illustrates that MIC or MBC are above 1 mg/ml.

better antibacterial effect than LA, and Thy was the principal antibacterial agent of the mixture. Compared with two Gram-negative bacteria, Thy showed a stronger antibacterial effect on two Gram-positive bacteria, among which the antibacterial effect against *L. monocytogenes* was best, so did Thy/LA. Moreover, the antibacterial effect against *L. monocytogenes* of Thy/LA with different proportions was comparable or better than those of LA and Thy alone. The MIC values for Thy/$LA_{25\%}$ (0.0625 mg/ml) and Thy/$LA_{50\%}$ (0.0625 mg/ml) were lower than LA (>1 mg/ml) and Thy (0.25 mg/ml) alone. The MBC values for Thy/$LA_{25\%}$ (0.25 mg/ml) and Thy/$LA_{50\%}$ (0.25 mg/ml) were lower than LA (>1 mg/ml) and Thy (0.5 mg/ml) alone, which were equivalent to a quarter of Thy alone, indicating that Thy/$LA_{25\%}$ and Thy/$LA_{50\%}$ demonstrated more effects against *L. monocytogenes*. This result ties well with a previous study (24) wherein Thy and LA exhibited stronger antibacterial effects than Thy or LA alone in certain proportions. According to previous studies (41, 42). Thy, as a hydrophobic substance, easily interacts with the phospholipid bilayers of bacteria to increase membrane permeability, which will lead to the leakage of components inside microbial cells, resulting in cell death. LA is also an amphiphilic substance, which can damage the cell membranes of Gram-positive bacterial (43). A possible explanation might be that the antibacterial effect of LA and Thy is not a simple superposition, but a synergistic effect (24), which may be because it acts on different sites of the cell membrane to increase membrane permeability, enhancing the antibacterial effect.

Owing to the remarkable antibacterial effect, LA with the ratio of 25 and 50% was selected to perform the following experiments, and *L. monocytogenes* was also selected to detect the bacteriostatic effect of the samples.

Preparation, Characterization, and Stability of Thy/LA-Emulsion

The impact of the proportion Thy/LA in the oil phase (The ratios of LA are 0, 25, 50, 75, and 100 wt%.) on the mean particle diameter, stability, and microstructure by using cryo-SEM of the emulsions was evaluated. According to previous studies (32, 44), EOs are susceptible to Ostwald ripening (OR) causing instability in emulsions. OR is a common phenomenon in EO emulsions, based on the diffusion of components of dispersed phase from smaller to larger droplets through a continuous phase, leading to droplet growth, creaming, and oiling off. In several feasible solutions (37, 45), the simplest and most effective measure was to modify the oil composition by incorporating ripening inhibitors (corn oil) before homogenization to inhibit the OR. To increase the stability of the emulsion, corn oil was added to the oil phase to prepare emulsion, and the impact of LA on the physical stability of thymol-based emulsion was also studied. First, a series of emulsions (Φ = 10%) with different mass Thy/LA or Thy and corn oil ratios were prepared [corn oil (%):Thy/LA (%) or Thy alone (%) = 0:100, 10:90, 20:80, 40:60, 60:40]. After homogenization, the emulsions were stored for 3 days at room temperature, and their mean particle sizes were measured in **Figure 2**. A downward trend can be seen, where the mean particle size of the samples decreased as a higher proportion of corn oil added in the oil phase. The particle size of the emulsion prepared by the oil phase using only Thy (0% corn oil) was large and the emulsion was highly unstable as oil separation occurred in the emulsion after 1-week storage (**Figure 2**). The phase separation happened in Thy/$LA_{25\%}$-Emulsion and Thy/$LA_{50\%}$-Emulsion as well. The results are in line with previous research studies (46). Chang et al. investigated the impact of cationic surfactants (lauryl arginate) on the physical properties and antibacterial efficacy of thyme oil nanoemulsions. It was also found that the emulsions were highly unstable and rapidly separated at higher thyme oil levels (≥80 wt%), but emulsions with better stability could be attained by incorporating a ripening inhibitor (corn oil) to the oil phase before homogenization. This illustrates that the addition of corn oil does increase the stability of emulsions by inhibiting OR. There was a steep reduction in mean particle size of 0–20 wt%

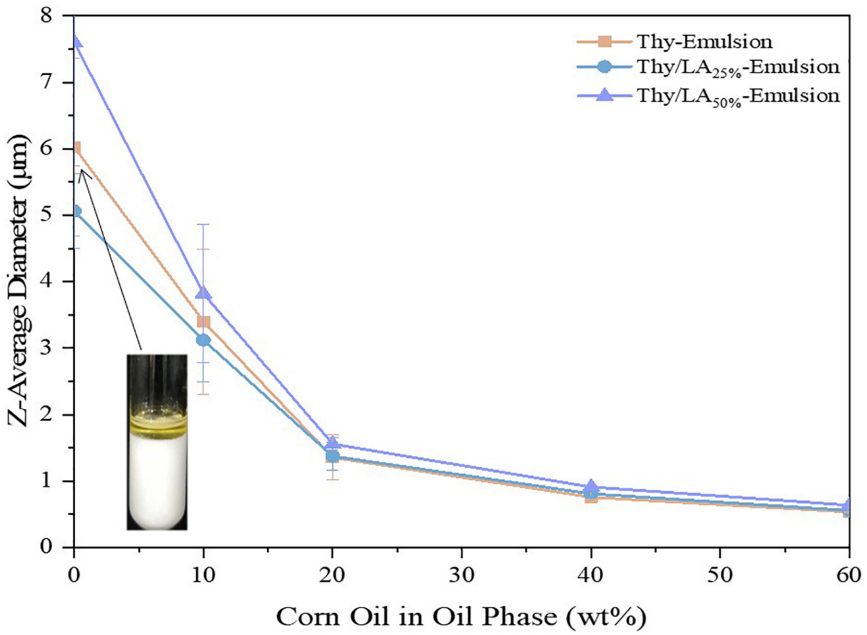

FIGURE 2 | Effect of corn oil concentration (0–60 wt%) on the mean particle sizes of Thy/$LA_{25\%}$-Emulsion, Thy/$LA_{50\%}$-Emulsion, and Thy-Emulsion. The photo in the graph shows that Thy-Emulsion appeared oil separation (0% corn oil). $n = 6$.

corn oil and a relatively gentle reduction in mean particle size of 20–60 wt% corn oil of all emulsions, indicating that all emulsions were more stable when the quantity of corn oil between 20 and 60 wt% in the oil phase, and the stability of emulsion was unaffected by the addition of LA. Prior research (32) has shown that the more corn oil is added, the more the antibacterial efficacy of emulsions is reduced. All in all, a ratio [corn oil (%):Thy/LA (%) or Thy (%) = 20:80] was selected for storage research and antibacterial experiments.

The mean particle size of three emulsions after 1-month storage at room temperature is shown in **Figure 3**. The mean particle size of emulsions is one of the critical factors to evaluate their physical stability (47). The mean particle size of Thy/$LA_{25\%}$-Emulsion and Thy-Emulsion did not appreciably change, illustrating that once an adequate quantity of ripening inhibitor is incorporated into the oil phase before homogenization, emulsions are highly stable against droplet growth over a period of time (48). These results are consistent with the volume fraction distribution of the particle size of Thy-Emulsion and Thy/$LA_{25\%}$-Emulsion exhibited in **Figure 4**. The volume fraction distribution of the particle size of Thy-Emulsion and Thy/$LA_{25\%}$-Emulsion were unimodal, and Thy-Emulsion and Thy/$LA_{25\%}$-Emulsion were stable after 28 days of storage. The mean particle size of Thy/$LA_{50\%}$-Emulsion increased from 1.44 ± 0.16 μm to 2.53 ± 0.08 μm after 1 week, and solidification appeared on the surface in the second week. Consequently, to ensure the storage stability of the emulsion, LA with the ratio of 25% was selected to perform the following experiments.

The ζ-Potential of an emulsion is generally related to the net surface electrical charge on the emulsion droplets and the stability of the emulsion (49, 50). The average ζ-potential values of Thy-Emulsion and Thy/$LA_{25\%}$-Emulsion were -33.47 ± 0.78 mV and -42.77 ± 0.81 mV, respectively. When pH was 6.5, which was higher than the isoelectric point of casein (pH 4.6), casein had a strong negative net charge (51). The emulsion droplets had a higher negative charge due to the absorption of casein at the oil–water (O/W) interface, so the ζ-Potentials of Thy-Emulsion and Thy/$LA_{25\%}$-Emulsion are negative. Moreover, with the addition of LA, the absolute value of zeta-potential of emulsion increased and

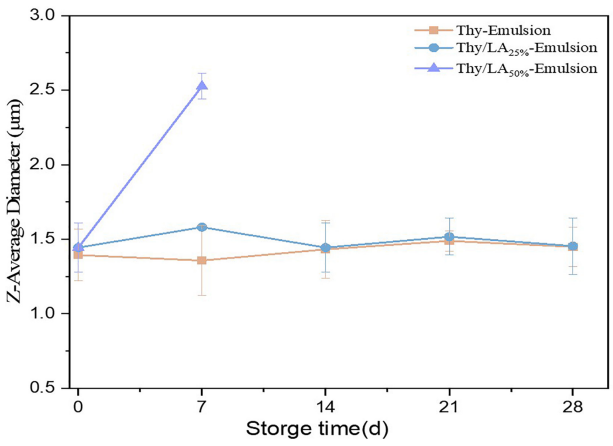

FIGURE 3 | Changes of the mean particle sizes of Thy/$LA_{25\%}$-Emulsion, Thy/$LA_{50\%}$-Emulsion, and Thy-Emulsion during storage for 4 weeks. As solidification appeared on the surface of Thy/$LA_{50\%}$-Emulsion in the second week, particle size could not be measured. $n = 3$.

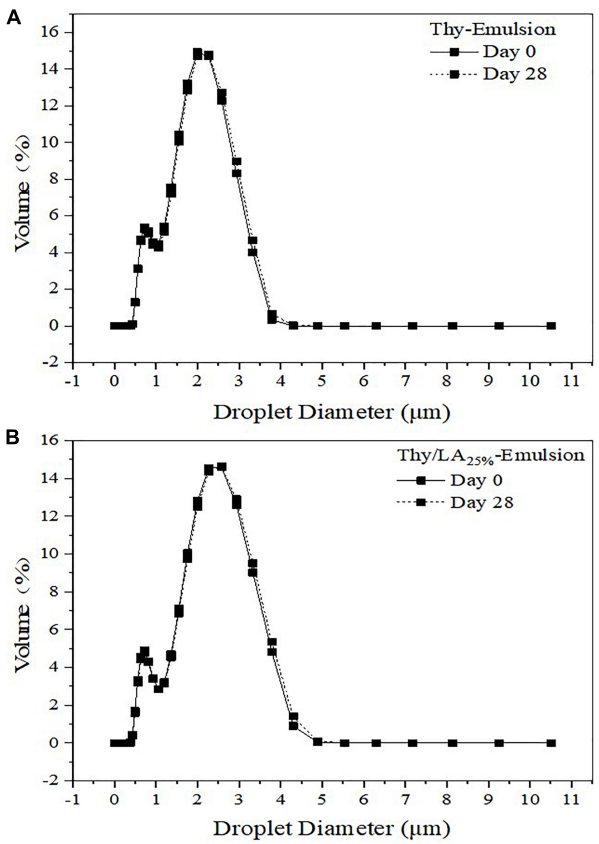

FIGURE 4 | Droplet size distributions in the volume of Thy-Emulsion **(A)** and Thy/$LA_{25\%}$-Emulsion **(B)**. The solid line represents the 0th day, and the dashed line represents the 28th day. *n* = 3.

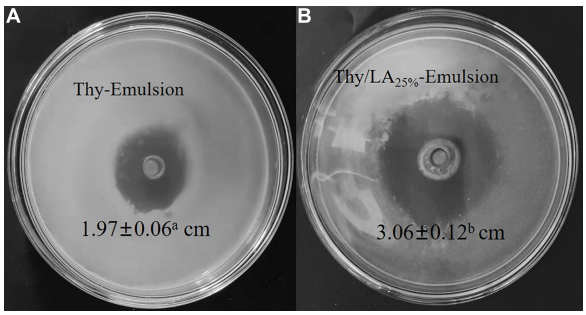

FIGURE 6 | The Zone of Inhibition of Thy-Emulsion **(A)** and Thy/$LA_{25\%}$-Emulsion **(B)** against *Listeria monocytogenes*. *n* = 6.

the Thy/$LA_{25\%}$-Emulsion might have higher stability than Thy-Emulsion. It has been reported that emulsions with higher zeta-potential exerted stronger electrostatic interaction and greater repulsive forces between oil droplets, which could prevent aggregation and improve the stability of the system (52).

Thy/$LA_{25\%}$-Emulsion and Thy-Emulsion were evaluated by cryo-SEM (**Figure 5**), which are consistent with the light scattering analysis of particle size. All the cryo-SEM images did exhibit that all emulsions with relatively small individual oil droplets (<2 μm) were evenly distributed throughout the samples, which also indicates that the stability of emulsions was not affected by the addition of LA.

Antibacterial Activity of Thy/LA-Emulsion

Antibacterial activity of two emulsions against *L. monocytogenes* was evaluated by using the zone of inhibition (**Figure 6**) and growth curves (**Figure 7**). As shown in **Figure 5**, the mean inhibition zone diameter of Thy/$LA_{25\%}$-Emulsion was 3.06 ± 0.12 cm, which was longer than the mean inhibition zone diameter of Thy-Emulsion (1.97 ± 0.06 cm). These results signified that Thy/$LA_{25\%}$-Emulsion exhibited a stronger antibacterial effect than Thy-Emulsion, indicating that the antibacterial effects of Thy and LA still demonstrate a synergistic effect in the emulsion delivery system (24). The concentration of Thy (**Figure 7A**) or Thy/LA (**Figure 7B**)

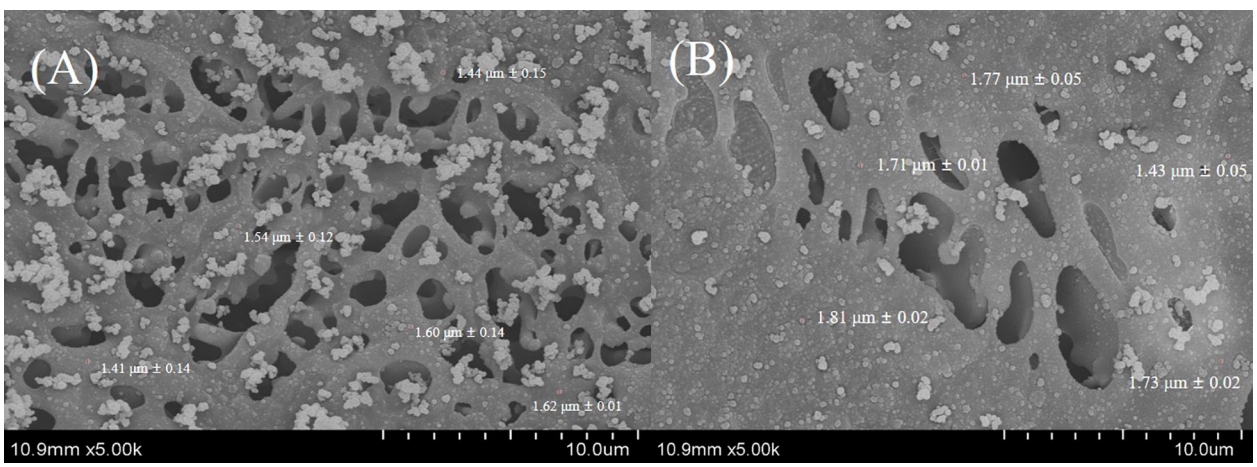

FIGURE 5 | The cryo-SEM micrographs of the Thy-Emulsion **(A)** and Thy/$LA_{25\%}$-Emulsion **(B)**. *n* = 3.

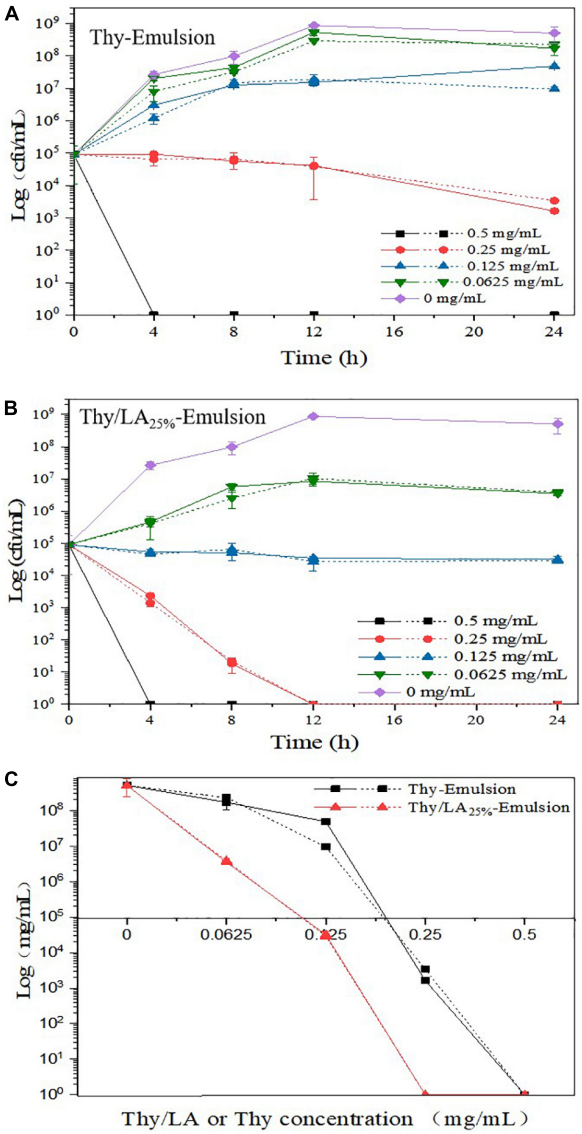

FIGURE 7 | The growth curves of Thy-Emulsion **(A)** and Thy/$LA_{25\%}$-Emulsion **(B)** incubated for 24 h at 37°C and **(C)** the number of colonies formed in Thy-Emulsion and Thy/$LA_{25\%}$-Emulsion after 24 h (the concentration of Thy or Thy/LA ranged from 0.625 to 0.5 mg/mL). The solid line represents the 0th day, and the dashed line represents the 30th day. $n = 6$.

in the oil phase ranged from 0.625 mg/ml to 0.5 mg/ml, and the higher the concentration of Thy or Thy/LA in the oil phase, the better the antibacterial effect of the emulsions possessed. After 24 h of cultivation, when the concentration of Thy or Thy/$LA_{25\%}$ was 0.125 mg/ml, the number of colonies in the Thy-Emulsion formed in the agar increased from approximately 9.0×10^4 cfu/ml to 4.9×10^7 cfu/ml, while the number of colonies in the Thy-Emulsion formed in the agar decreased from approximately 9.0×10^4 cfu/ml to 3.2×10^4 cfu/ml. The number of colonies in Thy-Emulsion formed in agar was approximately 10^4 times more than it was in Thy/$LA_{25\%}$-Emulsion (**Figure 7C**). Thy/$LA_{25\%}$-Emulsion could completely inhibit the growth of *L. monocytogenes*, while Thy-Emulsion demonstrated weak antibacterial activity. When the concentration of emulsions was 0.25 mg/ml, the number of colonies in Thy-Emulsion formed in agar was approximately 10^3 times more than it was in Thy/$LA_{25\%}$-Emulsion (**Figure 7C**). Thy/$LA_{25\%}$-Emulsion demonstrated a strong killing effect on *L. monocytogenes*, while Thy-Emulsion could only inhibit their growth. After 1-month of storage, the antibacterial activity of the two emulsions against *L. monocytogenes* was evaluated by using a growth curve (**Figure 7**), which is represented by a dashed line. The results showed that the antibacterial properties of Thy-Emulsion (**Figure 7A**) and Thy/$LA_{25\%}$-Emulsion (**Figure 7B**) did not decrease significantly after 1-month storage. These results indicated that Thy/$LA_{25\%}$-Emulsion demonstrated better antibacterial activity and physicochemical stability due to its long-term storage stability.

These results exhibited that the MIC values of Thy-Emulsion (0.5 mg/ml) were higher than those samples with Thy (0.25 mg/ml) alone, so did Thy/$LA_{25\%}$-Emulsion. These results were broadly in line with the findings of Chang et al. (32), where Thy emulsions were prepared as potential antimicrobial delivery systems and found that increasing the levels of ripening inhibitor in the oil phase reduced the antimicrobial efficacy of emulsions. This is because the partition of a lipophilic antibacterial agent between oil phase and aqueous phase hinges on their relative concentration and oil–water partition coefficient. After incorporating corn oil, the antibacterial agent will be more likely to partition into the oil phase of the emulsion, causing a decrease in the concentration of the antibacterial agent in the aqueous phase. Because microorganisms exist in the aqueous phase, the effective antibacterial concentration on the surface of microorganisms also decreases, thereby reducing the antibacterial effect (46, 47).

Above all, the incorporation of ripening inhibitor (corn oil) will reduce the antibacterial effect, but the antibacterial effect is still considerable due to the synergistic effect of LA and Thy. When the concentration of Thy was 0.0625 mg/ml (**Figure 7C**), the number of colonies in Thy-Emulsion formed in agar was approximately 1.7×10^8 cfu/ml, while Thy/$LA_{25\%}$-Emulsion demonstrated a strong killing effect. In summary, compared with Thy-Emulsion, Thy/$LA_{25\%}$-Emulsion reduced the content of Thy and enhanced its antibacterial activity. At the same time, Thy/$LA_{25\%}$-Emulsion not only lessens the unique odor and irritation of Thy, but also conforms to the prevailing market in terms of economic benefits due to the low price of MCFs.

CONCLUSION

We studied the antibacterial effects of LA addition on thymol-based emulsions. The incorporation of LA (25 and 50%) could improve the antibacterial activity of thymol-based emulsions against Gram-positive bacteria, especially *L. monocytogenes*. Compared with Thy-Emulsion, Thy/$LA_{25\%}$-Emulsion demonstrated a better antibacterial effect. Thy/$LA_{25\%}$-Emulsion exhibited a greater inhibition zone (3.06 ± 0.12 cm) than Thy-Emulsion (1.97 ± 0.06 cm). When a complete antibacterial

effect was achieved against *L. monocytogenes*, the concentration of the antibacterial components (Thy) in the Thy-Emulsion was 0.5 mg/ml, while the concentration of the antibacterial components (Thy and LA) in the Thy/$LA_{25\%}$-Emulsion was 0.25 mg/ml. The concentration of Thy in the Thy/$LA_{25\%}$-Emulsion was 0.19 mg/ml, which lessens unique odor and irritation and saves cost by reducing the amount of Thy. Owing to the long-term storage stability, Thy/$LA_{25\%}$-Emulsion demonstrated the best antibacterial activity and physicochemical stability. This study may provide a useful and novel antibacterial measure for food and drugs.

DATA AVAILABILITY STATEMENT

The original contributions presented in the study are included in the article/supplementary material, further inquiries can be directed to the corresponding authors.

AUTHOR CONTRIBUTIONS

QC and SL: designed and conceived the study. QC, YZ, and XF: performed the experiments. QC: analyzed the data and drafted the manuscript. SL, ZH, SP, and WL: contributed to the writing of the manuscript. WL: provided the funding and resources. All authors revised and approved the submitted version of the manuscript.

FUNDING

This research was financially support by the Natural Science Foundation of Jiangxi Province, China (20212BAB215035), "Shuangqian Project" of Scientific and the Technological Innovation of High-end Talents–Natural Science, Jiangxi Province (S2019GDKX2836), and the China Postdoctoral Science Foundation (2020M682111).

REFERENCES

1. World Health Organization. *Food Safety*. Geneva: World Health Organization (2020).
2. Wilking H, Lachmann R, Holzer A, Halbedel S, Flieger A, Stark K. Ongoing high incidence and case-fatality rates for invasive listeriosis, Germany, 2010-2019. *Emerg Infect Dis.* (2021) 27:2485–8. doi: 10.3201/eid2709.210068
3. Choi MH, Park YJ, Kim M, Seo YH, Kim YA, Choi JY, et al. Increasing incidence of listeriosis and infection-associated clinical outcomes. *Ann Lab Med.* (2018) 38:102–9. doi: 10.3343/alm.2018.38.2.102
4. Isman MB. Plant essential oils for pest and disease management. *Crop Prot.* (2000) 19:603–8. doi: 10.1016/S0261-2194(00)00079-X
5. Jackson WB. Integrated pest management. *Phytoparasitica.* (1992) 20:3–6. doi: 10.1007/BF02995628
6. Mutlu-Ingok A, Devecioglu D, Dikmetas DN, Karbancioglu-Guler F, Capanoglu E. Antibacterial, antifungal, antimycotoxigenic, and antioxidant activities of essential oils: an updated review. *Molecules.* (2020) 25:4711. doi: 10.3390/molecules25204711
7. Calo JR, Crandall PG, O'Bryan CA, Ricke SC. Essential oils as antimicrobials in food systems – a review. *Food Control.* (2015) 54:111–9. doi: 10.1016/j.foodcont.2014.12.040
8. Baser KHC. Biological and pharmacological activities of carvacrol and carvacrol bearing essential oils. *Curr Pharm Des.* (2008) 14:3106–19. doi: 10.2174/138161208786404227
9. Raut JS, Karuppayil SM. A status review on the medicinal properties of essential oils. *Ind Crop Prod.* (2014) 62:250–64. doi: 10.1016/j.indcrop.2014.05.055
10. Burt S. Essential oils: their antibacterial properties and potential applications in foods – a review. *Int J Food Microbiol.* (2004) 94:223–53. doi: 10.1016/j.ijfoodmicro.2004.03.022
11. Falleh H, Ben Jemaa M, Saada M, Ksouri R. Essential oils: a promising eco-friendly food preservative. *Food Chem.* (2020) 330:127268. doi: 10.1016/j.foodchem.2020.127268
12. Gholami-Ahangaran M, Ahmadi-Dastgerdi A, Azizi S, Basiratpour A, Zokaei M, Derakhshan M. Thymol and carvacrol supplementation in poultry health and performance. *Vet Med Sci.* (2022) 8:267–88. doi: 10.1002/vms3.663
13. Kachur K, Suntres Z. The antibacterial properties of phenolic isomers, carvacrol and thymol. *Crit Rev Food Sci.* (2020) 60:3042–53. doi: 10.1080/10408398.2019.1675585
14. Lammari N, Louaer O, Meniai AH, Elaissari A. Encapsulation of essential oils via nanoprecipitation process: overview, progress, challenges and prospects. *Pharmaceutics.* (2020) 12:5. doi: 10.3390/pharmaceutics12050431
15. Samperio C, Boyer R, Eigel WN, Holland KW, McKinney JS, O'Keefe SF, et al. Enhancement of plant essential oils' aqueous solubility and stability using alpha and beta cyclodextrin. *J Agric Food Chem.* (2010) 58:12950–6. doi: 10.1021/jf103275a
16. Radunz M, da Trindade MLM, Camargo TM, Radunz AL, Borges CD, Gandra EA, et al. Antimicrobial and antioxidant activity of unencapsulated and encapsulated clove (*Syzygium aromaticum*, L.) essential oil. *Food Chem.* (2019) 276:180–6. doi: 10.1016/j.foodchem.2018.09.173
17. Hadaruga DI, Hadaruga NG, Costescu CI, David I, Gruia AT. Thermal and oxidative stability of the *Ocimum basilicum* L. Essential oil/beta-cyclodextrin supramolecular system. *Beil J Org Chem.* (2014) 10:2809–20. doi: 10.3762/bjoc.10.298
18. Hyldgaard M, Mygind T, Meyer RL. Essential oils in food preservation: mode of action, synergies, and interactions with food matrix components. *Front Microbiol.* (2012) 3:12. doi: 10.3389/fmicb.2012.00012
19. Nikkhah M, Hashemi M, Najafi MBH, Farhoosh R. Synergistic effects of some essential oils against fungal spoilage on pear fruit. *Int J Food Microbiol.* (2017) 257:285–94. doi: 10.1016/j.ijfoodmicro.2017.06.021
20. Huang ZX, Pang DR, Liao ST, Zou YX, Zhou PF, Li EN, et al. Synergistic effects of cinnamaldehyde and cinnamic acid in cinnamon essential oil against S. pullorum. *Ind Crop Prod.* (2021) 162:113296. doi: 10.1016/j.indcrop.2021.113296
21. Dra LA, Brahim MAS, Boualy B, Aghraz A, Barakate M, Oubaassine S, et al. Chemical composition, antioxidant and evidence antimicrobial synergistic effects of *Periploca laevigata* essential oil with conventional antibiotics. *Ind Crop Prod.* (2017) 109:746–52. doi: 10.1016/j.indcrop.2017.09.028
22. Langeveld WT, Veldhuizen EJA, Burt SA. Synergy between essential oil components and antibiotics: a review. *Crit Rev Microbiol.* (2014) 40:76–94. doi: 10.3109/1040841X.2013.763219
23. Ju J, Xie YF, Yu H, Guo YH, Cheng YL, Qian H, et al. Synergistic interactions of plant essential oils with antimicrobial agents: a new antimicrobial therapy. *Crit Rev Food Sci.* (2022) 62:1740–51. doi: 10.1080/10408398.2020.1846494
24. Kim SA, Rhee MS. Highly enhanced bactericidal effects of medium chain fatty acids (caprylic, capric, and lauric acid) combined with edible plant essential oils (carvacrol, eugenol, beta-resorcylic acid, trans-cinnamaldehyde, thymol, and vanillin) against *Escherichia coli* O157:H7. *Food Control.* (2016) 60:447–54. doi: 10.1016/j.foodcont.2015.08.022
25. Zhang XW, Zhou DG, Cao YF, Zhang Y, Xiao XL, Liu FS, et al. Synergistic inactivation of *Escherichia coli* O157:H7 and *Staphylococcus aureus* by gallic acid and thymol and its potential application on fresh-cut tomatoes. *Food Microbiol.* (2022) 102:103925. doi: 10.1016/j.fm.2021.103925
26. Marten B, Pfeuffer M, Schrezenmeir J. Medium-chain triglycerides. *Int Dairy J.* (2006) 16:1374–82. doi: 10.1016/j.idairyj.2006.06.015
27. Sado-Kamdem SL, Vannini L, Guerzoni ME. Effect of α-linolenic, capric and lauric acid on the fatty acid biosynthesis in *Staphylococcus aureus*. *Int J Food Microbiol.* (2009) 129:288–94. doi: 10.1016/j.ijfoodmicro.2008.12.010

28. Kim SA, Kim HW, Rhee MS. Cranberry extract with enhanced bactericidal activities against uropathogenic *Escherichia coli* within one minute of treatment. *LWT Food Sci Technol.* (2019) 113:108318. doi: 10.1016/j.lwt.2019.108318
29. Van Immerseel F, Russell JB, Flythe MD, Gantois I, Timbermont L, Pasmans F, et al. The use of organic acids to combat *Salmonella* in poultry: a mechanistic explanation of the efficacy. *Avian Pathol.* (2006) 35:182–8. doi: 10.1080/03079450600711045
30. Zhu YL, Li CZ, Cui HY, Lin L. Encapsulation strategies to enhance the antibacterial properties of essential oils in food system. *Food Control.* (2021) 123:107856. doi: 10.1016/j.foodcont.2020.107856
31. Razola-Diaz MD, Guerra-Hernandez EJ, Garcia-Villanova B, Verardo V. Recent developments in extraction and encapsulation techniques of orange essential oil. *Food Chem.* (2021) 354:129575. doi: 10.1016/j.foodchem.2021.129575
32. Chang YH, McLandsborough L, McClements DJ. Physical properties and antimicrobial efficacy of thyme oil nanoemulsions: influence of ripening inhibitors. *J Agric Food Chem.* (2012) 60:12056–63. doi: 10.1021/jf304045a
33. McClements DJ. Emulsion design to improve the delivery of functional lipophilic components. *Annu Rev Food Sci Technol.* (2010) 1:241–69. doi: 10.1146/annurev.food.080708.100722
34. Miao JY, Xu N, Cheng C, Zou LQ, Chen J, Wang Y, et al. Fabrication of polysaccharide-based high internal phase emulsion gels: enhancement of curcumin stability and bioaccessibility. *Food Hydrocolloid.* (2021) 117:106679. doi: 10.1016/j.foodhyd.2021.106679
35. Peng SF, Zhou L, Cai QZ, Zou LQ, Liu CM, Liu W, et al. Utilization of biopolymers to stabilize curcumin nanoparticles prepared by the pH-shift method: caseinate, whey protein, soy protein and gum Arabic. *Food Hydrocolloid.* (2020) 107:105963. doi: 10.1016/j.foodhyd.2020.105963
36. Xu N, Wu XL, Zhu YQ, Miao JY, Gao Y, Cheng C, et al. Enhancing the oxidative stability of algal oil emulsions by adding sweet orange oil: effect of essential oil concentration. *Food Chem.* (2021) 355:129508. doi: 10.1016/j.foodchem.2021.129508
37. Ziani K, Chang YH, McLandsborough L, McClements DJ. Influence of surfactant charge on antimicrobial efficacy of surfactant-stabilized thyme oil nanoemulsions. *J Agric Food Chem.* (2011) 59:6247–55. doi: 10.1021/jf200450m
38. Yang RP, Miao JY, Shen YT, Cai N, Wan CP, Zou LQ, et al. Antifungal effect of cinnamaldehyde, eugenol and carvacrol nanoemulsion against *Penicillium digitatum* and application in postharvest preservation of citrus fruit. *LWT Food Sci Technol.* (2021) 141:110924. doi: 10.1016/j.lwt.2021.110924
39. Nouri M, Baghaee-Ravari S, Emadzadeh B. Nano-emulsified savory and thyme formulation show limited efficacy to suppress *Pectobacterium carotovorum* subsp. carotovorum compared with pure oil. *Ind Crop Prod.* (2021) 161:113216. doi: 10.1016/j.indcrop.2020.113216
40. Chun MK, Hossain K, Choi SH, Ban SJ, Moon H, Choi HK. Development of cataplasmic transdermal drug delivery system containing eutectic mixture of lidocaine and prilocaine. *J Pharm Investig.* (2012) 42:139–46. doi: 10.1007/s40005-012-0023-6
41. Gill AO, Holley RA. Disruption of *Escherichia coli*, *Listeria monocytogenes* and *Lactobacillus sakei* cellular membranes by plant oil aromatics. *Int J Food Microbiol.* (2006) 108:1–9. doi: 10.1016/j.ijfoodmicro.2005.10.009
42. Tian L, Wang XY, Liu RJ, Zhang D, Wang X, Sun RC, et al. Antibacterial mechanism of thymol against *Enterobacter sakazakii*. *Food Control.* (2021) 123:107716. doi: 10.1016/j.foodcont.2020.107716
43. Yang HT, Chen JW, Rathod J, Jiang YZ, Tsai PJ, Hung YP, et al. Lauric acid is an inhibitor of *Clostridium difficile* growth in Vitro and reduces inflammation in a mouse infection model. *Front Microbiol.* (2018) 8:2635. doi: 10.3389/fmicb.2017.02635
44. Kabalnov AS, Shchukin ED. Ostwald ripening theory: applications to fluorocarbon emulsion stability. *Adv Colloid Interface Sci.* (1992) 38:69–97. doi: 10.1016/0001-8686(92)80043-W
45. McClements DJ, Henson L, Popplewell LM, Decker EA, Choi SJ. Inhibition of Ostwald ripening in model beverage emulsions by addition of poorly water soluble triglyceride oils. *J Food Sci.* (2012) 77:C33–8. doi: 10.1111/j.1750-3841.2011.02484.x
46. Chang YH, McLandsborough L, McClements DJ. Fabrication, stability and efficacy of dual-component antimicrobial nanoemulsions: essential oil (thyme oil) and cationic surfactant (lauric arginate). *Food Chem.* (2015) 172:298–304. doi: 10.1016/j.foodchem.2014.09.081
47. Mirhosseini H, Tan CP, Hamid NSA, Yusof S. Optimization of the contents of arabic gum, xanthan gum and orange oil affecting turbidity, average particle size, polydispersity index and density in orange beverage emulsion. *Food Hydrocolloid.* (2008) 22:1212–23. doi: 10.1016/j.foodhyd.2007.06.011
48. Zhao YJ, Liu R, Qi CP, Li W, Rifky M, Zhang M, et al. Mixing oil-based microencapsulation of garlic essential oil: impact of incorporating three commercial vegetable oils on the stability of emulsions. *Foods.* (2021) 10:7. doi: 10.3390/foods10071637
49. Salvia-Trujillo L, Rojas-Graü A, Soliva-Fortuny R, Martín-Belloso O. Physicochemical characterization and antimicrobial activity of food-grade emulsions and nanoemulsions incorporating essential oils. *Food Hydrocolloid.* (2015) 43:547–56. doi: 10.1016/j.foodhyd.2014.07.012
50. Masum AKM, Chandrapala J, Adhikari B, Huppertz T, Zisu B. Effect of lactose-to-maltodextrin ratio on emulsion stability and physicochemical properties of spray-dried infant milk formula powders. *J Food Eng.* (2019) 254:34–41. doi: 10.1016/j.jfoodeng.2019.02.023
51. Ritzoulis C, Siasios S, Melikidou KD, Koukiotis C, Vasiliadou C, Lolakos S. Interactions between pig gastric mucin and sodium caseinate in solutions and in emulsions. *Food Hydrocolloid.* (2012) 29:382–8. doi: 10.1016/j.foodhyd.2012.04.005
52. Yu H, Byun Y, Chang P-S. Lipase-catalyzed two-step esterification for solvent-free production of mixed lauric acid esters with antibacterial and antioxidative activities. *Food Chem.* (2022) 366:130650. doi: 10.1016/j.foodchem.2021.130650

Conflict of Interest: ZH is employed by Jiangxi Danxia Biol Technol Co., Ltd.

The remaining authors declare that the research was conducted in the absence of any commercial or financial relationships that could be construed as a potential conflict of interest.

Publisher's Note: All claims expressed in this article are solely those of the authors and do not necessarily represent those of their affiliated organizations, or those of the publisher, the editors and the reviewers. Any product that may be evaluated in this article, or claim that may be made by its manufacturer, is not guaranteed or endorsed by the publisher.

frontiers | Frontiers in Nutrition

ORIGINAL RESEARCH
published: 26 April 2022
doi: 10.3389/fnut.2022.892845

Pickering Emulsions Stabilized by Tea Water-Insoluble Protein Nanoparticles From Tea Residues: Responsiveness to Ionic Strength

Zhongyang Ren[1,2,3], *Zhongzheng Chen*[2], *Yuanyuan Zhang*[2], *Xiaorong Lin*[2], *Wuyin Weng*[1,3] *and Bin Li*[2*]

[1] College of Ocean Food and Biological Engineering, Jimei University, Xiamen, China, [2] College of Food Science, South China Agricultural University, Guangzhou, China, [3] Collaborative Innovation Center of Provincial and Ministerial Co-construction for Marine Food Deep Processing, Dalian, China

Tea water-insoluble protein nanoparticles (TWIPNs) can be applied to stabilize Pickering emulsions. However, the effect of ionic strength (0–400 mmol/L) on the characteristics of Pickering emulsions stabilized by TWIPNs (TWIPNPEs) including volume-averaged particle size ($d_{4,3}$), zeta potential, microstructure and rheological properties is still unclear. Therefore, this work researched the effect of ionic strength on the characteristics of TWIPNPEs. The $d_{4,3}$ of TWIPNPEs in the aquatic phase increased with the increase in ionic strength (0–400 mmol/L), which was higher than that in the SDS phase. Furthermore, the flocculation index of TWIPNPEs significantly ($P < 0.05$) increased from 24.48 to 152.92% with the increase in ionic strength. This could be verified from the microstructure observation. These results indicated that ionic strength could promote the flocculation of TWIPNPEs. Besides, the absolute values of zeta potential under different ionic strengths were above 40 mV in favor of the stabilization of TWIPNPEs. The viscosity of TWIPNPEs as a pseudoplastic fluid became thin when shear rate increased from 0.1 to 100 s^{-1}. The viscoelasticity of TWIPNPEs increased with increasing ionic strength to make TWIPNPEs form a gel-like Pickering emulsion. the possible mechanism of flocculation stability of TWIPNPEs under different ionic strengths was propose. TWIPNs adsorbed to the oil-water interface would prompt flocculation between different emulsion droplets under the high ionic strength to form gel-like behavior verified by CLSM. These results on the characteristics of TWIPNPEs in a wide ionic strength range would provide the theoretical basis for applying Pickering emulsions stabilized by plant proteins in the food industry.

Keywords: tea residues, plant proteins, Pickering emulsions, ionic strength, rheological properties

OPEN ACCESS

Edited by:
Jianhua Liu,
Zhejiang University of Technology, China

Reviewed by:
Shilin Liu,
Huazhong Agricultural University, China
Aimin Shi,
Institute of Food Science and Technology (CAAS), China

***Correspondence:**
Bin Li
bli@scau.edu.cn

Specialty section:
This article was submitted to Food Chemistry, a section of the journal Frontiers in Nutrition

Received: *09 March 2022*
Accepted: *01 April 2022*
Published: *26 April 2022*

Citation:
Ren Z, Chen Z, Zhang Y, Lin X, Weng W and Li B (2022) Pickering Emulsions Stabilized by Tea Water-Insoluble Protein Nanoparticles From Tea Residues: Responsiveness to Ionic Strength. Front. Nutr. 9:892845. doi: 10.3389/fnut.2022.892845

INTRODUCTION

Emulsions are easily affected by external factors such as pH, temperature and ionic strength to lose stability (1, 2). In recent 10 years, numerous food-grade particles have been developed with the rise of food-grade Pickering emulsions. The development and application of plant proteins have aroused the interest of researchers to structure Pickering emulsions (3). Plant protein particles can combine oil and water to form stable emulsions (4, 5). However, some protein particles

only stabilize Pickering emulsions under a certain ionic strength (6).

Protein particles like nanoparticles, microgels and fibrils can manipulate the properties of Pickering emulsions like aggregation or flocculation with the change of ionic strength (7). Numerous raw proteins can form nanoparticles using simple methods. The interfacial behavior of protein nanoparticles from zeins, kafirins, soy proteins, wheat proteins, wheat protein/xanthan gum complexes in Pickering emulsions can be adjusted by ionic strength (8–11). Zein nanoparticles can produce stable o/w Pickering emulsions under moderate ionic strengths (1–10 mmol/L) (8). Protein microgels with soft and deformable properties can quickly swell and deswell reversibly under various external stimuli like ionic strength to form stimuli-responsive emulsions (12). Lots of protein nanoparticles need to be processed by thermal denaturation method, ion bridging method, solvent/antisolvent method to prepare stable Pickering emulsions. These protein nanoparticles must be carefully designed to reach the appropriate size and interface behavior before effectively stabilizing Pickering emulsions (3). Additionally, the performance of protein nanoparticles can be also improved by adjusting ionic strength in the protein nanoparticle solution to suitable interfacial properties (13). Pickering emulsions have been prepared by combining different protein nanoparticles with polysaccharides like gluten nanoparticle/xanthan gum complexes under suitable ionic strengths (11).

Tea proteins from tea residues account for 20–30% of dry tea are mainly tea water-insoluble proteins after the treatment of alkaline method (14) or enzyme method (15). Tea water-insoluble protein nanoparticles (TWIPNs) from tea residues include the uncharged amino acids and hydrophobic amino acids of more than 60% of amino acids gained by the alkali-solution and acid-precipitation method (16). At an oil-water ratio of 6:4, TWIPNs can be used to stabilize Pickering emulsions on the neutral condition, (17). Besides, TWIPNs can be applied to generate gel-like Pickering emulsions after high-pressure homogenization (18). Meanwhile, the flocculation of Pickering emulsions stabilized by TWIPNs (TWIPNPEs) is accelerated at high temperatures (100°C/120°C) (19). Furthermore, TWIPNPEs can exhibit a gel-like behavior at pH 7–11 (20) and as a template to prepare oil gels (21). However, few studies have systematically characterized the properties and colloidal behavior of TWIPNPEs under different ionic strengths. it is very necessary to characterize the ability of TWIPNPEs for responding to the environmental condition of ionic strength.

Therefore, this study aimed to reveal the effect of ionic strength (0–400 mmol/L) on the characteristics of TWIPNPEs under neutral conditions. The characteristics of TWIPNPEs under different ionic strengths were analyzed. We hypothesized that TWIPNs at the interface of oil and water would prompt the flocculation between different emulsion droplets under a high ionic strength, forming gel-like behavior. The gel-like behavior of TWIPNPEs was explored under different ionic strengths.

MATERIALS AND METHODS

Materials

Tea residues were gained from Shenzhen Shenbao Huacheng Tech. Co., Ltd. Soy oil was purchased from the local supermarket in Guangzhou of China. Sodium dodecyl sulfate (SDS, ≥99.0%) was purchased from Merck & Co., Inc. Other reagents were of analytical purity. All water was of deionized water.

Preparation of TWIPNs

TWIPNs were prepared according to a previous method (17). Briefly, tea residues (100 g) were extracted at 90°C for 1.5 h using a 3 L NaOH solution (0.3 mol/L) and centrifuged at 8,288 g for 15 min at 25°C. The supernatant was precipitated at pH 3.5 after decolorization using 30% H_2O_2. TWIPNs were gained after washing the precipitates to the neutral and frozen-drying via a freeze drier (Christ, ALPHA 1-2 LD Plus, Osterode, Germany). The TWIPNs (2 g) were dispersed with the different NaCl solutions (0–400 mmol/L) and hydrated for 24 h at 4°C for preparing emulsions.

Preparation of TWIPNPEs

TWIPNPEs were prepared according to a previous method (21). TWIPN suspension (40 mL) and soy oils (60 mL) were mixed using a shear emulsifying machine (SUOTN, AD500S-H, Shanghai, China) at 20,000 r/min for 2 min to form initial emulsions. The initial emulsions were homogenized at 40 MPa by a high-pressure homogenizer (AH-Basic-II, Suzhou, China) to obtain TWIPNPEs.

Measurements of Droplet Size and Flocculation Index of TWIPNPEs

The volume-average droplet size ($d_{4,3}$) and flocculation index of TWIPNPEs were determined by Mastersizer (Malvern 3000, Malvern, UK) according to a previous method (22). Water and 10 g/L SDS solution were used as dispersants. The flocculation index was calculated according to Eq. (1).

$$FI(\%) = (d_{4,3-W}/d_{4,3-S} - 1) \times 100 \quad (1)$$

where $d_{4,3-W}$ and $d_{4,3-S}$ represent the droplet size of emulsions in water and SDS dispersion, respectively.

Measurement of Zeta Potential of TWIPNPEs

The zeta potential of TWIPNPE was measured according to a previous method (23). TWIPNPEs (10 μL) were mixed using water (990 μL). The Malvern zetasizer (Nano ZS90, Malvern, UK) was equilibrated for 60 s after putting a disposable folded capillary cell. The testing condition was performed at 25°C.

Morphological Observation of TWIPNPEs

TWIPNPEs were observed via an optical microscope (Motic, BA310-T, Hong Kong, China) equipped with a 100 × lens. Then, the confocal laser scanning microscope (CLSM) with LSM 7 DUO dual confocal system was used to observe TWIPNPEs. The emulsions were stained before observation with Nile blue A for TWIPNs and Nile red for soybean oil. The TWIPNPEs were

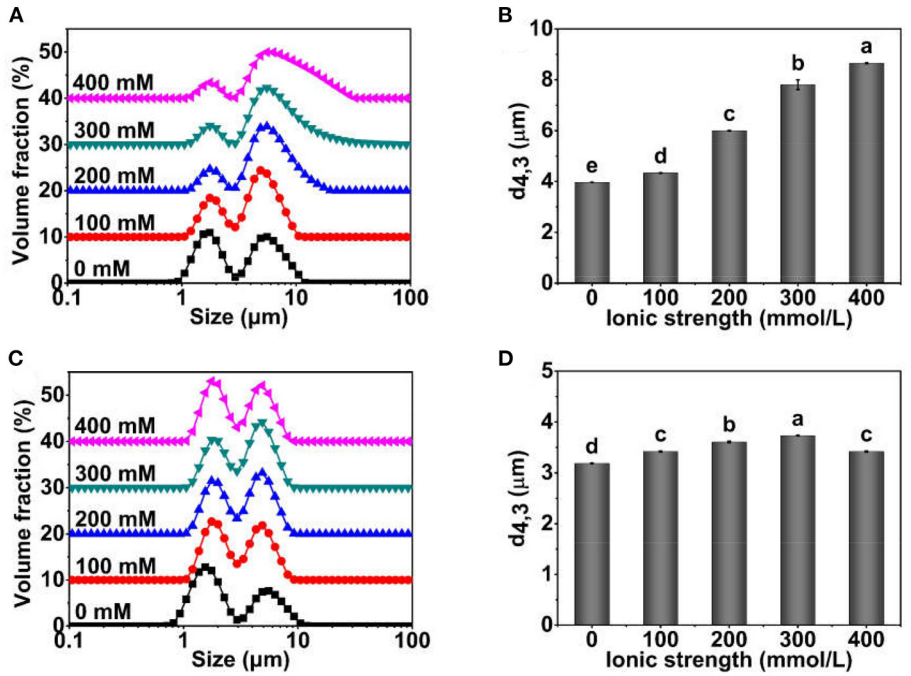

FIGURE 1 | Particle size distribution profiles and $d_{4,3}$ of Pickering emulsions stabilized by TWIPNs at different ionic strengths [**(A)** Particle size distribution in water; **(B)** $d_{4,3}$ in water; **(C)** Particle size distribution in 1.0% SDS; **(D)** $d_{4,3}$ in 1.0% SDS]. The lowercases indicate the significance of different Pickering emulsions by tea water-insoluble protein nanoparticles under different ionic strengths ($P < 0.05$).

stained with anhydrous ethanol containing 0.05% Nile blue A and 0.05% Nile red for 30 min. TWIPNPE samples were observed by Argon and He/Ne lasers with the excitation wavelengths of 488 nm and 633 nm.

Determination of Rheological Properties of TWIPNPEs

TWIPNPEs were determined by rheometer (Anton Paar, MCR-102, Graz, Austria) according to a previous method (24). The apparent viscosity of TWIPNPEs was analyzed at shear rates from 0.1 to 100 s^{-1} using a parallel plate (Φ50 mm). The frequency sweep of TWIPNPEs was tested at the angular velocity from 0.1 to 100 rad/s within a small amplitude oscillatory mode. The gap was fixed at 1.0 mm. All the tests were performed at 25 ± 0.1°C. The storage modulus (G') and loss modulus (G") were recorded.

Statistical Analysis

Data were expressed as the mean values ± standard deviation. Origin Pro 9.0.5 software was used to analyze the significance ($P < 0.05$).

RESULTS AND DISCUSSION

Stability of Pickering Emulsions Prepared Using TWIPNs Under Different Ionic Strengths

Droplet Size

The particle size distribution and $d_{4,3}$ of TWIPNPEs using TWIPNs under different ionic strengths are shown in **Figure 1**. The particle size distribution of TWIPNPEs in the aqueous phase presented two peaks. The volume fraction of peak 1 decreased with the increase in ionic strength, while the volume fraction of peak 2 increased, indicating that the droplets of TWIPNPEs in the aquatic phase increased with the increase in ionic strength (**Figure 1A**). The $d_{4,3}$ of TWIPNPEs in the aquatic phase increased with the increase from 0 to 400 mmol/L NaCl (**Figure 1B**), which was consistent with the particle size distribution in **Figure 1A**. It also has been reported that the size of emulsions stabilized by pea protein isolate nanoparticles increases with the increase in the ionic strength (25). The increase in droplet size of emulsions with the increase in ionic strength might be due to that the strong electrostatic screening induces coalescence (26). In addition, the particle size distribution and $d_{4,3}$ of TWIPNPEs dispersing in 1.0% SDS indicated that the particle size of TWIPNPEs increased with the increase of ionic strengths (0–300 mmol/L) and decreased under the ionic strength of 400 mmol/L. The $d_{4,3}$ of TWIPNPEs in 1.0% SDS was significantly smaller than those in the aquatic phase. This may result in the flocculation of Pickering emulsions, which could be verified by FI in **Figure 2**.

Flocculation Index

The FI of TWIPNPEs under different ionic strengths is shown in **Figure 2**. The FI of TWIPNPEs significantly ($P < 0.05$) increased from 24.48 to 152.92% with the increase in ionic strength. These results indicated that ionic strength could promote the flocculation of TWIPNPEs under the ionic strengths of 0–400 mmol/L. It has been indicated that the droplet flocculation of

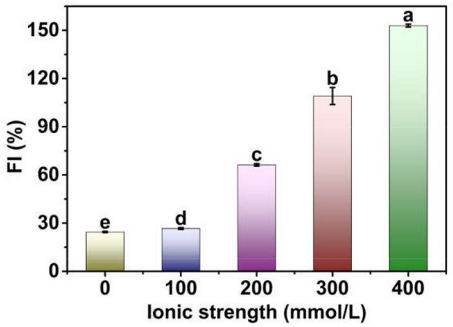

FIGURE 2 | FI of Pickering emulsions stabilized by tea water-insoluble protein nanoparticles under different ionic strengths. The lowercases indicate the significance of different Pickering emulsions by tea water-insoluble protein nanoparticles under different ionic strengths ($P < 0.05$).

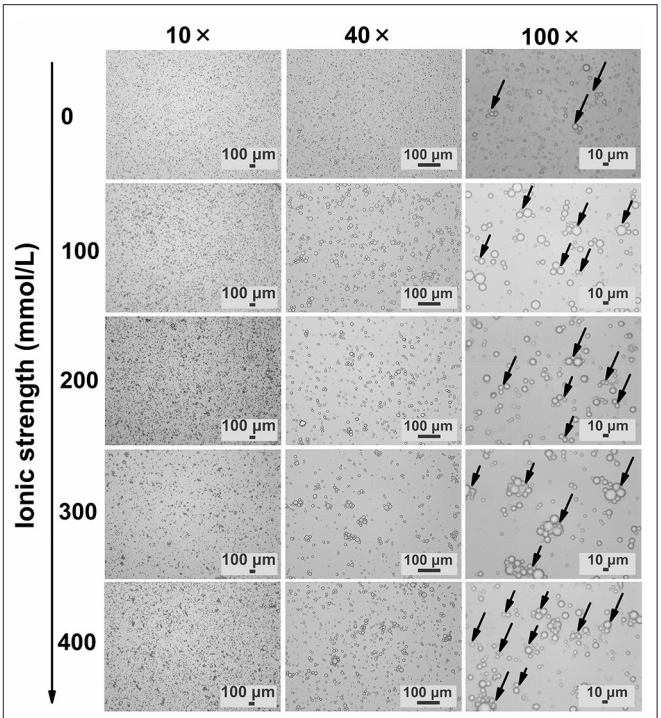

FIGURE 3 | Microscopic observation of Pickering emulsions stabilized by tea water-insoluble protein nanoparticles under different ionic strengths (left: ionic strength; upper: magnification times. Arrows indicate the flocculation).

Pickering emulsions stabilized by pea protein microgel particles can be observed after the addition of 100 mM NaCl (27). This can be attributed to that protein particles interact with each other at the surface of emulsion droplets with the increase in ionic strength, thereby increasing the flocculation of Pickering emulsions (28). Besides, salt ions can be applied to control the electrostatic interactions between the droplets of Pickering emulsions and affect the formation of emulsion gels (29). Meanwhile, ionic strength promoted the formation of aggregates of TWIPNs to increase the size of protein particles, which increased the aggregation of adjacent TWIPNs to improve the flocculation of emulsion droplets.

Microscope Observation

TWIPNPEs under different ionic strengths were further observed as shown in **Figure 3**. As indicated by the black arrow, the flocculation of emulsion droplets gradually increased with increasing ionic strength. This result was in agreement with the analysis of particle size (**Figure 1**) and flocculation of TWIPNPEs under different ionic strengths (**Figure 2**). According to the observation of TWIPNPEs in 100× objective lens in **Figure 3**, it could be observed that the flocculation of TWIPNPEs increased from 0 to 400 mmol/L NaCl as indicated using the arrows. This indicates the network formation of aggregated emulsion droplets among the adjacent emulsion droplets. The formation of inter-droplet particle networks at the high ionic strengths is verified like Pickering emulsions stabilized by zein (8), hydrophilically modified silica nanoparticles (30), silica nanoparticles coated with (3-glycidyloxypropyl) trimethoxysilane (31) and so on. Protein nanoparticles can be induced to form a network through salt ions.

Zeta Potential

The zeta potential of TWIPNPEs under different ionic strengths was also analyzed as shown in **Figure 4**. The zeta potential of TWIPNPEs under the ionic strength of 100 mmol/L had no significant change ($P > 0.05$) compared with that without the addition of salt (**Figure 4A**). However, the absolute zeta potential value of TWIPNPEs without SDS treatment increased with increasing ionic strength at above 100 mmol/L, which was higher than that under the ionic strength of no more than 100 mmol/L. In this study, the emulsions were prepared at pH 7, which is above the isoelectric point (pH 3.5) of TWIPNs (16). the zeta potential of the emulsions stabilized by proteins at pH above the isoelectric point with negative charges increases with the increase in ionic strength (32). When the ionic strength reached 400 mmol/L, the zeta potential of TWIPNPEs showed a slight decrease compared to that under the ionic strength of 300 mmol/L (**Figure 4A**). This may be attributed to the flocculation of TWIPNPE droplets under the high ionic strength, leading to the reduction of exposing charged residue groups at the surface of emulsion droplets. The decrease in negative charges of emulsions stabilized by proteins at pH above the isoelectric point could be attributed to electrostatic screening and ion binding effects (32, 33). The absolute value of zeta potential of TWIPNPEs in the SDS solution was higher than those in the deionized water as shown in **Figure 4B**. It is due to that SDS can destroy the emulsion flocculation, resulting in more exposure of anions at the droplet surface. The absolute values of zeta potential of TWIPNPEs under different ionic strengths were above 40 mV, which was beneficial to the stabilization of TWIPNPEs according to previous reports (17, 34).

Rheological Behavior of Pickering Emulsions Prepared Using TWIPNs Under Different Ionic Strengths

Ionic strength can also affect the rheological behavior of Pickering emulsions except for the particle size, zeta potential,

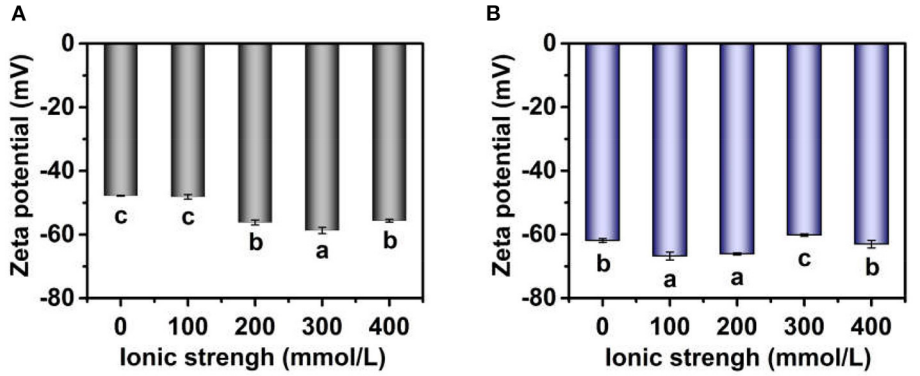

FIGURE 4 | Zeta potential of Pickering emulsions by tea water-insoluble protein nanoparticles under different ionic strengths [**(A)** emulsions in water; **(B)** emulsions in 1.0% SDS]. The lowercases indicate the significance of different Pickering emulsions by tea water-insoluble protein nanoparticles under different ionic strengths ($P < 0.05$).

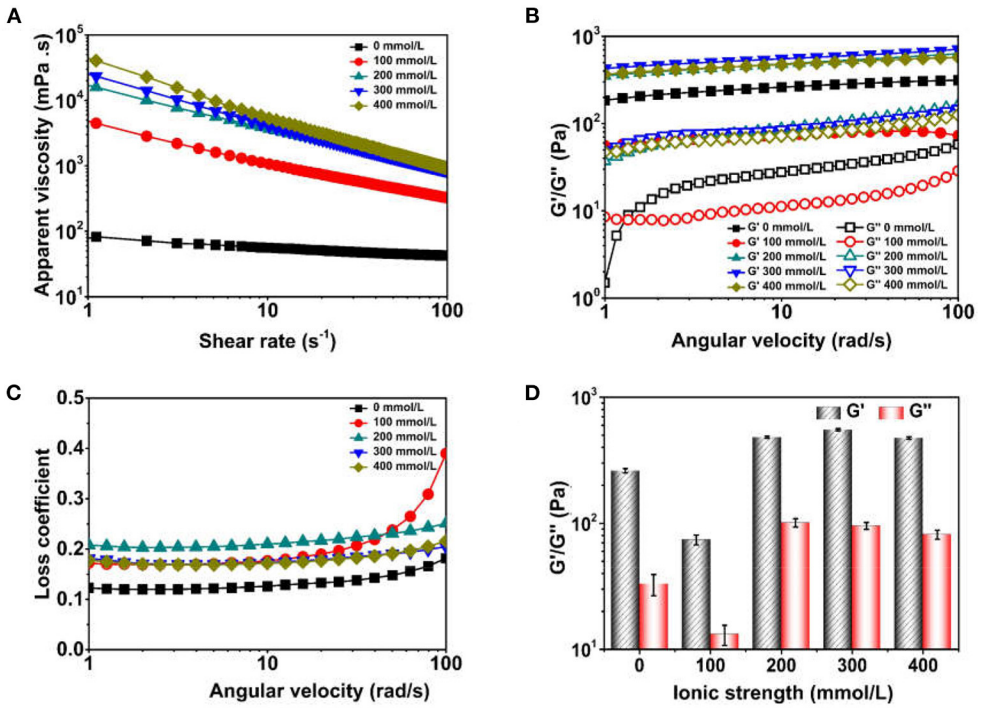

FIGURE 5 | Apparent viscosity and viscoelastic parameter of Pickering emulsions by tea water-insoluble protein nanoparticles under different ionic strengths [**(A)** apparent viscosity; **(B)** G'/G"; **(C)** Loss coefficient; **(D)** G'/G" at 10 rad/s].

flocculation of emulsions. The rheological behavior of TWIPNPEs under different ionic strengths is presented in **Figure 5**. The apparent viscosity of TWIPNPEs under different ionic strengths decreased with the increase in shear rate (**Figure 5A**), which showed the TWIPNPEs belonged to the pseudoplastic fluid as a previous report (35). The TWIPNPEs at the same shear rate became thick with the increase in ionic strength. Meanwhile, the apparent viscosity of TWIPNPEs increased under the ionic strength from 0 to 400 mmol/L at the same angular velocity. The particle size, flocculation and droplet interaction increased with the increase in ionic strength, resulting in the improvement of the apparent viscosity of TWIPNPEs (**Figures 1**, **2**). Besides, the thick emulsions under high ionic strengths contain no free solid particles in the emulsion system due to the aggregation of emulsion droplets together with each other (1).

The G', G"and loss coefficient of TWIPNPEs stabilized by TWIPNs at different ionic strengths were analyzed (**Figures 5B,C**). In the linear viscoelastic range, the G' and G" values of TWIPNPEs decreased below the ionic strength of

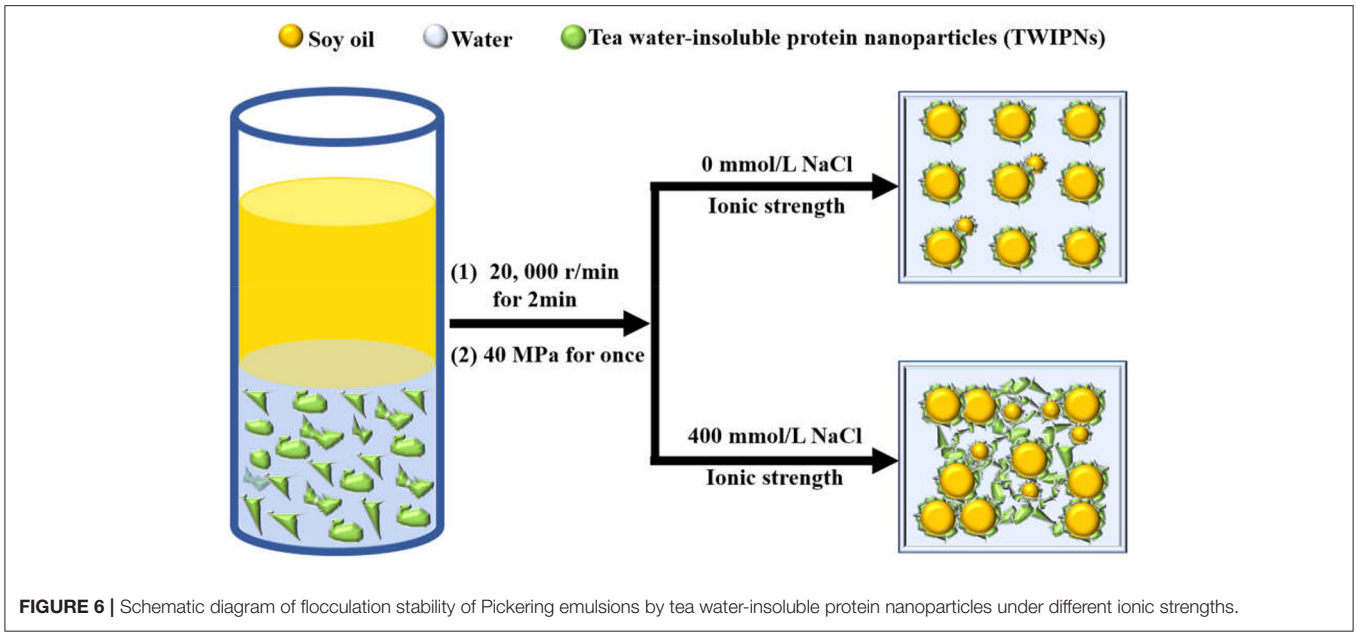

FIGURE 6 | Schematic diagram of flocculation stability of Pickering emulsions by tea water-insoluble protein nanoparticles under different ionic strengths.

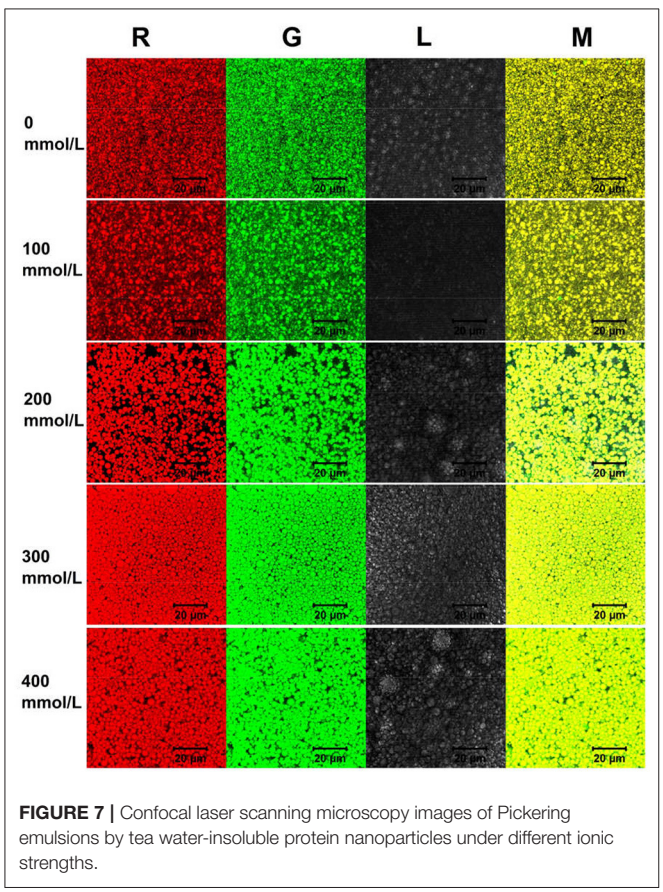

FIGURE 7 | Confocal laser scanning microscopy images of Pickering emulsions by tea water-insoluble protein nanoparticles under different ionic strengths.

100 mmol/L at the same angular velocities. However, the G' and G" values of TWIPNPEs under the ionic strength of more than 200 mmol/L were similar, which was higher than that of TWIPNPEs under the ionic strength below 100 mmol/L. The G' values of TWIPNPEs were higher than G", indicating that the TWIPNPEs under different ionic strengths possessed the gel-like behavior as previous reports (36). The loss coefficient of TWIPNPEs was no more than 0.5 (**Figure 5C**), implying that these emulsions possessed dominant elasticity to form gel-like behavior. The G' values of TWIPNPEs were much higher than G". As previously reported, this is beneficial for the formation of gel-like networks (37, 38). The viscoelasticity of TWIPNPEs could be also obtained at 10 rad/s (**Figure 5D**). However, Destroying the gel-like behavior of emulsions using shearing at high yield stress may induce the emulsion coalescence due to the network of flocculated solid particles (39). As shown in (**Figure 5A**), the viscosity of TWIPNPEs as a pseudoplastic fluid became thin when the shear rate increased from 0.1 to 100 s^{-1}. The yield stress of pseudoplastic fluid is increased with an increase in shear rate (40). According to previously reported, a suitable ionic strength can control the yield stress to reach the workability of emulsions with respect to its practical applications in the food industry (1).

Possible Mechanism of Pickering Emulsions Prepared Using TWIPNs Under Different Ionic Strengths

The addition of salt ions can change the ionic strength of the solution. Monovalent or polyvalent metal ions could effectively reduce the electrostatic shielding by reducing the dipole moment, thus reducing the zeta potential on the surface of the emulsion droplets to affect the emulsion stability (8). Monovalent, divalent and trivalent metal ions prompt the flocculation of different kinds of emulsions; meanwhile, univalent metal ion salts such as NaCl are usually used to analyze the effect of ionic strength on emulsion properties (41, 42). The change of ionic strength results in the different flocculation degrees of emulsions. In

this research, ionic strengths of 0–400 mmol/L were chosen to cause a certain amount of flocculation (**Figure 2**), which could improve the stability to some extent rather than destabilization of TWIPNPEs. As a previous report, walnut protein/xanthan gum complexes under the ionic strength of 500 mmol/L NaCl increase the degree of dissipative flocculation (43). A certain quantity of salt ions in the water phase inhibits electrostatic repulsion between protein nanoparticles to promote closer packing at the interface of emulsion droplets (44). The presence of a certain amount of salt ions is crucial for forming stable Pickering emulsions (45).

Here, the schematic diagram of flocculation stability of TWIP stabilized Pickering emulsions under different ionic strengths is shown in **Figure 6**. The viscosity and viscoelasticity of TWIPNPEs increased under the ionic strength from 0 to 400 mmol/L to benefit for forming gel-like TWIPNPEs (**Figures 5A,B**). The selection of appropriate ionic strength can control the yield stress, contributing to that Pickering emulsions meet the practical application of processability in the food industry (1). TWIPNs flocculated with each other to form gel-like stable emulsions in a certain concentration of ionic strengths (**Figure 5B**). The microstructures of TWIPNPEs under different ionic strengths of 0–400 mmol/L were also investigated by CLSM (**Figure 7**). A reinforcement of the flocculation of the TWIPNPEs was verified with the increase of ionic strengths, especially above 200 mmol/L. This is consistent with a previous report about the flocculated network due to the increase in ionic strengths (46). The formation of a gel-like network in TWIPNPEs was certainly due to relate with ionic strengths in this study. However, it should be carefully considered that shearing could damage the gel system above the yield stress to destruct gel-like structures of Pickering emulsions, leading to the coalescence and further instability of Pickering emulsions (39).

When salt is added to the nanoparticle dispersion, salt ions are selectively adsorbed at the particle surface to neutralize the net charge to reduce the number of charges around the nanoparticles and the thickness of the double electric layer, furtherly forming the flocculation of emulsions (1). The valence of metal ions is closely related to the flocculation of emulsions. The flocculation degree of divalent and trivalent metal ions is more than approximately 10–100 times that of univalent metal ions at the same ionic strength (47). Within a certain range, improving ionic strength can increase the hydrophobicity of particles to promote the adsorption of particles at the oil and water interface (48). An appropriate amount of ionic strength can also reduce the electrostatic repulsion between particles, which is conducive to the accumulation of particles at the surface of emulsion droplets to form a layer (44). Protein particles effectively adsorbed to the surface of the emulsion droplets result in the change of the dependence of emulsion droplets on ionic strength, thus allowing emulsions to achieve the flocculation stability in a suitable ionic strength range (17).

CONCLUSION

This work researched the effect of ionic strength on the characteristics of TWIPNPEs under neutral conditions. First of all, the $d_{4,3}$ of TWIPNPEs in the aquatic phase increased more than that in the SDS phase. Besides, ionic strength promoted the aggregation of TWIPNs to increase the size of protein particles for improving the flocculation of emulsion droplets through the microstructure observation. With the increase in ionic strength, the apparent viscosity and viscoelasticity of TWIPNPEs increased, especially when the ionic strength was above 200 mmol/L, showing good gel-like properties. This was consistent with our hypothesis that TWIPNs adsorbed to the oil-water interface would prompt flocculation between different emulsion droplets under the high ionic strength to form gel-like behavior. These findings can be utilized in the food industry for improving the stabilization of Pickering emulsions stabilized by tea proteins from tea residues under a wide range of ionic strengths to broaden the utility and application of Pickering emulsions in different environments of food manufacture.

DATA AVAILABILITY STATEMENT

The raw data supporting the conclusions of this article will be made available by the authors, without undue reservation.

AUTHOR CONTRIBUTIONS

ZR: data curation, formal analysis, investigation, methodology, resources, software, validation, visualization, and writing—original draft. ZC: data curation, formal analysis, and writing—original draft. YZ: data curation, formal analysis, and methodology. XL: validation, visualization, and writing—original draft. WW: formal analysis and writing—review and editing. BL: funding acquisition, project administration, supervision, and writing—review and editing. All authors contributed to the article and approved the submitted version.

FUNDING

This study was funded by the Natural Science Foundation of Fujian Province in China (2021J01835), National Key Research and Development Program of China (2021YFD210020204), Fujian Science and Technology Project (2021N5013), Special Fund from the Modern Agricultural Industry of China (CARS-19), and the Scientific Research Foundation of Jimei University in China (ZQ2020011).

ACKNOWLEDGMENTS

We thank Shenzhen Shenbao Huacheng Tech. Co., Ltd. for kindly providing the tea leaves.

REFERENCES

1. Chevalier Y, Bolzinger MA. Emulsions stabilized with solid nanoparticles: Pickering emulsions. *Colloids Surf A.* (2013) 439:23–34. doi: 10.1016/j.colsurfa.2013.02.054
2. Li S, Zhang B, Li C, Fu X, Huang Q. Pickering emulsion gel stabilized by octenylsuccinate quinoa starch granule as lutein carrier: role of the gel network. *Food Chem.* (2020) 305:125476. doi: 10.1016/j.foodchem.2019.125476
3. Xiao J, Li Y, Huang Q. Recent advances on food-grade particles stabilized Pickering emulsions: fabrication, characterization and research trends. *Trends Food Sci Tech.* (2016) 55:48–60. doi: 10.1016/j.tifs.2016.05.010
4. Zhu X, Zheng J, Liu F, Qiu C, Lin W, Tang C. Freeze-thaw stability of Pickering emulsions stabilized by soy protein nanoparticles. Influence of ionic strength before or after emulsification. *Food Hydrocoll.* (2018) 74:37–45. doi: 10.1016/j.foodhyd.2017.07.017
5. Zhou F, Yu X, Zeng T, Yin S, Tang C, Yang X. Fabrication and characterization of novel water-insoluble protein porous materials derived from Pickering high internal-phase emulsions stabilized by gliadin-chitosan-complex particles. *J Agr Food Chem.* (2019) 67:3423–31. doi: 10.1021/acs.jafc.9b00221
6. McClements DJ. Protein-stabilized emulsions. *Curr Opin Colloid In.* (2004) 9:305–13. doi: 10.1016/j.cocis.2004.09.003
7. Bertoncarabin CC, Schroën K. Pickering emulsions for food applications: background, trends, and challenges. *Annu Rev Food Sci T.* (2015) 6:263–97. doi: 10.1146/annurev-food-081114-110822
8. De Folter JW, van Ruijven MW, Velikov KP. Oil-in-water Pickering emulsions stabilized by colloidal particles from the water-insoluble protein zein. *Soft Matter.* (2012) 8:6807–15. doi: 10.1039/c2sm07417f
9. Xiao J, Wang X, Gonzalez AJP, Huang Q. Kafirin nanoparticles-stabilized Pickering emulsions: Microstructure and rheological behavior. *Food Hydrocoll.* (2016) 54:30–9. doi: 10.1016/j.foodhyd.2015.09.008
10. Zhu YQ, Chen X, McClements DJ, Zou L, Liu W. Pickering-stabilized emulsion gels fabricated from wheat protein nanoparticles: Effect of pH, NaCl and oil content. *J Disper Sci Technol.* (2018) 39:826–35. doi: 10.1080/01932691.2017.1398660
11. Fu D, Deng S, McClements DJ, Zhou L, Zou L, Yi J, et al. Encapsulation of β-carotene in wheat gluten nanoparticle-xanthan gum-stabilized Pickering emulsions: enhancement of carotenoid stability and bioaccessibility. *Food Hydrocoll.* (2019) 89:80–9. doi: 10.1016/j.foodhyd.2018.10.032
12. Yan X, Ma C, Cui F, McClements DJ, Liu X, Liu F. Protein-stabilized Pickering emulsions: formation, stability, properties, and applications in foods. *Trends Food Sci Tech.* (2020) 103:293–303. doi: 10.1016/j.tifs.2020.07.005
13. Dai L, Sun C, Wei Y, Zhan X, Mao L, Gao Y. Formation and characterization of zein-propylene glycol alginate-surfactant ternary complexes: effect of surfactant type. *Food Chem.* (2018) 258:321–30. doi: 10.1016/j.foodchem.2018.03.077
14. Zhang C, Bozileva E, Klis FVD, Dong Y, Sanders JPM, Bruins ME. Integration of galacturonic acid extraction with alkaline protein extraction from green tea leaf residue. *Ind Crop Prod.* (2016) 89:95–102. doi: 10.1016/j.indcrop.2016.04.074
15. Shen L, Wang X, Wang Z, Wu Y, Chen J. Studies on tea protein extraction using alkaline and enzyme methods. *Food Chem.* (2008) 107:929–38. doi: 10.1016/j.foodchem.2007.08.047
16. Ren Z, Chen Z, Zhang Y, Zhao T, Ye X, Gao X, et al. Functional properties and structural profiles of water-insoluble proteins from three types of tea residues. *LWT-Food Sci Technol.* (2019) 110:324–31. doi: 10.1016/j.lwt.2019.04.101
17. Ren Z, Chen Z, Zhang Y, Lin X, Li B. Novel food-grade Pickering emulsions stabilized by tea water-insoluble protein nanoparticles from tea residues. *Food Hydrocoll.* (2019) 96:322–30. doi: 10.1016/j.foodhyd.2019.05.015
18. Ren Z, Chen Z, Zhang Y, Lin X, Li B. Characteristics and rheological behavior of Pickering emulsions stabilized by tea water-insoluble protein nanoparticles via high-pressure homogenization. *Int J Biol Macromol.* (2020) 151:247–56. doi: 10.1016/j.ijbiomac.2020.02.090
19. Ren Z, Chen Z, Zhang Y, Lin X, Li Z, Weng W, et al. Effect of heat-treated tea water-insoluble protein nanoparticles on the characteristics of Pickering emulsions. *LWT-Food Sci Technol.* (2021) 149:111999. doi: 10.1016/j.lwt.2021.111999
20. Ren Z, Chen Z, Zhang Y, Lin X, Weng W, Liu G, et al. Characteristics of Pickering emulsions stabilized by tea water-insoluble protein nanoparticles at different pH values. *Food Chem.* (2022) 375:131795. doi: 10.1016/j.foodchem.2021.131795
21. Ren Z, Li Z, Chen Z, Zhang Y, Lin X, Weng W, et al. Characteristics and application of fish oil-in-water Pickering emulsions structured with tea water-insoluble proteins/κ-carrageenan complexes. *Food Hydrocoll.* (2021) 114:106562. doi: 10.1016/j.foodhyd.2020.106562
22. Liu F, Tang CH. Soy glycinin as food-grade Pickering stabilizers: Part. I structural characteristics, emulsifying properties and adsorption/arrangement at interface. *Food Hydrocoll.* (2016) 60:606–19. doi: 10.1016/j.foodhyd.2015.04.025
23. Xue J, Wang T, Hu Q, Zhou M, Luo Y. Insight into natural biopolymer-emulsified solid lipid nanoparticles for encapsulation of curcumin: effect of loading methods. *Food Hydrocoll.* (2018) 79:110–6. doi: 10.1016/j.foodhyd.2017.12.018
24. Feng X, Tjia JYY, Zhou Y, Liu Q, Fu C, Yang H. Effects of tocopherol nanoemulsion addition on fish sausage properties and fatty acid oxidation. *LWT.* (2020) 118:108737. doi: 10.1016/j.lwt.2019.108737
25. Li X, Liu W, Xu B, Zhang B. Simple method for fabrication of high internal phase emulsions solely using novel pea protein isolate nanoparticles: stability of ionic strength and temperature. *Food Chem.* (2022) 370:130899. doi: 10.1016/j.foodchem.2021.130899
26. Zhong Y, Xiang X, Wang X, Zhang Y, Hu M, Chen T, et al. Fabrication and characterization of oil-in-water emulsions stabilized by macadamia protein isolate/chitosan hydrochloride composite polymers. *Food Hydrocoll.* (2020) 103:105655. doi: 10.1016/j.foodhyd.2020.105655
27. Zhang S, Holmes M, Ettelaie R, Sarkar A. Pea protein microgel particles as Pickering stabilisers of oil-in-water emulsions: Responsiveness to pH and ionic strength. *Food Hydrocoll.* (2020) 102:105583. doi: 10.1016/j.foodhyd.2019.105583
28. Dickhout JM, Kleijn JM, Lammertink R, De WV. Adhesion of emulsified oil droplets to hydrophilic and hydrophobic surfaces-effect of surfactant charge, surfactant concentration and ionic strength. *Soft Matter.* (2018) 14:5452–60. doi: 10.1039/C8SM00476E
29. Zhu Y, McClements DJ, Zhou W, Peng S, Zhou L, Zou L, et al. Influence of ionic strength and thermal pretreatment on the freeze-thaw stability of Pickering emulsion gels. *Food Chem.* (2020) 303:125401. doi: 10.1016/j.foodchem.2019.125401
30. Griffith C, Daigle H. Manipulation of Pickering emulsion rheology using hydrophilically modified silica nanoparticles in brine. *J Colloid Interf Sci.* (2018) 509:132–9. doi: 10.1016/j.jcis.2017.08.100
31. Hatchell D, Song W, Daigle H. Examining the role of salinity on the dynamic stability of Pickering emulsions. *J Colloid Interf Sci.* (2022) 608:2321–9. doi: 10.1016/j.jcis.2021.10.154
32. Sriprablom J, Luangpituksa P, Wongkongkatep J, Pongtharangkul T, Suphantharika M. Influence of pH and ionic strength on the physical and rheological properties and stability of whey protein stabilized o/w emulsions containing xanthan gum. *J Food Eng.* (2019) 242:141–52. doi: 10.1016/j.jfoodeng.2018.08.031
33. Griffin K, Khouryieh H. Influence of electrostatic interactions on the formation and stability of multilayer fish oil-in-water emulsions stabilized by whey protein-xanthan-locust bean complexes. *J Food Eng.* (2020) 277:109893. doi: 10.1016/j.jfoodeng.2019.109893
34. Dickinson E. Hydrocolloids as emulsifiers and emulsion stabilizers. *Food Hydrocoll.* (2009) 23:1473–82. doi: 10.1016/j.foodhyd.2008.08.005
35. Kumar Y, Roy S, Devra A, Dhiman A, Prabhakar PK. Ultrasonication of mayonnaise formulated with xanthan and guar gums: Rheological modeling, effects on optical properties and emulsion stability. *LWT-Food Sci Technol.* (2021) 149:111632. doi: 10.1016/j.lwt.2021.111632
36. Yang D, Gao S, Yang H. Effects of sucrose addition on the rheology and structure of iota-carrageenan. *Food Hydrocoll.* (2020) 99:105317. doi: 10.1016/j.foodhyd.2019.105317
37. Yang Z, Yang H, Yang H. Effects of sucrose addition on the rheology and microstructure of κ-carrageenan gel. *Food Hydrocoll.* (2018) 75:164–73. doi: 10.1016/j.foodhyd.2017.08.032

38. Wang JJ, Wang Y, Wang Q, Yang J, Hu S, Chen L. Mechanically strong and highly tough prolamin protein hydrogels designed from double-cross-linked assembled networks. *Acs Appl Mater Inter.* (2019) 1:1272–9. doi: 10.1021/acsapm.9b00066
39. Whitby CP, Fischer FE, Fornasiero D, Ralston J. Shear-induced coalescence of oil-in-water Pickering emulsions. *J Colloid Interf Sci.* (2011) 361:170–7. doi: 10.1016/j.jcis.2011.05.046
40. Yin M, Yang D, Lai S, Yang H. Rheological properties of xanthan-modified fish gelatin and its potential to replace mammalian gelatin in low-fat stirred yogurt. *LWT.* (2021) 147:111643. doi: 10.1016/j.lwt.2021.111643
41. Kulmyrzaev AA, Schubert H. Influence of KCl on the physicochemical properties of whey protein stabilized emulsions. *Food Hydrocoll.* (2004) 18:13–9. doi: 10.1016/S0268-005X(03)00037-7
42. Feng X, Chen L, Lei N, Wang S, Xu X, Zhou G, et al. Emulsifying properties of oxidatively stressed myofibrillar protein emulsion gels prepared with (–) -epigallocatechin-3-gallate and NaCl. *J Agr Food Chem.* (2017) 65:2816–26. doi: 10.1021/acs.jafc.6b05517
43. Tan Y, Deng X, Liu T, Yang B, Zhao M, Zhao Q. Influence of NaCl on the oil/water interfacial and emulsifying properties of walnut protein-xanthan gum. *Food Hydrocoll.* (2017) 72:73–80. doi: 10.1016/j.foodhyd.2017.05.031
44. Fei Y, Liu S, Jian X, Qiang L, Fang W, Sun D. Pickering emulsions stabilized solely by layered double hydroxides particles: the effect of salt on emulsion formation and stability. *J Colloid Interf Sci.* (2006) 302:159–69. doi: 10.1016/j.jcis.2006.06.015
45. Wu J, Shi M, Li W, Zhao L, Wang Z, Yan X, et al. Pickering emulsions stabilized by whey protein nanoparticles prepared by thermal cross-linking. *Colloids Surf B.* (2015) 127:96–104. doi: 10.1016/j.colsurfb.2015.01.029
46. Xu D, Zheng B, Che Y, Liu G, Cao Y. The stability, microstructure, and microrheological properties of *Monascus* pigment double emulsions stabilized by polyglycerol polyricinoleate and soybean protein isolate. *Front Nutr.* (2020) 7:543421. doi: 10.3389/fnut.2020.543421
47. Dickinson E. Flocculation of protein-stabilized oil-in-water emulsions. *Colloids Surf B.* (2010) 81:130–40. doi: 10.1016/j.colsurfb.2010.06.033
48. Shen R, Lin D, Liu Z, Zhai H, Yang X. Particles for the stabilization of high internal phase Pickering emulsions by anti-solvent precipitation and their application in the delivery of curcumin. *Front Nutr.* (2021)1: 734620. doi: 10.3389/fnut.2021.734620

Conflict of Interest: The authors declare that the research was conducted in the absence of any commercial or financial relationships that could be construed as a potential conflict of interest.

Publisher's Note: All claims expressed in this article are solely those of the authors and do not necessarily represent those of their affiliated organizations, or those of the publisher, the editors and the reviewers. Any product that may be evaluated in this article, or claim that may be made by its manufacturer, is not guaranteed or endorsed by the publisher.

frontiers | Frontiers in Nutrition

REVIEW
published: 17 May 2022
doi: 10.3389/fnut.2022.890188

Engineering Emulsion Gels as Functional Colloids Emphasizing Food Applications: A Review

Abdullah[1†], *Lang Liu*[1†], *Hafiz Umer Javed*[2] *and Jie Xiao*[1*]

[1] *Guangdong Provincial Key Laboratory of Functional Food Active Substances, College of Food Sciences, South China Agricultural University, Guangzhou, China,* [2] *School of Chemistry and Chemical Engineering, Zhongkai University of Agricultural and Engineering, Guangzhou, China*

Gels are functional materials with well-defined structures (three-dimensional networks) assembled from the dispersed colloids, and capable of containing a large amount of water, oil, or air (by replacing the liquid within the gel pores), known as a hydrogel, oleogel, and aerogel, respectively. An emulsion gel is a gelled matrix filled with emulsion dispersion in which at least one phase, either continuous phase or dispersed phase forms spatial networks leading to the formation of a semisolid texture. Recently, the interest in the application of gels as functional colloids has attracted great attention in the food industry due to their tunable morphology and microstructure, promising physicochemical, mechanical, and functional properties, and superior stability, as well as controlled release, features for the encapsulated bioactive compounds. This article covers recent research progress on functional colloids (emulsion gels), including their fabrication, classification (protein-, polysaccharide-, and mixed emulsion gels), and properties specifically those related to the gel-body interactions (texture perception, digestion, and absorption), and industrial applications. The emerging applications, including encapsulation and controlled release, texture design and modification, fat replacement, and probiotics delivery are summarized. A summary of future perspectives to promote emulsion gels' use as functional colloids and delivery systems for scouting potential new applications in the food industry is also proposed. Emulsion gels are promising colloids being used to tailor breakdown behavior and sensory perception of food, as well as for the processing, transportation, and targeted release of food additives, functional ingredients, and bioactive substances with flexibility in designing structural and functional parameters.

Keywords: biopolymer-based colloids, emulsion gels, delivery systems, functional material, gel-body interactions, food applications

OPEN ACCESS

Edited by:
Jianhua Liu,
Zhejiang University of Technology, China

Reviewed by:
Husnain Raza,
Shenzhen University, China
Muhammad Umair Ijaz,
University of California, Davis, United States
Zia-ud-Din,
University of Swabi, Pakistan
Hongcai Zhang,
Shanghai Jiao Tong University, China

****Correspondence:***
Jie Xiao
xiaojieacademic@163.com

[†]These authors have contributed equally to this work

Specialty section:
This article was submitted to Food Chemistry, a section of the journal Frontiers in Nutrition

Received: *05 March 2022*
Accepted: *25 March 2022*
Published: *17 May 2022*

Citation:
Abdullah, Liu L, Javed HU and Xiao J (2022) Engineering Emulsion Gels as Functional Colloids Emphasizing Food Applications: A Review. Front. Nutr. 9:890188. doi: 10.3389/fnut.2022.890188

INTRODUCTION

A gel is an advanced material possessing three-dimensional (3D) networks with the ability to incorporate large amount of water (hydrogel), oil (oleogel), or air (aerogel), due to its spatial structure and unique properties, including high surface area, porosity, and loading capacity (1, 2). A gel can also be defined as "an intermediate (semisolid) product between a solid and a liquid possessing both elasticity and viscosity characteristics" (3). An emulsion gel is also known as emulsion-filled gel or emulgel is "an emulsion dispersion filled gel matrix, wherein at least one

phase either continuous phase or dispersed phase of emulsion forms the 3D network structure leading to the gel formation". These gels possess superior stabilities against chemical reactions (e.g., hydrolysis and oxidation), physical processes (e.g., phase inversion and/or separation), and environmental changes such as pH, temperature, and ionic strength (4–8) compared to traditional emulsions, which tend to break down with time by gravitational separation, droplets aggregation, and Ostwald ripening (1, 9–11).

The biopolymers (e.g., polysaccharides and proteins) based emulsion gels produced by different gelation methods and coupled with a wide range of functionalities had the capability of forming complex microstructures such as single continuous phase-, double continuous phase-, uniform continuous-, and nonhomogeneous as well as several other gelled systems (**Figure 1**) (12, 13), making them diverse biomaterial and efficient delivery vehicles for versatile industrial applications. Functional food additives, bioactive phytochemicals, essential oils, and lipophilic compounds including carotenoids, phenolic acids, flavonoids, stilbenes, vitamins, and unsaturated fatty acids exhibit health-promoting characteristics but have difficulty being incorporated into food matrixes due to their low chemical stability, limited water solubility and dispersibility, as well as poor cell adsorption (12, 14–18). During the past 10 years (**Figure 2**), emulsion gels have emerged as a promising biomaterial with desirable features and flexible fabrication potential to be employed for the protection and transportation of health-promoting functional ingredients and designing heathier formulations with improved desired sensorial textures, digestion, bioaccessibility, and bioavailability (8, 12, 17, 19, 20).

In recent years, many studies have reported the potential of emulsion gels to effectively encapsulate, protect, and targeted release of functional ingredients and nutraceuticals against adverse environmental conditions by modifying their dispersibility and stability in the food, controlling their release time and rate, as well as improving bioavailability. To date, emerging applications of emulsion gels to encapsulate and deliver hydrophilic and lipophilic nutraceuticals (7, 21, 22), controlled release of bioactives (12, 23), low fat foods with reduced lipolysis (24, 25), reducing fat, sugar, and salt in foods (26–28), probiotics delivery in the gastrointestinal tract with improved viability (29), desired sensorial textures with improved physical stability (30, 31), structuring plant-oils as animal-fat replacer and substitute of partially hydrogenated oils (32–34), and designing complex food structures (textures, shapes, and nutritional contents) using 3D printing (35) have attracted tremendous attentions for designing safer, healthier, and sustainable food products.

This review summarizes the latest developments in engineering biopolymers (e.g., polysaccharides and proteins) based food gels, emphasizing their food applications. The gels fabrication, their classification according to the composition of the gel matrix (protein-, polysaccharide-, and mixed emulsion gels), and properties, specifically those related to the gel-body interactions (texture perception, digestion, and absorption), are all discussed (**Figure 3**). The emerging industrial applications, including encapsulation and controlled release, texture design and modification, fat replacement, and probiotics delivery are highlighted. A summary of conclusions and future perspectives for scouting potential new applications of emulsion gels in the food industry is also presented.

EMULSION GELS: FABRICATION AND CLASSIFICATION

The formation of an emulsion gel takes place *via* gelation of the following: (i) continuous phase or (ii) dispersed phase in the precursor solution through different methods, including emulsification, heating, heating and cooling, enzymatic treatment, pH adjustment, salt induced, *etc*. It has been established that gels formed *via* gelation usually had superior stability against environmental stresses due to their strong networks (3D) developed by the interconnected biopolymer molecules (1, 12). The gelation process that leads to the formation of gel matrix plays a key role in determining the final properties (physicochemical, mechanical, and functional) of emulsion gels. Briefly, the biopolymer type and concentration, processing conditions (pH, temperature, and ionic strength), Pickering particles, such as emulsifiers (size, wettability, surface charge, and amount), and cooling temperature, as well as the aging period after gelation, are the key points that strongly influence the emulsion gels properties. The emulsion gels can be classified into three categories based on biopolymers composition in a gel matrix, including the following: (i) protein-based emulsion gels (e.g., caseins, gelatin, soy, and whey proteins), (ii) polysaccharide-based emulsion gels (e.g., alginate, starch, pectin, and xanthan gum), and (iii) mixed emulsion gels (e.g., soy protein isolate-beet pectin, xanthan gum-guar gum, and zein-sodium caseinate-propylene glycol alginate). In recent years, researchers have mostly focused on the formation of protein-based emulsion gels, which might be due to their excellent emulsifying properties, relatively easy processing (gelation), and inheritable nutritional composition (19, 36).

PROTEIN-BASED EMULSION GELS

Protein emulsion gels usually had a relatively high protein concentration in the gel matrix, and caseins, gelatin, soy, and whey proteins are the widely used biopolymers in emulsion gels production due to their abundance, renewable resources, and promising emulsifying and gelling properties. Gelation techniques including heat-set (heating), and cold-set such as acidification (acid-induced), ethanol-induced, enzyme treatment, salt addition (salt-induced), and hydrostatic pressure-induced approaches have been applied to synthesize the protein-based emulsion gels (12, 37).

Recently, Luo et al. (19) synthesized whey protein emulsion gels and then microgel particles with an average size of 0.5 $\pm$ 0.05 μm *via* heating (90°C for 20 min) followed by cooling (4°C for overnight) method to enhance the bioaccessibility of capsaicinoids. The optimized formula includes whey protein (10 wt%), soybean oil (19.98 wt%), and capsaicinoids (0.02 wt%) used in the preparation of emulsion gels. The *in vitro* study results suggested that emulsion gels as a delivery system significantly

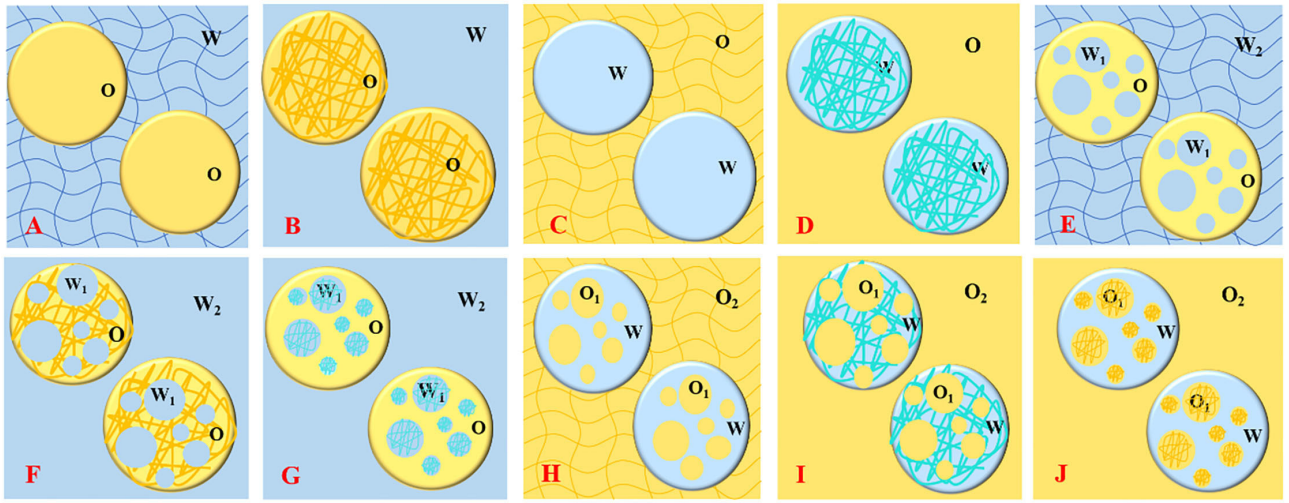

FIGURE 1 | Schematic representation of different types of emulsion gels; oil/hydrogel **(A)**, oleogel/water **(B)**, water/oleogel **(C)**, hydrogel/oil **(D)**, water/oil/hydrogel **(E)**, water/oleogel/water **(F)**, hydrogel/oil/water **(G)**, oil/water/oleogel **(H)**, oil/hydrogel/oil **(I)**, and oleogel/water/oil **(J)**.

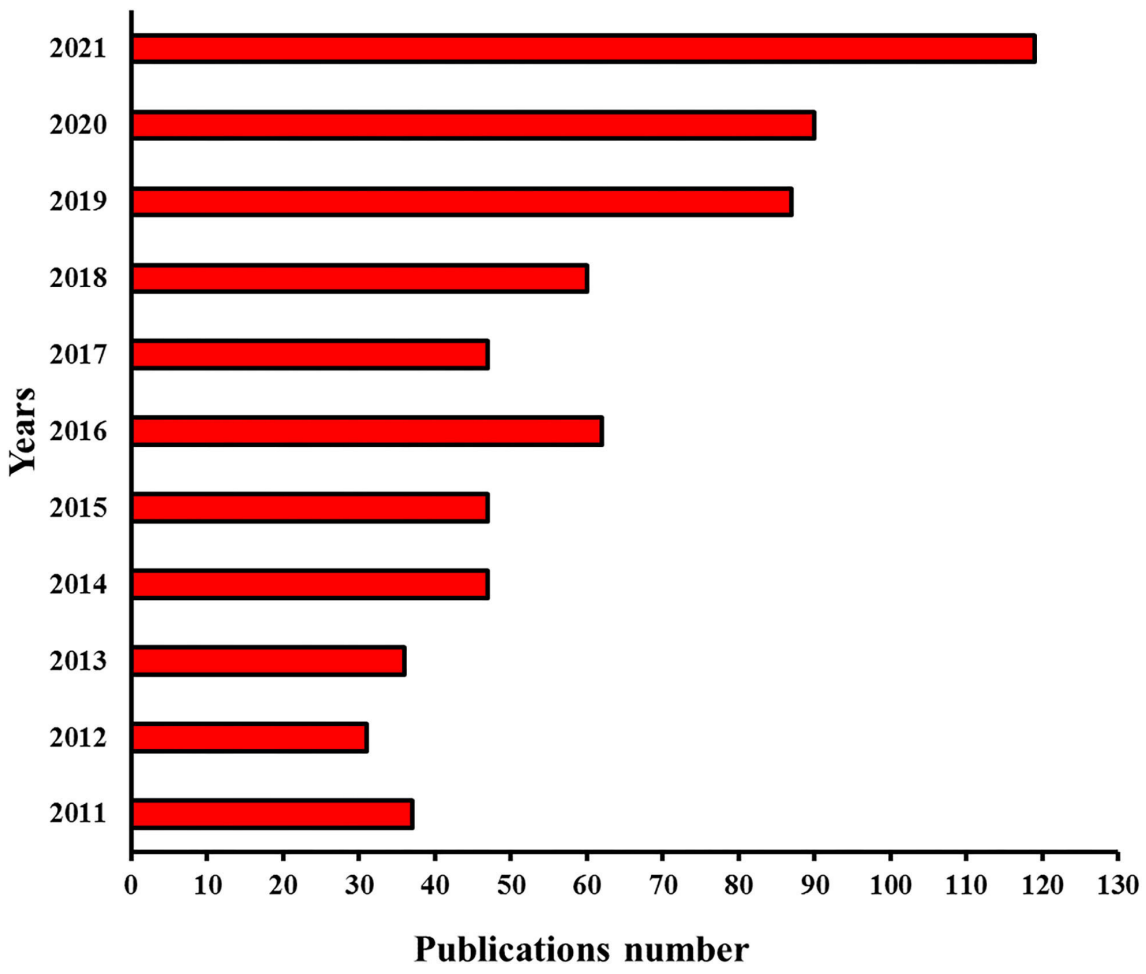

FIGURE 2 | Publications per year during the last 10 years (2011-2021) were analyzed by "Sci-finder" using "emulsion gel" as the keyword for searching.

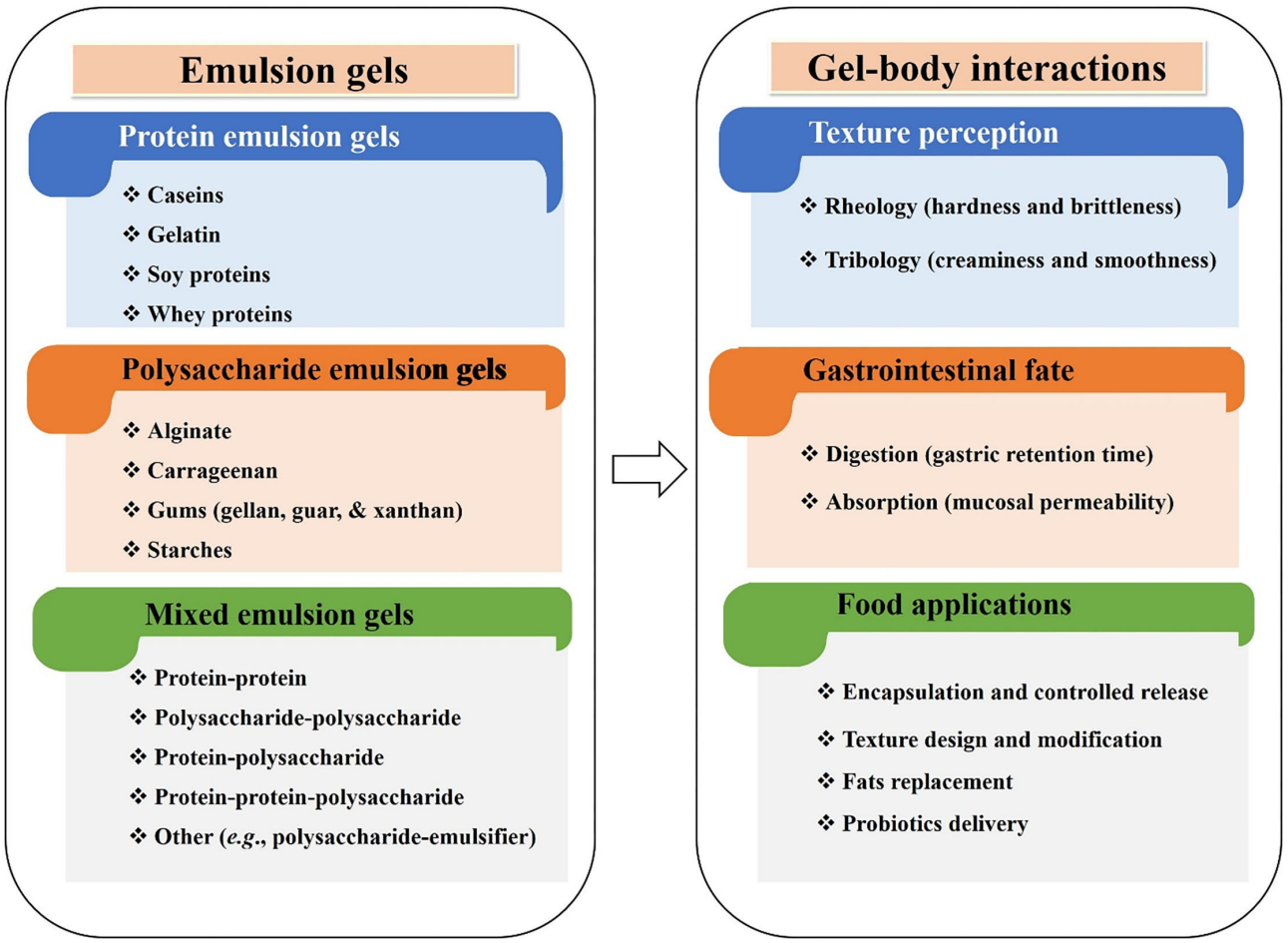

FIGURE 3 | An overview of emulsion gels, indicating their classification, gel-body interactions (texture perception, digestion, and absorption), and emerging industrial food applications.

increased the bioaccessibility of encapsulated capsaicinoids and showed a positive correlation with the extent of lipid digestion. The bioaccessibility indicated the release of capsaicinoids from gel matrix during digestion and their solubilization in the aqueous phase in the gastrointestinal tract. Fu et al. (36) fabricated whey protein emulsion gels containing medium chain triglyceride and cinnamaldehyde oils by the heating method. The scanning electron microscopy results showed that cross-linking occurred between the whey proteins and cinnamaldehyde at the oil-water interfaces leading to an effective reduction in viscosity, an increase in viscoelasticity, and smaller and uniform pore size in emulsion gels. The *in vitro* study on gastrointestinal fate showed that protein-based gel had slower disintegration than protein-cinnamaldehyde gel and revealed a faster disintegration due to the addition of cinnamaldehyde that softened the gel.

Lv et al. (38) produced Pickering emulsion gels containing canola oil stabilized by whey protein isolate gelled particles aimed to encapsulate curcumin. The formed gels had the highest loading efficiency of 90.3%, which contributed to the gel's compact structure (solid-like) that retained the maximum percentage of curcumin. The *in vitro* release under the gastric and intestinal conditions revealed that emulsion gel had a slower release rate than liquid emulsion ascribed to the gel-like structure which showed a better resistance against the hydrolysis by pepsin. Moreover, the emulsion gel encapsulating curcumin hindered the degradation and showed remarkable stability, i.e., >70% amount remained compared to only 7% of control (without any protection) during storage of 240 min under the light. Tan and his team prepared highly concentrated emulsion gels as nutraceuticals cargos by encapsulating 80% sunflower oil by employing gelatin particles (∼200 nm) as the emulsifiers at concentrations of 0.3–1.5 wt%. The formed gels remained stable even after 90 days of storage and embedded β-carotene showed a very high retention rate (90%) than that of bulk oil (8%) recorded after 27-days (39, 40). Xu et al. (41) produced emulsion gels containing 80% dodecane stabilized by β-conglycinin Pickering particles (0.2–1 wt%), and formed gels showed excellent stability during 60-days storage as well as heating at 100°C for 15 min. Furthermore, a progressive decrease was observed in the size of the droplets from 60 to 24 μm with an increase in particle

concentration from 0.2 to 1 wt%. Thus, emulsion gels and Pickering emulsion gels can improve the digestion process along with providing protection to the embedded lipophilic compounds attributed to the compact gel structure.

POLYSACCHARIDE-BASED EMULSION GELS

These emulsion gels comprise polysaccharide food polymers with the gelation capacity that depends on their source and structure, and alginate, agarose, modified starches (e.g., octenyl succinic anhydride), carrageenan, curdlan, inulin, konjac gum, and xanthan gum were the commonly employed biopolymers in the formation of emulsion gels. Various methods, including heating, heating and cooling, high shear, freeze-thaw cycles, pH, ions induced (Ca^{2+} and K^{+}), and salts addition ($CaCl_2$) can be applied to induce gelation leading to the formation of emulsion gels (1, 37). Polysaccharide-based emulsion gels are thermoreversible and their derived colloidal particles are also considered less efficient emulsifiers to produce emulsion gels compared to protein-based emulsion gels that exhibit long-term stability because of protein molecules that not only act as gel substrates but are excellent stabilizers (1, 10, 12, 28). However, polysaccharide-based biopolymers are more effective to increase viscosity and also exhibit inherent resistance to digestive enzymes, such attributes make them particularly suitable as delivery vehicles for bioactive compounds that require a prolonged digestive journey for the encapsulates (20, 42, 43).

Torres et al. (30) fabricated starch-based emulsion gels through heat-induced gelation, containing sunflower oil volume fraction (5–20 wt%), wheat starch (15–20 wt%), and octenyl succinic anhydride (OSA) https://www.sciencedirect.com/topics/biochemistry-genetics-and-molecular-biology/modified-starch modified starch (0.5–2 wt%). The results indicated that when starch was used at a concentration of 20 wt% and oil at 5–15 wt%, the gel elastic modulus increased by 50%, whereas a further increase in oil content (20 wt%) strengthened the gel with an increment in the elastic modulus up to 70%. This reinforcement in the gel matrix is attributed to the hydrophobic interactions between oil droplets and interfacial starch, and hydrogen bonding among starch polymers specifically amylose molecules to form 3D networks. The authors also produced gel particles with a diameter ranging from 5 to 50 μm *via* a top-down shearing of the formed gels and suggested that these novel emulsion gels and derived microgel particles can be employed in the delivery of bioactive substances in various food and personal care products.

Mokhtari et al. (44) developed alginate nanogels *via* emulsification and internal gelation induced by https://www.sciencedirect.com/topics/chemistry/calcium-chloride calcium chloride to deliver nutraceuticals with high encapsulation efficiency. The results showed that sodium alginate (0.5%), canola oil (400 ml), calcium chloride (0.05 M), and Tween 80 (100 ml) were the optimized concentrations in formulating alginate-based gel nanoparticles. Moreover, the nanocarriers derived from gel showed a spherical shape and a higher encapsulation yield was obtained with the increasing alginate amount due to increased viscosity that imparted more cohesion property leading to high entrapment efficiency. Furthermore, the gel particle size and encapsulation yield were found highly proportional to the alginate concentrations as high amounts lead to higher while small amounts resulted in lower values. Zhang et al. (42) prepared emulsion gel using carrageenan as gel matrix stabilized by mixed colloidal Pickering nanoparticles made of zein-carboxymethyl dextrin biopolymers and *N*-ethyl-N-(3-dimethylaminopropyl) carbodiimide as the crosslinking agent. The *in vitro* digestion analysis suggested that the bioaccessibility of curcumin in crosslinked emulsion gel was decreased compared to emulsion due to the spatial networks developed in emulsion gel. Briefly, the network structure slowed down the digestive enzymes' diffusion into the gel matrix, thus delaying the https://www.sciencedirect.com/topics/biochemistry-genetics-and-molecular-biology/enzymatic-hydrolysis hydrolysis and digestion of oil droplets encapsulating curcumin and subsequently decreasing the bioaccessibility. In addition, this study's investigations revealed that photochemical and thermal stability of the impregnated curcumin in emulsion gel was significantly improved due to crosslinking and exhibited high retention rates of 90.7 and 82.2% under light and heat, respectively.

MIXED EMULSION GELS

Interest in the production of mixed gels has attracted more attention from researchers since they offer enriched gelling behaviors and more precise control on the physicochemical, rheological, and functional properties over the individual emulsion gels. Le et al. (20) reported that mixed gels (protein and polysaccharide) had outstanding water-holding properties (up to 600 g/g of mixed gel), and were also capable to produce a diverse range of microstructures that can be further exploited to bring desirable textures and sensory attributes. For instance, during the process of homogenization, the polysaccharide part imparts better stability against environmental conditions such as pH, temperature, and ionic strength, while the protein part contributes to producing fine droplets size through excellent emulsifying capacity leading to a homogenous structure (10). Gelation methods, including heating, cooling after heating, high shear, enzyme treatment, and coacervation can be applied to produce mixed emulsion gels (20, 45).

Particularly, coacervation is a commonly employed method in the formation of mixed gels from oppositely charged biopolymers, (e.g., protein-protein, polysaccharide-polysaccharide, and protein-polysaccharide), by regulating the mixture ratio (biopolymer type and concentration), temperature, pH, ionic strength, *etc*. During this process, the charged species (e.g., H^{+} and OH^{-}) adsorbed on biopolymers surfaces interact through electrostatic complexation and develop 3D networks leading to gel formation (1, 20). **Table 1** describes different mixed emulsion gels combinations that include the following: (i) protein-protein (72), (ii) polysaccharide-polysaccharide (43), and (iii) protein-polysaccharide, etc. (68).

TABLE 1 | Gel-based functional delivery systems, including protein-, polysaccharide-, and mixed emulsion gels (emulgels).

Delivery systems	Gel matrix	Oil phase	Bioactives	Applications	References
Protein-based emulsion gels	Whey protein isolate	Corn oil	Probiotics	Encapsulation and controlled release	Gao et al. (29)
	Soy protein isolate	Olive oil (40%)	Polyphenols	Encapsulation and controlled release	Munoz-Gonzalez et al. (46)
	Soy protein	Soybean oil (50%)	Inulin	Fat replacement	de Souza Paglarini et al. (33)
	Whey protein isolate	Soybean oil (50%, v/v)	…….	Functional food	Xi et al. (47)
	Whey protein isolat	Mixed oils (coconut & corn, 20% of emulsion)	β-carotene	Encapsulation and controlled release	Lu et al. (48)
	Whey protein isolat	Soybean oil (19.98 wt%)	Capsaicinoids	Encapsulation and controlled release	Luo et al. (49)
	Whey protein isolate	Soybean oil (30%)	…….	Encapsulation and controlled release	Mantovani et al. (50)
	Whey protein isolate	Soybean oil (30%)	Retinol (vit. A)	Encapsulation and controlled release	Beaulieu et al. (51)
	β-lactoglobulin	Sunflower oil (30%)	α-Tocopherol (vit. E)	Encapsulation and controlled release	Liang et al. (52)
	Soy protein isolate	…….	Riboflavin (vit. B2)	Encapsulation and controlled release	Maltais et al. (21)
	Wheat gluten	Corn oil (56%)	EGCG + quercetin	Encapsulation and controlled release	Chen et al. (53)
Polysaccharide-based emulsion gels	Carrageenan	Soybean oil (50%)	.....	Fat replacement	Paglarini et al. (28)
	Alginate	Canola oil (40, 60, and 80%)	Peppermint extract	Encapsulation and controlled release	Mokhtari et al. (44)
	Gellan gum	Soybean oil (60%)	Probiotics	Probiotics delivery	Picone et al. (54)
	Starch	Soy oil (85%)	.....	Texture design and modifications	Yang et al. (55)
	Rice starch	Sunflower oil (40%)	……	Texture design and modifications	Zhang et al. (56)
	Sodium alginate	Paraffin oil (0.2%)	Probiotics	Probiotics delivery	Qi et al. (57)
	Sodium alginate	Tea seed oil (0.2 g)	Curcumin	Encapsulation and controlled release	Xu et al. (58)
Mixed emulsion gels	Whey protein isolate-soy protein isolate	Sodium alginate (0.4%	.....	Texture design and modifications	Lin et al. (11)
Protein-protein					
	Whey protein- lactoferrin	Corn oil (30 g)	.....	Reduced-fat products	Yan et al. (59)
	Whey protein-soy protein	Olive oil, linseed oil, and fish oil (44.39, 37.87, and 17.74%	Fatty acids (n-3) and condensed tannins	Encapsulation and controlled release	Freire et al. (60)
Polysaccharide-polysaccharide	Alginate-konjac glucomannan	Rapeseed oil (5–30%)	…..	Fat replacement	Yang et al. (61)
	Gellan gum- Pectin-carrageenan-xanthan Gum	Corn oil (10%)	Quercetin	Encapsulation and controlled release	Chen et al. (53)
	Xanthan gum-guar gum	Sunflower oil (41%)	Probiotics	Probiotics delivery	Pandey et al. (43)
Protein-polysaccharide	whey protein isolate-carrageenan	MCT oil (4 mL)	Curcumin	Encapsulation and controlled release	Su et al. (62)
	black soybean protein-sodium alginate	Soybean oil	Insulin and quercetin	Encapsulation and controlled release	Han et al. (63)
	Whey protein isolate-sodium alginate	Corn oil (20% v/v)	Lycopene	Encapsulation and controlled release	Liu et al. (64)
	Soy proteinisolate-pectin	Soybean oil [6% (v/v)]	β-carotene	Encapsulation and controlled release	Zhang et al. (65)
	Whey protein isolate-alginate	Sunflower oil (0.5–20%)	α-Tocopherol + resveratrol	Encapsulation and controlled release	Feng et al. (66)

(Continued)

TABLE 1 | Continued

Delivery systems	Gel matrix	Oil phase	Bioactives	Applications	References
	Whey protein isolate-xanthan gum	Babacu oil and tristearin (4%)	Curcumin	Fat replacement	Geremias-Andrade et al. (67)
	Soy protein-sugar beet pectin	Corn oil (15%)	Ethyl butyrate	Encapsulation and controlled release	Hou et al. (68)
	Whey protein isolate- rice starch	Corn oil (2–8%)	Carotenoids	Encapsulation and controlled release	Mun et al. (69)
Polysaccharide-emulsifier	Kappa-carrageenan-polysorbate 80	Algae oil	Catechins	Encapsulation and controlled release	Alejandre et al. (70)
Protein-protein-polysaccharide	Zein- sodium caseinate-propylene glycol alginate	Soybean oil (80%)	……..	Texture design and modification	Sun et al. (71)

Pandey et al. (43) formulated mixed emulsion gel using sunflower oil and a combination of xanthan gum and guar gum for the delivery of https://www.sciencedirect.com/topics/biochemistry-genetics-and-molecular-biology/lactobacillus-plantarum *Lactobacillus plantarum* 299v. The mechanical strength and disintegration investigations on formed gel showed significant improvements in the mechanical stability and gastric acid resistance due to the combination of the xanthan gum and guar gum in the dispersed phase of the formulation. Moreover, the natural gums-based emulsion gel stored at different conditions including 4, −20, and −196°C, revealed higher survival rates of encapsulated probiotics in the emulsion gels compared to control. Hou et al. (68) designed mixed emulsion gels *via* the enzymatic (mTGase) gelation method, comprising flavored corn oil and stabilized by soy protein isolate-sugar beet pectin complexes. Briefly, complex emulsified emulsion gels presented more compact structures due to the formation of strong interfacial networks ascribed to higher emulsifier absorption at the oil-water interfaces. In addition, gas chromatography analysis revealed that the ethyl butyrate release rate was significantly lower before and after the mastication process in emulsion gels due to their compact structure.

Zou et al. (73) prepared Pickering emulsion gels containing corn oil volume fraction of 50% stabilized by complex Pickering particles (zein-tannic acid- 1-1.5 wt%) having a three-phase contact angle value of ∼86° and high interfacial activity. The formed emulsion gels stabilized by complex Pickering particles showed homogeneous structure and good stability over 30-days of storage without any signs of oiling-off (creaming and phase separation) due to their transformation from a liquid state to a semisolid state ascribed to particles networks. Wei et al. (72) produced highly concentrated emulsion gels using ovotransferrin-lysozyme complex Pickering particles as the stabilizers, and by increasing particle concentration from 0.5 to 2 wt% the size of the droplets decreased from 81.4 to 42.4 μm at a fixed oil phase (75%). The formed emulsion gels presented excellent stability during long-term storage and inhibited the phase separation phenomenon because of particles networks ascribed to electrostatic interactions. The Pickering particles stabilized emulsion gels enhanced the bioaccessibility of the impregnated curcumin by 22.2%, indicating gels as an effective delivery system for lipophilic bioactive substances. (74) fabricated Pickering emulsion gels by encapsulating medium chain triglyceride oil (50-60%) stabilized by complex colloidal particles (zein-pullulan - 2 wt%). The resultant gels showed excellent stability against coalescence and phase separation and no oil leakage was noticed even after 30-days of storage at room temperature. The stability of emulsion gels was due to the formation of compact interfacial layers by the colloidal particles around the oil droplets, indicating their potential as a delivery system for bioactive substances to design better food formulations.

GEL-BODY INTERACTIONS

Texture Perception During Oral Processing

Texture perception is a complex process that correlates with the properties of food such as chemical composition and structure as well as physiochemical, mechanical, and enzymatic changes that occur during oral processing (75, 76). Briefly, texture indicates the rheology (hardness and brittleness-chewing) and tribology (creaminess and smoothness-lubrication) related food attributes sensed at early and later stages of oral processing, respectively (1, 77–79). It has been found that the rheological properties were correlated with the fracture stress and strain and determined by the hardness and brittleness of food, whereas tribological properties were linked with the friction coefficient perceived by creaminess or smoothness (76, 80, 81). The rheological and tribological properties of gels can be finely tuned by the gel composition (biopolymer type and concentration), structure, and mesh size to obtain the desired sensory attributes.

In recent years, interest in the application of emulsion gels as a potential tool to mimic the food texture without affecting their sensory perception by designing gels with reduced fat, sugar, and salt has rapidly increased. The incorporation of emulsion gel or derived particles into semisolid food formulations could mimic the perception of fat because of the significant reduction in friction coefficient through ball-bearing in the case of whey proteins (82, 83) and enzymatic reactions for starch particles (84). Interestingly, mouth-melting gels (e.g., gelatin-based gels)

had excellent potential to increase the surface lubrication of foods to achieve the desired mouthfeel of fat perception (85). For instance, gelatin-based gels remain in a gel state at room temperature but start melting at mouth temperature (37°C), thus could be effectively used in many food formulations to mimic fat perception. In addition, emulsion gels can also avoid undesirable sensory attributes of drugs or bioactive compounds by separating them from the taste bud receptors in the mouth and delaying their release in the digestive tract (26, 27).

Zhang et al. (56) used enzymatically hydrolyzed rice starch (20 g) and sunflower oil (40 g) to fabricate emulsion-filled gels, and the resulting gels showed a comparable texture including hardness and cohesiveness similar to fat. Moreover, the concentration of starch in the formulation directly influenced the textural properties and flow behavior of formed gels. Briefly, the firmness of emulsion gels was strengthened with the increase in the concentration of starch, since the high content of amylose and longer chains of amylopectin led to the formation of harder emulsion gels. Luo et al. (49) prepared whey protein-based emulsion gels comprising whey protein isolate 895 (10 wt%), soybean oil (19.98 wt%), and capsaicinoids (0.02 wt%), and evaluated their oral breakdown behavior and mouth burn perception. The capsaicinoids-loaded whey protein emulsion gels revealed a lower mouth burn perception due to higher mechanical strength that resulted in a slower diffusion rate of the encapsulates from the gel matrix and subsequently a lower mouth burn. These results suggested that emulsion gels had promising textural potentials which could be utilized to mimic desirable sensorial perceptions as well as for masking the undesirable flavors of bioactive compounds in food formulations while maintaining their consumer acceptability.

Digestion

The digestion kinetics of food-grade polymer-based gels are mainly influenced by the gelation process, for instance, gelation (acid and heat) of milk proteins slowed down their digestion rate and prolonged the gastric retention time without affecting the enzymatic cleavage sites (86, 87). Likewise, the majority of polysaccharides (dietary fiber form) in the gel state can significantly increase the gastric emptying time due to the thickening effect that becomes prominent upon their transformation from polymer to gel particles (88). Moreover, gelation also delays the diffusion of digestive enzymes into the gel matrix, thus digestion process of bioactive compounds can be substantially delayed by encapsulating into food gels (42). Therefore, *via* decreasing the digestion rate and prolonging gastric retention time, gels impart health-promoting effects, including enhanced satiety to attenuate obesity, good control of glucose and cholesterol metabolism to prevent chronic disorders, etc. (26, 88, 89).

The gels digestion process leads to the release of the encapsulated bioactive compounds that takes place through different mechanisms, including disintegration, swelling, molecular interactions, and erosion (1, 17, 18). In the process of gel erosion, the human enzymes work synergistically with the pH responses (e.g., oral cavity, stomach, small intestine, and colon) to initiate the controlled release of embedded bioactive agents at the target sites such as the small intestine and colon. The pH differences of the gastrointestinal tract bring changes to the overall charge on the surface of biopolymers, thus, charge shifting and different digestion behaviors in combination with the interior environment make gels promising vehicles for the efficient delivery of sensitive bioactive substances. For small intestine delivery, a protein can be entrapped in calcium alginate gel particles at pH 3 due to the opposite charges on protein and alginate biopolymers, and protein can be easily released in the small intestine at pH 7 because at this pH both biopolymers possess negative charges (90). Therefore, the enzymes diversity and pH responses show the potential to develop functional delivery systems for the encapsulation, protection, and release of bioactive at targeted sites, that could be further fine-tuned by manipulating the differences in the ionic strengths between the food gels formulations and the gastrointestinal environment (17, 91, 92).

Lin et al. (11) fabricated alginate-based emulsion gels stabilized by proteins (whey protein and soy protein isolates as emulsifiers) and tomato-derived lycopene was encapsulated in gels to study the *in vitro* digestion and its release behavior. The results showed a delayed release of the encapsulated lycopene from emulsion gels; whey protein isolate stabilized alginate emulsion gel release commenced at 4-4.5 h, soy protein isolate stabilized gel at 3.5-4 h, whereas an early release of 2.5-3 h was observed in alginate-based gel without any protein. The release corresponds to the start point of the structural collapse and degradation of gel networks after swelling during *in vitro* digestion of the emulsion gels. The whey protein had a better emulsifying capacity and also developed stronger interactions with alginate, thus improving the gel properties such as increasing Young's modulus of emulsion gel. A higher Young's modulus could retard the swelling process and subsequently prevents the collapse of gel structure during the *in vitro* gastric digestion. Thus, controlled release of encapsulated lycopene was achieved *via* delayed degradation of gel matrix during the *in vitro* intestinal digestion. Therefore, emulsion gels can be employed to protect the health-promoting substances from the harsh conditions of the gastrointestinal tract and deliver them to specific target sites with improved digestion and bioaccessibility (93, 94).

Absorption

It is a proven fact that undigested food is difficult to transport leading to poor absorption of the inheritable nutrients into the body because of barriers in the gastrointestinal tract epithelial cells and especially the mucous layer. The mucous layer comprises a 3D network of mucin glycosylated protein fibers with an average mesh size of ∼100 nm (45, 95, 96). In this regard, emulsion gels and derived particles with optimum surface attributes (e.g., size, shape, surface charge, and hydrophilicity/hydrophobicity) had the potential to enhance the mucosal permeability and maximize the bioavailability of embedded bioactive compounds (37, 94). Among the biopolymers, chitosan exhibits the potential to adhere and travel through the mucous layers to improve cellular uptake *via* reversible depolymerization of cellular actin and strong

interactions with the protein molecules. Thus, chitosan emulsion gels are popular delivery cargos with the superiority of enhancing cellular permeability without damaging epithelial cells (93, 96). For particles traversing through the epithelial cells, the main pathways include paracellular migration and transcellular translocation through tight junctions and enterocytes or M cells, respectively. Therefore, increasing the translocation of loaded gel particles is an important strategy for efficient delivery of the biomolecules with low mucosal permeability, including proteins, peptides, antimicrobial agents, nutraceuticals, and functional food ingredients (37, 93, 94, 97).

Haug et al. (98) designed gelatin-based emulsion gels and investigated their capability as delivery vehicles to boost the bioavailability of omega-3 fatty acids including eicosapentaenoic acid (EPA) and docosahexaenoic acid (DHA). The study's findings revealed that emulsion gels significantly increased the EPA and EPA + DHA levels in the blood plasma by 44.9 and 43.3%, respectively, as compared to gelatin capsules oral intake. This significant increase was attributed to the pre-emulsification of the fish oil as well as the design of the delivery vehicles (chewable and soft (emulsion gels) vs. intact and solid (capsules). Compared to gel capsules consumption, EPA and EPA + DHA loaded emulsion gels showed the highest increase of 100.4 and 105.6%, respectively, indicating gels' potential as efficient delivery systems in improving the bioavailability of gel matrix embedded functional ingredients.

Food Applications

Emulsion gels and derived particulates have emerged as promising delivery systems for industrial food applications due to their unique properties such as protection of functional food additives, controlled release of bioactive substances, and improved digestion and absorption of macro- and micronutrients in the gastrointestinal tract (37, 75, 99, 100). The industrial food applications of emulsion gels, including encapsulation and controlled release, texture design and modification, fat replacement, and probiotics delivery with enhanced viability are discussed in the following section.

Encapsulation and Controlled Release

Encapsulation is a promising technique widely employed for the protection and targeted delivery of bioactive compounds due to the superior stability of embedded substances against chemical, physical, and environmental stresses, and their desired controlled release (e.g., fast or sustained). To date, different delivery systems have been successfully developed with desirable structures and characteristics such as protected encapsulation and delivery of various bioactive nutrients with improved health benefits (17, 37, 101). In recent years, emulsion gels have garnered considerable attention as promising encapsulation and delivery cargos due to their superior properties for many food applications.

Xu et al. (41) prepared alginate-based nanoemulsion-filled gels fabricated by a facial approach of self-emulsification and sodium alginate ionic gelation. The formed gel loaded with curcumin showed an average particle size of 0.46 ± 0.02 mm, a loading capacity of 7.25 ± 3.16 mg/g, and encapsulation efficiency of 99.15 ± 0.85%, and the release rate was found significantly higher at pH 9 than at pH 7. The results showed that the alkaline condition (pH 9) achieved the half-release time of curcumin (50% release) in just 3 h due to an accelerated corrosion process compared to the neutral environment (pH 7) that provided stability to the curcumin loaded emulsion filled gels. Zhang et al. (102) produced gel as a delivery system from whey protein isolate through heat gelation (24 h at 85°C) for the encapsulation of β-carotene. The encapsulation efficiency was greatly improved from 76.55 to 92.11% than that of untreated whey protein isolate. The layers of protein isolate enhanced the protection of β-carotene, resulting in improved digestion resistance and subsequently increased bioavailability. Chen et al. (103) produced Pickering particle-stabilized emulsion gels *via* emulsification and pH adjustment and coencapsulated (-)-epigallocatechin-3-gallate (EGCG-hydrophilic bioactive) in the inner water phase, whereas quercetin (lipophilic bioactive) in the oil phase (**Figure 4**). The formed gels used to coencapsulate bioactives showed an encapsulation efficiency of 65.5 and 97.2% for (-)-epigallocatechin-3-gallate and quercetin in the aqueous phase and oil phase, respectively. Furthermore, *in vitro* study revealed that gels improved the bioaccessibility by 48.4 and 49% compared to control (water suspension) by 25.8 and 15%, for epigallocatechin-3-gallate and quercetin, respectively. Thus, emulsion gels as delivery systems had the potential for the encapsulation and coencapsulation of hydrophilic and lipophilic bioactive along with high encapsulation efficiency and controlled release features to enhance their bioaccessibility. In summary, gels are efficient cargos that could be used in improving the digestion, bioaccessibility, and bioavailability of bioactive compounds, functional ingredients, and pharmaceuticals.

Texture Design and Modification

The increasing consumers' awareness and industrial demands for clean-label food products have challenged the use of traditional synthetic food additives (e.g., thickeners, moisture absorbers, and emulsifiers) in designing food structures with desired properties. Employing emulsion gels is appropriate for various industrial food applications, for instance, they can be employed for modifying the texture and designing safer and healthier functional foods with improved physicochemical properties. Furthermore, the texture of emulsion gels can be fabricated by varying the biopolymer type and concentration, Pickering particles concentration (emulsifier), addition of functional additives, and processing conditions such as pH, ionic strength, and temperature (8, 12).

Zhang et al. (56) prepared emulsion-filled gels (EFGs) using enzymatically hydrolyzed rice starches (ERS) instead of native rice starch. The amount of starch in the gel medium had a direct impact on the final properties of ERS-EFGs. The addition of starch was found responsible for increasing the storage modulus (G′) and loss modulus (G″), as well as improving the firmness and freeze-thaw stability of resultant ERS-EFGs. On the other hand, the higher amount of emulsion droplets diluted the starch concentration, causing a reduction in both G′ and G″, freeze-thaw stability, and firmness. Taktak et al. (8) synthesized the gelatin-based emulsion gels from

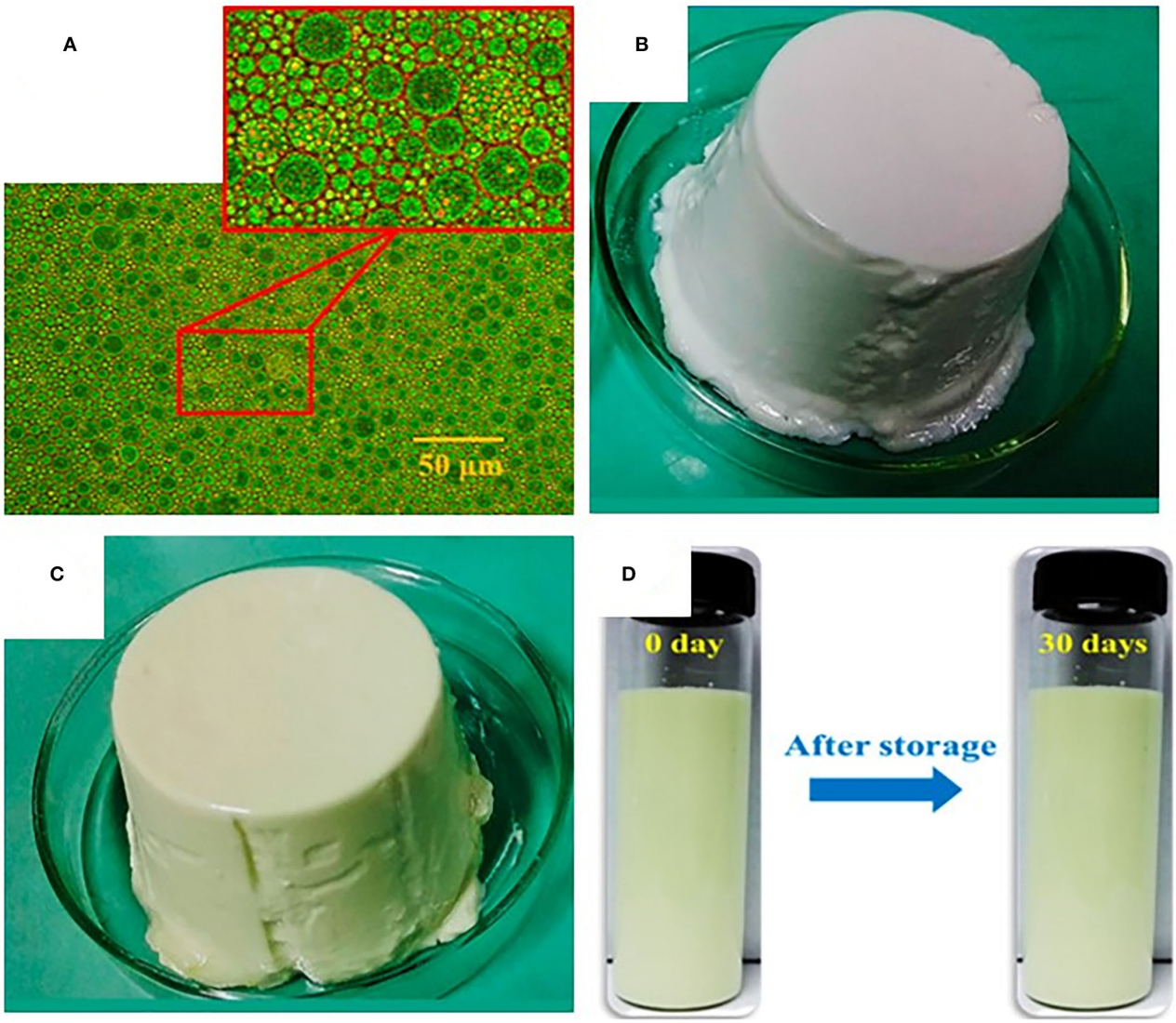

FIGURE 4 | Optical microscopic image and visual appearances of emulsion gels; **(A)** Emulsion dispersion droplets, **(B)** Blank emulsion gel, and **(C)** Epigallocatechin-3-gallate and quercetin co-loaded emulsion gel. The formed gel showed an encapsulation efficiency of 65.5 and 97.2%, whereas enhanced the bioaccessibility by 48.4 and 49% for (-)-epigallocatechin-3-gallate and quercetin, respectively. In addition, emulsion gel showed lower release rates of 73.3 and 31.7% and improved stability by 63.6 and 82.3% for epigallocatechin-3-gallate and quercetin after 8-h incubation in specific environmental conditions (simulated intestinal fluid) and remained stable to phase separation during 30-days storage at 4°C **(D)** (103).

European eel skin gelatin (ESG) and European oil (EO). The emulsion gels were prepared using the weight of EO:ESG in 1:2 and 1:4 (w/w) ratio through the homogenization process or homogenization followed by sonication. The textural properties such as hardness (7.87 N), masticability (35.94 Nmm), breaking strength (4.72 N), and rigidity (1.29 N/mm) were higher in gelatin gel (control) compared to gelatin based emulsion gels, indicating that emulsion gels were more flexible than gelatin gel. Gao et al. (29) synthesized high internal phase emulsion gels, prepared by whey protein isolate and pectin, and gelled by the addition of D-(+)-gluconic acid δ-lactone and calcium to form double networks high internal phase emulsion gels. The structural properties, such as hardness (220.77 ± 11.07 g), adhesiveness (168.4 ± 31.18 g/s), gumminess (129.98 ± 4.63 g), and chewiness (108.41 ± 23.91 g) of the internal phase emulsion gel (whey protein isolate and 2% pectin), were significantly higher as compared to hardness (125.59 ± 18.64 g), adhesiveness (35.2 ± 8.1 g/s), gumminess (51.02 ± 16.85 g), and chewiness (50.79 ± 17.04 g) of a hydrogel (prepared with similar composition as in internal phase emulsion gel). Thus, the incorporation of emulsion gels in foods as functional colloids exhibits the potential to regulate textural (rheology and tribology) and functional properties such as reduced sugar, salt, or cholesterol contents.

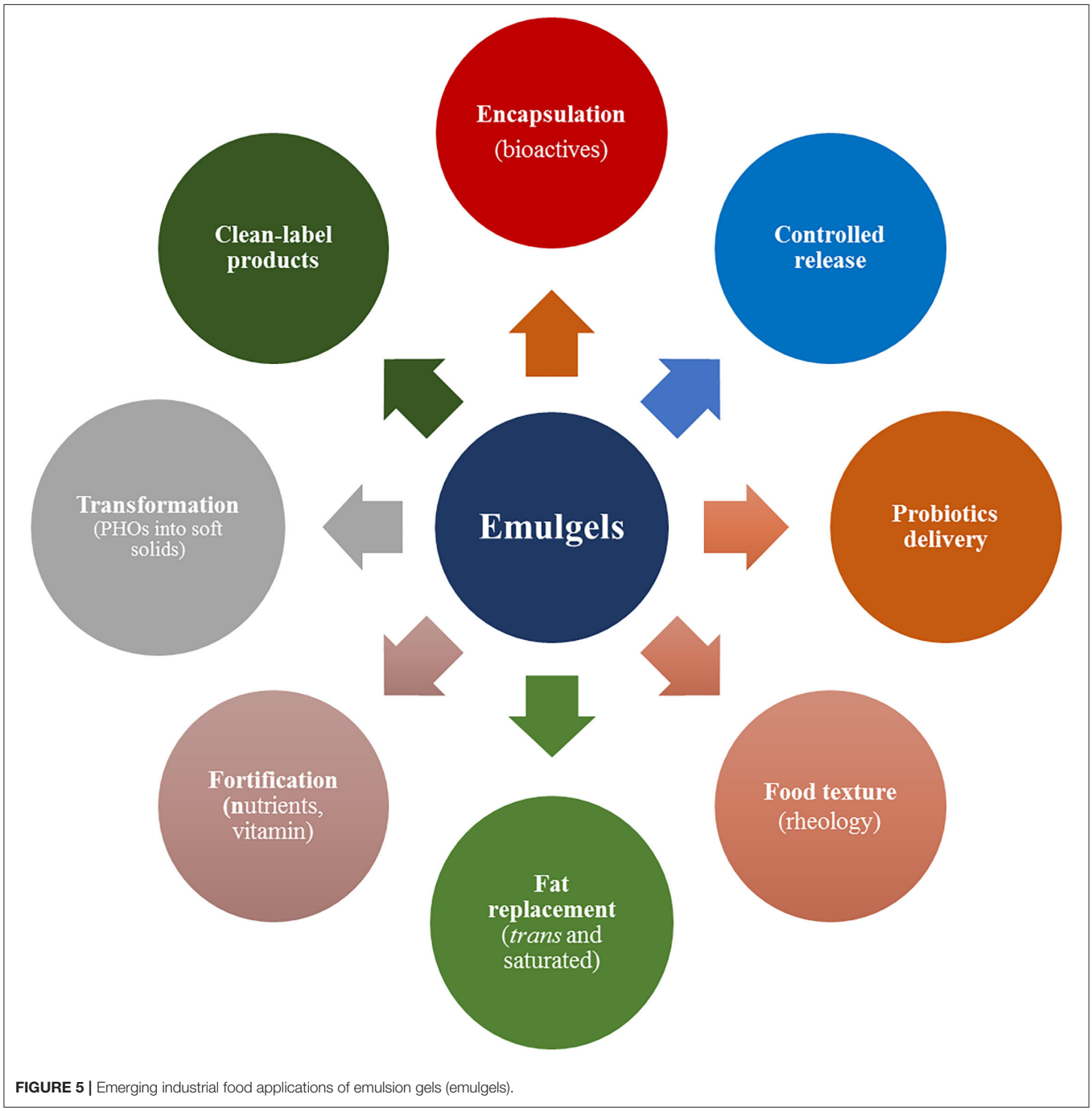

FIGURE 5 | Emerging industrial food applications of emulsion gels (emulgels).

Fat Replacement

Worldwide, cardiovascular diseases developed due to excessive intake of trans-fats are considered a major cause of morbidity and mortality (104). Mozaffarian et al. (105) reported that consumption of processed foods rich in saturated and artificial trans-fats elevated the prevalence of coronary heart disease from 23 to 29% when energy intake was increased by only 2% from foods containing trans-fats. Moreover, the United States Food and Drug Administration had also put a ban on partially hydrogenated oils used in processed foods, since they are a major source of trans-fats (106). Thus, the consumers' concerns about the harmful effects of fat consumption and the recent policy of the FDA related to the exclusion of trans-fat from food products have together attracted increased attention for needed innovation (107). In this regard, emulsion-gel technology may be employed to develop food products without trans fats and also to transform partially hydrogenated oils into semi-solid forms such as viscoelastic gels with zero trans fats or less saturated fats as a substitute for solid fats.

Nacak et al. (34) prepared emulsion gel comprising oil phase [peanut oil:linseed oil (10:1) and polyglycerol polyricinoleate (3.2 g)], and aqueous phase [water (37 g), inulin (8 g), egg white powder (3 g), and gelatin (2 g)], per 100 g of emulsion by heating at 55°C in water bath followed by emulsification at 700 rpm for 3 min. The formed gel was utilized to replace the beef fat partially/completely (50 and 100%) in sausages and found a 40% reduction in total fat content and 27% in case of energy content. Interestingly, the content of total saturated fatty acids (21.46 ± 0.4) and cholesterol (27.32 ± 0.6) was successfully decreased, while obvious boosts were seen in mono-unsaturated fatty acids (45.95 ± 0.14) and poly-unsaturated fatty acids (29.78 ± .22) in sausages containing emulsion gels (100% beef fat replacement) as compared to control. Likewise, de Souza Paglarini et al. (33) produced emulsion gels by encapsulating 50% soybean oil in the soy protein isolate (4%) and inulin (16.5%) as gel substrate to replace animal fat. A decline in fat (11 to 34%) was calculated in the reformulated products, furthermore, the least total fat content (190.4 ± 6.3), higher fiber content (2.97 %), and high amount of polyunsaturated fatty acid (80.37 ± 3.72) observed in emulsion gels incorporated sausages. Notably, the incorporation of emulsion gel replacing animal fat also offered better sensory properties such as texture, flavor, aroma, and overall liking. These findings indicated that emulsion gels had potential as animal fat substitutes and could be used in formulating healthier food products with a better fatty acids composition and sensory score. Liu et al. (108) used wheat gluten protein particles (1 wt%) as Pickering emulsifiers and prepared emulsion gels by encapsulating sunflower oil as a mayonnaise substitute. The formed gels presented excellent thermal stability at 90°C for 30 min than the mayonnaise, which showed a complete collapse with oil leakage. These findings suggested that emulsion gels have had better nutritional ratios, healthier lipid composition, and acceptable sensory features which could be used to replace animal fat and as a safe alternative to partially hydrogenated oils.

Probiotics Delivery

Probiotics are the viable microorganisms in the human gastrointestinal tract that impart health-promoting characteristics by regulating the balance of gut microflora (e.g., *Bifidobacterium* and *Lactobacillus*) (109, 110). For example, probiotics present in the intestinal tract exert multiple health benefits e.g., improved gastrointestinal tract health, enhanced immunity, reduced bad-cholesterol levels, and harmful microorganisms growth inhibition (111, 112). However, environmental and processing conditions such as high relative humidity and high temperatures greatly affect probiotics viability (113). Recently, biopolymer-based emulsion gels have emerged as a promising delivery system for probiotics targeted delivery with enhanced viability by protecting them from harsh environmental conditions during processing and digestion.

Gao et al. (29) developed high internal phase emulsion gels from whey protein isolate and pectin biopolymers to encapsulate and deliver *Bifidobacterium lactis*. The results showed that the viability of encapsulated probiotics was significantly higher in high internal phase emulsion gel (5.31 log CFU/ml) than hydrogel (4.66 5.31 log CFU/ml) after a heat treatment at 65°C for 30 min ascribed to the fact that gel pores filled with oil droplets effectively protected and minimized the effect of heating on probiotics. In addition, the strength, shear viscosity, water holding capacity, and stability of gels increased with an increase in the concentration of pectin from 0 to 2%. Qi et al. (57) developed smooth and spherical shaped micro-beads by emulsion-gelation method with sizes ranging from 300 to 500 μm as a delivery system for *Saccharomyces boulardii* and *Enterococcus faecium*. The formed gels showed that *S. boulardii* and *E. faecium* grew well and their survival rate improved by 25 and 40%, respectively, compared to controls under high temperature and high humidity. The survival rate in gastric juice for *S. boulardii* (60%) was significantly higher than *E. faecium* (25%), but in the case of intestinal juice, a higher rate was noticed for *E. faecium* (20%) than *S. boulardii* (15%). Picone et al. (54) synthesized gellan gum-based spherical microbeads with a diameter of 1.85 μm *via* the emulsion-gelation method to deliver *Lactobacillus rhamnosus* with a higher survival rate. The formed emulsion gel showed the encapsulated probiotics viability as 77% which was significantly higher than the non-gelled emulsion of 66%. The *in vitro* study findings suggested that emulsion-gelation improved the resistance of the embedded probiotics which remained stable to oral and gastric digestions. Based on the aforementioned findings, emulsion gels have emerged as model probiotics delivery systems that not only protected the encapsulated probiotics from adverse *in vitro* and *in vivo* conditions but also ensured their targeted delivery with enhanced viability. In addition, biopolymers as wall material also provide nutrients to probiotics and the host due to biopolymers' inheritable nutrient profiles, suggesting their potential to deliver probiotics in the gastrointestinal tract and development of functional formulations such as fermented foods.

CONCLUSIONS AND FUTURE TRENDS

Emulsion gel is an emulsion dispersion-filled gel matrix, wherein at least one phase either continuous phase or dispersed phase of emulsion creates 3D networks leading to the formation of semisolid texture. In this review, the authors have discussed the classification of emulsion gels based on their constitutive nature of the polymers (i.e., proteins, polysaccharides, and mixed emulsion gels), and gel-body interactions including sensorial textures, digestion, and absorption. The tunable attractive properties (morphology, mechanical, and functional) and unique characteristics (biocompatible, biodegradable, eco-friendly, and cost-competitive sustainable biomaterials) make emulsion gels promising functional colloids and delivery vehicles for different food applications (encapsulation, controlled release, texture design, fat replacement, probiotics delivery, designer foods, and so on). Based on their properties and characteristics emulsion gels could be effectively utilized in the processing, transportation, and targeted delivery of food additives, nutraceuticals, probiotics, and functional ingredients such as flavors, natural pigments, minerals, and vitamins (**Figure 5** and **Table 1**). In addition, emulsion gels can tailor breakdown behavior and sensory perception of food, protect the bioactive substances against

adverse conditions, modify their dispersible status in the food matrixes, control their release time and rate, and eventually enhance their bioavailability.

Emulsion gels could possibly be used to develop innovative stimuli-responsive gels which may alter their morphology and properties upon exposure to any external stimuli such as enzymes, light, temperature, pressure, and pathogenic microorganisms. Moreover, a combination of stimuli-responsive gels with biological entities (e.g., bacteria and viruses) can help in designing advanced bio-systems with high efficiency and sensitivity to monitor and control the safety and quality of the food products. Although biopolymer-derived emulsion gels had many advantages (cell biocompatibility and biodegradability, source renewability, inherent nutritional composition, *etc.*) over synthetic polymers-based gels, however some properties such as mechanical strength may not fully match. In this regard, the presence of charged species (H^+ and OH^-) and different functional groups on biopolymers such as amino, carboxyl, and hydroxyl groups impart huge fabrication potentials that would be utilized in designing gels with superior properties according to the needs.

To further explore the scope of emulsion gels in the food industry, cross-disciplinary studies emphasizing their physicochemical, rheological and tribological, and functional properties are needed to better design effective food formulations. Moreover, detailed investigations both *in vitro* and *in vivo* studies focusing on gel-body interactions specifically gastrointestinal physiology (digestion, biochemical transformations, absorption, and excretion) could help in promoting emulsion gels applications in edible food formulations. For instance, gels with desired sensorial textures and flavors may help in eradicating obesity-related problems by minimizing the intake of fats and sugars and consequently an effective control of cholesterol and glucose metabolism. Moreover, emulsion gels can be used to tailor the sensory perception of bioactive compounds such as phenolic substances and capsaicinoids that had pungent and astringent tastes during oral processing.

AUTHOR CONTRIBUTIONS

A and JX: conceptualization. A, LL, and HJ: writing-original draft preparation. A and JX: writing-review and editing. JX: supervision and resources, and funding acquisition. All the authors have read, revised, and agreed to manuscript publication.

FUNDING

The authors would like to recognize the financial support of the Guangdong Introducing Innovative and Entrepreneurial Teams under Grant (Project No. 2019ZT08N291) and the Foreign Technology Cooperation Plan of Guangzhou (No. 201907010031).

ACKNOWLEDGMENTS

We acknowledge the support of the South China Agricultural University, China.

REFERENCES

1. Cao Y, Mezzenga R. Design principles of food gels. *Nat Food*. (2020) 1:106–18. doi: 10.1038/s43016-019-0009-x
2. Abdullah, YuCheng Z, Farooq S, Walayat N, Zhang H, Faieta M, et al. Bio-aerogels: Fabrication, properties and food applications. *Crit Rev Food Sci Nutr*. (2022) 14:1–23. doi: 10.1080/10408398.2022.2037504
3. Banerjee S, Bhattacharya S. Food gels: Gelling process and new applications. *Crit Rev Food Sci Nutr*. (2011) 52:334–46. doi: 10.1080/10408398.2010.500234
4. Ma L, Zou L, McClements DJ, Liu W. One-step preparation of high internal phase emulsions using natural edible Pickering stabilizers: Gliadin nanoparticles/gum arabic. *Food Hydrocoll*. (2020) 100:105381. doi: 10.1016/j.foodhyd.2019.105381
5. Wang PX, Tan J, Zhang T, Zhai K, Zhang F, Wang P. Thermoresponsive starch-based particle-stabilized Pickering high internal phase emulsions as nutraceutical containers for controlled release. *Int J Biol Macromol*. (2020) 146:171–8. doi: 10.1016/j.ijbiomac.2019.12.269
6. Zhou ZT, Yin SW, Tang CH, Yuan DB, Yang XQ. Development of antioxidant gliadin particle stabilized Pickering high internal phase emulsions (HIPEs) as oral delivery systems and the *in vitro* digestion fate. *Food Funct*. (2018) 9:959–70. doi: 10.1039/C7FO01400G
7. Ma L, Wan Z, Yang X. Multiple water-in-oil-in-water emulsion gels based on self-assembled saponin fibrillar network for photosensitive cargo protection. *J Agric Food Chem*. (2017) 65:9735–43. doi: 10.1021/acs.jafc.7b04042
8. Taktak W, Hamdi M, Chentir I, Boughriba S, Ben Y, Li S, et al. Development of emulsion gelatin gels for food application : Physicochemical, rheological, structural and thermal characterization. *Int J Biol Macromol*. (2021) 182:1–10. doi: 10.1016/j.ijbiomac.2021.03.141
9. McClements, and Gumus CE. Natural emulsifiers — Biosurfactants, phospholipids, biopolymers, and colloidal particles: Molecular and physicochemical basis of functional performance. *Adv Colloid Interface Sci*. (2016) 234:3–26. doi: 10.1016/j.cis.2016.03.002
10. Abdullah, Weiss J, Ahmad T, Zhang C, and Zhang H. A review of recent progress on high internal-phase Pickering emulsions in food science. *Trends Food Sci Technol*. (2020) 106:91–103. doi: 10.1016/j.tifs.2020.10.016
11. Lin D, Kelly AL, Maidannyk V, Miao S. Effect of structuring emulsion gels by whey or soy protein isolate on the structure, mechanical properties, and in-vitro digestion of alginate-based emulsion gel beads. *Food Hydrocoll*. (2021) 110:106165. doi: 10.1016/j.foodhyd.2020.106165
12. Lu Y, Mao L, Hou Z, Miao S, Gao Y. Development of emulsion gels for the delivery of functional food ingredients: from structure to functionality. *Food Engineering Reviews*. (2019) 11:245–58. doi: 10.1007/s12393-019-09194-z
13. van de Velde F, de Hoog EH, Oosterveld A, Tromp RH. Protein-polysaccharide interactions to alter texture. *Annu Rev Food Sci Technol*. (2015) 6:371–88. doi: 10.1146/annurev-food-022814-015558
14. Abdullah A, Algburi A, Huang Q, Ahmad T, Zhong H, Javed HU, et al. Anti-biofilm potential of *Elletaria cardamomum* essential oil against *Escherichia coli* O157:H7 and *Salmonella* Typhimurium JSG 1748. *Front Microbiol*. (2021) 12:620227. doi: 10.3389/fmicb.2021.620227
15. Abdullah A, Asghar A, Huang Q, Mustfa W, Javed HU, Zehm S, et al. Black cardamom essential oil prevents *Escherichia coli* O157:H7 and *Salmonella* Typhimurium JSG 1748 biofilm formation through inhibition of quorum sensing. *J Food Sci Technol*. (2021). 58: 3183–91 doi: 10.1007/s13197-020-04821-8
16. Abdullah, A.sghar A, Butt MS, Shahid M, Huang Q. Evaluating the antimicrobial potential of green cardamom essential oil focusing on quorum

sensing inhibition of *Chromobacterium violaceum*. *Journal of Food Science and Technology*. (2017) 54, 2306–2315. doi: 10.1007/s13197-017-2668-7
17. McClements DJ. Designing biopolymer microgels to encapsulate, protect and deliver bioactive components: Physicochemical aspects. *Adv Colloid Interface Sci.* (2017) 240:31–59. doi: 10.1016/j.cis.2016.12.005
18. McClements DJ. Encapsulation, protection, and release of hydrophilic active components: potential and limitations of colloidal delivery systems. *Adv Colloid Interface Sci.* (2015) 219:27–53. doi: 10.1016/j.cis.2015.02.002
19. Luo N, Ye A, Wolber FM, Singh H. Effect of gel structure on the *in vitro* gastrointestinal digestion behaviour of whey protein emulsion gels and the bioaccessibility of capsaicinoids. *Molecules*. (2021) 26:1379. doi: 10.3390/molecules26051379
20. Le XT, Rioux LE, Turgeon SL. Formation and functional properties of protein-polysaccharide electrostatic hydrogels in comparison to protein or polysaccharide hydrogels. *Adv Colloid Interface Sci.* (2017) 239:127–35. doi: 10.1016/j.cis.2016.04.006
21. Maltais A, Remondetto GE, Subirade M. Tabletted soy protein cold-set hydrogels as carriers of nutraceutical substances. *Food Hydrocoll.* (2010) 24:518–24. doi: 10.1016/j.foodhyd.2009.11.016
22. Torres O, Sarkar A, Murray T. Emulsion microgel particles: Novel encapsulation strategy for lipophilic molecules *Trends Food Sci Technol*. (2016) 55:98–108. doi: 10.1016/j.tifs.2016.07.006
23. Mao L, Roos YH, Miao S. Study on the rheological properties and volatile release of cold-set emulsion-filled protein gels. *J Agric Food Chem.* (2014) 62:11420–8. doi: 10.1021/jf503931y
24. Guo Q, Rousseau D, Bellissimo N. Role of gel structure in controlling *in vitro* intestinal lipid digestion in whey protein emulsion gels. *Food Hydrocoll.* (2017) 69:264–72. doi: 10.1016/j.foodhyd.2017.01.037
25. Mao L, Miao S, Yuan F, Gao Y. Study on the textural and volatile characteristics of emulsion filled protein gels as influenced by different fat substitutes. *Food Res Int.* (2018) 103:1–7. doi: 10.1016/j.foodres.2017.10.024
26. Stieger M and van de Velde F. Microstructure, texture and oral processing: New ways to reduce sugar and salt in foods. *Curr Opin Colloid Interface Sci.* (2013) 18:334–48. doi: 10.1016/j.cocis.2013.04.007
27. Sala G, Stieger M, van de Velde F. Serum release boosts sweetness intensity in gels. *Food Hydrocoll.* (2010) 24:494–501. doi: 10.1016/j.foodhyd.2009.12.001
28. Paglarini Cd S, Furtado GF, Biachi JP, Vidal VAS, Martini S, Forte MBS, et al. Functional emulsion gels with potential application in meat products. *J Food Eng.* (2018) 222:29–37. doi: 10.1016/j.jfoodeng.2017.10.026
29. Gao H, Ma L, Sun W, Julian D, Cheng C, Zeng H, et al. Impact of encapsulation of probiotics in oil-in-water high internal phase emulsions on their thermostability and gastrointestinal survival. *Food Food Hydrocoll.* (2022) 126:107478. doi: 10.1016/j.foodhyd.2021.107478
30. Torres O, Tena NM, Murray BS, Sarkar A. Novel starch based emulsion gels and emulsion microgel particles: Design, structure and rheology. *Carbohydr Polym.* (2017) 178:86–94. doi: 10.1016/j.carbpol.2017.09.027
31. Renard D, Fvande V, Visschers RW. The gap between food gel structure, texture and perception *Food Hydrocoll.* (2006) 20:423–31. doi: 10.1016/j.foodhyd.2005.10.014
32. Foggiaro D, Dominguez R, Pateiro M, Cittadini A, Munekata PES, Campagnol PCB, et al. Use of healthy emulsion hydrogels to improve the quality of pork burgers. *Foods*. (2022) 11:596. doi: 10.3390/foods11040596
33. de Souza Paglarini C, Vidal VAS, Ribeiro W, Badan Ribeiro AP, Bernardinelli OD, Herrero AM, et al. Using inulin-based emulsion gels as fat substitute in salt reduced Bologna sausage. *J Sci Food Agric.* (2020) 101:505–17. doi: 10.1002/jsfa.10659
34. Nacak B, Öztürk-Kerimoglu B, Yildiz D, and Çagind,i Ö, Serdaroglu M. Peanut and linseed oil emulsion gels as potential fat replacer in emulsified sausages. *Meat Sci*. (2021) 176:108464. doi: 10.1016/j.meatsci.2021.108464
35. Godoi FC, Prakash S, Bhandari BR. 3d printing technologies applied for food design: status and prospects. *J Food Eng.* (2016) 179: 44-54. doi: 10.1016/j.jfoodeng.2016.01.025
36. Fu W, Chen E, McClements DJ, Cao Y, Liu S, Li B, et al. Controllable viscoelastic properties of whey protein-based emulsion gels by combined cross-linking with calcium ions and cinnamaldehyde. *ACS Appl Bio Materials.* (2019) 2:311–20. doi: 10.1021/acsabm.8b00604
37. Light K, Karboune S. Emulsion, hydrogel and emulgel systems and novel applications in cannabinoid delivery: a review. *Crit Rev Food Sci Nutr.* (2021) 22:1–31. doi: 10.1080/10408398.2021.1926903
38. Lv P, Wang D, Dai L, Wu X, Gao Y, Yuan F. Pickering emulsion gels stabilized by high hydrostatic pressure-induced whey protein isolate gel particles: Characterization and encapsulation of curcumin. *Food Res Int.* (2020) 132:109032. doi: 10.1016/j.foodres.2020.109032
39. Tan H, Sun G, Lin W, Mu C, Ngai T. Gelatin particle-stabilized high internal phase emulsions as nutraceutical containers. *ACS Appl Materials Interfaces.* (2014) 6:13977–84. doi: 10.1021/am503341j
40. Tan H, Zhao L, Tian S, Wen H, Gou X, Ngai T. Gelatin particle-stabilized high-internal phase emulsions for use in oral delivery systems: protection effect and *in vitro* digestion study. *J Agric Food Chem.* (2017) 65:900–7. doi: 10.1021/acs.jafc.6b04705
41. Xu YT, Liu TX, Tang CH. Novel Pickering high internal phase emulsion gels stabilized solely by soy β-conglycinin. *Food Hydrocoll.* (2019) 88:21–30. doi: 10.1016/j.foodhyd.2018.09.031
42. Zhang B, Meng R, Li XL, Liu WJ, Cheng JS, Wang W. Preparation of Pickering emulsion gels based on κ-carrageenan and covalent crosslinking with EDC: Gelation mechanism and bioaccessibility of curcumin. *Food Chem.* (2021) 357:129726. doi: 10.1016/j.foodchem.2021.129726
43. Pandey S, Senthilguru K, Uvanesh K, Sagiri SS, Behera B, Babu N, et al. Natural gum modified emulsion gel as single carrier for the oral delivery of probiotic-drug combination. *Int J Biol Macromol.* (2016) 92:504–14. doi: 10.1016/j.ijbiomac.2016.07.053
44. Mokhtari S, Jafari SM, Assadpour E. Development of a nutraceutical nano-delivery system through emulsification/internal gelation of alginate. *Food Chem.* (2017) 229:286–95. doi: 10.1016/j.foodchem.2017.02.071
45. Liu L, Tian C, Dong B, Xia M, Cai Y, Hu R, et al. Models to evaluate the barrier properties of mucus during drug diffusion. *Int J Pharm.* (2021) 599:120415. doi: 10.1016/j.ijpharm.2021.120415
46. Munoz-Gonzalez I, Ruiz-Capillas C, Salvador M, Herrero AM. Emulsion gels as delivery systems for phenolic compounds: Nutritional, technological and structural properties. *Food Chem.* (2021) 339:128049. doi: 10.1016/j.foodchem.2020.128049
47. Xi Z, Liu W, McClements DJ, Zou L. Rheological, structural, and microstructural properties of ethanol induced cold-set whey protein emulsion gels: Effect of oil content. *Food Chem.* (2019) 291:22–9. doi: 10.1016/j.foodchem.2019.04.011
48. Lu Y, Mao L, Cui M, Yuan F, Gao Y. Effect of the solid fat content on properties of emulsion gels and stability of β-carotene. *J Agric Food Chem.* (2019) 67:6466–75. doi: 10.1021/acs.jafc.9b01156
49. Luo N, Ye A, Wolber FM, Singh H. Structure of whey protein emulsion gels containing capsaicinoids: Impact on in-mouth breakdown behaviour and sensory perception. *Food Hydrocoll.* (2019) 92:19–29. doi: 10.1016/j.foodhyd.2019.01.019
50. Mantovani RA, Cavallieri ALF, Cunha RL. Gelation of oil-in-water emulsions stabilized by whey protein. *J Food Eng.* (2016) 175:108–16. doi: 10.1016/j.jfoodeng.2015.12.011
51. Beaulieu L, Savoie L, Paquin P, Subirade M. Elaboration and characterization of whey protein beads by an emulsification/cold gelation process: application for the protection of retinol. *Biomacromolecules.* (2002) 3:239–48. doi: 10.1021/bm010082z
52. Liang L, Line VLS, Remondetto GE, Subirade M. *In vitro* release of α-tocopherol from emulsion-loaded β-lactoglobulin gels. *Int Dairy J.* (2010) 20:176–81. doi: 10.1016/j.idairyj.2009.09.008
53. Chen X, McClements DJ, Zhu Y, Zou L, Li Z, Liu W, et al. Gastrointestinal fate of fluid and gelled nutraceutical emulsions: impact on proteolysis, lipolysis, and quercetin bioaccessibility. *J Agric Food Chem.* (2018) 66:9087–96. doi: 10.1021/acs.jafc.8b03003
54. Picone CSF, Bueno AC, Michelon M, Cunha RL. Development of a probiotic delivery system based on gelation of water-in-oil emulsions. *LWT Food Sci Technol.* (2017) 86:62–8. doi: 10.1016/j.lwt.2017.07.045
55. Yang T, Zheng J, Zheng B-S, Liu F, Wang S, Tang C-H. High internal phase emulsions stabilized by starch nanocrystals. *Food Hydrocoll.* (2018) 82:230–8. doi: 10.1016/j.foodhyd.2018.04.006
56. Zhang X, Chen D, Zhao Z, Wan J, Prakash S. Rheological and textural properties of emulsion-filled gel based on enzymatically

hydrolyzed rice starch. *Food Hydrocoll.* (2022) 126:107463. doi: 10.1016/j.foodhyd.2021.107463
57. Qi W, Liang X, Yun T, Guo W. Growth and survival of microencapsulated probiotics prepared by emulsion and internal gelation. *J Food Sci Technol.* (2019) 56:1398–404. doi: 10.1007/s13197-019-03616-w
58. Xu W, Huang L, Jin W, Ge P, Shah BR, Zhu D, et al. Encapsulation and release behavior of curcumin based on nanoemulsions-filled alginate hydrogel beads. *Int J Biol Macromol.* (2019) 134:210–5. doi: 10.1016/j.ijbiomac.2019.04.200
59. Yan C, Fu D, McClements DJ, Xu P, Zou L, Zhu Y, et al. Rheological and microstructural properties of cold-set emulsion gels fabricated from mixed proteins: whey protein and lactoferrin. *Food Res Int.* (2019) 119:315–24. doi: 10.1016/j.foodres.2019.02.012
60. Freire M, Cofrades S, Pérez-Jiménez J, Gómez-Estaca J, Jiménez-Colmenero F, Bou R. Emulsion gels containing n-3 fatty acids and condensed tannins designed as functional fat replacers. *Food Res Int.* (2018) 113:465–73. doi: 10.1016/j.foodres.2018.07.041
61. Yang X, Gong T, Lu YH, Li A, Sun L, Guo Y. Compatibility of sodium alginate and konjac glucomannan and their applications in fabricating low-fat mayonnaise-like emulsion gels. *Carbohydr Polym.* (2020) 229:115468. doi: 10.1016/j.carbpol.2019.115468
62. Su J, Wang L, Dong W, Wei J, Liu X, Yan J, et al. Fabrication and characterization of ultra-high-pressure (uhp)-induced whey protein isolate/κ-carrageenan composite emulsion gels for the delivery of curcumin. *Front Nutr.* (2022) 9:839761. doi: 10.3389/fnut.2022.839761
63. Han L, Zhou S, Lu K, Zheng Y, Qi B, Li Y. Effects of inducer type and concentration on the formation mechanism of W/O/W double emulsion gels. *Food Chem.* (2022) 379:132166. doi: 10.1016/j.foodchem.2022.132166
64. Liu F, Liang X, Yan J, Zhao S, Li S, Liu X, et al. Tailoring the properties of double-crosslinked emulsion gels using structural design principles: Physical characteristics, stability, and delivery of lycopene. *Biomaterials.* (2022) 280:121265. doi: 10.1016/j.biomaterials.2021.121265
65. Zhang X, Chen X, Gong Y, Li Z, Guo Y, Yu D, et al. Emulsion gels stabilized by soybean protein isolate and pectin: Effects of high intensity ultrasound on the gel properties, stability and β-carotene digestive characteristics. *Ultrason Sonochem.* (2021) 79:105756. doi: 10.1016/j.ultsonch.2021.105756
66. Feng W, Yue C, Wusigale, Ni Y, Liang L. Preparation and characterization of emulsion-filled gel beads for the encapsulation and protection of resveratrol and α-tocopherol. *Food Res Int.* (2018) 108:161–71. doi: 10.1016/j.foodres.2018.03.035
67. Geremias-Andrade IM, Souki NPDBG, Moraes ICF, Pinho SC. Rheological and mechanical characterization of curcumin-loaded emulsion-filled gels produced with whey protein isolate and xanthan gum. *LWT.* (2017) 86:166–73. doi: 10.1016/j.lwt.2017.07.063
68. Hou JJ, Guo J, Wang JM, Yang XQ. Effect of interfacial composition and crumbliness on aroma release in soy protein/sugar beet pectin mixed emulsion gels. *J Sci Food Agric.* (2016) 96:4449–56. doi: 10.1002/jsfa.7656
69. Mun S, Kim Y, Mcclements DJ. Control of β-carotene bioaccessibility using starch-based filled hydrogels. *Food Chem.* (2015) 173:454–61. doi: 10.1016/j.foodchem.2014.10.053
70. Alejandre M, Ansorena D, Calvo MI, Cavero RY, Astiasaran I. Influence of a gel emulsion containing microalgal oil and a blackthorn (Prunus spinosa L.) branch extract on the antioxidant capacity and acceptability of reduced-fat beef patties. *Meat Sci.* (2019) 148:219–22. doi: 10.1016/j.meatsci.2018.05.022
71. Sun C, Gao Y, Zhong Q. Properties of ternary biopolymer nanocomplexes of zein, sodium caseinate, and propylene glycol alginate and their functions of stabilizing high internal phase Pickering emulsions. *Langmuir.* (2018) 34:9215–27. doi: 10.1021/acs.langmuir.8b01887
72. Wei Z, Cheng Y, Huang Q. Heteroprotein complex formation of ovotransferrin and lysozyme: Fabrication of food-grade particles to stabilize Pickering emulsions. *Food Hydrocoll.* (2019) 96:190–200. doi: 10.1016/j.foodhyd.2019.05.024
73. Zou Y, Guo J, Yin SW, Wang JM, Yang XQ. Pickering Emulsion Gels Prepared by Hydrogen-Bonded Zein/Tannic Acid Complex Colloidal Particles. *J Agric Food Chem.* (2015) 63:7405–14. doi: 10.1021/acs.jafc.5b03113
74. Liu Q, Chang X, Shan Y, Fu F, Ding S. Fabrication and characterization of Pickering emulsion gels stabilized by zein/pullulan complex colloidal particles. *J Sci Food Agric.* (2021) 101:3630–43. doi: 10.1002/jsfa.10992
75. Funami T, Nakauma M. Instrumental food texture evaluation in relation to human perception. *Food Hydrocoll.* (2022) 124:107253. doi: 10.1016/j.foodhyd.2021.107253
76. Pascua Y, Koç H, Foegeding EA. Food structure: Roles of mechanical properties and oral processing in determining sensory texture of soft materials. *Curr Opin Colloid Interface Sci.* (2013) 18:324–33. doi: 10.1016/j.cocis.2013.03.009
77. Krop EM, Sarkar A, Hetherington MM, Holmes H, Miquel S. On relating rheology and oral tribology to sensory properties in hydrogels. *Food Hydrocoll.* (2019) 88:101–13. doi: 10.1016/j.foodhyd.2018.09.040
78. Chen J, Stokes JR. Rheology and tribology: Two distinctive regimes of food texture sensation. *Trends Food Sci Technol.* (2012) 25:4–12. doi: 10.1016/j.tifs.2011.11.006
79. de Lavergne MD, Tournier C, Bertrand D, Salles C, Van de Velde F, and Stieger M. Dynamic texture perception, oral processing behaviour and bolus properties of emulsion-filled gels with and without contrasting mechanical properties. *Food Hydrocolloids.* (2016) 52:648–60. doi: 10.1016/j.foodhyd.2015.07.022
80. Srivastava R, Stieger M, Scholten E, Souchon I, Mathieu V. Texture contrast: Ultrasonic characterization of stacked gels' deformation during compression on a biomimicking tongue. *Curr Res Food Sci.* (2021) 4:449–59. doi: 10.1016/j.crfs.2021.06.004
81. Stokes JR, Boehm M, Baier SK. Oral processing, texture and mouthfeel: from rheology to tribology and beyond. *Curr Opin Colloid Interface Sci.* (2013) 18:349–59. doi: 10.1016/j.cocis.2013.04.010
82. Liu K, van der Linden E, van de Velde F, Stieger M, Tian Y. Evidence for ball-bearing mechanism of microparticulated whey protein as fat replacer in liquid and semi-solid multi-component model foods. *Food Hydrocoll.* (2016) 52:403–14. doi: 10.1016/j.foodhyd.2016.03.036
83. Sarkar A, Kanti F, Gulotta A, Murray BS, Zhang S. Aqueous lubrication, structure and rheological properties of whey protein microgel particles. *Langmuir.* (2017) 33:14699–708. doi: 10.1021/acs.langmuir.7b03627
84. Torres O, Andablo-Reyes E, Murray BS, Sarkar A. Emulsion microgel particles as high-performance bio-lubricants. *ACS Appl Materials Interfaces.* (2018) 10:26893–905. doi: 10.1021/acsami.8b07883
85. Hayakawa F, Kazami Y, Ishihara S, Nakao S, Nakauma M, Funami T, et al. Characterization of eating difficulty by sensory evaluation of hydrocolloid gels. *Food Hydrocoll.* (2014) 38:95–103. doi: 10.1016/j.foodhyd.2013.11.007
86. Dupont D, Souchon I, Marze S, Feunteun SL. Structuring food to control its disintegration in the gastrointestinal tract and optimize nutrient bioavailability Innovative. *Food Sci Emerg Technol.* (2018) 46:83–90. doi: 10.1016/j.ifset.2017.10.005
87. Barbé F, Ménard O, Le Gouar Y, Buffière C, Famelart MH, Laroche B, et al. The heat treatment and the gelation are strong determinants of the kinetics of milk proteins digestion and of the peripheral availability of amino acids. *Food Chem.* (2013) 136:1203–12. doi: 10.1016/j.foodchem.2012.09.022
88. Capuano E. The behavior of dietary fiber in the gastrointestinal tract determines its physiological effect. *Crit Rev Food Sci Nutr.* (2017) 57:3543–64. doi: 10.1080/10408398.2016.1180501
89. Mudgil D, Barak S. Composition, properties and health benefits of indigestible carbohydrate polymers as dietary fiber: a review. *Int J Biol Macromol.* (2013) 61:1–6. doi: 10.1016/j.ijbiomac.2013.06.044
90. Zhang Z, Zhang R, Zou L, McClements DJ. Protein encapsulation in alginate hydrogel beads: Effect of pH on microgel stability, protein retention and protein release. *Food Hydrocoll.* (2016) 58:308–15. doi: 10.1016/j.foodhyd.2016.03.015
91. McClements DJ, Xiao H. Is nano safe in foods? Establishing the factors impacting the gastrointestinal fate and toxicity of organic and inorganic food-grade nanoparticles. *npj Sci Food.* (2017) 1:6. doi: 10.1038/s41538-017-0005-1
92. Garcia-Gonzalez CA, Alnaief M, Smirnova I. Polysaccharide-based aerogels-Promising biodegradable carriers for drug delivery systems. *Carbohydr Polym.* (2011) 86:1425–38. doi: 10.1016/j.carbpol.2011.06.066
93. des Rieux A, Fievez V, Garinot M, Schneider YJ, Preat V. Nanoparticles as potential oral delivery systems of proteins and

vaccines: a mechanistic approach. *J Control Release*. (2006) 116: 1–27. doi: 10.1016/j.jconrel.2006.08.013
94. Chaturvedi K, Ganguly K, Nadagouda MN, Aminabhavi TM. Polymeric hydrogels for oral insulin delivery. *J Control Release*. (2013) 165:129–38. doi: 10.1016/j.jconrel.2012.11.005
95. Johansson ME, Sjovall H, Hansson GC. The gastrointestinal mucus system in health and disease. *Nat Rev Gastroenterol Hepatol.* (2013) 10:352–61. doi: 10.1038/nrgastro.2013.35
96. Cone RA. Barrier properties of mucus. *Adv Drug Deliv Rev*. (2009) 61:75–85. doi: 10.1016/j.addr.2008.09.008
97. Yun Y, Cho YW, Park K. Nanoparticles for oral delivery: targeted nanoparticles with peptidic ligands for oral protein delivery. *Adv Drug Deliv Rev*. (2013) 65:822–32. doi: 10.1016/j.addr.2012.10.007
98. Haug IJ, Sagmo LB, Zeiss D, Olsen IC, Draget KI, Seternes T. Bioavailability of EPA and DHA delivered by gelled emulsions and soft gel capsules. *Eur J Lipid Sci Technol.* (2011) 113:137–45. doi: 10.1002/ejlt.201000450
99. Hu X, Karthik P, Chen J. Enhanced oral oil release and mouthfeel perception of starch emulsion gels. *Food Res Int.* (2021) 144:110356. doi: 10.1016/j.foodres.2021.110356
100. Norton JE, Gonzalez Espinosa Y, Watson RL, Spyropoulos F, Norton IT. Functional food microstructures for macronutrient release and delivery. *Food Funct*. (2015) 6:663–678. doi: 10.1039/C4FO00965G
101. Premjit Y, Pandhi S, Kumar A, Rai DC, Duary RK, Mahato DK. Current trends in flavor encapsulation: A comprehensive review of emerging encapsulation techniques, flavour release, and mathematical modelling. *Food Res Int.* (2022) 151:110879. doi: 10.1016/j.foodres.2021.110879
102. Zhang C, Fu Y, Li Z, Li T, Shi Y, Xie H, et al. Application of whey protein isolate fibrils in encapsulation and protection of β-carotene. *Food Chem.* (2021) 346:128963. doi: 10.1016/j.foodchem.2020.128963
103. Chen X, McClements DJ, Wang J, Zou L, Deng S, Liu W, et al. Coencapsulation of (-)-epigallocatechin-3-gallate and quercetin in particle-stabilized w/o/w emulsion gels: controlled release and bioaccessibility. *J Agric Food Chem.* (2018) 66:3691–9. doi: 10.1021/acs.jafc.7b05161
104. Restrepo BJ, Rieger M. Denmark's Policy on Artificial Trans Fat and Cardiovascular Disease. *Am J Prev Med.* (2016) 50:69–76. doi: 10.1016/j.amepre.2015.06.018
105. Mozaffarian D, Katan MB, Ascherio A, Stampfer MJ, Willett WC. Trans Fatty Acids and Cardiovascular Disease. *N Engl J Med.* (2006) 354:1601–13. doi: 10.1056/NEJMra054035
106. Patel AR, Dewettinck K. Edible oil structuring: an overview and recent updates. *Food Funct.* (2016) 7:20–9. doi: 10.1039/C5FO01006C
107. Patel AR. Edible "Oleocolloids": The Final Frontier in Food Innovation? *J Agric Food Chem.* (2017) 65:3432–3. doi: 10.1021/acs.jafc.7b01421
108. Liu X, Guo J, Wan Z-L, Liu Y-Y, Ruan Q-J, Yang X-Q. Wheat gluten-stabilized high internal phase emulsions as mayonnaise replacers. *Food Hydrocoll.* (2018) 77:168–75. doi: 10.1016/j.foodhyd.2017.09.032
109. Ooi LG, Liong MT. Cholesterol-lowering effects of probiotics and prebiotics: a review of *in vivo* and *in vitro* findings. *Int J Mol Sci.* (2010) 11:2499–522. doi: 10.3390/ijms11062499
110. Su J, Wang X, Li W, Chen L, Zeng X, Huang Q, et al. Enhancing the viability of Lactobacillus plantarum as probiotics through encapsulation with high internal phase emulsions stabilized with whey protein isolate microgels. *J Agric Food Chem.* (2018) 66:12335–43. doi: 10.1021/acs.jafc.8b03807
111. Cueto C, Aragon-Rojas S. Evaluation of probiotic potential of lactic acid bacteria to reduce *in vitro* cholesterol. *Sci Agropecuaria.* (2012) 3:45–50. doi: 10.17268/sci.agropecu.2012.01.06
112. Perdigon G, Fuller R, Raya R. Lactic acid bacteria and their effect on the immune system. *Curr Iss Intestinal Microbiol.* (2001) 2:27–42.
113. Higl B, Kurtmann L, Carlsen CU, Ratjen J, Först P, Skibsted LH, et al. Impact of water activity, temperature, and physical state on the storage stability of Lactobacillus paracasei ssp. paracasei freeze-dried in a lactose matrix. *Biotechnol Prog.* (2007) 23:794–800. doi: 10.1002/bp070089d

Conflict of Interest: The authors declare that the research was conducted in the absence of any commercial or financial relationships that could be construed as a potential conflict of interest.

Publisher's Note: All claims expressed in this article are solely those of the authors and do not necessarily represent those of their affiliated organizations, or those of the publisher, the editors and the reviewers. Any product that may be evaluated in this article, or claim that may be made by its manufacturer, is not guaranteed or endorsed by the publisher.

frontiers | Frontiers in Nutrition

ORIGINAL RESEARCH
published: 13 June 2022
doi: 10.3389/fnut.2022.808351

Effects of Proteins and Mineral Ions on the Physicochemical Properties of 1,3-Dioleoyl-2-Palmitoylglycerol Emulsion to Mimic a Liquid Infant Formula

Qi Wang[1†], *Yuxi Xu*[2†], *Yanchen Liu*[1], *Fang Qian*[1], *Guangqing Mu*[1*] *and Xuemei Zhu*[1*]

[1] School of Food Science and Technology, Dalian Polytechnic University, Dalian, China, [2] State Key Lab of Food Science and Technology, Nanchang University, Nanchang, China

OPEN ACCESS

Edited by:
Weilin Liu,
Zhejiang Gongshang University, China

Reviewed by:
Aiqian Ye,
Massey University, New Zealand
Jayani Chandrapala,
RMIT University, Australia
Anant Dave,
Fonterra Research and Development Centre (FRDC), New Zealand

***Correspondence:**
Guangqing Mu
GuangqingMu@163.com
Xuemei Zhu
zhuxuemei2005@aliyun.com

[†] These authors have contributed equally to this work and share first authorship

Specialty section:
This article was submitted to Food Chemistry, a section of the journal Frontiers in Nutrition

Received: 03 November 2021
Accepted: 29 April 2022
Published: 13 June 2022

Citation:
Wang Q, Xu Y, Liu Y, Qian F, Mu G and Zhu X (2022) Effects of Proteins and Mineral Ions on the Physicochemical Properties of 1,3-Dioleoyl-2-Palmitoylglycerol Emulsion to Mimic a Liquid Infant Formula. Front. Nutr. 9:808351. doi: 10.3389/fnut.2022.808351

Proteins and minerals in infant formula not only serve as nutrients, but also have important effects on the physical and chemical stability of emulsions. In this study, calcium carbonate (0 or 9.08 mM) and potassium chloride (0 or 15.96 mM), as representatives of divalent and monovalent minerals, were added to 1,3-dioleoyl-2-palmitoylglycerol (OPO) emulsions in different ratios (10:0, 9:1, 6:4, 5:5, and 0:10) of whey protein isolate (WPI) and sodium caseinate (CN). The influence of proteins and minerals on emulsion stability was investigated by analyzing particle size, zeta potential, creaming index, rheological properties, storage stability, and lipid oxidation. 1,3-dioleoyl-2-palmitoylglycerol (OPO) emulsions could be destabilized by adding Ca^{2+}, as shown by the increase in particle size index, creaming index, and the decrease in zeta potential magnitude. Divalent ions could affect the electrostatic interactions between lipid droplets and the interactive effects of ion surface adsorption. In addition, the effect of different protein ratios on the physical stability of emulsions was not significant under the same ion-type conditions. In terms of chemical stability, higher oxidized values were found in emulsions stabilized with only CN than in those containing WPI. Our study showed that protein ratios and minerals played an important role in the stability of OPO emulsions, which might provide a reference for the development and utilization of liquid infant formula.

Keywords: calcium, potassium, OPO emulsion, stability, lipid oxidation

INTRODUCTION

In the first 6 months of life, breast milk from healthy and well-nourished mothers is regarded as the best food for infants (1). In addition, it contains nutrients that aid in the protection and maturation of the infant intestine (2). Breast milk contains 3–5% fat, 0.8–0.9% protein, 6.9–7.2% carbohydrate, and 0.2% minerals, and other physiologically active components (IgA, bifidus factor, etc.) (3). Among the macronutrients, breast milk lipids are the primary source of energy and vital nutrients for the newborn. In terms of the composition of breast milk fat, triglycerides account for 98% of the fat content and oleic acid, palmitic acid, and linoleic acid are the three most abundant fatty acids, followed by stearic and myristic acids, where 70% of palmitic acid is esterified at the sn-2 position and unsaturated fatty acids (oleic acid, linoleic acid, etc.) are located at the sn-1,3 position.

The unique composition and distribution of fatty acids leads to a representative human milk fat named 1,3-dioleoyl-2-palmitoylglycerol (OPO) (4, 5).

Human milk fat substitutes refer to the triglyceride mixture synthesized by modern enzymatic modification technology. It modifies animal and vegetable fats according to the nutritional composition, fatty acid composition, and fat distribution of human milk (6, 7). It is intended to meet the nutritional needs of infants and their growth and development. Carnielli et al. provided solid evidence that breastfed newborns absorbed palmitic acid at the sn-2 position (8). López-Lópe et al. compared the total fatty acid compositions with the sn-2 positional fatty acid compositions of colostrum, transitional milk, mature milk, and infant formula. They found that infant formula containing sn-2 positional palmitic acid is more easily absorbed than regular formula (9). Koo et al. demonstrated that palmitic acid in the sn-2 position of infant formula had a physiological function, including enhancing calcium absorption in the small intestine and decreasing bone mass (10). OPO, as a triglyceride typical of breast fat, influences infant digestion and absorption, making OPO a value-added ingredient in commercial powder infant milk.

Currently, liquid infant formula is a potential popular product because it is easier to drink and has brighter packaging that appeals to infants and young children. For the development of liquid infant formula products, the physical and chemical stability of these products are just as crucial as their nutritional content. The emulsifier has a significant impact on emulsion stability. As main milk proteins, whey protein (WP) and casein are important emulsifiers in liquid infant formula products, which have also been widely used in the food industry (11). The ratio of WP to casein in breast milk varied depending on the stage of breastfeeding, for example, it could be as high as 9:1 in early lactation and subsequently decline to 5:5 in late lactation. An overall ratio of roughly 6:4 is used in most infant formula products. Milk proteins adsorb at the interface between the two phases of the oil-in-water (O/W) system, forming a protective layer on the surface of the lipid droplet before and after homogenization and inhibiting interfacial tension to maintain emulsions. It is well known that WP and casein have different properties, which have an impact on the physical and chemical stability of liquid infant formula.

Minerals in infant formula have a significant impact on the physical and chemical stability of emulsions, in addition to the complex fat structure and protein composition. Minerals boost the ionic strength in the aqueous phase, lowering the electrostatic repulsion between droplets and promoting phase separation (12–15). Some minerals bind to oppositely charged groups on the surface of emulsion droplets, decreasing their zeta potential and thus reducing electrostatic repulsion (16). In several commercial emulsions, calcium-induced flocculation and creaming have been identified as the sources of long-term destabilization (17).

Previous studies have shown that the creaming stability of emulsions with 0.5% protein decreased, while the emulsion with 3% protein was not affected by the addition of $CaCl_2$ to 0.5% (18, 19). In this study, an OPO emulsion was prepared to imitate liquid infant formula. We investigated the effect of a series of protein ratios (10:0, 9:1, 6:4, 5:5, and 0:10) and ion types on the physicochemical properties of the OPO emulsion. The ratios were selected based on the content of WP and casein in breast milk throughout the lactation period and the combined effect of monovalent (represented by K^+) and divalent (represented by Ca^{2+}) ions in infant formula milk powder. This study may provide a theoretical basis for the physical stability of liquid infant formula.

MATERIALS AND METHODS

Materials

1, 3-dioleic-2-palmitate triglyceride-type human milk fat substitutes (triglycerides > 98%) were kindly donated by Renzhichu Technology Group Ltd. (Jiangxi, China), which would be used directly for producing infant formula. Provon® whey protein isolates (WPI, purity 90%) were purchased from Glanbia Nutritionals Ltd. (Ireland). Sodium caseinate (CN, BR, from bovine milk) was purchased from Macklin Biochemical Co., Ltd. (Shanghai, China). Other solvents and reagents were of analytical grade.

Preparation of O/W Emulsions

Oil-in-water emulsions were prepared according to previous reports with simple modifications. Briefly, an aqueous solution consisting of WPI: CN (1% w/v in total) and phosphate buffered saline (PBS, 0.01 M, pH 7.0) was stirred for 5 h to ensure complete dissolution of the protein. After storing the emulsion at 4°C overnight, Ca^{2+} and K^+concentrations (9.08 and 15.96 mM) were added once the protein dispersion had returned to room temperature. The solutions were stirred for 10 min using a DS-101S magnetic stirring apparatus (Yarong Instrument Ltd., Zhengzhou, China) to ensure complete dissolution of the salts. To make a fresh emulsion, 10% (v/v) of OPO human milk fat substitutes were mixed with sufficient dissolution at 12,000 rpm for 3 min, homogenized 2 times at 30 MPa, and loaded with sodium azide (0.02% w/v) as an antibacterial agent. The pH of the emulsion was adjusted to 7.0 with 1 M NaOH and/or 1 M HCl for analysis.

Average Particle Size and Zeta Potential

The particle size distributions and zeta potential of infant formula emulsion samples were measured using a nano-ZSE laser particle size analyzer (Malvern Instruments Ltd., England) according to dynamic light scattering. Infant formula (×100 dilution) emulsion samples were prepared to avoid multiple scattering effects, and the absorption of 0.01 was used to calculate particle size distributions as described previously (20). Each sample was tested three times, and the data are presented as average ± standard deviation (SD).

Creaming Index

The infant formula emulsion sample (pH 7.0) was transferred to a test tube [internal diameter (Φ) = 20 mm, height (H) = 500 mm], and then stored at room temperature for 4 months. After storage, several samples were separated into a thin "cream" layer at the top and a transparent "serum" layer at the bottom (21). The creaming

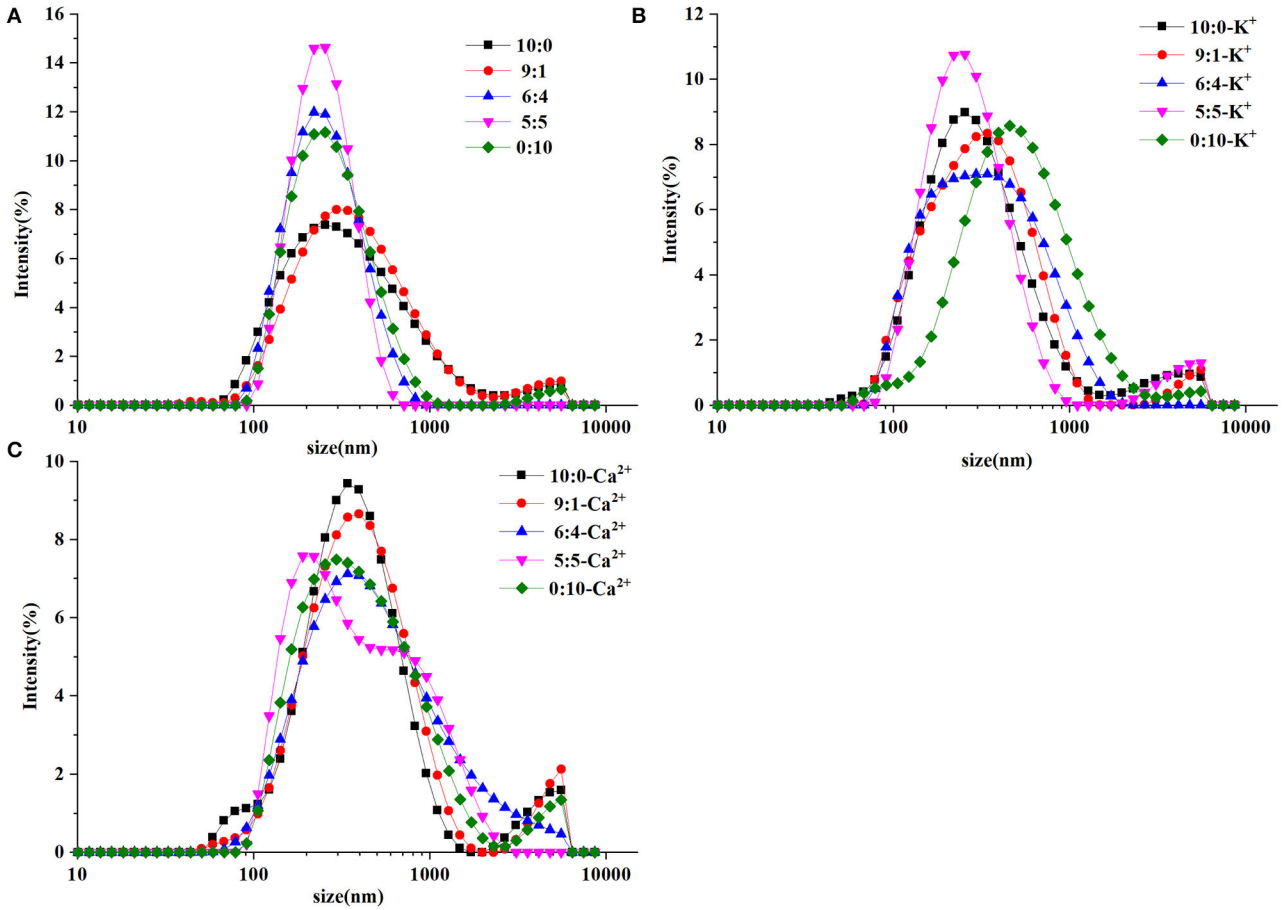

FIGURE 1 | Particle size distribution of control **(A)**, containing K^+ **(B)**, and Ca^{2+} **(C)** of 1,3-dioleoyl-2-palmitoylglycerol (OPO) emulsions (10% v/v OPO human milk fat substitutes) with different ratios of whey protein isolate (WPI) and caseinate (CN; 10:0, 9:1, 6:4, 5:5, 0:10, 1% w/v in total) as emulsifiers.

destabilization kinetics was evaluated by measuring creaming index as the percentage of serum layer height (H_S) from the total emulsion height (H_T) (22).

$$Creaming\ \ index = \frac{H_S}{H_T} \times 100\%$$

Rheological Properties

Rheological properties were carried out in a DHR-2 rheometer (TA Instruments Ltd., New Castle, DE, USA). The temperature was maintained at 25 ± 0.5°C. The apparent viscosity of the emulsion sample was measured upon shear rate ramp-up from 5 to 100 s^{-1} according to the modified method as described previously (23). The exposed surfaces of the samples were covered with a thin layer of silicone oil to prevent dehydration. The shear rate was then recorded as the shear stress was increased.

Storage Stability

The infant formula emulsion sample (2 ml) was poured into a cuvette and then stored at room temperature for 40 days, and 5 μl of each sample was taken out at the time intervals of 0, 8, 16, 24, 32, and 40 days for analysis. The physical stability of emulsions during storage was characterized by regular sampling and measuring their average particle size and zeta potential.

Lipid Oxidation

The method for characterizing the oxidation stability of oil is based on the method of Qiu et al. (24) and slightly modified. The emulsion sample was placed in an oven at 60°C, and the samples were taken out at different time periods (0, 10, 20, 30, and 40 days) for the analysis of oxidation state.

Primary Oxidation Product Hydrogen Peroxide Value

Primary oxidation product hydrogen peroxide value (POV) was measured according to the report of Zeng et al. (25) with slight modifications. Briefly, 1 ml of the emulsion sample was vortexed vigorously three times with 5 ml of isooctane: isopropanol (2:1 v/v) followed by centrifugation for 5 min at 2,800 × g (FA-45-6-30 rotor, centrifuge 5804R, Eppendorf AG, Hamburg, Germany). Then, 0.2 ml of the isooctane: isopropanol extract was mixed with 4.8 ml of methanol: butanol (2:1 v/v). This mixture was then reacted with 20 μl of 3.94 M potassium thiocyanate and 20 μl of ferrous iron solution. The mixture was allowed to react for 20 min at room temperature in the dark before measuring the absorbance of the sample at 510 nm using a TU-1900

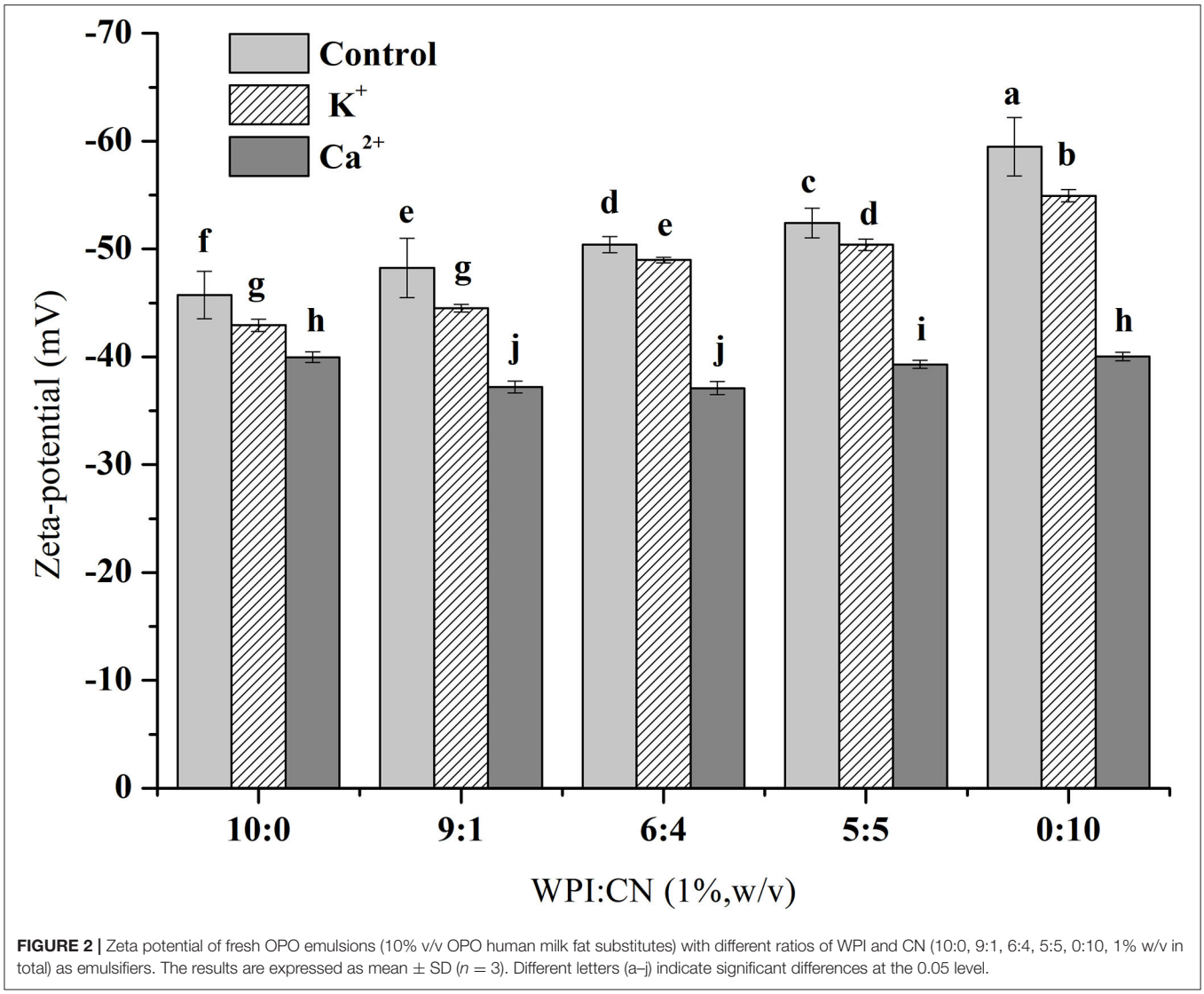

FIGURE 2 | Zeta potential of fresh OPO emulsions (10% v/v OPO human milk fat substitutes) with different ratios of WPI and CN (10:0, 9:1, 6:4, 5:5, 0:10, 1% w/v in total) as emulsifiers. The results are expressed as mean ± SD ($n = 3$). Different letters (a–j) indicate significant differences at the 0.05 level.

spectrophotometer (Baiqi Biotechnology Ltd., Jinan, China). The concentration of hydroperoxides was determined based on a standard curve of hydroperoxide.

Thiobarbituric Acid Reactive Substances

Thiobarbituric acid reactive substances (TBARS) were measured according to Xu et al. (26). The infant formula emulsion sample (0.6 ml) was combined with 4.0 ml of TBA (thiobarbituric acid) solution (prepared by mixing 15 g of trichloroacetic acid, 0.375 g of TBA, 1.76 ml of 12 M HCl, and 82.9 ml of H_2O) in test tubes and placed in a boiling water bath for 30 min. The tubes were cooled to room temperature for 10 min and then centrifuged at 860 × g (2,500 rpm) for 20 min followed by measuring the absorbance at 532 nm. TBARS were calculated from a standard curve prepared with 1,1,3,3-tetraethoxypropane.

Statistical Analysis

The results are presented as means ± SD using SPSS 18.0 software (IBM Corporation, NY, USA) and Origin 85 software (Microsoft Corporation, Redmond, WA, USA). The statistical analysis was performed by one-way ANOVA followed by Duncan's test at $p < 0.05$.

RESULTS

Particle Size and Zeta Potential Analysis

Particle size distribution in the OPO emulsion samples is illustrated in **Figure 1**. In **Figure 1A**, the emulsion in the control (without ions) with a higher WPI ratio (10:0 and 9:1) was characterized with larger particles and a tail peak in peak distribution. The result indicated that a number of original droplets had accumulated. Emulsions with increasing CN ratios (6:4, 5:5, and 0:10) showed a single peak distribution and a tight particle size distribution, indicating a good symmetry dispersion. Compared with the control, the particle size distribution of the ion groups showed a bimodal distribution. The size distribution was control group < K^+ group < Ca^{2+} group, indicating that the

TABLE 1 | The creaming index of fresh 1,3-dioleoyl-2-palmitoylglycerol (OPO) emulsions (10% v/v OPO human milk fat substitutes and whey protein isolate (WPI): CN/10:0, 9:1, 6:4, 5:5, 0:10, 1% w/v in total) for 120 days.

WPI: CN (1%, w/v)	20 days	40 days	60 days	120 days
10:0	ND	ND	ND	0.78 ± 0.41
9:1	ND	ND	3.72 ± 0.59^{b}	26.71 ± 5.14^{a}
6:4	ND	2.90 ± 0.16^{b}	8.04 ± 1.08^{b}	40.34 ± 2.73^{a}
5:5	ND	5.05 ± 2.02^{b}	7.07 ± 1.00^{b}	43.60 ± 1.34^{a}
0:10	ND	3.80 ± 0.94^{c}	6.63 ± 0.09^{b}	38.15 ± 5.62^{a}
10:0-K^+	ND	ND	ND	1.96 ± 0.13
9:1-K^+	ND	1.55 ± 0.43^{c}	7.01 ± 3.98^{a}	13.04 ± 1.94^{a}
6:4-K^+	7.92 ± 0.71^{c}	6.38 ± 2.06^{c}	39.98 ± 2.46^{b}	71.84 ± 6.63^{a}
5:5-K^+	13.59 ± 0.43^{c}	10.58 ± 6.05^{c}	28.95 ± 4.34^{b}	65.23 ± 7.11^{a}
0:10-K^+	ND	21.81 ± 4.71^{c}	77.99 ± 4.02^{b}	81.69 ± 1.84^{a}
10:0-Ca^{2+}	ND	ND	ND	2.49 ± 0.42
9:1-Ca^{2+}	ND	3.67 ± 2.07^{c}	5.39 ± 4.06^{b}	23.43 ± 10.28^{a}
6:4-Ca^{2+}	10.79 ± 2.76^{d}	18.27 ± 5.00^{c}	31.33 ± 4.66^{b}	64.92 ± 6.32^{a}
5:5-Ca^{2+}	7.13 ± 1.24^{d}	16.51 ± 3.36^{c}	32.11 ± 1.42^{b}	72.58 ± 5.56^{a}
0:10-Ca^{2+}	ND	16.09 ± 2.30^{c}	78.03 ± 4.64^{b}	82.02 ± 6.44^{a}

$^{a-d}$ Different small letters represent the significance of the difference ($p < 0.05$); ND means not detected.

large particles in emulsions were gradually increased and formed by droplet aggregation.

The zeta potential values of emulsions with various WPI and CN ratios are shown in **Figure 2**. The zeta potential amplitude of the control samples (without ionic addition) decreased as the CN concentration in emulsions increased. When adding K^+ and Ca^{2+} into emulsions, the absolute zeta potential value did not change significantly with increasing CN ratio. Under the conditions of different or same protein ratios, the absolute zeta potential value was K^+ group > Ca^{2+} group and the change in the absolute zeta potential value was Ca^{2+} group > K^+ group > control group.

Creaming Index During Storage

According to **Table 1**, the impacts of different protein ratios and mineral ions in emulsions did not show layering behavior when emulsions were placed at room temperature for 20 days, except the 6:4 and 5:5 (WPI:CN) emulsions after adding K^+ and Ca^{2+}, which showed a slight alteration (7.92 ± 0.71, 13.59 ± 0.43, 10.79 ± 2.76, and 7.13 ± 1.24%, respectively). However, varying degrees of cream layer separation were found from 20 to 120 days. Emulsions emulsified by WPI were stable, whereas emulsions with K^+ and Ca^{2+} showed the most obvious layering phenomenon (81.69 ± 1.84 and 82.02 ± 6.44%). It is shown that the overabundance of unabsorbed biopolymers resulted in higher droplet accumulation, larger particles, and more pronounced stratification behavior after longer storage time.

Viscosity Analysis

The rheological behavior of the OPO emulsion system was examined as a function of different protein ratios and ionic strength. In particular, the flow behavior of the emulsion sample was investigated taking into account the dependence of the shear stress on the sample viscosity. The effect of different protein ratios and ionic strength on the rheological properties of emulsions was examined (**Figures 3A–D**). The flocculated emulsions exhibited strong shear thinning behavior (**Figure 3**). Viscosity decreased with increasing shear rate. When the shear rate was in the range of 5–10 s^{-1}, the viscosity of each emulsion group decreased rapidly as shear stress increased. Then, the viscosity tended to be consistent within the shear rate of 20–100 s^{-1}. Compared with **Figure 3A**, the viscosity of the K^+ and Ca^{2+} groups was higher than the control group in the range of 5–10 s^{-1}. This difference could be attributed to factors such as flocculated volume fraction of the droplets, flocculation size, and spatial distribution or intensity of interaction between flocculated droplets (27). Different protein ratios were found to be insensitive to changes in emulsion viscosity.

To understand the relationship between shear stress and viscosity of emulsions by the addition of K^+ and Ca^{2+}, only the ratio of 6:4 (WPI:CN) was chosen for viscosity analysis. **Figure 3D** shows that the viscosity of the 6:4 emulsion without salt ions is lower than that of the emulsion with K^+ and Ca^{2+}, which was Ca^{2+} group > K^+ group > control group in the range of 5–20 s^{-1}.

Physical Stability of Emulsions During Storage

The storage stability (particle size and zeta potential) of emulsions after 40 days is shown in **Table 2**. The results showed that the emulsion particle size gradually increased with storage time. It was also demonstrated that the absolute value of the zeta potential gradually decreased as the emulsion storage time increased. In detail, the particle size of emulsions without ions and with K^+ or Ca^{2+} were 355–460, 426–507, and 424–514 nm, respectively, after storage for 40 days. In addition, the zeta potential in the control, K^+, and Ca^{2+} groups was −41.53∼-51.27, −39.53∼-52.33, and −29.67∼-36.10 mV, respectively, after storage for 40 days. According to the analysis with or without K^+ and Ca^{2+}, the trend of the physical stability of emulsions during storage decreased in the following order: control group > K^+ group > Ca^{2+} group.

Lipid Oxidation of Emulsions

In this study, the rate of lipid oxidation in different emulsions containing K^+ or Ca^{2+} was measured. All samples were kept at 60°C for 40 days to accelerate lipid oxidation. To investigate the rate of lipid oxidation, primary and secondary lipid oxidation products were measured as POV and TBARS (**Figure 4**), respectively. The results showed that the rate of lipid oxidation increased at first and then decreased as the storage time was prolonged. Due to its more compact structure and lack of phosphate groups, WPI might limit its iron-binding ability and thus promote oxidation (28). In addition, the relative oxidation value of emulsions with CN alone as the emulsifier was greater than that of other emulsions with

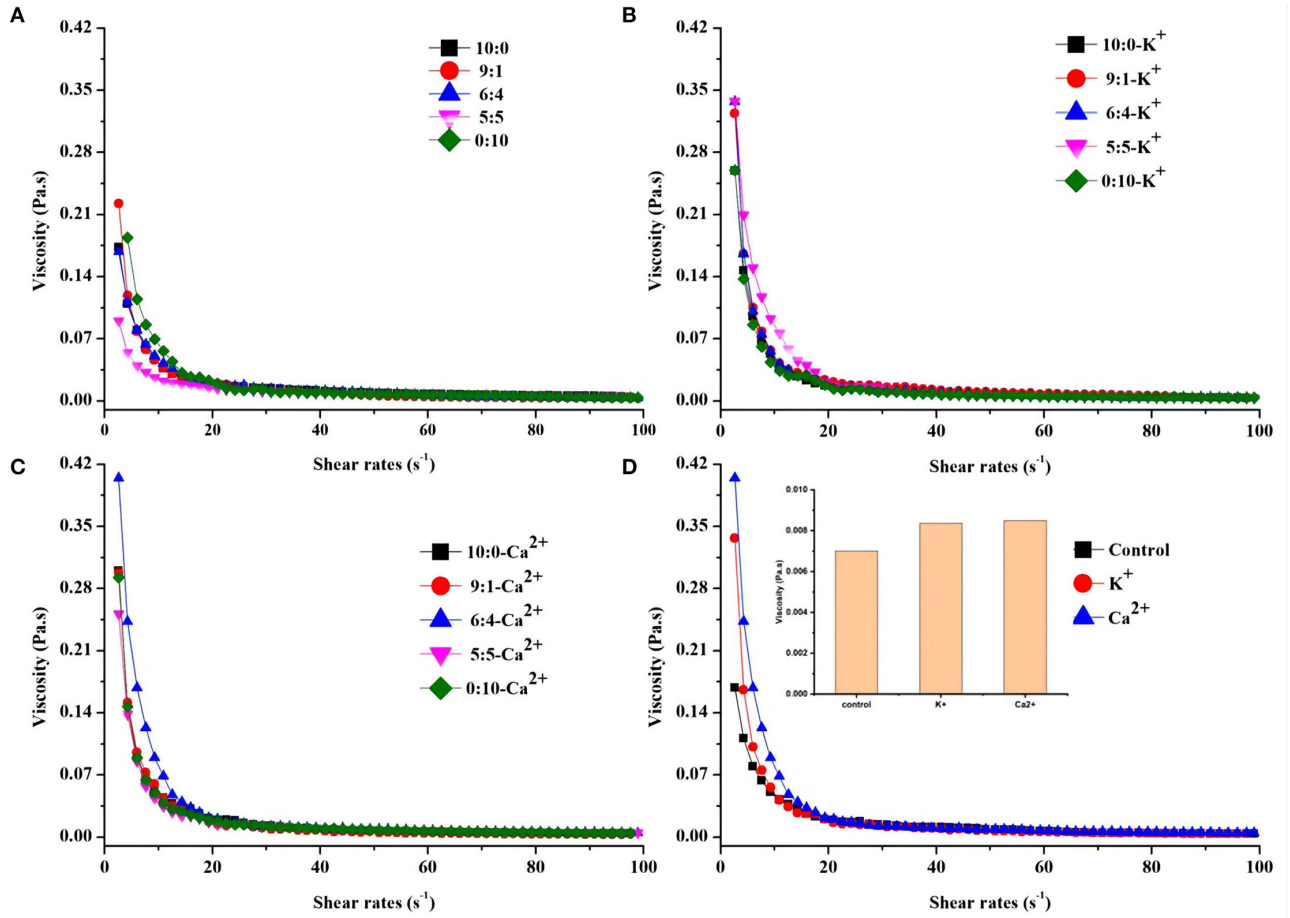

FIGURE 3 | Shear stress and viscosity relationships of OPO emulsions (10% v/v OPO human milk fat substitutes) at different protein ratios (WPI:CN/10:0, 9:1, 6:4, 5:5 and 0:10, 1% w/v in total; **(A)** either in the presence of K^+ **(B)** or Ca^{2+} **(C)**. **(D)** Comparison of the shear stress and viscosity relationship of OPO emulsions for WPI:CN/6:4 (control) with K^+ or Ca^{2+}.

varied ratios of WPI, based on the POV and TBARS content in **Figure 4**. The higher oxidation rate might be because the affinity of phosphate groups of casein molecules for iron was better than that of carboxylic acid groups of other proteins (29). In the 30-day oxidation stage, the POV content at different protein ratios (10:0, 9:1, 6:4, 5:5, and 0:10) without and with K^+ and Ca^{2+} was 3.39–9.39, 10.73–13.52, and 11.41–15.18 μg/ml and the TBARS content was 0.05–0.16, 0.06–0.35, and 0.08–0.56 μg/ml, respectively. These data indicated that K^+ and Ca^{2+} can promote the oxidation of emulsions, possibly because these ions destabilize the physical state of emulsions as mentioned above.

DISCUSSION

Whey protein isolate and CN are typical protein-type emulsifiers, which can exert their emulsification and adsorption properties in emulsions and are improved by electrostatic or three-dimensional repulsive forces to maintain emulsion stability (30). CN, characterized by its disordered structure and hydrophobic properties, possesses greater adsorption at the oil–water interface than a tiny, compact, and globular WPI (31).

As represented in **Figures 1B,C**, K^+ and Ca^{2+} binding may induce the aggregation of emulsion droplets as salt ions reduce the repulsive force between droplets (32). However, the particle size distribution peak of the samples shifted toward larger particle size with the addition of potassium ions, except for the ratio 5:5 in **Figure 1B**. According to Keowmaneechai et al., surfactants such as casein to replace the WP absorbed from the droplet surface, the aggregation induced by metal ions was found to be almost reversible (33). In addition, the homogenized proteins were exposed to more calcium binding sites, which might accelerate particle aggregation (34).

Therefore, compared with K^+, emulsions with Ca^{2+} produce extensive droplet aggregation resulting in an unstable emulsion. The absolute value of the zeta potential was the highest when the proportion of CN was the highest, as shown in **Figure 2**. Amino acid side chains from protein dissociation are more conducive to induce electrostatic repulsion to enhance emulsion

TABLE 2 | Effects of K^+ and Ca^{2+} on storage stability (particle size and zeta potential) in different OPO emulsions (10% v/v OPO human milk fat substitutes and WPI: CN/10:0, 9:1, 6:4, 5:5, 0:10, 1% w/v in total).

WPI: CN(1%, w/v)	0 day	8 days	16 days	24 days	32 days	40 days
Particle size						
10:0	276.57 ± 3.29^{c}	253.10 ± 1.87^{d}	285.93 ± 1.50^{c}	330.33 ± 13.65^{b}	351.80 ± 4.65^{a}	355.87 ± 3.50^{a}
9:1	307.43 ± 6.02^{d}	344.27 ± 3.37^{c}	347.37 ± 4.22^{c}	373.30 ± 4.55^{b}	429.23 ± 3.34^{a}	435.00 ± 2.82^{a}
6:4	233.70 ± 3.22^{f}	342.83 ± 0.81^{e}	379.07 ± 5.05^{d}	403.37 ± 5.77^{c}	443.77 ± 3.77^{b}	467.70 ± 1.85^{a}
5:5	229.10 ± 1.18^{d}	322.37 ± 2.81^{c}	365.60 ± 2.50^{b}	380.00 ± 16.10^{b}	402.97 ± 7.11^{a}	409.70 ± 9.26^{a}
0:10	253.27 ± 1.68^{d}	253.47 ± 2.17^{d}	311.27 ± 3.02^{c}	335.17 ± 3.60^{b}	348.80 ± 0.46^{b}	395.23 ± 4.77^{a}
10:0-K^+	259.30 ± 2.26^{e}	269.77 ± 2.61^{e}	329.93 ± 7.97^{d}	353.17 ± 3.52^{c}	383.90 ± 5.84^{b}	429.93 ± 6.08^{a}
9:1-K^+	265.77 ± 1.04^{e}	273.40 ± 3.15^{e}	356.60 ± 4.08^{d}	386.03 ± 4.66^{c}	403.40 ± 3.22^{b}	426.60 ± 4.50^{a}
6:4-K^+	266.80 ± 1.84^{d}	254.07 ± 2.95^{e}	347.70 ± 3.76^{c}	363.83 ± 2.91^{c}	426.60 ± 9.28^{b}	452.83 ± 10.07^{a}
5:5-K^+	250.20 ± 2.91^{e}	288.90 ± 4.03^{d}	343.33 ± 5.09^{c}	358.33 ± 8.74^{c}	424.17 ± 0.81^{b}	487.13 ± 3.81^{a}
0:10-K^+	281.33 ± 7.69^{e}	339.77 ± 1.44^{d}	381.67 ± 8.52^{c}	423.33 ± 2.89^{c}	469.17 ± 10.08^{b}	507.30 ± 1.65^{a}
10:0-Ca^{2+}	317.97 ± 6.06^{d}	331.27 ± 3.18^{c}	354.60 ± 5.81^{c}	387.17 ± 3.00^{b}	413.73 ± 5.05^{a}	424.33 ± 2.16^{a}
9:1-Ca^{2+}	355.40 ± 4.16^{c}	343.17 ± 6.62^{d}	369.13 ± 3.17^{c}	451.83 ± 13.27^{b}	464.30 ± 4.11^{b}	491.93 ± 2.53^{a}
6:4-Ca^{2+}	361.47 ± 5.70^{e}	397.30 ± 2.46^{d}	454.67 ± 3.45^{c}	479.07 ± 2.80^{b}	486.73 ± 20.76^{b}	514.10 ± 1.74^{a}
5:5-Ca^{2+}	304.13 ± 3.30^{e}	380.60 ± 6.31^{d}	408.60 ± 2.96^{c}	418.67 ± 12.17^{b}	427.2 ± 18.76^{b}	500.90 ± 13.00^{a}
0:10-Ca^{2+}	352.63 ± 9.18^{d}	363.90 ± 7.20^{c}	376.53 ± 12.08^{c}	462.50 ± 4.52^{b}	465.17 ± 3.36^{a}	460.90 ± 14.30^{b}
Zeta potential						
10:0	−45.73 ± 2.21^{a}	−43.87 ± 2.80^{b}	−43.47 ± 2.90^{b}	−42.43 ± 0.21^{c}	−42.20 ± 0.26^{c}	−41.53 ± 1.00^{d}
9:1	−48.23 ± 2.75^{a}	−45.10 ± 0.26^{b}	−44.70 ± 2.35^{c}	−43.47 ± 0.29^{d}	−43.03 ± 0.85^{d}	−42.43 ± 1.65^{e}
6:4	−50.40 ± 0.75^{a}	−50.10 ± 0.69^{a}	−47.83 ± 0.45^{b}	−47.73 ± 0.99^{b}	−47.07 ± 2.66^{b}	−45.67 ± 1.30^{c}
5:5	−52.40 ± 1.37^{a}	−52.07 ± 3.99^{a}	−48.47 ± 0.32^{b}	−47.13 ± 0.68^{c}	−46.43 ± 0.35^{d}	−46.23 ± 1.16^{d}
0:10	−59.47 ± 2.72^{a}	−56.77 ± 3.17^{b}	−56.43 ± 0.87^{b}	−52.13 ± 0.38^{c}	−51.63 ± 1.40^{d}	−51.27 ± 4.30^{d}
10:0-K^+	−42.93 ± 0.57^{a}	−41.37 ± 0.93^{b}	−41.27 ± 0.12^{b}	−40.10 ± 0.61^{c}	−39.57 ± 0.49^{d}	−39.53 ± 0.59^{d}
9:1-K^+	−44.50 ± 0.35^{a}	−44.27 ± 0.31^{a}	−42.93 ± 0.82^{b}	−41.50 ± 0.23^{c}	−41.17 ± 0.40^{c}	−40.87 ± 0.72^{c}
6:4-K^+	−48.97 ± 0.25^{a}	−48.30 ± 0.70^{a}	−47.07 ± 1.10^{b}	−46.03 ± 0.31^{c}	−45.07 ± 1.00^{d}	−43.97 ± 0.91^{e}
5:5-K^+	−50.40 ± 0.53^{a}	−50.07 ± 0.42	−47.03 ± 0.45	−46.37 ± 0.12	−46.00 ± 0.75	−45.97 ± 0.40
0:10-K^+	−54.93 ± 0.57^{b}	−56.83 ± 0.06^{a}	−53.90 ± 0.70^{c}	−53.17 ± 0.80^{c}	−52.37 ± 0.49^{d}	−52.33 ± 0.66^{d}
10:0-Ca^{2+}	−39.97 ± 0.50^{a}	−34.63 ± 0.72^{b}	−34.20 ± 0.36^{b}	−33.73 ± 0.75^{c}	−32.90 ± 0.21^{d}	−30.47 ± 0.52^{e}
9:1-Ca^{2+}	−37.20 ± 0.56^{a}	−37.13 ± 0.67^{a}	−35.53 ± 0.68^{b}	−35.13 ± 0.61^{b}	−34.63 ± 0.55^{c}	−31.77 ± 0.60^{d}
6:4-Ca^{2+}	−37.10 ± 0.62^{a}	−36.80 ± 0.44	−36.63 ± 0.66	−35.90 ± 0.00	−35.70 ± 0.50	−34.90 ± 0.78
5:5-Ca^{2+}	−39.30 ± 0.36^{a}	−37.80 ± 0.62^{b}	−37.40 ± 0.87^{b}	−36.80 ± 1.10^{c}	−36.10 ± 0.10^{c}	−29.67 ± 0.40^{d}
0:10-Ca^{2+}	−40.03 ± 0.40^{a}	−38.73 ± 0.74^{b}	−37.67 ± 0.55^{c}	−37.37 ± 0.50^{c}	−37.17 ± 0.80^{c}	−36.10 ± 0.61^{d}

$^{a-f}$*Different small letters represent the significance of the difference ($p < 0.05$).*

stability when the pH (the pH of emulsions is seven) is further away from the emulsifier's isoelectric point (35, 36). At pH values above the isoelectric point, protein molecules have more $-COO^-$ groups than $-NH3^+$ groups, so protein molecules present more negatively charged groups. It has been reported that Ca^{2+} can bind to the two main proteins of whey protein through the free carboxylic groups of aspartic and glutamic acids (35, 37). Therefore, Ca^{2+} could combine with the $-COO^-$ groups to reduce the negative charge on the surface of emulsion droplets in this study. In the absence of K^+, emulsions might lead to a less extensive diffuse double layer, interdroplet repulsion, and eventually droplet aggregation (38). The effect of ion valence on emulsion zeta potential in this study indicated that multivalent ions in the emulsion were more effective than monovalent ions combined with countercharge in the interaction effects of electrostatic shielding and ion surface adsorption. Our results were consistent with the conclusions of previous studies (39).

Creaming index is an important indicator to measure the degree of aggregation of lipid droplets in the emulsion. Lipid droplet network layout, structural rearrangement, and final phase separation kinetics are the critical aspects, which impact emulsion instability, and depletion flocculation is one of the main causes (40–42). Emulsions with a high creaming index are generally unstable (16). According to Srinivasan et al., a high CN emulsion content resulted in low stability due to depletion flocculation generated by the unabsorbed CN in the aqueous phase (43). Our results showed that the addition of K^+ and Ca^{2+} plays an important role in emulsion stability. The electrostatic repulsion between the droplets was gradually shielded by the anti-ions around the droplets, and the small particulate matter adsorbed on each other, so that the large

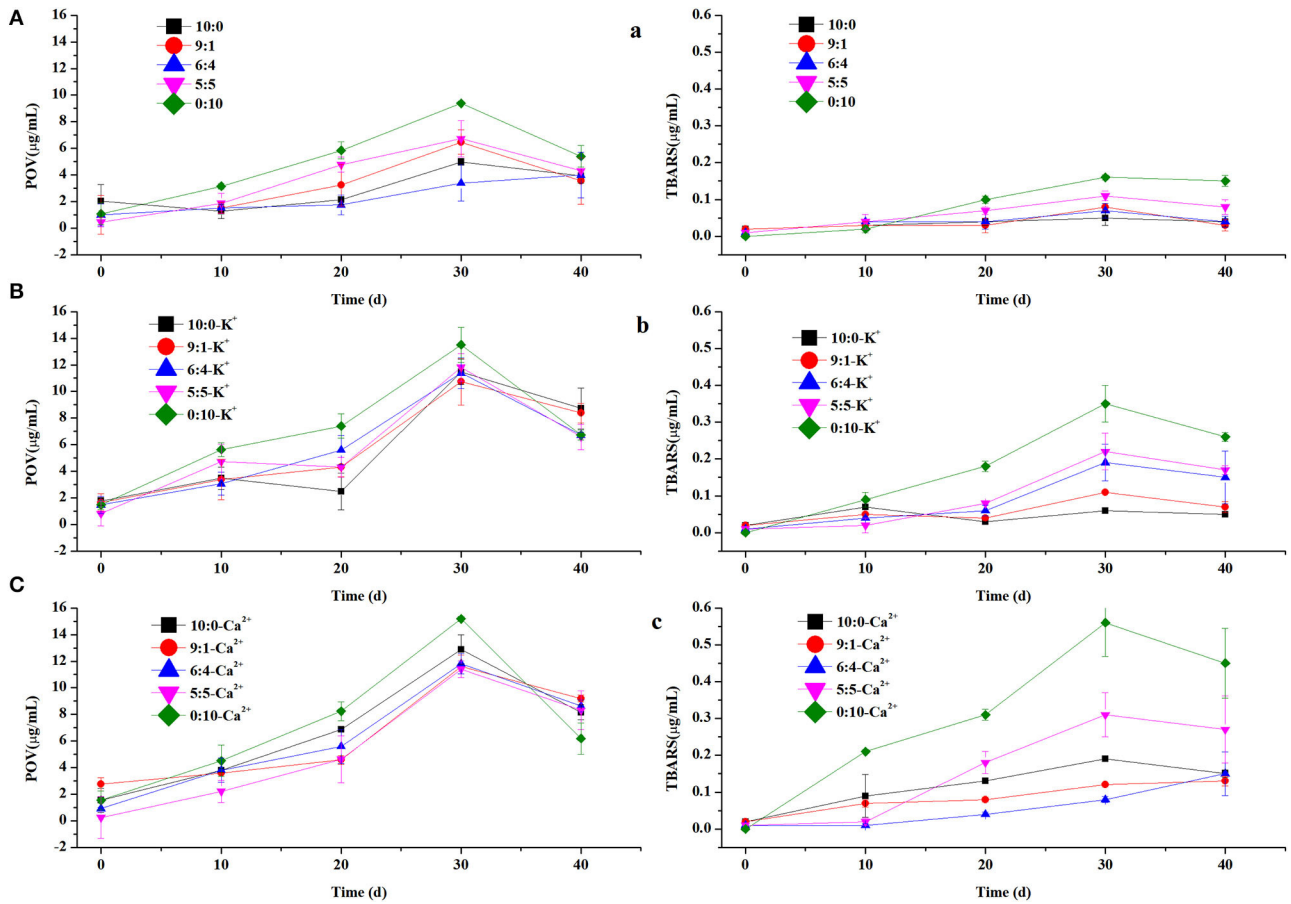

FIGURE 4 | The peroxidevalue (POV) and thiobarbituric acid reactive substances (TBARS) of control, containing K^+ **(A–C)** and containing Ca^{2+} **(a–c)** in OPO emulsions (10% v/v OPO human milk fat substitutes and WPI: CN/10:0, 9:1, 6:4, 5:5, 0:10, 1% w/v in total) as emulsifiers.

particles aggregated and the fat floated upward with the addition of K^+ and Ca^{2+} (44). In addition, the effects of K^+ and Ca^{2+} on creaming index might be gradually increasing particle size and making droplet aggregation to result in flocculation with storage days. A higher degree of flocculation is preferable to a higher degree of creaming in emulsions (45). Creaming instability measurements in the absence of K^+ and Ca^{2+} support the result of particle size and zeta potential measurements.

The rheological property is also a key factor to consider in O/W emulsion stability. Previous research showed that the floccules created in the emulsion trapped water molecules in the two oil–water phases. This increased the effective volume fraction of particles and promoted the flocculated emulsion to have a higher viscosity than the unflocculated emulsion (45, 46). Our results indicated that the Ca^{2+}- containing emulsion has a higher viscosity, as shown in **Figure 3D**. It would be expected that Ca^{2+} could promote the flocculation of droplets to a greater extent and increase its strength due to electrostatic screen interactions, reduce droplet charge, and act as ionic bridges, while potassium ion could only play a role of electrostatic screen interactions, with weak strength and low emulsion viscosity (33).

Emulsion destabilization is often due to various physical phenomena. As shown in **Table 2**, the emulsion particle size in each group increased to different degrees and the Ca^{2+} group had the highest particle size on day 40 of the storage period. Previous studies have indicated that flocculation, rather than coalescence, is the cause of droplet aggregation of emulsions with calcium (19) and potassium (47). Flocculation occurs because the metal ions reduce the electrostatic repulsion between the droplets, thus these droplets get closer. According to Ray and Rousseau, droplet aggregation caused by electrostatic action is blocked when the absolute value of the zeta potential of the emulsion is higher than 30 mV (58) (48). In contrast, the absolute value of the zeta potential of a calcium ion was 29.67 ± 0.40, which is the smallest among the three groups. This result showed that the emulsion of adding Ca^{2+} would be unstable, which was consistent with the previous results. The emulsion particle size and zeta potential during the 40 days of study indicated that the storage stability of each emulsion is different due to factors such as protein ratios and ionic

strength, which is consistent with the results reported by Ye (49). The above results indicated that K^+ and Ca^{2+} affect the long-term stability of OPO emulsions, which may have significant effects on the formulation of potassium- and calcium-enhanced emulsion-based products with a long expected shelf-life.

In addition to physical properties, lipid oxidation is a major issue in food storage and consumption, influencing the flavor, odor, and color of food (11). Our results showed that lipid oxidation might be caused by the different structures of WPI and CN, enabling their affinity for iron to be different. However, during the oxidation process, the principal product, hydroperoxide, dissociates into secondary oxidation products, such as malondialdehyde and hexanal, resulting in a decrease in the oxidation content of POV (50).

As shown in **Figures 4B-b,C-c**, our results indicated that both POV and TBARS values increase after adding K^+ and Ca^{2+} into the emulsion, which can promote the oxidation of emulsions enabling emulsions to be unstable. The results were the same as particle size and creaming index.

We chose the different ratios of WPI and CN to better simulate the different stages of breastfeeding, and added OPO human milk fat substitute, which was conducive to the digestion and absorption of breast milk by infants. Furthermore, minerals are also essential, and K^+ and Ca^{2+} account for a high proportion of minerals in infant formula. Thus, macronutrients and micronutrients complement each other. However, this infant formula was not ideal, which might be related to the concentration of added minerals. Therefore, the effect of varying mineral ion concentrations on the physicochemical properties of the OPO emulsion must be thoroughly explored to prepare a stable liquid infant formula. In addition, from a nutritional point of view, *in vitro* gastrointestinal digestion would be ideal, and could be further investigated.

CONCLUSIONS

This study demonstrates the impact of protein ratios and mineral ions on the stability of OPO emulsions as mimics of a liquid infant formula. Changes in WPI to CN ratios had a significant impact on the zeta potential but not on particle size. The addition of Ca^{2+} increased the average particle size and decreased the zeta potential. It caused emulsion instability, possibly because Ca^{2+} reduced the charge of the droplets and acted as an ionic bridge by shielding the interaction between static electricity and ions. These interactions promoted flocculation of the droplets and subsequently failed to prevent oil oxidation.

DATA AVAILABILITY STATEMENT

The raw data supporting the conclusions of this article will be made available by the authors, without undue reservation.

AUTHOR CONTRIBUTIONS

QW finished the conceptualization, set the methodology, and wrote the original draft. YX finished the methodology and analyzed the data with the software. YL finished the investigation and validation. FQ guided the methodology and supervised the results. GM and XZ participated in project administration, acquired funding, and reviewed and edited this manuscript. All authors have read and accepted the published version of this manuscript.

ACKNOWLEDGMENTS

This research was funded by the National Natural Science Foundation of China (Nos. 31901614, 31660470).

REFERENCES

1. Walker A. Breast milk as the gold standard for protective nutrients. *J Pediatr.* (2010) 156:S3–7. doi: 10.1016/j.jpeds.2009.11.021
2. He S, Liu G, Zhu X. Human breast milk-derived exosomes may help maintain intestinal epithelial barrier integrity. *Pediatr Res.* (2021) 90:366–72. doi: 10.1038/s41390-021-01449-y
3. Demmelmair H, Koletzko B. Lipids in human milk. Best practice & research. *Clin Endocrinol Metab.* (2018) 32:57–68. doi: 10.1016/j.beem.2017.11.002
4. Qin XL, Zhong JF, Wang YH, Yang B, Lan DM, Wang FH. 1,3-Dioleoyl-2-palmitoylglycerol-rich human milk fat substitutes: Production, purification, characterization and modeling of the formulation. *Eur J Lipid Sci Technol.* (2014) 116:282–90. doi: 10.1002/ejlt.201300343
5. Wei W, Feng Y, Zhang X, Cao X, Feng, F. Synthesis of structured lipid 1,3-dioleoyl-2-palmitoylglycerol in both solvent and solvent-free system. *LWT-Food Sci. Technol.* (2015) 60:1187–94. doi: 10.1016/j.lwt.2014.09.013
6. Wei W, Jin Q, Wang X. Human milk fat substitutes: past achievements and current trends. *Prog Lipid Res.* (2019) 74:69–86. doi: 10.1016/j.plipres.2019.02.001
7. Ilyasoglu H, Gultekin-Ozguven M, Ozcelik, B. Production of human milk fat substitute with medium-chain fatty acids by lipase-catalyzed acidolysis: optimization by response surface methodology. *LWT-Food Sci Technol.* (2011) 44:999–1004. doi: 10.1016/j.lwt.2010.11.027
8. Carnielli VP, Luijendijk I, Vangoudoever JB, Sulkers EJ, Sauer P. Structural position and amount of palmitic acid in infant formulas: effects on fat, fatty acid, and mineral balance. *Pediatr Res.* (1994) 36:10–10. doi: 10.1203/00006450-199407000-00047
9. López-López A, López-Sabater MC, Campoy-Folgoso C, Rivero-Urgell M, Castellote-Bargalló AI. Fatty acid and sn-2 fatty acid composition in human milk from Granada (Spain) and in infant formulas. *Eur J Clin Nutr.* (2002) 56:1242–54. doi: 10.1038/sj.ejcn.1601470
10. Koo WW, Hockman EM, Dow M. Palm olein in the fat blend of infant formulas: effect on the intestinal absorption of calcium and fat, and bone mineralization. *J Am Coll Nutr.* (2006) 25:117–22. doi: 10.1080/07315724.2006.10719521
11. Ries D, Ye A, Haisman D, Singh, H. Antioxidant properties of caseins and whey proteins in model oil-in-water emulsions. *Int Dairy J.* (2010) 20:72–8. doi: 10.1016/j.idairyj.2009.09.001
12. Ji J, Zhang J, Chen J, Wang Y, Dong N, Hu C, et al. Preparation and stabilization of emulsions stabilized by mixed sodium caseinate and soy protein isolate. *Food Hydrocoll.* (2015) 51:156–65. doi: 10.1016/j.foodhyd.2015.05.013

13. Liang Y, Gillies G, Patel H, Matia-Merino L, Ye A, Golding M. Physical stability, microstructure and rheology of sodium-caseinate-stabilized emulsions as influenced by protein concentration and non-adsorbing polysaccharides. *Food Hydrocoll.* (2014) 36:245–55. doi: 10.1016/j.foodhyd.2013.10.006
14. Yerramilli M, Ghosh S. Long-term stability of sodium caseinate-stabilized nanoemulsions. *J Food Sci Technol.* (2017) 54:82–92. doi: 10.1007/s13197-016-2438-y
15. Zembyla M, Murray BS, Radford SJ, Sarkar A. Water-in-oil Pickering emulsions stabilized by an interfacial complex of water-insoluble polyphenol crystals and protein. *J Colloid Interf Sci.* (2019) 548:88–99. doi: 10.1016/j.jcis.2019.04.010
16. Abdolmaleki K, Mohammadifar MA, Mohammadi R, Fadavi G, Meybodi NM. The effect of pH and salt on the stability and physicochemical properties of oil-in-water emulsions prepared with gum tragacanth. *Carbohydr Polym.* (2016) 140:342–8. doi: 10.1016/j.carbpol.2015.12.081
17. Erxleben SW, Pelan E, Wolf B. Effect of ethanol on the stability of sodium caseinate stabilised emulsions. *Food Hydrocoll.* (2021) 121:107058. doi: 10.1016/j.foodhyd.2021.107058
18. Ye A, Singh H. Interfacial composition and stability of sodium caseinate emulsions as influenced by calcium ions. *Food Hydrocoll.* (2001) 15:195–207. doi: 10.1016/S0268-005X(00)00065-5
19. Ye A, Singh H. Influence of calcium chloride addition on the properties of emulsions stabilized by whey protein concentrate. *Food Hydrocoll.* (2000) 14:337–46. doi: 10.1016/S0268-005X(00)00010-2
20. Qian C, Decker EA, Xiao H, McClements DJ. Physical and chemical stability of β-carotene-enriched nanoemulsions: Influence of pH, ionic strength, temperature, and emulsifier type. *Food Chem.* (2012) 132:1221–9. doi: 10.1016/j.foodchem.2011.11.091
21. Ravindran S, Williams MAK, Ward RL, Gillies G. Understanding how the properties of whey protein stabilized emulsions depend on pH, ionic strength and calcium concentration, by mapping environmental conditions to zeta potential. *Food Hydrocoll.* (2018) 79:572–8. doi: 10.1016/j.foodhyd.2017.12.003
22. Owens C, Griffin K, Khouryieh H, Williams K. Creaming and oxidative stability of fish oil-in-water emulsions stabilized by whey protein-xanthan-locust bean complexes: impact of pH. *Food Chem.* (2018) 239:314–22. doi: 10.1016/j.foodchem.2017.06.096
23. Castel V, Rubiolo AC, Carrara CR. Droplet size distribution, rheological behavior and stability of corn oil emulsions stabilized by a novel hydrocolloid (Brea gum) compared with gum arabic. *Food Hydrocoll.* (2017) 63:170–7. doi: 10.1016/j.foodhyd.2016.08.039
24. Qiu C, Zhao M, Decker EA, McClements DJ. Influence of protein type on oxidation and digestibility of fish oil-in-water emulsions: gliadin, caseinate, and whey protein. *Food Chem.* (2015) 175:249–57. doi: 10.1016/j.foodchem.2014.11.112
25. Zeng T, Wu ZL, Zhu JY, Yin SW, Tang CH, Wu LY, et al. Development of antioxidant Pickering high internal phase emulsions (HIPEs) stabilized by protein/polysaccharide hybrid particles as potential alternative for PHOs. *Food Chem.* (2017) 231:122–30. doi: 10.1016/j.foodchem.2017.03.116
26. Xu X, Liu W, Luo L, Liu C, McClements DJ. Influence of anionic polysaccharides on the physical and oxidative stability of hydrolyzed rice glutelin emulsions: impact of polysaccharide type and pH. *Food Hydrocoll.* (2017) 72:185–94. doi: 10.1016/j.foodhyd.2017.05.018
27. Dickinson E. Introduction to food colloids. *J Study Relig Ideol.* (1992) 64:22–23.
28. Guzun-Cojocaru T, Koev C, Yordanov M, Karbowiak T, Cases E, Cayot P. Oxidative stability of oil-in-water emulsions containing iron chelates: Transfer of iron from chelates to milk proteins at interface. *Food Chem.* (2011) 125:326–33. doi: 10.1016/j.foodchem.2010.08.004
29. Sugiarto M, Ye A, Singh H. Characterisation of binding of iron to sodium caseinate and whey protein isolate. *Food Chem.* (2009) 114:1007–13. doi: 10.1016/j.foodchem.2008.10.062
30. Kellerby SS, McClements DJ, Decker EA. Role of proteins in oil-in-water emulsions on the stability of lipid hydroperoxides. *J Agric Food Chem.* (2006) 54:7879–84. doi: 10.1021/jf061340s
31. Hu M, McClements DJ, Decker EA. Impact of whey protein emulsifiers on the oxidative stability of salmon oil-in-water emulsions. *J Agric Food Chem.* (2003) 51:1435–9. doi: 10.1021/jf0203794
32. Shao Y, Tang CH. Characteristics and oxidative stability of soy protein-stabilized oil-in-water emulsions: influence of ionic strength and heat pretreatment. *Food Hydrocoll.* (2014) 37:149–58. doi: 10.1016/j.foodhyd.2013.10.030
33. Keowmaneechai E, McClements DJ. Effect of CaCl2 and KCl on physiochemical properties of model nutritional beverages based on whey protein stabilized oil-in-water emulsions. *J Food Sci.* (2002) 67:665–671. doi: 10.1111/j.1365-2621.2002.tb10657.x
34. Radford SJ, Dickinson E, Golding M. Stability and rheology of emulsions containing sodium caseinate: combined effects of ionic calcium and alcohol. *J Colloid Interface Sci.* (2004) 274:673–86. doi: 10.1016/j.jcis.2003.12.045
35. Pappas CP, Rothwell J. The effects of heating, alone or in the presence of calcium or lactose, on calcium binding to milk proteins. *Food Chem.* (1991) 42:183–201. doi: 10.1016/0308-8146(91)90033-K
36. Walker HW, Grant SB. Influence of surface charge and particle size on the stabilization of colloidal particles by model polyelectrolytes. *Coll Surf A.* (1998) 135:123–33. doi: 10.1016/S0927-7757(97)00226-4
37. Baumy JJ, Brule G. Binding of bivalent cations to a-lactalbumin and b-lactoglobulin: effect of pH and ionic strength. *Lait.* (1988) 68:33–48. doi: 10.1051/lait:198813
38. Kulmyrzaev AA, Schubert H. Influence of KCl on the physicochemical properties of whey protein stabilized emulsions. *Food Hydrocoll.* (2004) 18:13–9. doi: 10.1016/S0268-005X(03)00037-7
39. Shao P, Ma H, Zhu J, Qiu Q. Impact of ionic strength on physicochemical stability of o/w emulsions stabilized by Ulva fasciata polysaccharide. *Food Hydrocoll.* (2017) 69:202–9. doi: 10.1016/j.foodhyd.2017.01.039
40. Cuevas-Bernardino JC, Lobato-Calleros C, Román-Guerrero A, Alvarez-Ramirez J, Vernon-Carter EJ. Physicochemical characterisation of hawthorn pectins and their performing in stabilising oil-in-water emulsions. *React Funct Polym.* (2016) 103:63–71. doi: 10.1016/j.reactfunctpolym.2016.03.024
41. Hu HY, Xing LJ, Hu YY, Qiao CL, Wu T, Zhou GH, et al. Effects of regenerated cellulose on oil-in-water emulsions stabilized by sodium caseinate. *Food Hydrocoll.* (2016) 52:38–46. doi: 10.1016/j.foodhyd.2015.06.019
42. Liang Y, Gillies G, Matia-Merino L, Ye A, Patel H, Golding M. Structure and stability of sodium-caseinate-stabilized oil-in-water emulsions as influenced by heat treatment. *Food Hydrocoll.* (2016) 66:307–17. doi: 10.1016/j.foodhyd.2016.11.041
43. Srinivasan M, Singh H, Munro PA. The effect of sodium chloride on the formation and stability of sodium caseinate emulsions. *Food Hydrocoll.* (2000) 14:497–507. doi: 10.1016/S0268-005X(00)00030-8
44. Xiao J, Wang X, Gonzalez AP, Huang, QR. Kafirin nanoparticlesstabilized Pickering emulsions: Microstructure and rheological properties. *Food Hydrocoll.* (2016) 54:30e3943. doi: 10.1016/j.foodhyd.2015.09.008
45. Sriprablom J, Luangpituksa P, Wongkongkatep J, Pongtharangkul T, Suphantharika M. Influence of pH and ionic strength on the physical and rheological properties and stability of whey protein stabilized o/w emulsions containing xanthan gum. *J Food Eng.* (2019) 242:141–52. doi: 10.1016/j.jfoodeng.2018.08.031
46. Dickinson E. Properties of emulsions stabilized with milk proteins: overview of some recent developments. *J Dairy Sci.* (1997) 80:2607–19. doi: 10.3168/jds.S0022-0302(97)76218-0
47. Hunt JA, Dalgleish DG. The effect of the presence of KCl on the adsorption behavior of whey protein and caseinate in oil-in-water emulsions. *Food Hydrocoll.* (1996) 10:159–65. doi: 10.1016/S0268-005X(96)80030-0
48. Ray M, Rousseau D. Stabilization of oil-in-water emulsions using mixtures of denatured soy whey proteins and soluble soybean polysaccharides. *Food Res Int.* (2013) 52:298–307. doi: 10.1016/j.foodres.2013.03.008
49. Ye A. Interfacial composition and stability of emulsions made with mixtures of commercial sodium caseinate and whey protein concentrate. *Food Chem.* (2008) 110:946–52. doi: 10.1016/j.foodchem.2008.02.091

50. Chen B, McClements DJ, Decker EA. Role of continuous phase anionic polysaccharides on the oxidative stability of menhaden oil-in-water emulsions. *J Agric Food Chem.* (2010) 58:3779–84. doi: 10.1021/jf9037166

Conflict of Interest: The authors declare that the research was conducted in the absence of any commercial or financial relationships that could be construed as a potential conflict of interest.

Publisher's Note: All claims expressed in this article are solely those of the authors and do not necessarily represent those of their affiliated organizations, or those of the publisher, the editors and the reviewers. Any product that may be evaluated in this article, or claim that may be made by its manufacturer, is not guaranteed or endorsed by the publisher.

Advantages of publishing in Frontiers

OPEN ACCESS
Articles are free to read for greatest visibility and readership

FAST PUBLICATION
Around 90 days from submission to decision

HIGH QUALITY PEER-REVIEW
Rigorous, collaborative, and constructive peer-review

TRANSPARENT PEER-REVIEW
Editors and reviewers acknowledged by name on published articles

Frontiers
Avenue du Tribunal-Fédéral 34
1005 Lausanne | Switzerland

Visit us: www.frontiersin.org
Contact us: frontiersin.org/about/contact

REPRODUCIBILITY OF RESEARCH
Support open data and methods to enhance research reproducibility

DIGITAL PUBLISHING
Articles designed for optimal readership across devices

FOLLOW US
@frontiersin

IMPACT METRICS
Advanced article metrics track visibility across digital media

EXTENSIVE PROMOTION
Marketing and promotion of impactful research

LOOP RESEARCH NETWORK
Our network increases your article's readership